THE DYNAMICS OF PACKED BEDS WITH INTRAPHASE HEAT TRANSFER

by

C. P. JEFFRESON, B.E., M. Eng. Sci..

DEPARTMENT OF CHEMICAL ENGINEERING

UNIVERSITY OF ADELAIDE

A T H E S I S

Submitted for the degree of Doctor of Philosophy

in the

Faculty of Engineering, University of Adelaide.

February, 1971

DECLARATION.

This is to certify that all ideas and results presented in this thesis are products of the writer's own work except where due acknowledgement is given.

The thesis contains no material previously submitted by the writer for a degree in this University or any other.

C. P. Jeffreson.

ABSTRACT.

An exploratory experimental study and theoretical analysis of the relationships between various mathematical descriptions or 'models' of linear packed bed heat transfer dynamics has been carried out. Some contributions have also been made to the theory and practice of dynamic testing.

Physical phenomena allowed for included fluid phase axial dispersion, inter and intra-phase heat transfer and bulk fluid convection. 'Two phase' finite stage and continuous models were compared and shown to yield close correspondence over a wide range of parameters.

The conditions under which a single parameter may be used to characterise the dynamic response of a packed bed were clarified. It was found that the 'equivalent conductivity' model of Babcock and co-workers could be used only when a parameter known as the 'heat capacity ratio', V_H was near unity. For large values of heat capacity ratio, the Schumann model could be applied, lumping axial dispersion and solids conductivity effects into an equivalent Schumann heat transfer parameter by means of a simple equation, provided the 'bed length parameter', γx, defined by Babcock was greater than 5 to 10.

The criterion proposed by Handley and Heggs for assessing the importance of 'intraparticle' (or internal particle conduction)

effects on breakthrough curves was examined. The criterion was found to be incorrect since it did not distinguish between 'dispersive' and 'curve shape' effects.

General integral formulae for determining breakthrough curves in a packed bed from any linear transfer function were derived and used, through an orthogonal polynomial Fourier transform inversion procedure, to obtain theoretical breakthrough curves for a wide range of parameters. Points on the curve were then correlated empirically against the single parameter referred to above, allowing rapid construction of any breakthrough curve satisfying the constraints on bed length parameter and heat capacity ratio.

Relationships between frequency response testing and moments analysis were derived and orthogonal polynomial approximation procedures for pulse to frequency response conversion developed. A critical assessment of errors inherent in various methods of dynamic testing has been presented with emphasis on the cyclic test method of frequency response and on two step response procedures.

A technique for improving the reliability of pulse testing experiments was developed and used to apply thermal pulse and step inputs to packed beds of lead, soda glass and Perspex through which air was flowing. Theoretical conclusions regarding the effect of the bed length parameter γx on curve shape were verified although anomalous results were obtained for small values of γx. It is suggested that the models considered do not provide a good

description of packed bed dynamics in this case. Comparison of experimental values of the Stanton number with those predicted by the steady state heat transfer correlations of Denton and others led to the conclusion that these correlations are 'contaminated' by axial fluid dispersion effects. Correction for axial fluids dispersion would therefore be expected to yield erroneous results in predictions of breakthrough curves, when those correlations are used. The theoretical effects of fluid phase axial dispersion on various steady state packed bed experiments were also considered by use of the F-factor approach of Epstein.

ACKNOWLEDGEMENTS

I would like to thank the University of Adelaide for allowing me the opportunity to complete a Ph.D. degree whilst paying me for the execution of my normal duties as a member of the Academic staff.

Thanks are also due :

to Professor R.W.F. Tait, Head of the Chemical Engineering Department for his tolerance and helpful criticisms,

to Michael Hutchison who carried out physical property determinations and some of the illustrations,

to members of the workshop staff of the Chemical Engineering Department,

to the Australian Institute of Nuclear Science and Engineering for financial assistance and the opportunity to test out my ideas at a number of symposia,

and to my wife Mary, whose help cannot be measured.

TABLE OF CONTENTS

Contents (Contd.)

Contents (contd.)

Contents (contd.)

Contents (contd.)

Contents (contd.)

Contents (contd.)

LIST OF ILLUSTRATIONS

ILLUSTRATIONS (contd.)

ILLUSTRATIONS (contd.)

CHAPTER V

CHAPTER VI

ILLUSTRATIONS (contd.)

ILLUSTRATIONS (contd.)

APPENDICES

Appendix 11

LIST OF TABULATIONS

CHAPTER II

CHAPTER IV

CHAPTER VI

CHAPTER VII

TABULATIONS (contd.)

TABULATIONS (contd.)

APPENDICES

INTRODUCTION - OVERALL OBJECTIVES OF STUDY

(a) Mathematical Modelling

The objects of this study have been to examine various mathematical models of packed bed dynamics, to compare the predictions of each and to extend them so that a wide range of physical phenomena might be included in the description. Experimental verification has been limited to a heat transfer system. Nevertheless the writer has been conscious of the wider applications of the theory to mass transfer systems such as ion exchange beds, adsorption columns and gas chromatographic columns. Much of the work in the latter field, for example the extraction of data concerning internal particle diffusivities and the determination of adsorption isotherms by dynamic testing, relies on the validity of various mathematical models of the system. It has been felt that a detailed study of the (analogous) heat transfer system where physical properties are relatively easy to measure would allow more detailed verification of the models to be carried out. The effects of axial conduction and 'dispersion' have been chosen for detailed study from a theoretical viewpoint whilst intraparticle heat transfer resistance has also been studied experimentally.

(b) Dynamic Testing Methods

Interpretation of the results of a dynamic experiment depend not only on the validity of an assumed mathematical description of the system but on the data reduction technique used and the actual

organisation of the test itself. Therefore, a parallel investigation was undertaken into several of the testing methods commonly used, in order to assess the importance of various errors and to eliminate these where possible. It was hoped that the results of such a study might find applications wider than the particular heat transfer system under study.

(c) Prediction of Breakthrough Curves

A potentially useful application of the work is to the prediction of breakthrough curves of linear adsorbers and thermal regenerators. The most rigorous and general solution to the problem to date has been that of J.B. Rosen [1952]. Unfortunately, the complexity of the computations involved has limited its practical value in design whilst a potentially important phenomenon, that of fluid phase axial dispersion had, because of mathematical difficulties, to be ignored.

The 'equivalent conductivity' model of Babcock and co-workers [1966, 1967] yields a mathematically-simple form for the breakthrough curve whilst including axial dispersion in its description. A parallel task has been to test assumptions inherent in the equivalent conductivity model and to provide more rigorous yet computationally simple solutions to the breakthrough curve problem.

(d) Heat Transfer in Packed Beds

Whilst most of the physical parameters of a heat transfer system are readily measured, one remains, despite an enormous

literature on the subject, still open to question. This parameter is the average fluid-particle heat transfer coefficient. It is necessary to establish heat transfer correlations which have a general physical meaning rather than correlations which merely ensure a good fit to a particular experimenter's mathematical model under rigidly defined conditions. In other words, in order to test a particular mathematical description, the physical parameters must be measurable by techniques which are independent of the description. An assessment of the reliability of literature correlations hence became necessary. Whilst a definitive evaluation is not yet possible, it was hoped that the range of choice might at least be narrowed down. Further contributions to this field are likely to come from the (more fundamental) work of fluid mechanists and heat transfer specialists.

CHAPTER I

PHYSICAL PROCESSES IN PACKED BEDS

SCOPE OF THE CHAPTER

In this chapter, the physical basis for the mathematical theories of packed bed dynamics developed in later chapters is reviewed. No attempt is made to derive the usual equations for the continuous or axial dispersion model of packed bed dynamics since these have been presented many times in the literature. A mathematical treatment of the finite stage or mixing cell model is also deferred until later.

In Section A, evidence for axial dispersion in the fluid phase is reviewed, together with a brief discussion of the influence of axial solids conduction from the continuous model point of view. This discussion is continued in greater detail in Chapter III. The effects of velocity and voidage variations are also considered.

In Section B, the literature on fluid-particle heat transfer is reviewed in an attempt to establish reliable correlations against which mathematical models may be later tested at least in the high Reynolds number range.

In Section C, the physical assumptions usually made in formulating "mathematical models" of packed bed dynamics are summarised.

A. AXIAL CONDUCTION IN PACKED BEDS

1. Effective Axial 'Conductivity'

Estimates of axial and radial 'conductivity' of packed beds through which a fluid is flowing steadily are of importance in the design of packed bed chemical reactors. Considering a plane of fluid regarded for the moment as moving at an effectively uniform velocity v_a, then heat may be transferred normal to the direction of fluid flow as a result of heat transfer into and within the solid packing. In the fluid phase, heat may be transferred in the direction of fluid flow by random molecular motion relative to the plane of fluid flow (molecular conductivity) and by parallel paths through the boundary layers surrounding the particles and thence through the solid by conduction.

It was natural, given such a physical picture, to postulate an effective axial conductivity k_a such that the flux of thermal energy relative to the bulk motion would be given by

$$F = - k_a \frac{\partial T}{\partial z} \qquad \ldots \quad (1.1)$$

where $k_a = \varepsilon . k_m + (1 - \varepsilon) \times$ (fluid-solid-fluid conductivity)

k_m = molecular conductivity

and ε is the mean area porosity of the bed.

Similar expressions could also be written for radial 'effective conductivity'. In postulating the existence of such

a 'conductivity' the obviously heterogeneous medium is regarded as homogeneous. It may be expected that this approach will yield incorrect results when an exothermic reaction occurs on or in the particles so that local particle temperatures differ markedly from that of the fluid. Axial 'conduction' is difficult to measure from steady state experiments unless radial heat transfer is occurring or heat is generated by chemical reaction. Nonetheless, it was soon realised [Argo, 1953] that, however imprecise the experiments, effective conductivity in the axial direction was considerably larger than radial conductivity for superficial particle Reynolds numbers greater than 10. The axial conductivity approach is used (in section 5) to qualitatively establish the importance of fluid-solid-fluid conduction.

2. Mixing Cell Theory

Kramers and Alberda [1953] and later, more rigorously Aris and Amundson [1957] showed that differential motion due to mixing in the voids of a packed bed, this time on the scale of particle diameters, yielded a further apparent component of axial fluid conductivity which explained the differences in radial and axial effective conductivity referred to above. On the assumption that fluid flowed through a packed bed via a series of well mixed voids separated by a distance γd_p (where γ is roughly 1.0 for a randomly packed bed), they obtained an equation relating the concentration c_j of a tracer material in a perfectly mixed

'cell' a distance $j.\gamma.\ d_p$ from the bed inlet to the concentration c_{j-1} coming from a preceding cell:

$$v_a\ (c_{j-1} - c_j) = \gamma\ d_p \frac{dc_j}{dt'} \quad , j = 1, 2, \ldots N \qquad \ldots \quad (2.1)$$

where v_a is the axial interstitial velocity and t' is time (not normalised). The solution $c_N(t')$ was obtained for various inlet concentration variations, $c_0(t')$, and compared with the solution to the corresponding axial dispersion equation:-

$$\frac{\partial c}{\partial t'}\ (z,t) = - v_a \frac{\partial c}{\partial z'} + D_e \frac{\partial^2 c}{\partial z'^2} \qquad \ldots \quad (2.2)$$

where z', the length $= j.\gamma.\ d_p$,

v_a is the interstitial fluid velocity

and D_e = eddy dispersivity of tracer in the bulk fluid.

The result was that, for N large enough,

$$D_e = v_a.d_p.\ \frac{\gamma}{2}$$

$$\text{i.e.} \qquad Pe = \frac{v_a d_p}{D_e} = \frac{2}{\gamma} \simeq 2.0 \qquad \ldots \quad (2.3)$$

where Pe is defined as the fluid-phase axial dispersion Peclet number.

Kramers and Alberda used a sinuisoidal inlet concentration variation whilst Aris and Amundson considered an impulsive input.

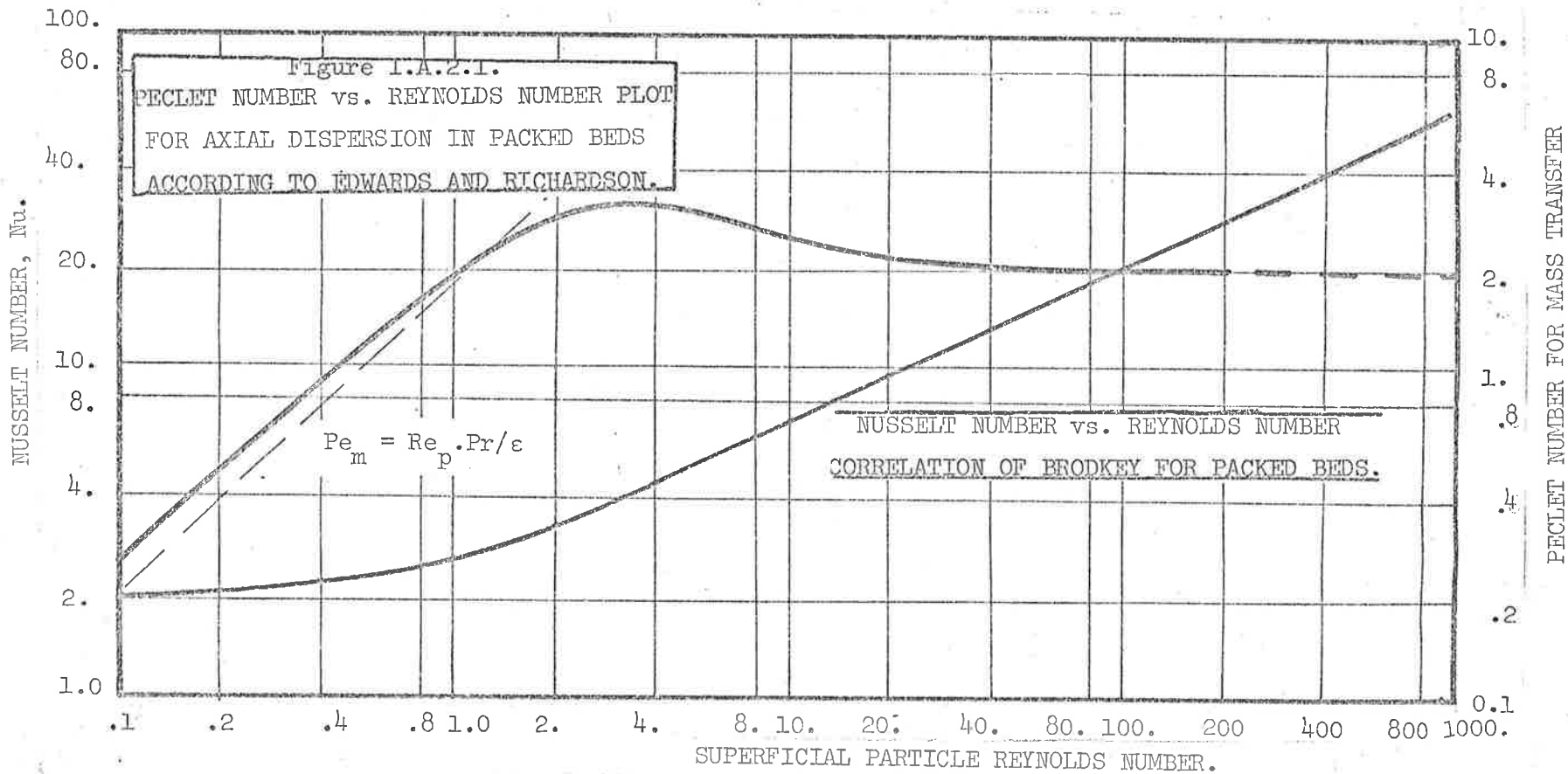
Figure I.A.2.1.
PECLET NUMBER vs. REYNOLDS NUMBER PLOT
FOR AXIAL DISPERSION IN PACKED BEDS
ACCORDING TO EDWARDS AND RICHARDSON.
NUSSELT NUMBER, Nu.
PECLET NUMBER FOR MASS TRANSFER
$Pe_m = Re_p.Pr/\varepsilon$
NUSSELT NUMBER vs. REYNOLDS NUMBER
CORRELATION OF BRODKEY FOR PACKED BEDS.
SUPERFICIAL PARTICLE REYNOLDS NUMBER.
100.
80.
40.
20.
10.
8.
4.
2.
1.0
10.
8.
4.
2.
1.
.8
.4
.2
0.1
.1
.2
.4
.8
1.0
2.
4.
8.
10.
20.
40.
80.
100.
200
400
800
1000.

The argument, applied to the dispersion of thermal energy assuming interphase transfer to be negligible predicts that the diffusivities (and hence Peclet numbers) for thermal and for mass dispersion should be identical, i.e.,

$$\frac{k_e}{\rho_f c_f} = D_e \qquad \ldots \quad (2.4)$$

where k_e is the effective eddy conductivity and ρ_f, c_f are the density and specific heat of the fluid respectively.

The limiting value of 2.0 for the flow of gases through packed beds at superficial particle Reynolds numbers, Re_p, greater than 10 has been well established for mass dispersion. Brodkey [1966] has summarised the experimental evidence to that date, whilst Edwards and Richardson [1968] discuss the transition from molecular diffusion to eddy mixing regions in greater detail. A plot of Edwards and Richardson's data is given in Figure 2.1. together with the calculated low Reynolds number line for a fluid having a Prandtl number of 0.74 and a bed porosity of 0.37. The introduction of porosity is necessary since superficial particle Reynolds number is used in the correlation.

3. Evidence for the Mixing Cell Model

Successful prediction of an axial Peclet number for dispersion of 2.0 presents quite strong evidence for the mixing cell approach. At an intuitive level, the discussion presented

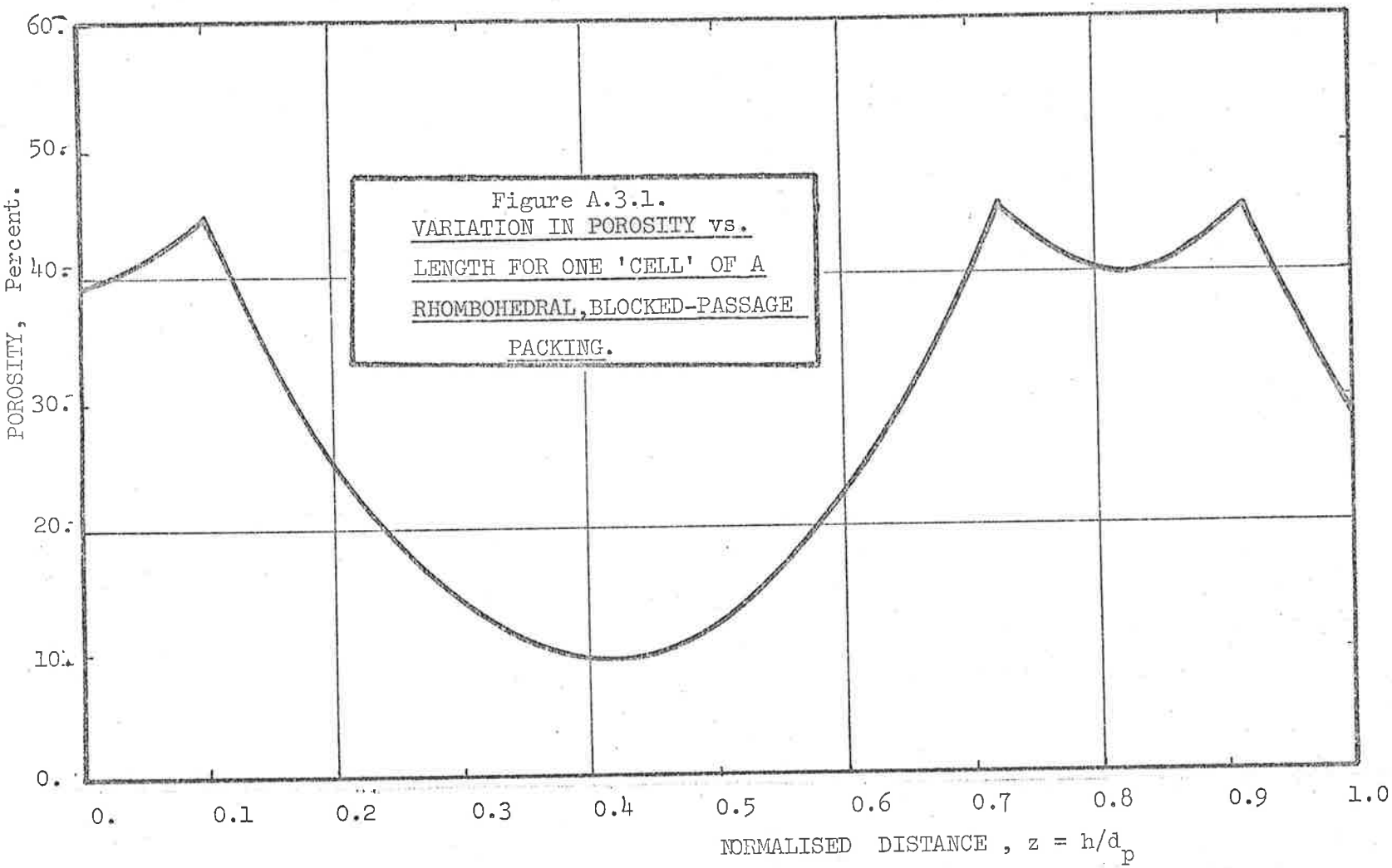

Figure A.3.1.
VARIATION IN POROSITY vs. LENGTH FOR ONE 'CELL' OF A RHOMBOHEDRAL, BLOCKED-PASSAGE PACKING.

by Aris and Amundson based on the structural characteristics of a packed bed is convincing. Thus, as shown by Figure 3.1, the area available for fluid flow varies, for a rhombohedral blocked-passage arrangement, from about 9% to 45% for a mean porosity of 26.5%. Fluid may be pictured as accelerating through areas of low porosity into regions of high porosity, giving rise to jet mixing effects in the void. As pointed out by Baron [1952] and Ranz [1952] fluid enters each void from a number of other voids radially displaced relative to the mixing void under consideration. These writers have been successful in predicting the radial Peclet number for eddy dispersion from consideration of such side-stepping action.

Mickley, Smith and Korshak [1965] have demonstrated, by measurement of velocity profiles and turbulence parameters in the voids of a regularly packed bed of 1-1/2 inch spheres, that eddy diffusivities in the voids were much smaller than predicted from the overall axial dispersion coefficient of 2.0 at least at Reynolds numbers of 4800 and 7000.

This, when combined with the evidence reviewed above, lends weight to the theory that overall structural considerations are dominant in determining effective dispersion rather than local turbulent diffusion processes when Reynolds numbers are "high enough."

4. Statistical Approach to Fluid Phase Dispersion

The conclusion of Kramers and Alberda, and of Aris and

Amundson, is, in fact, closely related to the Einstein theory of diffusion. The one-dimensional exposition has been well summarised by Feller [1957] as an example of a restricted random walk with one barrier. Thus the following assumptions are made:

(a) a particle of fluid will, with equal probability, either stay in a mixing cell or move to the next within an average transition time,

(b) the average time between transitions is equal to the cell holdup time and the average distance between displacements is $\gamma\, d_p$,

and (c) a sufficient number of steps is required to occur to ensure convergence.

Assumption (a) is consistent with a residence time or probability distribution function for a particular cell of the Poisson type, e.g.

$$g(t) = U(t).\, e^{-t/T}/T$$

where $T = \gamma\, d_p / v_a$ and U(t) is the unit step function. Such a distribution function corresponds to statistically perfect mixing.

The result obtained in the present nomenclature is

$$\frac{(\gamma\, d_p)^2}{\gamma d_p / v_a} = 2.\, D_e$$

i.e.

$$\frac{d_p v_a}{D_e} = \frac{2}{\gamma} ,$$

the result obtained by Aris and Amundson (equ. 2.3).

It should be noted that according to (c) the diffusion or continuous model will only approximate to the finite stage model for long bed lengths.

5. Influence of Axial Solids Conduction

According to the effective conductivity approach to packed beds, axial conduction of heat may occur through the packing:-

(i) via point contacts of adjacent particles

or

(ii) via a path pictured as one of fluid-solid-fluid conduction.

The experiments of numerous workers concerned with steady-state radial 'effective conductivity' in packed beds eliminate (i) as a significant mechanism because of the high contact resistance between solid particles [Masamune and Smith, 1963].

A rough estimate of the importance of fluid-solid-fluid transfer may be obtained from Argo and Smith's [1953] effective radial conductivity expression translated into a form suitable for evaluation of longitudinal conductivity. Thus, on the assumption that fluid molecular conductivity and turbulent mixing 'conductivity' are in parallel with series fluid-solid-fluid conduction they derive the following expression for

equivalent effective axial conductivity, $k_{a_{eff}}$:-

$$k_{a_{eff}} = \varepsilon\left(k_m + \frac{c_f . G . d_p}{\varepsilon . Pe_a}\right) + \frac{(1-\varepsilon) . h_p . k_s . d_p}{2k_s + h_p . d_p} \quad \ldots (5.1)$$

where h_p is the fluid-solid heat transfer coefficient and k_s the solids conductivity and Pe_a represents eddy or structural-type contributions of the type discussed in section A.2.

Re-arranging (5.1) into dimensionless group form, we have

$$k_{a_{eff}} = k_m \left[\frac{Pr. Re_p}{Pe} + (1-\varepsilon) . \frac{Nu}{2(1 + Bi)} \right] \quad \ldots (5.2)$$

where Bi is the Biot number defined here in terms of particle radius:-

$$Bi = \frac{h_p d_p}{2 k_s}$$

and Pe combines molecular and 'structural' contributions.

The third term in equation (5.2) represents the contribution due to axial fluid-solid-fluid conduction.

In the low Reynolds number region we have

$$Pe = Pe_m \simeq Re_p . Pr./\varepsilon$$

(if tortuosity is assumed to be 1.0) whilst the Nusselt number should approach 2.0. Hence, for Bi=0, the ratio

$$\beta = \frac{\text{Axial fluid-solid-fluid conductivity}}{\text{Total effective axial conductivity}}$$

approaches 1-ε or about 60 to 70% for packed beds.

In Figure 5.1, the ratio β is plotted assuming the Nusselt number correlation recommended by Brodkey [1964]. This correlation has the advantage that a limiting Nusselt number of 2.0 is approached at low Reynolds numbers as predicted by theory for an infinite fluid.
It is included on Figure 2.1 with Edwards and Richardson's Peclet number correlation also used in the calculation. The object of the calculations presented here is to suggest that this heat transfer mechanism may be ignored for superficial particle Reynolds numbers greater than 100. It may be noted that the Biot number has been assumed zero since this maximises the predicted effect of axial fluid-solid-fluid conduction.

A further discussion of the predicted effects of this mechanism and that of fluid phase axial dispersion on average heat transfer measurements in the low Reynolds number region is presented in III.D.1.

6. Radial Voidage and Velocity Variations Across a Packed Bed

The known increase in porosity near the wall of a randomly packed bed [Ridgeway and Tarbuck, 1963, 1968] may be expected to give rise to variations in velocity across the section of a packed bed which combined with radial diffusion, would be expected to have a considerable influence on the effective eddy thermal dispersivity. Such voidage variations apparently extend 1-1/2 to 2-1/2 particle diameters in from the wall. The

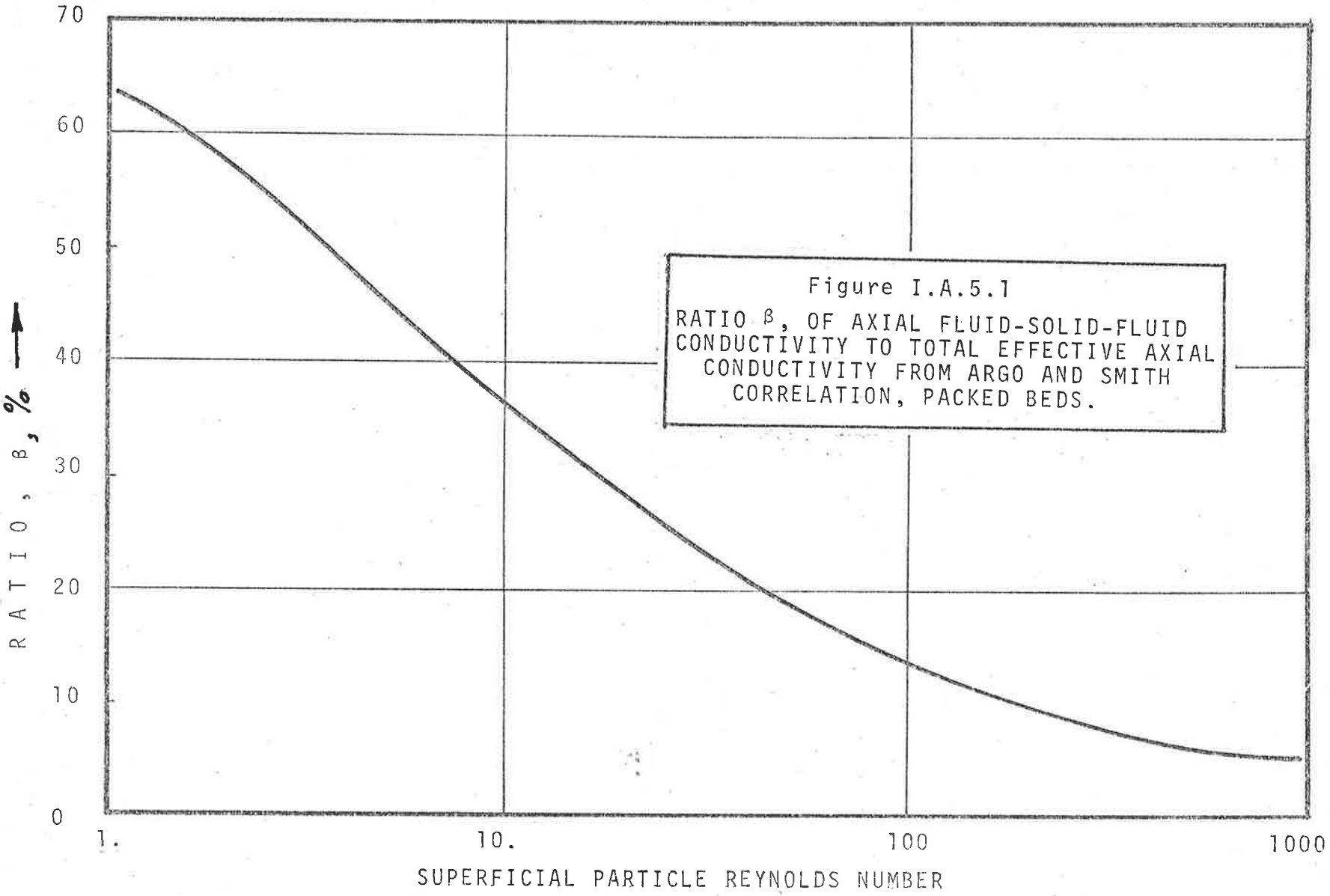

Figure I.A.5.1

RATIO β, OF AXIAL FLUID-SOLID-FLUID CONDUCTIVITY TO TOTAL EFFECTIVE AXIAL CONDUCTIVITY FROM ARGO AND SMITH CORRELATION, PACKED BEDS.

remarkable radial velocity variations of Schwartz and Smith [1953] rising (even for tube to particle diameter ratios of 16 or greater) to a pronounced maximum one or two diameters from the wall have been quoted by many writers. Beek [1963] for example, concludes that "there is no obvious reason for the velocity to drop off farther than some small fraction of a particle diameter from the wall" whilst Gillespie, Crandall and Carberry [1968] could find no correlation between rates of heat transfer to spheres in a packed bed as a function of radial position and the Schwartz and Smith profiles although they noted an increase in heat transfer coefficient in the near vicinity of the wall.

Fortunately, recent careful experimental work by Price [1968] has established that the region of high velocity in beds of randomly packed spheres is limited for $1470 \leq Re_p \leq 4350$, to one half a sphere diameter from the wall for tube to particle diameter ratios in the range 12 to 48. A similar result was reported by Mickley, Smith and Korshak for ordered spheres half sectioned at the wall to avoid voidage variations. In the present experimental work, tube to particle diameter ratios were greater than 14.

B. FLUID-PARTICLE HEAT TRANSFER IN PACKED BEDS

1. Introduction

Since most mathematical descriptions or models of packed bed dynamics yield impulse responses which approximate to Gaussian distributions at long bed lengths [Klinkenberg, 1956], a good fit between the model and experimental data is no proof of the validity of a model in itself. A parameter common to each of the models to be discussed is the fluid particle heat transfer coefficient. A basic requirement in testing the validity of any model is that such coefficients may also be obtained by measurements which do not assume the 'truth' of the model to be tested.

The extensive survey published by Barker [1965] presents a discouraging picture of the measurements made up to that date. The correlation of Colburn j_H factor against superficial particle Reynolds number for randomly packed beds of spheres shows j_H factors varying from about 0.01 up to about 0.13 at a Reynolds number of 1000, i.e. a thirteen-fold variation, although a majority of the results lie in the range 0.053 to 0.13. Such a variation makes the results unacceptable as an independent check on the validity of a model. It may perhaps be concluded that surface-averaged heat transfer coefficients are of little practical value in computing overall heat transfer rates in packed beds.

Fortunately, the range of variation is considerably reduced when the criteria discussed below are applied. Before presenting these criteria, a brief qualitative discussion of the mechanisms involved in fluid particle heat transfer will be given.

2. Factors Influencing Fluid-Particle Heat Transfer

(i) Isolated Spheres

The factors influencing heat or mass transfer to isolated spheres in an infinite medium have been well discussed in the literature. A very full review of the literature concerning experimentally measured surface-averaged heat transfer coefficients for spheres has been given by Rowe, Claxton and Lewis [1965]. They conclude that for air, where superficial particle Reynolds numbers Re_p range from 20 to 2000, the Nusselt number Nu may be obtained from

$$Nu = 2.0 + 0.69 \cdot Pr^{0.33} \cdot Re_p^{0.5} \quad \ldots \quad (2.1)$$

yielding the expected minimum value of 2.0 for an infinite stagnant fluid and that the Reynolds number exponent increases slowly from 0.4 at $Re_p = 1$ to 0.6 at $Re_p = 10^4$. The exponent of 0.5 agrees with numerical solutions of the Navier-Stokes equations for heat transfer [Bennett and Myers, 1962].

More recent work by Lavender and Pei [1967] has again attempted to establish the effect of turbulence intensity and

scale on the critical Reynolds number or point at which the boundary layer becomes turbulent. Studies have also been made of local variations in Nusselt number relative to the forward stagnation point using internally heated spheres. The most recent of these was by Gillespie, Crandall and Carberry [1968]. These show clearly the characteristic minimum at the point of boundary layer separation (for $Re_p > 10$), the maximum occurring at the forward stagnation point, and the shift forward of the point of separation towards 90° (measured from the forward point) as Reynolds numbers increase. Surface averaged Nusselt numbers obtained by graphical integration of the local distributions agree quite well with the above correlation.

(ii) In Packed Beds

Unfortunately, the tidy picture presented by the isolated sphere data is by no means reproduced in a packed bed. Most of the additional factors to be taken into account in developing a predictive theory based on the fundamentals of transport phenomena naturally arise from the structure of a packed bed. Some of these are listed below.

(a) Radial velocity variations due to wall effects. These have been shown to occur even when care is taken to eliminate wall voidage variations by placing sectioned particles in the wall region. For example, Mickley, Smith and Korchak [1964] measured velocity and

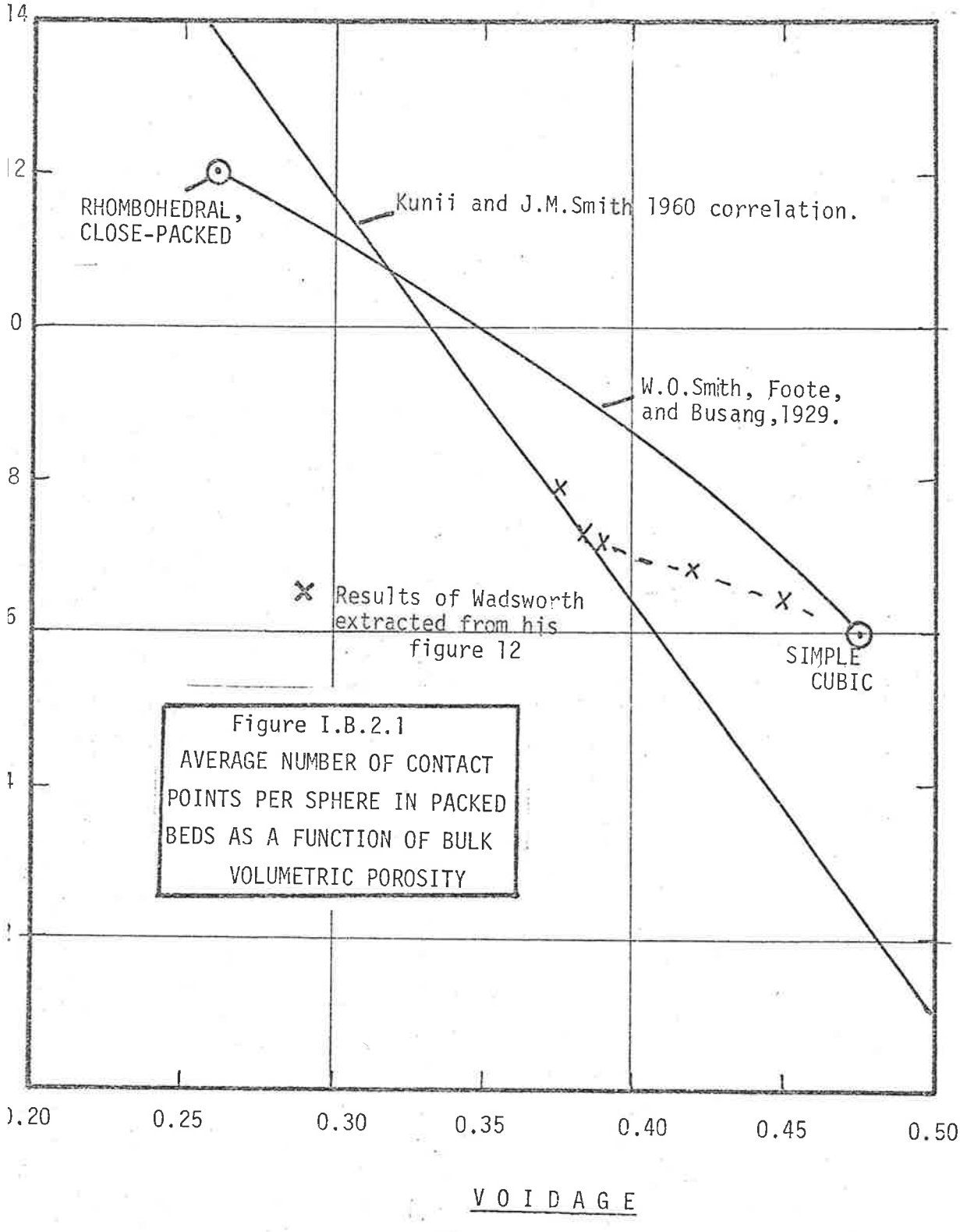

Figure I.B.2.1
AVERAGE NUMBER OF CONTACT POINTS PER SPHERE IN PACKED BEDS AS A FUNCTION OF BULK VOLUMETRIC POROSITY

turbulence profiles in the voids of such a carefully arranged bed and found significantly higher velocities in a void located one particle diameter from the wall despite the fact that gross voidage variations were eliminated. Ridgeway and Tarbuck [1968] noted that the actual voidage disturbances due to the wall in a randomly packed bed extended about 1-1/2 to 2 diameters in from the wall.

(b) Actual point contacts due to adjacent particles. These interfere with the development of velocity profiles around the particles. Wadsworth's data [1960a] for the average number of contact points per sphere has been calculated from his figure 12 and plotted as a function of voidage on Figure 2.1. For the range of porosities in the present work, a little over 7 contact points per sphere may be expected. That each contact point is a point of stagnation and low heat transfer rate was also shown by Wadsworth [1960].

(c) Wide local variations in porosity [see Figure A.3.1]. These result in high velocity streams impinging from a number of directions on each particle.

(d) The shielding effect of upstream particles on the forward points of each particle. This results in

local heat transfer rates which do not necessarily reach a maximum at these so-called 'stagnation' points. See, for example, the recent work of Gillespie, Crandall and Carberry [1968].

(e) High turbulence levels in packed beds. Mickley, Smith and Korchak [1965] report very high turbulence intensities in ordered packed beds at least at superficial particle Reynolds numbers of 4500 to 7000.

Despite the formidable complications introduced by the above factors, Leclair and Hamielec [1968] have attempted to compute both local and surface-averaged Nusselt number - Reynolds number correlations as a function of bed voidage. The computations were based on a model which assumes each particle to be surrounded by an envelope of fluid, the volume (but not the shape) of which is directly related to the overall bed voidage. The results of the computations are compared with the experimental results of Gupta and Thodos [1963] obtained from expanded beds, that is, assemblages of particles held apart by wires. In view of the criticisms which may be made of the experimental techniques of these workers, (see section 4.i), agreement, except perhaps in the 'creeping flow' region, may be regarded as fortuitous. In support of this claim, the experimental local Nusselt number plots of Denton [1951] and more recently of Gillespie and others [1968] obtained from isolated spheres at

various points in a bed bear little resemblance to Leclair and Hamielec's computations.

No attempt will therefore be made to consider fluid-particle heat transfer from a fundamental point of view. Instead, criteria will be developed which will reduce the range of variation between the various empirical literature correlations, so that the bed conditions (such as tube to particle diameter ratio, bed shape, length and porosity) more closely approach those of the present study. In the process, some of the factors mentioned above will be discussed in greater detail. It will also be necessary to discuss the experimental techniques of some of the workers, although, fortunately, application of the criteria will eliminate most of these correlations.

It should be re-stated that the object here is to obtain correlations which are independent of the mathematical pictures proposed for the system so that these models may be tested rigorously.

3. General Criteria for Selection of Literature Correlations

(a) Steady-state measurements preferred. Since correlations obtained from unsteady state methods depend in general for their validity on an assumed mathematical model of the system, steady state methods are, in general, to be preferred. Nonetheless the dynamic

test methods of

(i) Handley and Heggs [1968]

(ii) various cyclic test method investigators

and discussed in later chapters with reference to axial dispersion errors and to errors inherent in dynamic methods, respectively.

(b) Turbulent conditions. Superficial particle Reynolds numbers in excess of 100 are of interest in this study. Jolls and Hanratty [1966] have shown, by observation of the behaviour of dye filaments and records of diffusion-limited reaction rates on the surfaces of test spheres, that a sudden transition from steady to unsteady flow conditions over the sphere surface occurs at a superficial particle Reynolds number of 110 to 150, although the transition is not accompanied by a marked change in surface-averaged mass transfer rate. Nonetheless a discussion of the theoretical effects of axial fluids dispersion and fluid-solid-fluid conduction on measured fluid-particle coefficients at very low Reynolds numbers is presented in section III.A.2 since some anomalous results have been reported in this region.

(c) Elimination of 'wall effects'. Because of 'wall effects', the ratio of tube diameter d_T to particle

diameter d_p should be greater than about 16. Both Denton [1951] and Baumeister and Bennett [1958] found that the coefficient, a, and exponent, b, in a correlation of surface averaged Nusselt number Nu versus particle Reynolds number Re remained essentially constant for d_T/d_p greater than 16. Similar conclusions were reached by Gillespie, Crandall and Carberry [1968]. For reasons outlined below, Baumeister and Bennett's absolute values will be rejected however.

(d) Random packing preferred. Porosities should be of the order of 0.35 to 0.40 and the beds should be randomly packed.

(e) Elimination of entrance effects. Bed lengths should be greater than three particle diameters to eliminate entrance effects. Gillespie, Crandall and Carberry verified that the bed entrance effect was limited to about two particle diameters whilst Malling and Thodos [1967] obtained similar results in experiments on evaporation from porous spheres.

(f) Circular section preferred. Bed sections should be circular rather than square since effective velocity distributions in square sectioned beds are known to even smaller accuracy than distributions in circular sections.

(3) Spherical particles are required since the effects of sharp edges and surface roughness on fluid-particle heat transfer has not yet been quantitatively established.

The application of the above criteria to the twenty-eight references listed by Barker in his Table 1 eliminates all but one, Baumeister and Bennett [1958]. Other correlations not referred to in Barker's survey and/or appearing after the survey will be considered below together with the results obtained by workers using the 'evaporation from porous spheres' technique originally of Gamson, Thodos and Hougen,[1943]. The experimental conditions of these workers do not, in general, satisfy all the above criteria but will be considered nonetheless since their results are quoted so widely in the literature.

4. Steady State Measurements in Packed Beds

(i) Note on Choice of Characteristic Dimension in Packed Bed Heat Transfer Correlations

In the work reported here and in the bulk of the heat transfer literature, a Reynolds number Re_p based on particle diameter dp and superficial mass velocity G over the empty bed section is defined:

$$Re_p = \frac{d_p G}{\mu_f} \qquad \ldots(4.1)$$

As pointed out by Seidel [1965] the use of the interstitial mass velocity $v_a \rho_f$ and an equivalent, or effective diameter d_e is more logical, where

$$de = \frac{4 \times \text{free volume of fluid}}{\text{wetted area for heat transfer}} \qquad \ldots(4.2)$$

Hence, for a packed bed of spherical or right cylindrical particles (surface to volume ratio, $a_p = 6/d_p$) and bulk porosity ε, equation (4.2) becomes

$$de = \frac{2.\ \varepsilon.\ d_p}{3\ (1-\varepsilon)} \qquad \ldots(4.3)$$

so that

$$Re_h = \frac{de\ v_a\ \rho_f}{\mu_f} \qquad \ldots(4.4)$$

where Re_h is Seidel's 'hydraulic' Reynolds number.

Substitution of $\varepsilon = 0.33$ in equation (4.3) yields $de = \varepsilon\ d_p$ so that Re_h and Re_p become identical. For the bulk of the packed bed correlations reported in the literature, porosity is in the range 35 to 38% yielding hydraulic Reynolds numbers which are 11% to 23% higher than corresponding superficial particle Reynolds numbers Re_p. Attempts to devise a general packed bed heat transfer correlation which satisfactorily accounts for varying porosity have been largely unsuccessful to date (see Malling and Thodos [1967] for one attempt) so that there appears to be little point in using a more sophisticated definition of Reynolds number than that given by equation (4.1).

(ii) Evaporation from Porous Spheres

This technique of measurement was originally developed by Gamson, Thodos and Hougen [1943] to test the proposed analogy between heat and mass transfer introduced by Chilton and Colburn [1934]. The method has been refined by the various Ph.D. studens of Thodos. Their packed sections have had low tube to particle diameters ratios (for experimental reasons) and generally do not satisfy criterion (c) above.

The method depends on the establishment of constant drying rate conditions at the surface of porous Celite spheres initially soaked in water. Inlet and outlet air wet and dry bulb temperatures are measured, as are selected particle surface temperatures, and the whole bed is removed at intervals to establish the constant drying rate condition and as a check on the rate of heat and mass transfer. It is apparent from an examination of 'typical' results of Gupta and Thodos [1964] that problems arise due to saturation of the outlet air at long bed lengths, so that 'active' bed lengths are generally short. Since temperatures change as the air moves through the bed, elimination of heat losses or gains by means of control over water jacket temperature surrounding the test section is not strictly possible. For example, McConnachie and Thodos [1963] report calculated heat losses of 6% at one particular flowrate from radiation alone.

In addition to the effects of undetected heat losses, small errors in measurement of steady state temperature differences may also introduce large relative errors in the final computed heat transfer coefficient especially at low flows. For instance, McConnachie and Thodos [1963] report ratios of inlet to outlet temperature difference of 10 to 1 at a Reynolds number of 200. Such ratios mean that great emphasis is placed on the accuracy of temperature difference measurements at the outlet of the bed.

Both De Acetis and Thodos [1960] and Bradshaw and Myers [1963] report that, for low Reynolds numbers, the wet bulb and sphere surface temperature are not identical although this should influence mass transfer experiments more than heat transfer.

Despite experimental difficulties, the results of a particular investigator appear to be internally consistent. However, the marked differences which exist between the results of Malling and Thodos [1967], Gupta and Thodos [1964, 1963] and Gamson, Thodos and Hougen [1943] do not appear to be explicable solely by entrance turbulence as suggested by Malling and Thodos. Furthermore, since the air flow was stopped 'every 6-8 minutes' and the bed removed for weighing, it is likely that the re-establishment of steady state will cause systematic errors.

Nonetheless, some valuable qualitative results have been obtained by Malling and Thodos who used cylindrical beds, $d_T/d_p \simeq 4$ to 5. It was found that the coefficient a in correlations of the form $Nu = 2.0 + a\, Re_p^b$ increased for $200 \leq Re_p \leq 8000$ as the number of layers of spheres above and below the active layer increased from zero to three. This was attributed to increasing turbulence levels. Malling and Thodos applied a correction to their logarithmic mean temperature difference which allows for axial dispersion in the fluid phase. The correction was first introduced by Epstein [1958] and is based on a steady state version of the mixing cell model. The

theoretical implications will be further discussed later, in section III.A.2 since similar corrections are required for dynamic experiments.

Despite the lack of general applicability of the results of the above workers, they appear to have established the approximate ratio of 1.0 to 1.2 between the j_D and j_H factors (both heat and mass transfer experiments are subject to similar errors).

Another objective of these investigations was to link the data for heat transfer to isolated spheres to the data for packed beds by the use of expanded beds of decreasing porosity. In this they seem to have been less successful for the reasons mentioned above.

Bradshaw and Meyers [1963] employed a similar method to that of Thodos and co-workers and since they used higher tube to particle diameter ratios (above 17) their conclusions should be more applicable to larger diameter beds, of interest industrially and in the present work.

Their work satisfies all the criteria listed earlier in this section, with the exception of bed length. At low flows, bed lengths of about 3 particle diameters were used (although, at higher flows, bed lengths of up to 18 particle diameters were used).

Their j_H correlation for $400 \leq Re_p \leq 4000$ was, for

spheres,

$$j_H = 0.725/Re_p^{0.322}$$

with a standard deviation of ± 3.3%.

They also outline some experimental errors which arise in this type of test in addition to those mentioned above. For example, unless the measurements were carried out over the last 60% of the constant drying rate period, droplets of water were torn from the packing, causing high apparent coefficients. As a further example, they found that a 90% approach to saturation gave 'unreliable results' and that logarithmic mean calculations gave outlet temperatures which were too high for intermediate lengths. For longer bed lengths, the area under a plot of height against temperature difference was therefore used.

In summary, it appears that the lack of agreement amongst workers using the evaporation from porous spheres method and the already known errors of the method are sufficient to reject the bulk of the data from this source. The experiments of Bradshaw and Meyers, however, satisfy nearly all the criteria outlined earlier, with the result that some degree of reliability may be assigned to their work.

(ii) Induction Heating of Steel Spheres

Baumeister and Bennett [1958] carried out steady state measurements of the temperature of air and steel spheres as a

function of radial position at the inlet and outlet of a bed encased in a dielectric medium and heated by an induction coil surrounding the whole. Since the temperature of both air and spheres varied across the section due to radially non-uniform inductive fields, it was necessary to integrate graphically across the section, that is, to evaluate $\int_0^R r^2.T(r)\,dr$. An examination of a 'typical profile' across the tube shows the radial gradients to be marked, with a pronounced discontinuity at the centre. Similar lack of uniformity may be expected in a longitudinal direction. Their calculations of overall heat transfer coefficient required estimation of heat loss by imperfectly-established literature correlations. The results obtained are very considerably higher than those of other investigators and may be largely explained by the ~~axial~~ radial gradients mentioned above. Such gradients would render the logarithmic mean temperature difference approach invalid. Their results are hence rejected as an independent heat transfer correlation.

(iii) Generation of Heat Within Isolated Spheres

The heating of an isolated sphere which may be located anywhere within a bed of inert spheres is the most simple and obvious method of measurement available. Because of mixing of air streams from adjacent 'cells' the bulk fluid temperature is little affected by the heating of one sphere, so that measurement of this temperature is not subjected to a large

error. It may be thought that contact by adjacent (unheated) spheres would result in an error in average particle surface temperature. The work of Masamune and Smith [1963] on the effective static conductivity of packed beds (under high vacuum conditions) shows that heat transfer across the points of contact themselves would be very small at high flows, relative to bulk convection and heat transfer across the boundary layer. It should be noted however that at low flows, it has been suggested that heat transfer could occur through the relatively 'stagnant' gas surrounding the contact points. If this were so, then absolute particle size would be of importance and more complex expressions than derived in section I.A.5 would be required for axial fluid-solid-fluid conductivity.

The work of Denton [1950]still appears to provide a reliable standard against which other work may be evaluated. His measurements were carried out over a wide range of Reynolds numbers which were also high enough to make particle-particle conduction unimportant (Re_p was between 500 and 50,000). Spherical particles and long cylindrical beds were used ($25<L/d_p<85$). Tube to particle diameter ratios of 10,17.5,23 and 34 were used. Differences between average particle surface temperature and mean fluid temperature were measured by thermocouple thermometry directly, thus avoiding errors due to cold junctions, whilst total heat input to each test sphere was found accurately by electrical means. Measurements made on isolated spheres agreed well with literature correlations available at the time. No mentions is made of errors due to radiations losses although such losses would have been accounted for to

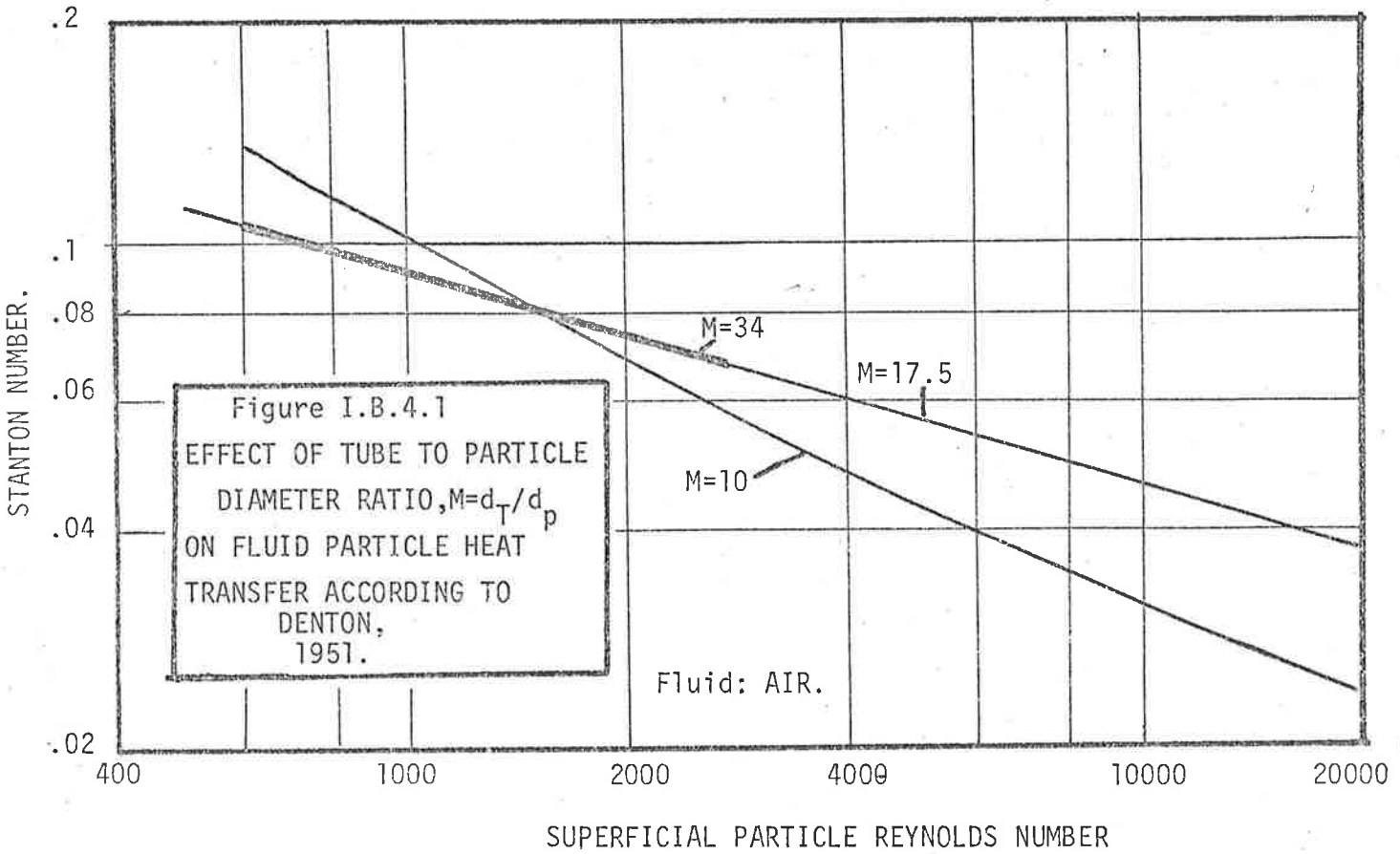

Figure I.B.4.1
EFFECT OF TUBE TO PARTICLE DIAMETER RATIO, $M=d_T/d_p$ ON FLUID PARTICLE HEAT TRANSFER ACCORDING TO DENTON, 1951.

a large extent by tests carried out to determine the correction for particle-to-particle conduction heat transfer at zero fluid flow rate. No systematic attempt was made to correlate surface-averaged heat transfer coefficients with radial or axial location in the bed - test spheres were located at random positions 'to within three sphere diameters of the upper and lower surfaces of the bed'. The effect of tube to particle diameter ratio on the averaged j_H factor correlation was pronounced for d_T/d_p less than about 16 (see Figure 4.1). The exponent in a Nusselt number- Reynolds number correlation increased from the isolated sphere value of 0.5 to a limiting value of 0.7 showing the decreasing importance of the wall on overall heat transfer.

The final correlation for air (Pr ≈ 0.73) where $L/d_p > 3$, $d_T/d_p > 20$, $500 \leq Re_p \leq 50{,}000$ and $\varepsilon \approx 0.37$ was

$$St = 0.72 / Re_p^{0.30} \quad \ldots \quad (4.1)$$

with a standard deviation of ± 5%.

Gillespie, Crandall and Carberry [1968] have reported similar experiments to Denton using one inch diameter metal spheres immersed in a 12" square sectioned bed of 1 inch randomly-packed cork spheres, $120 \leq Re_p \leq 1700$. The main objective was to determine the effect of position in the bed on average (and local) heat transfer coefficients. The correlation obtained is not strictly comparable, except for

spheres located at the centre of the bed where it was concluded that:-

$$Nu = 0.63\ Re_p^{0.65}.$$

that is, for air,

$$St = 0.864/\ Re_p^{0.35} \quad \text{(std deviation } \pm 9\%).$$

Nonetheless, their results clearly show that the entrance region is limited to the top two layers of the bed, and that the rate of heat transfer increases as the wall region is approached. Gillespie, Crandall and Carberry's work does not, from a practical point of view, significantly improve on Denton's measurements made 18 years earlier.

(iv) Summary

In summary, it appears that for the restrictions imposed by the following conditions:-

(a) $Re_p \geq 500$

(b) $d_T/d_p \geq 15$

(c) $0.35 \leq \varepsilon \leq 0.40$ (randomly packed)

(d) $L/d_p > 3$

(e) spherical particles and circular section,

Denton's correlation is the most reliable available. Since we may reasonably expect the limiting Nusselt number of 2.0 to be

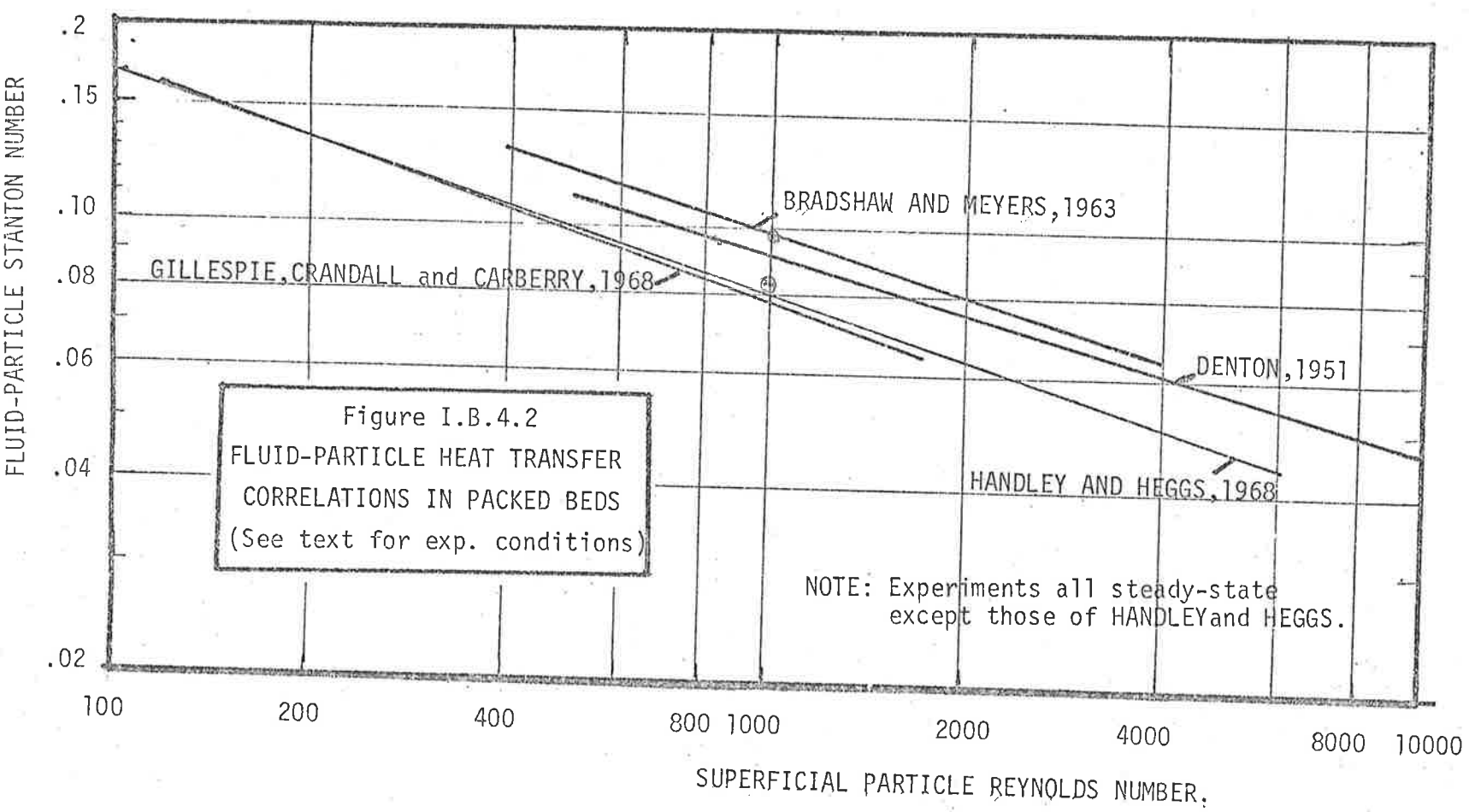

Figure I.B.4.2
FLUID-PARTICLE HEAT TRANSFER CORRELATIONS IN PACKED BEDS
(See text for exp. conditions)

approached at low flowrates, the slope of a Stanton number-Reynolds number correlation may be expected to increase for $Re_p < 500$.

A number of the correlations discussed in this section are presented graphically on Figure 4.2.

C. PHYSICAL ASSUMPTIONS IN FORMULATION OF MATHEMATICAL MODELS OF PACKED BED DYNAMICS

Much of the evidence leading to the physical assumptions made in either continuous or finite stage (mixing cell) models of packed bed dynamics have been discussed in sections B and C of this chapter. These assumptions are summarised below.

(a) Negligible Heat Transfer Through Vessel Walls

The vessel containing the bed will be assumed to be well insulated. Unfortunately, the use of lagging increases wall capacitance which, in itself, may influence dynamic behaviour. A rudimentary analysis based on the finite stage model (Appendix 4) yields the not-unexpected result that a reasonably large tube-to-particle diameter ratio is required to make either wall heat loss or capacitance effects negligible.

(b) Radial Uniformity of Voidage and Velocity Profiles

The evidence for this assumption has been discussed in Section B, part 6.

(c) Uniformity of Surface and Fluid Temperatures over a Particle Length at a Given Bed Depth

Surface temperature variations must arise in fact, since surface heat transfer rates vary around a sphere. However, since fluid-solid heat transfer data are reported on this assumption, it will be assumed valid here.

A fluid temperature which is constant over most of a sphere length is consistent with the finite stage model, since voids are assumed well mixed. This particular assumption involves the continuous or axial dispersion model in a contradiction, since each particle is assumed surrounded by a uniform field whilst at the same time postulating continuity of the fluid phase within the bed.

(d) Molecular Conduction

Molecular conduction is assumed to have negligible effect on fluid phase dispersion in the case of the finite stage model, although this could be allowed for by varying the mixing cell length. See Section B, part 7.

(e) Fluid-Solid-Fluid Conduction Negligible

The evidence for this has been discussed in Section B, part 5. It is, in fact, a consequence of assumption (c).

(f) Symmetry of Internal Particle Temperature Distributions

This is also a consequence of (c) above.

(g) Constant Fluid-Particle Heat Transfer Coefficient

As noted in section B, surface-averaged fluid-particle heat transfer coefficients vary with bed position. However since most of the variation is in the top three layers and near the tube wall it will be assumed constant. The assumption seems a reasonable one when tube to diameter ratios are large and bed lengths long.

(h) Thermal and Transport Properties Constant

In heat transfer terminology temperature changes will be small enough to allow fluid density and specific heat to be regarded as constant. Solids diffusivity is also assumed to be independent of temperature. This is a reasonable assumption in the case of heat transfer systems but may be hard to justify in the case of mass transfer systems. A further assumption inherent in the above is that pressure drop has negligible effect on density.

CHAPTER II

MATHEMATICAL MODELS OF PACKED BED DYNAMICS

SCOPE OF THE CHAPTER

In this chapter, two techniques are used to compare various mathematical descriptions or 'mathematical models' of packed bed dynamic behaviour. The techniques (frequency response and moments analysis) have been widely used in experimental studies - their applications to and limitations in testing will be discussed in detail in Chapter V. Here, they are used purely as mathematical techniques. It should be noted that neither requires actual computation of time or transient response, merely derivation of the transfer function of the system (defined in A.1). Transfer functions are generally easier to derive than transient responses and do contain much valuable information. Actual 'time domain' comparisons are presented in the chapter on breakthrough curve prediction (Chapter IV).

In Section A various mathematical properties of linear systems are reviewed. The relationships between frequency response analysis and moments analysis are also traced using a well known result from the theory of mathematical statistics. The connection between the moments analysis and frequency response approaches to modelling and dynamic testing has not been hitherto clearly presented in the literature. It will be shown in later

Chapters that a useful unification of theory is achieved.

In Section B various 'two phase, continuous' models of packed bed dynamics are discussed. Rather than review existing models in chronological order, the writer's most recent extension is presented first and then compared with the earlier models of Rosen, Pulsifer, Chao and Hoelscher and Schumann. Such simplified models are, of course, often of greater utility than more comprehensive ones. One of the objectives of the present work is to establish when these simplified approaches are adequate for engineering purposes.

In Section C, the predictions of the two phase finite stage model are compared with those of the two phase continuous models. The comparison, via the transfer function has theoretical implications with regard to the confidence which may be placed in the finite stage model of Deans and Lapidus when applied to non-linear adsorption and simultaneous heat and mass transfer.

In Section D the 'one phase, equivalent conductivity' model of Babcock and co-workers is discussed since this approach appears to offer both mathematical simplicity and physical comprehensiveness. A comparison is made between the predictions of this model and those of the others presented in sections B and C.

A. MATHEMATICAL REVIEW

1. The 'Transfer Function'

In the present work, the differential equations of packed bed dynamics are ultimately to be solved so as to yield the temperature $T(z,t)$ of the fluid in the bed at axial distance z and time t in response to prescribed changes in fluid temperature $T_i(t)$ at the inlet of the bed. In this case, $T(z,t)$ mathematically is the dependent variable and will be referred to as the output of the system. Another dependent variable which is often of interest is the temperature $T_p(z,r,t)$ of a particle at axial distance z and radial distance r from the centre of a particle. The forcing function, or independent variable $T_i(t)$ is referred to as the input to the system.

Variables z and r are included when the equations are formulated as partial differential rather than as ordinary differential equations. In the first formulation, the system is viewed as a distributed parameter system, the second views the system as a lumped parameter system. A more complete discussion of the differences between the two is given from the control engineering point of view in a paper by the writer [1969] which is included in Appendix 3 (paper 2).

Time and distance variables, t, z and r, are in general normalised, or rendered non-dimensional. Time and distance

variables which are superscripted with a prime represent dimensional quantities, e.g. t', in minutes.

For a complete solution, initial conditions are required which, in the distributed parameter case, must also be specified as a function of distance. Boundary conditions are, of course, also necessary. In this work, the initial conditions will be, throughout, $T(z,t=0) = T_p(z,r,t=0) = 0$. It will be noted that T and T_p are, in fact, deviations from steady state or initial values.

The ratio of the Laplace transform of the output of a system assumed initially at steady state to the Laplace transform of the input is defined as the transfer function of the system and is denoted by $G(z,s)$ or $G(s)$. The transfer function is usually relatively easy to obtain, compared with the time response of the system. The definition of transfer function is, in mathematical form:-

$$\frac{\mathcal{L}\, T(z,t)}{\mathcal{L}\, T_i(t)} = \frac{T(z,s)}{T_i(s)} = G(z,s) = \mathcal{L}[g(z,t)]$$

$$= \int_0^\infty g(z,t).\, e^{-st}.\, dt \qquad \ldots \quad (1.1)$$

The Laplace transform variable s is a complex number $s = \sigma + j\omega$ where σ is chosen to be large enough to ensure convergence of the integral of equation (1.1). See Doetsch

[1961,a] for a more rigid definition. Equation (1.1) implies that the output, $T(z,t)$, is obtained by convolution. This operation is only applicable to the linear systems as in the present work. Convolution, or multiplication in the Laplace transform domain, is defined by the convolution integral in the time domain, i.e. for the case of $T_i(t) = T(z,t) = 0$, $t < 0$:

$$T(z,t) = \{T_i(t) * g(z,t)\} \overset{\text{def}}{=} \int_0^t g(t-\tau).T_i(\tau)d\tau$$

$$= \mathcal{L}^{-1} [T_i(s) \,.\, G(z,s)] \qquad \ldots \quad (1.2)$$

The symbol $\mathcal{L}^{-1}$ denotes Laplace transform inversion.

When the input is an impulse or Dirac function, $\delta(t)$, [Bracewell, 1963,a] then, $\mathcal{L}\, T_i(t) = \mathcal{L}\, \delta(t) = 1$ and for this reason the inverse of the transfer function, $g(z,t)$ will be referred to as the 'impulse response'. As explained in Chapter V, a good approximation to an impulsive input may be obtained physically by inputs which are of short duration relative to the impulse response.

The time integral of the impulse response represents the response to a unit step input and is defined as the step response $u(t)$ of the bed. A plot against time defines the breakthrough curve of a packed bed.

$$u(t) \overset{\text{def.}}{=} \int_0^t g(\tau),d\tau = \mathcal{L}^{-1} \frac{G(s)}{s} \qquad \ldots \quad (1.3)$$

Consideration of breakthrough curves is deferred until Chapter IV.

2. Relations Between Frequency Response and Moments Analysis

As is well known, the replacement of s by the pure imaginary variable $j\omega$ in the transfer function of a stable, linear system yields the ratio in magnitude and phase of the steady-state sinusoidal output resulting from a steady state sinusoidal input. For a rigorous proof see Doetsch [1961,b]. Thus expressing the resultant complex function $G(z,j\omega)$ in modulus $|G(z,j\omega)|$ and argument $/G(z,j\omega)$ form, the modulus represents the ratio between output amplitude and input amplitude whilst the argument represents the phase shift between output sine wave of frequency ω and the input sine wave. This is the mathematical principle behind the cyclic method of testing (V.A.1).

In this chapter, plots of the frequency response function $G(z,j\omega)$ against frequency, ω in modulus and argument form will be used (merely as a mathematical technique) for comparing two or more proposed models of a system. Experimental frequency response methods will be discussed in greater detail in Chapter V. As noted above (section 1) 'transfer functions' are more easy to obtain than the response to actual input functions, so that frequency response plotting becomes particularly useful in comparisons of complex systems.

The technique of moments analysis may be used as an alternative method of comparing the mathematical predictions of various models or as a tool in analysis of dynamic experiments as in chapter V.

For a stable system, the response g(t), to an impulsive input when all initial conditions are zero, returns eventually to zero and has a finite integral. This "impulse response" may be treated mathematically as a one-sided density function defined by:

$$g(t) = o, \quad t < o,$$

$$\lim_{t \to \infty} g(t) = o \qquad \ldots(2.1)$$

and $$\mu'_o = \int_o^\infty g(t).dt = \text{finite}$$

Where μ'_o is defined as the zero 'th moment of the density function.

The length variable, z has for convenience been dropped from definition of the impulse response function g (t). In addition, the other absolute moments μ'_n, n = 1, 2 ... may be defined:

$$\mu'_n = \int_o^\infty t^n.g(t).dt \qquad \ldots(2.2)$$

and these moments define the shape of the density function. It is assumed that for the physical systems considered here, the moments μ'_n of all orders exist. The question of the existence of the moments of g(t) is bound up with the question of the convergence and existence of the Fourier transform or characteristic function of g(t) [Moran, 1968.]

Thus in the present notation we define

$$\left.\begin{aligned} \mathcal{F}[g(t)] &= \int_{-\infty}^{\infty} g(t).\, e^{-j\omega t}\, dt \\ &= \int_{0}^{\infty} g(t).e^{-j\omega t}\, dt \end{aligned}\right\} \qquad \ldots(2.3)$$

when $g(t) = 0,\ t < 0$

It will be noted that the Fourier transform of g(t) is, in fact, the transfer function G(s) with the complex variable replaced by the pure imaginary variable $j\omega$.

Expanding exp $(-j\omega t)$ in the usual infinite series, (convergent for all ω) we obtain the relation presented in texts on mathematical statistics:

$$\begin{aligned} G(j\omega) &= \int_{0}^{\infty} g(t) \sum_{n=0}^{\infty} \left[\frac{(-j\omega t)^n}{n!}\right] dt \\ &= \sum_{n=0}^{\infty} \frac{\mu_n'}{n!} (-j\omega)^n \end{aligned} \qquad \ldots(2.4)$$

The expansion of equation (2.4) will, in general, be convergent only within a particular radius of convergence.

Equation (2.4) also leads to the formulae of equations (2.5) which are frequently used in deriving the moments of density function from either transfer function G(s) or $G(j\omega)$:

$$\mu_n' = \lim_{\omega \to 0} (\div j)^n \frac{d^n G(j\omega)}{d\omega^n} \qquad \ldots(2.5)$$

$$\text{or} \qquad \mu_n' = \lim_{\omega \to 0} (-1)^n \frac{d^n G(s)}{ds^n}$$

It is also sometimes valuable to expand $G(j\omega)$ which we will henceforth call the "frequency response transfer function" in terms of the cumulants κ_n of the density function g(t) where the cumulants are defined by:

$$\ln G(j\omega) = \sum_{n=o}^{\infty} \kappa_n (-j\omega)^n = \ln(|G| \; e^{-j\underline{/G}})$$

$$= \ln |G(j\omega)| + j \; \underline{/G(j\omega)} \qquad \ldots(2.6)$$

As for the moments expansion, equation (2.4) it will in general, be necessary to examine the circle of convergence of the cumulant expansion, equation (2.6).

Extensive tabulations of the relations between the cumulants κ_n and the absolute moments μ'_n and also between κ_n and the <u>central moments</u> μ_n of g(t) defined for n = 1,2,3, ... by

$$\mu_n = \int_o^{\infty} (t-\mu'_1)^n g(t) \, dt \qquad \ldots(2.7)$$

have been presented by Kendall and Stuart [1958.]

When the zero'th moment μ'_o is unity (or is normalised to unity) we obtain:

$$\kappa_o = \ln \mu'_o = 0$$

$$\kappa_1 = \mu'_1$$

$$\kappa_2 = \sigma^2 = \mu_2 = \mu'_2 - \mu^2$$

$$\kappa_3 = \pi^3 = \mu_3 = \mu'_3 - 3\mu.\mu'_2 + 2\mu^3$$

$$\kappa_4 = \mu'_4 - 4\mu'_3 \mu + 6\mu^2\mu'_2 - 3\mu^4 \qquad \ldots(2.8)$$

In equations (2.8) as elsewhere, we denote the first absolute moment μ'_1 more simply by μ the second central moment or variance by σ^2 and the third central moment (often loosely called the 'skewness) by π^3.

Two other useful expansions are obtained from equations (2.6). Thus, equating real and imaginary parts we obtain:

$$\ln|G(j\omega)| = \kappa_o - \kappa_2 \frac{\omega 2}{2!} + \kappa_4 \frac{\omega^4}{4!} - \ldots \qquad \ldots(2.9)$$

and $\underline{/G(j\omega)} = -\kappa_1\omega + \kappa_3 \frac{\omega^3}{3!} - \kappa_5 \frac{\omega^5}{5!} + \ldots$ (2.10)

The above results will be used in chapter V. It is sufficient to sa at this stage that since the cumulants define the frequency response over its circle of convergence, comparisons between models may be carried out by comparing $G(j\omega)$ or the cumulants κ_n. Equations (2.9) and (2.10) also yield most valuable insights into the likely shape of an impulse (or step) response; given the frequency response or vice-versa.

3. Additivity Under Convolution

If x(t) and y(t) are distribution functions in the present sense (equ. 2.1) and z(t) is formed by the convolution of x and y (see A.1) i.e.

$$Z(t) = [X(t) * Y(t)]$$

or

$$Z(j\omega) = X(j\omega) \cdot Y(j\omega),$$

then $Z(j\omega)$ may be obtained from $X(j\omega)$ and $Y(j\omega)$ by the following additivity relations (from the properties of complex numbers):

$$\ln |Z(j\omega)| = \ln|X(j\omega)| + \ln|Y(j\omega)| \quad \ldots \quad (3.1.)$$

and

$$\underline{/Z(j\omega)} = \underline{/X(j\omega)} + \underline{/Y(j\omega)} \quad \ldots \quad (3.2)$$

These additive relations are used in experimental frequency response analysis and in theoretical derivations.

The corresponding additive relations for the first three central moments of x(t), y(t) and z(t) are widely used in experimental and

theoretical analysis. They are more generally expressed in terms of the corresponding cumulants of x(t), y(t) and z(t).

Thus from (3.1) and (2.10) and from (3.2) and (2.11)

$$\kappa_{z_n} = \kappa_{x_n} + \kappa_{y_n} \qquad \ldots \quad (3.3)$$

for n=0,1,2,3 .... where κ_{x_n} denotes the n'th cumulant of the density function x(t). Setting n = 1,2 and 3 we obtain

$$\mu_Z = \int_o^\infty t.z(t)\, dt$$

$$= \mu_X + \mu_Y ,$$

$$\sigma_Z^2 = \sigma_X^2 + \sigma_Y^2 ,$$

and $$\pi_Z^3 = \pi_X^3 + \pi_Y^3 .$$

A discussion of the application of equ. (3.3) to the experimental technique of moments analysis is given in Chapter V. Basically the method is one of estimating the moments of the impulse response g(t) from the corresponding cumulants of an input x(t) to and of output y(t) from the system.

B. TWO PHASE CONTINUOUS MODELS OF PACKED BED DYNAMICS

1. Introduction

The mathematical models considered in this section are described as 'two phase' since they make separate allowance

in their formulation for temperatures (or concentrations) in fluid and solid phases. This distinguishes them from the equivalent conductivity approach of Babcock and co-workers who have treated the (two phase) bed as though it were one, continuous medium (see section D). The term 'continuous' distinguishes this group of models from the discontinuous, cell model or finite stage approach applied in section C to the fluid phase.

The equations solved by Rosen [1952] for a step input at the bed entrance represent the most complete and rigorous physical description of linear adsorbers and thermal regenerators available in a practical form. Amundson [1956] has, in fact, presented step response solutions to models which are even more comprehensive. Nonetheless his work has been totally ignored in the literature on adsorber dynamics since his solutions involve multiple infinite series which are difficult and tedious to evaluate. The disadvantage of infinite series solutions will become obvious when cylindrical particles are considered.

The model used by Rosen accounts for

(a) convective transport in the fluid phase

(b) interphase resistance

and (c) intraparticle diffusional resistance.

Other physical assumptions are as summarised in section I.C.

It will be noted that axial fluid phase dispersion has been ignored as has fluid-solid-fluid conduction.

Axial dispersion in the fluid phase has been added to Rosen's model and transfer functions derived in Appendix 1 for two boundary conditions. This more complete model will thus be considered first and the more restrictive models of Rosen, Pulsifer [1965], Chao and Hoelscher [1966] and Schumann[1929] reviewed later.

2. Formulation of the Extended Model Equations

(i) Fluid Phase Equations

In the present notation, a material balance over an increment of bed length $\delta z'$ yields, for the fluid phase:

$$\varepsilon k_e \frac{\partial^2 T}{\partial z'^2} - v_a \varepsilon \rho_f c_f \frac{\partial T}{\partial z'} + h_p . a_p (1-\varepsilon)[T_s - T] = \varepsilon \rho_f c_f \frac{\partial T}{\partial t'} \quad \ldots \quad (2.1)$$

$$0 \leq z' \leq L$$

where $T \equiv T(z',t')$: fluid temperature at distance z', time t'.

$$T_s \equiv T_s(z',t') \overset{\text{def.}}{=} \lim_{r' \to R} T_p(z',r',t')$$

= particle surface temperature

ρ_f and c_f are fluid density and specific heat respectively

v_a is the interstitial fluid velocity through the bed,

ε is the mean volume (and mean area) porosity,

h_p is the surface-averaged fluid particle heat transfer coefficient,

a_p is the surface area to volume ratio of the particles,

($a_p = 6/d_p$ for both spheres and right cylinders)

L is the bed length = N dp

and k_e is the effective axial fluids conductivity including the effects of molecular conduction and turbulent mixing 'conduction'.

Normalising equation (1.1) with respect to bed length L and mean fluid holdup time $\bar{T} = L/v_a$ so that

$$z = z'/L$$

$$t = t'/\bar{T} ,$$

equation (2.1) becomes

$$\boxed{\frac{1}{Pe'} \cdot \frac{\partial^2 T}{\partial z^2} - \frac{\partial T}{\partial z} + KV_H(T_s - T) = \frac{\partial T}{\partial t}} \quad \ldots \quad (2.2)$$

where

$$Pe' = \frac{Lv_a}{D_e} = Lv_a \frac{\rho_f c_f}{k_e} = N.Pe$$

$\equiv$ axial dispersion Peclet number based on bed length,

Pe is the axial dispersion Peclet number based on particle diameter,

and $KV_H = \dfrac{h_p . a_p . (1-\varepsilon) . L}{\rho_f \, c_f \, \varepsilon \, v_a}$.

The parameter KV_H may be preferably written in terms of the fluid-particle Stanton number St where

$$St = \frac{h_p}{Gc_f}$$

and $G = \varepsilon v_a \rho_f$ is the superficial mass velocity over the section.

Thus

$$KV_H = St.a_p.L.(1-\varepsilon)$$

For spheres or right cylinders, $a_p = 6/d_p$ and

$N = L/d_p$ = bed length in particle diameters,

so that

$$\boxed{KV_H = 6NSt(1-\varepsilon)} \qquad \ldots \quad (2.3)$$

This is a fundamental parameter in all packed bed models and has the physical interpretation [Klinkenberg and Mooy, 1948]

$$St \equiv \frac{\text{Rate of heat transfer normal to fluid flow per unit surface}}{\text{Maximum rate of convective heat transfer}} \qquad \ldots \quad (2.4)$$

or,

$$KV_H \equiv \frac{\text{Rate of heat transfer normal to fluid flow over entire bed packing}}{\text{maximum rate of convective heat transfer}}$$

The parameter $V_H = \dfrac{\rho_s c_s (1-\varepsilon)}{\rho_f c_f \varepsilon}$ $\qquad \ldots \quad (2.5)$

defined as the '<u>heat capacity ratio</u>' gives the ratio of the solid packing volumetric thermal capacity to that of the interstitial fluid. The importance of this parameter was first noted by Saunders and Ford [1940].

Hence

$$K = \frac{h_p.a_p.\bar{T}}{\rho_s c_s} \qquad \ldots \quad (2.6)$$

K may be regarded as the equivalent normalised 'diffusivity' of the external heat transfer resistance.

The other fundamental parameter in equation (2.2), the Peclet number Pe where $Pe' = N\,Pe$ may be visualised as

$$Pe \equiv \frac{\text{Maximum rate of axial convective heat transfer}}{\left[\begin{array}{c}\text{Rate of axial heat transfer by eddy and} \\ \text{molecular conduction}\end{array}\right]}$$

so that the numerical value of the product St.Pe should yield a measure of the extent to which a heat front is dispersed axially, that is, a small value of St and/or of Pe should result in a large axial spreading.

(ii) Solid Phase

Assuming radial symmetry, thermal diffusion within spherical particles may be written:-

$$\rho_s c_s \frac{\partial T_p(r',z',t')}{\partial t'} = \frac{2k_s}{r'}\cdot\frac{\partial T_p}{\partial r'} + k_s\cdot\frac{\partial^2 T_p}{\partial r'^2} \qquad \ldots \quad (2.7)$$

$$0 \leq r' \leq R$$

where ρ_s and c_s are solids density and specific heat,

R is the particle radius $(= d_p/2)$

and k_s is the solids thermal conductivity.

In normalised form equation (2.7) becomes

$$\frac{1}{\alpha}\frac{\partial T_p(r,z,t)}{\partial t} = \frac{2}{r}\frac{\partial T_p}{\partial r} + \frac{\partial^2 T_p}{\partial r^2} \qquad \ldots \quad (2.8)$$

where α is a non-dimensional diffusivity parameter, more usually defined in the present calculations in terms of K and the Biot number Bi:-

$$\alpha = \frac{k_s \bar{T}}{\rho_s c_s R^2} = \frac{K}{3.Bi} \qquad \ldots \quad (2.9)$$

The boundary conditions linking fluid and solid may be, before normalisation either:-

$$k_s \frac{\partial T_p(z',r',t')}{\partial r}\Bigg|_{r'=R} = h_p(T-T_s) \qquad \ldots \quad (2.10a)$$

or

$$\frac{\partial \bar{q}}{\partial t'} = h_p a_p (T-T_s) \qquad \ldots \quad (2.10b)$$

where $\bar{q}$ is the volumetrically averaged total quantity of heat in the particle.

Boundary condition (2.10b) was used in Rosen's treatment. It involves integration over the whole particle volume. Boundary condition (2.10a) is far simpler to use and has been used in the present treatment.

In normalised form, equation (2.10a) becomes

$$\frac{\partial T_p(z,r,t)}{\partial r}\Bigg|_{r=1} = Bi\,[T - T_s] \qquad \ldots \quad (2.11)$$

In cases where the particle Biot number is effectively zero or particle temperatures are about uniform equation (2.10b) is preferable, becoming in normalised form:-

$$\frac{d}{dt} T_p(z,t) = K [T(z,t) - T_p(z,t)] \quad \ldots \quad (2.12)$$

where $T_p(z,t) = T_s(z,t)$

(iii) Overall Boundary Conditions

The presence of axial dispersion makes the correct bed inlet and exit boundary conditions difficult to decide, strictly. The fluid dispersion coefficients upstream and downstream of the bed are required yielding, for example, at the bed inlet

$$\left[T_i - \frac{1}{Pe'_i} \frac{\partial T_i}{\partial z} \right]_{z=0-} = \left[T - \frac{1}{Pe'} \frac{\partial T}{\partial z} \right]_{z=0+}$$

where the subscript i refers to 'inlet' conditions just upstream of the bed. However the physical conditions at the inlet are not predictable with accuracy and the solution becomes exceedingly complex.

Pulsifer [1965] used the Danckwerts' boundary conditions [1953]. At the entrance of the bed:

$$T_i(t) = \left[T(z,t) - \frac{1}{Pe'} \frac{\partial T}{\partial z} \right]_{z \to o}$$

At the bed exit (z=1), . . . (2.13)

$$\left[\frac{\partial T}{\partial z} \right]_{z \to 1} = 0$$

These boundary conditions have been widely discussed in the literature. Van Cauwenberghe [1966] concluded that the conditions represent plug flow in both entrance and exit piping, that is, negligible dispersion in either inlet or exit sections. The second boundary condition appears to be unduly restrictive for transient operation of a packed bed.

The solution given in Appendix 1 uses these conditions. A more simple set of boundary conditions has been used by Chao and Hoelscher [1966]. These are:-

$$T_i(t) = \lim_{z \to o} T(z,t) \qquad \ldots \quad (2.14)$$

and

$$\lim_{z \to \infty} T(z,t) = \text{finite (or zero)}$$

In the present work, diffusion is never dominant and in view of uncertainty concerning the actual physical conditions at the bed inlet and exit, there seems little justification for using any conditions other than the simplest (2.14).

3. Transfer Function of Extended Continuous Model

(i) Fluid Particle Transfer Function

In Appendix 1 transfer functions for the extended continuous model are derived for both sets of boundary conditions referred to in 2.iii. The key to the solution is the derivation of $G_p(s)$, the fluid-particle transfer function. This relates the surface temperature of a particle at any distance z to the assumed uniform fluid temperature surrounding the particle, i.e.

$$\frac{T_s(z,s)}{T(z,s)} \stackrel{\text{def.}}{=} G_p(s) \qquad \ldots \quad (3.1)$$

The transfer function is independent of distance z and is simple to derive in the case of zero Biot number or uniform particle temperature. Thus, Laplace transformation of equation (2.12) for zero initial conditions quickly yields

$$G_p(s) = \frac{K}{s+K} \qquad \ldots \quad (3.2)$$

When the Biot number is non zero the solution becomes more complex. In an earlier paper on the finite stage model the writer [1968] obtained the non zero Biot number particle transfer function in open form:-

$$G_p(s) = \sum_{n=1}^{\infty} \frac{K_n/\overline{T}}{(T_n/\overline{T})s+1} \qquad \ldots \quad (3.3)$$

A similar form may be obtained for cylindrical particles with uniform surface temperature (see Appendix of paper 1). The use of the open form considerably lengthens calculations and places undue emphasis on the convergence of equation 3.3. In calculations with both spherical and cylindrical particles the criterion

$$\lim_{N\to\infty} \sum_{n=1}^{N} \frac{K_n}{T} = 1$$

was used to decide a reasonable point at which to truncate the series.

A number of computations have been carried out to compare the predicted response of beds packed with cylindrical particles with beds of spheres. A few of these are reported in Section II.E.3 and illustrate both the excessive computation time and programme complexity which results from the use of the open form of $G_p(s)$.

Fortunately, Rosen [1952] has already derived equation (3.3) in closed form for spherical particles, in the guise of "admittance functions". Since writing paper 1 the relationship between the "admittance function for solid diffusion only", $Y_D(s)$ and the transfer function $G_p(s)$ has been clarified. Thus:

$$G_p(s) = \frac{K}{K+Y_D(s)} \qquad \ldots \quad (3.4)$$

where in the present notation,

$$Y_D(s) = \frac{K}{Bi}(p \cot p - 1) \quad ,$$

$$p = j(s/\alpha)^{1/2} \quad , \qquad \ldots \quad (3.5)$$

$$j = \sqrt{-1} \quad ,$$

and as before, $\alpha = K/(3Bi)$.

The validity of this solution has been checked in some detail both numerically by comparison with (3.3) and mathematically. It will not be re-derived in this work.

As noted before, in the case where internal particle diffusivity is infinite, (i.e. Bi=0) equation (2.2) is appropriate.

The closed form solution above greatly simplifies derivation of the moments of the impulse response. A discussion of methods of computing the complex functions $G_p(j\omega)$ and $N_D(j\omega)$ for frequency response plotting is presented in section B.3.iv.

(ii) Overall Bed Transfer Function and Moments

Danckwerts' Boundary Conditions

The transfer function obtained in this case (see Appendix I for derivation), is, for z=1 (bed exit):

$$G(s) = \frac{4NPe.\ e^{NPe/2}.\sqrt{X}}{\exp(\frac{1}{2}\sqrt{X}).(NPe+\sqrt{X})^2 - \exp(-\frac{1}{2}\sqrt{X}).(NPe-\sqrt{X})^2} \qquad \ldots \quad (3.6)$$

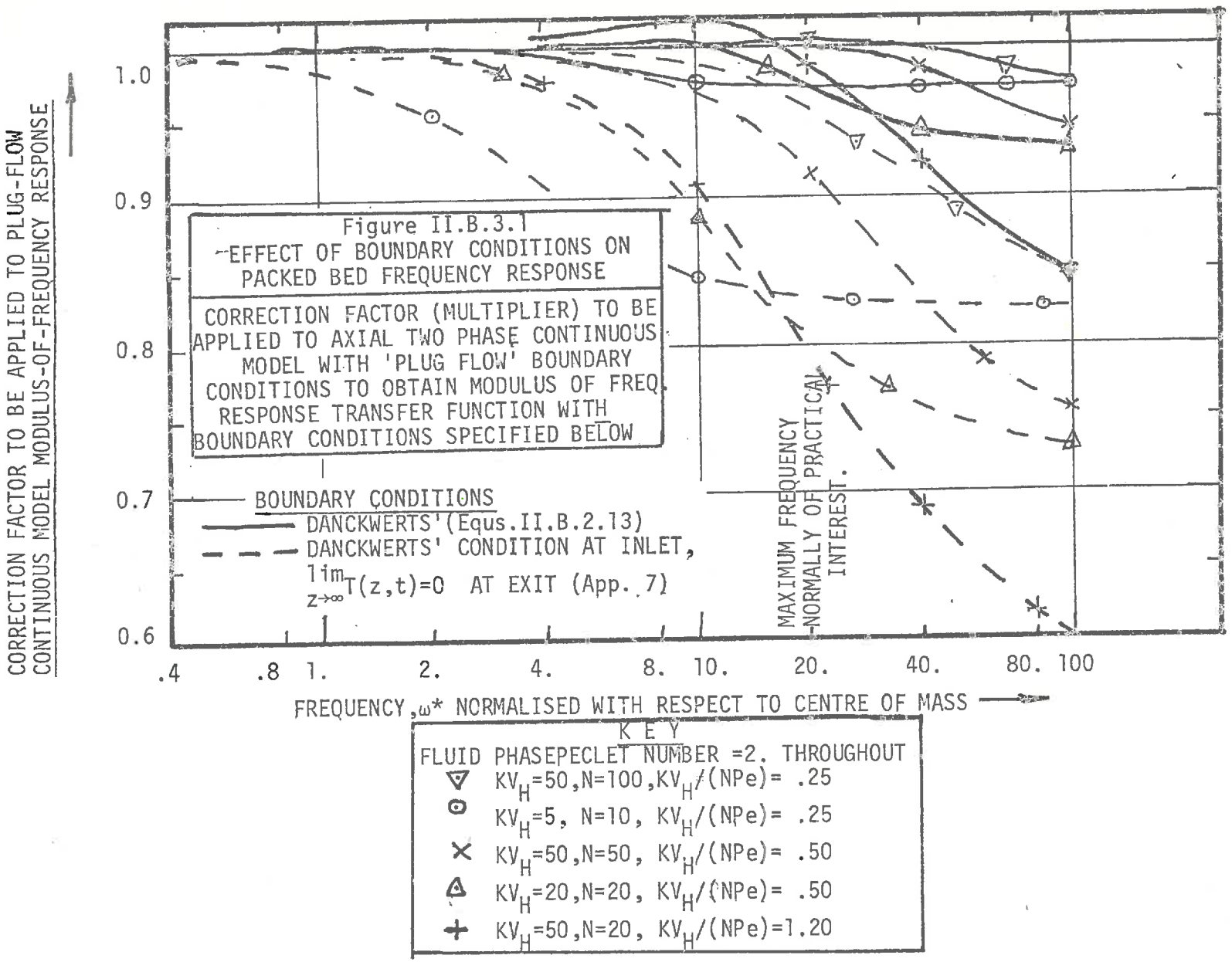
CORRECTION FACTOR TO BE APPLIED TO PLUG-FLOW CONTINUOUS MODEL MODULUS-OF-FREQUENCY RESPONSE
1.0
0.9
0.8
0.7
0.6
.4
.8
1.
2.
4.
8.
10.
20.
40.
80.
100
FREQUENCY, ω* NORMALISED WITH RESPECT TO CENTRE OF MASS
Figure II.B.3.1
EFFECT OF BOUNDARY CONDITIONS ON PACKED BED FREQUENCY RESPONSE
CORRECTION FACTOR (MULTIPLIER) TO BE APPLIED TO AXIAL TWO PHASE CONTINUOUS MODEL WITH 'PLUG FLOW' BOUNDARY CONDITIONS TO OBTAIN MODULUS OF FREQ. RESPONSE TRANSFER FUNCTION WITH BOUNDARY CONDITIONS SPECIFIED BELOW
BOUNDARY CONDITIONS
DANCKWERTS'(Equs.II.B.2.13)
DANCKWERTS' CONDITION AT INLET, lim T(z,t)=0 AT EXIT (App. 7)
z→∞
MAXIMUM FREQUENCY NORMALLY OF PRACTICAL INTEREST.
KEY
FLUID PHASEPECLET NUMBER =2. THROUGHOUT
KV_H=50,N=100,KV_H/(NPe)= .25
KV_H=5, N=10, KV_H/(NPe)= .25
KV_H=50,N=50, KV_H/(NPe)= .50
KV_H=20,N=20, KV_H/(NPe)= .50
KV_H=50,N=20, KV_H/(NPe)=1.20

where

$$X = N^2Pe^2 + 4NPe\,[s + KV_H(1-G_p(s))], \qquad \ldots \quad (3.7)$$

$G_p(s)$ is defined by equations (3.4) and (3.5),

$$NPe = \frac{Nd_p v_a}{D_e} \quad \text{and} \quad Nd_p = L.$$

Attempts to derive formulae for the moments of the impulse response were abandoned after the first moment had been obtained:

$$\mu = 1 + V_H$$

because of the excessively tedious and complicated algebra involved. A number of computations were carried out to compare the frequency response of this model with that of the simplified boundary condition model discussed below. The result of some of these computations is presented on Figure 3.1. It may be seen that little difference is noticeable except, as expected, at low values of KV_H and N. As noted in B.2.iii, lack of knowledge about actual physical conditions at bed entrance and exit and the excessive computational complications introduced makes the use of these boundary conditions unjustified.

(iii) Overall Bed Transfer Function and Moments-
Simplified Boundary Conditions

The boundary conditions used by Chao and Hoelscher [1966] [equations B.2.14] lead, according to the derivation in Appendix 1 to a more simple transfer function. When z=1,

$$G(s) = e^{NPe/2} \cdot \exp\left[-\frac{1}{2}\sqrt{X}\right] \quad \ldots \quad (3.8)$$

where X has been defined by equation (3.7).

The first, second and third moments of the impulse response are derived in Appendix 2. Expressed in terms of fluid phase axial dispersion Peclet number Pe, the Biot number Bi and KV_H (see section B.2.i) we have

$$\mu = 1 + V_H$$

$$\sigma^2 = \frac{2\mu^2}{NPe} + \frac{2(\mu-1)^2}{KV_H}\cdot\frac{Bi+5}{5} \quad \ldots \quad (3.9)$$

$$\pi^3 = \frac{12\mu^3}{N^2Pe^2} + \frac{12\mu(\mu-1)^2}{N.Pe.KV_H}\cdot\frac{Bi+5}{5} + \frac{6(\mu-1)^3}{(KV_H)^2}\cdot\frac{2Bi^2+14Bi+35}{35}$$

Note that the centre of mass of the impulse response is not a function of the dispersive parameters Pe, KV_H and Bi. Variance and skewness are increased by reducing KV_H, increasing Biot number, or reducing bed length. These conditions correspond physically to high flows (small St), large diameter particles and/or low conductivity particles.

Relative to a centre of mass of 1.0, i.e. redefining the time scale to be 1.0 at $\frac{L}{v_a}(1+V_H)$ time units, equations (3.9) become:

$$\mu^* = 1$$

$$\sigma^{*2} = \frac{2}{N.Pe} + \frac{2}{KV_H} \cdot \left(\frac{\mu-1}{\mu}\right)^2 \cdot \frac{Bi+5}{5}$$

$$\pi^{*3} = \frac{12}{N^2Pe^2} + \frac{12}{N.Pe.KV_H} \cdot \left(\frac{\mu-1}{\mu}\right)^2 \cdot \frac{Bi+5}{5}$$

$$+ \frac{6}{(KV_H)^2} \cdot \left(\frac{\mu-1}{\mu}\right)^3 \cdot \frac{2Bi^2+14Bi+35}{35} \quad \ldots \quad (3.10)$$

It will be noted that dispersion about the centre of mass is predicted to be approximately independent of the heat capacity ratio V_H when V_H is large, i.e. when $\mu \simeq \mu-1$.

(iv) Computational Considerations in Frequency Response Comparisons

As pointed out above [section 3.(i)] closed form expression of the particle transfer function $G_p(s)$ derived by Rosen [1952] has been used in the present work. Unfortunately the expressions for the frequency response transfer function $G_p(j\omega)$ are rather complicated and involve the definition of various subsidiary functions. This complexity has, it is believed, somewhat limited the application of Rosen's other results.

In fact, the substitution of $j\omega$ for s and computation of $G(j\omega)$ and $/G(j\omega)$ offers few difficulties where the computer

used has extensive facilities for complex arithmetic. In particular, it should be possible to evaluate directly

$$p(j\omega) = j\sqrt{[j\omega/\alpha]} \quad \ldots \quad (3.11)$$

and

$$\cot[p(j\omega)] \quad \ldots \quad (3.12)$$

using appropriate complex number subroutines.

A few such sophisticated systems are at present available.

If limited facilities are available, (3.11) must be converted to a complex number more explicitly:-

$$p(j\omega) = -\frac{\gamma}{\sqrt{2}}(1-j) \quad \ldots \quad (3.13)$$

where $\gamma = \sqrt{(\omega/\alpha)}$

whilst the cotangent may be expressed in terms of sine and cosine functions with real arguments for example

$$\cot[p(j\omega)] = \frac{A + jB}{C + jD} \quad \ldots \quad (3.14)$$

where

$$A = -e^{-\gamma/\sqrt{2}}[\cos(\gamma/\sqrt{2}) - j \sin(\gamma/\sqrt{2})]$$

$$B = e^{-\gamma/\sqrt{2}}[\cos(\gamma/\sqrt{2}) + j \sin(\gamma/\sqrt{2})]$$

$$C = e^{-\gamma/\sqrt{2}}[\sin(\gamma/\sqrt{2}) + j \cos(\gamma/\sqrt{2})]$$

$$D = e^{\gamma/\sqrt{2}}[\sin(\gamma/\sqrt{2}) - j \cos(\gamma/\sqrt{2})]$$

Since transfer functions of the type of eq. (3.8) appear, it is obviously also necessary to be able to compute the exponent of a complex quantity. This method has been applied

in the present work.

If no complex arithmetic facilities are available, real and imaginary parts must be evaluated using the rather difficult hyperbolic functions listed by Rosen.

4. Transfer Functions of Simplified Models

(i) Rosen's Model

The model proposed by J.B. Rosen [1952, 1953] assumes fluid phase axial dispersion to have negligible effect on the axial spreading of an impulse or step function input to the bed. Substitution of $^1/Pe = 0$ in equation B.2.2 yields the model equation for the fluid phase whilst the solid phase equation remains unchanged. The assumption may be seen to be theoretically valid when the contribution in equations (3.10) of terms involving Pe is small relative to terms involving the Stanton and Biot numbers only. This corresponds physically to situations of high flow, or poorly conductive, large particles.

Substituting $^1/Pe = 0$ we obtain the following transfer function for $0 \leq z \leq 1$,

$$G(z,s) = e^{-sz} \cdot \exp\{-KV_H[1-G_p(s)]z\} \qquad \ldots \quad (4.1)$$

The term e^{-sz} represents a perfect time delay of z units i.e. z'/v_a minutes. The solution predicts that nothing will

happen to the output for this time after making a change in input.

It may be shown from the initial value theorem that:

$$\lim_{t \to 0+} f(t) = \lim_{s \to \infty} s.F(s)$$

Applying this to the delayed version of equation (4.1) (obtained after eliminating e^{-sz}) we find,

$$\lim_{s \to \infty} s.\exp[G_p(s).z] = \exp[-KV_H.z]$$

Hence the initial response predicted is as sketched in the following figure for z = 1, i.e.,z'=L:

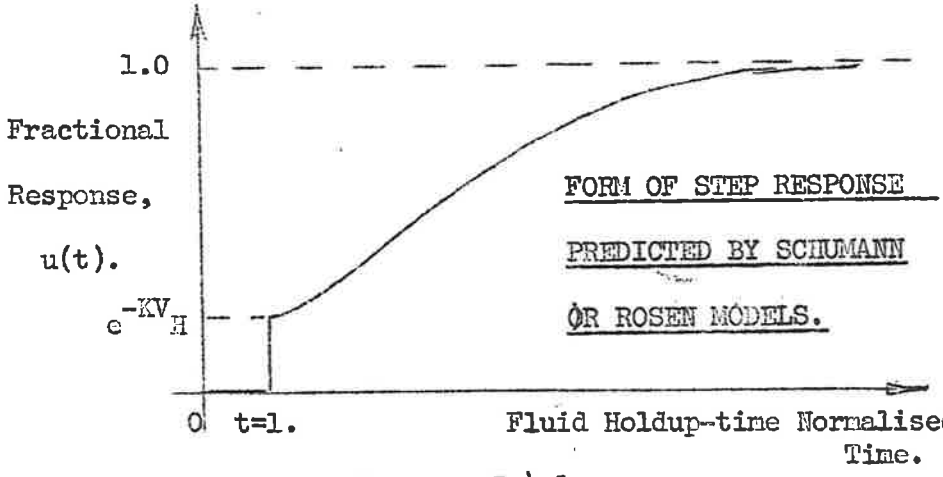

Figure B.4.1.

Such a situation is, strictly speaking, a physical impossibility. It results from the assumption of perfect plug flow and postulates that a proportion,$\exp[-KV_H]$, of a step input ,(or an identical area of an impulsive input) appears ,without any axial spreading, one fluid holdup time after administering the input. When V_H is large (e.g. a highly 'adsorptive' packing) the delay period is small, relative to the overall response. At the same time, a large value of KV_H

i.e. large Stanton number or low flow implies that exp $[-KV_H]$ will be small. However under this condition, according to equations (3.10), terms involving the Peclet number may assume importance so that more detailed computation is evidently required to establish the range of physical parameters over which the model is valid.

A corresponding frequency domain result is obtained by substituting $j\omega$ for s in equation (4.1) and allowing $\omega \to \infty$ noting that

$$\lim_{\omega \to \infty} \quad G_p(j\omega) = 0$$

The result obtained is

$$\lim_{\omega \to \infty} \quad G(z,j\omega) = e^{-KV_H} \cdot e^{-j\omega z} \qquad \ldots \quad (4.2)$$

or

$$|G(z,j\omega)| \to e^{-KV_H} \cdot \qquad \ldots \quad (4.3)$$

Such a result implies infinite 'band width', i.e. the system will respond to any signal, no matter how fast with an attenuation given by (4.3). This result is also a physical impossibility. Equation (4.3) has, nonetheless been extensively used in the application of cyclic test methods (Section V.A. 1.) to the determination of heat transfer coefficients in packed beds.

The Rosen model will be discussed in greater detail in Chapter IV in connection with breakthrough curve prediction. The first three moments are obtained by substituting $1/Pe=0$ in equations (3.9) and (3.10).

It is useful to note, from a study of equations (4.1) and (3.4) that frequency response plots need only contain the parameters KV_H and Bi provided the pure time delay factor e^{-sz} is eliminated from the phase angle curves, when $V_H\omega$ is the independent variable. To demonstrate this, substitute $j\omega$ for s in the expression for p, equ. (3.5):

$$p(\omega) = j\left[\frac{j\omega V_H}{\alpha V_H}\right]1/2 = j\left[\frac{3.Bi.j\omega V_H}{KV_H}\right]1/2$$

Equation (3.4) may also be written:

$$G_p(j\omega) = \frac{KV_H}{KV_H + \frac{KV_H}{Bi}[p(\omega).\cot p(\omega)-1]}$$

$$= \frac{Bi}{Bi+p(\omega).\cot p(\omega) - 1}$$

which is a function of ωV_H with Bi and KV_H as parameters. Substituting $j\omega$ for s in the full equation (4.1) we obtain

$$G(j\omega) = e^{-j\omega}.e^{-KV_H}.\exp[G_p(j\omega)] \quad , \quad Z=1$$

The factor $e^{-j\omega}$ remains a function of ωV_H with V_H as an additional parameter. However, this factor may be shown to

have an effect only on the phase angle curves. Thus

$$|G(j\omega)| = e^{-KV_H} \cdot |\exp[G_p(j\omega)]|,$$

is a function of KV_H, Bi and $V_H\omega$ only,

whilst $$\underline{/G(j\omega)} = -\frac{\omega V_H}{V_H} - KV_H - \underline{/\exp[G_p(j\omega)]}$$

is a function of V_H as well.

The first term in the phase angle curve may be subtracted as a correction from generalised plots excluding this.

Physically, this justifies the usual practice of plotting breakthrough curves as a function only of reduced time t/V_H with KV_H as a parameter for the case of intraphase resistance provided a dead time equal to the holdup time of the bed is added.

The property referred to above unfortunately does not hold when axial dispersion is added to the model.

(ii) The Model of Schumann

The Schumann [1929] model makes the further simplification of infinite solids conductivity, i.e. Bi=0. In this case the transfer function of equation (4.1) further reduces to

$$G(z,s) = e^{-sz} \cdot e^{-KV_H} \cdot \exp\left[\frac{K^2 V_H}{S + K}\right] \quad \ldots \quad (4.4)$$

whilst moments become

$$\mu = 1 + V_H$$

$$\sigma^2 = \frac{2}{KV_H}(\mu-1)^2 \qquad \ldots \quad (4.5)$$

$$\pi^3 = \frac{6(\mu-1)^3}{(KV_H)^2}$$

Analytical solutions to (4.4) for the case of a step input have been discussed by Klinkenberg [1954, 1960]. See also Section IV.3. The remarks made above concerning the physical limitations of the Rosen model also apply here. The model has been extensively applied to the analysis of cyclic method experiments (V.A. 1,) and even recently [Handley and Heggs, 1968] to the determination of heat transfer coefficients from the breakthrough curve or step response of a packed bed. The heat capacity ratio V_H is also eliminated as a separate parameter in frequency response and time response plots in a similar way to the Rosen model.

(iii) Axial Dispersion Models of Pulsifer and of Chao and Hoelscher

Pulsifer [1965] in his studies of fluid-particle heat transfer at low Reynolds numbers ($5 \leq Re_p \leq 100$) made use of the fact that at low Reynolds numbers, the Biot number

$$Bi = \frac{R.h_p}{k_s} = St.\ Re_p.Pr.\ \left(\frac{k_f}{2k_s}\right) \qquad \ldots \quad (4.6)$$

becomes very small, at least in gas-solid systems. Thus, assuming a limiting Nusselt number of roughly 2.0, equation (4.4) yields for very low flows,

$$Bi \to k_{f/k_s} \qquad \ldots \quad (4.7)$$

No allowance was made therefore for intraphase resistance although the more complex Danckwerts' boundary conditions were assumed. His transfer function may be obtained from equations (3.6) and (3.7) by substituting

$$G_p(s) = \frac{K}{s+K} \quad .$$

Pulsifer extended his model to allow for wall heat capacity (but not wall heat loss) although no allowance was made for radial gradients within the bed. A slightly extended version of this approach will be applied to the finite stage model analysis in Appendix 4. It may be noted that Pulsifer, in common with other investigators quoted by Pulsifer [Bar-Ilan and Resnick, 1957; Eichhorn and White, 1952; Kunii and Smith, 1961] arrived at the conclusion that Nusselt numbers considerably less than the theoretical minimum of 2.0 were obtainable at low Reynolds numbers. In another paper [Littman, Barille, Pulsifer, 1968] further results obtained from Pulsifer's modified apparatus have been reported after application of corrections for fluid-solid-fluid conduction and elimination of 'channelling'.

As a result of these corrections, higher Nusselt numbers are now reported and it is suggested that a limiting Nusselt number in the range of 1. to 2. would be achieved, given sufficient information about axial solids conduction in the low Reynolds number region.

Chao and Hoelscher [1966] used a similar model to that of Pulsifer in their studies of the dispersion which occurs when a pulse of hydrogen is administered to a bed packed with activated charcoal through which hydrocarbon mixtures are flowing. By simplifying the boundary conditions in Pulsifers model and ignoring the kinetics of the adsorption, they were able to obtain a transfer function, the moments of which were relatively easily extracted. As in Pulsifer's model, the resistance of the solid phase to, in this case, mass transfer, was assumed to be negligible. The simplified boundary conditions have been given by equations (B.2.14).

Substitution of Bi=0. in equations (B.3.8) and (B.3.7) yields Chao and Hoelscher's transfer function whilst their moments are obtained in a similar manner from equations (B.3.9):

$$\mu = 1 + V_H$$

$$\sigma^2 = \frac{2\mu^2}{NPe} + \frac{2(\mu-1)^2}{KV_H} \qquad \ldots (4.6)$$

$$\pi^3 = \frac{12\mu^3}{N^2Pe^2} + \frac{12\mu(\mu-1)^2}{N.Pe.KV_H} + \frac{6(\mu-1)^3}{(KV_H)^2}$$

In Appendix 3, in a paper by the writer [paper 1, 1968] the correspondences between the terminology of mass transfer used by Chao and Hoelscher and the present heat transfer terminology have been compared.

Chao and Hoelscher obtained estimates for each of the three moments listed above assuming diffusivity in the solid phase to be infinite. They arrived at the yet unexplained conclusion that a considerable decrease in apparent Peclet number occurred (from about 1.4 to 0.1) as the fraction of hydrocarbon in the 'carrier gas' increased.

It may be noted that the frequency response form of the transfer functions of all the axial dispersion models presented so far give the physically correct result that

$$\lim_{\omega \to \infty} G(j\omega) = 0$$

unlike either the Rosen or Schumann models.

(iv) Moments Analysis Approach of Schneider and Smith

Recently and subsequent to the publication of the writer's paper 1 [1968] and submission of paper 2 [1969] Schneider and Smith [1968] have presented, in mass transfer terminology, the first, second and third moments of the extended model with simplified boundary conditions. The solutions obtained appear to be identical to equations (3.9) although a detailed translation from their terminology to the present notation has not

yet been attempted. In their analysis of their experimental results, only the first and the second central moments were used yielding as would be expected the equilibrium constant equivalent to V_H and by varying the flowrate, the other constants in the variance equation.

C. FINITE STAGE MODEL OF PACKED BED DYNAMICS

1. Introduction

At the time of commencing the present research, the finite stage model of Deans and Lapidus [1960] offered the most complete and comprehensive description of packed bed dynamics. Because of the potential practical value of the model it seemed desirable rigorously to compare it with existing and proposed continuous models and with experimental results.

The finite stage model as extended by Deans and Lapidus made use of the random walk model of Baron [1952] and others to allow for the effects of the radial dispersion of heat and matter. Their work was based on the purely computational thesis of Deans and included such complications as simultaneous heat and mass transfer with an exothermic reaction, together with heat transfer through the walls of the reactor. They point out that the use of the finite stage model, where fluid phase axial dispersion is significant, reduces the solution from an iterative one requiring the simultaneous satisfaction

of boundary conditions at both ends of the reactor to a sequential one. The model would seem to find its greatest potential use in the solution of breakthrough curves where adsorption isotherms are non-linear and heat generation occurs. The method also eliminates instability problems since the finite differencing scheme represents, presumably, the actual physical mixing processes occurring in the bed. Lai and Roth [1967] applied the model to the dynamic simulation of a gas chromatographic column.

In section C.2, a linear version of the model excluding radial transfer has been derived in transfer function form so that a rigorous comparison between the predictions of both finite stage and continuous models could be made where both interphase and intraphase heat transfer occur.

2. Model Formulation and Derivation of Transfer Function

The derivation of paper 1 (Appendix 3) will be followed except that an effective mixing stage height H and number of stages M will be used consistently throughout instead of assuming that the effective height is one particle diameter d_p.

Note that

$$L = M.H. = N.d_p$$

Writing a heat balance for the well mixed fluid in stage i where the distance z from bed inlet = i.H:-

$$H\varepsilon\rho_f c_f \frac{dT_i}{dt'} = v_a \varepsilon \rho_f c_f [T_{i-1} - T_i] + h_p a_p H(1-\varepsilon)[T_{s_i} - T_i] \quad \ldots \quad (2.1)$$

where T_i and T_{s_i} refer to the fluid temperature and particle surface temperature in stage i respectively. Other symbols have been defined in sub-section B.1.(i).

Normalising time so that

$$t' = t.\frac{L}{v_a} = t.\ \frac{MH}{v_a} = t.\ \bar{T}$$

$$\frac{dT_i}{dt} = M\,T_{i-1} - M\,T_i + KV_H[T_{s_i} - T_i] \quad \ldots \quad (2.2)$$

where, as before,

$$KV_H = \frac{h_p a_p}{\rho_f c_f} \cdot \frac{1-\varepsilon}{\varepsilon} \cdot \bar{T} = 6\ St\ N(1-\varepsilon) \text{ for spherical particles,}$$

$$V_H = \frac{\rho_s c_s (1-\varepsilon)}{\rho_f c_f \varepsilon} = \text{heat capacity ratio.}$$

Laplace transforming (2.2) with initial conditions zero and substituting

$$\frac{T_{s_i}(s)}{T_i(s)} = G_p(s)\ ,$$

i.e., the particle transfer function, the fluid temperature T_i in stage i is related to upstream fluid temperature T_{i-1} by

$$\frac{T_i(s)}{T_{i-1}(s)} = \frac{M}{s + [1-G_p(s)]\ KV_H + M} \stackrel{def}{=} G_1(s) \qquad \ldots \quad (2.3)$$

The temperature at stage i may also be related to the temperature at stage i-2 by

$$\frac{T_i(s)}{T_{i-2}(s)} = \frac{T_i(s)}{T_{i-1}(s)} \cdot \frac{T_{i-1}(s)}{T_{i-2}(s)} = [G_1(s)]^2 \stackrel{def}{=} G_2(s)$$

Extending the process to computation of the M'th stage temperature in response to inlet temperature variations $T_o(s)$ ('stage zero'):-

$$\frac{T_M(s)}{T_o(s)} = G_M(s) = \left[\frac{M}{s + (1-G_p(s))KV_H + M}\right]^M \qquad \ldots \quad (2.4)$$

Computation of the frequency response of the bed using the above transfer function is simpler than either continuous model since exponentiation of complex quantities is not required. The difficulties which arise in computing $G_p(j\omega)$ are identical to those which arise in computing the frequency response of the extended two phase continuous model and have been discussed in section B.3.iv. Plots of modulus, $|G(j\omega)|$ and phase angle $\underline{/G}$ against normalised frequency, $V_H\omega$

require the solid-fluid capacity ratio V_H as a parameter in addition to $6St(1-\varepsilon)N$, M (equivalent to stating a Peclet number) and Biot number Bi. The number of parameters may be reduced by plotting only $G_1(j\omega)$ and noting that

$$|G_M(j\omega)| = [|G_1(j\omega)|]^M$$
$$\underline{/G_M(j\omega)} = M.\ \underline{/G_1(j\omega)} \qquad \ldots \quad (2.5)$$

3. Moments Analysis

Moments of the finite stage model have been derived in Appendix 2 making use of the additive property of cumulants under convolution referred to in Section II.A.3.

The resulting moments are

$$\mu = 1 + V_H$$
$$\sigma^2 = \frac{\mu^2}{M} + \frac{2(\mu-1)^2}{KV_H} \cdot \frac{Bi+5}{5} \qquad \ldots \quad (3.1)$$
$$\pi^3 = \frac{2\mu^3}{M^2} + \frac{6\mu(\mu-1)^2}{M.KV_H} \cdot \frac{Bi+5}{5} + \frac{6(\mu-1)^3}{(KV_H)^2} \cdot \frac{(2Bi^2+14Bi+35)}{35}$$

It will be noted that as in all other models, the first moment is predicted to be $1 + V_H$.

Comparing equations (3.1) with (B.3,9), the variance for the extended axial dispersion model with simplified boundary condition will be seen to be identical with the extended finite stage model, provided:

$$\frac{N\ Pe}{2} = M$$

i.e.

$$Pe = 2.\frac{M}{N} = 2.\frac{d_p}{H} = \frac{2}{\gamma}$$

which is the conclusion reached by Aris and Amundson [1957] for the simple axial dispersion model without interphase transfer (see Section I.A.2).

Substituting $Pe = \frac{2M}{N}$ in the equation for skewness we have

$$\pi^3 = \frac{8\mu^3}{N^2Pe^2} + \frac{12\mu(\mu-1)^2}{N.Pe.KV_H}.\frac{Bi+5}{5} + \frac{6(\mu-1)^3}{(KV_H)^2}.\frac{(2Bi^2+14Bi+35)}{35} \quad \ldots \quad (3.2)$$

Comparison of equations (3.2) and (B.3.9) reveals that the skewnesses are identical except for the term involving axial dispersion alone.

In paper 1 (Appendix 3), p.516, the ratio (π^3, finite stage)/(π^3, continuous) has been computed for various combinations of KV_H, V_H and N assuming zero Biot number. Since computing these ratios, more realistic estimates of likely parameter combinations in packed beds of spheres (assuming air to be the flowing fluid) have been made for $100 \leq Re_p \leq 10{,}000$ using literature correlations. Thus for μ large, substituting $6NSt(1-\varepsilon)$ for KV_H, and Bi=0 equation (3.2) becomes, approximately,

$$\pi^3 = \frac{\mu^3}{N^2}\left[\frac{8}{Pe^2} + \frac{2}{Pe.St.(1-\varepsilon)} + \frac{1}{6St^2(1-\varepsilon)^2}\right]$$

The relative contribution of the first term becomes large when St is large (i.e. at low Reynolds numbers) and again when Pe falls below 2.0 at Reynolds numbers less than 10. Considering Re = 10, Pe = 2, St = 0.8 and $\varepsilon \simeq 0.35$, the relative contribution of the first term to skewness becomes 39.4%. If the continuous model is assumed correct, an increase in skewness of 12% would be predicted. Under these conditions, the coefficient of skewness, defined in statistical texts by

$$\gamma_1 = \pi^3/\sigma^3$$

is of the order of $2.40/\sqrt{N}$ for the finite stage model or $2.87/\sqrt{N}$ for the continuous. This may be compared with $2/\sqrt{N}$ for a Gamma distribution (towards which the finite stage model tends when $St \to \infty$) and represents a very slight difference in shape, at least for $N > 20$.

When μ becomes small (e.g. steel spheres/water system) then differences will be more marked. It is doubtful whether the finite stage approach is physically appropriate in the case of liquids flowing in packed beds in any case.

In summary, the above comparison indicates that some confidence may be placed in the results of a packed bed simulation using the finite stage model over quite a wide range of

parameters assuming the continuous model to be valid in any case.

In the same paper, a comparison has been made using frequency response plots. Further comparisons are presented in Section E.

4. Contribution of A. Pethö

Since submission of the above treatment for publication (June, 1967), a similar extension of the finite stage model has been published by A. Pethö [1967] of the Central Research Institute of the Hungarian Academy of Sciences. An identical result was obtained although Pëtho's treatment did not allow for intraphase diffusional resistance.

D. 'EQUIVALENT CONDUCTIVITY' MODEL OF PACKED BED DYNAMICS

1. Introduction

Babcock [1964] and co-workers [Green, Perry and Babcock, 1964; Babcock, Green and Perry, 1966; Babcock, Perry and Crosser, 1967] have developed an approximate model of packed bed dynamics which attempts to allow for the following phenomena:

(a) axial fluid-phase dispersion

(b) interphase resistance

(c) intraphase resistance

(d) bulk plug flow convective transport

(e) fluid-solid-fluid conductivity.

The model assumes uniform fluid and solid temperatures at a given distance z' from the bed inlet, a concept which, it should be noted, is incompatible with allowance for inter and intraphase resistances. In later chapters, the ability of the model to adequately predict breakthrough curves in thermal and other adsorbers is examined. In this section, the model will be compared with the other models presented thus far from the moments analysis and frequency response viewpoints. Attractive features of the model are:

(i) only one parameter is required to completely specify the dynamic response of the bed

and

(ii) the step response solution obtained is relatively simple.

2. Fundamental Equations

In the present notation, the fundamental equation for Babcock's model is obtained by writing a heat balance over fluid and solid together assuming both to be at the same temperature. The result is given by equation (2.2).

$$\frac{(1 + V_H)\ \partial T}{\partial t} = -\frac{\partial T}{\partial z} + \frac{1}{Pe_a}\ \frac{\partial^2 T}{\partial z^2} \qquad \ldots \quad (2.2)$$

where time and distance have been normalised with respect to average fluid holdup time and bed length.

Pe_a, the effective axial Peclet number is defined by

$$Pe_a = \frac{v_a L}{(1+V_H) D_e} \quad . \quad . \quad . \quad (2.3)$$

where D_e is the 'effective axial diffusivity' of the combined fluid and solid phases.

i.e.,

$$D_e = \frac{ke}{\rho_f c_f \varepsilon + \rho_s c_s (1-\varepsilon)}$$

$$= \frac{ke}{\rho_f c_f \varepsilon . (1+V_H)} \quad .$$

The effective conductivity, ke is supposed to be formed additively from

k_e^o = fluid-solid-fluid conductivity

k_{ha} = interphase conductivity contribution

$k_{s(ha)}$ = intra-particle conductivity contribution

$k_{fm}.\varepsilon$ = component of fluid phase conduction.

The component k_e^o is given by:

$$k_e^o = \frac{k_f [k_s + 2k_f - 2(1-\varepsilon)(k_f - k_s)]}{k_s + 2k_f + (1-\varepsilon)(k_f - k_s)} \quad . \quad . \quad . \quad (2.4)$$

There seems to be little theoretical justification for including this term when fluid is flowing through the bed. It is of the same order as the fluid molecular conductivity k_f and will consequently be disregarded in the following analysis.

After translation into the present terminology, the other components of effective conductivity are substituted into equation (2.3) to yield

$$\frac{1}{Pe_a} = \frac{1}{NPe} + \frac{1}{KV_H}\left[\frac{V_H}{1+V_H}\right]^2 + \frac{Bi}{5KV_H}\left[\frac{V_H}{1+V_H}\right]^2 \quad \ldots \quad (2.5)$$

The transfer function implied by Babcock's equation (2.2) may be derived by an identical process to that of Appendix 1. The result, using the simplified boundary conditions of Chao and Hoelscher is, for $0 \leq z \leq 1.$,

$$G(z,s) = \exp[zPe_a/2\,1. \quad \exp\{-\tfrac{1}{2}z\sqrt{[Pe_a^2+4Pe_a(1+V_H)j\omega]}\} \quad \ldots \quad (2.6)$$

3. Physical Implications of the Model

The physical conditions which are implied by the assumption of uniform fluid and solid temperature at a given length z are, intuitively:

(a) thermal capacities of fluid and solid phases approximately equal i.e. $V_H \simeq 1.$

(b) negligible intra-particle gradients, i.e. Bi small or zero

(c) thermal resistance between fluid and solid small relative to total convective axial heat transfer, i.e. $KV_H = 6\ N\ St(1-\varepsilon)$ large. This requires a

small Reynolds number or large bed length.

Combining (b) and (c), we require KV_H/Bi to be large. This parameter as defined by Babcock [Babcock, Green and Perry, 1966] was called the 'bed length parameter' and given, in Rosen's notation the symbol γx. Their condition for the validity of the equivalent conductivity model is that γx should be greater than 2. In the present notation,

$$\gamma x = \frac{KV_H}{Bi} = \frac{6N(1-\varepsilon)}{Re_p.Pr} \cdot \frac{2k_s}{k_f} \qquad \ldots (3.1)$$

It will be noted that the bed length parameter is independent of Stanton number and that moment equations derived thus far may be expressed as functions of V_H, KV_H and γx instead of V_H, KV_H and Bi.

Although Babcock imposes other conditions as well as the one considered above, this is the principal one The possible effect of heat capacity ratio was not considered by Babcock and will be investigated in section E.

4. Moments of Equivalent Conductivity Model.

Equation (2.2) is in fact the widely used axial dispersion model Clements,[1969]. The 'doubly infinite' boundary condition transfer function solution, equation(2.6) may, for z=1 be also written

$$G(j\omega^*) = \exp((Pe_a/2).[1 - \sqrt{(1 + w)}]) \qquad \ldots (4.1)$$

where $\omega^* = \omega.(1 + V_H)$,

$$w = 4\frac{j\omega^*}{Pe_a}$$

The cumulant expansion of equation (A.2.6) may be used to obtain all the cumulants of this model. Thus, taking logarithms of both sides of equation (4.1):

$$\ln [G(j\omega^*)] = \frac{Pe_a}{2} [1 - \sqrt{(1 + w)}] \qquad ...(4.2)$$

The expansion for $\sqrt{(1 + w)}$, i.e.:

$$(1 + w)^{\frac{1}{2}} = 1 + \tfrac{1}{2} w + \tfrac{1}{2} (\tfrac{1}{2} - 1) w^2/2! + \ldots$$

where $|w| \leq 1$, or $\omega^* \leq Pe_a/4$,

may be substituted into equation (4.2) which is then compared, term by term with the cumulant expansion equ.(A.2.6) yielding:

$$\kappa_o^* = 1 \qquad \kappa_1^* = 1$$

and

$$\kappa_n^* = [1.3.5\cdots(2n-3)] \frac{2^{n-1}}{Pe_a^{n-1}}, \quad n = 2,3,\ldots \qquad ...(4.4)$$

Where the asterisk indicates that the time scale of the cumulants is normalised with respect to $(1+V_H)$ times the fluid holdup time. The first three cumulants become:

$$\kappa_1^* = \mu^* = 1, \quad \kappa_2^* = \sigma^{*2} = 2/Pe_a, \qquad ...(4.5)$$

$$\kappa_3^* = \pi^{*3} = 12/Pe_a^2$$

or in holdup times units as for the other models, using equn. (D.2.5):

$$\mu = 1 + V_H$$

$$\sigma^2 = \frac{2\mu^2}{Pe_a} = \frac{2\mu^2}{N\ Pe} + \frac{2(\mu-1)^2}{KV_H} \frac{Bi + 5}{5} \qquad ...(4.6)$$

(cont)

$$\text{and} \quad \pi^3 = \frac{12\mu^3}{N^2Pe^2} + \frac{12\mu(\mu-1)^2}{N.Pe.KV_H} \cdot \frac{Bi + 5}{5} + \frac{12\,(\mu-1)^4}{\mu(KV_H)^2} \cdot \frac{Bi^2 + 10Bi + 25}{25} \qquad \ldots(4.6)$$

Comparison of equations (4.6) with the moments of the extended axial dispersion and finite stage models, equns. (B.3.9) and (C.3.1) reveals that the first moments and the variances are identical. As before the normalised moments σ^{*2} and π^{*3} are practically independent of the heat capacity ratio V_H when $V_H >> 1$.

E. COMPARISON OF MODELS

1. Moments Comparisons

(1) Low Order Moments - Since according to equation (D.4.4) all the cumulants of the equivalent conductivity model are a function of the single parameter Pe_a, it is useful to determine whether the other (two phase) models may be reduced approximately to single parameter models. The first moments of all are identical, as are the variances σ^2 so that since $\sigma^2 = 2\mu^2/Pe_a$ or $\sigma^{*2} = 2/Pe_a$, σ^{*2} may be used as an alternative parameter to Pe_a. This parameter has the possible advantage of giving a more clear idea of the ralative dispersion of an impulse response about its centre of mass μ.

The -skewnesses' π^{*3} will be compared as a function of σ^{*2}, since predicted skewnesses differ, according to equations (B.3.9) (C.3.1) and (D.4.6). The 'coefficient of skewness' γ_1 is defined, in statistical texts as

$$\gamma_1 = \frac{\pi^3}{\sigma^3} = \frac{\pi^{*3}}{\sigma^{*3}} = \frac{\kappa_3^*}{\kappa_2^{*\,3/2}} \qquad \ldots(1.1)$$

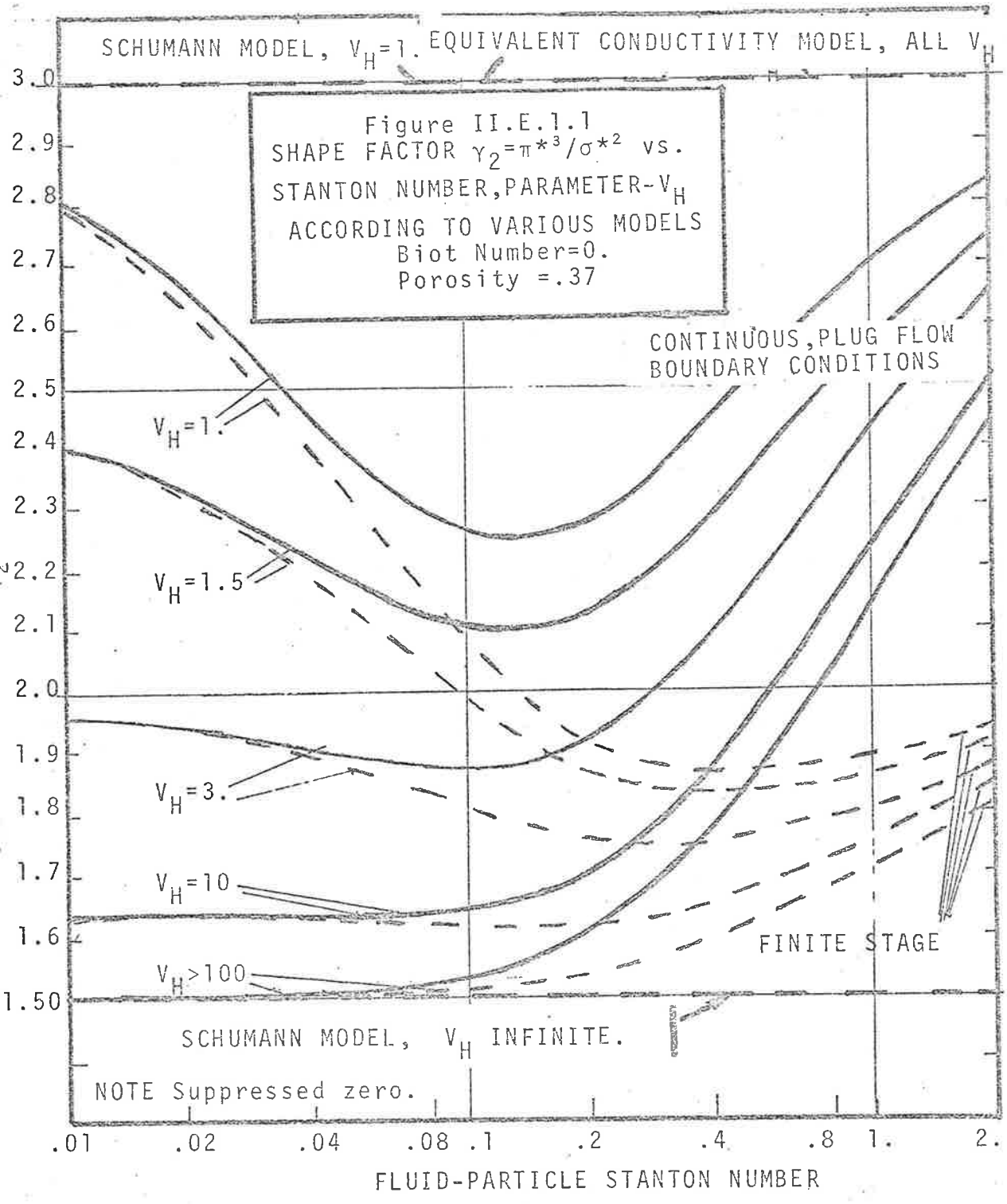
SCHUMANN MODEL, V_H=1.
EQUIVALENT CONDUCTIVITY MODEL, ALL V_H
Figure II.E.1.1
SHAPE FACTOR $\gamma_2=\pi^{*3}/\sigma^{*2}$ vs.
STANTON NUMBER, PARAMETER-V_H
ACCORDING TO VARIOUS MODELS
Biot Number=0.
Porosity =.37
CONTINUOUS, PLUG FLOW
BOUNDARY CONDITIONS
V_H=1.
V_H=1.5
V_H=3.
V_H=10
V_H>100
FINITE STAGE
SCHUMANN MODEL, V_H INFINITE.
NOTE Suppressed zero.
3.0
2.9
2.8
2.7
2.6
2.5
2.4
2.3
2.2
2.1
2.0
1.9
1.8
1.7
1.6
1.50
.01
.02
.04
.08
.1
.2
.4
.8
1.
2.
FLUID-PARTICLE STANTON NUMBER

The coefficient of skewness gives a good measure of the asymmetry of the impulse response, g(t). In the present work another coefficie involving the third cumulant may be found useful in comparing models. The ratio γ_2 is defined by equation (1.2):

$$\gamma_2 = \frac{\pi^{*3}}{\sigma^{*4}} = \frac{\pi^3 \cdot \mu}{\sigma^4} = \frac{\kappa^*_3}{\kappa^{*2}_2} \qquad \ldots (1.2)$$

Although this coefficient no longer is a good measure of asymmetry, it may be noted that the equivalent conductivity model predicts that γ_2 will be constant, having the value of 3.0 for any combinatic of physical parameters.

According to all three models (the two-phase continuous, finite stage and equivalent conductivity models) the parameter is predicted to be independent of bed length, N. This may be seen more clearly if the equation for KV_H, derived in section B.2 is substituted in equations (B.3.9) and (D.4.6) i.e.,

$$KV_H = a_p \cdot L \cdot St \cdot (1-\varepsilon)$$

$$= 6N.St.(1-\varepsilon) ,$$

for spherical or right cylindrical particles.

In this case, N disappears and γ_2 becomes a function of the Stanton number and porosity, the fluid phase axial Peclet number, the Biot number and the heat capacity ratio V_H. In figure E.1.1, values of γ_2 predicted by all three models are plotted as a function of Stanton number for a porosity of .37 and a Peclet number of 2., with V_H as parameter, Bi=0. Equation (1.5) on page 53 shows that for the Schumann model γ_2 is fixed at 1.5 for V_H, the heat capacity ratio very large, but becomes 3. when V_H=1. It may be seen that , as suggested in section D.3, V_H is an important parameter.

The range of Stanton numbers chosen corresponds, according to the Denton Correlation (section I.E.4) to superficial particle Reynolds numbers ranging from about 50 to about 50,000. As the value of V_H increases, γ_2 approaches a limiting value of about 1.5 at a Stanton number of 0.1.

In Table II. E.1.1 typical values of heat capacity ratio are listed for either water or air passing through beds of various materials. It may be seen that for the experiment carried out by Babcock and co-workers, using water as the fluid, V_H values will be low enough to ensure good agreement between the models.

TABLE II E.1.1.

TYPICAL HEAT CAPACITY RATIOS, 70°F

BED POROSITY ASSUMED : 0.40

Fluid	Pressure psig	Heat Capacity Ratio V_H, for Packings Indicated			
		Glass	Perspex	Lead	Steel
Water	-	0.76	0.62	0.54	1.28
Air	0	6100	5000	4300	10,300
"	50	1410	1150	1000	2400
"	100	800	650	560	1340
"	200	420	350	300	720

The specific heat c_f of air at constant pressure is taken as 0.234 BTU/(lb) (°F). A compressibility of 1.0 has been assumed.

Whilst γ_2 is predicted to be independent of bed length N, the skewness parameter γ_1 is supposed, for all three models, to vary inversely with the square root of the bed length N, i.e.

$$\gamma_1 \propto {}^{1}/\sqrt{N}.$$

Hence at long bed lengths, when all three models predict increasingly symmetrical impulse responses, (i.e. $\gamma_1 \to o$) the fact that γ_2 differs may be rather important. Nonetheless heat capacity ratio V_H does appear to be a more important factor than realised by Babcock and co-workers.

(ii) High Order Moment Comparisons

The normalised cumulants κ^*_n of the single parameter axial conduction model were derived in section D.4 (eq.D.4.4). The general cumulants of the Schumann model may also be derived in a similar manner. Thus, normalising equation (B.4.4) in terms of the centre of mass or first moment, setting z = 1 and taking natural logarithms we have:

$$\ln\left[G(j\omega^*)\right] = -KV_H - \frac{j\omega^*}{V_H + 1} + \frac{KV_H}{w + 1} \qquad \ldots(1.3)$$

where $$w = \frac{j\omega^*}{KV_H} \cdot \frac{V_H}{V_H + 1},$$

and $$\omega^* = \omega\,(1 + V_H).$$

The last term may, as before be expanded in an infinite series:

$$\frac{KV_H}{w + 1} = KV_H\,(1 - w + w^2 - \omega^3 + \ldots) \qquad \ldots(1.4)$$

where $|w| \leq 1$, or $\omega^* \leq KV_H\left[\frac{V_H + 1}{V_H}\right]$.

Comparing, as before, the expanded form of equation (1.3) with the cumulant expansion, equation (A.2.6), we have:

$$\kappa_0^* = 0 \, , \; \kappa_1^* = 1$$

and $$\kappa_n^* = \frac{n!}{(KV_H)^{n-1}} \cdot \left[\frac{V_H}{V_H + 1} \right]^n \quad n = 2,3, \qquad \ldots(1.5)$$

When equation (D.2.5) is substituted into the corresponding equation for the cumulants of the equivalent conductivity model (equ.D.4.4) with negligible fluid phase axial dispersion (Pe = ∞) and infinite particle conductivity (Bi = 0) we have

$$\kappa_0^* = 0,$$

$$\kappa_n^* = [1.3.5...(2n-3)] \frac{2^{n-1}}{(KV_H)^{n-1}} \left[\frac{V_H}{V_H + 1} \right]^{2n-2} \qquad \ldots(1.6)$$

When n = 0, 1 and 2, it has been shown (section D.4) that the cumulants of the equivalent conductivity and two phase models are identical. This is confirmed by equations (1.5) and (1.6). From physical considerations, the equivalent conductivity (single phase) model may be expected to yield close agreement with the Schumann (two phase) model when the thermal capacities of solid and fluid are equal, i.e. when $V_H = 1$, we have

Schumann two phase model:

$$\kappa_n^* = \frac{n!}{(KV_H)^{n-1}} \cdot \frac{1}{2^{n-1}} \, ,'$$

Equivalent conductivity model:

$$\kappa_n^* = \frac{[1.3.5.\cdots (2n-3)]}{(KV_H)^{n-1}} \cdot \frac{1}{2^n}$$

Substituting n = 3, 4 and 5 we have, Schumann model:

$$\kappa_3^* = 0.75/(KV_H)^2, \kappa_4^* = 1.5/(KV_H)^3, \kappa_5^* = 3.75/(KV_H)^4$$

Equivalent conductivity model:

$$\kappa_3^* = 0.75/(KV_H)^2, \kappa_4^* = 1.875/(KV_H)^3, \kappa_5^* = 6.56/(KV_H)^4$$

As the heat capacity ratio V_H becomes large i.e. $V_H \to \infty$ we have $V_H/(V_H+1) \to 1$ and divergence between the models increases. For this limiting case,

Schumann Model:

$$\kappa_3^* = 6/(KV_H)^2, \quad \kappa_4^* = 24/(KV_H)^3, \quad \kappa_5^* = 120/(KV_H)^4$$

whilst for the equivalent conductivity model:

$$\kappa_3^* = 12/(KV_H)^2, \quad \kappa_4^* = 120/(KV_H)^3, \quad \kappa_5^* = 1680/(KV_H)^4$$

In the following section, frequency response analysis is used to compare the two phase and single phase models more generally.

2. Frequency Domain Comparisons.

Comparisons of the frequency response transfer functions $G(j\omega)$ predicted by both two phase models and by the single phase or equivalent conductivity model yields a more detailed picture of the similarities and differences between the models. As for moments analysis, actual inversion to obtain the time response is not required although this type of comparison will also be carried out in chapter IV.

The choice of variance σ^{*2} as a single unifying parameter is a fortunate one since it effectively tends to reduce the more complex multiparameter models to single parameter models.

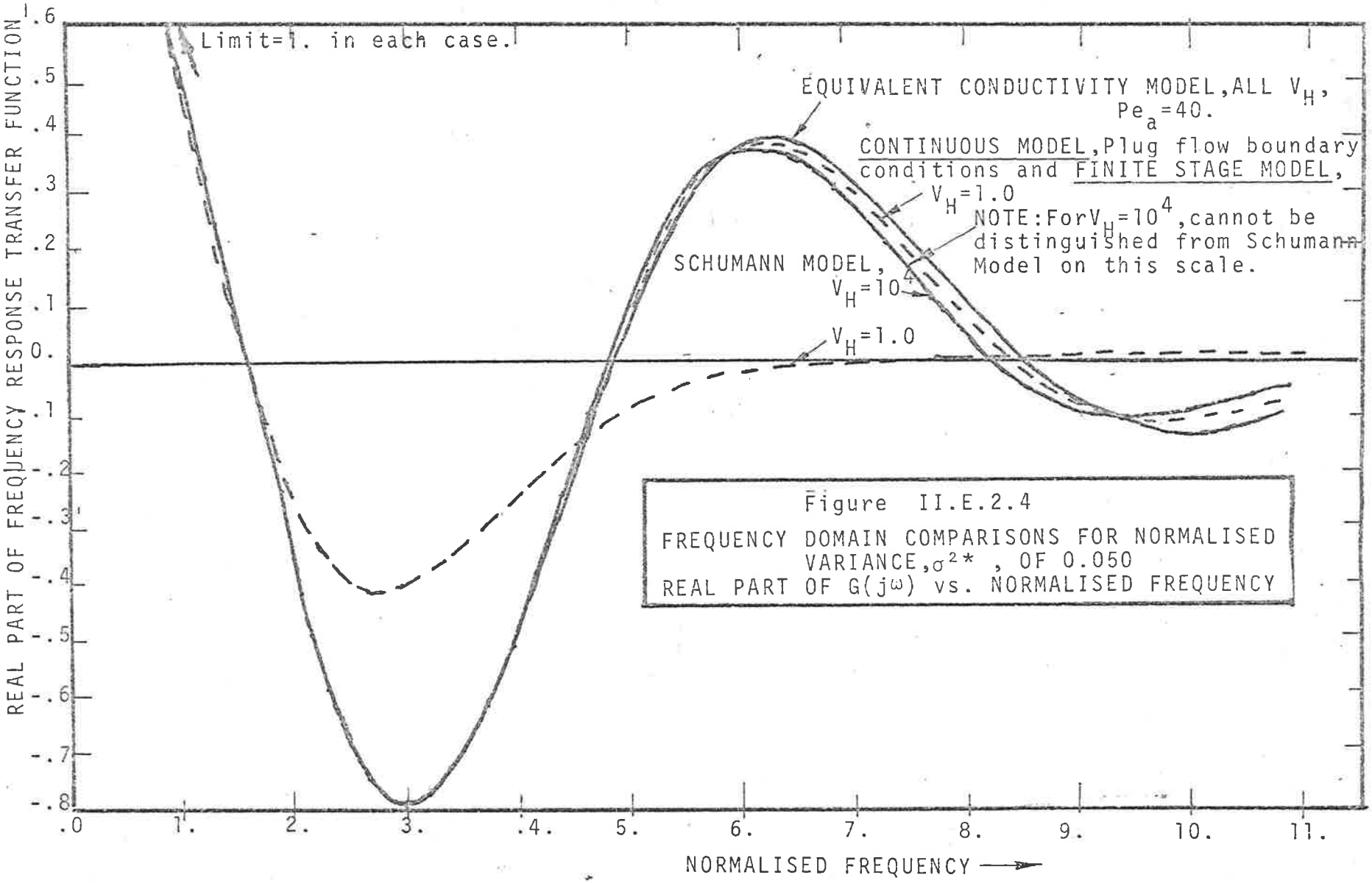

Figure II.E.2.4

FREQUENCY DOMAIN COMPARISONS FOR NORMALISED VARIANCE, σ^{2*}, OF 0.050
REAL PART OF $G(j\omega)$ vs. NORMALISED FREQUENCY

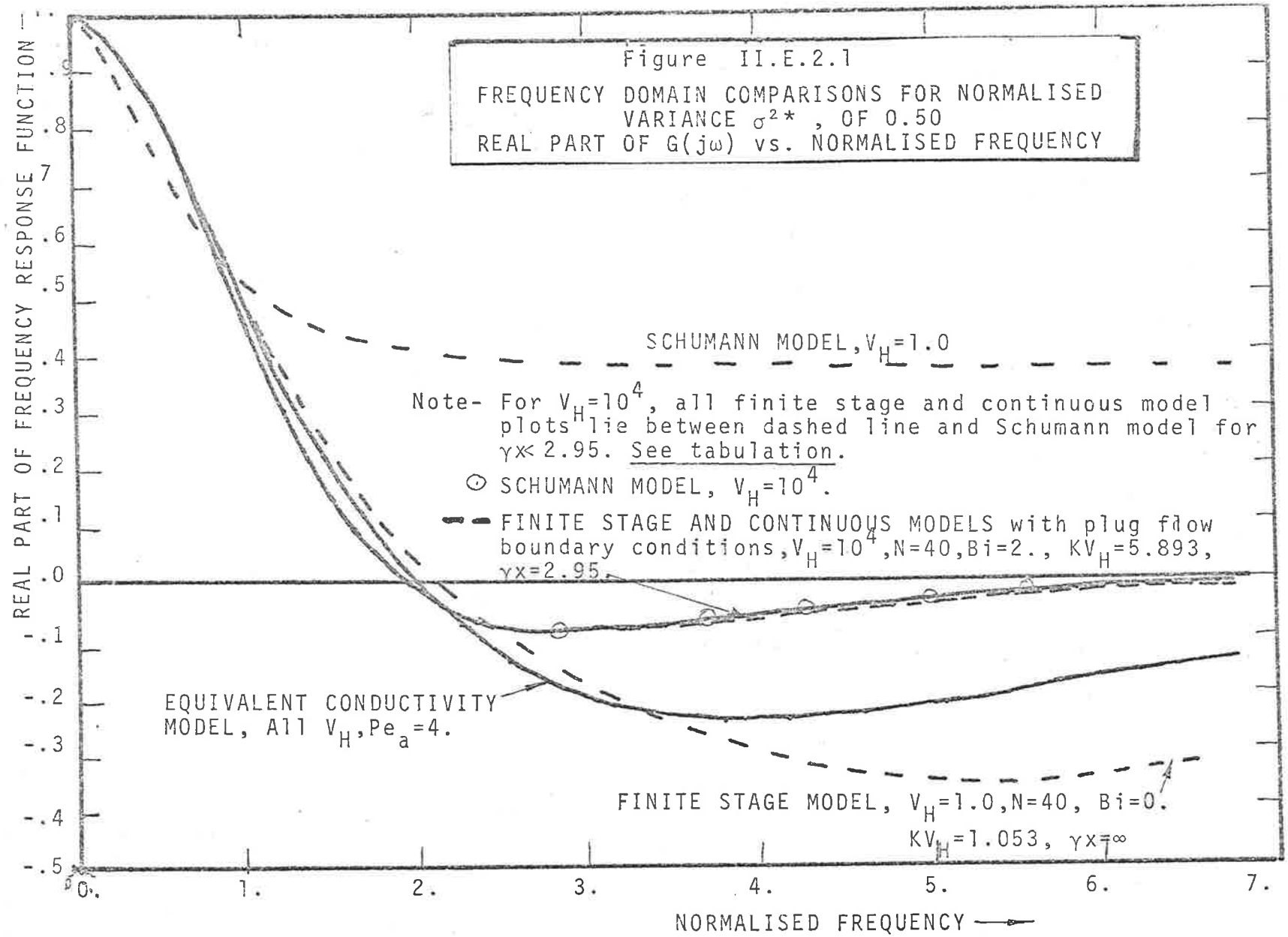
Figure II.E.2.1
FREQUENCY DOMAIN COMPARISONS FOR NORMALISED VARIANCE σ^{2*} , OF 0.50
REAL PART OF G(jω) vs. NORMALISED FREQUENCY
REAL PART OF FREQUENCY RESPONSE FUNCTION
NORMALISED FREQUENCY
SCHUMANN MODEL, V_H=1.0
Note- For $V_H=10^4$, all finite stage and continuous model plots lie between dashed line and Schumann model for γx< 2.95. See tabulation.
SCHUMANN MODEL, $V_H=10^4$.
FINITE STAGE AND CONTINUOUS MODELS with plug flow boundary conditions, $V_H=10^4$, N=40, Bi=2., KV_H=5.893, γx=2.95.
EQUIVALENT CONDUCTIVITY MODEL, All V_H, Pe_a=4.
FINITE STAGE MODEL, V_H=1.0, N=40, Bi=0. KV_H=1.053, γx=∞
.9
.8
.7
.6
.5
.4
.3
.2
.1
.0
-.1
-.2
-.3
-.4
-.5
0.
1.
2.
3.
4.
5.
6.
7.

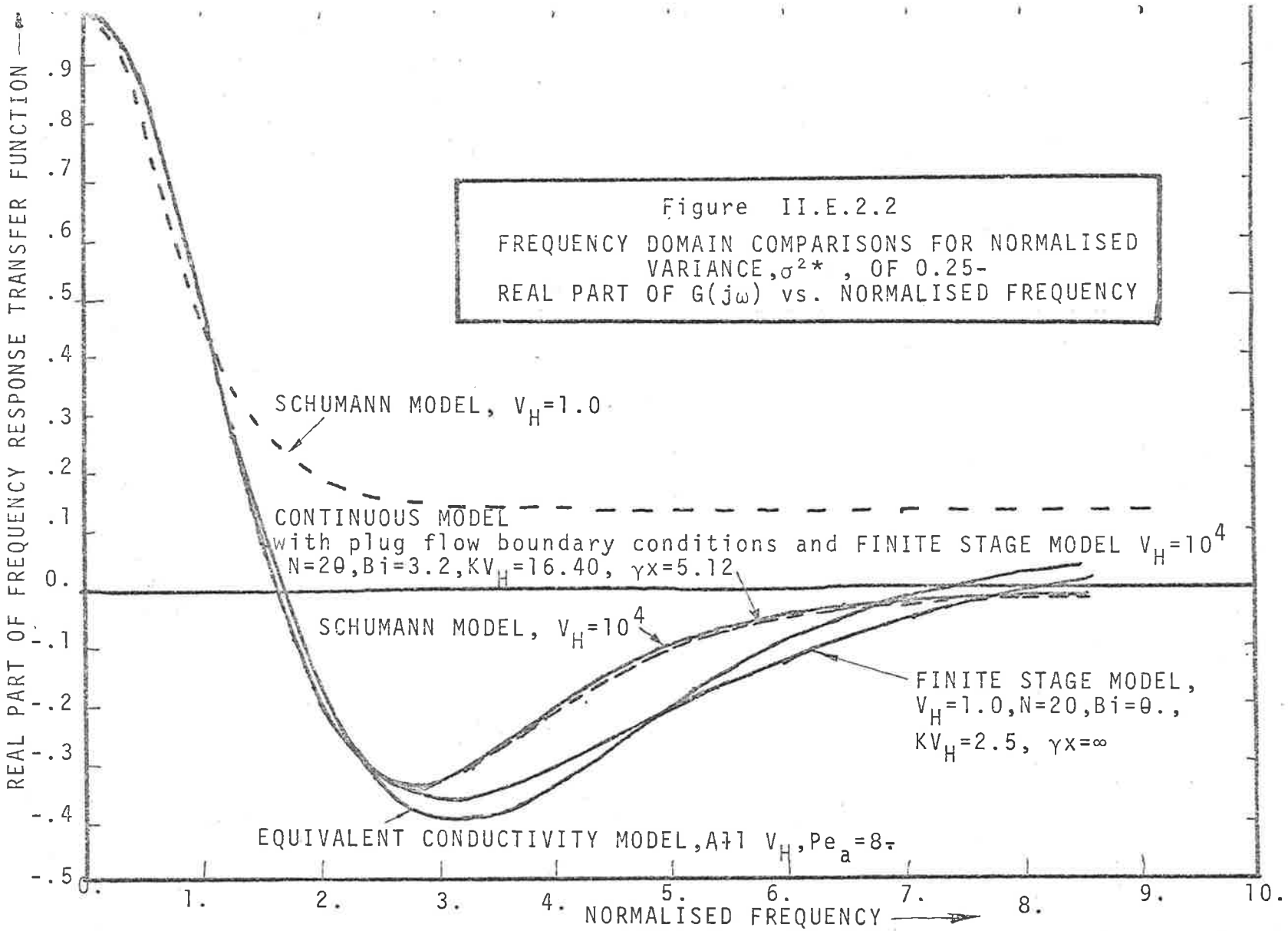

Figure II.E.2.2

FREQUENCY DOMAIN COMPARISONS FOR NORMALISED VARIANCE, σ^{2*} , OF 0.25- REAL PART OF $G(j\omega)$ vs. NORMALISED FREQUENCY

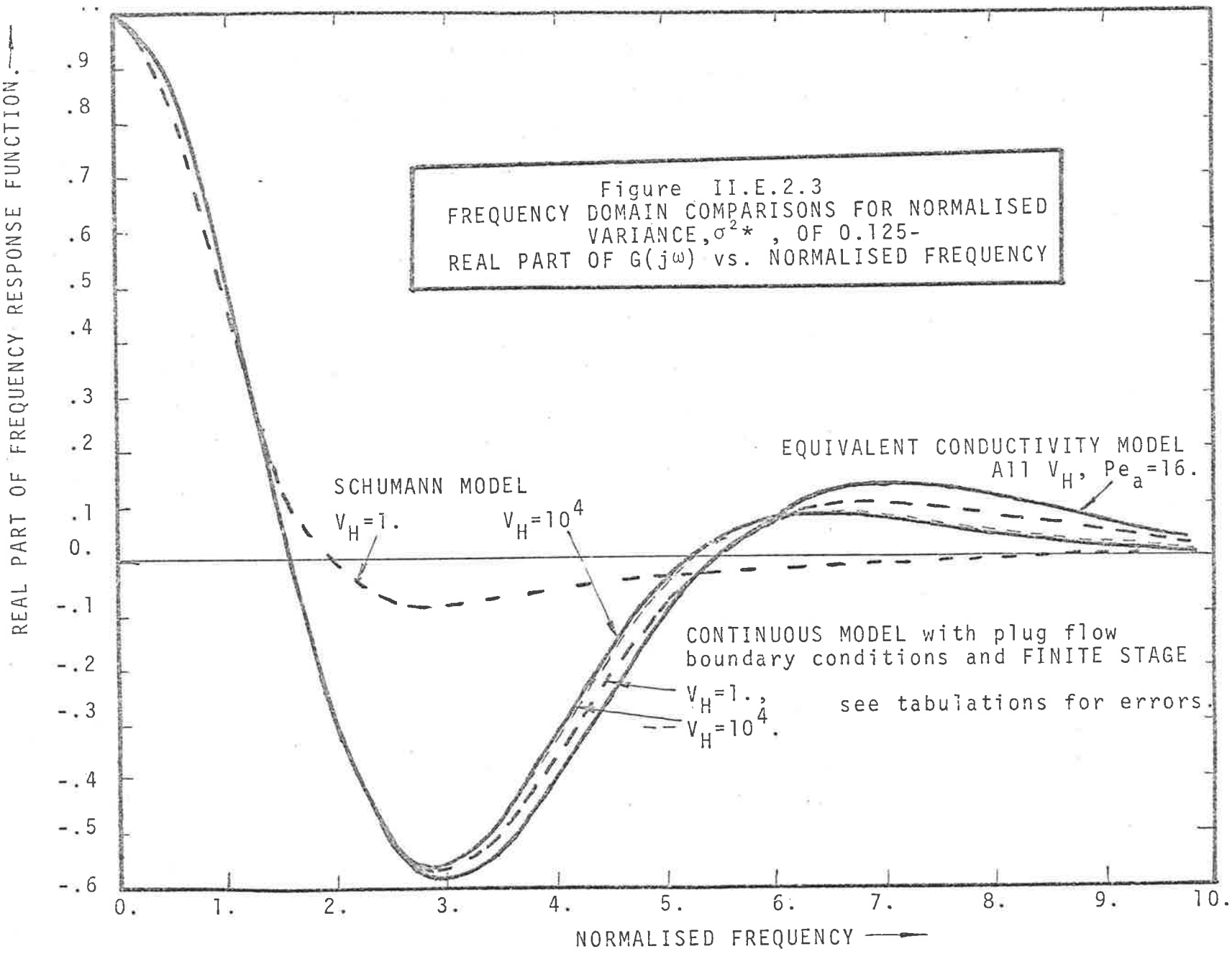
REAL PART OF FREQUENCY RESPONSE FUNCTION.
.9
.8
.7
.6
.5
.4
.3
.2
.1
0.
-.1
-.2
-.3
-.4
-.5
-.6
0.
1.
2.
3.
4.
5.
6.
7.
8.
9.
10.
NORMALISED FREQUENCY
Figure II.E.2.3
FREQUENCY DOMAIN COMPARISONS FOR NORMALISED VARIANCE, $\sigma^{2}*$, OF 0.125-
REAL PART OF G(jω) vs. NORMALISED FREQUENCY
SCHUMANN MODEL
V_H=1.
V_H=10^4
EQUIVALENT CONDUCTIVITY MODEL
All V_H, Pe_a=16.
CONTINUOUS MODEL with plug flow boundary conditions and FINITE STAGE
V_H=1.,
V_H=10^4.
see tabulations for errors.

Figures E.2.1 to E.2.4 illustrate the results of a series of computations carried out, for constant values of σ^* , at two values of V_H : 1.0, corresponding to liquid flowing through a packed bed and 1000, corresponding to the flow of gases (table E.1.1)

A marked deviation is revealed (as expected from moments analysis) between the equivalent conductivity and the two phase models at the higher value of heat capacity ratio. For the modulus curves, this is indicative, according to the cumulent expansion, [equations (A.2.9) and (A.2.10)] of the differences between the fourth cumulants κ_4^* or Kurtoses of the models.

It may be seen that the simple Schumann model differs little from the other two phase models, for V_H large, over a wide range of parameters, provided σ^{*2} is kept constant. Values of σ^{*2} or σ^2 may be obtained.

for the Schumann model: from equation (B.4.5),
for the Rosen model: from equation (B.3.9) with N very large i.e. with Pe $\rightarrow \infty$,
for the extended axial dispersion model: from equation (B.3.9)
and for the finite stage model: from equation (C.3.1).

When the heat transfer parameter KV_H is large (i.e. for long lengths or high Stanton numbers) intra particle conduction effects (indicated by the value of the Biot number) are predicted to cause little deviation from the Schumann solution provided as before the effect of the greater curve spread resulting is incorporated into σ^{*2}. The Schumann solution hence becomes an acceptable single - parameter model in an analogous way to the equivalent conductivity model, provided the ratio γx (or KV_H/Bi defined by Babcock, equation (D.3.1) is kept above about 10. This point is discussed further in section III. E.3

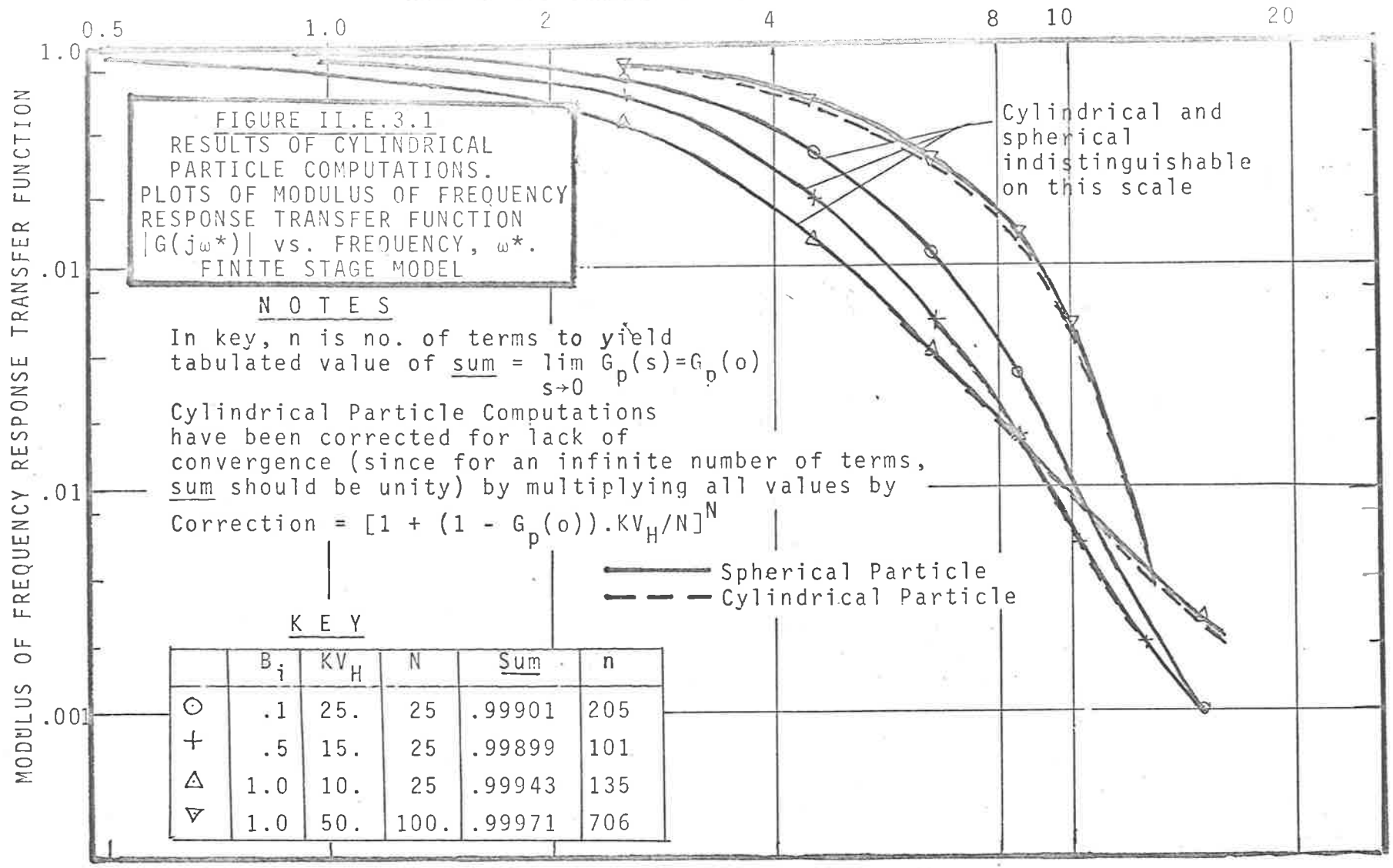

FIGURE II.E.3.1
RESULTS OF CYLINDRICAL PARTICLE COMPUTATIONS.
PLOTS OF MODULUS OF FREQUENCY RESPONSE TRANSFER FUNCTION
$|G(j\omega^*)|$ vs. FREQUENCY, ω^*.
FINITE STAGE MODEL

N O T E S

In key, n is no. of terms to yield tabulated value of sum = $\lim_{s \to 0} G_p(s) = G_p(o)$

Cylindrical Particle Computations have been corrected for lack of convergence (since for an infinite number of terms, sum should be unity) by multiplying all values by

Correction = $[1 + (1 - G_p(o)).KV_H/N]^N$

K E Y

	B_i	KV_H	N	Sum	n
⊙	.1	25.	25	.99901	205
+	.5	15.	25	.99899	101
△	1.0	10.	25	.99943	135
▽	1.0	50.	100.	.99971	706

Increasing distortion of the shape of the frequency responses becomes evident as γx decreases (i.e. as Bi increases and/or KV_H decreases) so that the Schumann solution is no longer a useful approximation.

At the lower end of the V_H scale, the equivalent conductivity model is likely to be a useful approximation provided, as shown by Babcock and co-workers, γx is kept large.

It also becomes obvious that it will be hard to differentiate experimentally between the effects of axial dispersion, heat transfer resistance between solid and fluid, and particle conductivity merely from a study of the shape of a transient or steady state frequency response test.

3. The Effects of Particle Shape

The results of a few computations of the frequency response transfer function of a bed packed with right cylindrical particle are presented in figure E.3.1. The computer program used for these computations is listed in appendix 6. It is evident that little difference is detectable between right cylindrical and spherical particles for the particular parameters chosen, and as the Biot number approaches zero the two become indistinguishable. It is obviously possible to extend the particle transfer function (or particle admittance function in Rosen's terminology approach to other geometries. This may be done by replacing Gp(s) throughout the chapter by, for example, the infinite plate transfer function provided solids axial conduction is zero or very small as in the case of regenerators constructed from a series of thin parallel plates.

This particular transfer function also fortunately is available in closed form.

F. SUMMARY OF CONCLUSIONS

This chapter has largely been devoted to statements of mathematical fact of use in later chapters and to a unification of nomenclature between alternative models of packed bed dynamics. The admittance functions of Rosen have been used, in the guise of 'particle transfer functions' to extend existing two phase continuous models and to simplify an extended finite stage model which has been shown to be of potential value in more complex non linear adsorber problems. The essential computational simplicity of the Rosen particle transfer function has also been demonstrated.

The theoretical importance of the heat capacity ratio V_H in prediction of a suitable limiting form of approximation to packed bed dynamics has been revealed. At high V_H values, the Schumann solution emerges as a satisfactory approximation to the more complex models, provided the normalised variance σ^{*2} is used as a parameter and provided the ratio $\gamma_X = KV_H/Bi$ is kept above about 10. Similar remarks apply to the equivalent conductivity solution for low values of V_H.

It was concluded that the effects of fluid phase axial dispersion and fluid particle heat transfer resistance will be difficult to separate experimentally even at relatively high values of the Biot number and that particle shape has little effect, mathematically at least, on the shape of a transient or frequency response plot.

CHAPTER III

AXIAL DISPERSION AND INTRA-PARTICLE CONDUCTION EFFECTS IN PACKED BEDS

SCOPE OF THE CHAPTER

In this chapter, the theoretical results of Chapter II are used to estimate the quantitative effects of fluid phase axial dispersion and intra-particle conduction.

In order to obtain an overall view of the importance of axial dispersion in packed beds, extensions of the theory to steady state conditions are made.

In Section A, a continuous version of the finite stage 'F factor' approach of Epstein [1958] to steady state heat transfer measurements in packed beds is derived. The theoretical independence of axial dispersion corrections from bed length is also demonstrated at least for simplified boundary conditions.

In Section B, F factors are also derived for steady state fluid-wall heat transfer measurements in packed beds.

In Section C, the same approach is applied to unsteady state step, pulse or cyclic determinations of fluid-particle transfer coefficients in packed beds.

In Section D, the results derived in the above sections are applied to calculation of likely axial dispersion and

fluid-solid-fluid conductivity errors at various flowrates.

Section E uses results from Chapter II to discuss further the likely significance of particle conductivity with a view to deriving simple criteria for deciding whether intraparticle resistance is likely to be of importance.

A summary of conclusions is presented in Section F.

A. STEADY STATE FLUID-PARTICLE TRANSFER COEFFICIENT DETERMINATIONS

1. Introduction

The quantitative importance of axial fluid phase conduction in packed bed regenerators, adsorbers and reactors is still difficult to estimate despite the considerable literature on axial dispersion in the absence of interphase transfer.

Epstein [1958] has provided fluid-phase axial dispersion correction factors F, which have been applied to steady state measurements of fluid-particle heat or mass transfer coefficients in packed beds by the 'evaporation from porous spheres' method (see I.B.4). In this method, surface temperatures are maintained at a constant value by evaporation. Inlet and outlet temperature differences are used to calculate a logarithmic mean driving force ΔT_{LM} which then is applied in the usual way to calculation of overall average fluid-particle coefficients.

Epstein's correction factor F was derived from a steady state version of the finite stage or mixing cell model. It allows a true temperature difference ΔT, representing the actual integrated driving force, to be calculated, where

$$\Delta T = F. \Delta T_{LM} \quad \ldots \quad (1.1)$$

The resultant equation for F was expressed by Epstein as a function of R, the inlet-outlet temperature difference ratio and of N, the number of perfectly mixed tanks in series, usually regarded simply as the bed length in particle diameters (i.e. $N = L/d_p$):

$$F = \frac{\ln R}{N(R^{1/N}-1)} \quad \ldots \quad (1.2)$$

A plot of F against R and N is presented and it was concluded that at long bed lengths, axial dispersion corrections are negligible, or $F \to 1$. The present experimental programme was planned on the assumption that axial dispersion effects would be detectable only at short bed lengths.

2. Alternative Form for F Factors

An alternative and exactly equivalent form for equation (1.2) is, for a bed of spheres or right cylinders (see Appendix 7) in heat transfer notation:

$$F = \frac{\ln [1 + 6St(1-\varepsilon)]}{6St(1-\varepsilon)} \quad \ldots \quad (2.1)$$

It may be seen that F is, in fact, independent of bed length and is a function only of Stanton number which, at a fixed Prandtl number is generally accepted to depend primarily on Reynolds number.

The correction factor F may be regarded, more generally, as the ratio of the apparent Stanton number St_{calc} (calculated without correction for axial dispersion) to the 'actual' Stanton number St.

That is,

$$F = \frac{St_{calc}}{St} \quad \ldots \quad (2.2)$$

This is because the exact solution using the finite stage model takes the same form as the usual plug flow solution when St is replaced by St_{calc}/F.

Hence plots of St_{calc} against St may be prepared allowing corrections to be made in one step.

As pointed out in I.A.2, if the equivalent number of perfect mixers in a bed of length N particle diameter is M, where $M = N/\gamma$, Aris [1957] has shown that an equivalent continuous model Peclet number Pe is obtained, where $Pe = 2/\gamma$.

Equation (2.1), hence may be written, more generally: for $\gamma = 1$:

$$F = \ln [1 + 12\ St(1-\varepsilon)/Pe] . \frac{Pe}{12\ St(1-\varepsilon)} .$$

$$\ldots \quad (2.3)$$

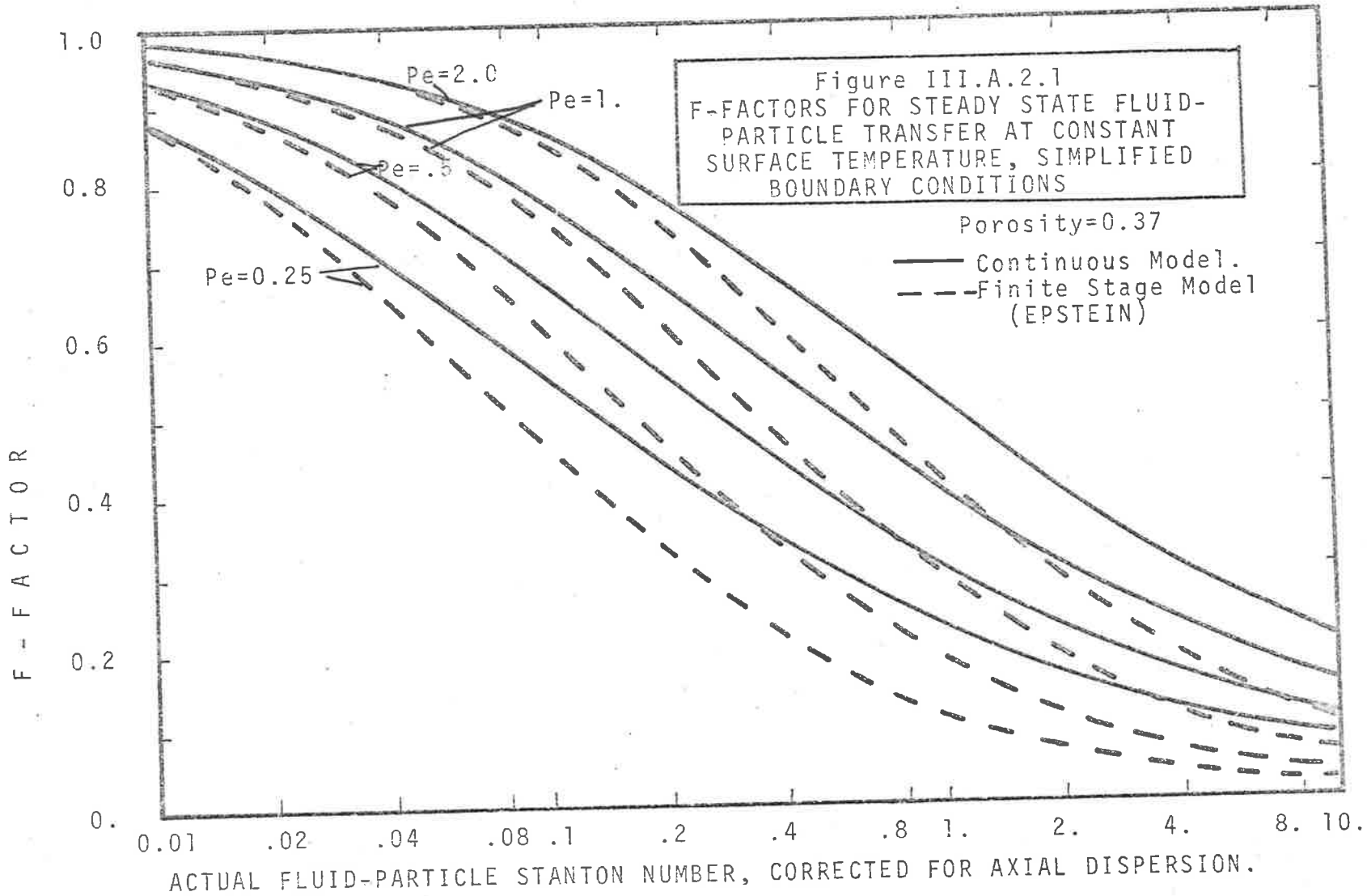
Figure III.A.2.1
F-FACTORS FOR STEADY STATE FLUID-PARTICLE TRANSFER AT CONSTANT SURFACE TEMPERATURE, SIMPLIFIED BOUNDARY CONDITIONS
Porosity=0.37
Continuous Model.
Finite Stage Model (EPSTEIN)
Pe=2.0
Pe=1.
Pe=.5
Pe=0.25
F-FACTOR
1.0
0.8
0.6
0.4
0.2
0.
0.01
.02
.04
.08
.1
.2
.4
.8
1.
2.
4.
8.
10.
ACTUAL FLUID-PARTICLE STANTON NUMBER, CORRECTED FOR AXIAL DISPERSION.

An alternative and more general treatment may also be made in terms of the steady state version of the continuous models considered in II.B.1 (obtained by setting $\partial T/\partial t = 0$ in equation 2.2). As in Chapter II, the solution may be made using either the Danckwerts' or the simplified boundary conditions (see II.B.2.iii). As before, the more complex conditions do not appear justified for work of the present accuracy. The F factor obtained using the continuous model with simplified boundary conditions is (Appendix 7)

$$F = \left[\sqrt{\left[\frac{1}{-} + \frac{24\ St\ (1-\varepsilon)}{Pe} \right]} - 1 \right] \cdot \frac{Pe}{12\ St(1-\varepsilon)} \qquad \ldots(2.4)$$

Equation (2.4) is again independent of N.

In figure 2.1, the F-factors predicted by both models have been plotted against 'true' Stanton number for a fixed porosity ε of 0.37 at Peclet numbers of 2.0 (as predicted by the finite stage model for γ=1) and at Pe = 1.0, 0.5 and 0.25. The solution for porosities other than 0.37 are readily obtained since F factors are actually a function of $St(1-\varepsilon)$ and not of St alone.

Since, by definition St = Nu/(Re.Pr), the Stanton number should become very large at low Reynolds numbers if, as for single spheres, a number of 2.0 is approached. Corrections may, therefore, become quite large.

Referring to the Peclet number-Reynolds number curve of Edwards and Richardson (figure I.A.2.1) it will be noted that, at very low Reynolds numbers, the drop off in Peclet number from the theoretical value of 2.0 will further increase axial dispersion corrections. In the present work, Reynolds numbers will be kept above about 100.

B. STEADY STATE FLUID-WALL HEAT TRANSFER

When heat is transferred from a wall at uniform temperature to a fluid flowing through a packed bed, calculation of fluid-wall coefficients may be complicated by the presence of significant radial gradients within the bed. Fortunately over the range of parameters of interest in the present work, the analysis of Appendix 7 shows radial gradients to be small so that the simplified treatment used below is appropriate.

In order to obtain some approximation to the axial dispersion errors involved, such radial gradients will be thus made zero in the bed. A similar treatment is applied in Appendix 4 to estimation of dynamic wall heat loss errors in the experimental programme.

The axial dispersion model equation is then very similar to that used for fluid-particle transfer:-

$$\frac{d^2\delta T}{dz^2} = N\,Pe.\,\frac{d\delta T}{dz} - \phi_{w'}\,N\,Pe.\delta T = 0 \qquad \ldots(1)$$

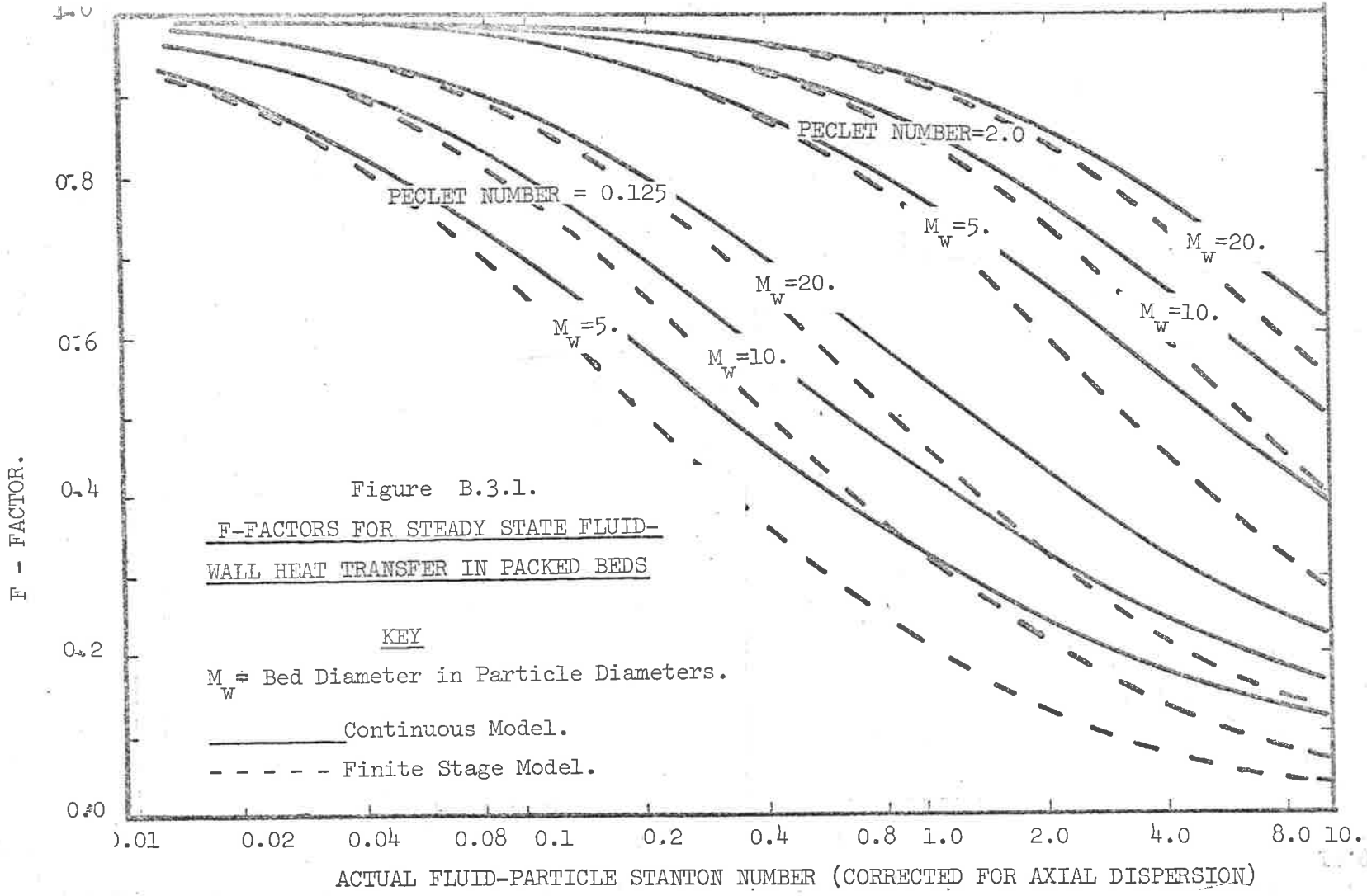

Figure B.3.1.

F-FACTORS FOR STEADY STATE FLUID-WALL HEAT TRANSFER IN PACKED BEDS

KEY

M_w = Bed Diameter in Particle Diameters.

_____ Continuous Model.

- - - - - Finite Stage Model.

In equation (1), δT represents the temperature difference between the wall and radially-averaged fluid or particle temperature,

$$\phi_w = 4 \frac{N}{M_w} St_w (1-\varepsilon) \quad \ldots \quad (2)$$

and M_w is the bed diameter (assumed circular) in particle diameters.

Applying the same simplified boundary conditions as before, we obtain:

$$F = \left[\left(1 + \frac{16\ St_w}{M_w\ Pe} \right)^{\frac{1}{2}} - 1 \right] \cdot \frac{M_w.Pe}{8\ St_w} \quad \ldots \quad (3)$$

A similar derivation for the generalised finite stage model yields equation (4).

$$F = \ln \left[1 + \frac{8\ St_w}{M_w.Pe} \right] \cdot \frac{M_w.Pe}{8\ St_w} \quad \ldots \quad (4)$$

The F-factors are thus also dependent on M_w. A few of these have been plotted on Figure B.1.

They show that axial dispersion corrections of a similar magnitude to those derived in section A arise.

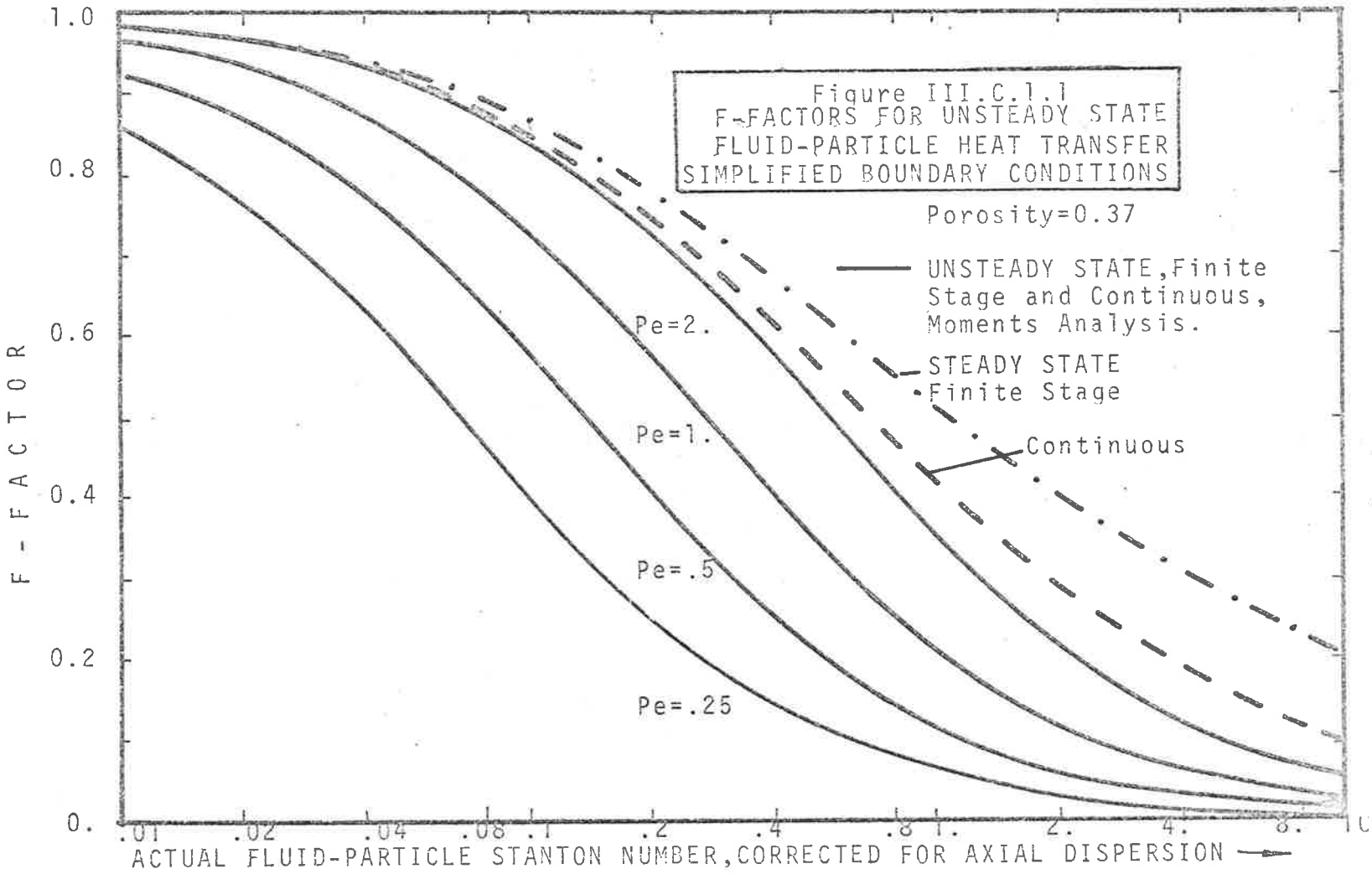
Figure III.C.1.1
F-FACTORS FOR UNSTEADY STATE
FLUID-PARTICLE HEAT TRANSFER
SIMPLIFIED BOUNDARY CONDITIONS
Porosity=0.37
UNSTEADY STATE, Finite Stage and Continuous, Moments Analysis.
STEADY STATE
Finite Stage
Continuous
Pe=2.
Pe=1.
Pe=.5
Pe=.25
F - F A C T O R
1.0
0.8
0.6
0.4
0.2
0.
.01
.02
.04
.08
.1
.2
.4
.8
1.
2.
4.
8.
ACTUAL FLUID-PARTICLE STANTON NUMBER, CORRECTED FOR AXIAL DISPERSION

C. UNSTEADY STATE PULSE STEP AND FREQUENCY RESPONSE

1. Step and Pulse Determinations

When a step or pulse change in inlet temperature is applied to a fluid flowing steadily through a packed bed, the resultant dispersion of the heat front may be used to estimate fluid-particle transfer coefficients. Calculation of the dispersion may be of importance in the design of thermal regenerators and adsorbers.

The application of pulse and step methods to packed bed dynamic testing will be discussed in detail in Chapter V. For the present purposes it will be enough to note that an estimate of the variance σ^2 may be obtained by these methods and used to determine the Stanton number. Assuming known particle conductivity, Peclet number, bed length, porosity and heat capacity ratio we have according to the continuous, finite stage or equivalent conductivity models, when Bi=0,

$$St = \frac{(\mu-1)^2}{3N(1-\varepsilon)\ [\sigma^2-2\mu^2/(NPe)]} \qquad \ldots (1.1)$$

When axial dispersion is assumed negligible as in the Schumann or Rosen models, an apparent or calculated Stanton number, St_{calc} results:

$$St_{calc} = \frac{(\mu-1)^2}{3N\sigma^2(1-\varepsilon)} \qquad \ldots (1.2)$$

Eliminating σ^2 between equations (1.1) and (1.2) and assuming μ to be large (i.e. $\mu - 1 \simeq \mu$) an F factor defined by A.2.2 results:

$$F = \frac{1}{1 + 6St(1-\varepsilon)/Pe} \quad \ldots \quad (1.3)$$

This relation has been plotted on Figure 1.1. Similar errors to those obtained before are predicted.

2. Cyclic Method Determinations

As pointed out in II.B.4, when fluid phase axial dispersion is ignored, a limiting large frequency value of the modulus or 'magnitude ratio' $|G(j\omega)|$ results, given by:

$$\lim_{\omega\to\infty} |G(j\omega)| = \exp [- KV_H]$$

$$= \{\exp [- 6St_{calc}.(1-\varepsilon)]\}^N \quad \ldots \quad (2.1)$$

(See II.A.2 for definition of magnitude ratio).

Although the introduction of axial dispersion ensures the more physically meaningful result:

$$\lim_{\omega\to\infty} |G(j\omega)| = 0,$$

it may be shown by computation that for V_H large, the axial dispersion and finite stage models tend to approximate to apparent limiting values given by equations (2.2) and (2.3) before tending

to zero at higher frequencies.

For the axial dispersion model, set $G_p(j\omega) = 0$ in equation II.B.3.8 and write $\omega \simeq 0$. Then, for ω large,

$$|G(j\omega)| \simeq \{\exp\left[\frac{Pe}{2} - \frac{1}{2}\sqrt{(Pe^2+24Pe.St(1-\varepsilon))}\right]\}^N \quad \ldots \quad (2.2)$$

For the finite stage model, set $G_p(j\omega) = 0$ in equation II.C.2.4 and write $\omega \simeq 0$. Then writing M=N (i.e. Pe = 2):

$$\underset{\text{large}}{\omega}, \quad |G(j\omega)| \simeq \left[\frac{NPe/_2}{KV_H + NPe/_2}\right]^M$$

$$= \left[\frac{1}{1 + 12St(1-\varepsilon)/Pe}\right]^M \quad \ldots \quad (2.3)$$

Comparison of equation (2.1) with equations (2.2) and (2.3) reveals that correction factors F are again independent of bed length, N. In fact identical F factors to those derived for the corresponding steady state situations result (equs. A.2.4 and A.2.3).

D. PREDICTED AXIAL DISPERSION EFFECTS IN PACKED BEDS

Heat Transfer Measurements

A study of the graphs presented so far indicates that errors in fluid-particle heat transfer coefficient measurements by steady or unsteady state methods will exceed 10% of the 'true' value only when the apparent Stanton number exceeds about 0.10, assuming a Peclet number of 2.0. This corresponds to a Reynolds number of

about 600 according to the Denton [1953] correlation. At this flow, β, the ratio of fluid-solid-fluid conductivity to total axial conductivity is estimated in Section I.A.5 as about 6-7%.

As the Reynolds number is reduced, combined axial fluids and fluid-solid-fluid conduction may be expected, according to the present theory, to introduce greater errors in methods which do not allow for these effects. The lowest experimental Reynolds number in this study has been about 100 at which point Brodkey's correlation referred to in I.A.5 predicts a Stanton number of about 0.27. Edwards and Richardson's Peclet number correlation suggests that a fluid-phase axial dispersion Peclet number of 2.0 may be expected whilst, according to Figure I.A.5.1, beta should be about 0.13. Hence, ignoring axial fluid-solid-fluid conduction, the F factor for step, pulse and cyclic method determinations will be 0.663 according to equ. D.1.3, when porosity is 37%. A calculation which ignores axial dispersion will under-estimate the Stanton number by 34%.

The precise way in which fluid-solid-fluid conduction may be expected to affect the measurement would be difficult to predict, however if β is 13%, then the 'equivalent' Peclet number could be regarded as $2/(1 + 0.13/_{0.87}) = 1.74$, so that F becomes 0.630 yielding an error of 37%. When measurements are carried out in the very low flow region (for example, $Re_p = 10$, $St \simeq 0.68$, $Pe \simeq 2$, $\beta \simeq 0.33$, equiv. Pe of 1.3, F = 0.336) even higher errors

may be expected. Furthermore, since the precise nature of axial conduction mechanisms is not known the 'true' value of Stanton number may be expected to be very difficult to determine especially by dynamic measurements.

It should be noted that the present experimental study cannot be expected to resolve the question of whether axial conduction effects even exist notwithstanding the elaborate theory developed above. No reliable measurements of fluid-particle heat transfer coefficient are available in the low Reynolds number region which are independent of axial conduction and dispersion effects. The fact that a number of investigators have reported fluid particle Nusselt numbers less than the isolated sphere limit of 2.0 [for example Williamson, Bazaire and Geankoplis, 1963] is some indication of the physical reality of these effects. The magnitude of the corrections is also a good indication of the likely practical implications for design of adsorbers, regenerative heat exchangers and similar equipment in the low flow, low pressure drop region.

E. INTRAPARTICLE CONDUCTION EFFECTS

1. Previous Work

Saunders and Ford [1940] have proposed that if the value of a dimensionless group:

$$v_a \, d_p \, \rho_f \, c_f \, / \, k_s$$

is less than 4.0, then particle conduction may be regarded as causing negligible error on fluid particle heat transfer coefficient measurements using the 'single blow' or step response technique, where the Schumann model (II.B.4.ii) is assumed correct.

The inequality

$$v_a \, d_p \, \rho_f \, c_f / k_s < 4.0 \qquad \ldots \quad (1.1)$$

may be replaced by

$$\frac{Bi}{St} < 2 \qquad \ldots \quad (1.2)$$

Chukhanov and Shapatina [1945] (quoted by Heggs [1967]) suggested that the Biot number should be less than 0.38 to 0.50 for negligible intraparticle conduction error.

More recently, Heggs [1969] has proposed that the parameter $\frac{k_s(1-\varepsilon)L}{G \, c_f \, d^2}$ be used as a criterion for deciding whether intraparticle conduction effects will cause an experimental step response to deviate from the response predicted by Schumann's solution. In the case of a packed bed of spheres d is the particle diameter so that the parameter becomes, in the present notation,

$$\frac{NSt(1-\varepsilon)}{Bi} = \frac{a_p \, L \, St(1-\varepsilon)}{6Bi} = \frac{KV_H}{6Bi} \qquad \ldots \quad (1.1)$$

where a_p is the surface to volume ratio of the packing. It is

suggested that the parameter should be greater than 60 for a spherical packing.

A similar parameter is proposed for a fixed 'bed' of parallel plates where d is now the plate thickness and here $a_p = 1/d$.

The criterion proposed for parallel plates becomes, in the present notation,

$$\frac{a_p L\, St(1-\varepsilon)}{Bi} = \frac{KV_H}{Bi} > 80 \qquad \ldots(1.2)$$

It will be noted that KV_H/Bi is in fact the parameter, γx, used by Babcock as a criterion for applicability of the single parameter equivalent conductivity model (see section II.D.3) and in section II.E.2 in relation to the Schumann model.

Heggs' criterion was obtained by solving the Rosen equations (section II.B.4) numerically, comparing the predicted responses with the Schumann solution for varying combinations of KV_H (Y in Heggs' notation) and Bi (or $1/K_r$ sphere, $1/K_t$, plate). [The Rosen analytical solution (Chapter IV) could have been used equally well although another form for $G_p(s)$, the particle transfer function would be required in the case of parallel plates Effectively, the closed form infinite slab solution would suffice].

2. Intraparticle Criterion from Present Models

The moments analysis equations derived in Chapter II for the extended axial dispersion or continuous finite stage model, and

equivalent conductivity models suggest that the variance or spread of the breakthrough curve about its centre of mass and its skewness are altered by multiplying factors which are a function only of the Biot number. This conclusion differs from both that of Heggs and of Saunders and Ford. Assume for the moment that the time taken for a step response to go from 20% to 80% of completion is directly proportional on a normalised time scale to the standard deviation calculated from equations II.B.3.9. This assumption will be investigated theoretically in Chapter IV. Then, when Reynolds numbers are sufficiently high to allow axial dispersion effects to be ignored,

$$\sigma^2 = \frac{(\mu-1)^2}{3N\ St(1-\varepsilon)} \cdot \frac{Bi+5}{5} \qquad \ldots(2.1)$$

It may be seen that according to this assumption, the time ΔT taken between 20% and 80% of response is proportional to $\sqrt{(1 + 0.2\ Bi)}$. Alternatively, Handley and Heggs' approach could be adopted, by defining a 'pseudo' Stanton number, St_{calc} defined by

$$St_{calc} = \frac{St}{1 + 0.2\ Bi} \qquad \ldots(2.2)$$

such that the Schumann solution correctly predicts ΔT when St_{calc} is used instead of St.

Then for agreement within 5% between ΔT computed by Schumann's solution and ΔT obtained from any of the other three models we

require

$$1 + Bi/5 \leq (1.05)$$

$$\text{i.e.} \quad Bi \leq 0.50$$

It may be seen that Chukhanov and Shapatina's criterion would, according to this theory be essentially correct provided γx is also greater than about 10.

3. Illustrative Example of Intraparticle Criteria

In order to make this point more clear, consider a packed bed of Perspex spheres through which air ($Pr = 0.73$) is flowing with a superficial particle Reynolds number of 1000, yielding, according to the Denton correlation, a Stanton number of about 0.09. The ratio, k_s/k_f of thermal conductivity of Perspex to that of air is about 8.08 so that the Biot number would be independent of bed length and given by

$$Bi = St.Re_p.Pr.\left[\frac{k_f}{2k_s}\right] = 4.1$$

Hence, the standard deviation of the impulse response about the centre of mass μ or, presumably, the spread of a breakthrough curve will be greater than that of a highly conductive material in the ratio $\sqrt{(1 + 4.1/5)} = 1.35$, i.e., the low thermal conductivity of Perspex is predicted to add 35% to the dispersion of a breakthrough curve, independently of bed length.

On the other hand, the parameter γx is dependent on length

and, for a porosity ε of 40% is given by

$$\gamma x = \frac{KV_H}{Bi} = \frac{KV_H}{4.1} = \frac{12.N.(1-\varepsilon)}{Re_p Pr} \cdot \left[\frac{k_s}{k_f}\right]$$

$$= 7.86 \times 10^{-2} \times N$$

where N is the bed length in particle diameters. In order to keep γx above 60 to 80 we require N to be about 760 to 1020, in which case Heggs would predict intraparticle effects to be absent. On the other hand, the computations of Chapter II suggest that intraparticle effects will definitely be present since curve spread will still be 35% greater, irrespective of γx.

Continuing with the above example, suppose we now keep γx greater than 10, or bed length greater than 127 diameters, then the computations of Chapter II suggest that curve shape (not curve spread) will become indistinguishable, for V_H large, from the Schumann solution. In order to obtain correspondence between the Schumann solution and the actual breakthrough curve, it will be necessary to use a pseudo value of KV_H:

$$KV_{H_{psd}} = \frac{KV_H}{1 + Bi/5} = \frac{KV_H}{1.82}$$

in other words, we will need to reduce KV_H by about 45% in order to obtain apparent agreement between the infinite conductivity solution and experiment.

4. Summary of Conclusions Regarding Intraparticle Conduction Effects.

The objective of this section and of section II.E.2 has been to clarify intraparticle effects by separating curve spread effects as measured by the standard deviation, σ^* from curve shape effects as measured by the 'bed length' parameter, γx. It appears that Handley and Heggs' criterion that the bed length parameter should be greater than 80 for intraparticle effects to be absent is incorrect, or rather it's success in the examples quoted by Handley and Heggs is fortuitous. For the values of KV_H chosen by Handley and Heggs, $\gamma x > 80$ also happens to ensure that the Biot number is small enough to limit the additional curve spread due to intraparticle effects. In summary, we find :

(a) The criterion $\gamma x = KV_H/Bi > 10$ is an appropriate one to use if we to ensure that the form (i.e. shape) of a frequency response or step response will be approximated, for V_H large, by the Schumann solution or for V_H small, by the equivalent conductivity solution.

(b) Irrespective of the value of γx, the value of the Biot number decides whether additional spreading or dispersion of an impulse response or breakthrough curve about its centre of mass need be accounted for. Thus, if $\gamma x > 10$, a pseudo Stanton number:

$$St_{psd} = St/(1 + Bi/5)$$

substituted into the Schumann solution may be expected to yield a good approximation when axial dispersion is absent.

It is also apparent that if we wish to design an experiment which separates intraparticle from fluid-particle and axial dispersion effects, we should keep γx small, i.e. bed length short at any particular value of the Biot number.

F. SUMMARY OF CONCLUSIONS

Axial dispersion and fluid-solid-fluid conduction were shown, at least theoretically, to influence the values of heat transfer coefficient obtained from a variety of steady state and unsteady state measurements especially at low superficial particle Reynolds numbers. It is probable that much of the literature data reported, especially at low Reynolds numbers, is 'contaminated' by the effects of axial dispersion.

In view of the conclusion reached in Chapter II about the difficulty in separating heat transfer and axial dispersion effects, this may not be of great practical importance, provided attempts are not made to correct again for axial dispersion when the empirical heat transfer correlation already incorporates its own axial dispersion 'correction'.

It was concluded that, for simplified boundary conditions appropriate to limited knowledge available about physical entrance conditions, axial dispersion effects should be independent

of bed length for both steady state and unsteady state measurements.

It was also concluded that the Biot number should be the main criterion for deciding whether intraparticle conduction is likely to influence heat transfer coefficient measurements by transient methods. This conclusion differs from that of Handley and Heggs.

CHAPTER IV

THEORETICAL PREDICTIONS OF BREAKTHROUGH CURVES IN LINEAR ADSORBERS

SCOPE OF THE CHAPTER

In this chapter, the problem of breakthrough curve prediction in linear adsorbers and packed bed thermal regenerators is considered. Existing solutions are reviewed and compared with the predictions of the finite stage model using an approximation method new to the engineering literature. An attempt is also made to simplify the problem of breakthrough curve prediction by the use of empirical correlations.

In Section A, the numerical Laplace transform inversion method of J.B. Rosen is simplified and generalised, through the Fourier transform, so as to be applicable to the extended models of chapter II.

Section B reviews using the present notation, the analytical breakthrough curve solutions of Schumann and of Babcock and co-workers.

In Section C, a new orthogonal polynomial approximation technique for breakthrough curve prediction is presented. The method has a number of advantages with regard to control over errors.

In Section D, the predictions of the various model solutions are compared using the 'standard deviation' of the impulse response as a parameter.

The solutions are used to develop empirical correlations of various points on a breakthrough curve against the parameter σ^{*2} proposed in Chapter II. This approach represents an extension to and a simplification of the Handley and Heggs 20% to 80% method of heat transfer coefficient determination.

Section E summarises the conclusions of the chapter.

A. EVALUATION OF BREAKTHROUGH CURVES BY NUMERICAL TRANSFORM INVERSION

1. Introduction

Breakthrough curves may be computed by numerical solution of the fundamental differential equations of the process [Heggs, 1967, Handley and Heggs, 1968; Heggs, 1969]. This may be the only practical method available when isotherms are nonlinear or where simultaneous heat and mass transfer processes are involved. These purely numerical techniques are prone to instabilities and estimation of the limits of error is a difficult procedure, although the workers referred to above have some success in overcoming these problems. As pointed out in Chapter II (II.C.4) the Deans and Lapidus finite stage model offers many advantages over conventional numerical schemes since it allows for the effects of axial dispersion and also is absolutely stable, numerically.

A more fundamental objection, from the point of view of design, is that reconstruction of the breakthrough curves for later use in hand calculations requires extensive tabulation over the range of all parameter combinations together with interpolation. A simple estimate of maximum likely error is also desirable.

Numerical methods of Laplace or Fourier transform inversion have similar disadvantages which will be discussed in this section.

2. Laplace Transform Inversion Technique of J.B. Rosen

Having obtained the transfer function of a packed bed, Laplace transform inversion is a possible next step in obtaining either the impulse response g(t) or its time integral, the step response u(t) which defines the 'breakthrough curve' of an adsorber or regenerator:

$$u(t) = \int_0^t g(t)\,dt = \mathcal{L}^{-1}\left[\frac{G(s)}{s}\right] \qquad \ldots \quad (2.1)$$

Carslaw and Jaeger [1953] have provided numerous examples of the use of the residue theorem in obtaining the inverse Laplace transform of the distributed parameter systems encountered in thermal conduction problems. The result is usually expressed in an infinite series form, the convergence of which may be slow. In the case of the transfer functions here, Rosen [1952] has pointed out that the residue theorem becomes impractical since the transfer functions have an infinite number of essential singularities on the negative real axis. The technique chosen was that of evaluation of the inversion integral along the path indicated

below, avoiding, for the step response, the pole due to 1/s at the origin.

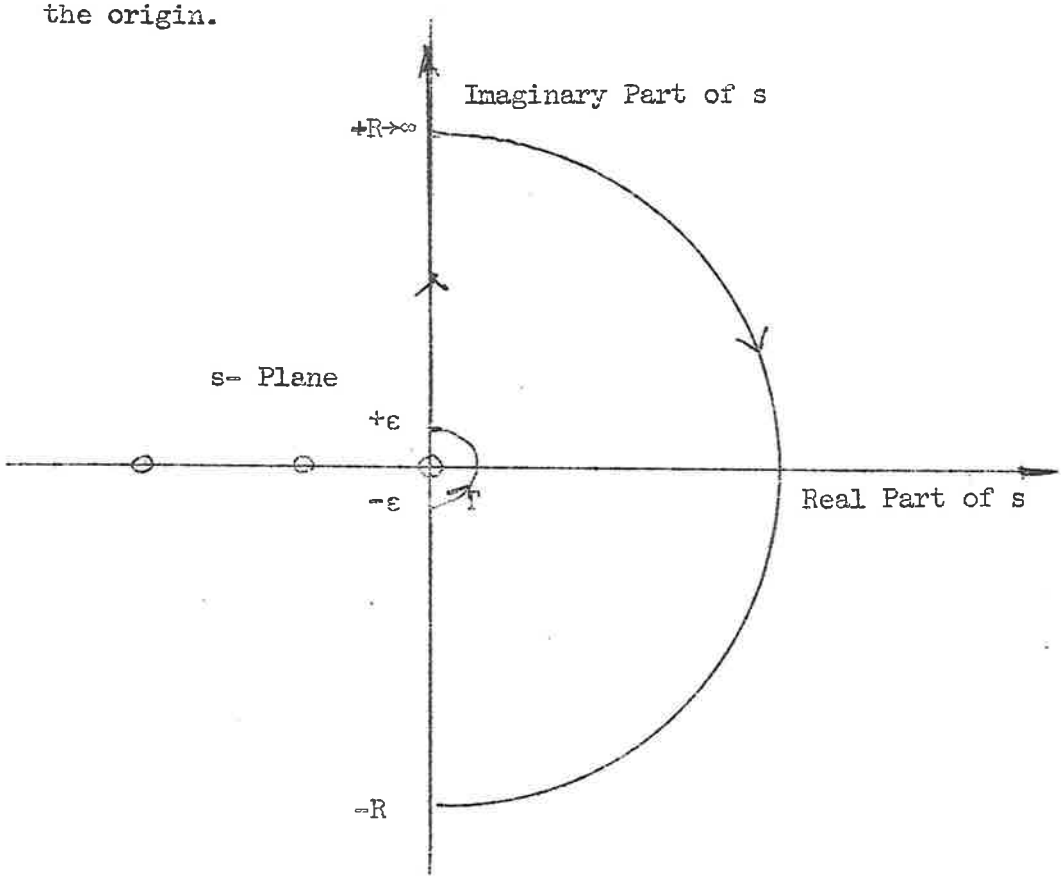

PATH TAKEN BY CONTOUR INTEGRATION IN LAPLACE TRANSFORM INVERSION OF ROSEN.

Figure A.2.1.

Following the contour indicated, which avoids the essential singularities on the negative real axis and the simple pole at the origin, the Laplace transform inversion integral becomes

$$\frac{1}{2\pi j}\oint \frac{G(s)}{s}.e^{st}.ds = \frac{1}{2\pi j}\left[\int_{-\infty}^{-\varepsilon} + \int_{\Gamma} + \int_{\varepsilon}^{\infty} + \int_{R}\right]\frac{G(s)}{s}.e^{st}.ds \quad \ldots \quad (2.2)$$

The integral on R vanishes for the stable linear systems considered here, whilst in the limit, as $\varepsilon \to 0$, the path Γ contributes exactly $1/2$ to integral. This is because

$$\lim_{s\to 0} \quad G(s) \quad = \quad 1$$

and

$$\lim_{\varepsilon\to 0} \quad \frac{1}{2\pi j} \quad \int_{\Gamma} \frac{e^{st}}{s}.ds \quad = \quad \frac{1}{2}$$

The integral of equation (2.2) reduces to

$$\mathcal{L}^{-1}\left[\frac{G(s)}{s}\right] = \frac{1}{2} + \frac{1}{2\pi j} \int_{-j\infty}^{j\infty} \frac{G(s)}{s} \cdot e^{st}.ds$$

$$= \frac{1}{2} + \frac{1}{2\pi} \int_{-\infty}^{\infty} \frac{G(j\omega)}{j\omega} \cdot e^{j\omega t} d\omega \qquad \ldots \quad (2.3)$$

If $R(\omega)$ and $I(\omega)$ are the real and imaginary parts, respectively of $G(j\omega)$, equation (2.3) may also be written:

$$u(t) = \frac{1}{2} + \frac{1}{\pi} \int_{0}^{\infty} \left[\frac{R(\omega)}{\omega}.\sin\omega t + \frac{I(\omega)}{\omega}.\cos\omega t\right] d\omega \qquad \ldots \quad (2.4)$$

This is because

$$\int_{-\infty}^{\infty} \frac{R(\omega)}{\omega} \cos\omega t \, d\omega \quad = \int_{-\infty}^{\infty} \frac{I(\omega)}{\omega}.\sin\omega t. \, d\omega = 0$$

since $R(\omega)$ and $I(\omega)$ are even and odd respectively (see Appendix 5).

The integrals of equation (2.4) are evaluated numerically in Rosen's treatment. Difficulties which arise in evaluating these integrals are discussed in section 4.

3. Alternative Numerical Fourier Transform Inversion Approach

An alternative method of obtaining the step response has been developed through the Fourier transform. It yields a more simple version of equation (2.4).

Direct evaluation of the step response,

$$u(t) = \int_0^t g(\tau)\, d\tau$$

by analytical or numerical Fourier transform inversion of $G(j\omega)/j\omega$ using the Fourier inversion integral:

$$\mathcal{F}^{-1}[G(j\omega)] = \frac{1}{2\pi}\int_{-\infty}^{\infty} G(j\omega).e^{j\omega t}.d\omega \qquad \ldots(3.1)$$

is not possible since the Fourier transform of u(t) does not, strictly speaking, exist. This is because $\int_{-\infty}^{\infty} u(t)\, dt$ is not finite.

Whilst u(t) is not Fourier transformable, U(t)[1-u(t)] is, where U(t) is the unit step function:

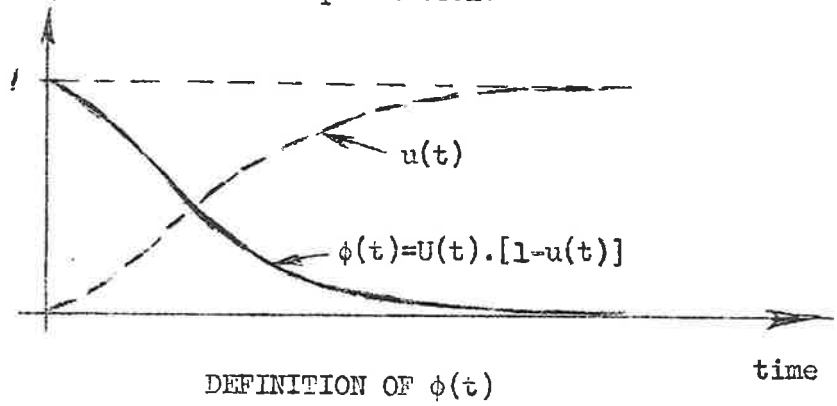

DEFINITION OF $\phi(t)$

FIGURE 3.1

Defining $\phi(t)$ as

$$\phi(t) = U(t)\,[1 - u(t)] \qquad \ldots(3.2)$$

the Fourier transform of $\phi(t)$ may be obtained, noting that

$$u(t) = \int_0^t g(\tau).\, d\tau$$

and

$$U(t) = \int_0^t \delta(\tau).\, d\tau \qquad \ldots(3.3)$$

where $g(t)$ is the impulse response defined in section II.A.2., and $\delta(t)$ is a delta or unit impulse function defined by

$$\delta(t) = 0, \quad t \lesseqgtr 0$$

$$\int_{-\infty}^{\infty} \delta(t)\, dt = 1. \qquad \ldots(3.4)$$

The Fourier transform of $\delta(t)$ is unity [Bracewell, 1965] and the Laplace transform integration theorem may be extended to the Fourier transform provided, as in this case, the definite integral is Fourier transformable.

Thus, if

$$\mathcal{F}[f(t)] = F(j\omega)$$

then $\mathcal{F}\int_{-\infty}^{t} f(\tau)\, d\tau = F(j\omega)/j\omega$

provided $\int_{-\infty}^{t} f(\tau)\, d\tau$ has a Fourier transform

Applying this to equations (3.3) and (3.2):

$$\mathcal{F}[\phi(t)] = \left[\int_0^t [\delta(\tau) - g(\tau)]\, d\tau\right]$$

$$= [1 - R(\omega) - j\, I(\omega)]\,/j\omega \qquad \ldots(3.5)$$

where $\mathcal{F}g(t) = G(j\omega) = R(\omega) + j\, I(\omega).$

In carrying out the reverse operation, i.e. inversion of the R.H.S. of equn. (3.5) we note that the real part of the transform to be inverted is:

$$R_\phi(\omega) = -\frac{I(\omega)}{\omega} \qquad \ldots(3.6)$$

whilst the imaginary part is

$$I_\phi(\omega) = -\left[\frac{1 - R(\omega)}{\omega}\right]$$

As shown in Appendix 5, the Fourier transform of the even part of $\phi(t)$ yields the real part of $\phi(t)$ where

$$E[\phi(t)] = \begin{cases} \tfrac{1}{2}\phi(t), & t \geq o \\ \tfrac{1}{2}\phi(-t), & t < o \end{cases} \qquad \ldots(3.7)$$

Hence

$$\underset{t \geq o}{\phi(t)} = \frac{j}{\pi}\int_{-\infty}^{\infty}\left[\frac{1 - R(\omega)}{\omega}\right]\left[\cos\omega t + j\sin\omega t\right]d\omega \qquad \ldots(3.8)$$

Since, as noted in section A.2., $R(\omega)$ is even, $[1 - R(\omega)]/\omega$ is odd, and hence the imaginary part (3.8) vanishes leaving

$$\underset{t \geq o}{\phi(t)} = +\frac{2}{\pi}\int_0^{\infty}\frac{1 - R(\omega)}{\omega}\cdot\sin\omega t\,.\,d\omega \qquad \ldots(3.9)$$

or, since $\int_{-\infty}^{\infty}\frac{\sin\pi x}{\pi x}\,.\,dx = 1$ [Bracewell, p.62].

$$\underset{t \geq o}{\phi(t)} = 1 - \frac{2}{\pi}\int_0^{\infty}\frac{R(\omega)}{\omega}\,.\,\sin\omega t\,.\,d\omega$$

Hence,

$$u(t) = \frac{2}{\pi}\int_0^{\infty}\frac{R(\omega)}{\omega}\cdot\sin\omega t\,.\,d\omega \qquad \ldots(3.10)$$

In a similar way we obtain

$$u(t) = 1 + \frac{2}{\pi}\int_0^{\infty}\frac{I(\omega)}{\omega}\cdot\cos\omega t\,.\,d\omega \qquad \ldots(3.11)$$

Equations (3.10) and (3.11) may be added and averaged to obtain Rosen's solution, equ. (2.4).

Equations (3.10) and (3.11) are simpler than equation (2.4). Since the treatment has been general for the stable, linear, real systems under consideration here, these equations may be applied, not only to Rosen's particular transfer function but to the extended models presented in Chapter II which incorporate axial dispersion.

4. Numerical Difficulties Experienced

In Rosen's version [1952] of equ. (2.4), the two trigonometric functions were condensed into one sine function by use of explicit equations for $R(\omega)$ and $I(\omega)$. This is avoided, where complex arithmetic is available by the use of equations presented in II.B.3.iv.

Difficulties in evaluating equation (2.4) numerically arise as a result of the unreal physical situation discussed in section II.B.4.i. That is, the output is required to change suddenly, at t=1, or one holdup time, from zero to $\exp[-KV_H]$. From a frequency response point of view, this means that both $R(\omega)$ and $I(\omega)$ cycle continuously to infinity (infinite 'band width'). As $t \to 1$, equation (2.4) becomes:

$$\lim_{t\to 1} u(t) = e^{-KV_H} = \frac{1}{2} + \frac{1}{\pi}\int_0^\infty \left[\frac{R(\omega)}{\omega}.\sin\omega + \frac{I(\omega).}{\omega}\cos\omega\right]d\omega \qquad \ldots(4.1)$$

Despite the presence of ω in the denominator, convergence of the integral of equation 4.1 may be slow.

Fortunately, when KV_H is large, $\exp[-KV_H]$ is small and then convergence is not so important.

Another difficulty arises for large time values since the integral of equation (2.4) becomes more and more oscillatory. The physical requirement that

$$\lim_{t\to\infty} \frac{1}{\pi}\int_0^\infty \left[\frac{R(\omega).}{\omega}\sin\omega t + \frac{I(\omega).}{\omega}\cos\omega t\right]d\omega = {}^1/_2 \qquad \ldots(4.2)$$

i.e. $\lim_{t\to\infty} u(t) = 1$ by definition of unit step response provides a check on convergence for t large. A good summary of the difficulties arising has been provided by Rosen [1954]:

> "Considerable care must be exercised in the choice of both the upper limit and the sum in order to keep the amount of computation to a minimum. In particular, the type of finite difference sum approximation to the integral and the length of the finite steps must be carefully chosen. If this is not done, the time required to compute the desired number of values (of u(t)) will be prohibitive, even with high-speed computation."

and

> "As an indication of the amount of computation required, a single value (of u(t)) requires that, on the average, 50,000 multiplications be performed."

It may be noted, that the "impossible" physical requirement mentioned above also causes difficulties in evaluation of breakthrough curves by direct numerical solution of the fundamental Schumann partial differential equations. Heggs [1967] discusses such difficulties in detail.

When axial dispersion is included in the model similar problems arise for KV_H small although in this case they are not so acute since $R(\omega)$ and $I(\omega)$ tend to zero for ω large. Nonetheless, in applying equations (3.5) or (3.6) the functions to be integrated need to be examined beforehand so as to decide the best strategy for the integration.

B. ANALYTICAL METHODS OF BREAKTHROUGH CURVE PREDICTION

1. Analytical Solutions to Schumann's Model

The transfer function for Schumann's model (see II.B.4.ii) is, in the present notation:

$$G(z,s) = e^{-sz} \cdot e^{-\phi} \cdot \exp\left[\frac{K\phi}{s+K}\right] \qquad \ldots(1.1)$$

where ϕ denotes $KV_H L/va$ and time, t is normalised with respect to mean fluid holdup time $V_H L/va$. As noted in sections II.B.4(i) and II.B.4(ii), the term e^{-sz} represents a time delay of z holdup time units, $0<z\leq 1$, so that it is convenient to consider the alternative transfer function for $\delta = 1$

$$G(s) = e^{-\phi} \cdot \exp\left[\frac{K\phi}{s+K}\right]$$

having a centre of mass or first moment of V_H instead of $1 + V_H$ holdup time units and to normalise time t+ with respect to V_H such that:

$$G(s^+) = e^{-\phi} \exp\left[\frac{\phi^2}{s^+ + \phi}\right] \qquad \ldots(1.2)$$

where $s+ = V_H \cdot s$.

Laplace transform inversion of equation (1.2) yields on this time scale:

$$u(t^+) = e^{-\phi}\left[1 + \phi \int_0^{t^+} \frac{e^{-\phi\tau}}{\sqrt{\tau}} \cdot I_1(2\phi\sqrt{\tau}) \cdot d\tau\right] \qquad \ldots(1.3)$$

where $I_1(x)$ denotes a modified Bessel function of the first kind, orde 1, argument x.

Equation (1.3) differs slightly in form from that presented by Schumann (and earlier by Anzelius [1926]. Klinkenberg [1954] has published a comprehensive survey of the various forms in which the step response may be represented, together with a discussion of various computational techniques available for its evaluation. In the present work, an accurate Bessel function subroutine from theC.S.I.R.O. library was used. For small values of ϕ ($\leq$ 10) rapid oscillation of the integrand of equation (1.3) occurs when t becomes large. It is then necessary to reduce the step size in order to ensure convergence.

2. Equivalent Conductivity Model Solution

The equivalent conductivity solution step response (see section II.D) is, in the present notation:

$$u(t) = \frac{1}{2}\left\{\operatorname{erfc}\left[\frac{1-\theta}{2\sqrt{(\theta/Pe_a)}}\right] + e^{Pe_a}\cdot \operatorname{erfc}\left[\frac{1+\theta}{2\sqrt{(\theta/Pe_a)}}\right]\right\} \quad \ldots \quad (2.1)$$

where $\theta = t/(1+V_H)$, (Also defined elsewhere as t^*),

$\operatorname{erfc}(x)$ represents the complementary error function:

$$\operatorname{erfc}(x) = 1 - \operatorname{erf}(x) = 1 - \frac{2}{\sqrt{\pi}} \int_0^t e^{-\tau^2} d\tau$$

and other symbols are defined in II.D.

Equation (2.1) may be obtained by Laplace transform inversion of equ. (II.D.4.4) using the standard transform pairs listed by Abramowitz and Stegun [1964,c]. It has a considerable advantage over solutions presented so far in that numerical integration is not necessary for evaluation since the error functions have been extensively tabulated.

The fact that the solution may be regarded as a function of

$$F = \sqrt{\theta} - 1/\sqrt{\theta}$$

and thus yields a straight line on arithmetic probability paper was used by Babcock in evaluation of Pe_a from experimental data. This method of plotting has been used in section IV.D.1. to compare predictions with other solutions.

C. PROPOSED APPROXIMATION METHOD

1. Basis of the Method

In paper 2, Appendix 3, the writer has presented a method which may be used to obtain the impulse response of the more complete models of packed bed behaviour derived in Chapter II. According to this method, the real part $R(\omega)$ of the frequency response function $G(j\omega)$ is approximated by a weighted sum of orthogonal basis functions $\phi_n(\omega)$, i.e.

$$R(\omega) \approx \bar{R}(\omega) = \sum_{n=0}^{N} a_n \cdot \phi_n(\omega) \qquad \ldots \quad (1.1)$$

When a good approximation of $R(\omega)$ by $\bar{R}(\omega)$ has been achieved as measured by direct comparison and evaluation of the error integral,

$$\bar{\varepsilon}^2 = \int_0^{\omega_{max}} [R(\omega) - \bar{R}(\omega)]^2 d\omega \qquad \ldots \quad (1.2)$$

it is then reasonable to assume that the exact inverse of $\bar{g}(t)$ given by:

$$\mathcal{F}^{-1}[\bar{R}(\omega)] = {}^1/_2\, \bar{g}(t), \quad t \geq 0 \qquad \ldots \quad (1.3)$$

is a good approximation to the impulse response $g(t)$. This is guaranteed by Rayleigh's Theorem [Bracewell, 1965] i.e.,

$$\bar{\varepsilon}^2 = \int_0^{\infty} [R(\omega) - \bar{R}(\omega)]^2 \, d\omega = \frac{\pi}{2} \int_0^{\infty} [g(t) - \bar{g}(t)]^2 \, dt \qquad \ldots \quad (1.4)$$

The basis functions $\phi_n(\omega)$ chosen here were Gaussian function weighted Hermite polynomials. These have a relatively simple

inverse [Arsac, 1966; Sz-Nagy, 1965]:

$$\mathcal{F}^{-1} \sum_{n=0}^{N} a_{2n} . H_{2n}(\omega) . \exp[-\omega^2/4]$$

$$= \sum_{n=0}^{N} \frac{(-1)^n}{(2n)!\ 2\pi} . a_{2n} . \exp(-t^2) . H_{2n}(2t) \quad \ldots \quad (1.5)$$

Other orthogonal basis functions having known transform pairs such as exponentially weighted Laguerre polynomials could have been chosen. The Hermite functions were chosen here since it was felt that the Gaussian envelope would correspond to the type of solutions expected from the particular distributed parameter systems under consideration.

2. Objectives of and Extensions to the Method

In developing the method it was hoped that extensive tabulation of the coefficients a_{2n} in equation (1.5) as a function of the parameters KV_H, Pe, Bi of the extended theoretical models would be of value to design engineers in predicting breakthrough curves. The difficulties involved in numerical integration mentioned in A.4 would be avoided, an estimate of error would be available through equ. (1.4) and the information would be in a more concise form than direct tabulation of breakthrough curves. A rather complex analytical expression for evaluation of the approximated breakthrough curve $\bar{u}(t)$ from the impulse response $\bar{g}(t)$ [equation 25 of Paper 2, Appendix 3] made evaluation of u(t) unwieldy.

Development of equation IV.A.3.11 allowed a simplification to be made since this equation is equivalent to

$$u(t) = 1 + 2.\mathcal{F}^{-1}\left[\frac{I(\omega)}{\omega}\right] \quad \ldots \quad (2.1)$$

Hence, $I(\omega)/\omega$ is approximated instead of $R(\omega)$. As pointed out in A.3 this relation also simplifies and extends Rosen's numerical integration procedure through equations (3.10)or (3.11). An approximate inequality, derived again in Appendix 8, relates the integral error squared of equation (1.2) (where $R(\omega)$ is replaced by $I(\omega)/\omega$) to the maximum error $|\varepsilon(t)|_{max}$ in the time solution:

$$|\varepsilon(t)|_{max} \leq \frac{2\sqrt{2}}{\pi} \sqrt{(\overline{\varepsilon^2}.\omega_c)} \quad \ldots \quad (2.2)$$

where ω_c is the maximum 'bandwidth' of the approximated transform. Inequality 2.2 cannot be justified rigorously except when $I(\omega)/\omega=0$, $\omega \geq \omega_c$. It provides, nonetheless, a useful estimate of maximum error.

Tabulation of the coefficients a_{2n} of the approximation to $I(\omega)/\omega$ now allows direct reconstruction of the breakthrough curve. The method of hand reconstruction, discussed in section IV.C.6 is surprisingly simple with the aid of a desk calculator.

3. Details of the Method

The procedure finally adopted was as follows:-

(a) Evaluate $I(\omega)/\omega$ over the whole bandwidth of the system at the mesh spacing chosen.

(b) Choose a suitable scale factor Z, so that for the number of terms N, desired in the approximation, the maximum bandwidth of the weighted Hermite polynomials exceeds that of $I(\omega)/\omega$. An 'automatic' method, less dependent on judgement is presented in the Addendum to this Chapter.
The scale factor Z is then used to expand the frequency scale of $I(\omega)/\omega$ (every mesh frequency ω_i is simply multiplied by Z). Use will later be made of the <u>similarity theorem</u>, [Bracewell, 1965,b] which states that for Z real,

$$\text{if } \mathcal{F}^{-1}[G(j\omega)] = g(t)$$

$$\text{then } \mathcal{F}^{-1}[G(j\omega Z)] = g(t/Z)/Z \qquad \ldots \quad (3.1)$$

Thus when $I(\omega Z)/(\omega Z)$ has been approximated, u(t) may be obtained from the inverse, $\bar{u}(t/Z)$.

(c) Starting with $H_o(\omega)$ and using the recurrence relation for Hermite polynomials:

$$H_n(\omega) = \omega . H_{n-1}(\omega) - (n-1)\, H_{n-2}(\omega),$$

$$H_o(\omega) = 1, \qquad H_1(\omega) = \omega \qquad \ldots \quad (3.2)$$

evaluate coefficients a_{2n} successively

$$a_{2n} = \frac{\sqrt{2}}{(2n)!\sqrt{\pi}} \int_o^{\omega_c} \frac{I(Z\omega)}{Z\omega} . e^{-\omega^2/4} . H_{2n}(\omega) . d\omega \qquad \ldots \quad (3.3)$$

using Simpson's or other rule for numerical integration where ω_c is the maximum frequency chosen.

(d) After each coefficient is evaluated, another term is added to

$$\frac{\overline{I(\omega)}}{\omega} = \sum_{n=0}^{N} a_{2n} . H_{2n}(\omega) . \exp(-\omega^2/4) \qquad \ldots \quad (3.4)$$

and the error integral of equation (1.4) evaluated. For continuous orthogonal approximations the integral square agreement between a function and its approximation monotonically improves as terms are added to the approximation. In practice, since continuous integrals are replaced by numerical approximations, a point is usually reached when the addition of further terms causes an increase in error. This may be overcome by:

reducing mesh spacing and starting again,
increasing scale factor and starting again,
or stopping further approximation at that point.

(e) When a sufficient number of terms have been added, the approximation and the errors remaining should be printed or plotted out since a study of the form of the error is often useful in predicting, after some experience, the likely location of the point of maximum error in the inverse.

(f) Using equations (3.1), (1.5) and (2.1) the step response approximation may be then printed or plotted out. Since the same weighted Hermite polynomials appear on both

sides of equ. (1.5) although with a different argument, these need not be evaluated again. In fact terms may be added successively to both sides of equation (2.5) with suitable change of scale factor, as they are evaluated. This reduces storage problems considerably since all N Hermite polynomials need not be stored simultaneously.

4. Further Details and Present Limitations

A disadvantage of the method becomes apparent when the function to be approximated is made up of two distinct regions, as when KV_H is small ($\lesssim 6$). In this case, a dispersed impulse or step applied at the entrance 'breaks through' shortly after t = 0 (centre of mass, one holdup time, L/v_a). This is analogous to the impulse of area $\exp[-KV_H]$ or step of height $\exp[-KV_H]$ which is predicted by the Schumann or Rosen models. The remainder of the step or pulse appears with a centre of mass V_H holdup times later. When V_H is large, as in the present work, these two regions are separated on a plot of $R(\omega)$ against ω by an apparent discontinuity. This is illustrated by Figure 5 of paper 2. The 'initial breakthrough' is represented by a damped cosine wave (having an approximately Gaussian envelope). The bulk of the response on a ωV_H time scale appears as a spike which is not approximated well.

Fortunately, over the range of parameters of interest in this work or in most practical cases (Table IV.B.4.1) this problem does not arise. A promising approach which will be pursued in later

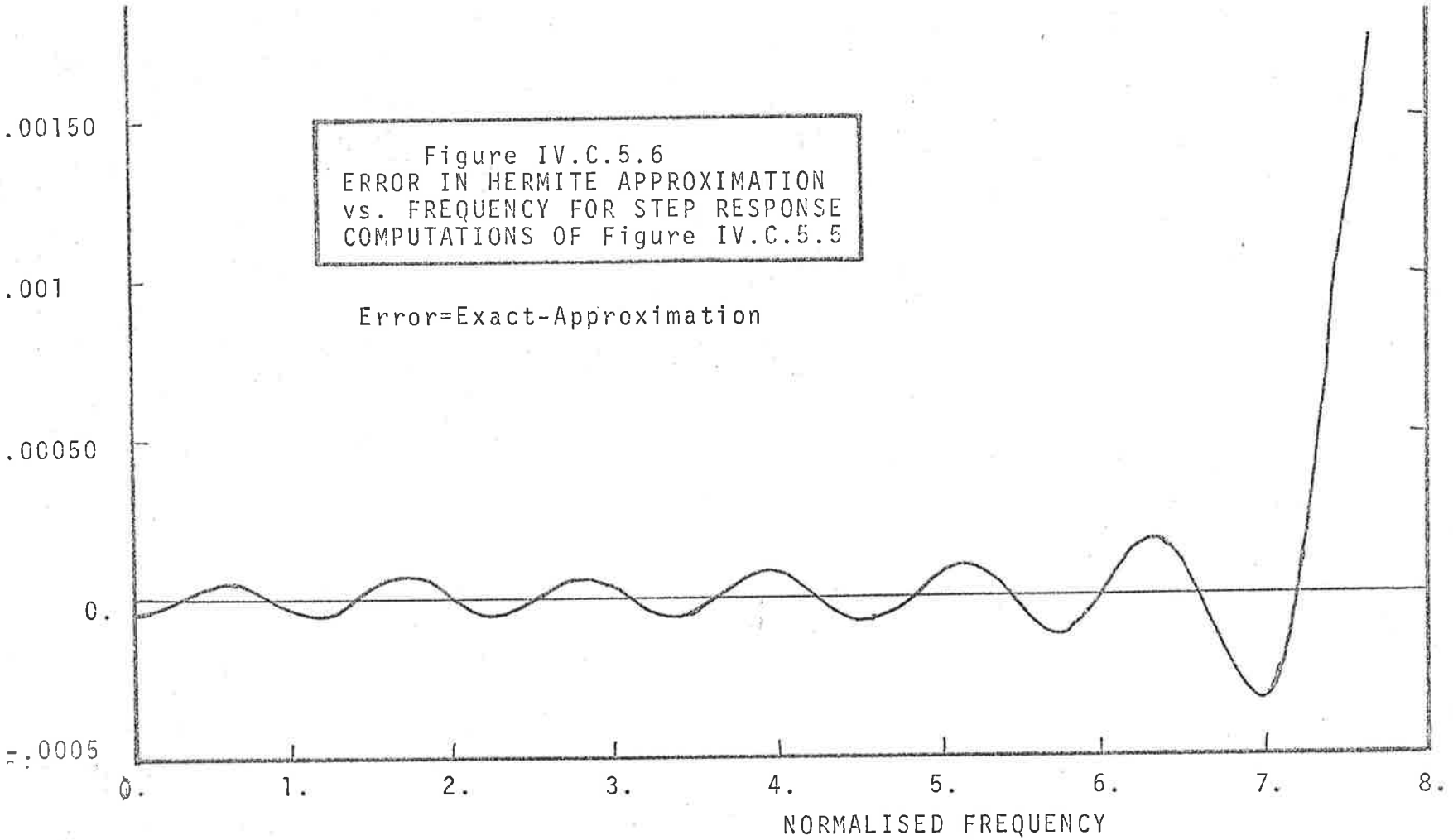

Figure IV.C.5.6
ERROR IN HERMITE APPROXIMATION
vs. FREQUENCY FOR STEP RESPONSE
COMPUTATIONS OF Figure IV.C.5.5

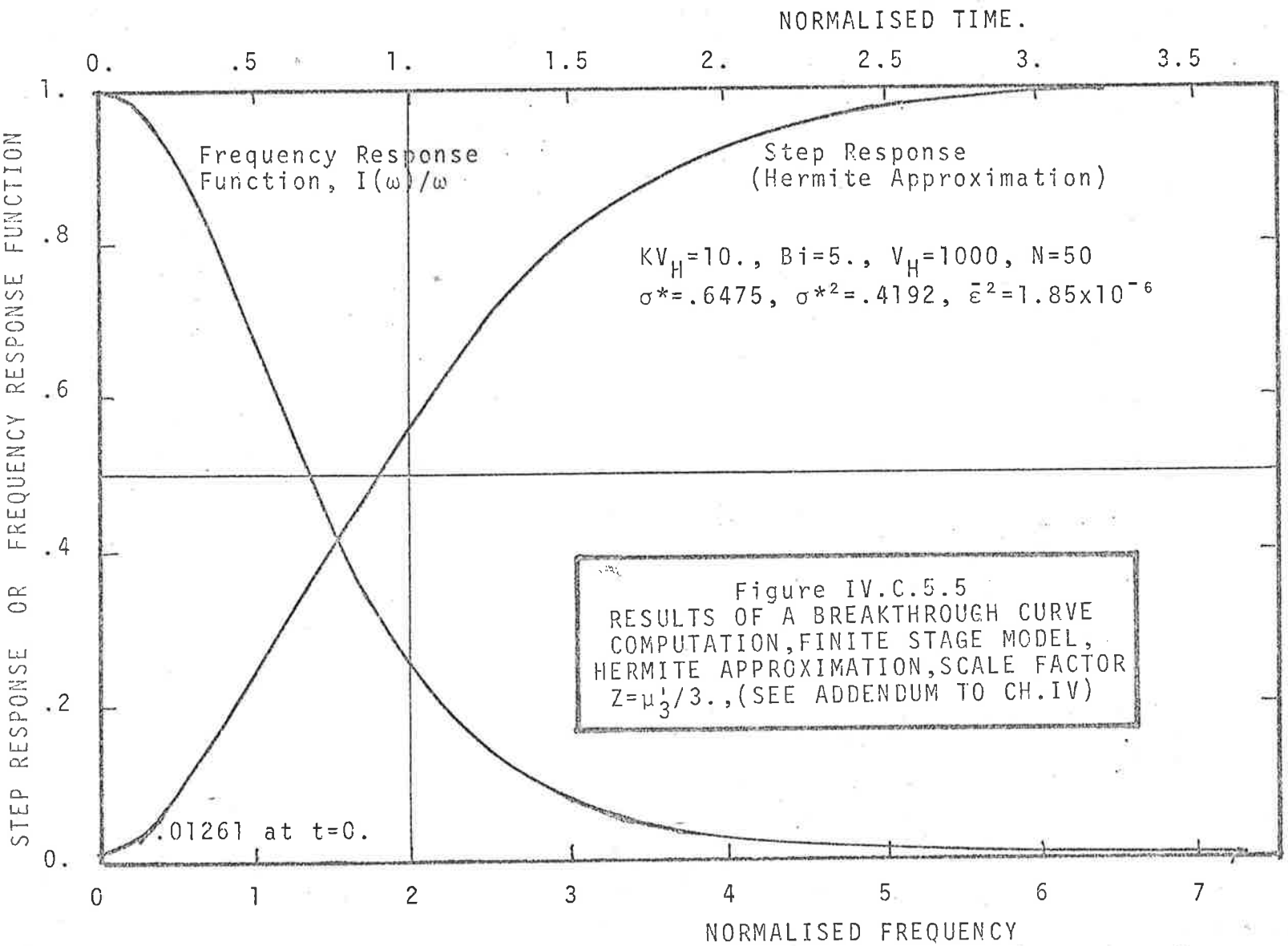

Figure IV.C.5.5
RESULTS OF A BREAKTHROUGH CURVE COMPUTATION, FINITE STAGE MODEL, HERMITE APPROXIMATION, SCALE FACTOR $Z=\mu_3'/3.$, (SEE ADDENDUM TO CH.IV)

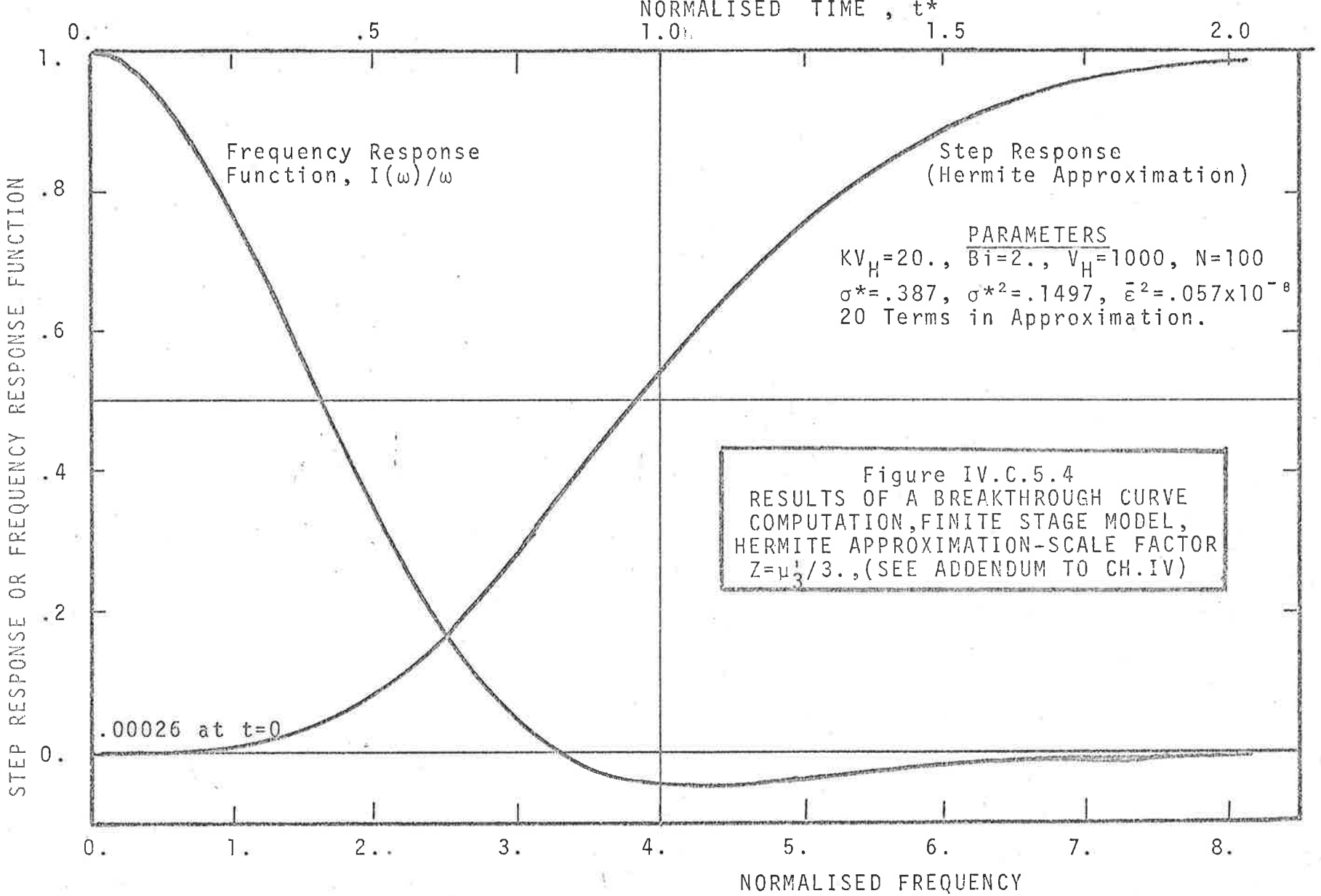

Figure IV.C.5.4
RESULTS OF A BREAKTHROUGH CURVE COMPUTATION, FINITE STAGE MODEL, HERMITE APPROXIMATION-SCALE FACTOR $Z=\mu_3'/3.$, (SEE ADDENDUM TO CH.IV)

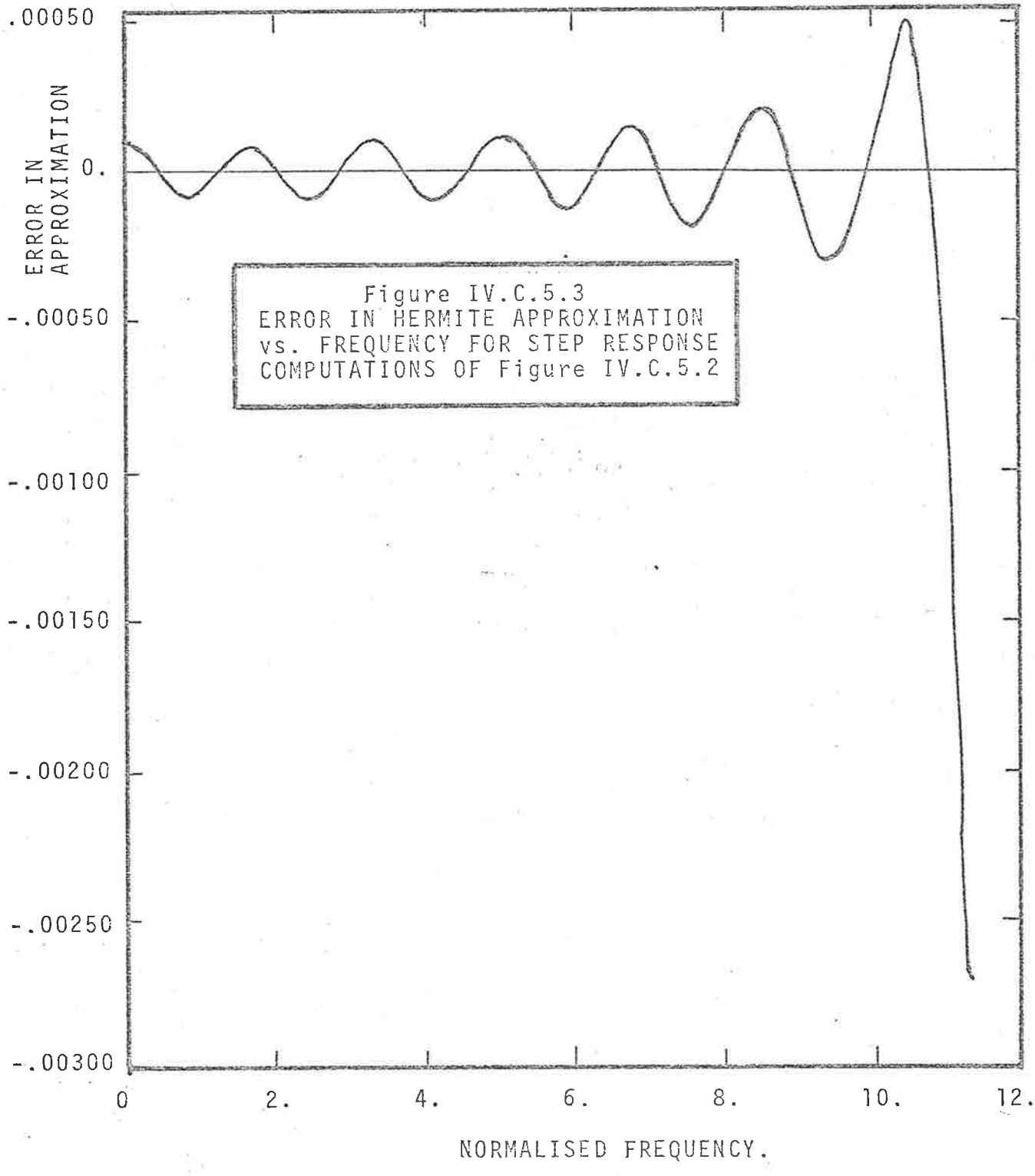

Figure IV.C.5.3
ERROR IN HERMITE APPROXIMATION
vs. FREQUENCY FOR STEP RESPONSE
COMPUTATIONS OF Figure IV.C.5.2

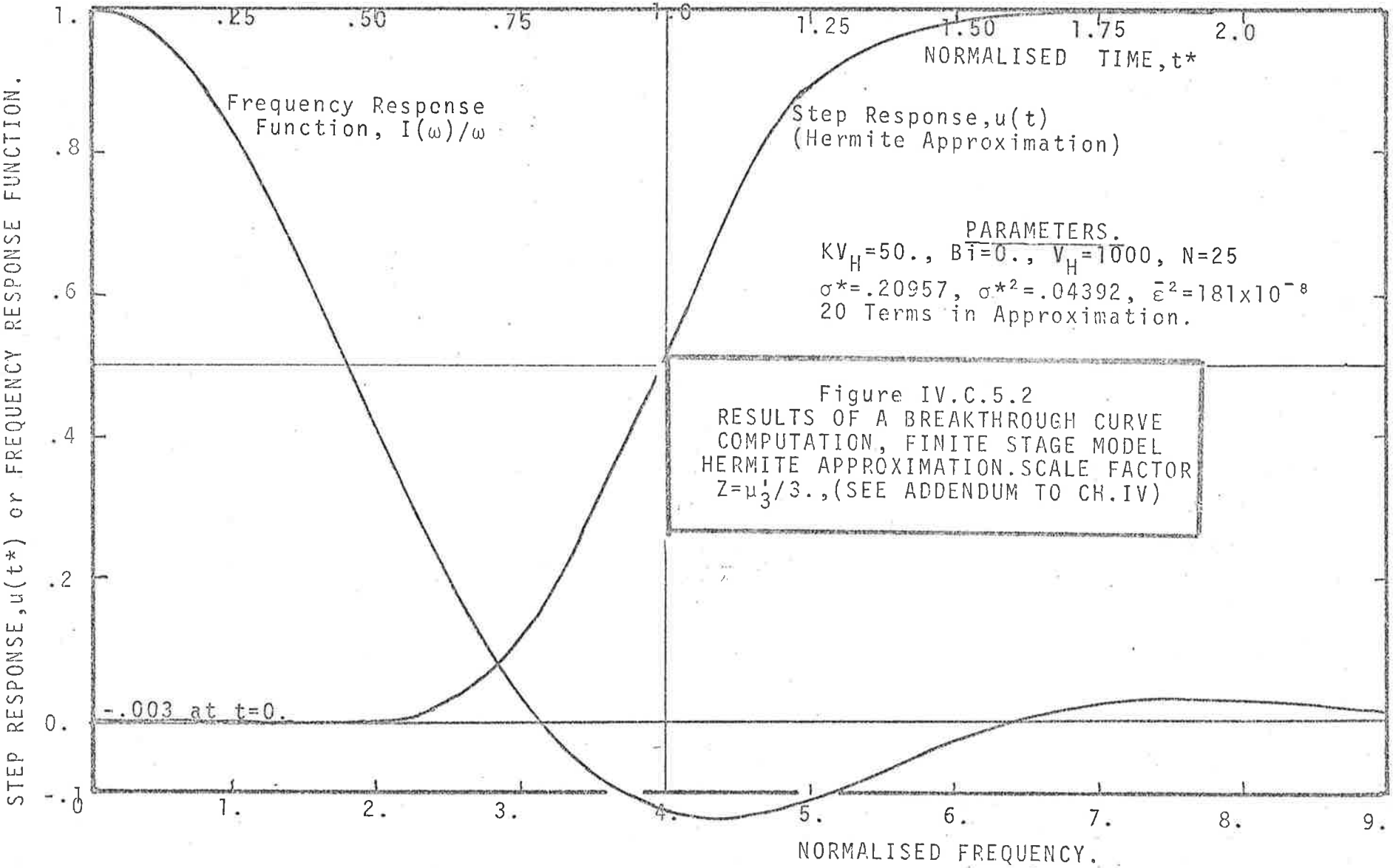

Figure IV.C.5.2
RESULTS OF A BREAKTHROUGH CURVE COMPUTATION, FINITE STAGE MODEL HERMITE APPROXIMATION. SCALE FACTOR $Z=\mu_3'/3.$, (SEE ADDENDUM TO CH. IV)

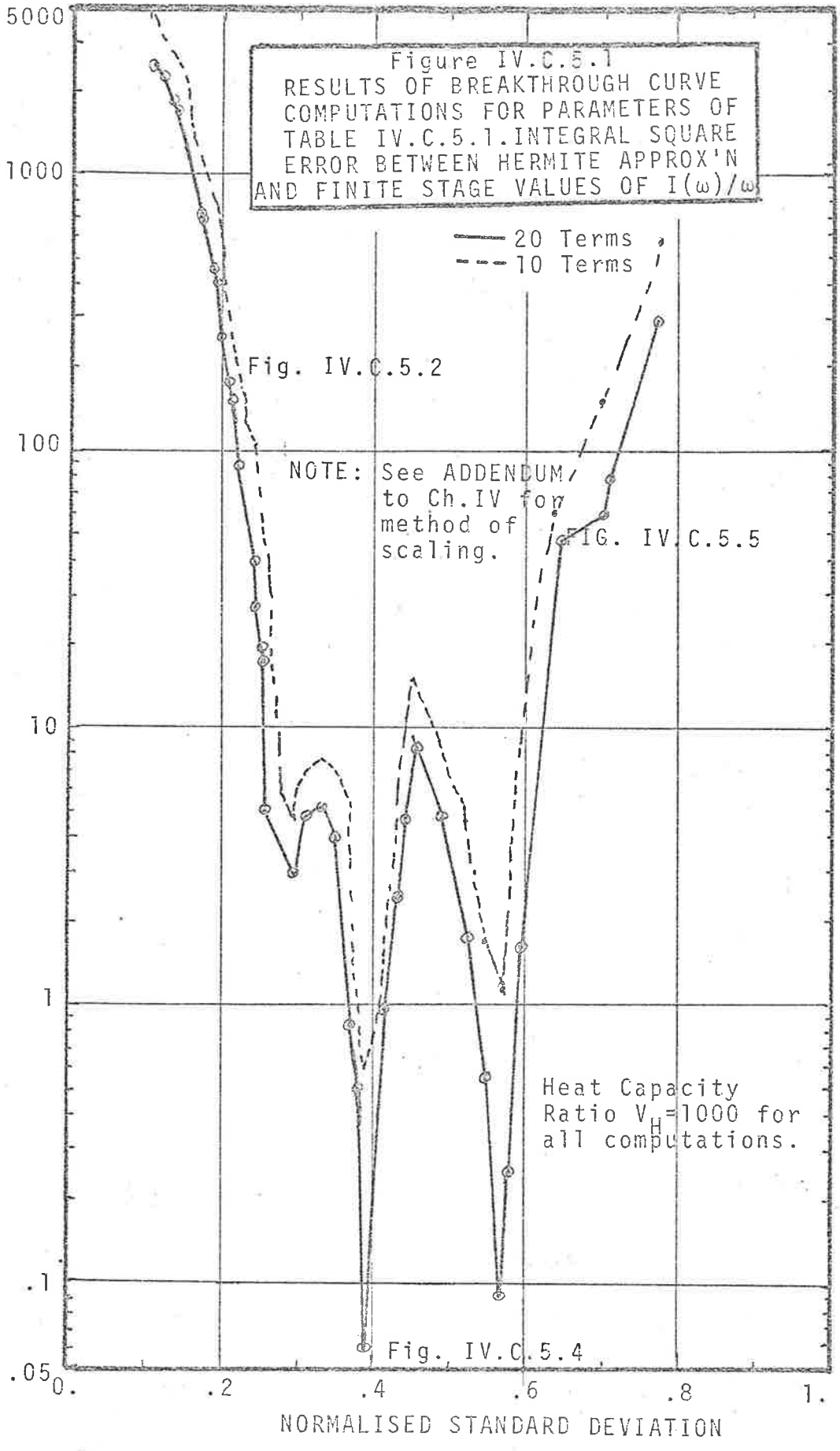

Figure IV.C.5.1
RESULTS OF BREAKTHROUGH CURVE COMPUTATIONS FOR PARAMETERS OF TABLE IV.C.5.1. INTEGRAL SQUARE ERROR BETWEEN HERMITE APPROX'N AND FINITE STAGE VALUES OF $I(\omega)/\omega$

work, is to subtract from the overall transfer function a simple tanks in series solution of area $\exp[-KV_H]$ and approximate the remainder.

5. Range of Parameters in Present Computations

In the present computations, breakthrough curves have only been studied via the finite stage model which virtually sets the Peclet number at a constant value of 2.0. Comparisons of the predicted and experimental breakthrough curves has been presented in Chapter VII, A systematic series of computations have been carried out in order to cover a range of Stanton numbers from about 0.05 to 0.26 i.e. for air, Reynolds numbers ranging from about 8000 down to 100. Bed lengths ranging from short (N=25 diameters) to medium (N=250) have been covered whilst Biot numbers range from zero to 5.0 at the lower Stanton numbers. A fixed value of V_H of 1000 has been chosen (the computations are insensitive to V_H variations for $V_H > 100$). The results of the computations are displayed on Figures 5.1 to 5.6 both in the form of selected $I(\omega)/\omega$ plots and breakthrough curves for the parameter combinations listed in Table 5.1. In most cases, the curves have been described by only 10 coefficients with a maximum estimated error of 0.5% although the results of the computations in the figures are for 20 terms.

In Appendix 9, the scale factors and coefficients for each parameter combination are tabulated together with integral $(\text{error})^2$ and estimated maximum error for each combination.

TABLE IV.C.5.1

PARAMETER COMBINATIONS IN BREAKTHROUGH CURVE PROGRAMME

PARAMETER				$KV_H = \phi$ at Bed lengths N indicated			
Approx. Re_p	Approx. St.	$6St(1-\varepsilon)$	Biot Numbers	N=25	N=50	N=100	N=250
100	0.265	1.0	0,0.1	25	50	100	250
	0.22	0.8	0,0.25	20	-	80	200
	0.16	0.6	0,0.5	15	30	-	150
	0.13	0.5	0,1.0	-	-	50	-
	0.11	0.4	0,1.0,2.0	10	20	-	100
8000	0.05	0.2	0,2.0,5.0	-	10	20	50

6. Reconstruction of Breakthrough Curves by Desk Calculation

In reconstructing a breakthrough curve from the data in Appendix 9 by hand computation the time values desired in units of V_H are first tabulated. Note that in the present computation, time has been normalised by dividing real time by $T_H(1+V_H)$ where T_H is the holdup time and V_H the heat capacity ratio. Each tabulated time value is divided by the scale factor, Z, listed and a table of values of exp $(-t^{*2})$ set up where

$$t^* = t/Z.$$

The first two weighted Hermite polynomials, $H_o(t^*).e^{-t^{*2}} = e^{-t^{*2}}$ and $H_1(2t^*).e^{-t^{*2}} = 2t^*.e^{-t^{*2}}$ are tabulated opposite each time value.

The even values are multiplied by a_o and divided by factorial 2n i.e. 1.

Next, the weighted polynomials $H_2(t^*).e^{-t^{*2}}$ and $H_3(t^*).e^{-t^{*2}}$ are tabulated at each time value from:

$$H_2(t^*).\ e^{-t^{*2}} = t^*.\ H_2(t^*).\ e^{-t^{*2}} - H_o(t^*).\ e^{-t^{*2}}$$

and

$$H_3(t^*).\ e^{-t^{*2}} = t^*.\ H_2(t^*).\ e^{-t^{*2}} - H_1(t^*).\ e^{-t^{*2}}.$$

The even polynomials are multiplied by a_2, divided by factorial 2n and the sign changed.

The process is continued changing the sign each time, until all N+1 values of

$$\sum_{n=0}^{N} \frac{(-1)^n}{(2n!)} \cdot a_{2_n} \cdot \exp(-t^{*2}).\ H_{2n}(2t^*)$$

have been calculated at each time value.

These are all summed at each time value and divided first by $\sqrt{2.\pi}$ and finally by Z.

Each value is then subtracted from 1.0 yielding the final dimensionless breakthrough curve.

It should be noted that the maximum error generally occurs at t=0 and will be detected by the value of the breakthrough curve at that point being some value other than exactly zero.

7. Comparison with Method of Kučera

Although the Hermite polynomial method was developed independently, an earlier treatment by Kučera [1965] has been recently brought to the writer's attention. Whilst the method has a number of disadvantages, some of its features could be used to extend and further simplify the Hermite polynomial method.

Kučera obtains the impulse response g(t) of a packed chromatographic column by expanding g(t) about the first moment μ_1' (see section II.A) and normalising with respect to the 'standard deviation' σ or $\sqrt{\mu_2}$ such that

$$g(t) = \sum_{n=o}^{\infty} a_n \cdot H_n(x) \cdot \exp(-x^2). \qquad \ldots(7.1)$$

where $x = \dfrac{t - \mu_1'}{\sqrt{2}\,\mu_2}$

Expansion in this manner makes even more efficient use of the Gaussian envelope e^{-x^2}. In a similar manner to before, the expansion coefficients are given by:

$$a_n = \frac{1}{2^n . n! \sqrt{\pi}} \int_0^{\infty} g(x) \cdot H_n(x)\, dx.$$

Expression of the Hermite polynomial H(x) explicitly in infinite series form:

$$H_n(x) = \sum_{k=o}^{\left[n/2\right]} \frac{(-1)^k . n!}{k!\,(n-2k)!} (2x)^{n-2k}$$

where $\left[n/2\right] = \begin{cases} n/2 & \text{, for n even} \\ \dfrac{n-1}{2} & \text{, for n odd,} \end{cases}$

leads to an equation for the coefficients a_n in terms of the central moments μ_n of the impulse response

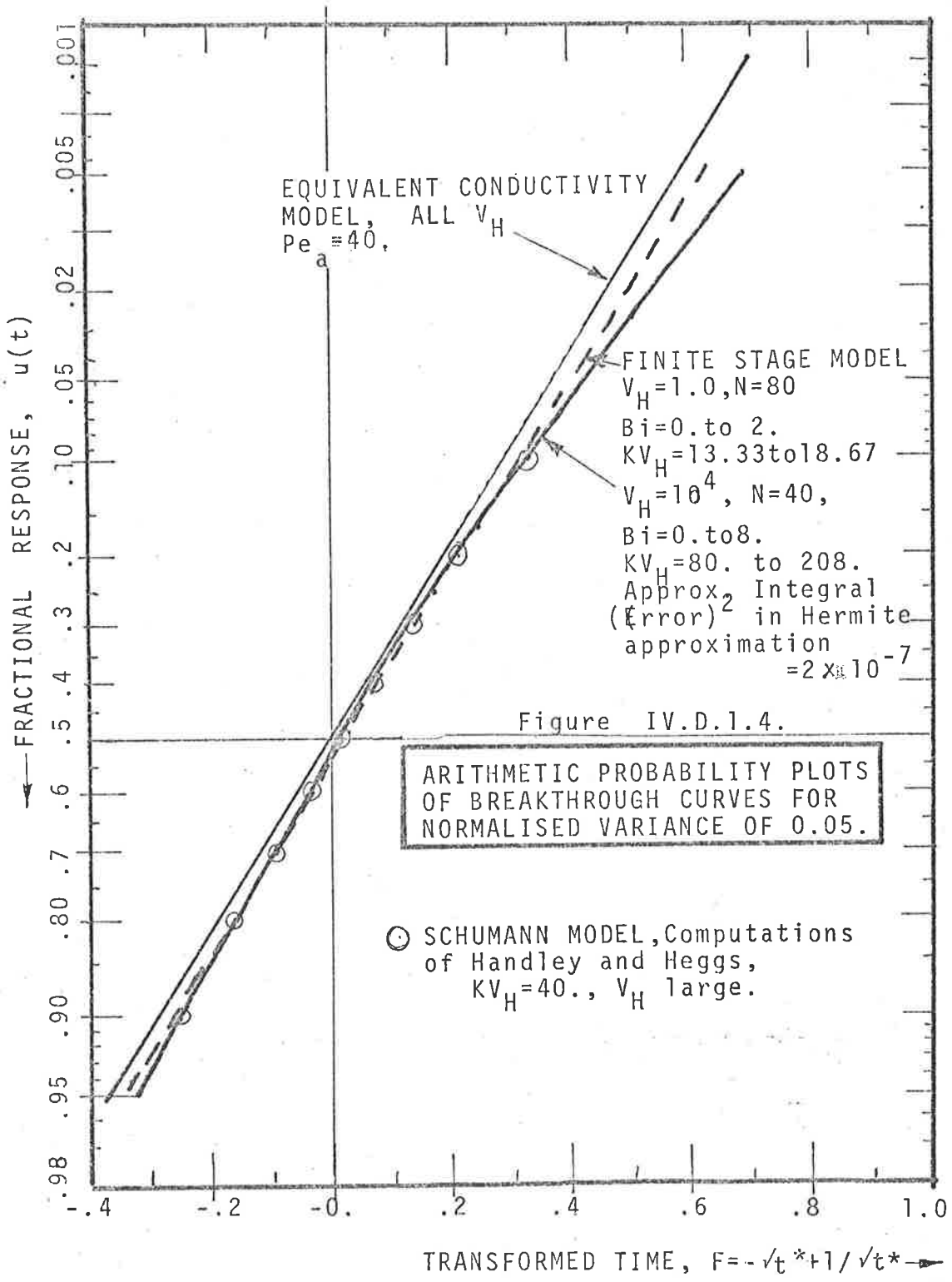

Figure IV.D.1.4.

ARITHMETIC PROBABILITY PLOTS OF BREAKTHROUGH CURVES FOR NORMALISED VARIANCE OF 0.05.

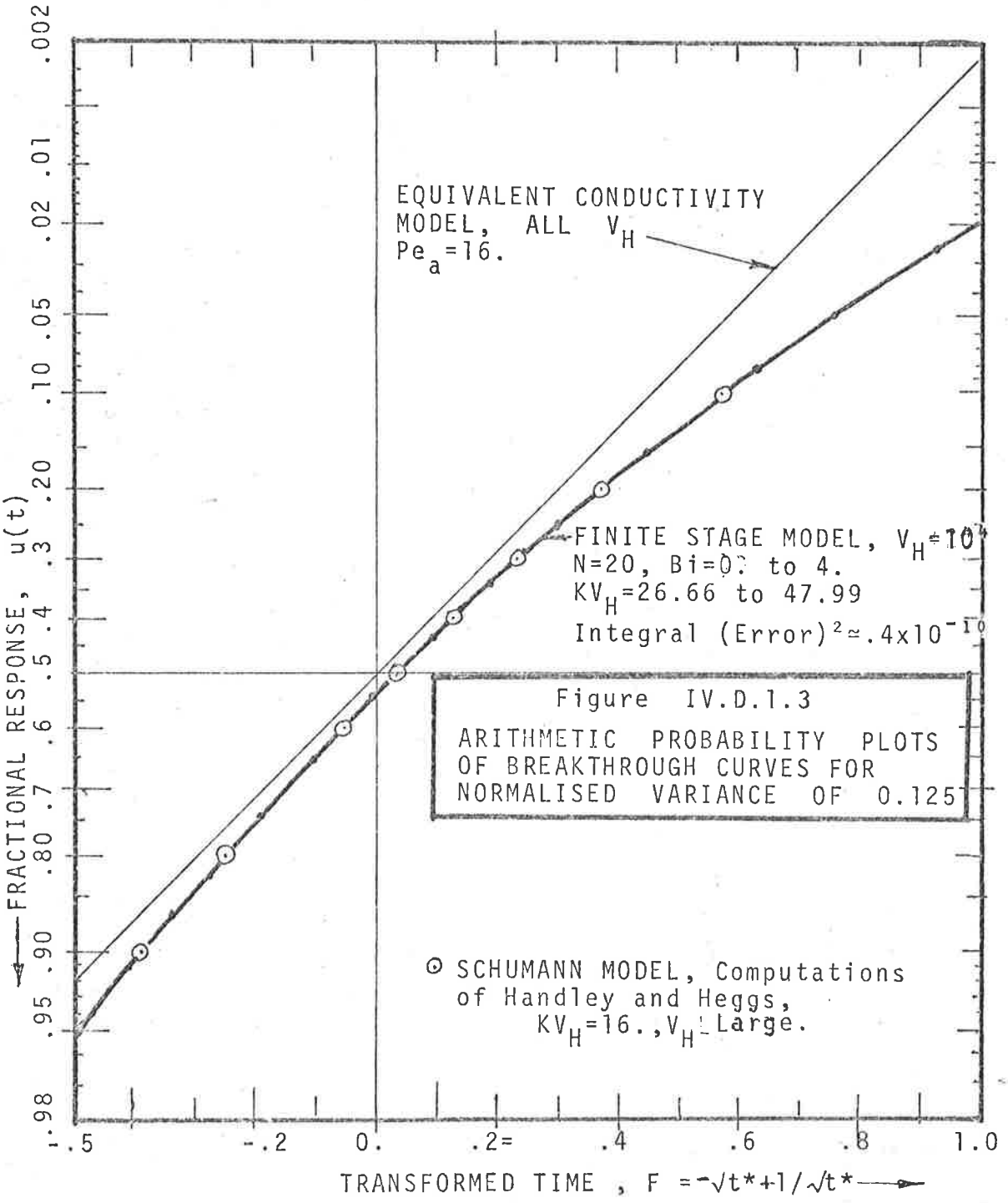

Figure IV.D.1.3

ARITHMETIC PROBABILITY PLOTS OF BREAKTHROUGH CURVES FOR NORMALISED VARIANCE OF 0.125

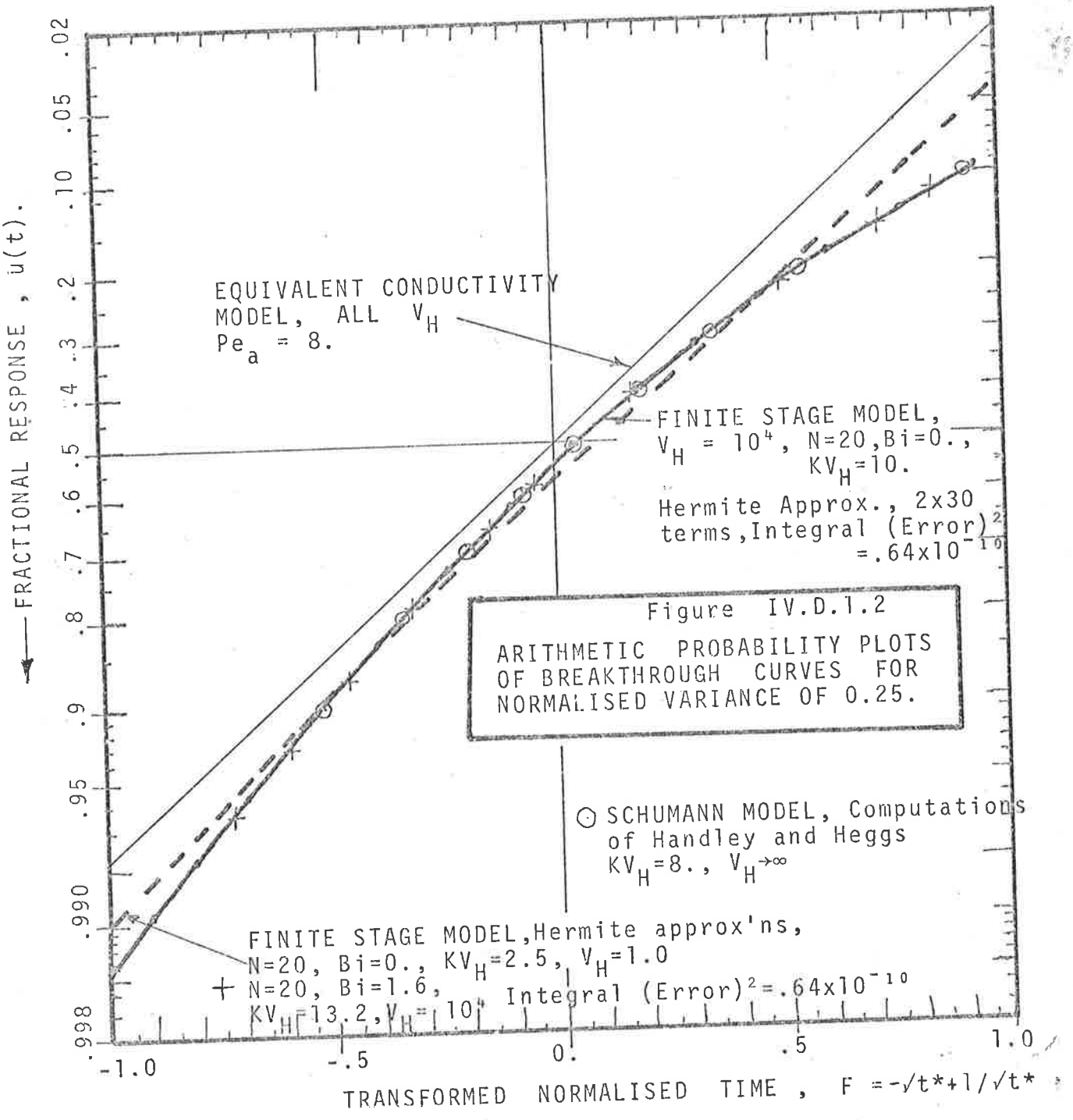

Figure IV.D.1.2

ARITHMETIC PROBABILITY PLOTS OF BREAKTHROUGH CURVES FOR NORMALISED VARIANCE OF 0.25.

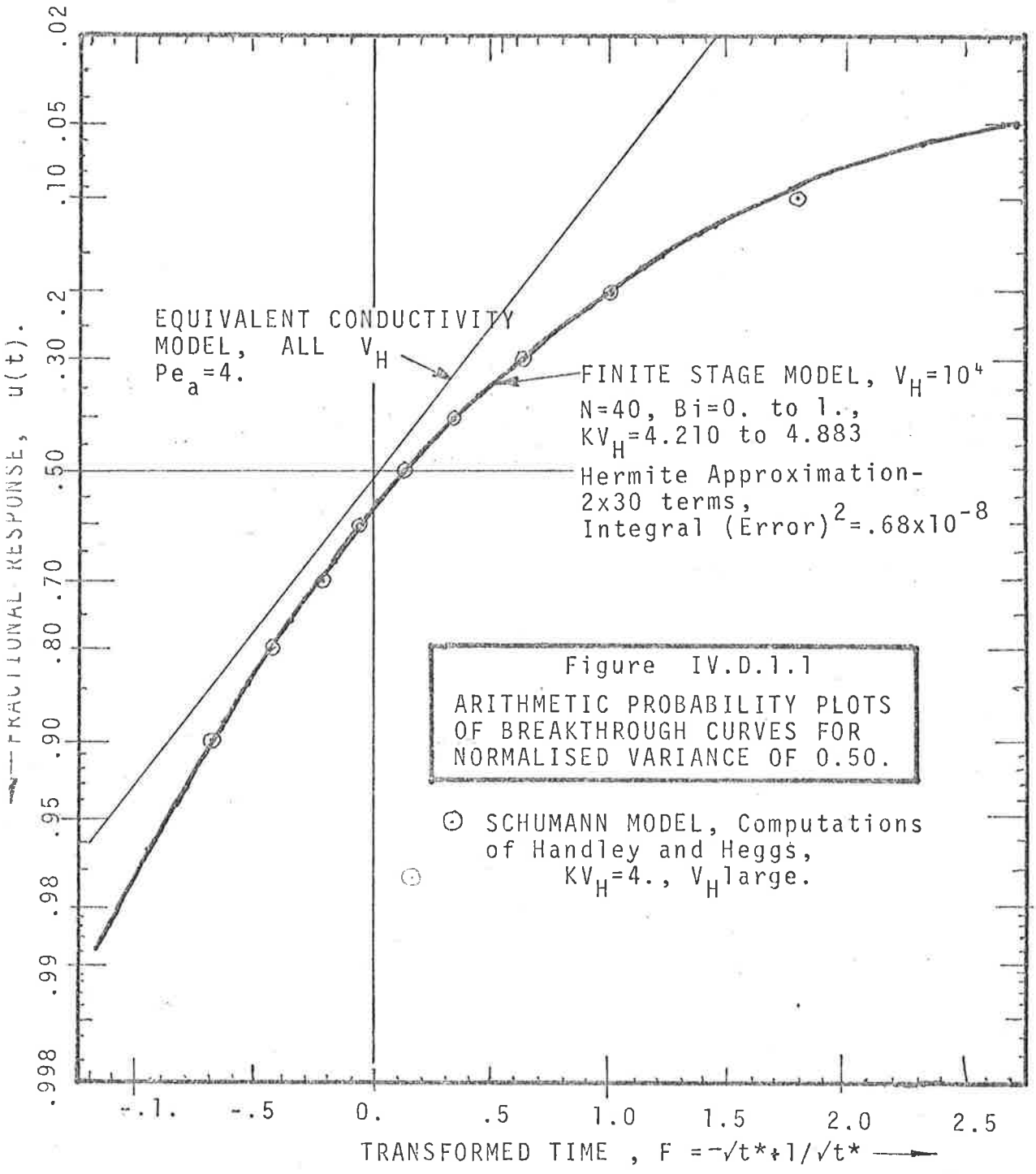

Figure IV.D.1.1

ARITHMETIC PROBABILITY PLOTS OF BREAKTHROUGH CURVES FOR NORMALISED VARIANCE OF 0.50.

$$a_n = \frac{1}{\sqrt{2\pi\,\mu_2}} \sum_{k=0}^{\left[n/2\right]} \frac{(-1)^k . \mu_{n-2k} . \mu_2^k}{2^k . k!\ (n-2k)\ !\ (2\mu_2)^{n/2}} \qquad \ldots(7.2)$$

Kučera presents lengthy expressions for the first ten central moments of the impulse response of a two phase continuous model of packed dynamics. It was found that even the first ten moments were insufficient to ensure convergence for certain parameter combinations. An error criterion was not developed.

In the present work, the step response u(t) is of greater interest than the impulse response. Nonetheless the concept of expansion about the centre of mass is a valuable one and if applied to the present Hermite polynomial method could be used, through equations A.3.10 or A.3.11 to obtain the coefficients a_{2n} in equation C.3.3 with greater efficiency since, presumably, fewer coefficients would be required.

D. ANALYSIS OF BREAKTHROUGH CURVES

1. Effects of Heat Capacity Ratio.

As shown in section II.E.2 the normalised variance σ^{*2}, predicted by the various models developed in chapter II, provides a single parameter for comparing frequency responses $G(j\omega^*)$ and, after inversion, step responses $u(t^*)$. In figures D.1.1 to D.1.4, step responses calculated by each model are compared, for constant σ^*, at two different values of heat capacity ratio V_H. on arithmetic probability plots. As expected from the results of II.E.2, the equivalent conductivity model differs markedly from the other models at high values of V_H, when the Schumann solution provides a useful approximation to the more complex(and more complete) solutions. The difference is revealed on this form of plot by curvature of the other solutions at small times and small values of KV_H.

Figure IV.D.2.1
CORRELATION OF NORMALISED TIME DIFFERENCES FOR BREAKTHROUGH CURVES IN PACKED BEDS vs σ^*, THE NORMALISED STANDARD DEVIATION, FOR HIGH VALUES OF V_H, OR HEAT CAPACITY RATIO, FOR THE PARAMETER COMBINATIONS OF TABLE IV.C.5.1

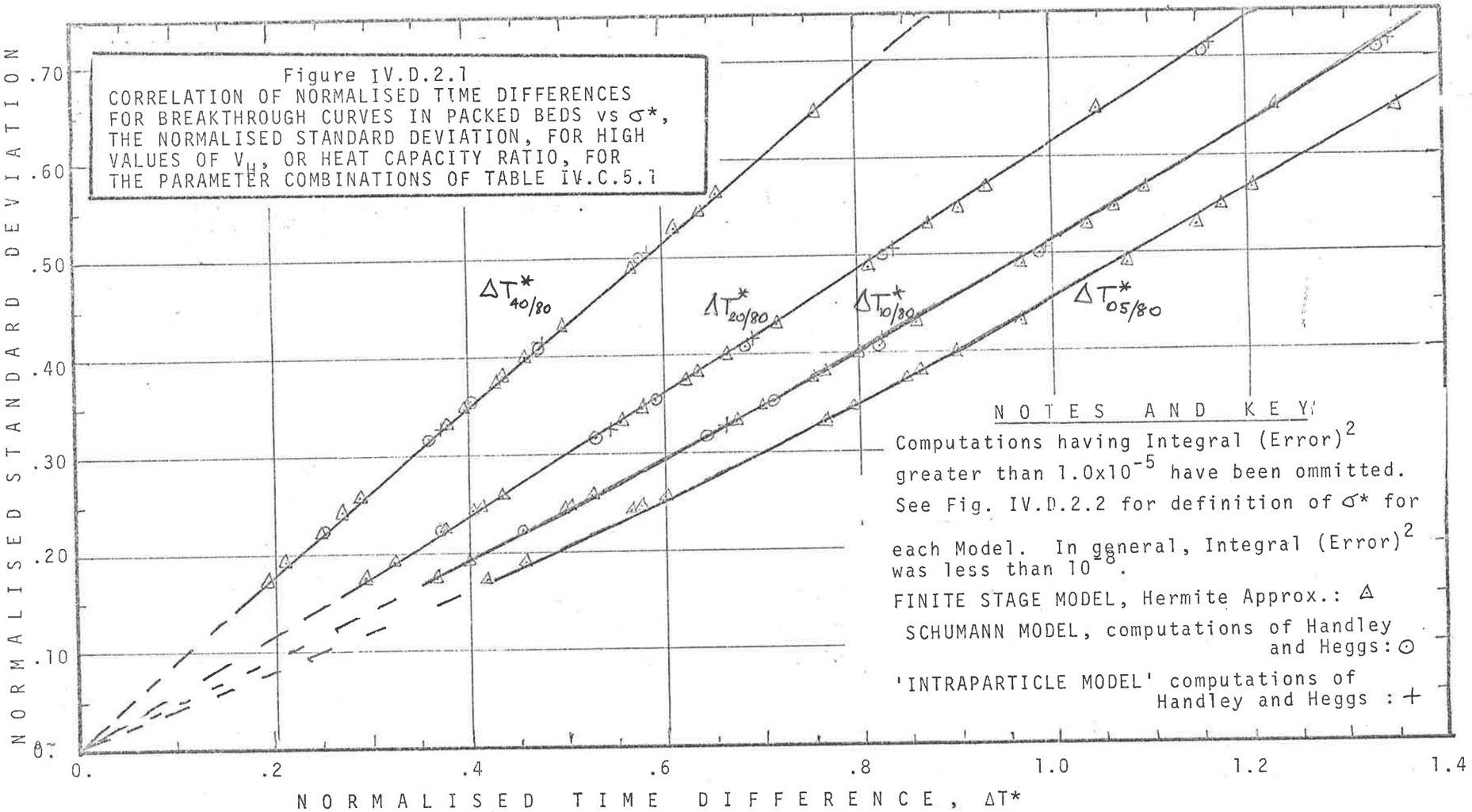

NOTES AND KEY

Computations having Integral $(Error)^2$ greater than 1.0×10^{-5} have been ommitted. See Fig. IV.D.2.2 for definition of σ^* for each Model. In general, Integral $(Error)^2$ was less than 10^{-8}.

FINITE STAGE MODEL, Hermite Approx.: Δ

SCHUMANN MODEL, computations of Handley and Heggs: $\odot$

'INTRAPARTICLE MODEL' computations of Handley and Heggs : +

As would be expected, straight line plots result at low values of V_H and the equivalent conductivity model provides the more useful approximation to the complex models. Once again, the fact that σ^* may be used as a single correlating parameter, for all models, over a wide range of parameters, demonstrates the difficulty likely to occur in separating the effects of axial dispersion, heat transfer resistance and particle conductivity.

2. Simplified Method of Breakthrough Curve Predictions

Since moments analysis predicts that impulse response, and hence step response curves will be symmetrical about their 'centres of mass' for KV_H and/or N large, it is apparent that the time taken, ΔT, for a step response to go from (say) 20% to 80% of completed response will be proportional, for σ^* small, to the 'standard deviation' σ^*. This was suggested in section III.E.2. Handley and Heggs [1969] have measured this particular time ΔT and used it by curve matching between the Schumann solution and the response curve to obtain estimates of KV_H and hence of the Stanton numbers.

Direct empirical correlations between various normalised times ΔT^* (5 to 80%, 10% to 80%, 20% to 80% and 40% to 80%) and the normalised standard deviation σ^* have been carried out using the computational results of this chapter. Straight or slightly curved lines are obtained over a wide range of parameter combinations, allowing rapid prediction of the actual spread of a breakthrough curve about its cente of mass in time units to reasonable accuracy. Since, for systems of practical interest (for example thermal regenerators) V_H values are high, the correlations have been carried out for $V_H = 1000$. Not surprisingly the equivalent conductivity model differs in its predicted curve spread correlations. The correlations obtained are presented graphically on figure 2.1 and are relatively insensitive, for practical purposes, to variations in the Biot number.

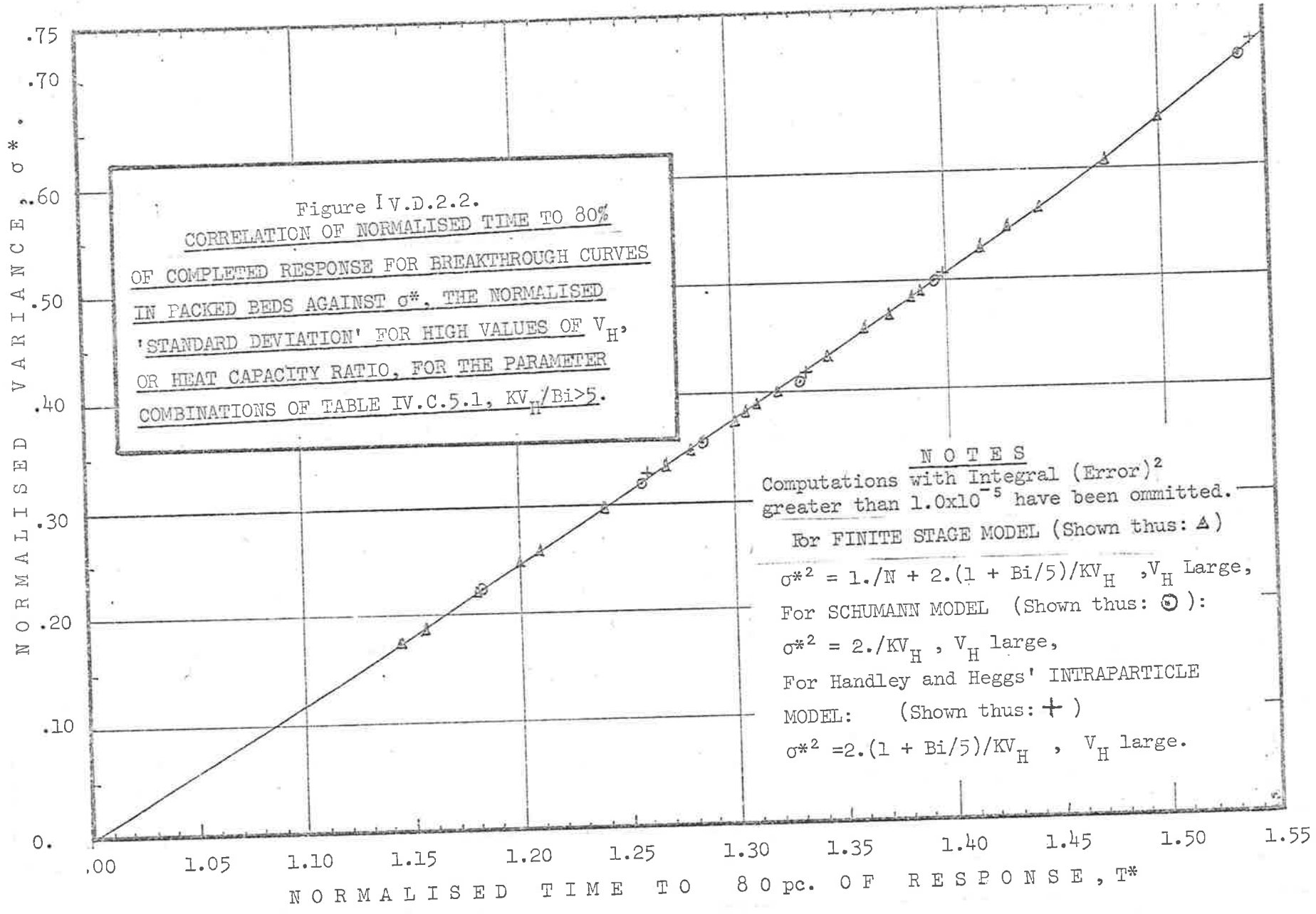

Figure IV.D.2.2.
CORRELATION OF NORMALISED TIME TO 80% OF COMPLETED RESPONSE FOR BREAKTHROUGH CURVES IN PACKED BEDS AGAINST σ*, THE NORMALISED 'STANDARD DEVIATION' FOR HIGH VALUES OF V_H, OR HEAT CAPACITY RATIO, FOR THE PARAMETER COMBINATIONS OF TABLE IV.C.5.1, $KV_H/Bi>5$.

On figure 2.2, the 80% point has been plotted as a function of σ^* allowing, with the correlation of figure 2.1 rapid sketching of the breakthrough curve in normalised time units.

In practical application to design, the "centre of mass" of the breakthrough curve may be calculated for a particular mass of packing and fluid flowrate.

Thus from the equation (applicable to all the models of Chapter II) for the first moment, expressed in actual time units we have

$$\mu(t) = (1+V_H).\frac{L}{v_a} = \left[\frac{\rho_f c_f \varepsilon + \rho_S c_S (1-\varepsilon)}{\rho_f c_f \varepsilon}\right].\frac{L}{v_a}.\frac{A_c}{A_c}$$

where A_c is the total cross sectional area of the bed.

i.e.

$$\mu(t) = \frac{M_f c_f + Mc_S}{Wc_f} \qquad \ldots(2.1)$$

where M_f = mass of fluid retained in the packing, lbs.

M = total mass of packing material, lbs.

and W = total weight flow of fluid, lb/min.

For practical purposes, $M_f c_f$ is usually much less than Mc_S, i.e. $V_H >> 1$, so that equation (2.1) becomes

$$\mu(t) \simeq \frac{Mc_S}{Wc_f} \qquad \ldots(2.2)$$

The normalised time T^*_{80} for 80% of completion is multiplied by $\mu(t)$ to convert to time units and using the particular values of Reynolds number, Stanton number and Biot number resulting from each particular cross sectional area chosen, σ^* is calculated and finally each ΔT in time units.

Since, for a particular combination of M and W, $\mu(t)$ is predicted to be independent of cross sectional area, the design problem becomes one of minimising the spread of the breakthrough curve, subject to economic constraints such as the power expended in pressure drop across the bed.

In order to allow a slightly more precise prediction of points on a breakthrough curve given a value of the estimated normalised 'standard deviation', least squares polynomials were fitted to the data displayed on Figures D.2.1 and D.2.2. The fit excludes those values for which the integral error square between Hermite approximation and the exact value of $I(\omega)/\omega$ exceeds 2×10^{-6} (figure C.5.1) and also three parameter combinations of Table C.5.1 for which $\gamma x = KV_H/Bi$ was less than or equal to 5.

Polynomials of the third degree were fitted in each case, i.e., for prediction of normalised times T* taken to reach a given fractional response, given σ^*:

$$T^* = a_o + a_1 \sigma^* + a_2(\sigma^*)^2 + a_3(\sigma^*)^3 \quad \ldots (2.3)$$

whilst for determining σ^*, given the normalised time differences ΔT^* between a point on the curve and the 80% response point:

$$\sigma^* = b_0 + b_1 \Delta T^* + b_2(\Delta T^*)^2 + b_3(\Delta T^*)^3 \quad \ldots (2.4)$$

The value of a_0 in equation (2.3) should, in each case be 1.0 theoretically since for zero curve spread, ($\sigma^*=0$), the breakthrough curve should become a unit step function located at $T^*= 1.0$, whilst , for a similar reason, b_0 should be zero. Other points on a curve could be correlated in a similar manner provided the one-parameter

model holds. Tables D.2.1 and D.2.2 list the appropriate coefficients in equations (2.3) and (2.4).

TABLE IV.D.2.1

COEFFICIENTS IN POLYNOMIALS OF EQUATION (D.2.3)

T^* on σ^*, where T^*_{10} denotes time to 10% of response, etc.

	a_0	a_1	a_2	a_3	Error Std. Dev'n. in predicted values
T^*_{10}	.9980	-1.302	.2776	-.0340	.00192
T^*_{20}	.9980	- .8551	.0132	-.0430	.00144
T^*_{40}	.9999	-.2504	-.2488	.0221	.00071
T^*_{80}	1.0046	.7874	.0430	-.1222	.0130

TABLE IV.D.2.2

COEFFICIENTS IN POLYNOMIALS OF EQUATION (D.2.4)

σ^* on ΔT^* where $\Delta T^*_{20/80}$ denotes time between 20% and 80% of response, etc.

	b_0	b_1	b_2	b_3	Error Std. Dev'n in predicted values
$\Delta T^*_{10/80}$	-.0029	.4862	.0031	.0232	.0068
$\Delta T^*_{20/80}$	-.0034	.6162	-.0309	.0263	.0080
$\Delta T^*_{40/80}$	.0024	.9677	-.2672	.1548	.0111

E. SUMMARY OF CONCLUSIONS OF CHAPTER IV.

The numerical Laplace transform inversion technique of Rosen has been generalised and simplified, in section A.3 so that it may be applied to breakthrough curve prediction for any model.

It was shown that greater control over error may be attained by use of an approximation method which allows direct comparison of the approximation in the frequency domain prior to analytical transform inversion. The method could be simplified by the application of a technique first presented by Kucera.

Analysis of the theoretical breakthrough curves thus obtained confirm the moments and frequency domain predictions of Chapter II:

1. The heat capacity ratio V_H is a primary criterion in deciding whether the equivalent conductivity model or the Schumann model is an appropriate single-parameter model to use as an approximation to the more complete two phase descriptions of packed bed dynamics.
2. The parameter σ^*, the normalised standard deviation of the impulse response may be used as such a single parameter, allowing for the effects of axial dispersion in the fluid phase, heat transfer resistance and internal particle conduction provided the ratio KV_H/Bi is kept less than about 5 to 10.

Simplified empirical correlations of the elapsed time between various fractional computed responses on a breakthrough curve were developed which may be of value in rapid estimation of these curves.

It was also found computationally that straight line arithmetic probability plots of breakthrough curves predicted by the equivalent conductivity model were obtained only for V_H small and $KV_{H/Bi}$ greater than about 10.

ADDENDUM TO CHAPTER IV

CHOICE OF SCALE FACTORS FOR HERMITE POLYNOMIAL BREAKTHROUGH CURVE APPROXIMATIONS.

The choice of scale factor Z used in computing breakthrough curves by the Hermite polynomial method is a somewhat arbitrary one when the method of section C.3. is used. A method has since been developed which is semi-automatic and does not require the decision to be made on subjective judgment. This method was found more suitable in programming the extensive computations required to obtain the results presented in Appendix 9 and displayed on figures C.5.1 to C.5.60.

The method requires knowledge of the first three cumulants of the impulse response of the system and ensures that the variance of the first term in the Hermite series is equal to variance of the even part of $\phi(t)$ where $\phi(t)$ is defined by

equation (A.3.2).

In computing a breakthrough curve, we approximate $I(Z\omega)/Z\omega$ by the series of equation (C.3.4). The first term of the series is $a_o.H_o(\omega).\ \exp(-\omega^2/4)$ which is a Gaussian function of 'variance' 4, since $H_o(\omega) = 1$. This process of approximation may also be regarded as approximating $I(\omega)/\omega$ by $a_o.\ \exp(-Z^2\omega^2/4)$ for a one term series, where the 'standard deviation' is 2/Z. Now

$$e^{-t^2/\sigma^2} = \frac{\sigma}{2}\sqrt{\pi}.\ e^{-\sigma^2\omega^2/4} \qquad \ldots(1)$$

and it may thus be seen that the inverse of $I(\omega)/\omega$ or $E[\phi(t)]$ is simultaneously approximated by a Gaussian function also, having a variance of Z. As in Appendix 5, E denotes 'the even part of'.

In section V.D.2, the fundamental equation linking the absolute moments μ'_{ϕ_n} of $\phi(t)$ to the absolute moments μ'_n of the impulse response is derived :

$$\mu'_{\phi_n} = \frac{\mu_{n+1}}{n+1}$$

Hence the variance $\sigma_\phi^{\,2}$ of $E[\phi(t)]$ may be obtained. Since $E[\phi(t)]$ is an even function, its variance is simply equal to the second absolute moment, and hence

$$\sigma_\phi^{\,2} = \mu'_{\phi_2} = \frac{\mu'_3}{3}. \qquad \ldots(2)$$

IV. ADDENDUM

The third absolute moment of g(t) may be obtained [Kendall and Stuart, 1958] from :

$$\mu_3' = \pi^3 + \mu_1'\mu_2' + 2\sigma^2\mu_1'$$

$$= \pi^3 + 3\mu_1'\sigma^2 + \mu_1'^3$$

The final method used in calculating the scale factor Z became one of calculating μ_3' for the particular parameters under consideration and then setting $Z = \sqrt{\mu_3'/3}$. The value of σ_ϕ calculated is also useful in deciding automatically the maximum frequency of interest in the computations and also the maximum time. The final computer program developed sets the maximum time equal to an arbitrary 3½ standard deviations σ_ϕ whilst the maximum frequency of interest is made equal to $3.5\sigma_\omega$ where

$$\sigma_\omega = 2/\sigma_\phi$$

The results obtained from the computations indicate that this choice of scale factor is, in general, a good one. Thus, in each case the approximations were repeated with scale factors of $0.9.Z_{opt}$ and $1.1.Z_{opt}$ where Z_{opt} is the 'optimum' scale factor obtained from

$$Z_{opt} = \sqrt{\mu_3'/3} \qquad \ldots(3)$$

In every case the integral $(\text{error})^2$ obtained with $Z = Z_{opt}$ was the smallest of the three for 10 terms.

CHAPTER V

METHODS OF DYNAMIC TESTING AND ANALYSIS

SCOPE OF THE CHAPTER

In this chapter, various methods of dynamic testing and analysis are examined in some detail. The basic objective is to reveal the considerations which led to the present experimental design (Chapter VI). An attempt is also made to unify some of the various theories of dynamic testing in current use in the Chemical Engineering literature.

In Section A (and Appendix 10) errors which have arisen in the application of cyclic test procedures are analysed chiefly to indicate why this procedure was rejected in the present experiments.

In Section B errors which may occur in application of the method of moments analysis are discussed from a general point of view together with alternative methods of moments analysis via frequency response. A preliminary error analysis is also presented for the technique when applied specifically to packed bed dynamic testing.

In Section C pulse to frequency response methods are analysed with emphasis on errors occurring in the use of the direct method of transformation. An approximation procedure to be used in the present experiments is proposed and compared with the Dooge

method of Laguerre polynomial approximation. The specific application of the proposed technique to packed bed dynamic testing is also discussed.

In Section D existing step response methods of error analysis are discussed and a new method presented which allows the moments of the impulse response to be obtained from step response data.

A summary of conclusions is presented in Section E.

A. CYCLIC METHODS OF DYNAMIC TESTING

1. Fundamental Relations

The cyclic method of testing has been widely applied to the determination of heat transfer coefficients in packed beds [Meek, 1961; Lindauer, 1967; Hart and Szomanski, 1968; Pulsifer, 1965]. As pointed out in section II.A.2 the method involves determination of the frequency response transfer function $G(j\omega)$ in magnitude $|G|$ and phase $/G$ at varying frequencies by administering a sinusoidal input temperature variation and measuring the resultant steady state variation in outlet temperature after all initial transients have ceased. Then if $|Y(j\omega)|$ and $|X(j\omega)|$ are the steady state complitudes of output and input sine waves respectively,

$$|Y(j\omega)| \; / \; |X(j\omega)| \; = \; |G(j\omega)| \qquad \ldots \quad (1.1)$$

whilst if $/Y(j\omega)$ and $/X(j\omega)$ are the phase shifts of output and input sine waves relative to some datum

$$/Y(j\omega) - /X(j\omega) = /G(j\omega) \quad \ldots \quad (1.2)$$

This principle has been applied to measurements of fluid-particle heat transfer coefficients in packed beds in two main ways.

(a) By measurement of frequency response at a number of frequencies from low to high followed by curve fitting of an assumed mathematical model to the data [Rosen and Winsche, 1950; Brodkey, 1964; Pulsifer, 1965; Littman and Barile, 1966; Littman, Barile and Pulsifer, 1968].

(b) By measurement of frequency response at a frequency or frequencies high enough to ensure that the supposed limiting value of equation II.B.4.3 is achieved i.e.

$$\lim_{\omega \to \infty} |G(j\omega)| = \exp[-6N\ St(1-\varepsilon)] \quad \ldots \quad (1.3)$$

Workers at various Government and semi-governmental research institutes have favoured this method [Dayton et al., Battelle Memorial Inst., U.S.A., 1952; Meek, National Engineering Laboratory, Lindauer, G.B., 1961; Brookhaven National Laboratory, 1967; Szomanski et al., Aust. Atomic Energy Commission, 1968, 1969].

2. Discussion of Errors

(i) General Remarks

In general, the cyclic method experiments take a long time to complete if a reasonable number of frequency points is to be

obtained. It has been suggested that since only one unknown is present in equation (1.3), only one frequency value need be tested [Hart and Szomanski, 1968]. For example, Turner [1967] has suggested that three unknowns (Stanton number, Biot number and Peclet number) may be obtained from only three frequency values. In view of the errors inherent in the method to be discussed below and in Appendix 10 such an approach may be regarded as impossible, experimentally. Even the second group of workers using equation (1.3) have not attempted to extract meaningful information from only one frequency test. The theoretical analysis of chapters II and IV also indicates that it is difficult to differentiate between these effects.

A more fundamental objection to the method arises from the experimental difficulty of generating a pure sine wave [Pulsifer, 1965: Brodkey, 1964: Manins and Szomanski, 1969]. Pulsifer has had some success in applying Fourier series analysis to the extraction of the fundamental frequency components using a periodic square wave input. Others [Manins and Szomanski, 1969] have ignored the effects of sine wave distortion despite the presence of obviously non sinusoidal wave forms at inlet and outlet.

A even more important objection arises from consideration of the effects of heat losses from the section and attenuation at high frequencies due to bed supports, wall capacitance, recorder bandwidth limitations and measurement lags (see Appendix 10).

The theoretical effects of heat loss (see Appendix 4) is to shift all apparent $|G(j\omega)|$ values downwards. According to the

models proposed so far (zero heat loss):

$$\lim_{\omega \to 0} |G(j\omega)| = 1 \qquad \ldots \quad (2.1)$$

When simple steady state heat loss occurs, the limiting value of the L.H.S. of equation (2.1) is less than unity. Since the dynamic effects of steady state heat loss are small (Appendix 4) all values of $|G|$ should be corrected upwards to ensure that the limit of equation (2.1) is satisfied. Steady state heat loss cannot be measured by cyclic methods since 'zero frequency' implies a non periodic input such as a step or pulse.

(ii) The Methods of Littman et al.

The Rosen and Winsche method of analysis [1950] was also used by Pulsifer [1965]. In his experiments great care was taken to eliminate heat losses. According to this approach, a plot of $\ln |G| / \underline{G}$ is made against frequency and this should result in a straight line.

An examination of equations II.A.2.10 and II.A.2.11 reveals that this condition is satisfied when skewness (π^3 or κ_3) is negligible, i.e. when:

$$\frac{\ln|G(j\omega)|}{/G(j\omega)} = \frac{\kappa_o - \kappa_2 \frac{\omega^2}{2!} + \kappa_4 \frac{\omega^4}{4!} - \ldots}{-\kappa_1 \omega + \kappa_3 \frac{\omega^3}{3!} - \ldots}$$

$$\simeq \frac{\sigma^2 . \omega}{2 \mu} \qquad \ldots \quad (2.2),$$

since, for zero heat loss,

$$\kappa_o = \lim_{\omega \to 0} \ln |G(j\omega)| = 0.$$

Such a limiting value is obtained according to equations II.B.3.9, II.C.3.2 or II.D.4.2 only for long bed lengths, small Biot numbers and high Stanton numbers. In general, the first group of workers in section 1 have applied this or a similar technique of curve fitting. Provided allowance is made for heat losses little criticism may be made of this approach since it does not place undue emphasis on high frequency values, where errors are largest.

(iii) Limiting Frequency Response Methods

The use of the limiting relation, equ. (1.3), introduces a number of serious errors into the measurement of fluid-particle heat transfer coefficient. These are analysed in greater detail in Appendix 10. Conclusions reached by the analysis are summarised below.

(a) Since measurable values of $\exp[-6NSt(1-\varepsilon)]$ are only achieved for short bed lengths and high Reynolds numbers when St is small, test sections must be only 5 to 12 particles in length. This means that transfer coefficients measured are not necessarily representative, entrance and exit conditions assume importance and it is difficult to achieve a true random packing. The use of short bed lengths generally leads to beds which are only

5 to 10 particles in width. This accentuates the dynamic effects of the wall (Appendix 4).

(b) At high frequencies, attenuation introduced by the packing support assumes considerable importance. Consideration of this error led to the experimental technique used in the present study (Chapter VI), that is, to immersion of the temperature measuring probe in the bed itself.

(c) Attempts to correct for high frequency attenuation by measurements on the empty test section may introduce even larger errors especially since corrections need to be very large.

B. MOMENTS ANALYSIS

1. Fundamental Relations

Aris [1959] has shown that the parameters of a flow system may be estimated (under conditions which are not explicitly stated) from the difference between moments measured at two points in a flow system when a pulse input is administered upstream of both measuring stations (Figure B.1).

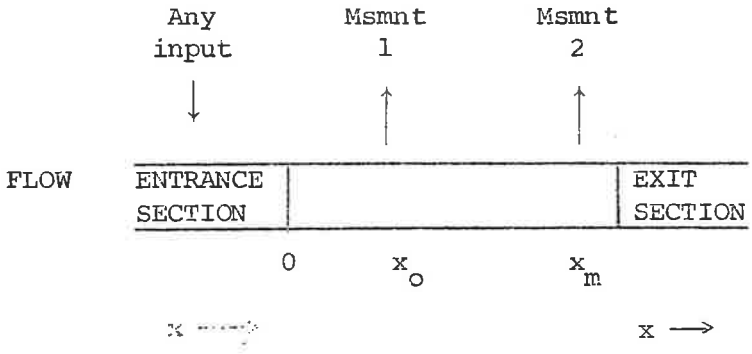

$$x_m(t) = \{x_o(t) * g(t, x_m - x_o)\}$$

FIGURE V.B.1

Aris' result follows more generally and may be extended by using the relations derived in section II.A.3 concerning the additivity of cumulants under convolution. Thus, for the situation of Figure V.B.1, provided the concentration or temperature $x_m(t)$ at measurement station 2 is formed by convolution of $x_o(t)$ and an impulse response between x_o and x_m then

$$\kappa_{G_n} = \kappa_{m_n} - \kappa_{o_n} \qquad \ldots \quad (1.1)$$

where κ_{G_n}, κ_{m_n}, κ_{o_n} are the n'th cumulants of the impulse response, $g(t, x_m - x_o)$ and of the measured distributions $x_m(t)$ and $x_o(t)$ respectively.

When an impulse $\delta(t)$ is applied at measurement station 1 all the cumulants κ_{o_n} become zero so that the measurement $x_m(t)$ is directly that of the impulse response i.e. $x_m(t) = g(t, x_m - x_o)$.

The cumulants are obtained experimentally by integration. For $x_m(t)$ we have, from equations II.A.2.6, II.A.2.7, II.A.2.8 and II.A.2.9:

$$\kappa_{m_o} = \ln \int_o^\infty x_m(t).dt \quad \ldots \quad (1.2)$$

$$\kappa_{m_1} = \mu_m = \int_o^\infty t.x_m(t).dt \quad \ldots \quad (1.3)$$

$$\kappa_{m_2} = \sigma_m^2 = \int_o^\infty (t - \mu_m)^2 . x_m(t).dt \quad \ldots \quad (1.4)$$

$$\kappa_{m_3} = \pi_m^3 = \int_o^\infty (t - \mu_m)^3 . x_m(t).dt \quad \ldots \quad (1.5)$$

2. Discussion of Errors

As many writers have pointed out, evaluation of the higher moments becomes prone to errors due to slow drift of the baseline since large time values are heavily weighted by successively higher powers of t [Curl, 1966; Gomezplata and Brown, 1968, Clements jr., 1969].

As noted in Chapter VI, early experiments in the present work resulted in a very wide variability in the estimated impulse response moments, particularly in the central third moment. A great improvement in reproducibility was achieved by controlling the input pulse so that 'tailing' of the input pulse did not occur. This improvement in experimental technique is discussed in Chapter VI., and results analysed in section VII.A.

As an example of the magnitude of the errors which may arise due to truncation of a measurement, assume the impulse response g(t) of a perfect mixer of unit holdup time is recorded. The transfer function is $G(s) = {}^{1}/_{(s+1)}$ and all cumulants are 1.0.

Then $g(t) = \exp(-t)$.

The effect of truncating the measurement after successively longer time values is illustrated by Table 2.1. The incomplete zero'th moment $\mu_o(t) = 1 - e^{-t}$ is used (following usual practice) to normalise the estimated first and second moments i.e.:-

$$\mu_{est} = \frac{\mu(t)}{\mu_o(t)} = \frac{\int_o^t t\, e^{-t}\, dt}{\int_o^t e^{-t}\, dt}$$

$$\sigma_{est}^2 = \frac{\sigma^2(t)}{\mu_o(t)} = \frac{\int_o^t [t-\mu_{est}]^2 . e^{-t}\, dt}{\int_o^t e^{-t}\, dt}$$

It may be seen that even if the record is truncated when the value of g(t) has fallen to 0.7% of its initial value, a 16% error remains in the normalised estimate of the variance and a 3.3% error in the estimated first moment. These errors will be accentuated if the normalisation of time is carried out incorrectly or if both input and output pulses are truncated (in this idealised example, the input is assumed to be a perfect Dirac or impulse function).

The last column of Table 2.1 presents the estimated value of σ^{*2} defined by

$$\sigma^{*2} = \sigma^2/\mu^2$$

It may be noted that truncation errors are not quite so important in estimates of σ^{*2} (see section B.4 for the use of this fact).

TABLE V.B.2.1

ERRORS IN ESTIMATED MOMENTS OF PERFECT EXPONENTIAL DECAY

t	$g(t) = e^{-t}$	$\mu_o(t)$	μ_{est}	σ_{est}^2	σ_{est}^{*2}
1	.3679	.6321	.418	.144	.635
2	.1353	.8647	.686	.341	.726
3	.0498	.9502	.842	.541	.762
4	.0183	.9817	.925	.706	.827
5	.0067	.9933	.967	.839	.898
6	.0025	.9975	.985	.914	.943
7	.0009	.9991	.994	.958	.970
∞	0.00	1.00	1.00	1.000	1.000

It is important to note that whilst estimates of system parameters (e.g. St, Pe, Bi) may be obtained from moments analysis, there is no guarantee that the system under test actually agrees with the theoretical model proposed. An independent check preferably using the whole of the estimated impulse or frequency response is necessary to test agreement between theory and experiment.

3. Other Methods of Moments Estimation

Early experience with the method of moments analysis applied to the present research led to adoption of least-squares analysis in the frequency domain (see section C) to supplement moments analysis. Clements [1969] has recently shown that fitting of a theoretical curve to an estimated frequency response produces a more accurate estimate of system parameters than does moments analysis. A recent paper by Østergaard and Michelson [1969] uses a form of frequency domain curve fitting to estimate the Peclet number in processes described by the axially dispersed piston flow model [Levenspiel and Bischoff, 1963]. This technique uses a particular mathematical property of the proposed model and is not generally applicable to all systems.

Another method has been recently proposed by Pëtho [1967, b]. According to this approach, a frequency response plot in magnitude $|G(j\omega)|$ and phase $\underline{/G(j\omega)}$ may be used to estimate the first moment μ and variance σ^2 from the first and second derivatives of $\underline{/G(j\omega)}$ and $|G(j\omega)|$ at $\omega = 0$:

$$\mu = - \lim_{\omega \to 0} \left[\frac{d/G}{d\omega} \right] \qquad \ldots \quad (3.1)$$

$$\sigma^2 = - \lim_{\omega \to 0} \left[\frac{d^2 \ln|G|}{d\omega^2} \right] \qquad \ldots \quad (3.2)$$

An examination of the relation between the frequency response and the cumulants of the impulse response presented in section II.A.2 (equs. II.A.2.10 and II.A.2.11) reveals that these results

may be generalised to:

$$\kappa_{2n+1} = \lim_{\omega \to 0} (-1)^{n+1} . (2n+1)! . \left[\frac{d^{2n+1} \angle G}{d\omega^{2n+1}} \right]$$

$$n = 0,1,2 \ldots \qquad \ldots \quad (3.3)$$

and

$$\kappa_{2n} = \lim_{\omega \to 0} (-1)^{n} . (2n)! . \left[\frac{d^{2n} |G|}{d\omega^{2n}} \right] \qquad \ldots \quad (3.4)$$

From a practical point of view, this approach must be rejected since it is extremely difficult to obtain derivatives of experimental data, especially high order derivatives, with any degree of accuracy.

The relation between direct moments analysis, which relies on the accuracy of large time values of data and this method which depends on the accuracy of small frequency values is nonetheless of interest.

Yet another alternative, which appears to be promising, is to fit, using conventional least squares regression techniques, equations of the form:

$$\ln |G(j\omega)| = a_o + a_2 \omega^2 + a_4 \omega^4 + \ldots \qquad \ldots \quad (3.5)$$

and

$$\angle G(j\omega) = a_1 \omega + a_3 \omega^3 + a_5 \omega^5 + \ldots \qquad \ldots \quad (3.6)$$

to the experimental data over a reliable frequency range. Moments may then be obtained from

$$\kappa_o = \ln \mu_o = a_o$$

$$\kappa_1 = \mu_1 = - a_1$$

$$\kappa_2 = \sigma^2 = -2! a_2 \quad \text{etc.}$$

This approach will be followed up in later work.

4. Application of Moments Analysis to Packed Bed Dynamic Testing

Chao and Hoelscher [1966] were the first to apply moments analysis to the dynamics of a packed bed system (mass transfer only in this case). The method of data reduction used has been described in Chao's thesis [1965]. A similar technique has been followed in the present work.

Thus the input pulse x'(t) and resulting output pulse y'(t) are first normalised to equal area using numerical integration. Thus whilst x'(t) may run from $0F^{o}$ to $4F^{o}$, x(t) goes from 0 to 1.0:-

$$x(t) = \frac{x'(t)}{\int_{o}^{\infty} x'(t)\ dt}$$

If the recording system were perfect and no heat losses occurred then

$$\int_{o}^{\infty} g(t)\ dt = \frac{\int_{o}^{\infty} y(t)\ dt}{\int_{o}^{\infty} x(t)\ dt}$$

$$= \lim_{\omega \to 0} G(j\omega) = 1.0$$

Normalisation in this manner has been justified in Appendix 4 since heat losses have a relatively small effect on the estimated system parameters. The estimated impulse response moments μ_G', σ_G^2 and π_G^3 may then be determined from equation B.1.1 through the

corresponding moments of input x(t) and output y(t). These values will have the units of time, $(\text{time})^2$ and $(\text{time})^3$ respectively. According to both finite stage and continuous models, the moments may be normalised in a similar way to equations II.B.3.10. Thus, assuming the validity of the extended continuous model (II.B.3):

$$N\sigma^{*2} = \frac{2}{Pe} + \frac{1 + 0.2Bi}{3St(1-\varepsilon)} \cdot \left(\frac{\mu-1}{\mu}\right)^2 \quad \ldots \quad (4.1)$$

$$N^2\pi^{*3} = \frac{12}{Pe^2} + \frac{2(1 + 0.2Bi)}{Pe\ St(1-\varepsilon)} \left(\frac{\mu-1}{\mu}\right)^2 + \frac{1 + 0.4Bi + 0.0572Bi^2}{6[St(1-\varepsilon)]^2} \cdot \left(\frac{\mu-1}{\mu}\right)^3 \quad \ldots \quad (4.2)$$

where $\sigma^{*2} = \sigma^2/\mu^2$

$\pi^{*3} = \pi^3/\mu^3$

When μ is large enough, (see Table II.D.4.1 for typical values) the ratio $1 - 1/\mu$ is close to unity so that the estimates of St and Bi (which are theoretically possible from equations (4.1) and (4.2), given an assumed value of Pe) are independent of μ. It may be noted, in fact that these estimates are independent of any assumptions about the holdup time or even of the recorder speed.

Setting Pe = 2 and defining a pseudo Stanton number St_{calc} in the manner of II.E.2.2 we obtain, from equation (4.1):

$$St_{calc} \simeq [3(1-\varepsilon).(N\sigma^{*2} - 1)]^{-1} \quad \ldots \quad (4.3)$$

The accuracy of the estimate of (4.3) depends on the accuracy of N and ε and on factors which influence the accuracy of the ratio σ^{*2}. It will be noted, from a study of Table V.B.2.1 that errors due to truncation are not likely to be quite so severe in this case. In the present work, V_H may be calculated from knowledge of the thermal properties of the system. When further normalisation with respect to holdup time L/v_a has been carried out we require $\mu = 1 + V_H$ to be satisfied to experimental accuracy. This is a first check on the validity of a model. As pointed out above however, an error in the first moment need not necessarily lead to an error in St_{calc}. This point is discussed further in Chapter VII., Section B.

In Chao and Hoelschers' work, Bi was assumed zero and equations (4.1) and (4.2) used to calculate the mass transfer analogies of St and Pe. In their work, μ was low (ranging from 1.2 to 1.9) so that estimates of these parameters depended on the accuracy of their time scale for μ as well as on the factors discussed above.

C. PULSE TO FREQUENCY RESPONSE METHODS

1. Fundamental Relations

The method of pulse to frequency response analysis has been widely discussed in the literature. For a recent literature survey, see Hays, Clements, jr. and Harris [1967]. According to this approach, the system transfer function $G(j\omega)$ is obtained by carrying

out numerical Fourier transforms of inlet and outlet pulses x(t) and y(t):

$$G(j\omega) = \frac{\int_0^{\infty} y(t).e^{-j\omega t}.dt}{\int_0^{\infty} x(t).e^{-j\omega t}.dt} \qquad \ldots (1.1)$$

The integrations of (1.1) actually cease when each pulse returns to zero say to T_y and T_x respectively. In evaluating equation (1.1) by direct methods the following trigonometric integrals are required:

$$A(\omega) = \int_0^{T_y} y(t).\cos \omega t.\ dt$$

$$B(\omega) = \int_0^{T_y} y(t).\sin \omega t.\ dt \qquad \ldots (1.2)$$

$$C(\omega) = \int_0^{T_x} x(t).\cos \omega t.\ dt$$

$$D(\omega) = \int_0^{T_x} x(t).\sin \omega t\ \ dt.$$

so that

$$G(j\omega) = \frac{A(\omega) - j\ B(\omega)}{C(\omega) - j\ D(\omega)} \qquad \ldots (1.3)$$

It is usual to then carry out, by parameter variation, a fitting of a theoretical model to the estimated or 'experimental' frequency response transfer function $G_e(j\omega)$ obtained from equation (1.3). In the control literature, methods of fitting 'lumped parameter' transfer functions to the modulus and argument form of $G_e(j\omega)$ have become highly developed. This approach is a logical and natural one when the data is already in this form as a result of a cyclic test (section A). Hays, Clements and Harris suggest that an alternative method of model or parameter fitting is more appropriate when the data is obtained by pulse testing. Their suggestion is discussed in some detail in section C.2 below.

2. Model Fitting in Time and Frequency Domains

Hays, Clements and Harris have discussed two methods of defining the error, ε between a model and experimental data. Assuming an impulse response (Section II A.1) may be obtained, then a comparison may be carried out in the time domain. The first method is to define the error $\varepsilon_1(t)$ by :

$$\varepsilon_1(t) = g_e(t) - g_p(t) \qquad \ldots (2.1)$$

where $g_e(t)$ is the experimental system impulse response and

$g_p(t)$ the model or predicted impulse response. For systems of the complexity discussed here, it should be apparent from the work in Chapter IV that computation of the impulse response may be difficult and prone to error. This is the main justification for carrying out modelling in the frequency domain, i.e. by comparing experimental and predicted frequency response transfer functions.

The second definition of error proposed is:

$$\varepsilon_2(t) = y_e(t) - y_p(t) \qquad \ldots (2.2)$$

where $y_e(t)$ and $y_p(t)$ are experimental and predicted system responses respectively. Both definitions become identical, of course, when the input pulse $x(t)$ is of short enough duration, relative to the impulse response, to be regarded as a perfect impulse. The convolution relations of section II.A.1 are used in computing $y_p(t)$ i.e.

$$y_p(t) = x(t) * g_p(t) \qquad \ldots (2.3)$$

An error criterion, $\phi = \phi[\varepsilon(t)]$, is required in the minimisation. Hays et al. suggest that since Rayleigh's Theorem [Bracewell, 1965, p.112] links the integral of the error squared in the time domain $\bar{\varepsilon}^2(t)$ with the corresponding integral in the frequency domain, model fitting may be performed in either domain according to convenience.

Thus, if

$$\mathcal{F}\,\varepsilon(t) = \varepsilon(j\omega) = R_\varepsilon(\omega) + jI_\varepsilon(\omega) \quad \ldots (2.4)$$

where, as indicated, $\varepsilon(j\omega)$ is a complex function of frequency, ω, then :

$$\phi(\varepsilon) = \int_{-\infty}^{\infty} |\varepsilon(t)|^2 .dt = \frac{1}{2\pi}\int_{-\infty}^{\infty} |\varepsilon(j\omega)|^2 .d\omega \quad \ldots (2.5)$$

As usual $|\ |$ denotes 'modulus of'.

Since $\varepsilon(t)$ is a real quantity, the modulus signs on the L.H.S. of equation (2.4) may be dispensed with and since $\varepsilon(t) = o, t < o$, the lower limit on the L.H.S. may be replaced by zero. Hays et al. then show that

$$\phi = \frac{1}{\pi}\int_{o}^{\infty} [R_\varepsilon^2(\omega) + I_\varepsilon^2(\omega)]\, dt, \quad \ldots (2.6)$$

so that "whilst ϕ depends on the squared scalar deviations in the time domain it depends upon the squared vectorial deviations in the frequency domain".

In fact, use may be again made of the Symmetry properties of the odd and even parts of $\varepsilon(t)$ (Appendix 5) to reduce equation (2.6) to

$$\phi = \int_{o}^{\infty} [\varepsilon(t)]^2 dt = \frac{2}{\pi}\int_{o}^{\infty} R_\varepsilon^2(\omega) d\omega$$

$$= \frac{2}{\pi}\int_{o}^{\infty} I_\varepsilon^2(\omega)\, d\omega, \quad \ldots (2.7)$$

so that <u>scalar</u> deviations based on <u>either</u> the real or

imaginary parts of the transformed errors may be used, since both are equivalent. This approach is used in the experimental work reported in Section VII.G.

If the second definition of error is used (equation 2.2) then since:

$$\varepsilon(j\omega) = X(j\omega) .[\, G_e(j\omega) - G_p(j\omega)] \,,$$

we have

$$\phi_2 = \frac{1}{\pi}\int_0^{\infty} [\,|X(j\omega)| \,.\, |G_e(j\omega) - G_p(j\omega)|\,]^2 \, d\omega \quad \ldots(2.8)$$

whilst equation (2.1) yields instead :

$$\phi_1 = \frac{1}{\pi}\int_0^{\infty} [\,|G_e(j\omega) - G_p(j\omega)|\,]^2 d\omega \quad \ldots (2.9)$$

Using equation (2.7) this then reduced to+

$$\phi_1 = \frac{2}{\pi}\int^{\infty} [R_e(\omega) - R_p(\omega)]^2 \, d\omega$$

$$= \frac{2}{\pi}\int_0^{\infty} [I_e(\omega) - I_p(\omega)]^2 \, d\omega \quad \ldots(2.10)$$

Hays then observes that when equations (2.8) and (2.9) are compared, $|X(j\omega)|$ may be "interpreted as a weighing function measuring the relative reliability of the deviations at each frequency". This observation assumes great practical importance when the inlet pulse x(t) is not short relative to the impulse

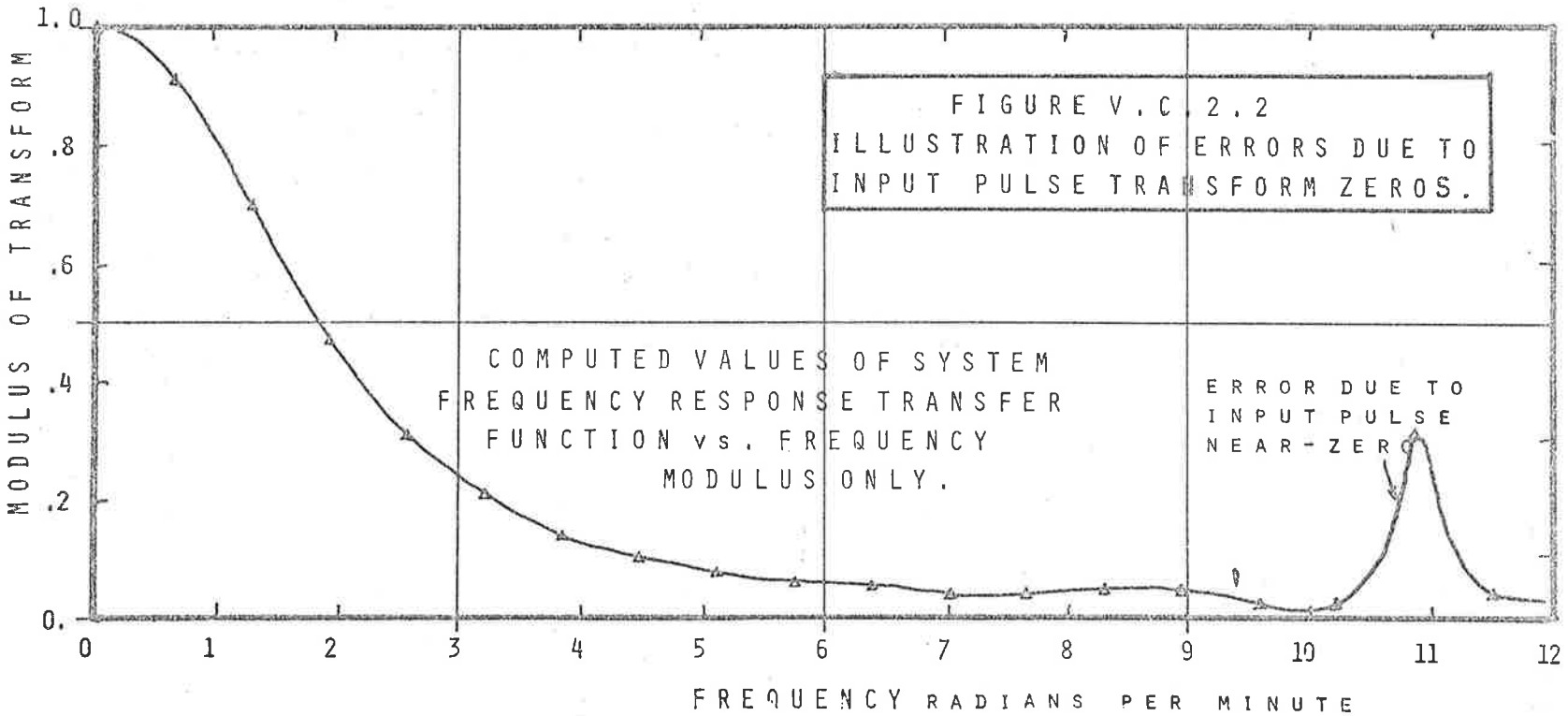
FIGURE V.C.2.2
ILLUSTRATION OF ERRORS DUE TO
INPUT PULSE TRANSFORM ZEROS.
COMPUTED VALUES OF SYSTEM
FREQUENCY RESPONSE TRANSFER
FUNCTION vs. FREQUENCY
MODULUS ONLY.
ERROR DUE TO
INPUT PULSE
NEAR-ZERO
MODULUS OF TRANSFORM
1.0
.8
.6
.4
.2
0.
0
1
2
3
4
5
6
7
8
9
10
11
12
FREQUENCY RADIANS PER MINUTE

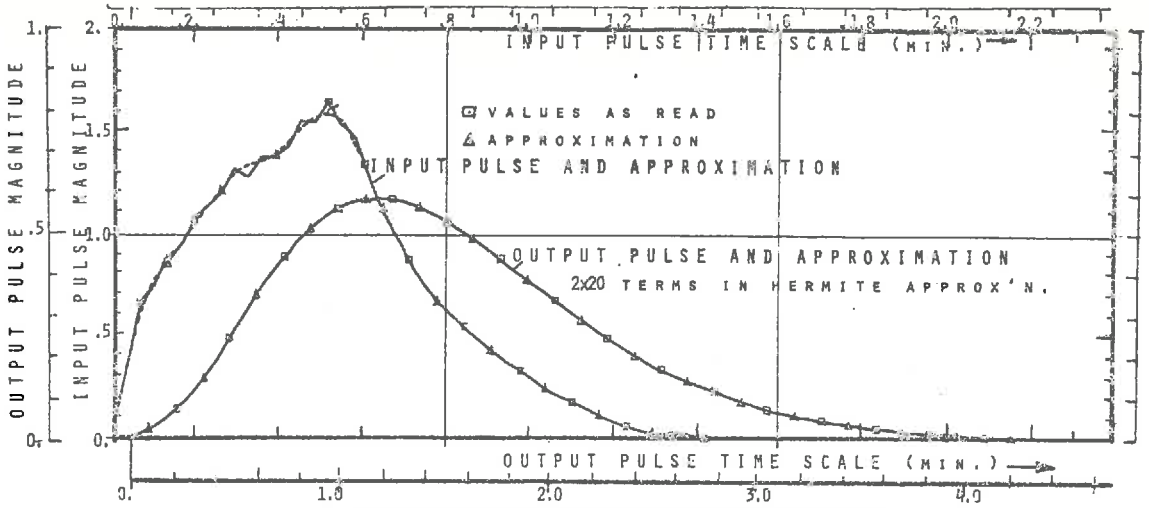

FIGURE V.C.2.1.
ILLUSTRATION OF ERRORS DUE
TO INPUT PULSE TRANSFORM ZEROS

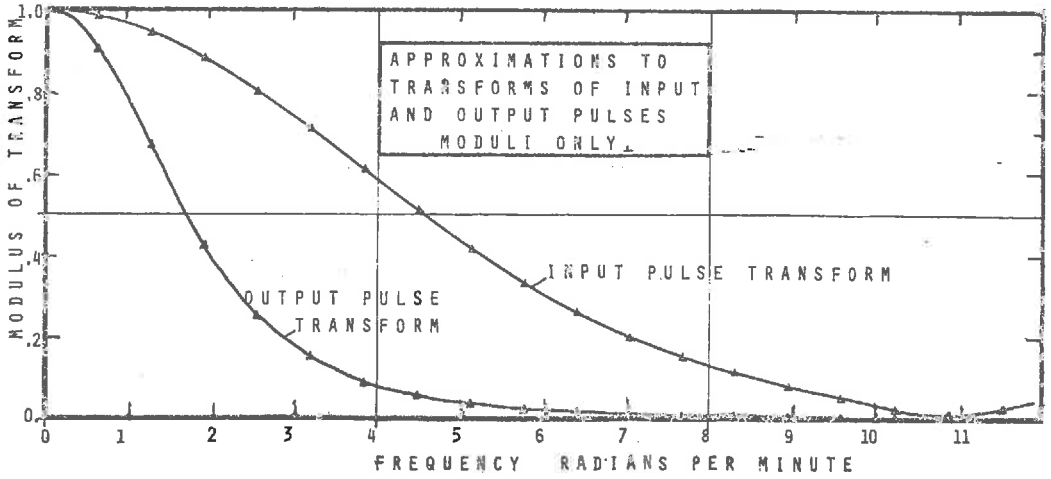

response of the system. In this case, zeros or near-zeros may occur in the estimated input pulse spectrum $\bar{X}(j\omega)$ in the frequency range of interest. Since the convolution relation holds for the system under test,

i.e. $Y(j\omega) = X(j\omega).\ G(j\omega)$,

any zeros in $X(j\omega)$ will theoretically occur at the same frequencies in $Y(j\omega)$, so that $G(j\omega)$ merely becomes indeterminant. From a practical point of view however, both $\bar{X}(j\omega)$ and $\bar{Y}(j\omega)$ are in error by (hopefully) small quantities $\varepsilon_x(j\omega)$ and $\varepsilon_y(j\omega)$. If $X(j\omega)$ is small, then the effect of $\varepsilon_x(j\omega)$ on the estimated transfer function $G_e(j\omega)$ may become large since

$$G_e(j\omega) = G(j\omega) \pm \varepsilon_G(j\omega) = \frac{Y(j\omega) \pm \varepsilon_y(j\omega)}{X(j\omega) \pm \varepsilon_x(j\omega)}$$

This is illustrated by an early experimental pulse test carried out at high flow on a short bed of soda glass prior to experimental modifications described in section VI.C.1. The run, carried out on 11.9.68 (and not included in Chapter VII) had an inlet pulse x(t) which was long relative to the system impulse response. The experimental pulses and their Fourier transforms, performed by the method of Hermite polynomial approximation developed in Section C.3, are plotted in figures C.2.1. and C.2.2.

It may be seen that at a frequency of 11.0 radians per minute, the input pulse magnitude or modulus, $|X(j\omega)|$

becomes nearly zero. When the estimated system impulse response Fourier transform or frequency response transfer function $G_e(j\omega)$ is evaluated, using equation (C.1.3) a spurious peak results in $|G_e(j\omega)|$ which would also be reflected in $R_e(\omega)$ and/or $I_e(\omega)$, (although these were not computed on this occasion). If the error criterion ϕ_2 of equation (2.8) is used instead of ϕ_1 , little weighting is given to the values of $G_e(j\omega)$ in the vicinity of ω = 11/min., since $X(j\omega)$ is itself small here.

It is concluded therefore that parameter fitting should in general be carried out by comparing predicted and measured outputs (or output transforms) rather than by comparing estimated impulse responses (or transfer functions).

3. Orthogonal Polynomial Methods of Fourier Transformation

(i) Hermite Polynomials

In evaluating the integrals of equation (C.1.1) by direct numerical methods, difficulty is experienced in devising a rational basis for error analysis. In addition to the problems described above, arising from zeros or near-zeros in the input pulse spectrum, certain oscillations have been reported in the evaluated integrals even when the input pulse may be regarded as an ideal impulse. Lees and Dougherty [1967] present an interesting discussion of this difficulty. They ascribed the problem to the use of finite summations to approximate the

continuous integrals and suggest the following empirical relationship between the maximum "reliable" frequency ω_{max} and the mesh spacing, δ, between samples :

$$\omega_{max} = 0.1\pi/\delta \qquad \ldots(3.1)$$

The criterion appears to yield a realistic estimate of ω_{max} for any given δ. See Jeffreson, [1970b] for the application of this technique to the analysis of the dynamics of an unstirred mixer .

Hays, Clements and Harris have suggested the application of more powerful numerical approximation procedures to the integration but do not present any suitable measure of the error between the approximation and the data.

As a result of the uncertainties revealed by Lees and Dougherty's paper, an alternative method of Fourier transformation was developed for the present experimental programme. The method is simply the reverse of that discussed in Chapter IV for Fourier transform inversion.

Thus each pulse is approximated by a finite sum of weighted Hermite polynomials which may be separated into odd and even parts. For example, for the input pulse x(t):

$$x(t) \simeq \bar{x}(t) = \sum_{n=0}^{2N} a_n \cdot H_n(t) \cdot e^{-t^2/4}$$

$$= \sum_{n=0}^{N-1} a_{2n+1} \cdot H_{2n+1}(t) \cdot e^{-t^2/4}$$

$$+ \sum_{n=0}^{N} a_{2n} \cdot H_{2n}(t) \cdot e^{-t^2/4}$$

$$= \emptyset [\bar{x}(t)] + E[\bar{x}(t)] \quad \ldots (3.2)$$

where, in a similar manner to before

$$a_n = \frac{1}{n\sqrt{(2\pi)}} \int_0^{T_{max}} e^{-t^2/4} \cdot x(t) \cdot H_n(t) \cdot dt \quad \ldots (3.3)$$

From symmetry considerations (Appendix 5) the odd and even parts of the approximation are Fourier transformed to the imaginary and real part of the approximation to $X(j\omega)$ respectively, that is, to approximations to $C(\omega)$ and $-D(\omega)$ of equations (1.2) and (1.3).

As in Chapter IV.C.3, a scale factor Z is chosen for each pulse which will ensure a good approximation for the number of terms used. When each pulse has been approximated, the integral $(\text{error})^2$ is calculated, together with the maximum error. The actual approximation and error is then printed out. This shows

up gross errors in reading the data and may suggest an alternative choice of scale factor to improve the approximation. The trend of the integral $(\text{error})^2$ as terms are added also suggests whether further improvement is possible and is useful in subsequent error analysis.

Having satisfactorily approximated input and output pulses, the Fourier transform of each is calculated using

$$\sum_{n=0}^{2N} a_n . H_n(t) . e^{-Z^2 t^2/4}$$

$$= 2\sqrt{\pi} \sum_{n=0}^{2N} a_n . e^{-\omega^2/\varepsilon^2} . (j)^n . H_n(2\omega/Z) \qquad \ldots .(3.4)$$

and the similarity theorem used to recover the approximations to $A(\omega)$, $-B(\omega)$, $C(\omega)$ and $-D(\omega)$ in equation (1.3).

The spectra of input and output pulses should be printed out and examined for zeros. Finally the Hermite polynomial approximation to $G(j\omega)$ is printed out in real or imaginary form or in modulus and argument form. Alternatively, the approximation to $X(j\omega)$ (the input pulse spectrum) is used, together with a suitable mathematical model, to obtain $Y_p(j\omega)$, the predicted output pulse spectrum.

(ii) Laguerre Polynomials .

Since developing the above technique, Anderssen and White [1969] have applied the Dooge method [1965] of pulse analysis to a mixing problem. According to this approach, each pulse is

approximated by an exponentially weighted sum of Laguerre polynomials computed in a similar way to equ. (3.2). Having carried out the approximations, the Laguerre coefficients for the estimated impulse response are obtained from the coefficients of the input and output approximations. Thus if

$$\bar{x}(t) = \sum_{n=0}^{N} a_n \psi_n(t)$$

$$\bar{y}(t) = \sum_{n=0}^{N} b_n \psi_n(t) \qquad \ldots (3.5)$$

then the coefficients c_n of

$$\bar{g}_e(t) = \sum_{n=0}^{N} c_n \cdot \psi_n(t) \qquad \ldots (3.6)$$

are obtained explicitly from the a_n and b_n, where the $\psi_n(t)$ are Laguerre functions, defined below.

In the present work, time domain modelling (for which the Dooge method is designed) would be difficult because of the complexity of the models considered. Now, transforming equations (3.5) and (3.6) and applying the convolution relation we have

$$\sum_{n=0}^{N} c_n \psi_n(j\omega) = \bar{G}_e(j\omega) = \frac{\bar{Y}(j\omega)}{\bar{X}(j\omega)} = \frac{\sum b_n \psi_n(j\omega)}{\sum a_n \psi_n(j\omega)} \qquad \ldots (3.7)$$

The values of $\bar{G}_e(j\omega)$ obtained by direct division of the two

series must be identical to those obtained from the c_n obtained by the Dooge method. Hence, we may expect that the values of ψ_1 of equation (2.9) will be identical whether obtained by the Dooge method (using time domain modelling) or by direct division using frequency domain modelling. Frequency domain modelling has the advantage however that the number of terms in the series in the numerator of equation (3.7) may differ from the number of terms in the denominator (this is not allowed by the Dooge approach). Furthermore, the direct method used in the present work allows differing scale factors to be used in numerator and denominator so that each approximation has a minimum integral error squared. Preliminary comparison between Hermite and Laguerre polynomials has been carried out using data of SectionVII.GThe Laguerre approximations had a slightly higher error than the Hermite in each case.

The procedure for use of Laguerre functions in frequency domain analysis is very similar to that for Hermite functions and the appropriate equations are listed below. These may be compared with equations (3.1) and (3.2).

$$x(t) \simeq \bar{x}(t) = \sum_{n=0}^{N} a_n . L_n(t) . e^{-t/2} \qquad \ldots (3.8)$$

where $L_n(t)$ is the Laguerre polynomial of degree n and defined by the recurrence relations :

$$\left.\begin{aligned} (n+1).L_{n+1}(t) &= (2n+1-t).L_n(t) - nL_{n-1}(t) \\ L_0(t) &= 1, \quad L_1(t) = 1-t \end{aligned}\right] \qquad \ldots (3.9)$$

V.C.3.
V.C.4.

$$\text{and } X(j\omega) \simeq \bar{X}(j\omega) = \sum_{n=0}^{N} a_n \cdot \frac{[j\omega - \tfrac{1}{2}]^n}{[j\omega + \tfrac{1}{2}]^{n+1}} = \sum_{n=0}^{N} a_n \, \psi_o(j\omega) \, [1 - \psi_o(j\omega)]^n \quad \ldots (3.10)$$

$$\text{where } \psi(j\omega) = L_o(t) \cdot e^{-t/2} = \frac{1}{j\omega + \tfrac{1}{2}} \quad \ldots (3.11)$$

The second form of equation (3.10) is most suitable for computer evaluation since each previous term may be simply multiplied by $(j\omega + \tfrac{1}{2})$ at each frequency value. Scale factors, Z_1 and Z_2 for input and output pulses are chosen and the Similarity Theorem used in an identical manner to the procedure described for Hermite polynomials.

4. Preliminary Suggestions for a Method of Error Analysis via Orthogonal Polynomial Approximation Procedures.

An important real and potential advantage of either orthogonal polynomial procedure over direct Fourier transformation when used for frequency domain analysis is that an estimate of the error in the approximation is available.

Thus, suppose we vary the parameters of a model, comparing the predicted output spectrum or frequency response transfer function with the corresponding experimental quantity until a minimum in an error criterion, such as that defined by equations (2.8) or (2.9), is achieved. Then, if the integral error squared between $R_e(\omega)$ and $R_p(\omega)$ is still 'significantly' larger than the

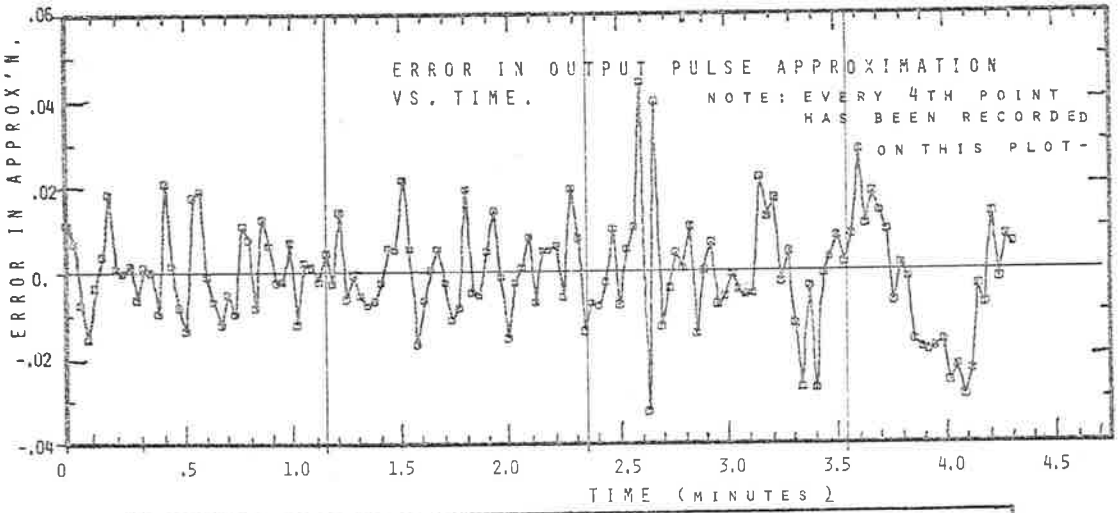

FIGURE V.C.4.1

RESIDUAL ERRORS REMAINING AFTER HERMITE APPROXIMATIONS TO PULSES OF FIGURES C.2.1 AND C.2.2

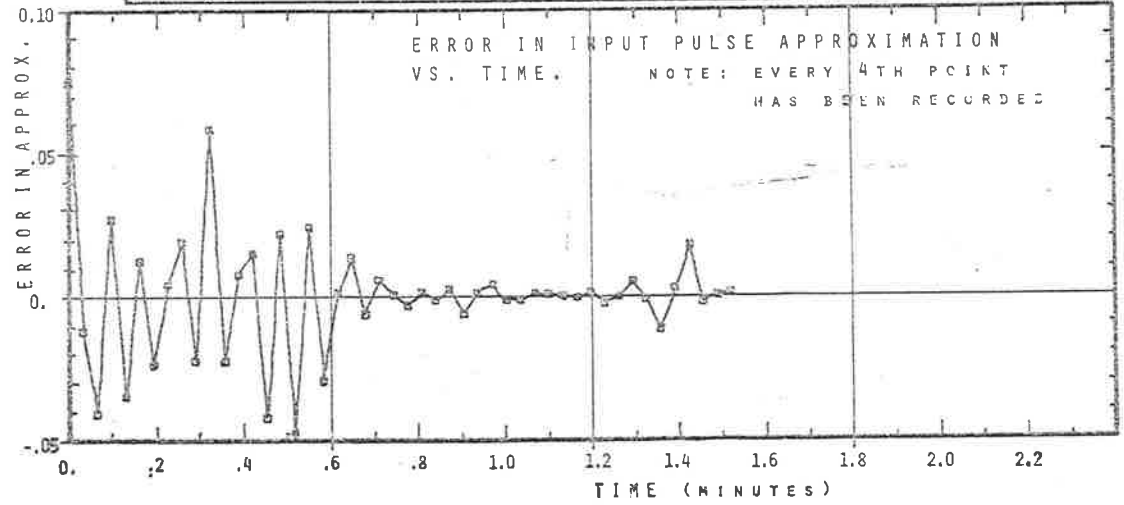

error between $R_e(\omega)$ and the experimental data, we may consider that the model does not give a very good fit to the data.

A further advantage of either approximation procedure is that when suitable scaling has been carried out, the residual error generally comprises random curve reading errors. This is because the operation of approximation is similar to that of passing the 'signal' through a low pass filter (in network theory terminology). This also ensures that random errors in reading and random 'noise' imposed on the data by external sources are 'smoothed' out objectively rather than subjectively, as occurs when the data is smoothed by eye. As a typical example of the random nature of error remaining after a good approximation has been achieved, plots of error in input and output approximations for the soda glass run quoted in Section C.2 are presented in figure C.4.1. The integral errors for input and output pulses were 7.14×10^{-4} and 6.89×10^{-6} respectively on a time scale normalised to the estimated first moment of the impulse response. Pulse $\hat{a}$reas were each normalised to an area of unity.

The precise nature of the statistical tests to be carried out have yet to be defined in detail. A simple variance-ratio analysis may perhaps be appropriate to test the significance of a parameter fit achieved, where the number of degrees of freedom would be related to the number of readings taken. The significance

of a parameter fit will be reduced by an excessive amount of 'noise' in the readings since this reduces the reliability of the data. A F ratio test would allow for this, provided the data is not smoothed beforehand. Further and more quantitative analysis along these lines is left for later work.

In addition to the above concepts, used qualitatively in the present work, an inequality, derived in Appendix 8, allows the maximum likely error in the frequency domain to be estimated, given the integral square approximation error $\bar{\varepsilon}^2(t)$ in the time domain :

$$R_\varepsilon(\omega) \leq 2\sqrt{[T_{max}.\bar{\varepsilon}^2(t)]} \qquad \ldots (4.1)$$

This inequality has not been rigorously derived - nonetheless, it does allow an estimate of the maximum 'reliable' frequency in the approximation to be made. If T_{max} is about 3. for example, then in order to keep the error in $R(\omega)$ less than 0.04, we require an integral error square less than 1.3×10^{-4}.

A useful feature of both the pulse methods discussed so far is that the ratio of the zero'th moments provides, for an accurately calibrated measuring system, an estimate of heat loss from the bed. As before both pulses are normalised to unit or equal area before commencing the analysis.

D. STEP RESPONSE ANALYSIS

1. Previous Work

Comparison of the experimental breakthrough curve u(t), or response to the perfect step input [equ. (II.A.1.3.)], with

theoretical solutions such as those discussed in chapter IV may be used to determine the applicability of a model and values of parameters in the model.

The arithmetic probability plot method of Babcock and co-workers has been introduced in section IV.B.2. Since the plots are expected to give straight lines the slopes may be used to determine the equivalent conductivity model Peclet number Pe_a. Curve matching, using the measured time between 20% and 80% of completion was used by Handley and Heggs to determine values of KV_H.

Other workers in the field of linear ion exchange [Colwell and Dranoff 1966] and adsorption [Stuart and Camp, 1967; Antonson and Dranoff, 1967; Rimpell, Camp, Kostecki and Canjar, 1968] have matched breakthrough curves against mass transfer versions of the Rosen solution (IV.A.2).

Yet another method, that of Fourier transformation of $\phi(t)$, the difference between the normalised step response and its final value [eqn. (IV.A.3.2.)] has been applied to heat transfer studies in packed beds by Healy [1967].

Each of the methods listed above assumes that a perfect or near perfect step function has been applied to the bed. This may be difficult unless the bed response is much slower than that of the apparatus used to administer the step. It should also be

noted that an independent estimate of the 'centre of mass' $\mu(t)$ of equation (IV.D.2.1) is usually required. Errors in estimating $\mu(t)$ may lead to errors in normalising the time scale and hence to errors in estimation of the other parameters. In section 2, the moments expansion of section II.A are used to increase the power of the step response technique.

2. Fundamental Relations

In section IV.A.3, the following relation between $\phi(t)$, where

$$\phi(t) = U(t) \quad [1 - u(t)]$$

and the real and imaginary parts $R(\omega)$ and $I(\omega)$ of the frequency response transfer function was derived:

$$\mathcal{F}[\phi(t)] = - \frac{I(\omega)}{\omega} - j \frac{[I - R(\omega)]}{\omega} \qquad \ldots (2.1)$$

A more general relation, when the 'gain' or zero'th moment μ_o' is not unity is obtained by replacing $[1-R(\omega)]/\omega$ by $[\mu_o' - R(\omega)]/\omega$ in equation (2.1). Numerical Fourier transformation of $\phi(t)$ was the method used by Healy to obtain $G(j\omega)$ from the step response or breakthrough curve.

If the moments expansion of $G(j\omega)$ given by equation (II.A.2.4.) is substituted into equation (2.1) we have

$$\frac{-I(\omega)}{\omega} = \mu'_1 - \frac{\mu'_3}{3} \cdot \frac{\omega^2}{2!} + \frac{\mu_5}{5} \cdot \frac{\omega^4}{4!} - \ldots$$

$$= \mu'_{\phi_0} - \mu'_{\phi_2} \cdot \frac{\omega^2}{2!} + \mu'_{\phi_4} \cdot \frac{\omega^4}{4!} - \ldots \ldots \ldots (2.2)$$

and

$$-\frac{1-R(\omega)}{\omega} = \frac{-\mu'_2}{2} \cdot \omega + \frac{\mu'_4}{4} \cdot \frac{\omega^3}{3!} - \ldots$$

$$= -\mu'_{\phi_1} \cdot \omega + \mu'_{\phi_3} \cdot \frac{\omega^3}{3!} - \ldots$$

where μ'_{ϕ_n} denotes the n'th absolute moment of $\phi(t)$.

Hence the following fundamental relation between the moments of $\phi(t)$ and of $g(t)$ is obtained :

$$\boxed{\mu^*_{\phi_n} = \frac{\mu'_{n+1}}{n+1}} \qquad n = 0,1,2, \ldots \ldots (2.3)$$

3. Application of the Fundamental Relationship

Equation (2.3) allows the perfect step response to be used to determine the moments of the impulse response. It is, in fact, a generalisation of a method used by Antonson and Dranoff to obtain the distribution coefficient for ethane adsorption onto molecular sieves and by Rimpell et al. to determine adsorption isotherms for propane on activated alumina.

It is instructive to translate their derivations into heat transfer terminology. Suppose a perfect step of $\delta T_i F^o$ is applied to a packed bed, all initial conditions zero and that this results in a step response δT_i. U(t) where U(t) is the unit step response.

Then at time t, total heat input is

$$q_i(t) = \delta T_i . W. c_f \int_o^t dt$$

where as before, W is the total weight flowrate of fluid through the section and c_f is the fluid heat capacity. Heat output from the bed, ignoring wall heat losses is given by

$$q_o(t) = \delta T_i W. c_f \int_o^t u(t)\, dt$$

As the response approaches completion ($t \to \infty$) we have

$$\lim_{t\to\infty} [q_i(t) - q_o(t)] = \text{Heat retained in packing and interstitial fluid.}$$

i.e. $$W.c_f . \delta T_i \int_o^\infty [1-u(t)]\, dt = [Mc_S + M_f c_f] . \delta T_i$$

$$\mu_{\phi_o} = \int_o^\infty \phi(t)\, dt = (1 + V_H) \frac{L}{v_a} = \mu(t) \quad \ldots (3.1)$$

Where $\mu(t)$ is the centre of mass of the impulse response expressed

in time units as in section IV.D.2. It may be seen that equation (2.3) is an extension of equation (3.1).

The central moments of g(t) may also be estimated from μ_{ϕ_n}. For example, since for $\mu'_o = 1$,

$$\sigma^2 = \mu'_2 - \mu'^2_1 \ ,$$

we have

$$\sigma^2 = 2\mu'_{\phi_1} - \mu'^2_{\phi_o}$$

where σ^2 is the variance of the impulse response density function. The above relations have been applied to analysis of the experimental data obtained using lead spheres, in section VII.C.3. whilst a rather detailed analysis of the effects of two common errors on the accuracy of the results is given in section VII.C.5.

4. Extension to and Simplification of the Method of Handley and Heggs .

The empirical relations obtained in section IV.D.2 may be used to estimate σ^* provided an accurate estimate of $\mu(t)$ is available. This method has the advantage of speed and simplicity for on the spot analysis of experimental data. As a check on the validity of a model it should be noted that the times 5 to 80% 10% to 80%, 20% to 80% and 40% to 80% should each give the same

value of σ^*, within experimental accuracy, for a particular model to be valid.

It should be noted however, the earlier values (5% and 10%) are likely to be distorted by the imperfect nature of an experimental 'step' input.

The main limitation of this approach is that when γx or KV_H/Bi is less than about 10 (as in the case of short beds of poorly conductive particles), the empirical correlations are not strictly valid. Also, since only two points are taken on a curve and since ΔT is squared to obtain St, errors are magnified. As noted above, the accuracy of the extended Handley and Heggs' method depends on the accuracy to which $\mu(t)$, the centre of mass of the impulse response is obtained. Heggs appears to have overcome this problem of inaccuracy in determining $\mu(t)$ by his 'analogous curve' check by allowing $\mu(t)$ to also vary until a double check is achieved. The method finally adopted (chapter VII) was to use equation (D.2.3) to obtain $\mu(t)$ for use with the empirical correlations.

In section VII.C.4, the extended method of breakthrough curve analysis is applied to experiments on a packed bed of lead spheres whilst in section VII.C.6 an attempt is made to assess the effects of two common experimental errors on the calculated values of σ^*.

E. SUMMARY OF CONCLUSIONS OF CHAPTER V.

It was concluded in section A and appendix 10 that frequency response methods of analysis using cyclic testing were subject to large errors at high frequencies. Methods of testing which relied on an assumed limiting value of the magnitude ratio $|G|$ were shown to be particularly prone to errors due to heat loss and support and wall capacitance (for heat transfer experiments) and to measurement probe and recorder limitations. Reliance on limiting high frequency behaviour also led to an experimental design with undesirable features, in particular a short and non-representative test section. It was concluded that cyclic test methods were of more general use under low flow conditions provided curve fitting was carried out over a range of frequencies so that undue emphasis was not placed on any particular part of the spectrum.

Consideration of the difficulty in generating pure sine waves and of the considerable time required to complete a test over a representative range of frequencies led to rejection of this method for the present experimental programme.

The fundamental relations derived in section II.A.2 were used to generalise the method of Rosen and Winsche and led to a more clear understanding of the reasons for the limitations of phase angle analysis in either cyclic or pulse to frequency response testing.

In section B, the fundamental relations of II.A.2 were used to generalise the imperfect pulse method of moments analysis of Aris and to generalise Pethö's method of frequency domain analysis. The practical disadvantages of each were also discussed.

In section C, methods of parameter fitting in the 'frequency domain' were discussed and a simplification made to the error criteria derived by Hays, Clements and Harris. The theoretical basis for the Fourier transformation of pulse data by either Hermite or Laguerre polynomial techniques was presented and it was concluded that this approach should allow (ultimately) a rigorous analysis of the significance of model fitting in either time or frequency domains. It was also concluded that parameter estimation and modelling based on a fitting of the Fourier transform of the output pulse from the system to a predicted (model) output pulse is less likely to introduce errors due near zeroes in the input pulse spectrum than comparisons based on the impulse response or frequency response transfer function.

A relation was derived for estimation of impulse response moments from a step response or breakthrough curve. The accuracy of the method is to be tested in Chapter VII.

An alternative method of step response parameter estimation, based on the empirical correlations of section IV.D.2 was proposed. The method is similar in principle to that used by Heggs but may be expected to be simpler.

CHAPTER VI

EXPERIMENTAL METHODS AND APPARATUS

SCOPE OF THE CHAPTER

This chapter discusses the design and operation of the experimental apparatus used in the test programme completed so far. The results obtained are presented in chapter VII.

In section A, the objectives of the experimental programme and their influence on the experimental design are outlined.

Section B describes the results of some preliminary work on the response of the thermocouples used in measuring temperature within the packed beds.

Section C describes the final experimental apparatus used and the operation of the baseline control system.

A. OVERALL DESIGN OF THE EXPERIMENTAL PROGRAM

1. General Objectives

The main objective of the experimental program was to test the validity of the various mathematical models discussed in earlier chapters. Establishment of a reliable fluid-particle heat transfer correlation was fundamental to the whole experimental design (see chapter I). Thus, fluid particle heat transfer coefficients must have the same meaning irrespective of the conditions of the experiment. The alternative, of using 'pseudo' Stanton numbers which ensure a good fit between a particular mathematical model and experimental results, is unacceptable if the model is to be of other than limited value.

It became apparent, as experiments proceeded, that a study of experimental techniques per se was also necessary.

The way in which particular objectives affected the experimental design is discussed in section 2. It will be seen that in some cases, these objectives had conflicting influences.

2. Detailed Objectives and Constraints

(a) Bed length and heat losses

It appeared, from early theoretical studies, that fluid phase axial dispersion effects would be most important at short bed lengths [Epstein, 1958]. To eliminate indeterminate end effects, it was decided to insert the temperature probes within the bed at varying axial distances along the bed.

It was expected that heat losses, if present, would cause distortion of the shape of the response curves. Significant heat losses would be detected by the presence of radial temperature gradients within the bed. Hence the probes were designed to provide either an averaged fluid temperature across a plane or point measurements at different radial distances from the centre line.

Thermocouple thermometry was chosen therefore, rather than a resistance wire method. It was found that for the range of flow-rate tested, radial gradients were not detectable even when comparison of steady temperature rise at the outlet with a steady inlet temperature increase indicated heat losses of 10% or more. Subsequent theoretical analysis (Appendix 4) suggested that distortion of the response due to heat loss would be insignificant.

According to assumption (b) of section I. C, the temperature changes administered were to be small in order to minimise density and other fluid property changes. Thermocouples were therefore arranged in thermopile and a high sensitivity (100μ V / inch) recorder used by courtesy of the Australian Institute of Nuclear Science and Engineering.

(b) Intraparticle Conduction Effects

In order to determine experimentally the effects of Biot number on the shape of step and pulse responses, packing materials of differing thermal conductivity were chosen. Lead was used as a high thermal conductivity control, and soda glass and 'Perspex' beads were used to yield intermediate and high Biot numbers, respectively. Since probes were inserted in the bed, electrical short circuiting was avoided, for lead experiments, by means of soda glass beads packed around the particular layer of interest

The influence of support screens on the dynamic response at high frequencies (see Appendix 10) was another reason for inserting wires into the bed rather than downstream of the packing support. Downflow was chosen to prevent fluidisation at high velocities.

(c) Influence of Heat Capacity Ratio

At the time of designing the experimental apparatus, (1967) a rigorous analysis of the influence of heat capacity ratio, V_H, was not available. Previous experiments in the literature at the time had used air at atmospheric or near-atmospheric pressure. It was considered that the simplest way to vary V_H would be to vary operating pressure i.e. to vary the gas density, ρ_f in

$$V_H = \frac{\rho_s . c_s . (1-\varepsilon)}{\rho_f . c_f . \varepsilon} .$$

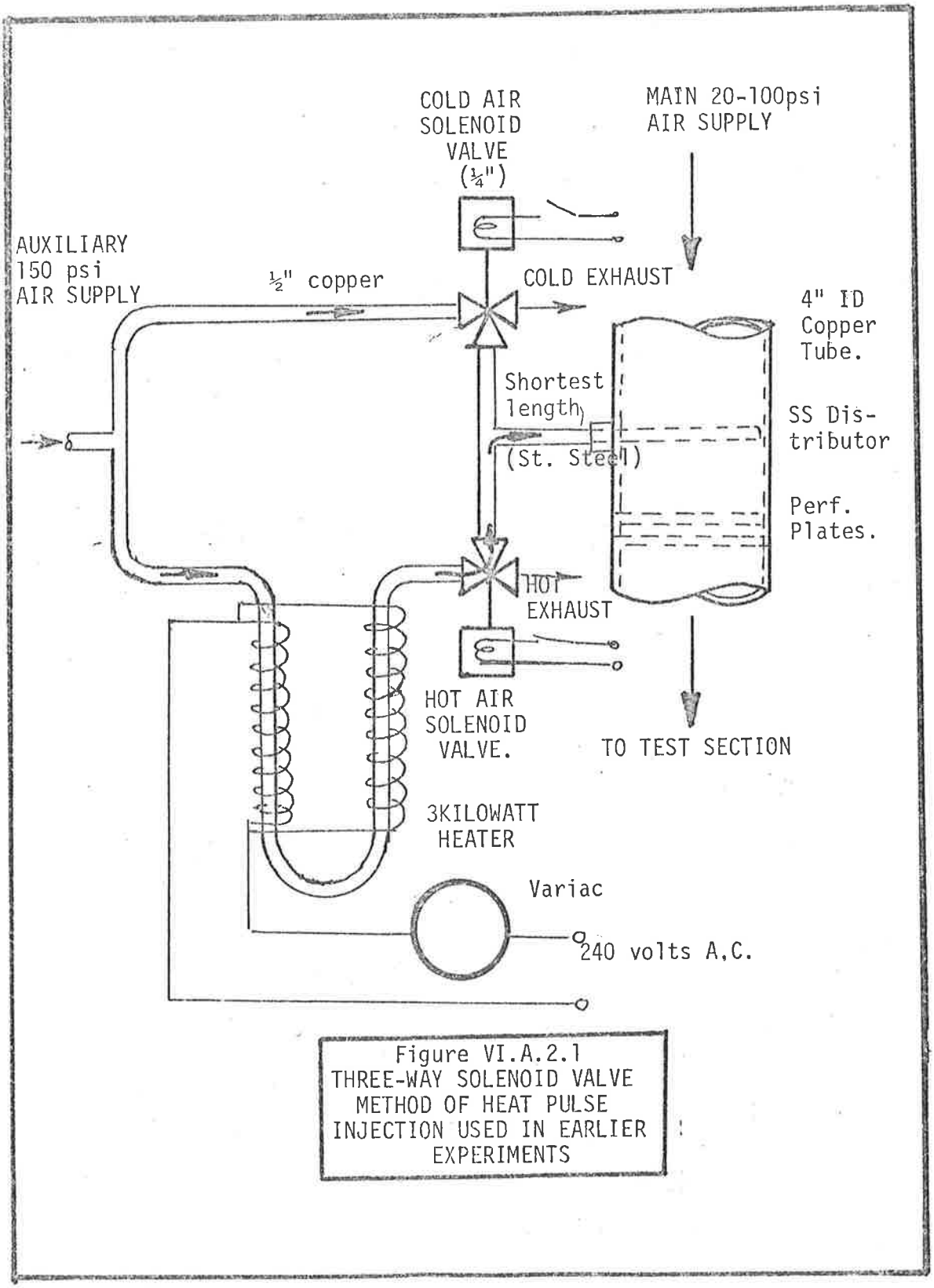

Figure VI.A.2.1
THREE-WAY SOLENOID VALVE
METHOD OF HEAT PULSE
INJECTION USED IN EARLIER
EXPERIMENTS

A 7:1 variation in V_H would thus be achieved by varying absolute operating pressure from 15 p.s.i.a. to 105 p.s.i.a. This resulted in a rather heavy (1/8") wall and required internal thermal insulation with a P.V.C. liner to minimise heat loss and capacitance effects.

(d) Dynamic Testing Techniques - Effects of Tailing

Because of the difficulty in generating suitable 'pure'sine waves, [section V.A.2.(i)] pulse test and step test methods were chosen.

Pulses were applied in early tests by the method illustrated in figure A.2.1. Either hot or cold air could be administered through the two simultaneously - operated three way solenoid valves illustrated. It was found that, whilst initial rise and fall times were very fast, the heat capacity of the fittings resulted in a large drawn-out'tail'on the input pulse. This resulted in an even more elongated output pulse and made determination of the correct 'cut-off' point, difficult.

A slow 'drift' in compressor air temperature made tailing even more serious so that the reproducibility of moments analysis experiments was very poor, particularly for the third moment or skewness (see section VII.B.4)

After the solenoid switching gear was replaced by a fine wire Nichrome heater, tailing was still present despite the small wire thermal capacity. The results were, in fact very similar to those reported by Healy [1967], who also used a fine wire electrical heater in studies of the dynamics of packed and fluidised beds. The experimental record obtained by Healy shown on figure A.2.2 is typical of the 'tailing'which occurred in the present experiments.

The solution to this problem - base line feedback control is described in section C.1.

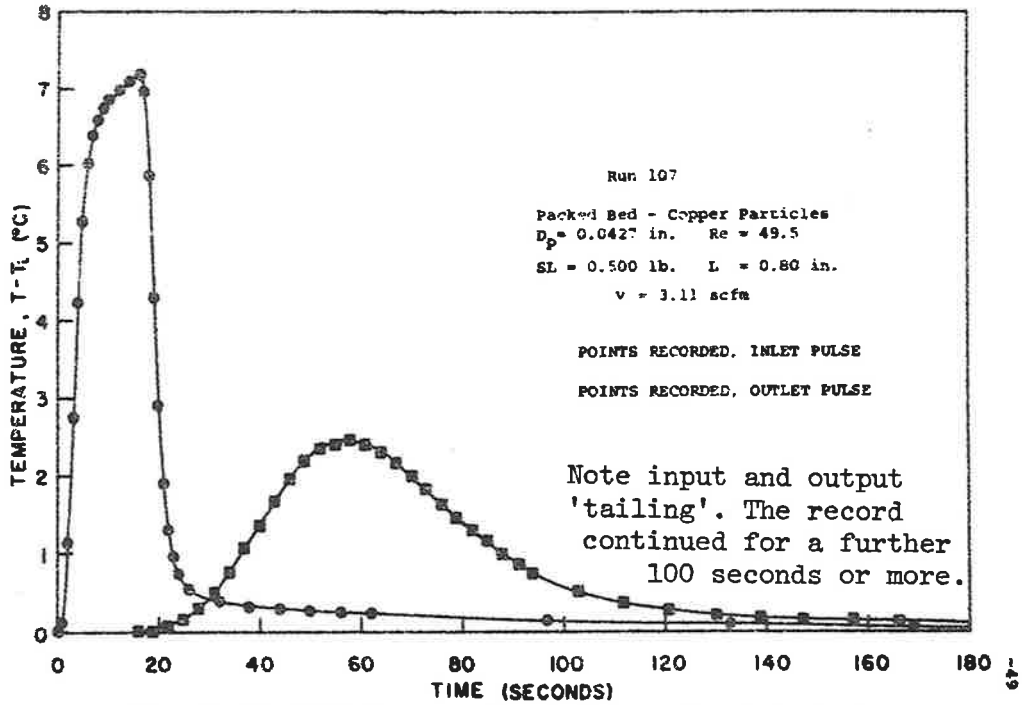

Figure 5. Time-temperature record for a typical run using a pulse input

FIGURE IV. A.2.2

EXPERIMENTAL PULSE RESULTS OF HEALY (1967)

(e) Packing Methods And Porosity

Since fine wires were used for temperature measurement, it was necessary to develop a reproducible method of packing which avoided breakage. The bed was placed under suction by means of a vacuum cleaner and the packing injected into the bed through an injection tube passing between the wires. Separate porosity measurements on a simulated test section (Appendix 11.1) showed that good reproducibility resulted, with negligible voidage variations due to the thermocouple wires.

The porosity resulting was very low for a random packing (35.6%), presumably because the beads were injected rather than poured in. Near the support grid, porosity further decreased to 33% and there was some evidence of a regular packing structure. Similar results were reported by Wadsworth [1954]. Sufficient distance was allowed between the support screen and the lowest layer of thermocouples to allow the packing to become random.

(f) Tube to Particle diameter ratio

A large diameter (3.75") container was chosen for the bed. This allowed the use of larger diameter glass beads of good sphericity and size uniformity without an undesirable reduction in tube to particle diameter ratio. As a result of the large tube diameter, superficial particle Reynolds numbers were limited to about 1800 for 6.2 mm spheres. This constraint is being overcome by installation of a larger compressor. The relatively large packing sizes used ensured that the influence of thermocouples would be small since the ratio of packing diameter to wire diameter was about 35:1.

B. THERMOCOUPLE EXPERIMENTS

1. Objectives and Theoretical Analysis

Before using internal probes with any confidence, it was necessary to establish whether the temperature measured was that of the gas rather than some intermediate temperature between solid and gas. It was also necessary to determine the extent of the high frequency attenuation introduced, since according to the calculations of appendix 10, the maximum allowable time constant would be about 0.6 seconds for a superficial particle Reynolds number of 2000 if short bed length measurements (N=10) were to be carried out. The basis of this figure is an allowable attenuation of 10% at a frequency $.(V_H+1)\ \omega$ of 10.

To reduce thermal capacity at the thermocouple junction a special butt welding technique was developed. Chromel-Alumel thermocouples were used, of diameter 0.0067 inches and the junctions made under argon using an electric arc. In most cases, magnification was necessary subsequently to locate the junction.

It may be shown, that provided wire temperature is uniform across a section, the transfer function relating fluid temperature variations δT_f (t) from steady state to resultant wire temperature variations δT_w (t) is given by equations (1.1):

$$\frac{\mathcal{L}[\ \delta T_w\ ]}{\mathcal{L}[\ \delta T_f\ ]} = \frac{T_w\ (s)}{T_f\ (s)} = \frac{1}{Ts + 1} \qquad \ldots(1.1)$$

where T, the time constant of the wire is related to the fluid - wire heat transfer coefficient h, the wire diameter d and volumetric thermal capacity $\rho_s\ c_s$ by

$$T = \frac{\rho_s . c_s . d}{4\ h} \qquad \ldots(1.2)$$

A step change in fluid temperature is practically impossible to achieve. It is simple however to vary heat input to the wire in a near stepwise manner by electrical heating. If the wire is heated to an initial temperature ϕ above the fluid and the power then turned off at $t = 0$ an exponential decay in wire temperature is predicted :-

$$\delta T_w\ (t) = \phi .\ \exp[\ -t/T\ ] \qquad \ldots(1.3)$$

A record of δT_w against time allows T to be determined experimentally.

A further assumption of the analysis is that axial conduction along the wire is of negligible importance. In this case, $^L/_d$ was about 500:1 so that the assumption appears reasonable.

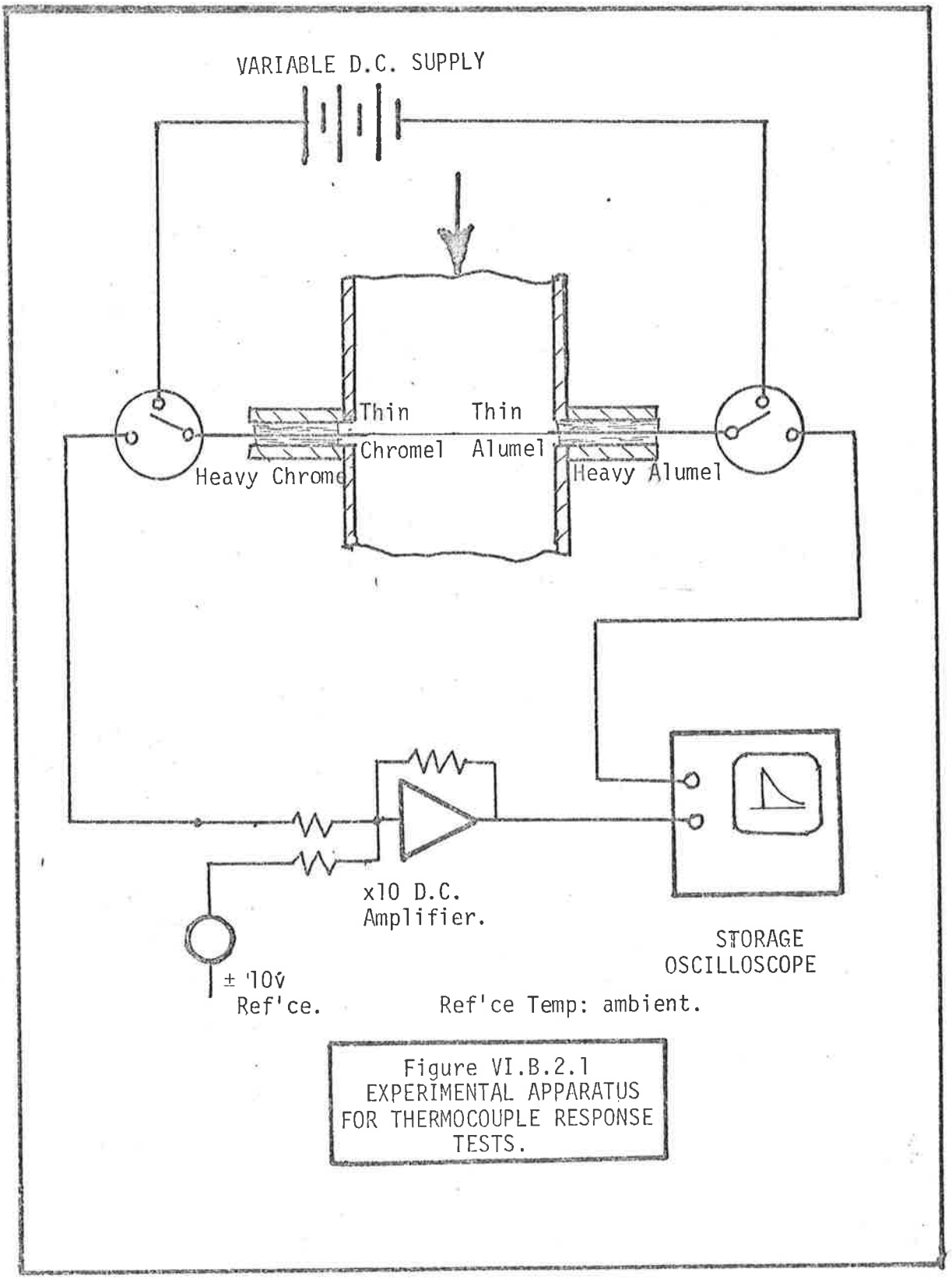

Figure VI.B.2.1
EXPERIMENTAL APPARATUS FOR THERMOCOUPLE RESPONSE TESTS.

2. Experimental Technique and Results

The unlined 4" tube was used and flow measured by rotameters as described in section C. A control thermocouple was located in the free air stream one inch above the packed section (see figure VI.B.2.1) which was packed with 5 m.m. lead glass spheres, 18"deep. Average bed porosity was 37%, determined by weighing and height measurement and the packed section thermocouple was located at the bed centre line, 5" from the top of the bed. Flow straighteners described in section C were inserted above the free thermocouple.

After heating the thermocouple to a steady temperature for 30 seconds, the switch was operated to turn off the current and throw the thermocouple voltage on to a D.C. amplifier (voltage gain 10) the output of which was recorded on the screen of a storage oscilloscope, beam deflection 6 cm at 1m V/cm.

The maximum voltage change at the thermocouple was 600μV which is equivalent to $26F^{o}$ above ambient. Radiant heat loss would therefore be expected to be negligible.

At each air flow, three transient tests were carried out and the time constants obtained from semilogarithmic plotting averaged. A straight line resulted in every case down to 5% of initial reading verifying the exponential cooling law of equn.(1.3).

The averaged time constants obtained have been listed in tables VI.B.2.1 and 2.2. In table 2.1 (open tube results) a wire Reynolds number Re_w has been defined based on mass velocity G in the open section with characteristic dimension, wire diameter. In table B.2.2 (packed bed results) the wire Reynolds number Re'_w has been based on interstitial mass velocity G/ε since this is representative of the local velocity across the wire itself.

The Nusselt numbers calculated in tables B.2.1 and B.2.2 are based on equation (1.2) and the thermal properties of chromel listed in table B.2.3. The thermal properties of chromel and of alumel differ widely and influence the calculated values of Nusselt number since these are calculated from the time constants T defined by equation (1.2).

In other words, since:

$$T, \text{ mins.} = \left[\text{Thermal Resistance}\right] \times \left[\text{Thermal Capacitance}\right],$$

$$^{\circ}F/_{(B.T.U/min)} \qquad B.T.U./_{F^{\circ}}$$

calculation of thermal resistance, $^{1}/_{(hS)}$, requires knowledge of the thermal capacitance of the probe.

Since the electrical resistance of chromel is more than twice that of alumel its properties are more appropriate. In any case, comparison is made between the experimental free-stream thermocouple and the packed bed couple so that the fact that each is in error by a constant amount relative to literature correlations is of negligible importance.

TABLE VI.B.2.1

HEAT TRANSFER TO THERMOCOUPLE WIRE - FREE AIR STREAM RESULTS

Air Flow Std.lpm 70°F,14.7psia	Pressure psig	Avg.Time constant, seconds	Reynolds number Re_w	Nusselt number Nu
66	37	0.875	1.46	1.10
112	82	0.739	2.48	1.31
116	83	0.785	2.58	1.23
180	26	0.644	4.00	1.50
308	80	0.522	6.84	1.85
760	54	0.368	16.9	2.62
930	50	0.348	20.6	2.77
1040	49	0.370	23.1	2.61
1080	48	0.341	24.0	2.83

TABLE VI.B.2.2

HEAT TRANSFER TO THERMOCOUPLE WIRE

PACKED SECTION RESULTS

Air Flow, std.lpm 70°F,14.7psia	Pressure, p.s.i.g.	Avg.Time Constant, seconds	Modified Reynolds No. Re'_w	Nusselt Number Nu
62	60	0.567	3.60	1.70
105	60	0.510	7.58	1.89
195	60	0.460	10.7	2.10
410	80	0.355	24.6	2.72
640	61	0.297	38.5	3.25
774	62	0.266	46.5	3.62
970	58	0.236	58.2	4.09
1080	48	0.234	64.8	4.12

TABLE VI.B.2.3

PROPERTIES OF CHROMEL (P) and ALUMEL (P)

at 100°F [Herzfeld, 1962]

	CHROMEL P	ALUMEL P
Density, gm/cc	8.73	8.60
Specific heat, BTU/(lb.°F)	0.107	0.125
Resistance, ohms/cmf	425	177
Volumetric thermal capacity, $\rho_S C_S$, BTU/(ft³ °F)	58.4	67.0

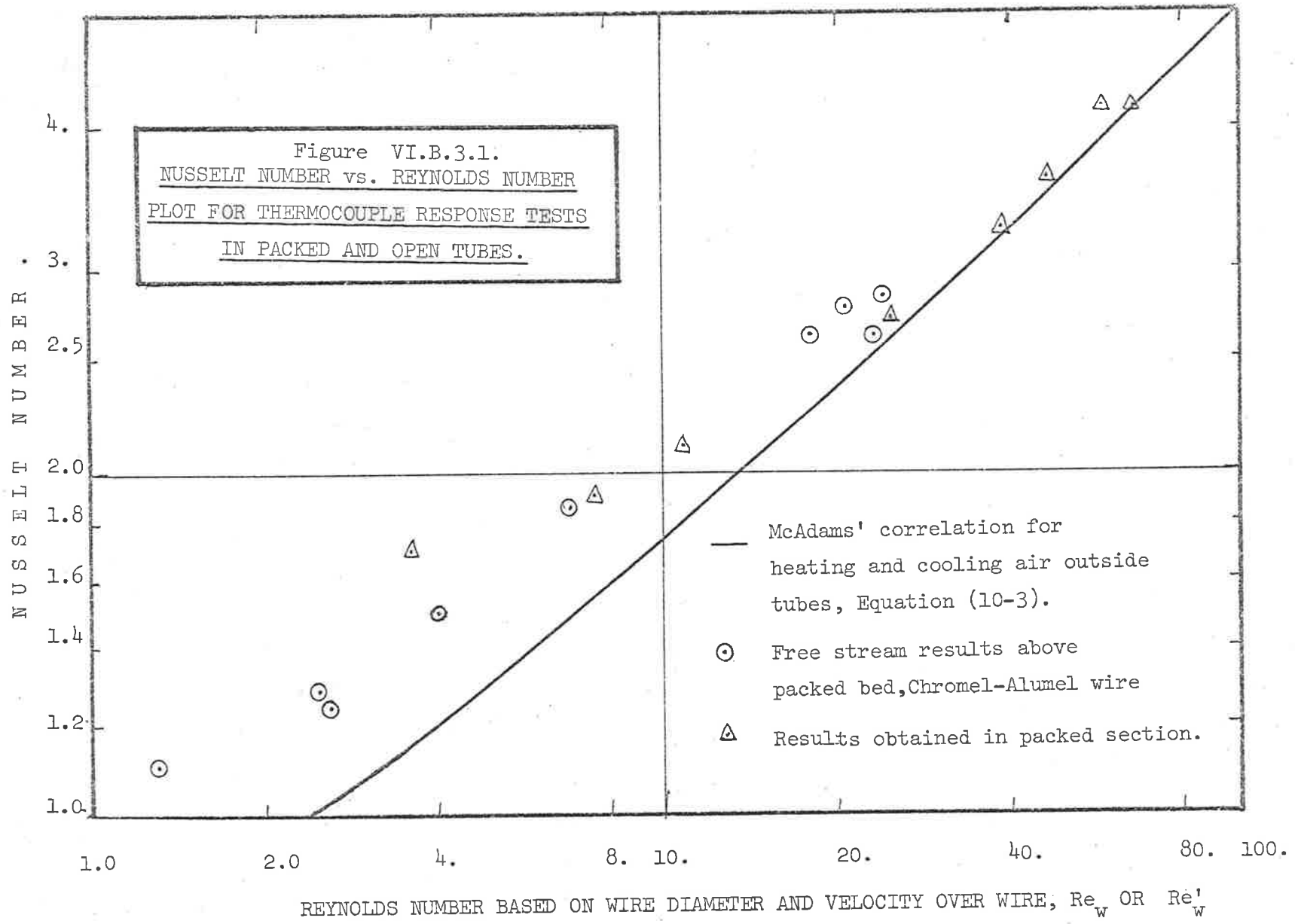
Figure VI.B.3.1.
NUSSELT NUMBER vs. REYNOLDS NUMBER
PLOT FOR THERMOCOUPLE RESPONSE TESTS
IN PACKED AND OPEN TUBES.
NUSSELT NUMBER
4.
3.
2.5
2.0
1.8
1.6
1.4
1.2
1.0
1.0
2.0
4.
8.
10.
20.
40.
80.
100.
McAdams' correlation for heating and cooling air outside tubes, Equation (10-3).
Free stream results above packed bed, Chromel-Alumel wire
Results obtained in packed section.
REYNOLDS NUMBER BASED ON WIRE DIAMETER AND VELOCITY OVER WIRE, Re_w OR Re'_w

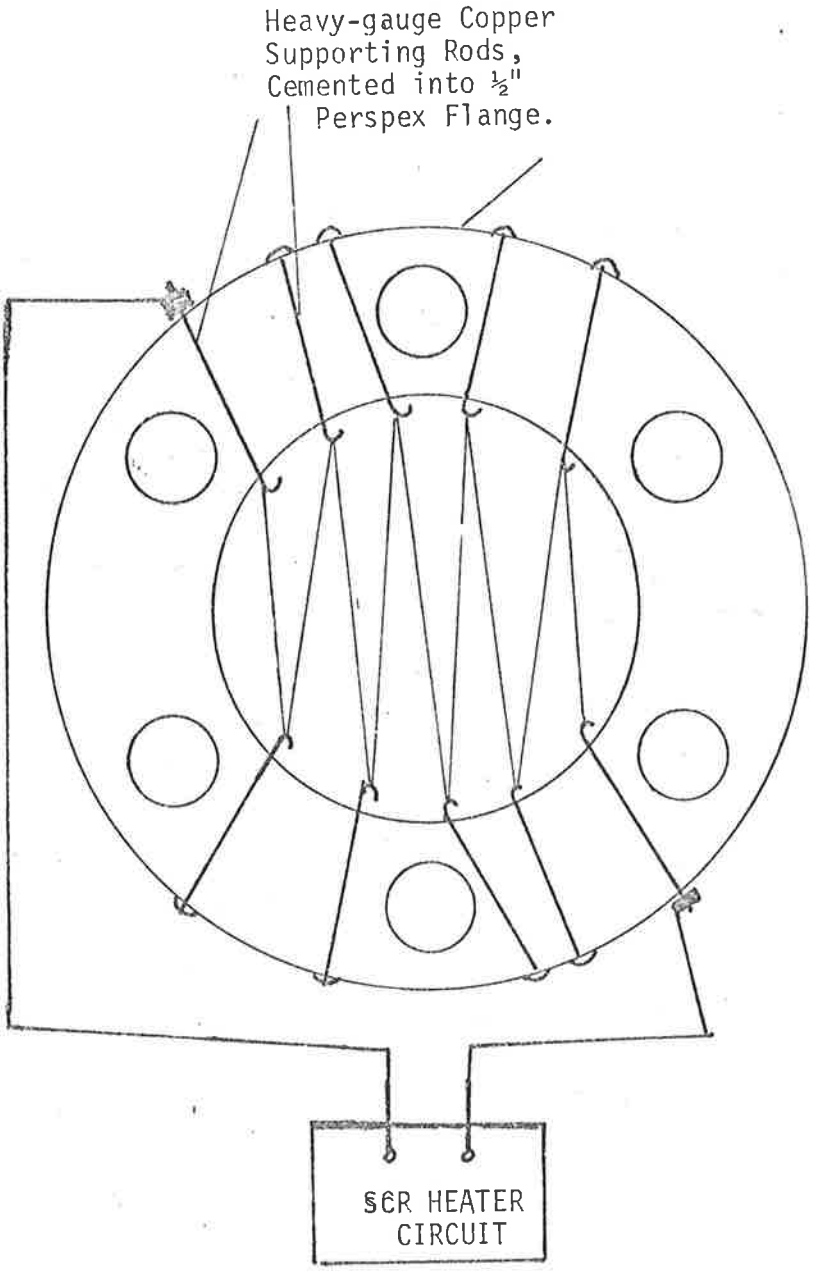

Figure VI.C.1.1
SCHEMATIC ARRANGEMENT OF A
NICHROME WIRE HEATER (3off)

3. Discussion of Results

In figure B.3.1, the Nusselt number - Reynolds number plots resulting from each experiment have been compared with each other and with the McAdams [1954] heat transfer correlation for flow normal to cylinders. While the agreement between absolute values is largely fortuitous, it is significant to note that the slopes of the plots are in general agreement with each other. When the good 'first order' behaviour of the packed bed thermocouples is taken into account also, it becomes apparent that thermocouple probes in the packed section are, indeed, measuring gas temperature and that response speeds are sufficient for present requirements. This is perhaps less surprising when the diameter of a thermocouple is compared with that of a particle on a scale drawing. It is evident that the number of contact points per unit length is extremely small, relative to the wire diameter.

C. FINAL DESIGN

1. Pulse Injection and Baseline Control System

As noted in A.2.e., replacement of the solenoid pulse injection system by wire heaters of 0.010 inch Nichrome strung in a zig-zag manner across the section (figure C.1.1.) did not eliminate 'tailing' of the input pulse.

Both tailing and drift were virtually eliminated by maintaining inlet air temperature a few degrees above the compressor air temperature with an electronic controller, before and after administering the inlet air temperature pulse or step change. Some residual drift occurred as a result of stratification resulting frommelting of the ice bath surrounding the kerosene cold junctions of the thermopiled temperature measurement system during the course of a series of experiments.

This is not surprising, since a change of one chart division or 1% of F.S.D. represents a temperature change of about $0.08F^{o}$.

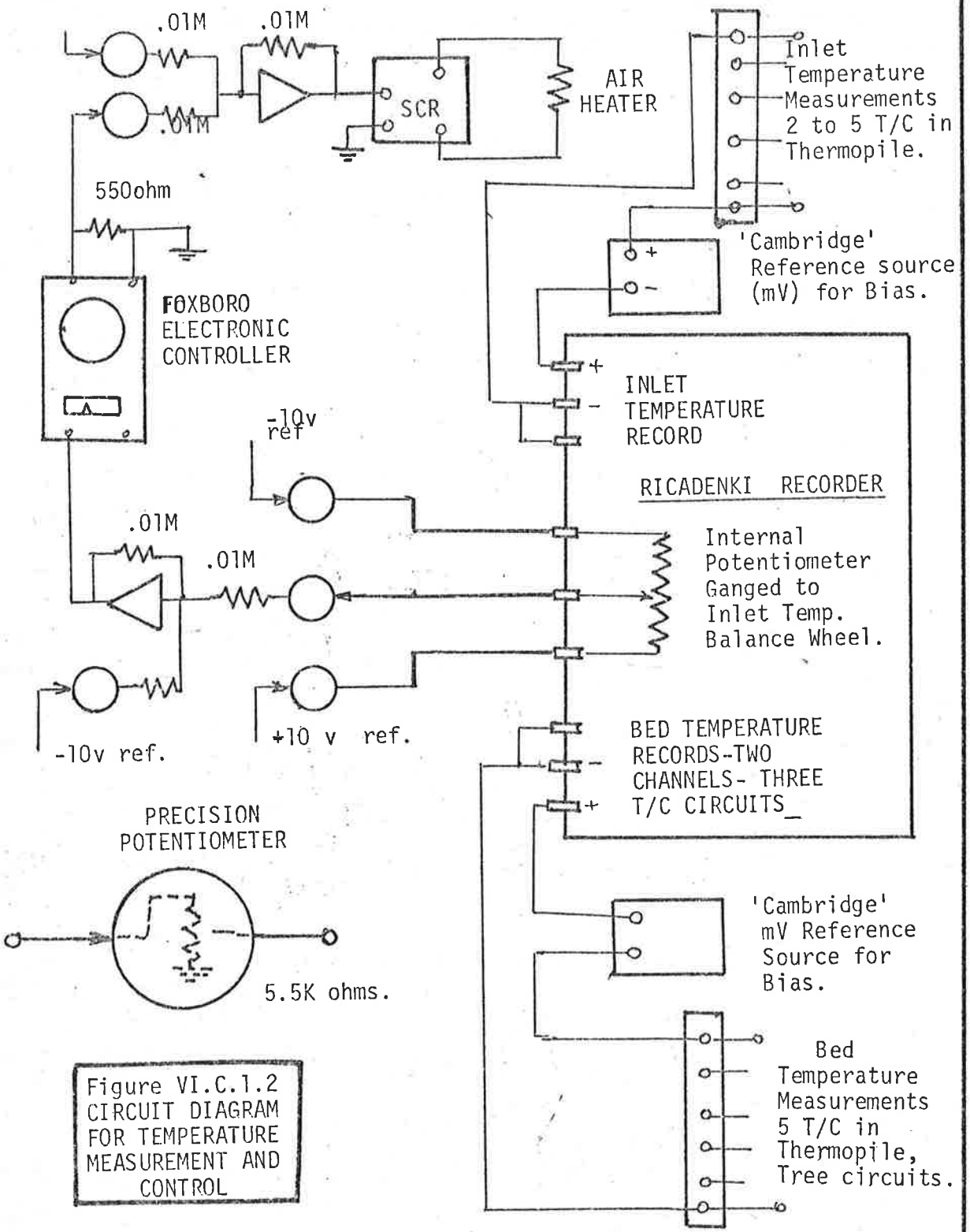

Figure VI.C.1.2 CIRCUIT DIAGRAM FOR TEMPERATURE MEASUREMENT AND CONTROL

This may be calculated as follows:

> One chart division at 1m V span = 10μV change in thermocouple voltage,
> for five thermocouples in thermopile this represents 2μV or 0.08F^{o} at 23μV per F^{o} for chromel - alumel.

In the final series of tests, using lead packing, even this small temperature change was smoothed out by replacement of the ice-water bath by a Leeds and Northrup automatic thermoelectric ice point device.

The resultant, approximately 5mV to 6mV thermocouple input and output signals were biased to 0. to 1. m V range for recording, by a Cambridge potentiometric reference supply aranged in series on each channel (see figure C.1.2).

Stable, high gain D.C. amplification of the low level input temperature signal was required in order to actuate the baseline control system. Such amplification was not to 'load' the thermocouple circuit. This was achieved by fitting a 'servo pot' to the balancing wheel shaft of the Rikadenki recorder. Motion of the shaft was directly proportional to temperature, so that when a stable 10 volt d.c. reference voltage was placed across the 'servo-potentiometer' a zero to 1.0 mV thermocouple signal was converted with a gain of 10,000 to a zero to 10 volt control signal. The servopot had a resistance of 500 ohms so that negligible loading occurred when this signal was fed to an operational amplifier of unity forward path gain having a 100,000 ohm input resistor. Stable reference supplies and the operational amplifiers required for 'signal conditioning' were obtained from a small Electronics Associates (E.A.I) TR-20 electronic analogue computer.

The resultant d.c. output signal was biased as shown in figure C.1.2 and dropped through a 100 ohm input resistor to yield a 6 to 18m A input signal for the model 62 Foxboro electronic controller. The bias was arranged to ensure that 0 to 100% on the controller set point dial corresponded to 0 to 100% deflection on the recorder.

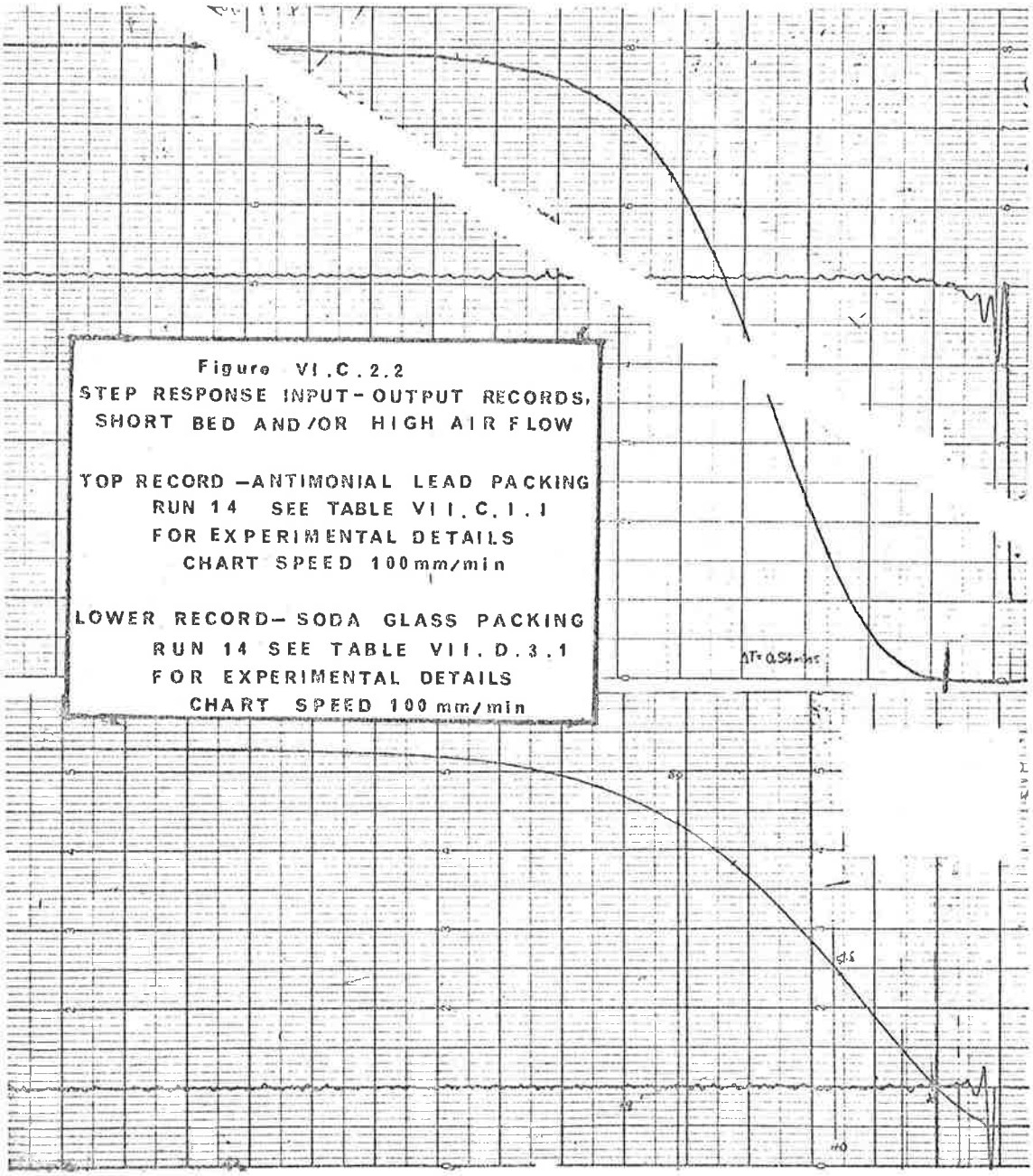

Figure VI.C.2.2
STEP RESPONSE INPUT-OUTPUT RECORDS,
SHORT BED AND/OR HIGH AIR FLOW

TOP RECORD –ANTIMONIAL LEAD PACKING
RUN 14 SEE TABLE VII.C.1.1
FOR EXPERIMENTAL DETAILS
CHART SPEED 100 mm/min

LOWER RECORD– SODA GLASS PACKING
RUN 14 SEE TABLE VII.D.3.1
FOR EXPERIMENTAL DETAILS
CHART SPEED 100 mm/min

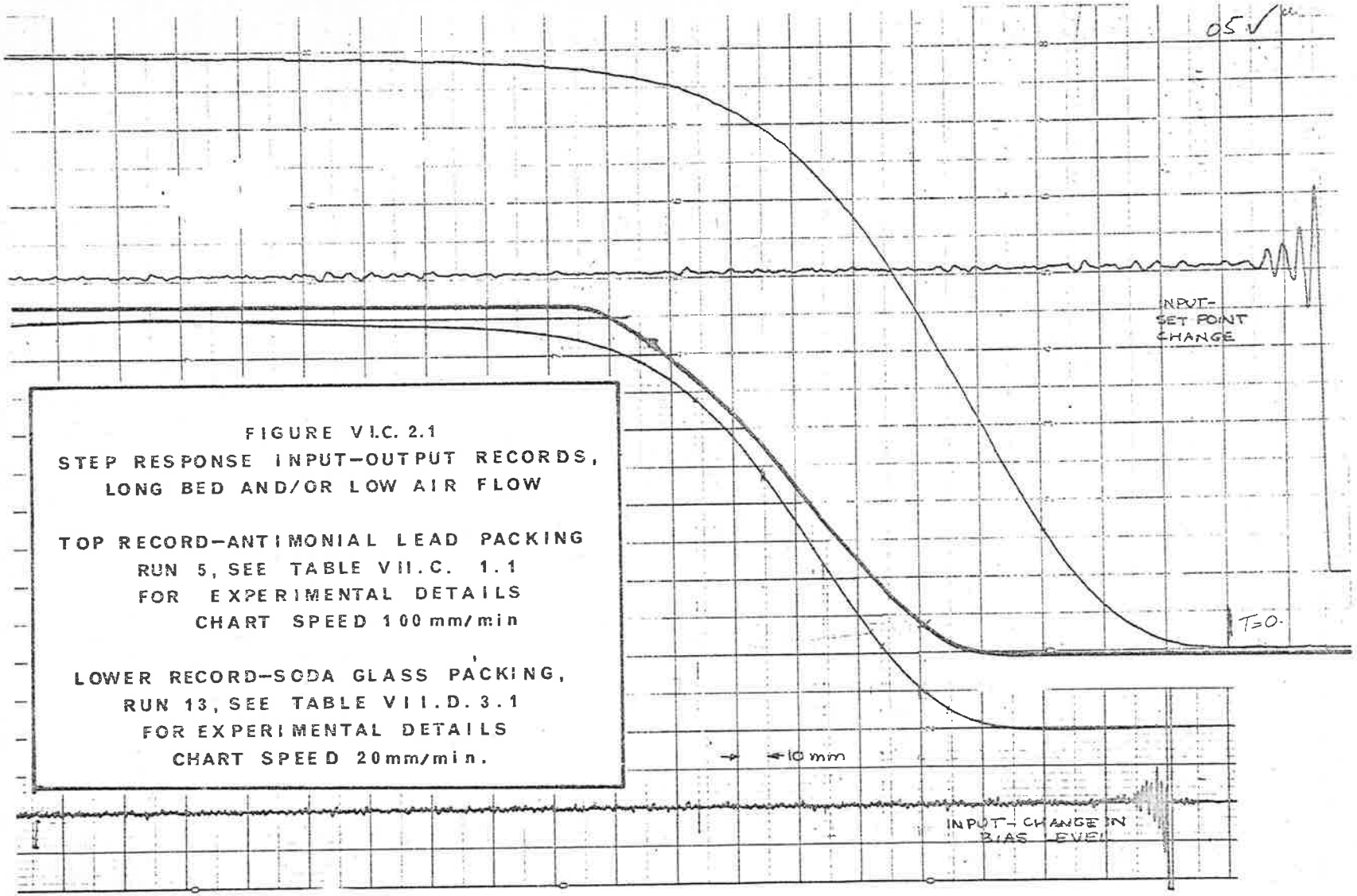

FIGURE VI.C. 2.1
STEP RESPONSE INPUT-OUTPUT RECORDS,
LONG BED AND/OR LOW AIR FLOW

TOP RECORD-ANTIMONIAL LEAD PACKING
RUN 5, SEE TABLE VII.C. 1.1
FOR EXPERIMENTAL DETAILS
CHART SPEED 100 mm/min

LOWER RECORD-SODA GLASS PACKING,
RUN 13, SEE TABLE VII.D.3.1
FOR EXPERIMENTAL DETAILS
CHART SPEED 20mm/min.

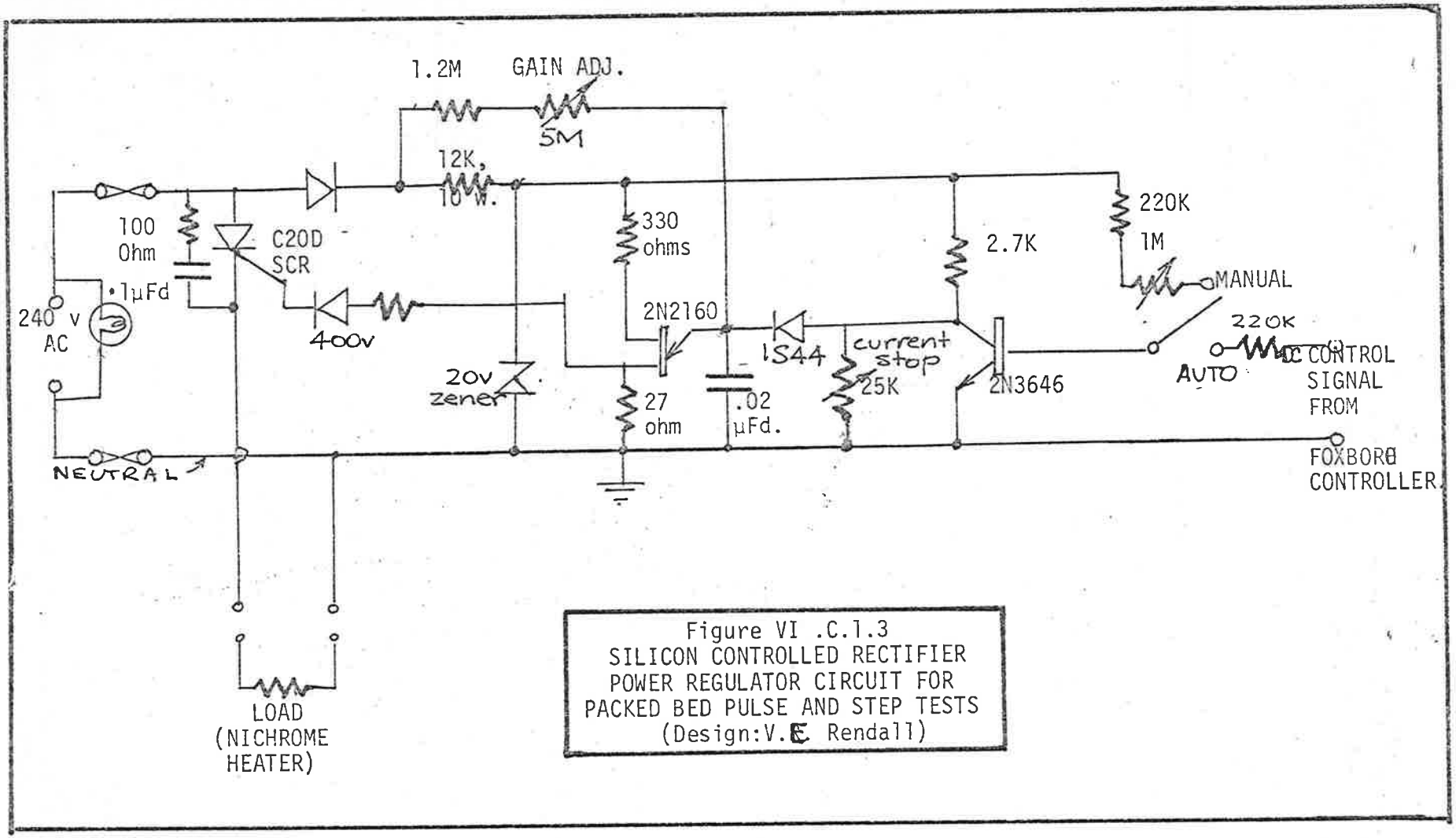

Figure VI .C.1.3
SILICON CONTROLLED RECTIFIER
POWER REGULATOR CIRCUIT FOR
PACKED BED PULSE AND STEP TESTS
(Design: V. E. Rendall)

The control signal from the Foxboro controller was then dropped across a 300 ohm load resistor and passed through a unity gain D.C. amplifier to become the actuating signal for a Silicon controlled rectifier power regulator circuit, figure C.1.3. The chopped A.C. power signal to the Nichrome wire heater was monitored on an oscilloscope.

2. Performance of Baseline Control System

Although continual random fluctuations in inlet temperature occurred about the control point, observation of outlet temperatures from the packed bed over prolonged periods of operation showed that long term temperature control was accurate to near the limit of resolution of the recorder (about 0.1% F.S.D.).

In applying a step change in inlet temperature, the controller set point was changed quickly to its new value and provided the controller was well 'tuned' i.e. the correct combination of controller gain and integral or reset time chosen, inlet temperature, after a period of overshoot and oscillation settled down to its new value. For long bed lengths and/or moderate air flows, this period of oscillation was short enough to appear to the bed to be an effective step change (see figure C.2.1). At very high flows and short bed lengths this period became larger, relative to the response time of the system so that small time values of the response were affected by the overshoot and oscillation of the controller (figure C.2.2). This was not significant in the majority of the experimental runs. Another method used to administer a step change was to change the bias of the input temperature measurement circuit by a fixed amount at a fixed set point.

It was found undesirable to apply pulse changes in input temperature by either of the methods mentioned above since overshoot and oscillation made exact Fourier transformation of the input pulse difficult; instead, the controller was placed on manual, and the input pulse applied by manually changing the input power above the baseline power level, returning to approximately the same level and switching back to manual.

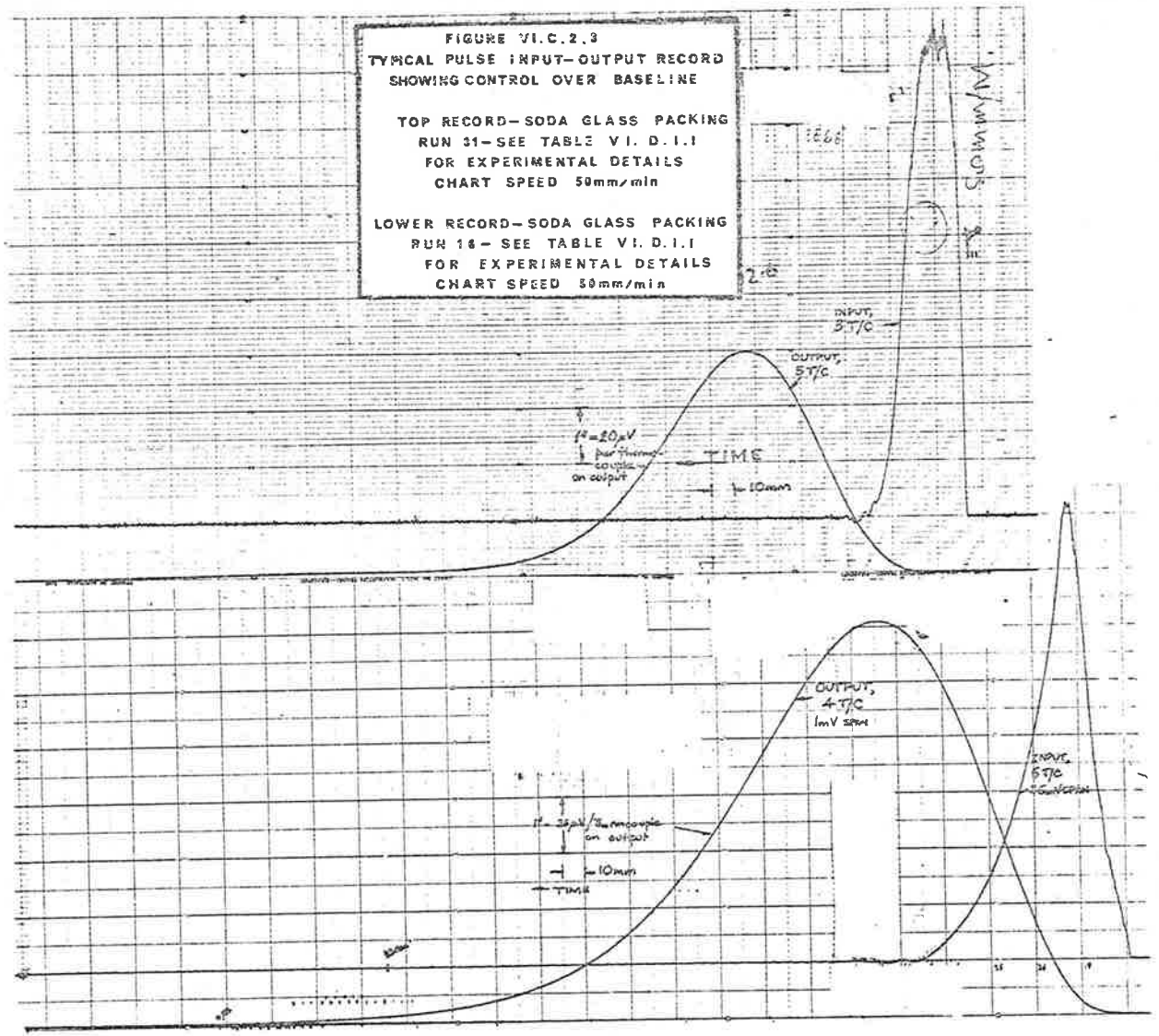

FIGURE VI.C.2.3
TYPICAL PULSE INPUT-OUTPUT RECORD SHOWING CONTROL OVER BASELINE

TOP RECORD - SODA GLASS PACKING
RUN 31 - SEE TABLE VI. D. 1. 1
FOR EXPERIMENTAL DETAILS
CHART SPEED 50mm/min

LOWER RECORD - SODA GLASS PACKING
RUN 18 - SEE TABLE VI. D. 1. 1
FOR EXPERIMENTAL DETAILS
CHART SPEED 50mm/min

A controller having 'bumpless change over' (i.e.internal matching of controller and manual output during the transition from manual to set point operation) was found desirable here since at high flows and short bed lengths insufficient time was available for matching controller and manual signals.

In general, a lower sensitivity (2.5m V span) was used on the input recording than on the output which was left at 1.0 m V span. This allowed a pulse to be applied which was as close an approximation to an 'impulse function' as possible, i.e. one which was of high intensity for a short duration relative to the response of the bed. Nonetheless input temperature changes were limited to a maximum of $35F^{o}$ with a resultant maximum output temperature change of about $15F^{o}$ (figure C.2.3).

3. Possible Improvements to the Control System

a) The non-linearity of the S.C.R. regulator meant that controller settings for a low power level were not always satisfactory at high power inputs, when the sensitivity of power input to changes in control signal (or firing angle) became large. This could be improved by modification of the S.C.R. circuit to ensure that a plot of power against control signal would be linear.

b) Overshoot and oscillation during pulse and step tests would be eliminated by using the controller only for steady control of baseline temperature and for elimination of long term drift prior to and after administration of the step or pulse.

The actual changes in power level would be best made by a programmed series of power changes preset by means of a series of comparators controlling a sequence of 'flip flops' or electronic switches. This would have been particularly useful at high flowrates and short bed lengths when rapid changes were difficult to apply manually.

c) The addition of a remote set point station to the Foxboro controller would be valuable in applying a few steady state cyclic tests (see section V.A.1) at selected frequencies as a check on pulse and step response results.

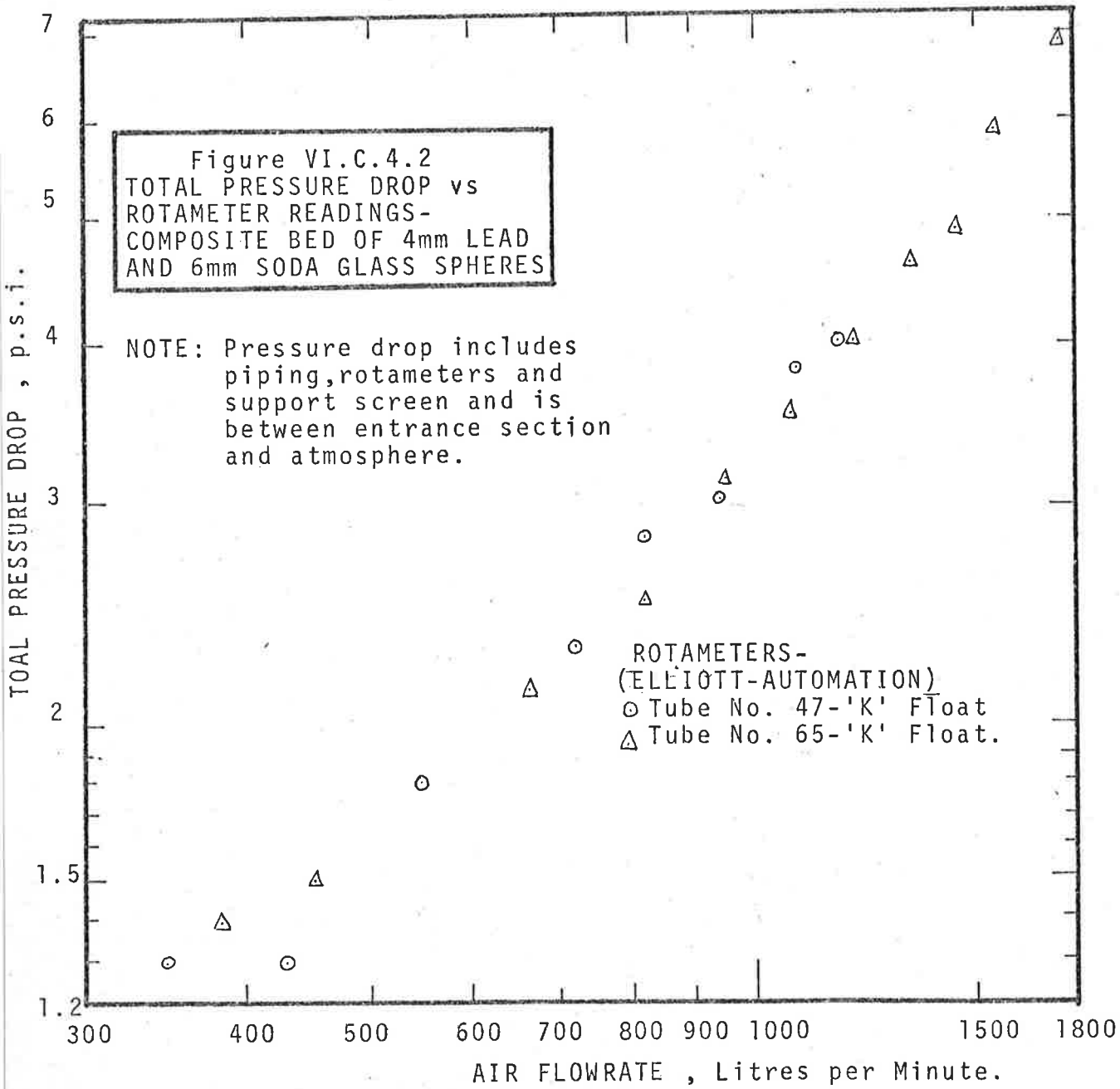
Figure VI.C.4.2
TOTAL PRESSURE DROP vs
ROTAMETER READINGS-
COMPOSITE BED OF 4mm LEAD
AND 6mm SODA GLASS SPHERES
NOTE: Pressure drop includes
piping, rotameters and
support screen and is
between entrance section
and atmosphere.
ROTAMETERS-
(ELLIOTT-AUTOMATION)
⊙ Tube No. 47-'K' Float
△ Tube No. 65-'K' Float.
TOAL PRESSURE DROP , p.s.i.
7
6
5
4
3
2
1.5
1.2
300
400
500
600
700
800
900
1000
1500
1800
AIR FLOWRATE , Litres per Minute.

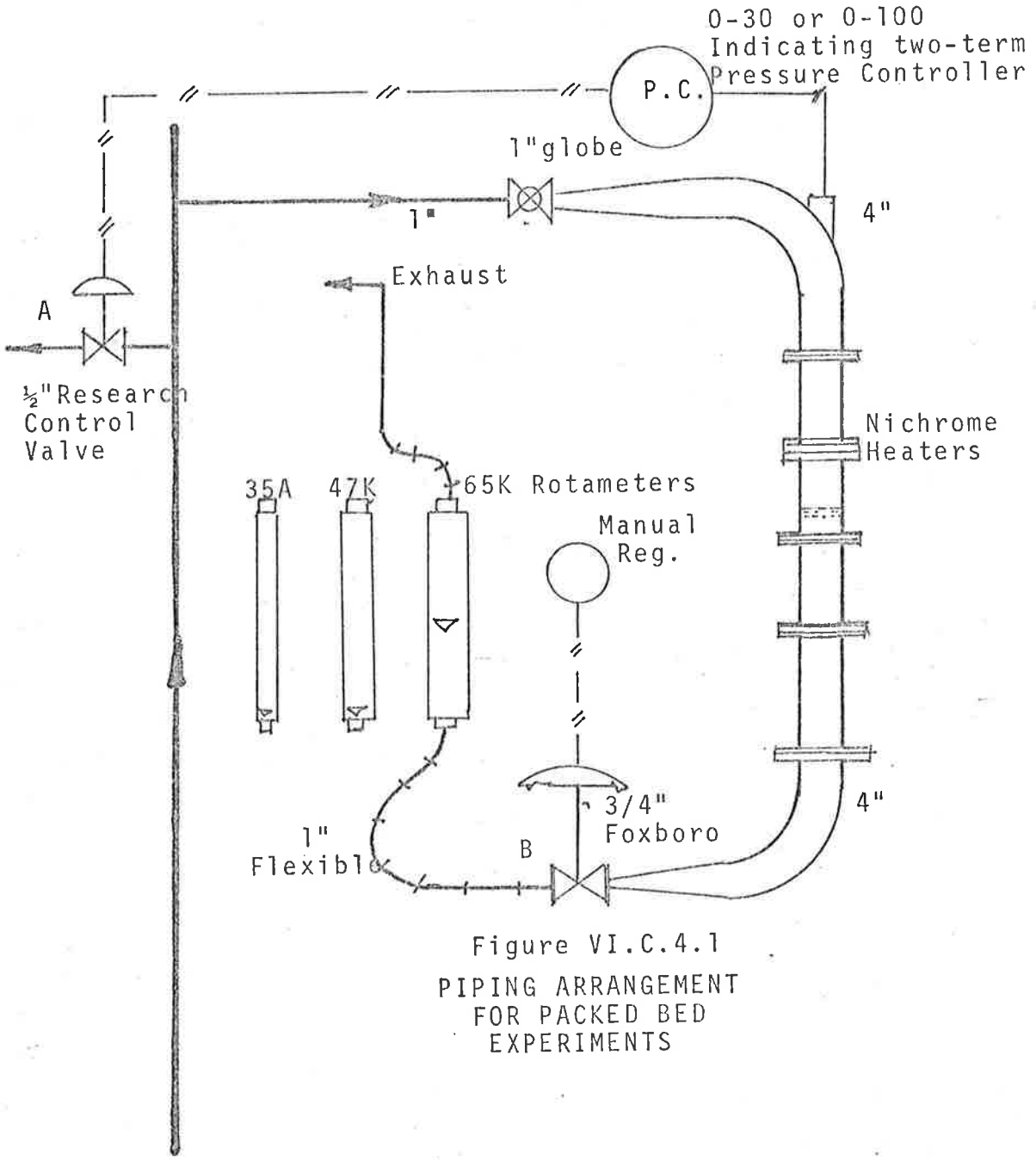

Figure VI.C.4.1

PIPING ARRANGEMENT
FOR PACKED BED
EXPERIMENTS

4. Other Constructional Details

The overall piping layout finally adopted is illustrated in figure C.4.1.

(i) Compressor Air

Compressed air was passed through a cooler and knockout drum to remove oil and water and thence through one of two silica gel driers. At the inlet to the bed, a 0 - 100 psig, or 0.-30 psig Foxboro pressure controller (calibrated by dead weight test) was used to bleed off a small amount of air through a ½" 'Research' control valve (A), on figure C.4.1. Another control valve (B) on the outlet was set at fixed opening appropriate to the flow and pressure required for each run. In later experiments on 4 m.m. lead beads further investigation of the effects of the heat capacity ratio, V_H was dispensed with and this valve by-passed in order to maximise throughput.

The Foxboro pressure controller and valve served to keep flow constant during a run and to minimise the effects of other users of compressor air.

Air flow was measured by one of three Elliott-Automation 'rotameters' with overlapping ranges. It was not possible to calibrate these rotameters against a standard flowmetering device, since excessive oscillation of the bobs occurred when installed in the test rig. Instead, a strain gauge differential pressure transducer was used to obtain a plot of overall bed pressure drop against flowrate indicated by the three rotameters. The curve was continuous on a log-log scale and no systematic difference between the readings was noted, figure C.4.2.

(ii) Test Section

Air to the test section was expanded from a 1" to a 4" pipe and then passed over the Nichrome wire heaters. In order to flatten the velocity profile and to reduce temperature gradients, air was then passed through a series of five perforated plates spaced 1/8" apart axially along the tube.

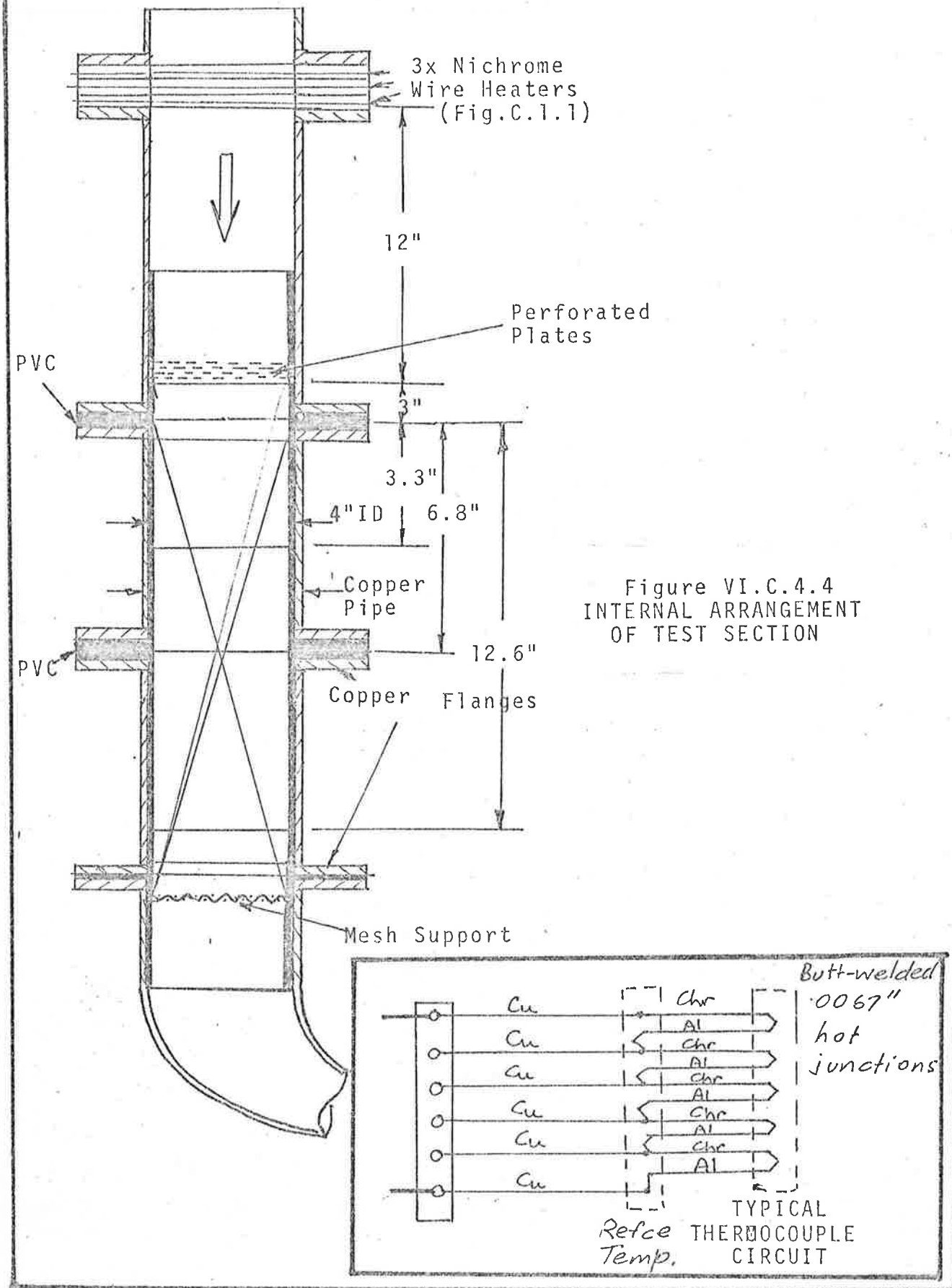

Figure VI.C.4.4
INTERNAL ARRANGEMENT
OF TEST SECTION

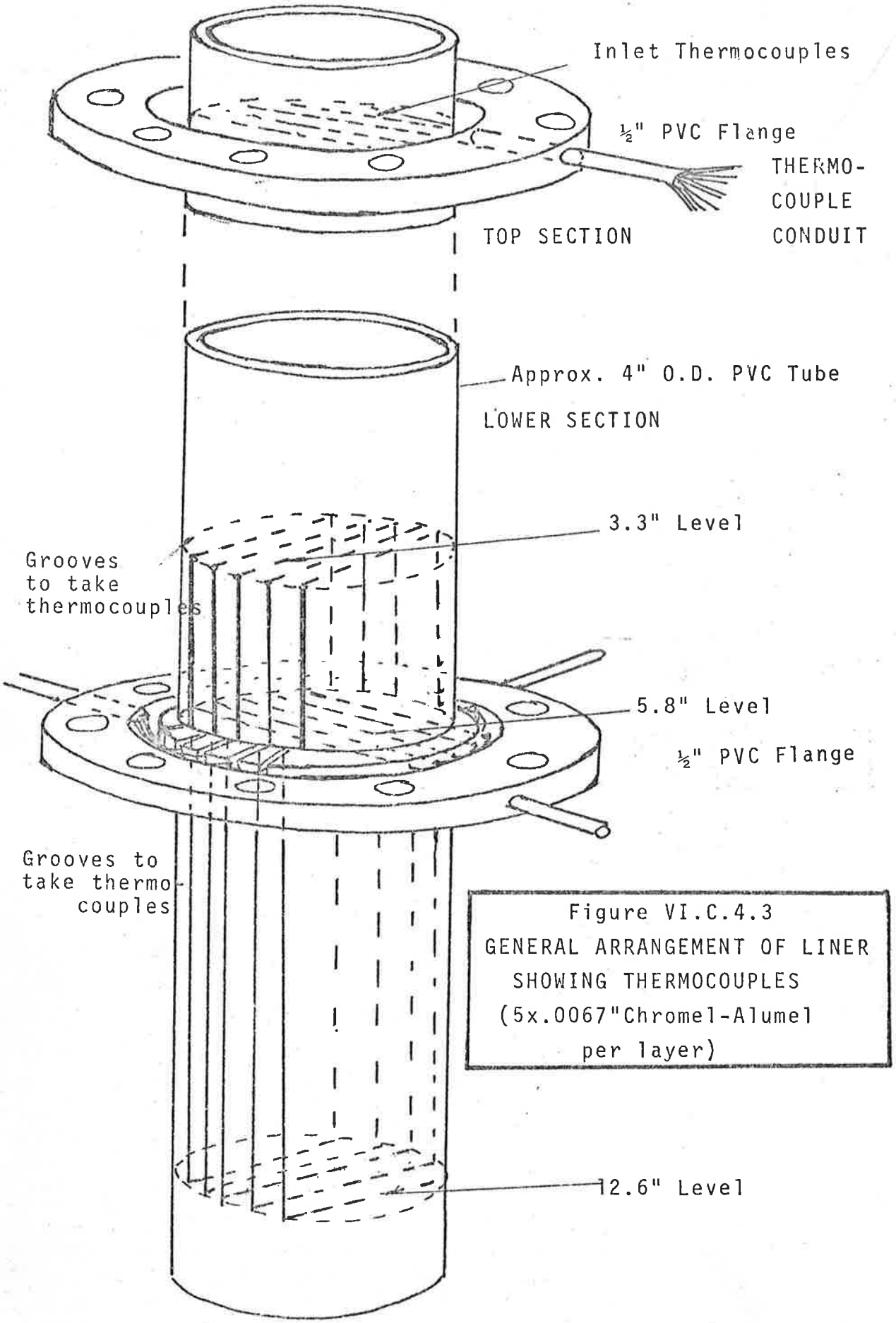

Figure VI.C.4.3
GENERAL ARRANGEMENT OF LINER
SHOWING THERMOCOUPLES
(5x.0067"Chromel-Alumel
per layer)

Perforations were 1/16" on 1/8" triangular pitch. The lowest pipe Reynolds number in this section was about 1700 so that elaborate flow straighteners appeared unnecessary.

In any case, it was considered desirable to minimise the thermal capacitance of fittings between the heater and the bed inlet so that the initial rise time of a step or pulse would be fast. (This consideration is, in fact not so important when a baseline control system is used since high initial speed of response may be obtained by increasing power level). The plates which were made from electrical circuit 'Zephir' board rested on the top of the 3.77" I.D. x 1/8" thich P.V.C. tube liner which in turn fitted tightly into the 4" I.D. copper external pressure tube. Insulated thermocouple wires were run through a P.V.C. flange attached to the liner and thence, via grooves along the outside of the liner, between the liner and containing tube to each layer of thermocouples (figure C.4.3). The P.V.C. flange was sandwiched between the flanges of the copper pressure tube.

Figure C.4.4 illustrates the spacing and arrangement of each thermocouple layer relative to the supporting stainless steel mesh. See appendix 11.1 for porosity determinations.

CHAPTER-VII. VII. SCOPE

EXPERIMENTAL RESULTS

SCOPE OF THE CHAPTER

In this chapter, the results of experimental step and pulse tests on soda glass, 'Perspex' and lead packings are analysed using some of the techniques of Chapter V. Comparisons are made with the predictions of the theoretical models discussed in Chapters II, III and IV and with the results of experiments by Handley and Heggs. A fairly detailed analysis of some of the errors inherent in the step test methods used is presented and an initial comparison of two criteria for frequency domain modelling carried out.

Section A comprises a chronology of the experiments carried out in the (continuing) research programme.

Section B discusses the effects which modifications to the experimental apparatus had on the reliability of pulse tests analysed by the method of moments. Lead glass and soda glass packings were used in the experiments.

In Section C the results of step tests on beds packed with 4 m.m. antimonial lead are reported. The data is analysed by the method of moments suggested in section V.D. and by the empirical correlation of points on the breakthrough curve. An error analysis is presented for each. Arithmetic probability plots are also presented for comparison with the predictions of the equivalent conductivity model.

VII SCOPE
VII.A.

Pulse and step tests performed on beds of soda glass are reported in section D whilst in Section E some results obtained by Handley and Heggs [1963] in similar experiments are analysed using present techniques.
In Section F, Perspex packing experiments are reported.

Orthogonal polynomial techniques of frequency domain analysis are applied, in section G, to some of the pulse test results. The objective of the analysis is to determine the accuracy with which various physical effects may be separated. Section H summarises the conclusions reached in this chapter.

A. CHRONOLOGICAL SEQUENCE OF EXPERIMENTS.

The way in which the original objects of the experimental programme affected the design of the experimental apparatus has been discussed in chapter VI. Many of these objectives became redundant as experimental work and theoretical analysis proceeded and as the published work of other experimenters became available. In retrospect, a fundamental error was made in not carrying out control experiments using highly conductive packing at the beginning of the programme. A series of step tests with antimonial lead as a packing was finally completed in June 1970. These experiments are reported, before earlier soda glass and Perspex experiments, in section C.

Preliminary pulse tests using the original three - way solenoid valve arrangement and soda glass packing were completed in 1967. These are reported in section B.2. The bulk of the soda glass and Perspex pulse and step tests, using the modified apparatus, were performed in 1968 - 9 and are presented in sections D and F.

B. EXPERIMENTS PRIOR TO AND AFTER EQUIPMENT MODIFICATIONS.

1. Pulse Test Data Analysis Method

(i) Zero'th and First Moments

In the presence of heat loss, it is necessary first to normalise input and output pulse areas (zero'th moments) to equality. This procedure is justified in Appendix 4.

In this chapter, the estimated dimensional first moment of the impulse response is written $\mu(t)$ after normalising areas and has units of time. From equation (V.D.3.1), independently of the model :

$$\mu(t) = (1+V_H)L/v_a = \frac{Mc_s + M_f c_f}{Wc_f} = \frac{Mc_s}{Wc_f} >> 1. \quad . . . (1.1)$$

Hence, to test consistency, one may plot $\mu(t)$ against flowrate W on log log paper.

Simple measurement, by weighing, of M, the total mass of solid between the two temperature measurement stations yields the most direct check against theory. This was done in later

experiments on lead packing. A more indirect (and less satisfactory) approach was used in earlier soda glass and 'Perspex' experiments. Here M was estimated from the bed diameter, length, porosity and packing density ρ_s. This method obviously may lead to an undesirable accumulation of error in the calculation of M.

To allow for the effects of differing bed lengths, $\mu(t)/N$ is plotted instead of $\mu(t)$, where N is bed length in particle diameters. Note that $\mu(t)$ is obtained from the area-normalised first moments of the input pulse $x(t)$ and of the output pulse $y(t)$:

$$\mu(t) = \mu_Y(t) - \mu_X(t). \qquad \ldots (1.2)$$

(ii) Variance and Skewness

The next two estimated central moments or cumulants are then normalised with respect to the dimensional first moment $\mu(t)$ yielding:

$$\sigma^{*2} = \sigma^2(t) / \mu^2(t)$$
$$\text{and} \quad \pi^{*3} = \pi^3(t) / \mu^3(t) \qquad \ldots (1.3)$$

where, as before, $\sigma^2(t)$ and $\pi^3(t)$ are obtained by difference from the corresponding cumulants of input and output and have units of $(\text{time})^2$ and $(\text{time})^3$ respectively.

According to the equations developed in chapter II for σ^{*2} (for example equs. II.B.3.10) both $N\sigma^{*2}$ and $N^2\pi^{*3}$ should, for the simplified boundary conditions assumed, be

independent of bed length Nd_p. Both these non dimensional moments are expected to depend only on Stanton number, porosity and Biot number and (weakly, where V_H is large), on heat capacity ratio V_H. Hence, for experiments carried out on beds of differing length N, it may be expected that entrance or bed length effects may be revealed by differing values of $\sqrt{N}.\sigma^*$ at the same flowrate for the same packed bed.

Since the parameter γ_2 was shown, in section II.E.1, to be theoretically insensitive to flowrate and since this parameter should be 3.0 for the equivalent conductivity model, γ_2 is calculated, instead of plotting $N^{2/3}\pi^*$ against flowrate.

According to the previous definition of γ_2:

$$\gamma_2 = \mu(t).\ \pi^3(t) \ /\ \sigma^4(t) \quad = \quad \pi^{*3} \ /\ \sigma^{*4} \qquad \ldots (1.4)$$

2. Results of Preliminary Experiments Prior to Modifications

Eleven pulse experiments were carried out using the original solenoid valve pulse injection equipment described in section VI.A.2.(d). Approximate conditions are given in Table B.2.1 although detailed physical properties were not determined for the nominal 5 m.m. 'lead glass' packing used.

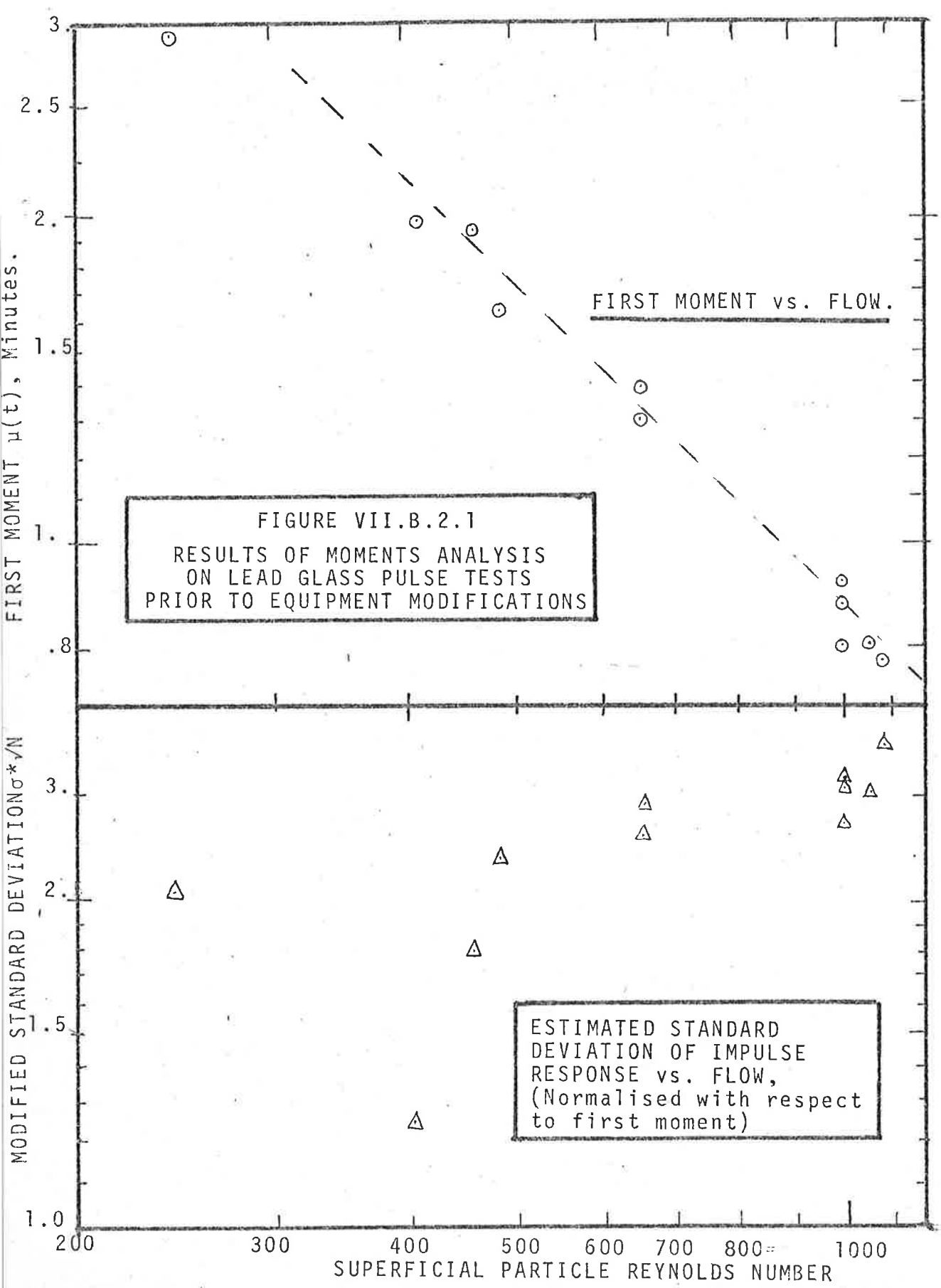
FIRST MOMENT vs. FLOW.
FIGURE VII.B.2.1
RESULTS OF MOMENTS ANALYSIS
ON LEAD GLASS PULSE TESTS
PRIOR TO EQUIPMENT MODIFICATIONS
ESTIMATED STANDARD
DEVIATION OF IMPULSE
RESPONSE vs. FLOW,
(Normalised with respect
to first moment)
FIRST MOMENT μ(t), Minutes.
MODIFIED STANDARD DEVIATION σ*√N
SUPERFICIAL PARTICLE REYNOLDS NUMBER
3
2.5
2.
1.5
1.
.8
3.
2.
1.5
1.0
200
300
400
500
600
700
800
1000

TABLE B.2.1

RESULTS OF MOMENTS ANALYSIS ON
LEAD GLASS PULSE TESTS
PRIOR TO MODIFICATIONS

Run number	Re_p (approx)	$\mu(t)$ (min)	σ^{*2}	σ^*	$\sigma^*\sqrt{N}$	π^{*3}	γ_2
1	462	1.940	0.106	.326	1.781	.0155	1.38
2	489	1.742	0.160	.400	2.182	.0118	0.46
3	656	1.389	0.158	.398	2.177	.0088	0.35
4	656	1.300	0.140	.374	2.04	- .0169	-0.86
5	1067	0.806	0.208	.456	2.49	- .0080	-0.069
6	1008	0.873	0.174	.418	2.28	- .0430	-1.42
7	1008	0.916	0.223	.472	2.58	.0928	1.86
8	1008	0.880	0.214	.462	2.52	.0454	0.99
9	1087	0.782	0.259	.509	2.78	.2820	4.21
10	410	1.980	0.052	.229	1.25	-.0435	-16.1
11	243	2.930	0.139	.373	2.04	.0062	0.32

Plots of $\mu(t)$ and $\sqrt{N}\sigma^*$ against calculated Reynolds number are presented on Figure B.2.1. It may be seen that whilst the first moments are reasonably consistent with equation (B.1.1), the variability of the standard deviation may be regarded as too great to establish a reliable functional relationship. The skewnesses π^{*3} reported in Table B.2.1, also vary widely and the theoretically

impossible result of a negative skewness occurs several times.

It appears likely that the variability in the moments was largely due to the excessively long tail on the input pulse and to drift in ambient temperature.

3. Reliability Experiments After Equipment Modifications

Immediately after modifications to eliminate tailing described in section VI.C.1. were installed, a series of pulse tests at similar flowrates were performed on two different bed lengths in order to test the repeatability of the results. Conditions of the experiments are summarised in table B.3.1 (see appendix 11 for details of physical property determinations).

TABLE B.3.1

EXPERIMENTAL CONDITIONS AND DATA FOR SODA GLASS TESTS AFTER EQUIPMENT MODIFICATIONS

Packing: 6.2 mm or .244 inch 'Englass' Ltd. soda glass spheres
Method of packing; vacuum injection (see appendix 11)
Nett bed diameter (1/8" thick P.V.C. liner was used); 3.77 ins.
Bed lengths: Short : 3.30 ins., N = 13.5
Long : 12.50 ins., N = 51.6
Tube to particle diameter ratio d_T/d_p = 15.5
Limiting porosity above support zone: 0.356
Particle specific gravity : 2.583 at 77°F
Particle thermal capacity: 0.184 B.T.U./(lb°F)
Particle volumetric thermal capacity: 29.6 B.T.U. /(ft.^{3} °F)
Particle thermal conductivity: 0.57 B.T.U. /(hr.ft.°F)
Assumed Prandtl number: 0.74
Assumed thermal capacity of air: 0.24 B.T.U./(lb.°F) at 75°F
Viscosity of air (75°F): 0.0448 lb./(hr.ft)
Thermal conductivity of air: 0.0145 B.T.U. / (hr.ft.°F)
Approximate temperatures in the bed ranged from 68°F to 78°F.

TABLE B.3.2

RESULTS OF PULSE TESTS AFTER EQUIPMENT MODIFICATIONS REPLICATE RUNS - 6.2 mm.

SODA GLASS

All runs at 40 p.s.i.g. (V_H = 775) except run 6 which was at 16 p.s.i.g., (V_H = 1380).

Run	Re_p	$\mu(t)/N$ (min)	σ^{*2}	π^{*3}	σ^*/N	$N.^{2/3}\pi^*$	γ_1	γ_2	$\beta_\%$
	Bed length N = 51.6 Date 9.9.68, L = 12.5:								
3	947	.0455	.120	.0192	2.48	3.71	.46	1.34	95.9
2	946	.0450	.110	.0154	2.38	3.45	.42	1.27	96.2
4	947	.0451	.112	.0152	2.41	3.44	.40	1.21	96.8
1	948	.0455	.119	.0185	2.48	3.66	.45	1.31	97.0
6	1080	.0401	.148	.0676	2.77	5.65	1.18	3.08	98.0
	Bed length N = 13.5., Date 2.10.68 , L - 3.3 ins:								
8	887	.0494	.434	. 264	2.42	3.64	.92	1.40	99.2
9	887	.0491	.422	. 227	2.39	3.46	.83	1.28	89.1
10	887	.0488	.426	.1238	2.40	3.52	.85	1.31	99.8
11	887	.0495	.435	. 271	2.42	3.67	.94	1.43	88.4
12	887.	.0489	.409	. 206	2.35	3.35	.79	1.23	99.2
5	889	.0475	.414	. 211	2.37	3.38	.79	1.23	96.4
14	894 mean	.0474	.420	. 226	2.38	3.46	.83	1.28	98.2
13	836	.0513	.402	. 199	2.33	3.32	.78	1.23	99.6
5	1245	.0351	.499	. 357	2.60	4.03	1.02	1.44	99.5

In table B.3.2, the ratio β represents the ratio (output pulse area)/(input pulse area) expressed as a percentage after correcting for recorder span and the number of thermocouples in thermopile at each level. 'Skewness' γ_1 has been defined by equation (II.E.1.1).

The following statistical quantities have been extracted from Table B.3.2 as a measure of the variability of $\mu(t)/N$, $\sqrt{N}\sigma^*$, γ_1, and γ_2 (Tables B.3.3 and B.3.4).

TABLE. B.3.3.

VARIABILITY OF PULSE TEST EXPERIMENTAL RESULTS AFTER EQUIPMENT MODIFICATIONS.

REPLICATE RUNS.

QUANTITY		VALUE		
		Long bed length	Short bed length	Pooled, long-short
Run numbers		1-4 incl.	5,8-12 incl. 14	14,1-5 incl. 8-12 incl.
Mean Reynolds numbers calc.		947	890	-
$\mu'_1(t)/N$, (minutes)	Mean	.0453	.0492	-
	Std. devn.	1.82×10^{-4}	9.46×10^{-4}	-
	95% confidence limits	.0450 to.0456	.0483 to.0501	-
$\sqrt{N}.\sigma^*$	Mean	2.44	2.33	
	Std. devn.	5.0×10^{-2}	3.7×10^{-2}	4.2×10^{-2}
	95% confidence limits	2.36 to 2.52	2.30 to 2.36	-
γ_1	Mean	.435	.850	-
	Std. devn.	.027	.062	.053
	95% confidence limits	.392 to .478	.788 to .912	-
γ_2	Mean	1.282	1.323	1.308
	Std. devn.	.046	.082	.098
	95% confidence limits	1.209 to 1.398	1.248 to 1.398	1.232 to 1.374

TABLE B.3.4

RESULTS OF STATISTICAL TESTS ON REPLICATE RUN DATA [Brownlee, 1949].

COMPARISONS BETWEEN LONG AND SHORT BED LENGTH RESULTS.

QUANTITY	TEST	SIGNIFICANCE LEVEL
$\mu_1'(t)/N$	t test between means	$p<0.001$
	F test for variability	$.01<p<.05$
$\sqrt{N}\sigma^*$	t test	$.001<p<.01$
	F test	$.05<p<.20$ (Non sig.)
γ_1	t test	$p<.001$
	F test	$.05<p<.20$ (Non sig.)
γ_2	t test	$p>.20$ (Non sig.)
	F test	$p>20$ (Non sig.)

4. Discussion of Results of Reliability Experiments.

It is unfortunate that the experiments reported in section B.3 were not carried out under the same conditions as the earlier ones. Nonetheless, it seems obvious without detailed statistical analysis that an improvement in consistency and reliability has occurred. The improvement in consistency is obvious from the absence of negative values of skewness whilst the ratio of skewness parameters γ_1 is equal

to the ratio of the square roots of the bed lengths N as predicted by theory for all theoretical models considered in earlier chapters. The parameter γ_2 is predicted to be independent of bed length and no significant difference was noted between the experiments at differing bed length.

The significant difference between the means of the length normalised centres of mass $\mu(t)/N$ is to be expected from the small differences in flowrate and is in the correct direction. The significant difference between the means of the curve spread parameter $\sqrt{N}\sigma^*$ at the two different bed lengths is also to be expected for the same reason.

An improvement in experimental technique was later made by using a greater inlet temperature change of shorter duration. This ensures that the outlet pulse response more nearly approaches the impulse response of the system. It will be noted that the difference in variability of the second and third moments was found to be 'non significant', i.e. $p>0.05$.

Further detailed analysis of these and other pulse test results is deferred until sections D and E.

C. LEAD PACKING STEP TESTS

1. Objectives of the Experiments and Experimental Conditions

The first objective of the lead packing experiments was to provide a control, uncontaminated by intraparticle conduction effects,

on the soda glass and Perspex experiments. A second objective was to test the validity of the moments analysis technique developed in section V.D.2.

A bed consisting of about 0.3 inch of 6 mm soda glass beads above and around the thermocouples (for electrical insulation) was used, the bulk of the bed (6.0 inches) being packed with I.C.I. Ltd. 'BB' shot (antimonial lead). Porosity of the lead section of the bed was checked by plotting bed depth against weight added and drawing a smoothed line through the data using the bed diameter and lead density given in Appendix 11. The calculated value of 0.361 differs by 2% from the value of 0.368 measured by kerosene displacement as recorded in Appendix 11. This is regarded as satisfactory agreement and an indication that the method of packing used was reasonably reproducible. In packing the bed, lead shot was added in teaspoon increments, distributing the packing as evenly as possible over the bed. This method of packing differed from the (earlier) method used in soda glass experiments and described in section VI.A.2. The lead shot as supplied had been packed in airtight polythene bags and appeared to be free from oxidation and to be of good sphericity.

In calculating theoretical values of $\mu(t)$, the 'centre of mass' of the impulse response, a mean value of $M.c_s$, (the bed thermal 'capacity' in B.T.U./$^{\circ}$F) was used, making allowance for the small amount of soda glass in the bed. Similarly the value of

N used in subsequent calculations is a composite one of glass and lead. Thus, in defining KV_H:

$$N = \frac{\text{Total Volume of bed}}{A_c \cdot d_p} \qquad \ldots (1.1)$$

Hence, if ε_1, M_1, ρ_1 and d_{p_1} refer to porosity mass, density and diameter of soda glass in the bed and ε_2, M_2, ρ_2 and d_{p_2} are the corresponding values for the lead, where A_c is the cross sectional area of the bed, then

$$N = \left[\frac{M_1}{(1-\varepsilon_1).\rho_1.d_{p_1}} + \frac{M_2}{(1-\varepsilon_2).\rho_2.d_{p_2}} \right] A_c \qquad \ldots (1.2)$$

TABLE C.1.1

EXPERIMENTAL CONDITIONS FOR

STEP TESTS ON 4 m.m. LEAD PACKING

Packing: 6.3 inch of 4.04 m.m. I.C.I. lead shot and

0.3 inch of 6.2 m.m. soda glass.

Weight of glass: 0.24 lbs

Weight of lead: 17.09 lbs.

Specific Gravity of lead: 11.2 at 65°F

Approximate heat capacity, Antimonial lead,

[Perry, Chemical Engineers Handbook, Fourth Edn.

Table 23-5, page 23] : 0.032 B.T.U./(lb.°F)

Porosity of lead in simulated section: 0.368

Check calculation based on length and weight in

test section: $\varepsilon = 0.361$

Nett bed diameter inside 1/8" P.V.C. liner: 3.77 inches

Calculated value of N: 39.0

Tube to particle diameter ratio, $d_T/d_p = 23.6$

Assumed lead thermal conductivity: 18 B.T.U./(hr.ft.°F),

[Perry, op. cit]

Method of packing: as described above.

Assumed Transport and other properties of air as listed in

Table B.3.1.

NOTE All runs carried out at 5.0 p.s.i.g.

Date of experiments June, 1970.

2. Lead Packing Step Tests - Data Analysis Methods.

(i) Step Response to Moments Analysis

In order to test the method for extraction of higher order moments from a step response as proposed in section V.D.3, sixteen lead packing step tests were processed using this method. This was also necessary in order to provide an independent estimate of $\mu(t)$, since the thermal capacity of the 4 m.m. antimonial lead spheres used was not measured.

Simpson's 1/3 rule integration of $\phi(t)$ to obtain the first two moments was carried out after normalising the breakthrough curve such that $0 < u(t) < 1$ i.e. $1 > \phi(t) > 0$. At least 100 equally spaced values were read from each response curve and $\mu(t)$ and σ^2 calculated from

$$\left.\begin{aligned} \mu(t) &= \mu_{\phi_0}, \\ \mu'_2(t) &= 2.\mu'_{\phi_1}, \\ \sigma^2(t) &= \mu'_2(t) - \mu^2(t), \\ \text{yielding} \quad \sigma^{*2} &= \sigma^2(t) \,/\, n\mu^2(t). \end{aligned}\right\} \quad \ldots(2.1)$$

(ii) Analysis of Points on The Breakthrough Curve.

This method provided an alternative estimate of the effective value of σ^*, the normalised impulse response standard deviation. The times for 5%, 10%, 20% and 40% of completed response were obtained from the curves and subtracted from the time to 80% of completed response. The value of $\mu(t)$, the impulse response centre of

mass for each run, was then used to convert the time differences ΔT to normalised time differences ΔT^*. Then the empirical plots of section IV.D.2 were used to obtain estimates of σ^* for each run. Where differences between estimates of σ^* for a particular run exceeded about 2% (i.e. a difference of 4% in σ^{*2}) the reason was generally found to be due to transcription errors and this led on occasions to a re-calculation of $\mu(t)$. This 'self check' on consistency seems rather similar to Handley's 'analogous curve' method of data analysis. It does, of course, assume that the breakthrough curves have the shape predicted by the Schumann solution. Since the breakthrough curves had already been 'sampled' for numerical integration, the points on the curves referred to above were obtained by Lagrange interpolation over 11 points in the vicinity of each value of interest.

As a rough check on the overall shape of the breakthrough curves and as a check on the effect of small errors in the location of the final value of the response, arithmetic plots of $u(t^*)$ against $F = 1/\sqrt{t^*} - \sqrt{t^*}$ were made (section IV.B.2). Results are discussed in section C.4 below.

3. Lead Packing Step Tests - Moments Analysis.

The results of the application of equation (C.2.1) to the lead packing step tests are shown in Table C.3.1. In computing the Stanton number, St, from the estimated values of σ^{*2} no correction is made for fluid phase axial dispersion at this stage. Thus assuming a Biot number of zero, we obtain from equations (II.B.3.10) and

(II.B.2.3) setting the axial dispersion term equal to zero :

$$St_{calc} = \frac{1}{3(1-\varepsilon).\ N\ \sigma^{*2}} \qquad \ldots(3.1)$$

TABLE C.3.1.

RESULTS OF STEP RESPONSE TO MOMENTS COMPUTATIONS

LEAD PACKING EXPERIMENTS.

N = 39.0, ε = 0.36

(See Table C.1.1 for Experimental Conditions).

Run No.	Re_p	$\mu(t)$ (min)		σ^{*2}	St	m	t^*_{max}	$\beta_{\%}$
		Calc.	Theory	Calc.	Calc.			
1	493	1.21	1.16	.1367	.098	149	3.03	103.0
2	478	1.26	1.19	.1591	.084	153	3.23	97.2
3	775	.74	.73	.1555	.086	161	2.83	100.0
4	213	2.62	2.64	.1069	.125	150	2.44	89.4
5	447	1.30	1.27	.1604	.083	164	3.36	97.6
6	405	1.48	1.40	.1123	.119	119	2.11	93.6
7	273	2.21	2.08	.1112	.120	182	2.35	91.4
8	275	2.16	2.17	.1102	.121	187	2.43	90.4
9	193	2.80	2.94	.0796	.168	181	2.16	89.7
10	91	6.10	6.22	.1124	.134	196	2.77	80.0
11	315	1.92	1.89	.1779	.075	281	3.78	94.0
12	950	.61	.60	.1572	.085	122	2.85	100.0
13	700	.84	.81	.1530	.087	89	2.86	100.5
14	700	.84	.81	.1603	.083	95	3.01	97.6
15	665	.87	.85	.1458	.092	162	2.41	99.7
16	649	.91	.87	.1579	.085	184	2.75	98.9

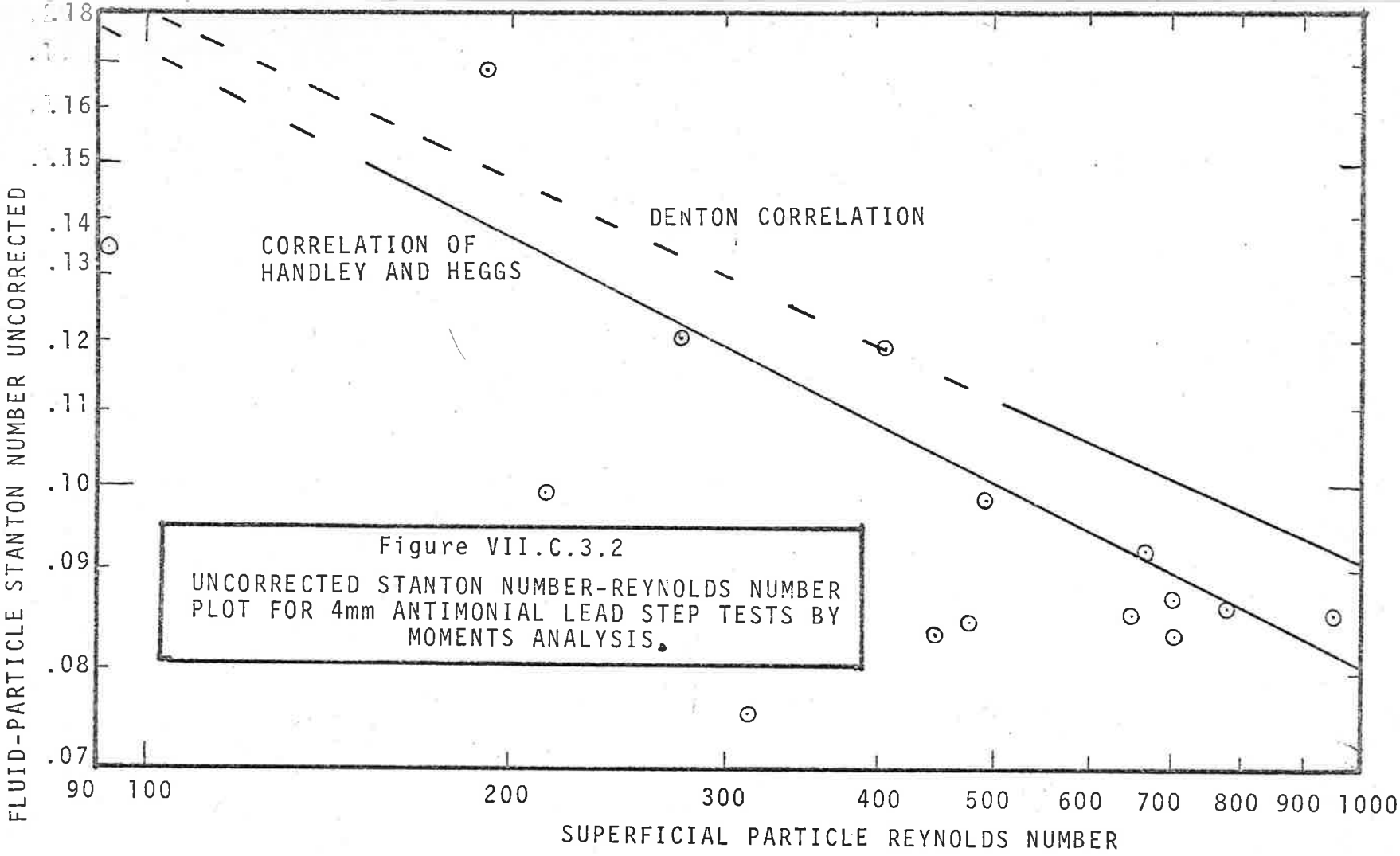

Figure VII.C.3.2

UNCORRECTED STANTON NUMBER-REYNOLDS NUMBER PLOT FOR 4mm ANTIMONIAL LEAD STEP TESTS BY MOMENTS ANALYSIS.

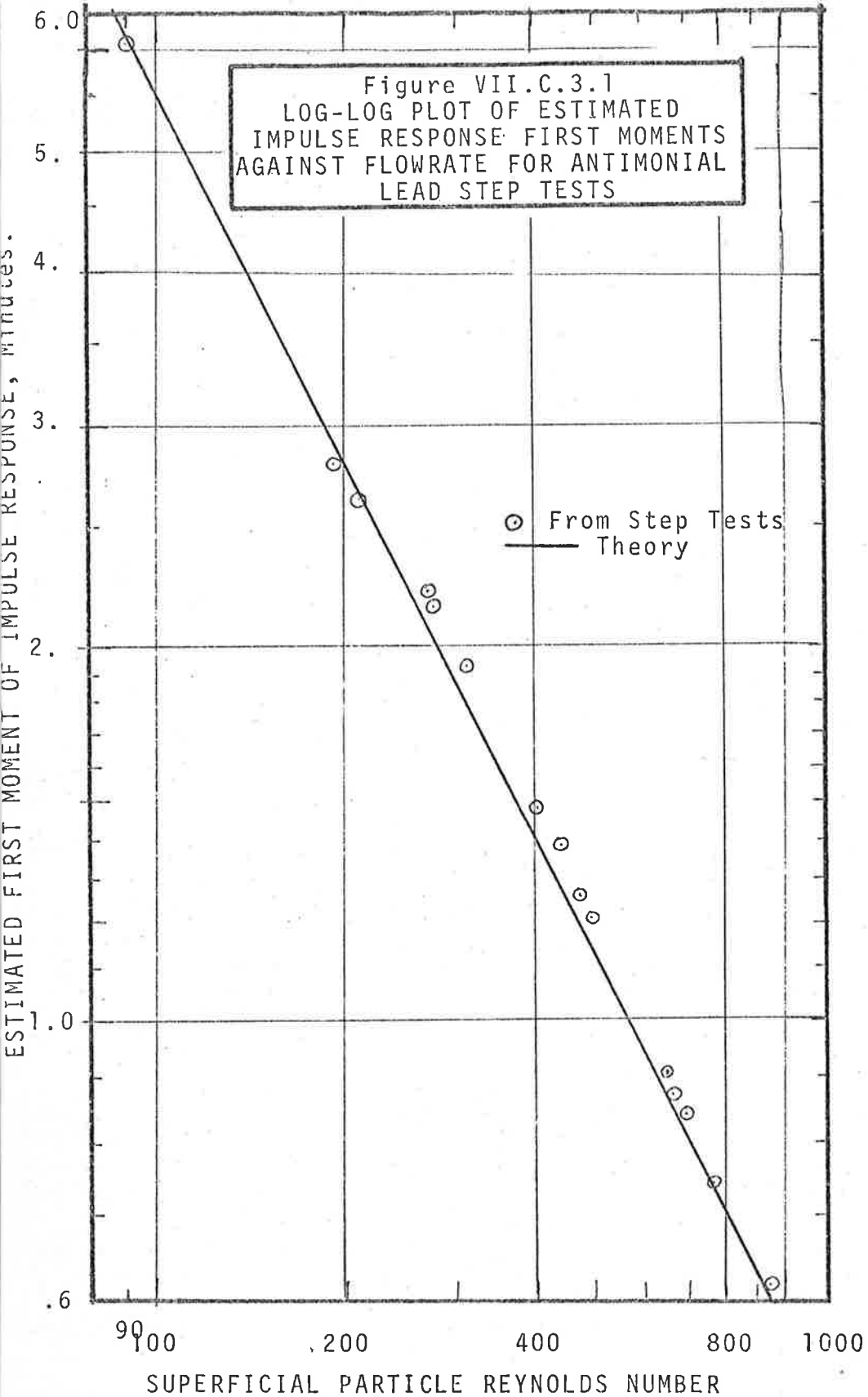
Figure VII.C.3.1
LOG-LOG PLOT OF ESTIMATED
IMPULSE RESPONSE FIRST MOMENTS
AGAINST FLOWRATE FOR ANTIMONIAL
LEAD STEP TESTS
From Step Tests
Theory
ESTIMATED FIRST MOMENT OF IMPULSE RESPONSE, Minutes.
6.0
5.
4.
3.
2.
1.0
.6
90
100
200
400
800
1000
SUPERFICIAL PARTICLE REYNOLDS NUMBER

In Table C.3.1, m is the number of data points read whilst t^*_{max} is the maximum time reading in normalised time units. Thus the mesh spacing, Δ, for numerical integration is given by $t^*_{max}/(m - 1)$.

The resultant log-log plot of estimated first moment $\mu(t)$ against flow is given in figure C.3.1 and compared with the values ($\mu(t)$ theory in table C.3.1) calculated from

$$\mu(t) = \frac{M.c_s}{W.c_f}$$

Agreement between the values is good despite the increasing heat loss from the section at low flows as shown by the reduced values of β. The results shown support the theory that the centre of mass is independent of transport parameters.

A plot of calculated Stanton number against flow on a log-log scale is given in figure C.3.2 and compared with the correlations of Denton (extrapolated back below its valid lower limit of $Re_p = 500$) and of Handley and Heggs. The data shows an unacceptable degree of scatter which was not present in either Denton's or Handley and Heggs' work since the correlation coefficient of log (St) on log (Re_p) is only -.722 with correspondingly wide 95% confidence limits.

Estimated Biot numbers, based on the assumed thermal conductivity given in Table C.1.1, never exceed 0.05 even at the maximum flowrate.

Hence the maximum contribution to variance from intraparticle heat transfer resistance is about 1% at the maximum flowrate according to equations (II.B.3.10).

An error analysis, given in section C.5 indicates that this variability is inherent in the moments technique and may be due to a small amount of residue baseline 'drift' and inaccuracies of integration.

4. Lead Packings Results - Breakthrough Curve Analysis

(i) Comparison with empirical correlations

The results obtained by using the empirical correlations of section IV.D.2 in the manner outlined in section C.2 (ii) above are listed in Table C.4.1. Analysis using (say) the 5/95%, 10/90%, 20/80% and 40/60% points rather than the 5/80%, 10/80%, 20/80% and 40/80% times would, no doubt, have given more consistent results and would have placed less reliance on a single value, the time to 80% of completed response.

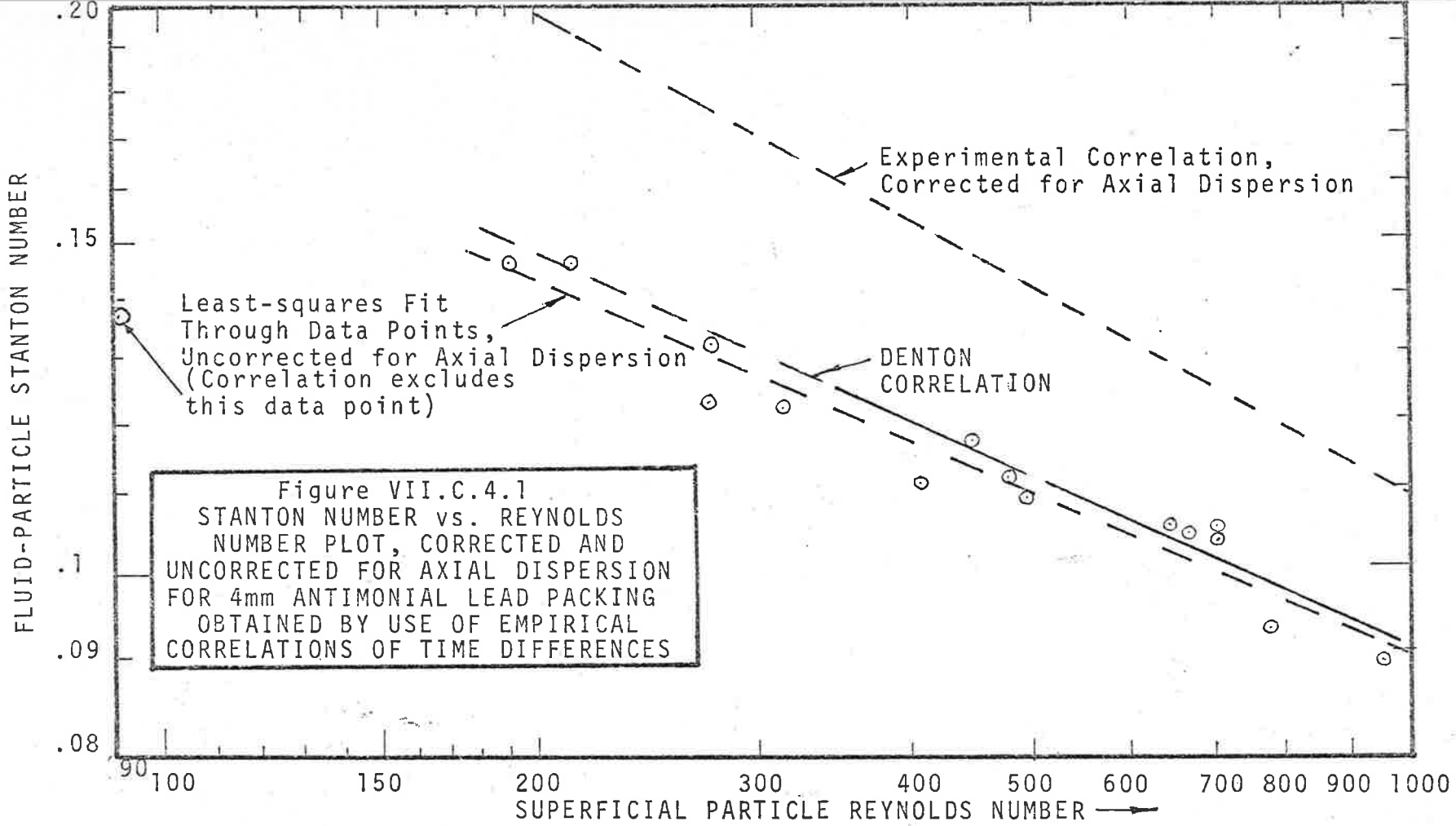

Figure VII.C.4.1
STANTON NUMBER vs. REYNOLDS NUMBER PLOT, CORRECTED AND UNCORRECTED FOR AXIAL DISPERSION FOR 4mm ANTIMONIAL LEAD PACKING OBTAINED BY USE OF EMPIRICAL CORRELATIONS OF TIME DIFFERENCES

TABLE C.4.1

RESULTS OBTAINED BY USE OF EMPIRICAL CORRELATIONS IN BREAKTHROUGH CURVE ANALYSIS.

4 mm. LEAD PACKING EXPERIMENTS

(See Table C.1.1 for Experimental Conditions)

Run No.	Re_p	σ^{*2} Estimated From --				Mean σ^{*2}	St calc.
		$\Delta T_{05/80}$	$\Delta T_{10/80}$	$\Delta T_{20/80}$	$\Delta T_{40/80}$		
1	493	.118	.129	.124	.119	.1225	.1087
2	478	.116	.118	.125	.119	.1194	.1116
3	775	.141	.147	.143	.143	.1436	.0927
4	213	.090	.094	.091	.092	.0918	.1455
5	447	.112	.120	.115	.112	.1147	.1161
6	405	.115	.121	.124	.119	.1197	.1112
7	273	.102	.116	.108	.107	.1083	.1223
8	275	.100	.104	.102	.099	.1099	.1319
9	193	.089	.093	.095	.095	.0932	.1450
10	91	.093	.103	.098	.097	.0977	.1362
11	315	.107	.114	.108	.108	.1091	.1220
12	950	.150	.149	.151	.149	.1497	.0892
13	700	.122	.132	.128	.122	.1262	.1055
14	700	.123	.136	.130	.127	.1291	.1032
15	665	.137	.144	.136	.135	.1381	.0964
16	649	.121	.128	.130	.128	.1267	.1051

The computed Stanton numbers, uncorrected for fluid phase axial dispersion, are plotted on figure C.4.1. Even a cursory comparison with figure C.3.2 shows that considerably less scatter

occurs in the values obtained from the empirical correlation and the computed first moment $\mu(t)$ than from pure moments analysis. The regression line of St_{calc} on Re_p obtained is, for $230 \leq Re_p \leq 950$:

$$St_{calc} = 0.652 \; / \; Re_p^{0.289}$$

with correlation coefficient -. on a log-log plot and 95% confidence limits of ±8.2%

Run number 10 has been omitted from the correlation since at this low Reynolds number (90) axial solids conduction is probably of importance.

The data, uncorrected for axial dispersion, is more nearly in agreement with the Denton correlation than with that of Handley and Heggs or Gillespie et al.

When the axial dispersion correction is applied, by use of the appropriate F factor (section III.C.1) the resultant heat transfer correlation (figure C.4.1) ranges from 40% down to 20% above the uncorrected correlation.

This may be seen by substituting $\varepsilon = 0.36$ and (i) $St_{calc} = 0.15$ (ii) $St_{calc} = 0.09$ in the equation for the F factor obtained by rearranging equation (III.C.1.3), i.e.

$$F = 1 - 3(1 - \varepsilon) St_{calc} = \frac{St_{calc}}{St}, \qquad \ldots(4.1)$$

where Pe is assumed equal to 2.0.

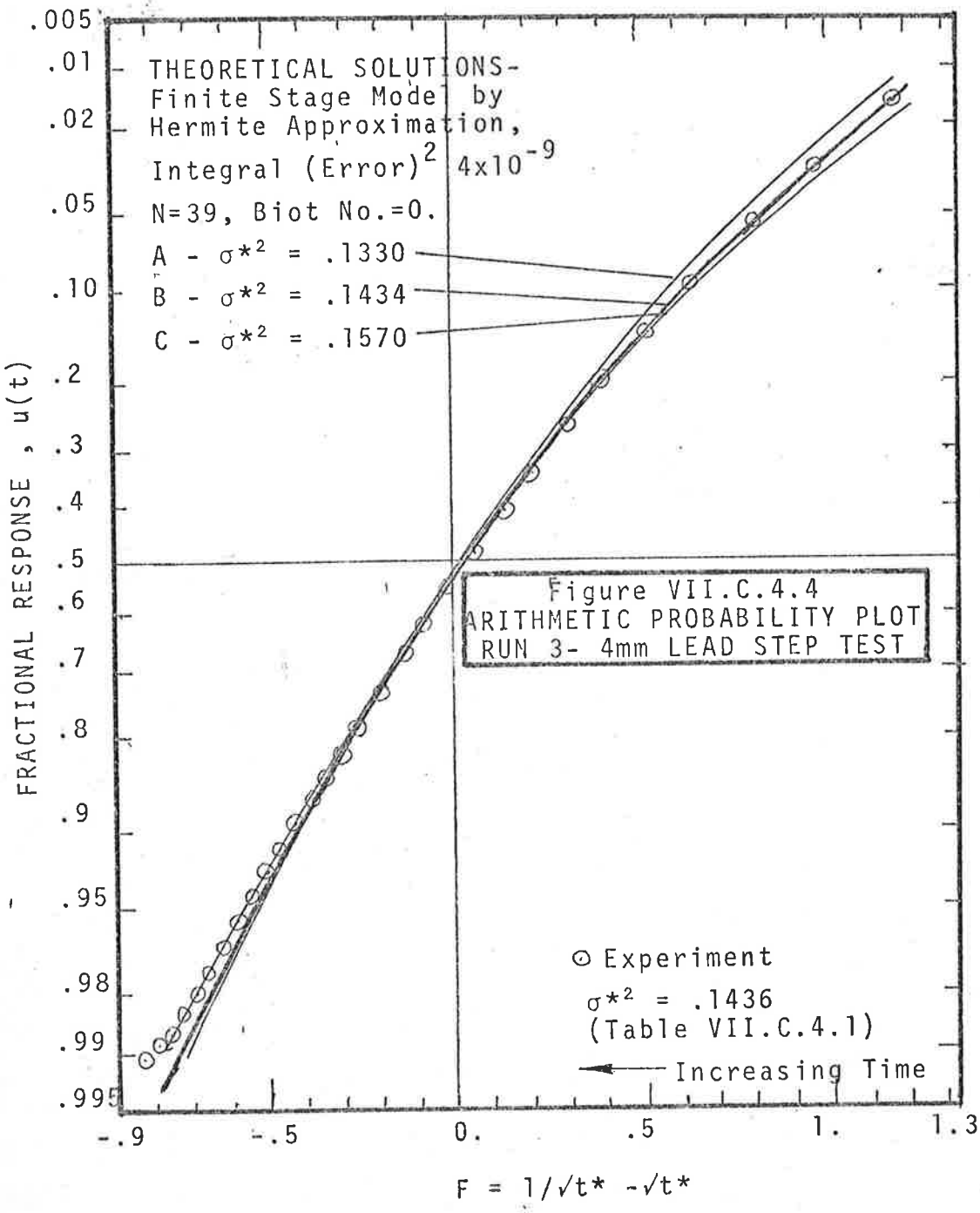
THEORETICAL SOLUTIONS-
Finite Stage Model by
Hermite Approximation,
Integral (Error)^2 4×10^{-9}
N=39, Biot No.=0.
A - σ^{*2} = .1330
B - σ^{*2} = .1434
C - σ^{*2} = .1570
Figure VII.C.4.4
ARITHMETIC PROBABILITY PLOT
RUN 3- 4mm LEAD STEP TEST
⊙ Experiment
σ^{*2} = .1436
(Table VII.C.4.1)
Increasing Time
FRACTIONAL RESPONSE , u(t)
.005
.01
.02
.05
.10
.2
.3
.4
.5
.6
.7
.8
.9
.95
.98
.99
.995
-.9
-.5
0.
.5
1.
1.3
F = 1/√t* -√t*

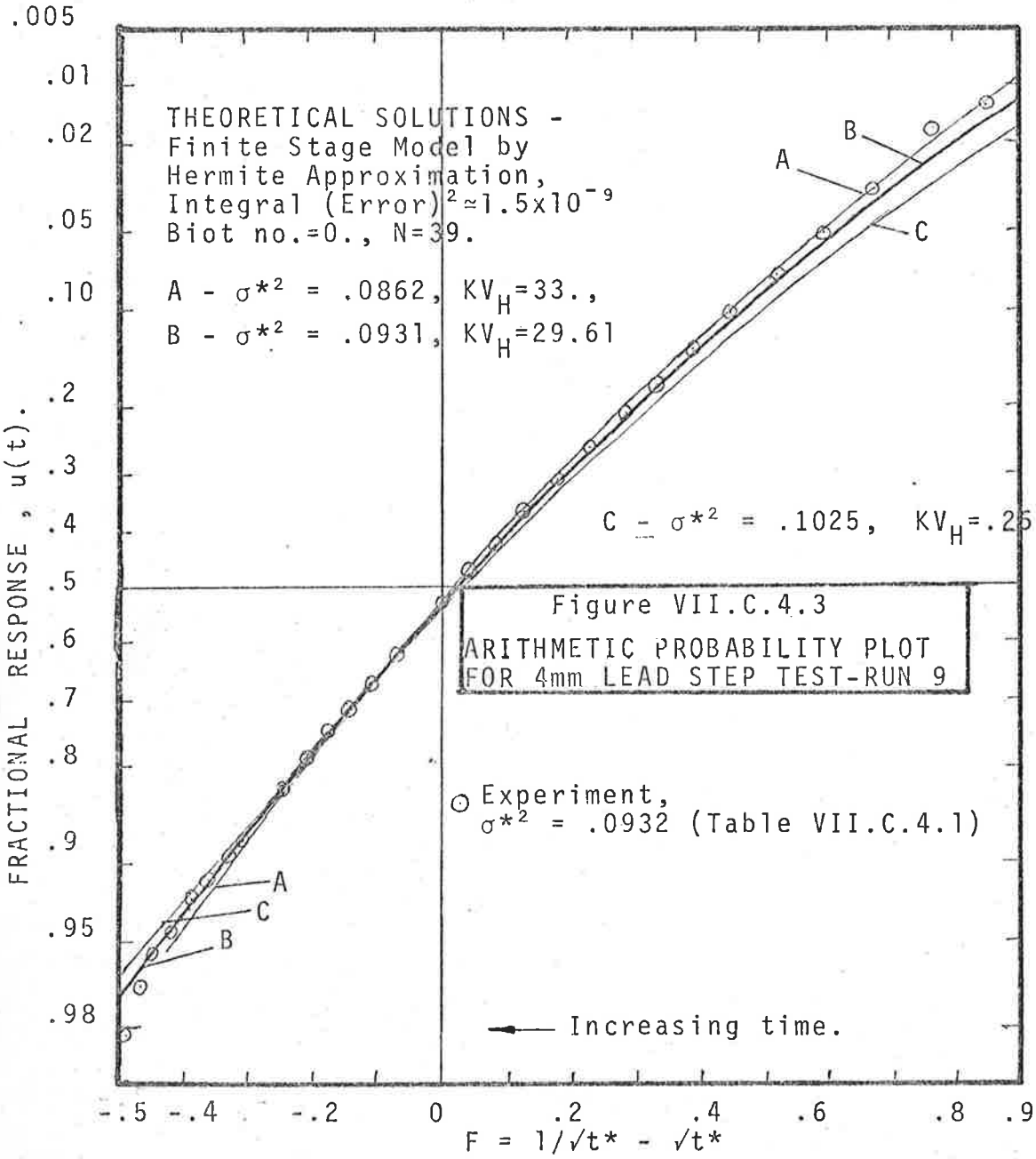
.005
.01
.02
.05
.10
.2
.3
.4
.5
.6
.7
.8
.9
.95
.98
FRACTIONAL RESPONSE , u(t).
THEORETICAL SOLUTIONS -
Finite Stage Model by
Hermite Approximation,
Integral (Error)$^2 \simeq 1.5 \times 10^{-9}$
Biot no.=0., N=39.
A - σ^{*2} = .0862, KV_H=33.,
B - σ^{*2} = .0931, KV_H=29.61
C - σ^{*2} = .1025, KV_H=.25
A
B
C
Figure VII.C.4.3
ARITHMETIC PROBABILITY PLOT
FOR 4mm LEAD STEP TEST-RUN 9
⊙ Experiment,
σ^{*2} = .0932 (Table VII.C.4.1)
Increasing time.
-.5 -.4 -.2 0 .2 .4 .6 .8 .9
F = $1/\sqrt{t^*} - \sqrt{t^*}$

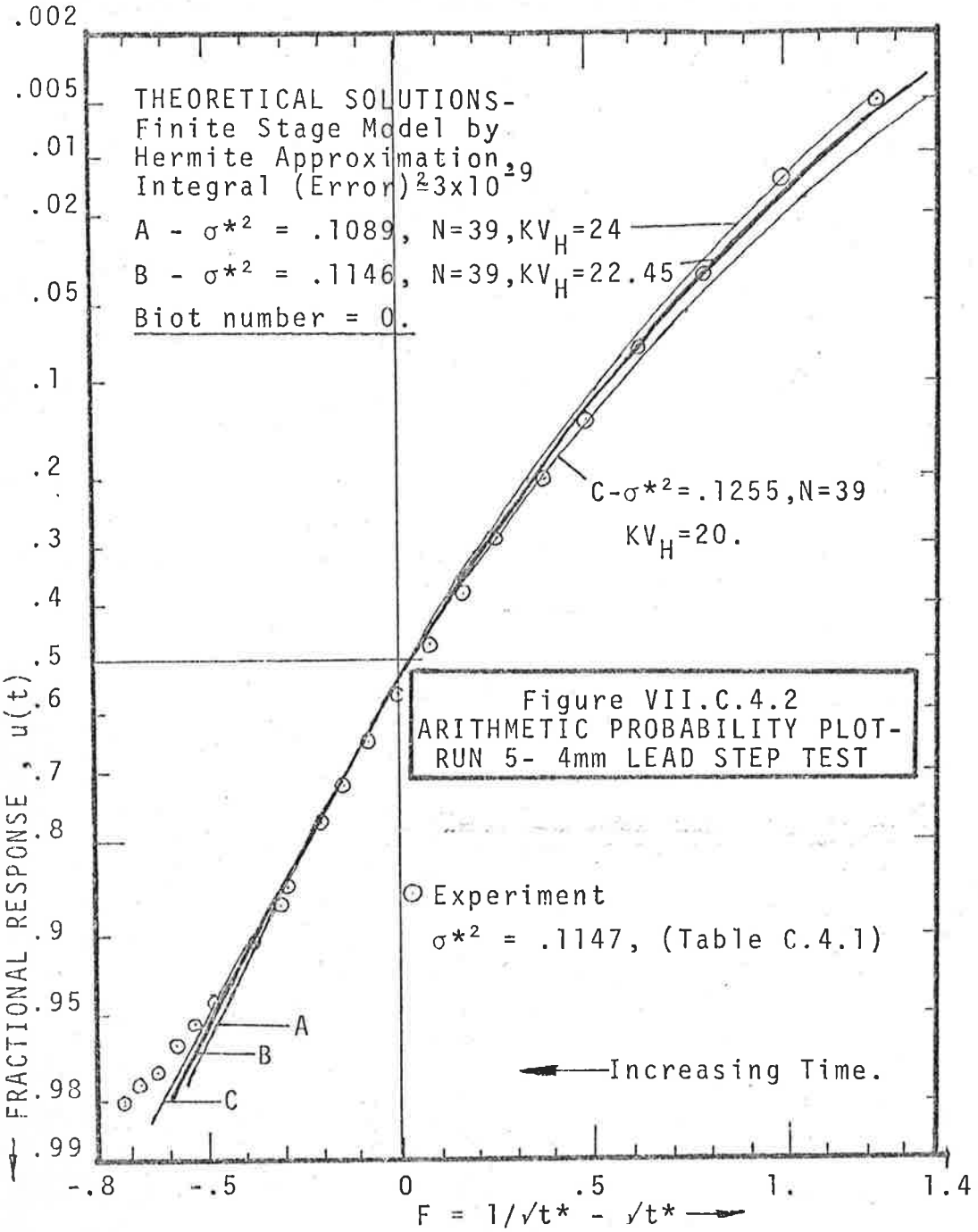
THEORETICAL SOLUTIONS-
Finite Stage Model by
Hermite Approximation,
Integral (Error)² ≅ 3x10⁻⁹
A - σ*² = .1089, N=39, KV_H=24
B - σ*² = .1146, N=39, KV_H=22.45
Biot number = 0.
C-σ*²=.1255, N=39
KV_H=20.
Figure VII.C.4.2
ARITHMETIC PROBABILITY PLOT-
RUN 5- 4mm LEAD STEP TEST
Experiment
σ*² = .1147, (Table C.4.1)
Increasing Time.
A
B
C
FRACTIONAL RESPONSE , u(t)
.002
.005
.01
.02
.05
.1
.2
.3
.4
.5
.6
.7
.8
.9
.95
.98
.99
-.8
-.5
0
.5
1.
1.4
F = 1/√t* - √t*

In equation (4.1) St is the corrected Stanton number and St_{calc} is the uncorrected value as listed in Table C.4.1.

Since theoretical analysis thus far has shown that axial dispersion and fluid-solid effects may be expected to be difficult to separate by analysis of the curve shape alone, it seems that, for this range of flowrates and V_H factors at least, practical prediction of breakthrough curves could be accomplished by using the simplest (i.e. Schumann's model and a heat transfer correlation which corresponds to the model, i.e. is uncorrected for axial fluid dispersion.

(ii) Arithmetic Probability Plots

Figures C.4.2. to C.4.4 display a number of arithmetic probability plots for the experimental runs compared with theoretical finite stage and equivalent conductivity plots having the same values of σ^*. It may be seen that as predicted (section IV.D.1) the experimental plots are curved, particularly for small times. For the experiments reported here, the heat capacity ratio V_H is high (apprpximately 1580). Some of the experimental curves also shown curvature for large times so that it would be difficult to extract accurate model parameters from the limiting large time slope of the curves. It appears likely from the discussion of errors given in section C.5 below that apparent curvature of the plots at large times results from small inaccuracies in

determination of the final steady state value of a breakthrough curve.

5. DISCUSSION OF ERRORS FOR STEP RESPONSE COMPUTATIONS

(i) Types of Error Considered

In this section we are concerned with the effects of small but systematic errors due to actual 'drift' in the measurement system or introduced by the operator in curve reading.

Firstly, other errors will be considered briefly. In computing normalised moments by integration, the actual time scale is irrelevant. The main error is that due to a 'blunder' in reading the flowrate since the calibration reported in section VI.C.4 suggests an error in reading of no more than about 2%. In computing the Stanton number from the normalised variance σ^{*2}, bed length in particle diameters N and porosity are used for highly conductive particles each with an estimated error of 2% yielding an overall maximum error of about 5% in St. If the first moment is determined directly from the flowrate, then the estimate of σ^{*2} and hence of Stanton number is affected, a + 2% error in flow yielding a -4% error in estimated Stanton number. The effect of flowrate errors on a final heat transfer correlation should be much smaller when the first moment is estimated from the response data. Similar remarks apply to pulse test analyses by either moments or pulse to frequency response.

The two most common errors arising in curve reading are :

(a) incorrect estimation of the final value of the response, resulting in a 'displacement' error. The estimated value of the normalised response $u(t)_{est}$ is related then to the ~~'true'~~ 'true' value $u(t)$ by

$$u(t)_{est} = \frac{u(t) \pm \varepsilon}{1 \pm \varepsilon} \qquad \ldots(5.2)$$

where ε is the fractional error in the final value.

(b) 'Drift' type error may occur either as a result of slow changes in thermocouple reference temperature or as a result of incorrect alignment of the chart record on the curve reader. In this case, we assume an error which is linear with time and which becomes the same as in (a) when $t = t_{max}$. In this case we have :

$$\phi_{est} = \frac{\phi(t)}{1 \pm \varepsilon} + \frac{\varepsilon}{1 \pm \varepsilon} \left(1 - t^*/t^*_{max}\right) \qquad \ldots(5.3)$$

where $t^* = t / \mu(t)$

= time normalised with respect to the first moment $\mu(t)$

and t^*_{max} = is similarly - normalised final time used in computations.

In addition to the above sources of error, a value may be inadvertently added or omitted during curve reading. If this occurs as a result of incorrectly estimating the location of $t = o$ on the chart, then since the response is generally effectively zero for

for $t \simeq o$, such an error has the effect of shifting the centre of mass without affecting the value of variance [in $min.^2$]. To a first approximation, a fractional error ε in $\mu(t)$ leads to an error of order 2ε in the normalised variance σ^{*2}.

(ii) Likely Magnitude of Errors.

Relative errors in the large time values (the 'tail' of a response) may be expected to become large when the reading approaches the final value to within the limit of resolution of the recorder. For the 'Rikadenki' potentiometric recorder used it was found that the rated resolution and repeatability of 0.2% of full scale (i.e. 0.02 inch) was not always achievable. A value of 0.04 inch seems more reasonable. This represents (for a 1 m V full scale deflection with 5 thermocouples in series and 23μV/^{o}F per thermocouple) a voltage change of 2μV or a temperature change of 0.03F^{o}. This is about equal to the 'typical stability' (.02F^{o}) expected by the Leeds and Northrup company of their 8435 Ice Reference System used in the lead packing experiments.

Errors also arise during curve reading.

All data for moments analysis was read from the curves using a 'Oscar' curve reader linked to an I.B.M. card punch. When cross hairs had been aligned, two three-decimal-digit numbers in the range 000 to 999 are punched onto a card representing the y and t coordinates of the point. This represents a nominal resolution of 0.1% or 0.01 inch for a 10 inch scale. In practice, a repreatability

of $\pm$ 2 parts in 1000 or $\pm$ 0.2% is the best attainable under good conditions.

In the calculations which follow, a likely overall error of $\pm$ 0.5% is assumed thus combining recorder, reference junction and curve reader errors.

It should be noted that whilst misalignment of the chart may be minimised with due care, actual temperature drift of the final value due to poor temperature control or slow changes in reference junction voltage is difficult to detect unless we assume the response to have, a priori , a particular form. For example a semilogarithmic plot of the data may be made and, as proposed by Sater and Levenspiel [1966] a pure exponential decay fitted to the data after a certain time, ignoring large time errors if present.

(ii) Estimated Errors in Moments.

Equations (5.2) and (5.3) may be used to determine fractional errors resulting in $\mu(t)_{est}$, $\mu_2(t)_{est}$ and σ^{*2}_{est}.

For displacement of the final value we obtain

$$\mu(t)_{est} = \frac{\mu(t)}{1 \pm \varepsilon} \quad ,$$

$$\mu_2(t)_{est} = \frac{\mu_2(t)}{1 \pm \varepsilon} \quad , \qquad \ldots (5.4)$$

and $$\sigma^{*2}_{est} = \sigma^{*2} \pm \varepsilon \mu_2^{*}$$

$$= \sigma^{*2} + \varepsilon \mu_2(t)/[\mu(t)]^2$$

Hence, a fractional error of ε in the final value of $u(t)$ leads to an identical fractional error in the estimated first and second absolute moments. When estimating the normalised variance σ^{*2} however, a very considerable magnification in the error may occur. As an example, assume $\varepsilon = 0.005$ and the true value of σ^{*2} is about 0.100 as in the lead packing experiments.

Then : $\sigma^{*2}_{est} = 0.100 + 0.005 \times 1.100$

$= 0.1055$

a + 5½% error, i.e. the original + 0.5% error in $u(t)$ has been magnified 10 times. On the other hand, the error in the dimensional first moment $\mu(t)$ is still only 0.5%, so that greater confidence may be placed in this result.

Errors resulting from drift (although smaller) may be added to the above. According to equation (5.3):

$$\frac{\mu(t)_{est}}{\mu(t)} = \frac{1}{1 \pm \varepsilon} \pm \frac{\varepsilon . t^*_{max} . (1 - \varepsilon/2)}{1 \pm \varepsilon}$$

and

$$\sigma^{*2}_{est} = \frac{\sigma^{*2} \pm \varepsilon \mu^*_2}{1 \pm \varepsilon t^*_{max} . (1 - \varepsilon/2)} \pm \frac{\varepsilon . t^*_{max} [(1 \pm \varepsilon) t^*_{max} /3. - 1 + \varepsilon/2]}{1 \pm \varepsilon t^*_{max} . (1 - \varepsilon/2)} \quad \ldots (5.5)$$

Using the same parameters as before, with $t^*_{max} = 3$ as in the lead experiments, we obtain

$$\mu(t)_{est} = \mu(t) \times 1.0099, \text{ about 1\% error}$$

and $\sigma^*_{est} = 0.1040$, a 4% error.

Hence the final fractional error of 0.5% in estimating u(t) has been multiplied 8 times in the estimated value of normalised variance. Further, for a fixed ε, an increase in t_{max} will lead to a quadratic increase in error, i.e. the reading of more and more values in an effort to achieve greater accuracy may be self defeating.

In section C.6 below an analysis of the effect which the same errors have on the breakthrough curve analysis method of section C.4.(i) is attempted.

(iv) Error Analysis for Breakthrough Curve Time Interval Fitting (i.e. Use of Empirical Correlations)

As before, a fractional error of $\pm\varepsilon$ in the final value of u(t) is assumed, yielding equations (5.2) and (5.3).

A first order estimate of the error $\delta(\Delta T^*)$ in computing the normalised difference in time between any two fractional responses u_1 and u_2 on a breakthrough curve may be made where $u_2 \equiv u(t_2^*)$, $u_1 \equiv u(t_1^*)$ and $\Delta T^* = t_2^* - t_1^*$. We obtain

$$\delta(\Delta T) = \varepsilon \left[\frac{1 - u_2}{g(t_2)} - \frac{1 - u_1}{g(t_1)} \right] \qquad \ldots(6.1)$$

where $g(t)$ = impulse response = $\dfrac{du(t)}{dt}$

Hence, it should be possible, knowing the likely shape of the curve in advance, to choose u_2 and u_1 so that for small errors ε, the nett error in ΔT^* is zero. Instead of using (6.1) however, a concrete example is chosen, using a theoretical (finite stage) breakthrough curve with $\sigma^{*2} = 0.1198$, $\sigma^* = 0.3462$, ΔT^* (20 to 80%) $= 0.5772$.

Taking $\varepsilon = +0.005$ as before, we obtain the following estimated and 'true' values.

	Value 1	Value 2	Difference
Assumed value of $u(t^*)$, i.e. $u(t^*)$ est, $= 0.005$	0.2	0.8	
Actual value of $u(t^*)$	0.196	0.799	
Values of time (measured) corresponding to actual values of $u(t^*)$	0.6982 x $\mu(t)$	1.2782 x $\mu(t)$	0.5800 x $\mu(t)$
Correct values of time	0.7024 x $\mu(t)$	1.2796 x $\mu(t)$	0.5772 x $\mu(t)$
Percentage errors in time reading	- 0.600	- 0.109	+ 0.485

If the estimated centre of mass $\mu(t)_{est}$ is correct, for then the resultant error of 0.48% in the normalised time difference ΔT^* yields an error of 0.97% in σ^{*2}. If, on the other hand, (as in this work) $\mu(t)$ is obtained by integration from the same data, the error of -0.5% in $\mu(t)_{est}$ increases the error in ΔT^* and hence in σ^{*2}, resulting in a final estimate of σ^{*2} which is about 2% high. This may be compared with 5½% error from moments analysis,

i.e. the time interval fitting method should be less sensitive to error in final value than the direct moments method.

Similar conclusions apply to the case of linear drift.

6. SUMMARY OF CONCLUSIONS - LEAD PACKING STEP TESTS

The first moment may be extracted from the step test data with satisfactory accuracy although estimates of the normalised second central moment are highly susceptible to small errors in curve reading and to baseline drift.

The time interval fitting method, using the empirical correlations of sections IV.D.2 gives more reproducable results and values of Stanton number obtained uncorrected for axial dispersion were consistent with Denton heat transfer correlations. Further results are required in the low Reynolds number region where heat losses from the test section makes the results open to doubt.

Good agreement between the finite stage model and the experimental breakthrough curves was obtained and arithmetic probability plots were not straight as required by the equivalent conductivity model, but curved as predicted from the finite stage, Schumann and Rosen models.

D. SODA GLASS PULSE AND STEP TESTS

1. Further Soda Glass Experiments - Pulse Tests

Tables D.1.1 and D.1.2 list experimental conditions and computed moments from the remainder of the soda glass experiments. The

'heat loss ratio' β is simply the ratio of input pulse area to output pulse area, i.e., the ratio of zero'th moments. As noted in B.1(i) input and output pulses are each normalised to a value of unity. For a discussion of the significance of the various computed parameters given in Table.D.1.2, the reader is referred back to section B.1. The statistical 'coefficient of skewness' γ_1 is defined by equation (II.E.1.1).

The bed and packing material was identical to that given in Table B.3.1.

TABLE D.1.1

EXPERIMENTAL CONDITIONS FOR FURTHER PULSE TESTS ON 6.2 mm. SODA GLASS

Notes: "Run designation" is arbitrary

"Run number" is the chronological run number on the the date shown.

Other conditions as in Table B.3.1.

Run Desig.	Run No. DATE	Re_p	Pressure p.s.i.g.	Approx V_H	BED LENGTH ins.	N	Heat loss Ratio, β %
16	4 - 18.11.68	310	20	1230	3.3	13.5	95.7
17	1 - 15.11.68	330	50	630	3.3	13.5	96.3
18	2 - 18.11.68	310	20	1230	12.5	51.6	97.0
19	2 - 15.11.68	337	50	630	12.5	51.6	89.0
20	7 - 18.11.68	134	20	1230	3.3	13.5	90.3
21	3 - 15.11.68	136	50	630	3.3	13.5	94.5
22	9 - 18.11.68	1700	20	1230	3.3	13.5	-
23	8 - 18.11.68	1700	20	1230	3.3	13.5	99.8
24	1 - 15.8.68	1130	16	1390	12.5	51.6	96.3
25	5 - 6.12.68	950	19.6	1420	12.5	51.6	96.2
26	4 - 6.12.68	1245	19.6	1150	3.3	13.5	99.7
27	3 - 6.12.68	927	30	970	3.3	13.5	99.0
28	2 - 6.12.68	930	30	980	3.3	13.5	99.2
29	3 - 19.1.69	367	60	570	12.5	51.6	90.3
30	7 - 20.4.69	365	60	595	12.5	51.6	94.5
31	14.4.69	1240	13.5	1510	12.5	51.6	98.2

TABLE D.1.2

MOMENTS ANALYSIS OF FURTHER PULSE TESTS ON

6.2 mm. SODA GLASS

Run Desig.	Re_p	$\mu(t)/_{\bar{t}}$ min.	σ^{*2}	π^{*3}	$\sigma^*\sqrt{N}$	$N^{2/3}\pi^*$	γ_1	γ_2
16	310	.143	.307	.151	2.040	3.02	.886	1.60
17	330	.130	.310	.148	2.040	3.02	.856	1.54
18	310	.139	.0812	.0141	2.040	3.34	.610	2.14
19	337	.128	.0839	.0128	2.080	3.24	.527	1.82
20	134	.333	.219	.0702	1.719	2.34	.689	1.47
21	136	.307	.274	.181	1.926	3.21	1.260	2.41
22	1700	.0253	.557	.375	2.744	4.09	.904	1.21
23	1700	.0250	.554	.371	2.739	4.08	.903	1.21
24	1130	.0384	.120	.0187	2.485	3.68	.450	1.30
25	950	.0455	.119	.0185	2.476	3.66	.451	1.31
26	1245	.0351	.499	.357	2.597	4.03	1.018	1.44
27	927	.0475	.460	.322	2.494	3.89	1.032	1.52
28	930	.0476	.473	.380	2.528	4.11	1.168	1.70
29	367	.115	.0880	.0134	2.123	3.28	.514	1.73
30	365	.120	.0898	.0197	2.144	3.72	.731	2.44
31	1240	.0349	.151	.0447	2.78	4.89	.756	1.95

In Table D.1.3 values of Stanton number, heat transfer KV_H and Biot number have all been calculated ignoring the effects (if any) of axial dispersion. In addition, the F factor from equation (C.4.1) has been calculated and used to obtain a 'corrected' value of Stanton number. It may be shown that

$$KV_H = KV_H \text{ (no axial dispersion)}/F$$

and $$Bi = Bi \text{ (no axial dispersion)}/F$$

so that the appropriate values F in Table D.1.3 may be used to obtain KV_H and Bi, both corrected for axial dispersion.

The ratio $\gamma x = KV_H/Bi$ which, according to earlier chapters, is required to be greater than about 10 for the shape of a breakthrough curve or impulse response to be approximated by the Schumann solution (V_H large), is independent of F, i.e.

$$\gamma x = \frac{KV_H \text{(no dispersion)}}{Bi \text{ (no dispersion)}} = \frac{KV_H}{Bi} \qquad \ldots(1.1)$$

$$= \frac{6N(1-\epsilon)\, k_s}{Pr.\, Re_p .\, k_f}$$

for spherical particles.

The calculated value of this quantity is also given in Table D.1.3.

TABLE D. 1. 3

FURTHER PARAMETERS COMPUTED

FROM SODA GLASS

PULSE TESTS

Run Desig.	Re_p	N	St (calc)	F	St (corr.)	KV_H calc.	Bi calc	γx
Mean, 1 - 4	947	51.6	.1029	.801	.128	20.5	.91	6.2
Mean, 5,8-12 14	890	13.5	.1134	.781	.145	5.91	.95	6.2
6	1080	51.6	.079	.848	.093	15.7	.65	24
5	1245	13.5	.090	.825	.109	4.72	.8	5.4
13	836	13.5	.112	.783	.143	5.85	.88	6.6
16	310	13.5	.135	.740	.182	7.03	.39	18
17	330	13.5	.134	.741	.181	6.99	.41	16
18	310	51.6	.133	.743	.179	26.5	.39	68
19	337	51.6	.129	.750	.172	25.8	.41	62
20	134	13.5	.183	.646	.283	9.55	.23	42
21	136	13.5	.145	.720	.202	7.57	.37	40
22	1700	13.5	.088	.829	.106	4.60	1.41	3.2
23	1700	13.5	.089	.828	.107	4.63	1.42	3.2
24	1130	51.6	.102	.804	.126	20.3	1.08	20
25	950	51.6	.099	.808	.123	19.8	.88	22
26	1245	13.5	.094	.819	.114	4.89	1.09	4.4
27	927	13.5	.097	.812	.120	5.08	.85	6.0
28	930	13.5	.094	.017	.115	4.93	.82	6.0
29	367	51.6	.121	.766	.158	24.1	.41	58
30	365	51.6	.121	.766	.158	24.1	.41	58
31	1240	51.6	.079	.848	.093	15.7	.91	11

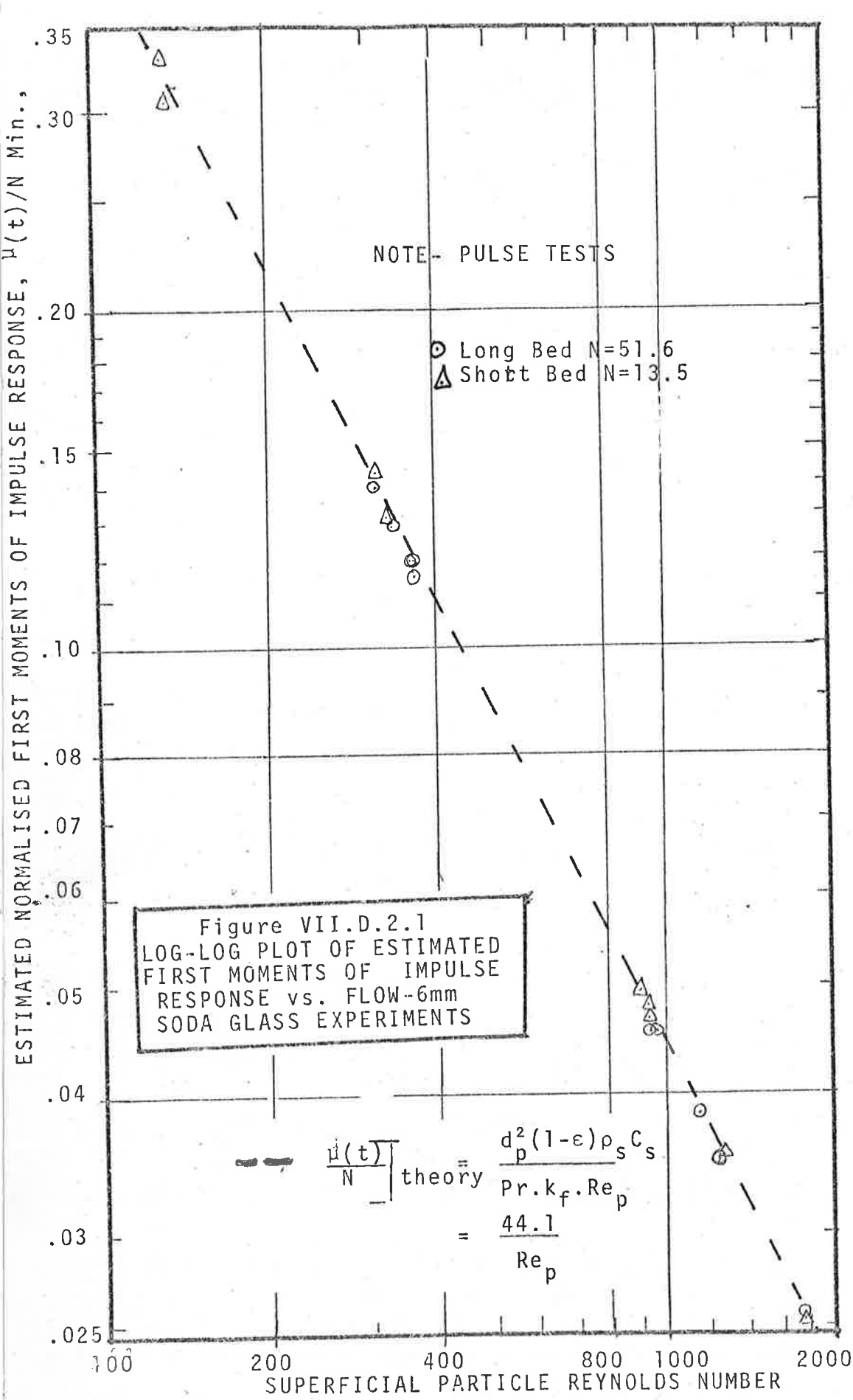
ESTIMATED NORMALISED FIRST MOMENTS OF IMPULSE RESPONSE, μ(t)/N Min.,
.35
.30
.20
.15
.10
.08
.07
.06
.05
.04
.03
.025
NOTE- PULSE TESTS
Long Bed N=51.6
Short Bed N=13.5
Figure VII.D.2.1
LOG-LOG PLOT OF ESTIMATED FIRST MOMENTS OF IMPULSE RESPONSE vs. FLOW-6mm SODA GLASS EXPERIMENTS
$\left[\frac{\mu(t)}{N}\right]_{theory} = \frac{d_p^2(1-\varepsilon)\rho_s C_s}{Pr.k_f.Re_p} = \frac{44.1}{Re_p}$
100
200
400
800
1000
2000
SUPERFICIAL PARTICLE REYNOLDS NUMBER

2. Preliminary Discussion of Soda Glass Pulse Tests

Figure D.2.1 shows the first moments obtained from the area-normalised pulse test data by difference between input and output pulses. A comparison is made with the theoretical centre of mass calculated, as mentioned in section D.1 (i) from individual measurements of ρ_s, c_s, ε bed diameter etc. The differences between the theoretical and experimental values are

for short bed length runs : 1.5%.

for long bed length runs : 2.0%

and despite the increased heat loss at low flows there is no significant departure from the -1 slope of the data on a log-log plot. This result appears satisfactory in view of possible errors in determining the above mentioned quantities and also flowrate. Long and short bed length values of $\mu(t)/N$ are indistinguishable.

Values of the parameter γ_2 obtained are again inconsistent with the value of 3.0 predicted by the equivalent conductivity model. An averaged overall value for all the soda glass results is 1.509 with 95% confidence limits of $\pm$ 0.125 compared with theoretical finite stage values of about 1.52 (section II.E.1). As predicted by theory, the skewness parameter γ_1 again decreases as bed length increases such that approximately, $\gamma_1 \propto 1/\sqrt{N}$.

A detailed discussion of the effects of solids conductivity on the response is deferred until section D.4, when pulse and step tests on soda glass are compared.

3. Soda Glass Step Tests

The soda glass step tests were analysed using the empirical time difference correlation method as for lead packing [C.2.(ii) and C.4.(i)]. In the present case, integration of the breakthrough curve to determine $\mu(t)$ was dispensed with and the pulse response first moments correlated allowing the step response values of $\mu(t)$ to be calculated. The correlations for the particular bed in use in both sets of experiments (Table B.3.1) were

Short bed length, $L = 3.30$ ins., $N = 13.5$:

$$\mu(t) = \frac{587}{Re_p}$$

Long bed length, $L = 12.50$ ins., $N = 51.6$:

$$\mu(t) = \frac{2227}{Re_p} .$$

As in Table C.4.2, the Stanton number St_{calc} in the final column of Table D.3.1 has not been corrected for fluid phase axial dispersion. Table C.4.3 gives the appropriate F factor calculated 'true' or corrected Stanton number and other parameters as in Table D.1.2 for the pulse tests.

For runs marked with an asterisk in Table D.3.2, the time difference correlations are not strictly applicable since the ratio $\gamma x = KV_R/Bi$ is not greater than 10. In most cases,

the error is only a few percent however, less than experimental error.

TABLE D.3.1

EXPERIMENTAL CONDITIONS FOR STEP TESTS

on 6.2 mm. SODA GLASS

Other conditions as in Table B.3.1

Run Desig.	Run No. DATE	Re_p	Pressure p.s.i.g.	V_H	$\mu(t)/N$ min. (calc)	BED LENGTH ins.	N
1	2 - 12.1.69	155	60	580	3.78	3.3	13.5
2	3 - 13.1.69	375	60	580	1.56	3.3	13.5
3	2 - 13.1.69	412	60	580	1.42	3.3	13.5
4	4A- 14.4.69	1240	13.5	1510	1.80	12.5	51.6
5	4B-14.4.69	1240	13.5	1510	.473	3.3	13.5
6	1 -18.12.68	156	60	580	3.76	3.3	13.5
7	4 - 13.1.69	374	60	580	1.57	3.3	13.5
8	1 - 13.1.69	477	60	580	1.23	3.3	13.5
9	5 - 13.1.69	381	60	580	5.84	12.5	51.6
10	7 - 13.1.69	1030	30	970	.569	3.3	13.5
11	6 - 14.4.69	220	10.7	200	2.93	3.3	13.5
12	1 - 12.1.69	153	60	580	3.83	3.3	13.5
13	3 - 20.1.69	354	60	580	6.29	12.5	51.6
14	2 -18.12.68	936	30	970	.627	3.3	13.5
15	3 - 19.4.69	128	10.9	200	4.58	3.3	13.5

TABLE D.3.2.

RESULTS OF USE OF EMPIRICAL CORRELATIONS

IN BREAKTHROUGH CURVE ANALYSIS

6 mm. SODA GLASS PACKING

(See Tables D.3.1 and B.3.1 for experimental conditions)

Run No.	Re_p	σ^{*2}, Estimated From --				Mean σ^{*2}	St calc
		$\Delta T_{05/80}$	$\Delta T_{10/80}$	$\Delta T_{20/80}$	$\Delta T_{40/80}$		
1	155	.265	.268	.268	.271	.268	.149
2	375	.343	.339	.343	.343	.342	.122
3	412	.376	.382	.374	.374	.377	.110
4	1240	.144	.147	.147	.151	.147	.0810
5*	1240	.546	.549	.543	.546	.546	.0839
6	156	.238	.242	.246	.228	.238	.169
7	374	.333	.334	.336	.340	.336	.124
8	477	.352	.365	.359	.354	.357	.119
9	381	.0882	.0894	.0912	.0912	.0897	.122
10*	1030	.585	.597	.590	.568	.585	.075
11	220	.279	.273	.278	.276	.276	.147
12	153	.235	.248	.260	.261	.251	.160
13	354	.0767	.0790	.0801	.0829	.0796	.137
14*	936	.489	.487	.489	.490	.489	.0910
15	128	.230	.232	.242	.245	.237	.168

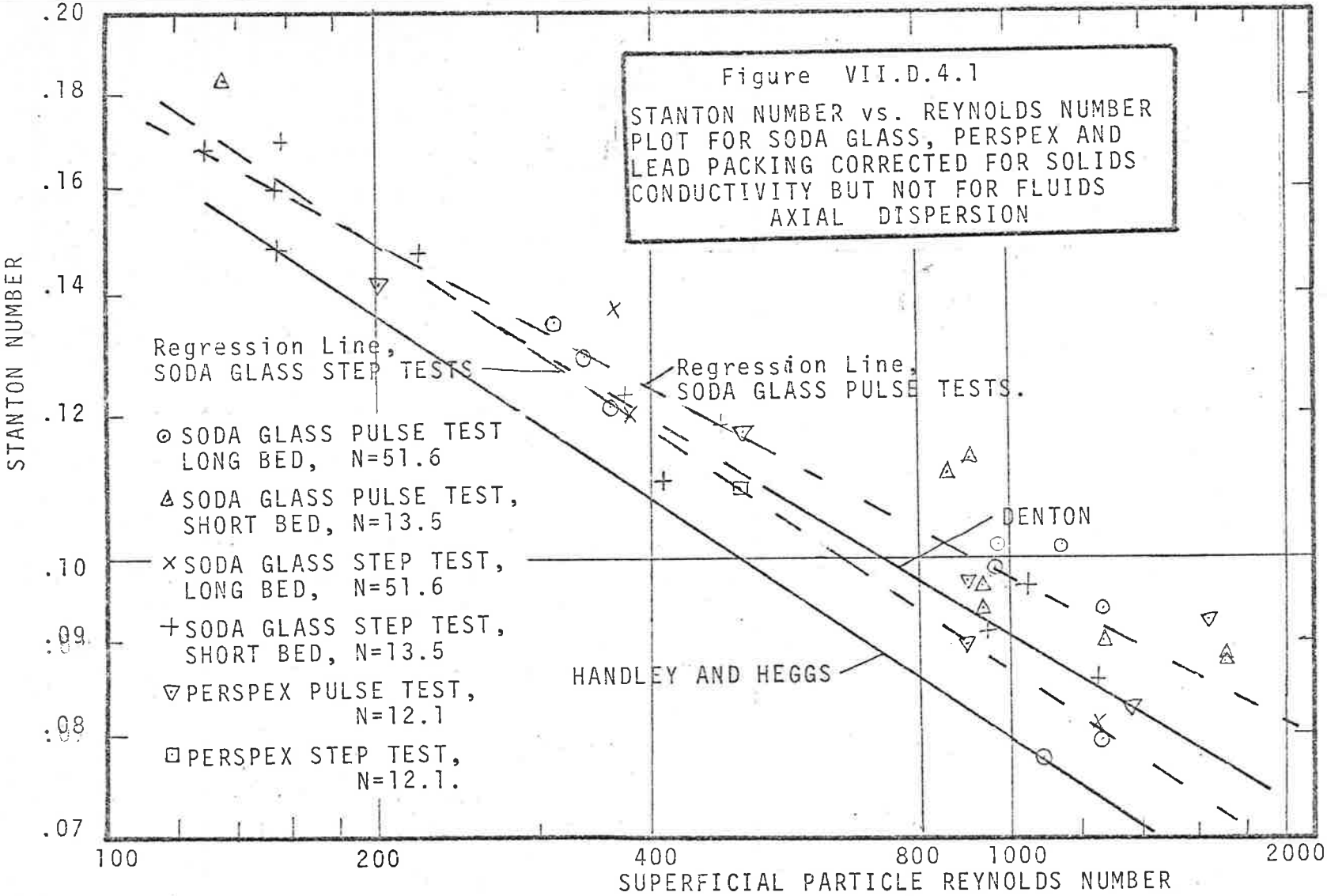
Figure VII.D.4.1
STANTON NUMBER vs. REYNOLDS NUMBER PLOT FOR SODA GLASS, PERSPEX AND LEAD PACKING CORRECTED FOR SOLIDS CONDUCTIVITY BUT NOT FOR FLUIDS AXIAL DISPERSION
STANTON NUMBER
.20
.18
.16
.14
.12
.10
.09
.08
.07
100
200
400
800
1000
2000
SUPERFICIAL PARTICLE REYNOLDS NUMBER
Regression Line, SODA GLASS STEP TESTS
Regression Line, SODA GLASS PULSE TESTS.
DENTON
HANDLEY AND HEGGS
⊙ SODA GLASS PULSE TEST LONG BED, N=51.6
△ SODA GLASS PULSE TEST, SHORT BED, N=13.5
× SODA GLASS STEP TEST, LONG BED, N=51.6
+ SODA GLASS STEP TEST, SHORT BED, N=13.5
▽ PERSPEX PULSE TEST, N=12.1
⊡ PERSPEX STEP TEST, N=12.1.

TABLE D.3.3

FURTHER PARAMETERS COMPUTED

FROM SODA GLASS

STEP TESTS

Run	Re_p	N	St (calc)	F	St (corr.)	KV_H (calc)	Bi (calc)	γx
1	155	13.5	.149	.712	.209	7.77	.21	36
2	375	13.5	.122	.765	.159	6.35	.43	15
3	412	13.5	.110	.786	.140	5.76	.42	13
4	1240	51.6	.0810	.843	.0960	16.1	.94	17
5	1240	13.5	.0839	.838	.100	4.38	.98	4.4
6	156	13.5	.169	.674	.250	8.79	.25	24
7	374	13.5	.124	.760	.163	6.47	.43	15
8	477	13.5	.119	.771	.154	6.19	.53	12
9	381	51.6	.122	.765	.159	24.2	.43	56
10	1030	13.5	.0750	.855	.0877	3.91	.72	5.4
11	220	13.5	.147	.715	.206	7.68	.30	26
12	153	13.5	.160	.691	.231	8.34	.23	36
13	354	51.6	.137	.734	.187	27.4	.45	60
14	936	13.5	.0910	.824	.110	4.75	.80	6
15	128	13.5	.168	.675	.249	8.76	.20	44

4. Discussion of Soda Glass Step and Pulse Tests

On figure D.4.1 the computed Stanton numbers, uncorrected for axial dispersion from the soda glass step and pulse experiments are plotted for comparison with the lead packing step test values.

The magnitude of the correction applied to account for solids conduction effects may be estimated from the Biot numbers shown on Tables D.1.3 and D.3.3. Thus, assuming axial dispersion to have negligible effect, we have

$$\sigma^{*2} = \frac{2}{KV_H} = (1 + Bi/5) \qquad \ldots(4.1)$$

where, as noted above, KV_H and Bi are uncorrected for axial dispersion. If particle thermal conductivity were ignored we would obtain a 'pseudo' value of KV_H from σ^{*2} and hence a 'pseudo' value of Stanton number St_{psd} such that

$$\frac{St_{psd}}{St} = \frac{1}{1 + Bi/5} \; . \qquad \ldots(4.2)$$

Hence, the value of Bi when divided by 5 gives the fractional correction applied to the pseudo Stanton number for solids conduction. It may be seen that the maximum correction is about 23% for the two readings at $Re_p = 1700$. For these particular experiments, the correction is evidently too large if the Denton correlation is regarded as giving correct values for Stanton numbers uncorrected for axial dispersion.

Comparing regression coefficients b in $St = a/Re_p^{\,b}$ for lead and for soda glass step tests, the result of a t test [Brownlee, p.66, 1954] is that/difference is not significant (t does not reach the 0.2 significance level). Hence, for the range

$155 \leq Re_p \leq 1240$, the correction for Biot number of equation (4.2) appears to be of the right order.

Curiously, however, the coefficient b in the soda glass pulse test correlation differs highly significantly (the difference exceeds the .001 significance level) from the soda glass step tests. The variability of the results computed from moments analysis of pulse data is also greater as indicated by the wider 95% confidence limits. Summarising, we have :

4mm lead step tests, $230 \leq Re_p \leq 950$:
$St_{calc} = .652/Re_p^{0.289}$ ± 8.2% (95% conf).
corr. coeff.: -.96

6 mm. Soda Glass step tests, $150 \leq Re_p \leq 1240$:
$St_{calc} = 0.874/Re_p^{0.334}$ ± 15% (95% conf.)
corr. coeff.: -.974

6 mm. Soda Glass pulse tests, $130 \leq Re_p \leq 1700$:
$St_{calc} = 0.599/Re_p^{0.263}$ ± 18% (95% conf.)
corr. coeff.: -.938

The difference still results even when the two runs at Re_p = 1700 are eliminated. Since no correction is made to step data for the spread of the input 'step' we could expect the estimated values of σ^{*2} from step tests to be high, or St_{calc} to be low. This is unlikely to be significant in the present experiments since the

rise time of the tuned input step was very fast because of the controller. Such a spread in the input step could, however explain the low values of St obtained by Handley and Heggs. Another suggestion is that the difference is caused by errors in the moments analysis.

Since Handley and Heggs [1968] have carried out a similar series of step test experiments over a wider range of flows, their results are compared with the present ones in section E.

E. COMPARISON OF PRESENT RESULTS WITH THOSE OF HANDLEY AND HEGGS.

1. Validity of the Present Methods Applied to Heggs' Data

The work of Heggs [1967] provides a useful source of data for comparison. A more recent publication [1969] not listed in the references and therefore footnoted below * gives details of a few individual runs and a few so called 'intraparticle' model solutions (numerical solutions to the differential equations solved analytically by Rosen(see IV.A.4.). These allow a check to be made on the validity of the present methods applied to the earlier, 1968 results. Solutions to the Schumann and 'Intraparticle' models listed in their tables 4 and 5 have been added to the plots of figures (IV.D.2.1) and (IV.D.2.2) It may be seen that the results are indistinguishable from the present computations.

*Handley D. and Heggs P.J., Int'l Jl Heat Mass Transfer.12: 549 (1969)

Two experimental runs have been reported in detail. Run 1 was a step test on a 6 inch long bed of 9 mm. lead having a tube to particle diameter ratio M of about 7.7. Using the data listed in Handley and Heggs' Table 6, the following quantities are obtained. The assumed value of c_s is 0.03 B.T.U./(lb.^{o}F.)

Reynolds number: 3695

Thermal capacity of bed, $M.c_s$: 0.277 B.T.U./^{o}F

Weight flow of air : 6.31×10^{-2} lb./sec.

Calculated centre of mass, for c_f = 0.24 B.T.U./(lb.^{o}F) becomes :

$$\mu(t) = \frac{0.277}{6.31 \times 10^{-2} \times 0.24} = 18.3 \text{ sec.}$$

Using the Handley and Heggs' correlation [1968] :

$$j_H.\varepsilon = \varepsilon.St.Pr^{2/3} = \frac{0.255}{Re_p^{0.335}} \quad \ldots(1.1)$$

or for Pr = 0.74, ε = .39:

$$St = \frac{0.801}{Re_p^{0.335}} \quad \ldots(1.2)$$

we obtain for Run 1, St = 0.0511. Since the bed length N and porosity ε for Run 1 are 17.1 and 0.37 respectively, we have :

$$KV_H = 6 \times 17.1 \times .0511 \times (1 - 0.37)$$
$$= 3.31$$

or since Bi ≃ 0,

$$\sigma^{*2} = {}^{2}/3.31 = .604$$
$$\sigma^{*} = 0.777$$

Using the tabulated data for the Schumann solution which Handley and Heggs have fitted to the data we obtain, from figure IV.D.2.1 :

$\Delta T^{*}_{10/80}$ = 1.4519 , σ^{*} = .783 (fig.IV.D.2.1)

$\Delta T^{*}_{20/80}$ = 1.2672 , σ^{*} = .782

$\Delta T^{*}_{40/80}$ = .9251 , σ^{*} = .781

Mean value of σ^{*} = .782

The value obtained differs by 0.6% from the value predicted by the correlation and by 0.2% from that predicted by the value of $Y = KV_H = 3.26$ of $\sigma^{*} = .783$ assumed by Handley and Heggs for this run.

For Run 2, a step test on an 8 inch long bed of 6 mm. soda glass, c_s = 0.189 B.T.U./(lb.^{o}F) [compare 0.184 B.T.U./(lb.^{o}F) obtained in present experiments], we obtain, by calculation, from Handley and Heggs' Table 2 :

Reynolds number : 2489

Thermal capacity of bed: 0.518 B.T.U./^{o}F

Weight flow of air : 6.38×10^{-2} lb/sec.,

Calculated centre of mass,

$\mu(t)$ = 34.0 sec.

Handley and Heggs fit two models to their data but unfortunately do not give the actual experimental readings.

For the Schumann solution, $KV_H = 8.25$, i.e. for V_H large, $\sigma^{*2} = 0.242$, $\sigma^* = 0.492$ whilst for the Intraparticle model $KV_H = 8.25$, Bi = 1.35, 1 + Bi/5 = 1.27 and $\gamma x = YK_r = KV_H/Bi = 6.1$ so that the Schumann curve shape is not strictly, valid. The predicted value of σ^* is 0.242 x 1.27 = 0.308 and hence $\sigma^* = 0.555$. From the values given in Table 7 of the paper we have,

	Schumann Handley and Heggs		'Intraparticle' Handley and Heggs	
$\Delta T^*_{10/80}$	.971		1.077	
σ^*		.491		.543
$\Delta T^*_{20/80}$	.815		.913	
σ^*		.492		.546
$\Delta T^*_{40/80}$	.570		.645	
σ^*		.492		.553
Mean σ^*		.4917		.5473
	(c.f. $\sigma^* = .492$)		(c.f. $\sigma^* = 0.555$ or 1.4% error)	

The above calculations are a further check on the validity of the proposed method. As a check on the calculation of KV_H, we have from equation (1.1), where $Re_p = 2489$ and $\epsilon = 0.37$ a Stanton number of 0.614, yielding for N = 34.3, a heat transfer parameter KV_H of 8.24 which compares with $KV_H = 8.25$ assumed by Handley and Heggs.

Assuming a thermal conductivity as quoted by Handley and Heggs of 0.60 B.T.U./(hr.ft.^{o}F), compared with 0.57 ± 8% measured on the soda glass used in the present experiments, we have:

$$Bi = St.Pr.Re_p . \frac{k_f}{2k_s} = 1.367,$$

compared with 1.35 assumed by Handley and Heggs.

2. Analysis of Heggs' Soda Glass Data

Having established that both methods of data analysis give similar values of the curve spread parameter σ^* (a not surprising conclusion in view of figure IV.D.2.1), the earlier 1968 data of Handley and Heggs may be analysed. Thus, the fitting of the Schumann model to a breakthrough curve gives a value of KV_H which, when the Biot number is non-zero, may be regarded as a pseudo heat transfer parameter, KV_{Hpsd}. As pointed out in chapters II andIII, such a curve shape fit may be achieved when KV_H/Bi is greater than 10 or so. Setting the axial dispersion term in equation (II.B.3.10) equal to zero, we obtain, for V_H large :

$$\sigma^{*2} = \frac{2}{KV_{H_{calc}}} . (1 + 0.2\ Bi_{calc}) \quad . . . (2.1)$$

where, as in equation (C.3.1), the subscripted 'calc' indicates that the quantity is not corrected for axial dispersion. We

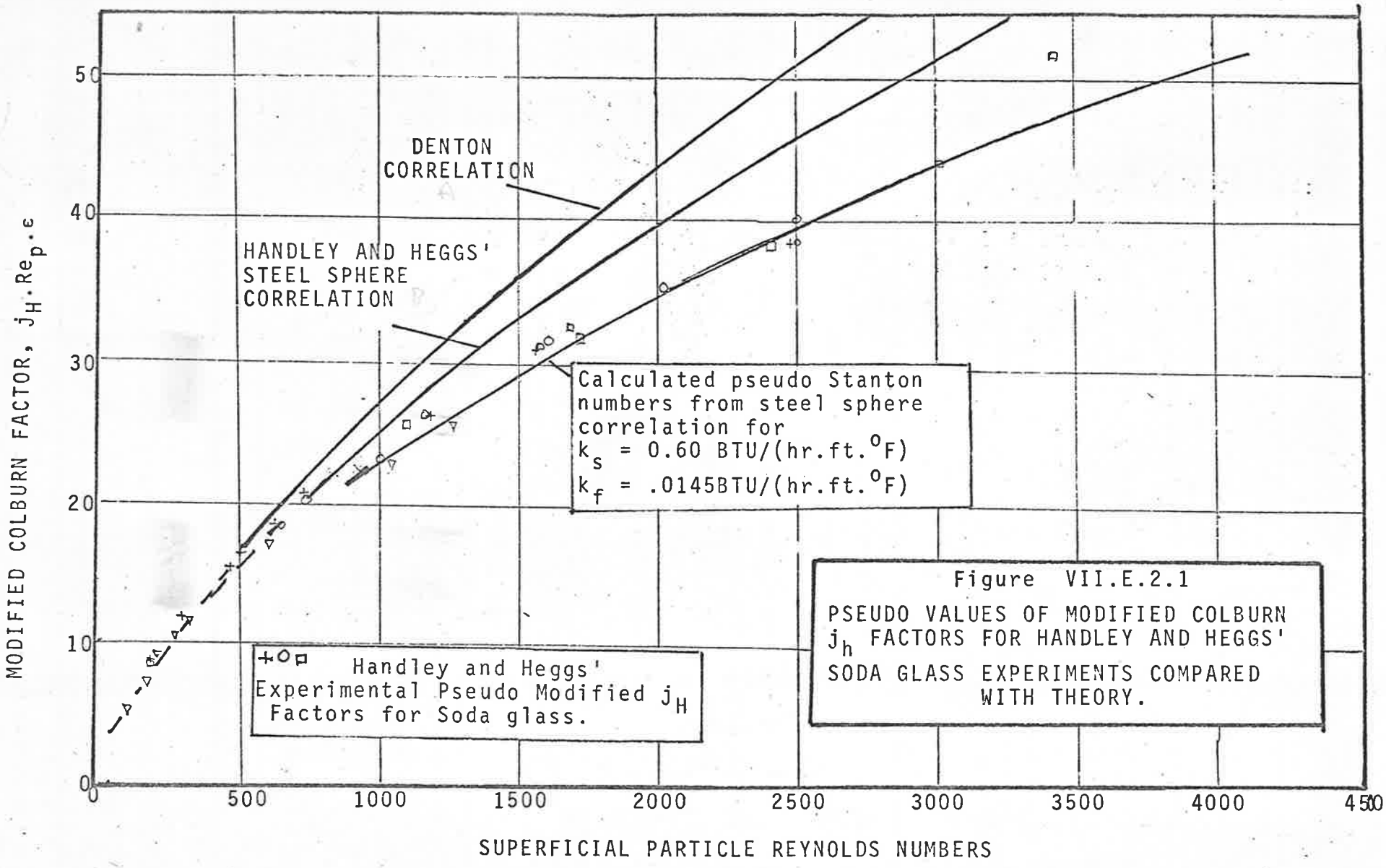

Figure VII.E.2.1

PSEUDO VALUES OF MODIFIED COLBURN j_h FACTORS FOR HANDLEY AND HEGGS' SODA GLASS EXPERIMENTS COMPARED WITH THEORY.

then obtain:

$$\frac{1}{St_{psd}} = \frac{1}{St_{calc}} + Pr.\ Re_p.\ \frac{k_f}{10k_s} \qquad \ldots (2.2$$

Setting k_f = 0.0145 B.T.U./(hr.ft.^{o}F),

and Pr = 0.74,

we obtain the following pseudo Stanton numbers and pseudo values of modified j_H factor, $j_H.Re_p.\varepsilon$ (Table E.2.1) using Handley and Heggs' correlation of equation (E.1.1) and (E.1.2).

TABLE VII.E.2

COMPUTED VALUES OF 'PSEUDO'

MODIFIED j_H FACTOR FROM

EQUATION E.2.2

Re_p	$j_H.Re_p.\varepsilon_{calc}$	$j_H.Re_p.\varepsilon$ psd.
100	5.47	5.28
400	17.0	15.3
1000	25.3	23.0
2000	40.2	34.9
2500	46.6	39.5
3000	52.8	43.8
3500	59.5	48.4
4000	63.5	50.9

These values are plotted on figure VII.E.2.1 and compared with Handley and Heggs' pseudo Stanton numbers obtained by fitting the Schumann model to the data. The pseudo modified j_H factors give excellent agreement with those obtained by experiment. The results illustrate the good internal consistency of Handley and Heggs' results. They also show that, at least for the range of conditions covered in these experiments, the correction factor of 1 + Bi/5 is appropriate.

3. Summary of Conclusions Reached in the Comparison with Handley and Heggs' Data.

The empirical correlation of points on the breakthrough curve method gives values of apparent or pseudo heat transfer parameter which are very close to those obtained by Handley and Heggs by fitting the numerically-determined Schumann solution to their experimental data.

The values of Stanton number obtained in the present highly conductive particle experiments (computed without correction for the supposed effects of fluid phase axial dispersion) were roughly 10% or more above those obtained by Handley and Heggs at $Re_p = 500$, the discrepancy increasing at higher flowrates. It seems likely that some of the difference may be traced to the increased relative importance of spreading of the input 'step' in Heggs' experiments, at least at higher flowrates.

This last assertion is based on experience with the packed beds used in the present study which are of a similar scale to those of Handley and Heggs.

The correction factor of 1 + Bi/5 applied to the calculated variance to allow for intraparticle conduction seems to have been verified in both sets of experiments although the present pulse test experiments do deviate significantly from the step test data.

Neither in the present experiments nor in the Handley and Heggs experiments was there any noticeable effect of heat capacity ratio V_H on the centre of mass or on the curve shape although this is to be expected since in all cases the heat capacity ratio was much larger than 1.

The use of a correction for fluid phase axial dispersion would make computed Stanton numbers much higher than those

predicted by the Denton correlation in either set of experiments. It seems possible that axial dispersion effects are present in instrumented-sphere experiments although this cannot be conclusively demonstrated at present.

F. PERSPEX PACKING EXPERIMENTS

1. Experimental Conditions and Results

To study the effects on response of higher values of Biot number a further limited series of experiments was performed using 6.9 mm. 'Perspex' or methyl methacrylate beads dumped into the bed on top of 12 inches of 6.2 mm soda glass spheres. A shortage of material limited the bed length to 3.3 inches. A higher porosity resulted (36.8% compared with 35.6%). Other physical properties are listed in table F.1.1. Test section temperatures were in the range 70 to 75°F.

TABLE F.1.1

EXPERIMENTAL CONDITIONS AND DATA-
6.9 mm PERSPEX EXPERIMENTS

Packing: 0.272 inch (6.9mm) clear Perspex spheres

Method of packing: dumped into bed in small increments, no shaking

Net bed diameter (1/8" thick P.V.C. liner): 3.77 ins.

Bed length: 3.30 ins, N = 12.1

Tube to particle diameter ratio : 13.9

Measured porosity in simulated bed : 0.368

Particle specific gravity : 1.193 at 70°F

Particle thermal capacity : 0.353 BTU/lb°F at approx.80°F

Particle volumetric capacity: 24.8 BTU/(ft³ °F)

Thermal conductivity 0.117 BTU/(hr.ft.°F)

Transport properties of air as in Table B.3.1.

Ratio k_s/k_f = 8.08

TABLE F.1.2

EXPERIMENTAL CONDITIONS

6.9 mm PERSPEX PULSE TESTS

Notes: Heat loss ratio not measured

All bed lengths : 3.30 ins

P: denotes pulse tests,

S: denotes step test

All experiments were performed on 25th April, 1969.

Run Desig.	Run No.	Expt. Type	Re_p	Pressure, p.s.i.g.	Approx. V_H
60	10	P	1640	17.6	1150
61	2	P	500	11.2	1500
62	7	P	1350	12.5	1310
63	6	P	890	11.2	1500
64	4	P	890	11.2	1500
65	8	P	200	17.6	1150
66	1	S	500	11.2	1500
67	3	S	500	11.2	1500
68	5	S	890	11.2	1500

TABLE F.1.3

RESULT OF CALCULATIONS

PERSPEX PULSE TESTS

Run Desig.	Re_p	$\mu(t)/N$ (min.)	σ^{*2}	π^{*3}	$\sigma^*\sqrt{N}$	$N^{2/3}\pi^*$	γ_1	γ_2
60	1640	.0293	1.059	1.600	3.59	6.18	1.47	1.43
61	500	.101	.538	.446	2.56	4.04	1.13	1.54
62	1350	.0342	1.005	1.415	3.50	5.94	1.39	1.40
63	890	.0546	.759	.856	3.04	5.02	1.29	1.48
64	890	.0567	.796	1.048	3.11	5.36	1.47	1.65
65	200	.237	.368	.198	2.11	3.07	1.01	1.46

TABLE F.1.4

PERSPEX STEP TEST ANALYSIS

Run Desig.	Re_p	σ^{*2}, Estimated From --				Mean σ^{*2}	St calc
		$\Delta T_{05/80}$	$\Delta T_{10/80}$	$\Delta_{20/80}$	$\Delta_{40/80}$		
66	500	.569	.576	.555	.578	.569	.109
67	500	.568	.564	.564	.578	.568	.109
68	890	.621	.656	.689	.702	.667	.126

TABLE F.1.5

FURTHER PARAMETERS COMPUTED FROM PERSPEX STEP AND PULSE TESTS, N = 12.1

Run Desig.	Re_p	St (calc.)	F	St (corr.)	KV_H calc.	Bi calc	γx
60	1640	.0934	.813	.115	4.51	1.40	3.2
61	500	.1176	.765	.154	5.68	.54	10
62	1350	.0827	.835	.099	4.00	1.02	3.9
63	890	.0971	.806	.120	4.69	.79	5.9
64	890	.0896	.821	.109	4.33	.73	5.9
65	200	.1417	.717	.198	6.85	.26	26
66	500	.1090	.782	.139	5.26	.50	10
67	500	.1093	.782	.140	5.28	.50	10
68	890	.126	Run Rejected				

Run 68 was rejected since at this high flow and short bed length, the curve shape differed markedly from that predicted by the Schumann and finite stage models. This is shown clearly

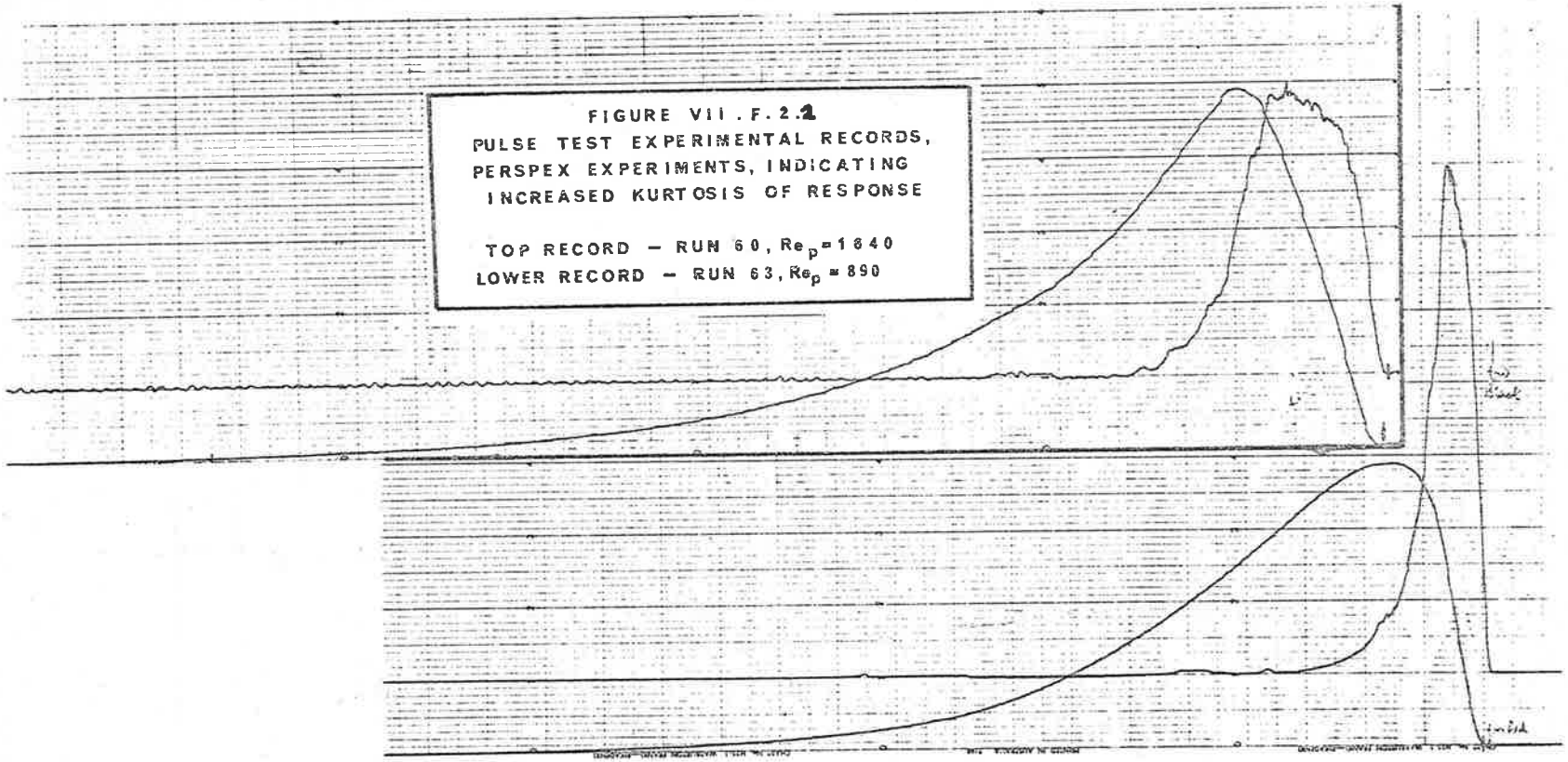

FIGURE VII.F.2.1
PULSE TEST EXPERIMENTAL RECORDS, PERSPEX EXPERIMENTS, INDICATING INCREASED KURTOSIS OF RESPONSE

TOP RECORD – RUN 60, $Re_p = 1640$
LOWER RECORD – RUN 63, $Re_p = 890$

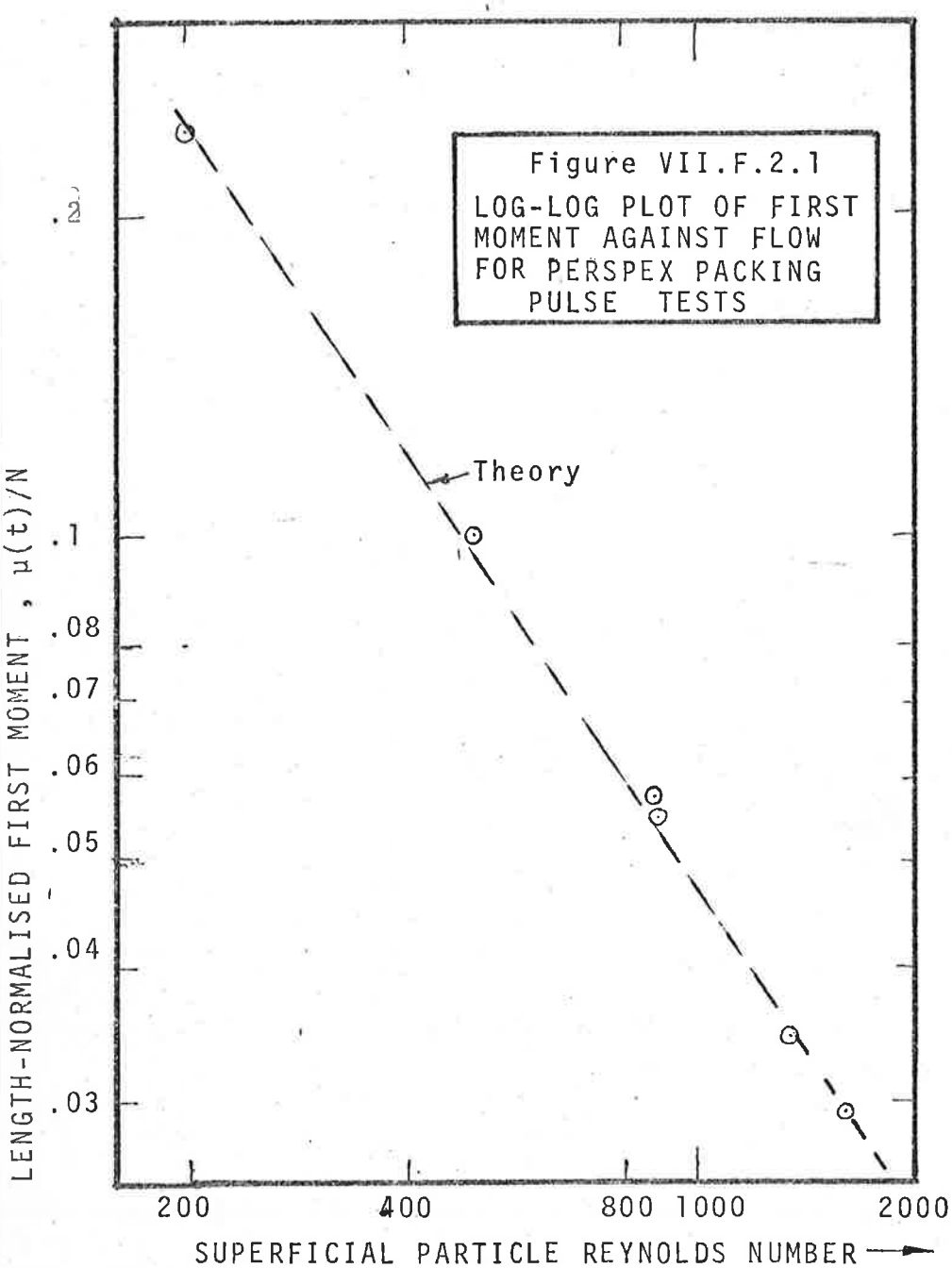
Figure VII.F.2.1
LOG-LOG PLOT OF FIRST MOMENT AGAINST FLOW FOR PERSPEX PACKING PULSE TESTS
Theory
.2
.1
.08
.07
.06
.05
.04
.03
200
400
800
1000
2000
LENGTH-NORMALISED FIRST MOMENT , μ(t)/N
SUPERFICIAL PARTICLE REYNOLDS NUMBER

by the differing estimates of σ^{*2} in Table F.1.4. At the same time, the short bed length and high flow meant that the inlet 'step' departed sufficiently from an ideal step to make a marked difference to the response. The pulse response results at this flow are, of course unaffected by inlet pulse shape deviations from an ideal impulse.

2. Discussion of Perspex Results

Figure F.2.1 indicates excellent agreement between experimental and theoretical first moments although because of the likely effect of separate errors in measurement of d_T, L, ε, ρ_S, c_S etc., agreement may be regarded as fortuitous. As for the soda glass experiments, the experimental value of $\mu(t)$ from the pulse tests was used in step test analysis.

The computed Stanton numbers, uncorrected for axial dispersion plotted on figure D.4.1 suggest that despite the increased size of the (1 + Bi/5) Biot number correction, the Denton correlation is recovered from the few experiments carried out.

An immediately noticeable effect of the substitution of low-conductivity Perspex for glass was the obvious increase in skewness and 'peakiness' (a function of the fourth cumulant κ_4). This is illustrated by a typical record (figure F.2.2).

Comparison of the curve shape parameter $\gamma_1 = \pi^{*3} / \sigma^{*3}$ with soda glass values at the same bed length should be made at the same flowaates since γ_1 is, theoretically, a function of flowrate.

Averaged values over the entire flowrange gave a highly significant difference between the means ($.01 > p > .001$):

Soda glass, L = 3.3 ins (19 observations)

mean $\gamma_1 = 0.995 \pm 0.093$ (95% conf.)

Perspex, L = 3.3 ins (6 observations)

mean $\gamma_1 = 1.296 \pm .186$ (95% conf.)

An F ratio test yielded a non significant difference in variability ($p > 0.2$).

Of greater interest, is a comparison of the second shape factor γ_2 between the two packings. According to the finite stage and axial dispersion models, a value of γ_2 of about 1.53 would be predicted for V_H large and $.01 < St < .1$, $0 < Bi < 2.0$, i.e. the shape factor is relatively independent of Biot number despite variations in γ_1.

Averaging over all Perspex experiments :

Mean $\gamma_2 = 1.493 \pm 0.158$ with 95% confidence. Comparing this value with the mean value of $1.500 \pm .125$ obtained for all soda glass experiments, the difference between the means is found to be non significant ($p > 0.2$) whilst once again no significant difference in variability was detected by an F ratio test.

The above calculations and measurements re-inforce the conclusion that for V_H large and $130 < Re_p < 1700$, the equivalent conductivity model provides a poor description of the shape of the impulse response and breakthrough curves since, as noted before, $\gamma = 3.0$ is predicted for all conditions by this model.

Further analysis of curve shape may be carried out by the pulse to frequency response method. A few such comparisons are performed in Section G.

G. PULSE TO FREQUENCY RESPONSE ANALYSIS OF EXPERIMENTAL DATA

1. Introduction.

Apart from determination of the fluid central moments and a number of arithmetic probability plots, the methods of data analysis used in previous sections have been concerned with dispersive rather than with curve shape effects.

The pulse to frequency response method is concerned with comparisons of the shape of either the experimental and predicted frequency responses or with the shape of the experimental and predicted outputs. As discussed in section V.C.2, the last named comparison is more likely to yield valid results, where the integral error square in either domain is used as a criterion for the excellence of the agreement. Both methods of comparison are used in this section. It is emphasised that (section V.C.4) quantitative methods for determining the significance of a 'fit' (obtained when the integral error square becomes minimal for a particular model) have not yet

been developed in detail. The results of this section should be regarded as preliminary, therefore. Many problems have been raised for further research - in the long term, it is believed that frequency domain analysis has a greater potential for extraction of the maximum amount of information from a transient test that has a step test or pulse to moments analysis.

2. Procedure Adopted in Analysis

A general outline of the procedure adopted in the use of orthogonal polynomial approximations to obtain the Fourier transform of either the frequency response transfer function $Ge(j\omega)$ and/or the input and output spectra $X(j\omega)$ and $Y_e(j\omega)$ has been presented in section V.C.3. Following are some specific points.

Input and output pulses were read at fixed (and equal) increments. As in the moments technique, zero'th and first moments were obtained numerically and the time scales normalised with respect to the first moment and the pulse areas to unity. The actual units of the time scale and recorder speed were immaterial.

A good starting value for the scale factors for both Hermite and Laguerre polynomial methods was obtained from

$$\lambda Z = 10./T_{max}$$

where T_{max} is the maximum normalised time for the pulse to become indistinguishable from its baseline, using 40 terms.

Having obtained either the estimated frequency response

transfer function or the output pulse transform approximation, a simple rectangular search procedure was used to obtain the combination of parameters which minimised the integral error square between model and experiment using either equation (V.C.2.8) or (V.C.2.9). Real parts only were used in each case as suggested by equation V.C.2.7.

In carrying out the search, the finite stage model was used, fixing first N, the number of mixing stages as required from $N = L/d_p$ and then the normalised variance σ^{*2} varied on either side of the estimate obtained previously from moments analysis. For each value of σ^{*2}, the Biot number was varied and equation II.B.3.10 used to obtain KV_H, i.e.

$$\sigma^{*2} = \frac{1}{N} + \frac{2}{KV_H} \cdot (1 + Bi/5) \cdot \left[\frac{V_H}{1 + V_H} \right]^2$$

The minima were determined simply by plotting the particular error criterion ϕ_1 or ϕ_2 against σ^{*2} at constant Biot number.

3. Results of Frequency Domain Analysis

Soda glass pulse tests 16 to 21 inclusive were chosen to represent medium to low flowrates and Biot numbers whilst higher Biot numbers were represented by soda glass runs 27 and 28 and Perspex pulse tests 60, 61, 62 and 63.

(i) Low to Intermediate Biot Number Runs

With the exception of run 21, all the low flow runs gave good agreement with the results of moments analysis. Since,

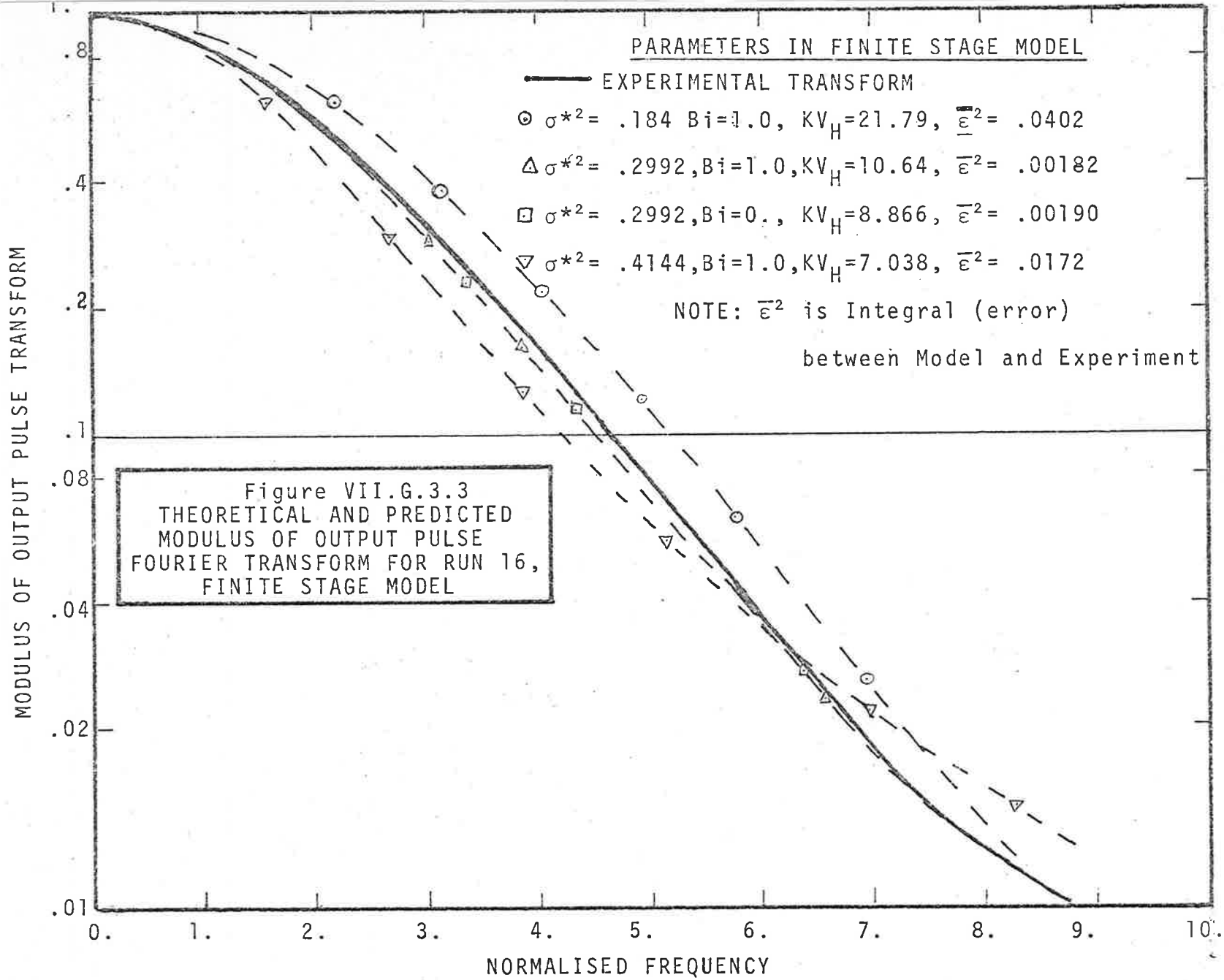

Figure VII.G.3.3
THEORETICAL AND PREDICTED
MODULUS OF OUTPUT PULSE
FOURIER TRANSFORM FOR RUN 16,
FINITE STAGE MODEL

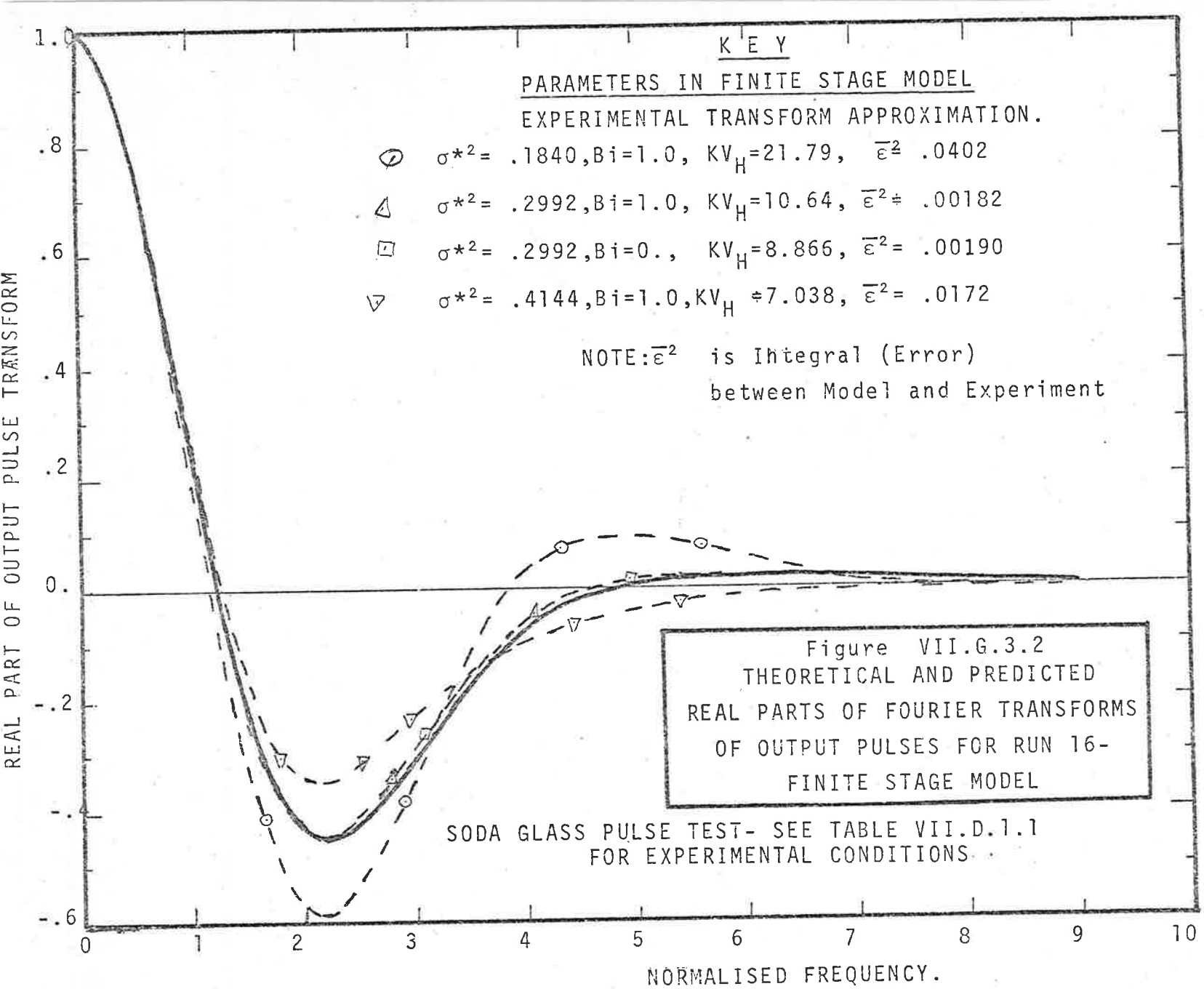

Figure VII.G.3.2
THEORETICAL AND PREDICTED
REAL PARTS OF FOURIER TRANSFORMS
OF OUTPUT PULSES FOR RUN 16-
FINITE STAGE MODEL

SODA GLASS PULSE TEST- SEE TABLE VII.D.1.1
FOR EXPERIMENTAL CONDITIONS

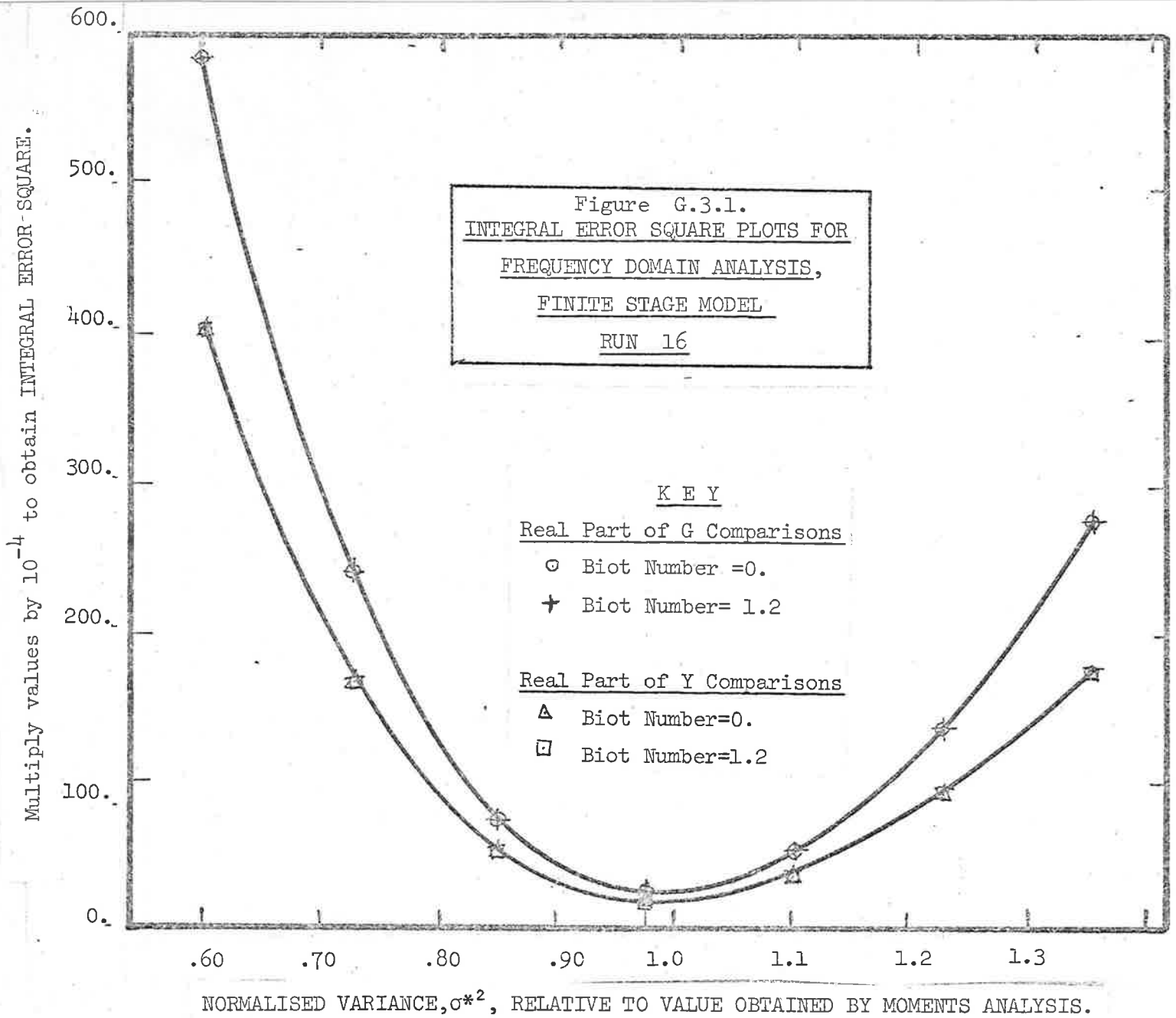
Figure G.3.1.
INTEGRAL ERROR SQUARE PLOTS FOR
FREQUENCY DOMAIN ANALYSIS,
FINITE STAGE MODEL
RUN 16
K E Y
Real Part of G Comparisons
Biot Number =0.
Biot Number= 1.2
Real Part of Y Comparisons
Biot Number=0.
Biot Number=1.2
Multiply values by 10^{-4} to obtain INTEGRAL ERROR-SQUARE.
600.
500.
400.
300.
200.
100.
0.
.60
.70
.80
.90
1.0
1.1
1.2
1.3
NORMALISED VARIANCE, σ^{*2}, RELATIVE TO VALUE OBTAINED BY MOMENTS ANALYSIS.

in each case, the input pulse duration was short relative to the input pulse (i.e. the value of $|X(j\omega)|$ large)so that no significant difference was noted between comparisons of experimental and predicted output pulse transforms through equ. (V.C.2.8) and comparisons of experimental and predicted transfer functions through equ. (V.C.2.9).

In each case very little difference between the integral errors ϕ_1 and ϕ_2 at differing values of Biot number was noted, for constant normalised variance σ^{*2}, i.e. the value of Biot number would not be extracted separately from the pulse shape. This is perhaps not surprising since the minimum value of $x = KV_H/Bi$ was about 5. The results of the frequency domain analysis hence confirm previous theoretical discussions in chapters II and III.

Run 16 is quite typical of the results obtained from these six runs - integral error square plots according to both criteria are given in figure 3.1 whilst figures 3.2 and 3.3 display direct comparisons between the experimental and theoretical transforms. Table 3.1 summarises the results. It should be noted that where the input pulse 'frequency content' is high, the integral error in the input pulse approximation has little effect on the over all error in $G_e(j\omega)$ or $Y_p(j\omega)$.

TABLE VII.G.3.1

RESULTS OF FREQUENCY DOMAIN COMPARISONS

FINITE STAGE MODEL - LOW BIOT NUMBERS

HERMITE POLYNOMIAL APPROXIMATIONS

TO PULSES

$\bar{\varepsilon}_x^2(t)$: Integral (error)^2 in input pulse Hermite approximation

$\bar{\varepsilon}_y^2(t)$: Integral (error)^2 in output pulse Hermite approximation

ϕ_1 : Minimum integral (error)^2 between predicted and experimental frequency response transfer functions

ϕ_2 : Minimum integral (error)^2 between predicted and experimental output pulse transforms

Run Desig.	INTEGRAL ERRORS				VARIANCES σ^{*2}		
	$\bar{\varepsilon}_x^2(t)$ X 10^5	$\bar{\varepsilon}_y^2(t)$ X 10^5	ϕ_1 X 10^4	ϕ_2 X 10^4	From Moments	From ϕ_1	From ϕ_2
16	55	.55	22	18	.307	.31	.31
17	132	1.05	14	10	.310	.31	.31
18	18	13.7	79	70	.0812	.079	.079
19	36	1.8	123	10	.0839	.083	.083
20	16	.55	40	30	.219	.22	.22
21	15	1.7		105	.274	.24	

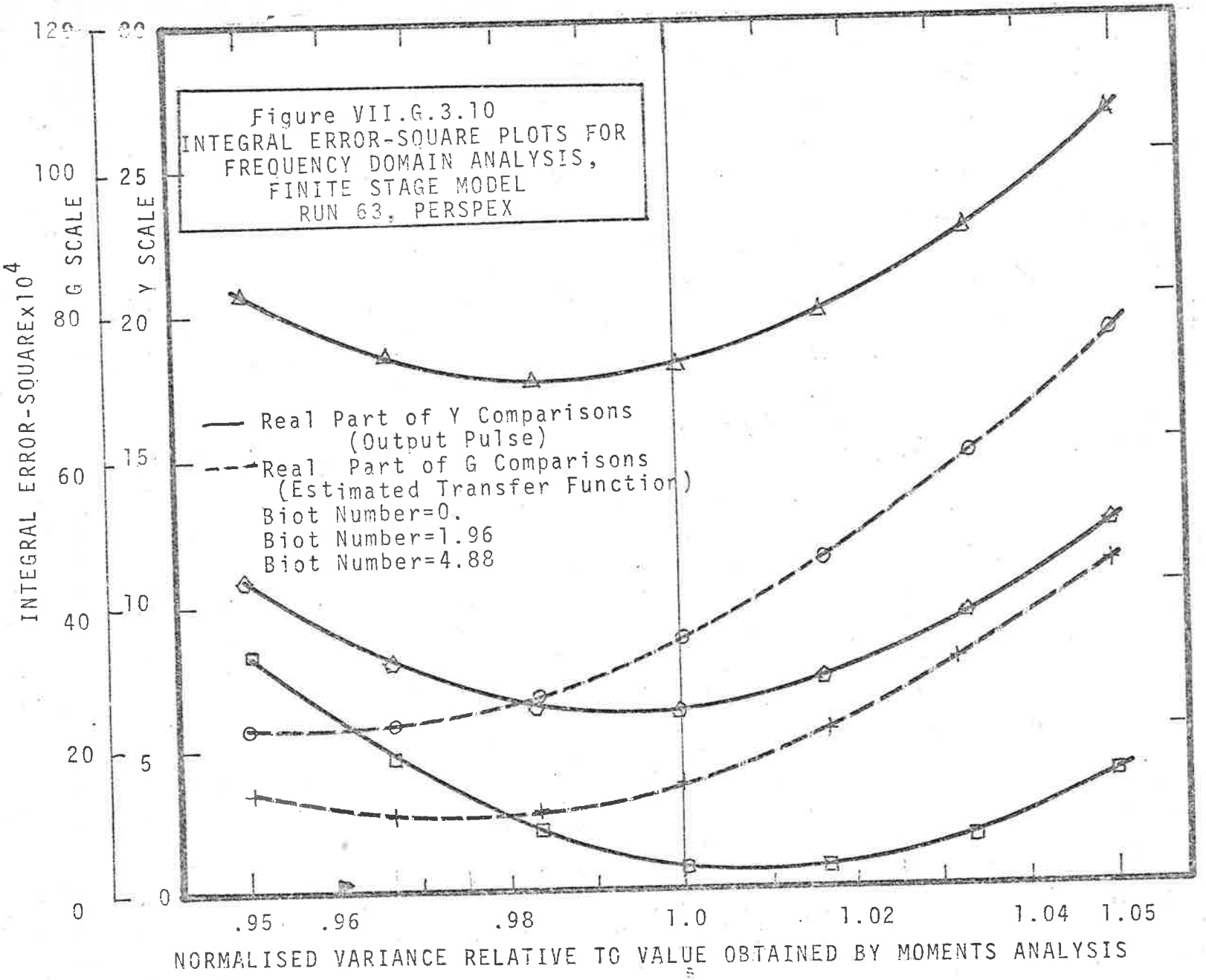
Figure VII.G.3.10
INTEGRAL ERROR-SQUARE PLOTS FOR
FREQUENCY DOMAIN ANALYSIS,
FINITE STAGE MODEL
RUN 63, PERSPEX
INTEGRAL ERROR-SQUAREx10^4
G SCALE
Y SCALE
120
100
80
60
40
20
0
25
20
15
10
5
0
Real Part of Y Comparisons
(Output Pulse)
Real Part of G Comparisons
(Estimated Transfer Function)
Biot Number=0.
Biot Number=1.96
Biot Number=4.88
.95
.96
.98
1.0
1.02
1.04
1.05
NORMALISED VARIANCE RELATIVE TO VALUE OBTAINED BY MOMENTS ANALYSIS

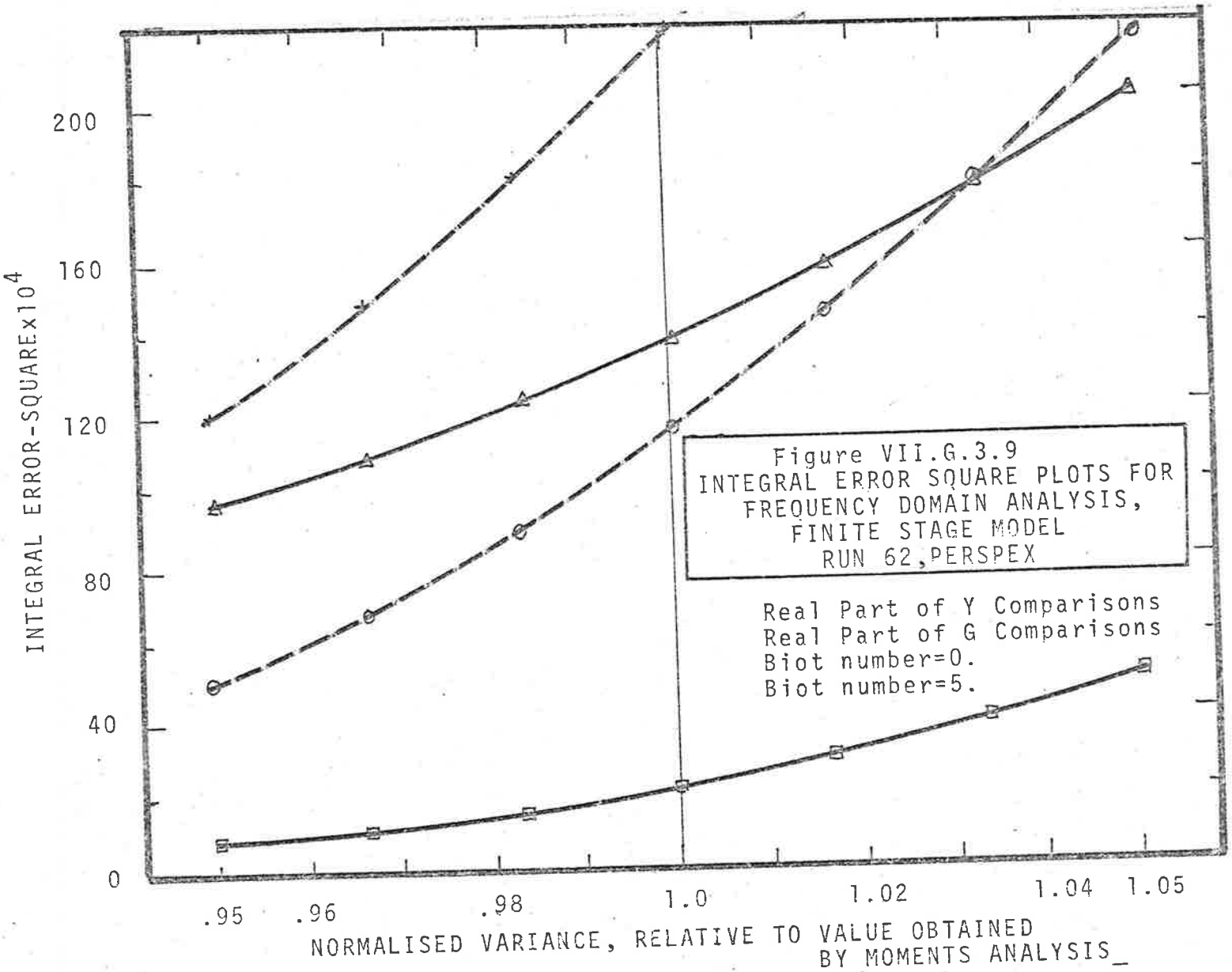

Figure VII.G.3.9
INTEGRAL ERROR SQUARE PLOTS FOR FREQUENCY DOMAIN ANALYSIS, FINITE STAGE MODEL
RUN 62, PERSPEX

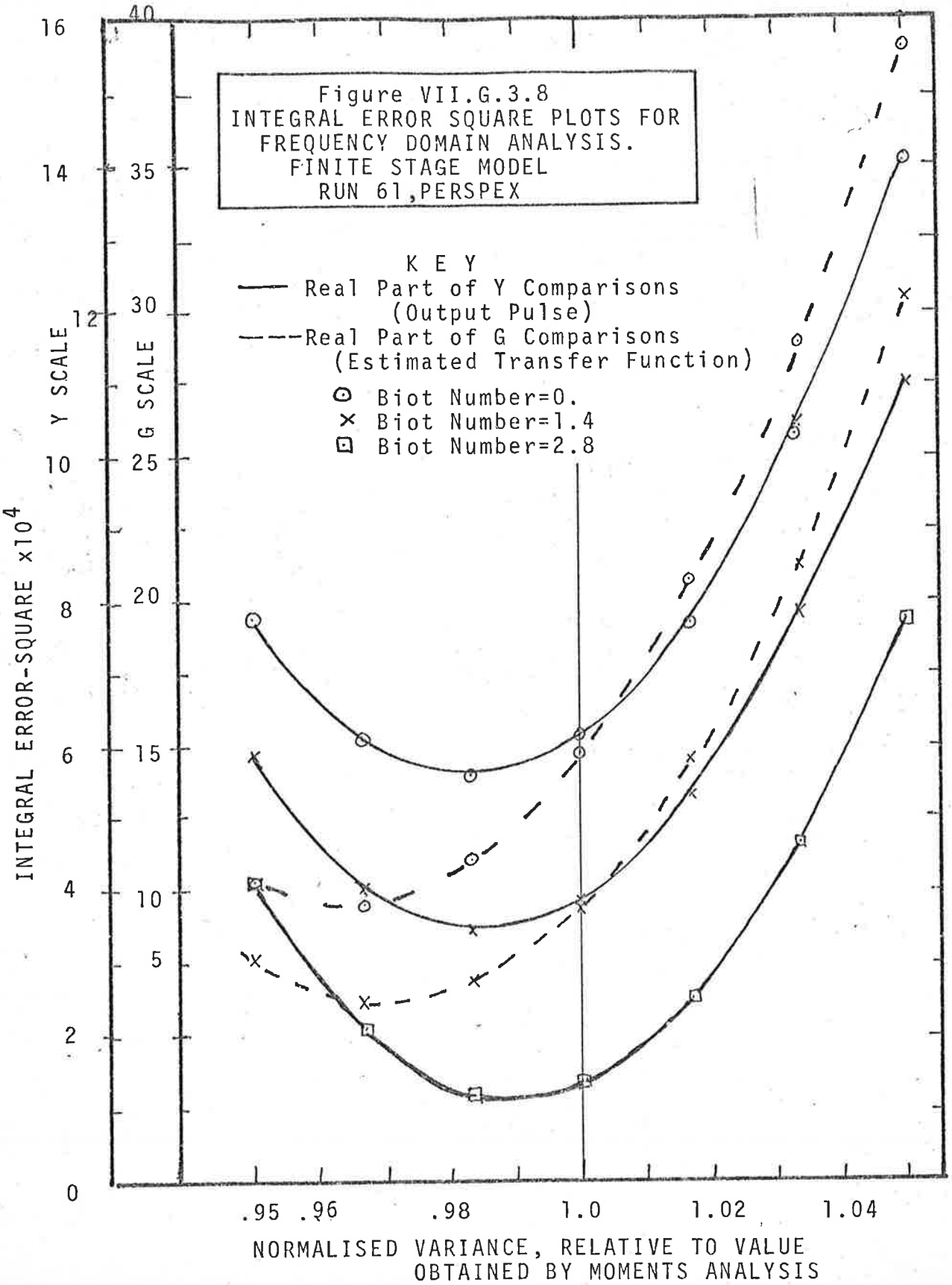
Figure VII.G.3.8
INTEGRAL ERROR SQUARE PLOTS FOR
FREQUENCY DOMAIN ANALYSIS.
FINITE STAGE MODEL
RUN 61, PERSPEX
K E Y
Real Part of Y Comparisons
(Output Pulse)
Real Part of G Comparisons
(Estimated Transfer Function)
Biot Number=0.
Biot Number=1.4
Biot Number=2.8
INTEGRAL ERROR-SQUARE x10^4
Y SCALE
G SCALE
0
2
4
6
8
10
12
14
16
5
10
15
20
25
30
35
40
.95
.96
.98
1.0
1.02
1.04
NORMALISED VARIANCE, RELATIVE TO VALUE
OBTAINED BY MOMENTS ANALYSIS

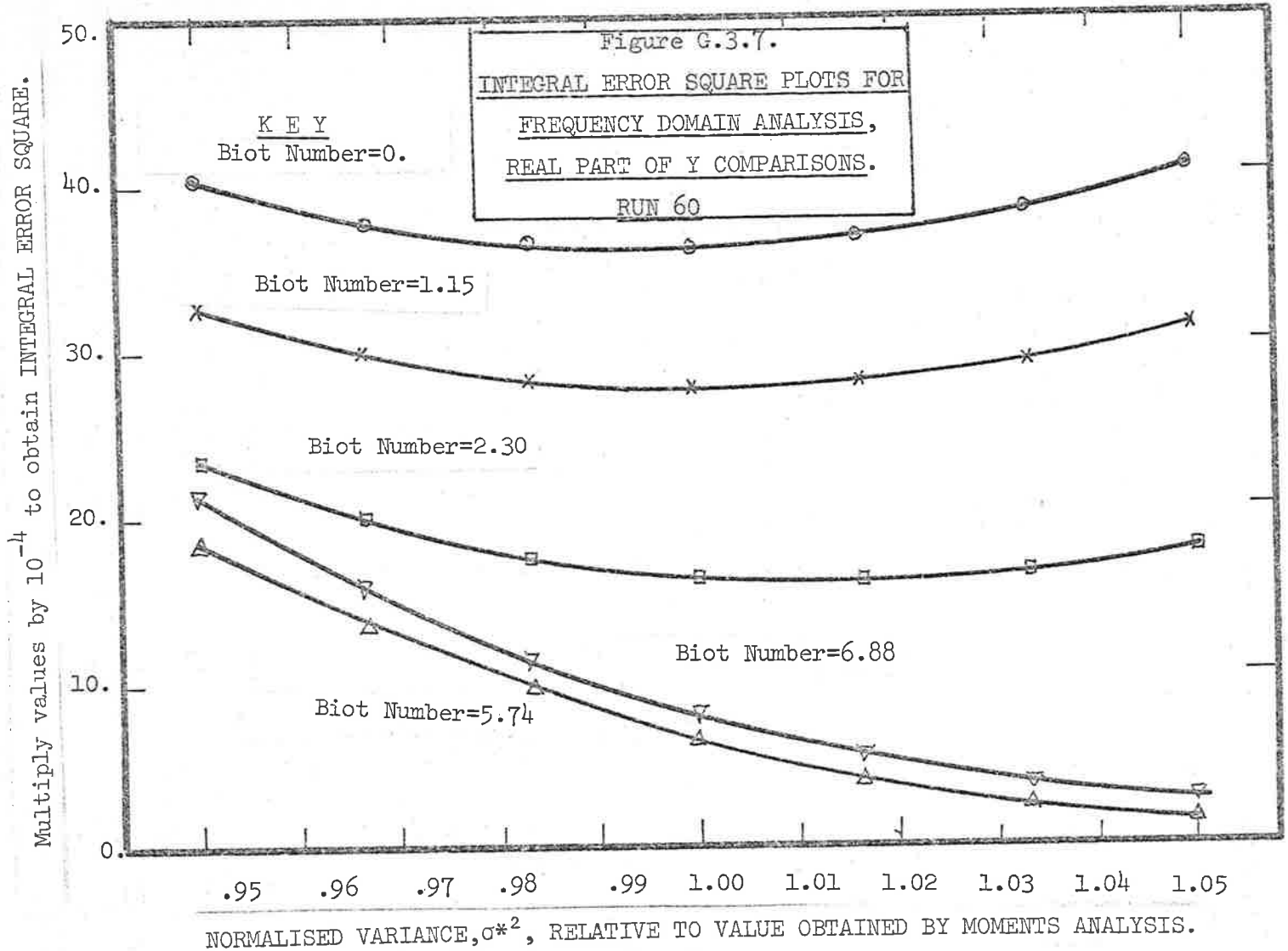
Figure G.3.7.
INTEGRAL ERROR SQUARE PLOTS FOR
FREQUENCY DOMAIN ANALYSIS,
REAL PART OF Y COMPARISONS.
RUN 60
K E Y
Biot Number=0.
Biot Number=1.15
Biot Number=2.30
Biot Number=6.88
Biot Number=5.74
Multiply values by 10^{-4} to obtain INTEGRAL ERROR SQUARE.
50.
40.
30.
20.
10.
0.
.95
.96
.97
.98
.99
1.00
1.01
1.02
1.03
1.04
1.05
NORMALISED VARIANCE, σ^{*2}, RELATIVE TO VALUE OBTAINED BY MOMENTS ANALYSIS.

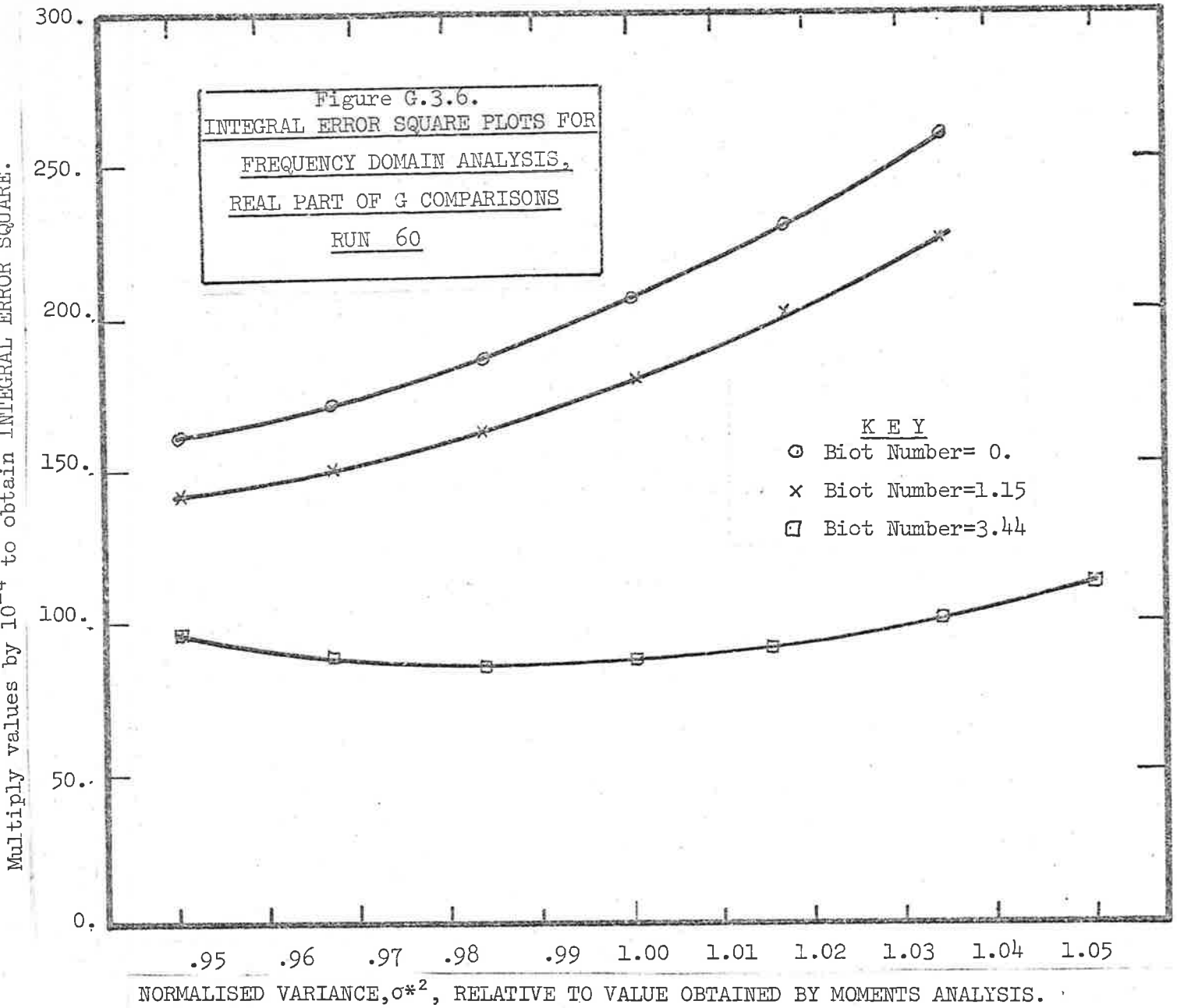
Figure G.3.6.
INTEGRAL ERROR SQUARE PLOTS FOR
FREQUENCY DOMAIN ANALYSIS,
REAL PART OF G COMPARISONS
RUN 60
KEY
Biot Number= 0.
Biot Number=1.15
Biot Number=3.44
Multiply values by 10^{-4} to obtain INTEGRAL ERROR SQUARE.
300.
250.
200.
150.
100.
50.
0.
.95
.96
.97
.98
.99
1.00
1.01
1.02
1.03
1.04
1.05
NORMALISED VARIANCE, σ^{*2}, RELATIVE TO VALUE OBTAINED BY MOMENTS ANALYSIS.

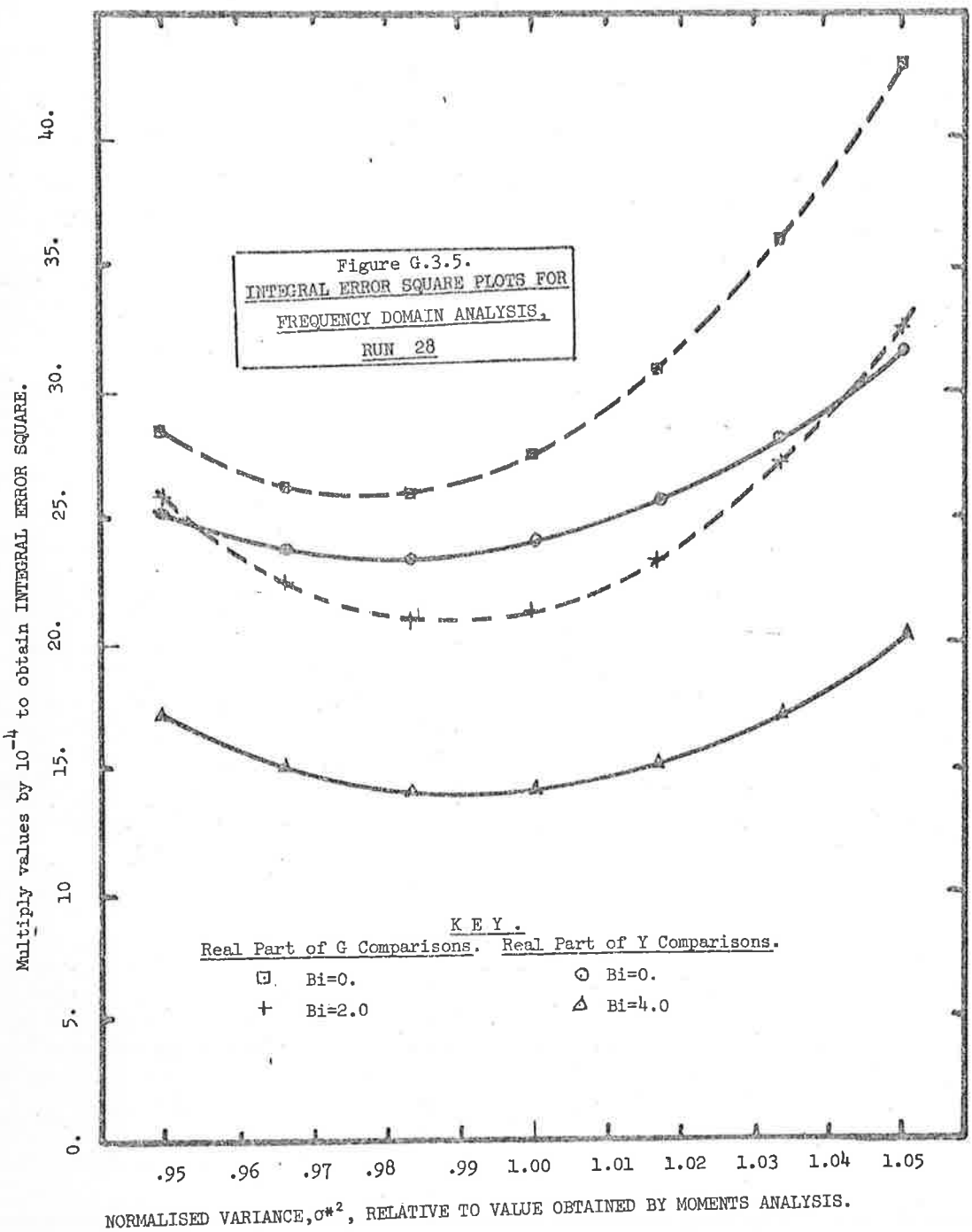
Figure G.3.5.
INTEGRAL ERROR SQUARE PLOTS FOR
FREQUENCY DOMAIN ANALYSIS,
RUN 28
Multiply values by 10^{-4} to obtain INTEGRAL ERROR SQUARE.
0.
5.
10
15.
20.
25.
30.
35.
40.
.95
.96
.97
.98
.99
1.00
1.01
1.02
1.03
1.04
1.05
NORMALISED VARIANCE, σ^{*2}, RELATIVE TO VALUE OBTAINED BY MOMENTS ANALYSIS.
K E Y .
Real Part of G Comparisons.
Bi=0.
Bi=2.0
Real Part of Y Comparisons.
Bi=0.
Bi=4.0

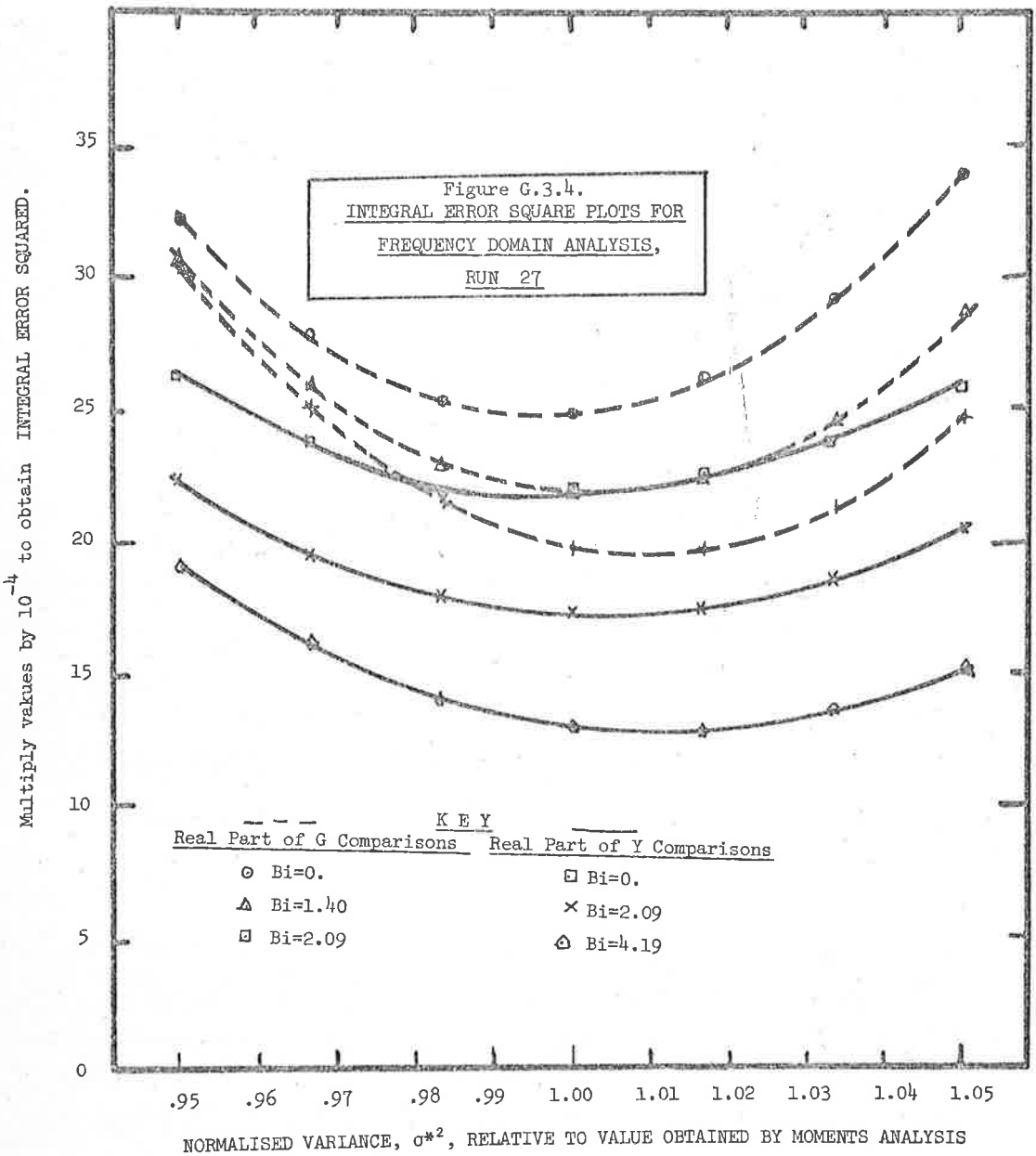
Figure G.3.4.
INTEGRAL ERROR SQUARE PLOTS FOR
FREQUENCY DOMAIN ANALYSIS,
RUN 27
Multiply values by 10^{-4} to obtain INTEGRAL ERROR SQUARED.
35
30
25
20
15
10
5
0
.95
.96
.97
.98
.99
1.00
1.01
1.02
1.03
1.04
1.05
NORMALISED VARIANCE, σ^{*2}, RELATIVE TO VALUE OBTAINED BY MOMENTS ANALYSIS
K E Y
Real Part of G Comparisons
Bi=0.
Bi=1.40
Bi=2.09
Real Part of Y Comparisons
Bi=0.
Bi=2.09
Bi=4.19

TABLE VII.G.3.1 (contd)

Run	Frequency Content $\lvert X(j\omega)\rvert$ of input pulse at $\omega = 10$
16	.34
17	.39
18	.74
19	.69
20	.54
21	.50

(ii) High Biot Number Runs

The results of the high Biot number runs were more ambiguous. Beacuse of the high flows and shorter bed lengths, the frequency content of input pulses was low in a few cases. Values of γx or KV_H/Bi were uniformly low at the Biot number predicted in tables D.3.3 and F.1.5. There were marked differences between the minimum error criteria ϕ_1 (or ϕ_2) for varying values of Biot number at fixed normalised variance σ^{*2}. At the same time, whilst one would expect the 'minimum minimum' value of ϕ_1 (or ϕ_2) to occur at the values of Biot number predicted by Tables D.3.3 and F.1.5, this was not found to be so. A continuous increase in Biot number resulted in a continuous decrease in the minimum value of ϕ_1 or ϕ_2.

In general, comparison of experimental and predicted values of output pulse transforms using the error criterion ϕ_2 gave values of σ^{*2} which were closer to the results of moments analysis. This

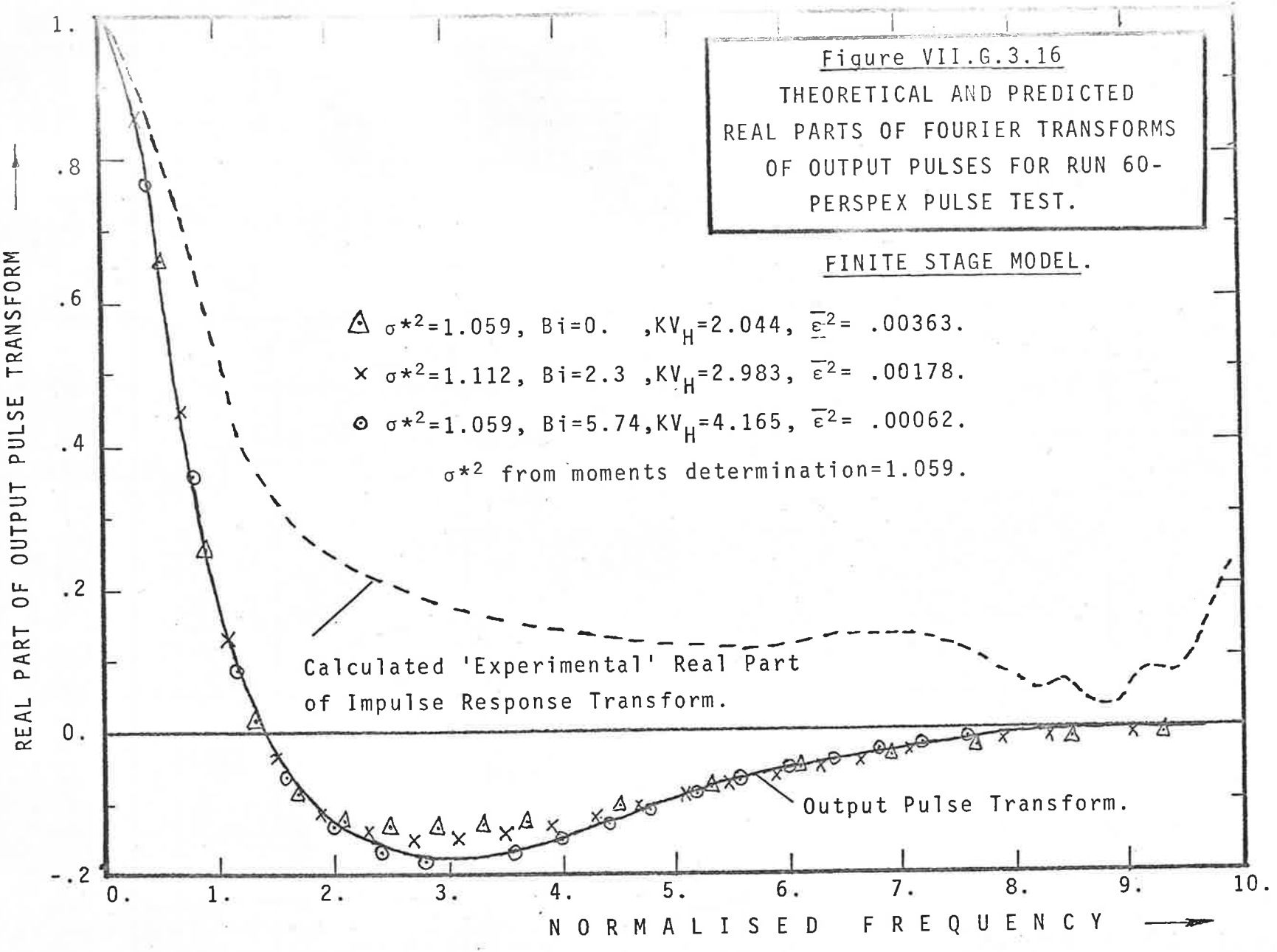
Figure VII.G.3.16
THEORETICAL AND PREDICTED
REAL PARTS OF FOURIER TRANSFORMS
OF OUTPUT PULSES FOR RUN 60-
PERSPEX PULSE TEST.
FINITE STAGE MODEL.
σ*²=1.059, Bi=0. ,KV_H=2.044, ε̄²= .00363.
σ*²=1.112, Bi=2.3 ,KV_H=2.983, ε̄²= .00178.
σ*²=1.059, Bi=5.74,KV_H=4.165, ε̄²= .00062.
σ*² from moments determination=1.059.
Calculated 'Experimental' Real Part
of Impulse Response Transform.
Output Pulse Transform.
REAL PART OF OUTPUT PULSE TRANSFORM
NORMALISED FREQUENCY
1.
.8
.6
.4
.2
0.
-.2
0.
1.
2.
3.
4.
5.
6.
7.
8.
9.
10.

would be expected, according to the discussion of section V.C.2, when the input pulse frequency content was low. On the other hand, the sensitivity (and reliability) of the estimated value of σ^{*2} was lower using output pulse transform analysis.

In summary, very poor agreement between theoretical and experimental curve shapes was obtained at high values of the Biot number and low values of the bed length parameter γx. The theoretical model was found inadequate for obtaining reasonable and consistent values of the Biot number.

Results of the frequency domain comparisons are displayed in figures 3.4 to 3.16 and in table 3.2.

TABLE VII.G.3.2

RESULTS OF FREQUENCY DOMAIN COMPARISONS

FINITE STAGE MODEL - HIGH BIOT NUMBERS

HERMITE POLYNOMIAL APPROXIMATIONS TO PULSES.

For Key to tabulation see Table G.3.1.

Run Desig.	INTEGRAL ERRORS				VARIANCES σ^{*2} at Bi = 0		
	$\bar{\varepsilon}_x^2(t)$ x 10^5	$\bar{\varepsilon}_y^2(t)$ x 10^5	ϕ_1 x 10^4	ϕ_2 x 10^4	Moments	ϕ_1	ϕ_2
27	239	1.12	28	21.9	.460	.45	.460
28	149	1.28	26.0	23.0	.473	.465	.465
60	108	57.0	150	36	1.059	<1.	1.04
61	50.	1.15	9.5	5.6	.538	.52	.528
62	927	38.	120	85	1.005	<0.9	<10.9
63	551	20.	20.	17.6	.0546	.535	.515

TABLE VII.G.3.1 (contd.)

Run	Frequency content, $\lvert X(j\omega) \rvert$ of input pulse at ω = 10
27	.308
28	.010
60	.043
61	.298
62	.651
63	.455

H. SUMMARY OF THE CONCLUSIONS OF CHAPTER VII.

An improvement in reliability and consistency of the experimental pulse (and step) results was achieved by the use of feedback control of the input temperature.

It was found that for step response or breakthrough curve testing, estimates of the normalised variance could be obtained simply and rapidly using the empirical breakthrough curve correlations combined with experimental determination of the first moment $\mu(t)$ of the impulse response from the zero'th moment of $1 - u(t)$. It was found that this method was less susceptible to small errors in the location of the final value of a breakthrough curve than was direct evaluation of higher moments from the breakthrough curve.

The Stanton numbers uncorrected for fluid phase axial dispersion gave close agreement with the Denton heat transfer

correlation for both sets of step response data. It was suggested that fluid phase axial dispersion effects may be included in steady state fluid-particle heat transfer measurements made by heating isolated spheres, as in the evaporation from porous spheres method discussed in chapter III. This is not surprising, on reflection, since axial dispersion, if present, would cause the 'true' temperature difference around an isolated sphere to differ from the apparent temperature difference in the same way as it is predicted to do in an assemblage of spheres. Since axial dispersion effects are supposed to be separated from other effect with difficulty due to the small effect on curve shape, then the question cannot be finally resolved at this stage.

It nonetheless apparent that, for lower Reynolds numbers especially, correction of a heat (or mass transfer)correlation which incorporates its own axial dispersion 'correction' could lead to errors in breakthrough curve prediction, so that from a practical point of view one might as well proceed as though axial dispersion were absent.

Whilst the experimental step responses for highly conducti and for poorly conductive particles appeared to be consisent with each other and with a Biot number correction of 1+Bi/5, the soda glass results were anomalous. In Section D.4, spreading of the input 'step' was rejected as a reason for the discrepancy and at the present stage of the investigation, no no alternative explanation has been found.

Despite this discrepancy, frequency domain analysis of

pulse tests for low Biot numbers and for bed length parameters greater than 5.0 gave similar estimates of the normalised variance those obtained by direct moments analysis. Hence the results appea to be internally consistent, at least.

In the case of experiments which had yielded low values of bed length parameter, very poor agreement between theory and experiment was obtained. It appears that further experiments would be desirable in the high Biot number region.

Experimental breakthrough curves did not yield straight lines on an arithmetic probability plot as predicted by the equiva conductivity model.

CHAPTER VIII.

DISCUSSION, PERSPECTIVE AND AREAS FOR FUTURE WORK.

Mathematical Models

The original objective in comparing finite stage and continuous models of packed bed dynamics was to establish more clearly the range of parameters for which the finite stage model would be regarded as a useful approximation to the continuous. This would allow more confidence to be placed in the results of a numerical simulation of packed bed dynamics in the more complex situations which arise in adsorption when the adsorption isotherm is non-linear. Continuous model solutions become very time consuming even on a digital computer, since iteration is necessary in order to satisfy both inlet and exit boundary conditions. The finite stage approach allows a more rapid solution since the transient response for each row of particles may be computed in full and used as an input to the next row without the need for iteration.

The correspondence demonstrated between the two models occurs, fundamentally, because the dynamics of individual particles is common to both and dominates the solution for a wide range of parameters. This is also the reason why, when the heat capacity ratio is large, the simple Schumann model which makes no allowance at all for axial dispersion provides a useful description of the situation. The recent

suggestion by D.J. Gunn * that neither model fits experimental data when Reynolds numbers are small and the packing structure is regular is therefore not quite so relevant as may be supposed except in the low Reynolds number region,

In comparing theoretical models three methods have been used in this thesis. In chapter II and paper I the finite stage and continuous models were compared by plotting the frequency response transfer function of each in magnitude and phase for similar parameter values and noting the correspondences. A similar procedure was adopted in comparing the predictions of the finite stage, Schumann and equivalent conductivity models at constant values of normalised variance σ^{*2}. A second method was to show that computed points on breakthrough curves fall on the same straight line when correlated against σ^{*4} whilst a third was to compare numerical values of the first three cumulants as in the comparison between the equivalent conductivity and Schumann models in section II.E.1.

None of these methods give a very exact and quantitative measure of the agreement between models, whilst direct comparison between points on a breakthrough curve as used by Handley and Heggs may also be misleading. A preferable method is suggested by the work of section V.C.2. Thus, computation of the integral error square between real parts of the frequency response transfer function

---

* Gunn, D.J., 'Dispersion in Packed Beds', Trans. Instn. of Chem. Eng. 47 T341 [1969].

yields the same quantity for the impulse response. A similar procedure may be adopted in comparing step responses. The values thus obtained give a numerical measure of the agreement between models and would be useful in detecting the effects of more subtle differences such as those due to boundary conditions. The above procedure will be adopted in future work.

Fluid-solid-fluid Axial Conduction

In the case of heat transfer, the predicted importance of fluid-solid-fluid conduction effects at low flowrates is likely to make analysis very complex. The discussion presented in section I.A.5, is, admittedly, highly simplified and it is probable that the actual particle size would need to be considered in computations of fluid-solid-fluid conductivity. The writing of separate equations for fluid and fluid-solid-fluid conduction leads to a fourth order differential equation in the Laplace transform domain [Littman, Barille and Pulsifer, 1968] so that we may expect breakthrough curves to assume a significantly different shape to those observed here. The situation is further complicated by the interaction between fluid-solid heat transfer and axial fluids dispersion and by the resultant unreliability of heat (and mass) transfer correlations. From the dynamic testing point of view, the complexity of the axial solids.

conduction equations leads to the conclusion that moments will be too unwieldy for practical evaluation. Hence frequency domain analysis should be useful, via pulse techniques.

Further experimental work in the low Reynolds number region is warrented together with a parallel development of pulse to frequency response analysis techniques. More rigorous methos of testing the statistical significance of a time or frequency domain fit are required.

APPENDIX 1

TRANSFER FUNCTION DERIVATION FOR EXTENDED AXIAL DISPERSION MODELS

1. With Danckwerts' Boundary Conditions

Defining equations:-

$$\frac{1}{Pe'}\frac{\partial^2 T}{\partial z^2} - \frac{\partial T}{\partial z} + KV_H(T_s - T) = \frac{\partial T}{\partial t} \qquad 0 \leq z \leq 1, \quad \ldots \quad (1.1)$$

$$\frac{1}{\alpha}\frac{\partial T_p}{\partial t} = \frac{2}{r}\frac{\partial T_p}{\partial r} + \frac{\partial^2 T_p}{\partial r^2} \qquad 0 \leq r \leq 1, \quad \ldots \quad (1.2)$$

$$\frac{1}{Bi}\left[\frac{\partial T_p}{\partial r}\right]_{r\to 1} = T - T_s \qquad \ldots \quad (1.3)$$

$$T_i(t) = \left[T(z,t) - \frac{1}{Pe'}\frac{\partial T}{\partial z}\right]_{z\to 0} \qquad \ldots \quad (1.4)$$

$$\left[\frac{\partial T}{\partial z}\right]_{z\to 1} = 0 \qquad \ldots \quad (1.5)$$

Laplace transforming (1.1) for zero initial conditions an ordinary differential equation results:-

$$\frac{1}{Pe'}\frac{d^2 T}{dz^2} - \frac{dT}{dz} - s\,T - KV_H(T - T_s) = 0 \qquad \ldots \quad (1.6)$$

Relating particle surface and fluid temperatures at any distance z by the particle transfer function $G_p(s)$ (see II.A.3.a), we have:-

$$Tp(z,r,s)]_{r=1} = T_s(z,s) = G_p(s).\,T(z,s) \qquad \ldots \quad (1.7)$$

Substituting (1.7) into (1.6):-

$$\frac{d^2T}{dz^2} - Pe' \frac{dT}{dz} - Pe'.\ T.\ \{s + KV_H[1 - G_p(s)]\} = 0 \quad \ldots \quad (1.8)$$

Equation (1.8) has the general form

$$\frac{d^2T}{dz^2} - A_1 \frac{dT}{dz} - A_2 T = 0$$

with general solution

$$T(z,s) = C_1 \exp(m_1 z) + C_2 \exp(m_2 z) \quad \ldots \quad (1.9)$$

where m_1 and m_2 are the roots of the indicial equation

$$m^2 - A_1 m - A_2 = 0$$

i.e.
$$m_1 = \frac{A_1}{2} - \frac{1}{2}\sqrt{[A_1^2 + 4A_2]}$$

$$m_2 = \frac{A_1}{2} + \frac{1}{2}\sqrt{[A_1^2 + 4A_2]}$$

Boundary condition (1.4) yields

$$T_i(s) = \lim_{z \to 0}[C_1 \exp(m_1 z) + C_2 \exp(m_2 z) - \frac{1}{Pe'} C_1 m_1 \exp(m_1 z) - \frac{1}{Pe'} C_2 m_2 \exp(m_2 z)]$$

or
$$T_i(s) = \frac{C_1}{Pe'}(Pe' - m_1) + \frac{C_2}{Pe'}(Pe' - m_2) \quad \ldots \quad (1.10)$$

From boundary condition (1.5):-

$$\lim_{z \to 1} [C_1 m_1 \exp(m_1 z) + C_2 m_2 \exp(m_2 z)] = 0$$

$$C_1 m_1 \exp m_1 + C_2 m_2 \exp m_2 = 0 \quad \ldots \quad (1.11)$$

Equations (1.10) and (1.11) may be solved for C_1 and C_2:-

$$C_1 = \frac{Pe' m_2 e^{m2} . T_i(s)}{m_2 (Pe'-m_1) e^{m2} - m_1 (Pe'-m_2) e^{m1}}$$

$$C_2 = \frac{Pe' m_1 e^{m1} . T_i(s)}{m_2 (Pe'-m_1) e^{m2} - m_1 (Pe'-m_2) e^{m1}} \quad \ldots \quad (1.12)$$

Whilst equations (1.12) and (1.9) could be left in their present form, dependent on z as a parameter a simplification is introduced if z is set equal to 1. The overall transfer function then results:-

$$\frac{T(s)}{T_i(s)} = G(s) = \frac{4.Pe' . e^{Pe'/2} . \sqrt{X}}{\exp(\frac{1}{2}\sqrt{X}) . (Pe'+\sqrt{X})^2 - \exp(-\frac{1}{2}\sqrt{X}) . (Pe'-\sqrt{X})^2} \quad \ldots \quad (1.13)$$

where

$$X = Pe'^2 + 4\, Pe' \{s + KV_H(1-G_p(s))\}$$

2. With Simplified Boundary Conditions

Replace equations (1.4) and (1.5) by

$$T_i(t) = \lim_{z \to 0} T(z,t) \quad \ldots \quad (2.1)$$

and

$$\lim_{z \to \infty} T(z,t) = \text{finite or zero} \quad \ldots \quad (2.2)$$

Then equation (2.2) requires that only the negative root in (1.9) is admissable, i.e.

$$T(z,s) = C_1 \exp(m_1 z)$$

From (2.1), $C_1 = T_i(s)$.

Hence

$$\frac{T(z,s)}{T_i(s)} = G(z,s) = e^{Pe'/2} \exp[-\tfrac{1}{2}\sqrt{X}] \quad . \ . \ . \quad (2.3)$$

where X has been defined by equation (1.13).

APPENDIX 2

DERIVATION OF MOMENTS

1. Rosen's Transfer Function

For z=1, equation II.B.4.1 gives

$$G(s) = e^{-s} . e^{-\phi} . \exp[\phi . G_p(s)] \quad \ldots \quad (1.1)$$

where (equations II.B.3.4 and II.B.3.5)

$$G_p(s) = \frac{K}{K + Y_D(s)} = \frac{Bi}{Bi + p\cot p - 1} \quad \ldots \quad (1.2)$$

$$p = j(s/\alpha)^{1/2}$$

Expanding (1.2) in power series:-

$$G_p(s) = \frac{Bi}{Bi - \frac{p^2}{3} - \frac{p^4}{45} - \frac{2p^6}{945} - \ldots}$$

$$= 1 + \frac{p^2}{3Bi} + \frac{p^4(Bi+5)}{45Bi^2} + \frac{p^6(2Bi^2+14Bi+35}{945Bi^3}$$

$$= a_o + a_2 p^2 + a_4 p^4 + a_6 p^6 + \ldots$$

$$\ldots \quad (1.3)$$

The moments of the particle impulse response are needed in determining the moments of the overall transfer function. These are obtained below using equation II. B.3.4

For the zero'th moment:-

$$\lim_{s \to 0} G_p(s) = 1$$

From (1.3):

$$\frac{dG_p(p)}{dp} = G_p'(p) = 2a_2p + 4a_4p^3 + 6a_6p^5 + \ldots \qquad \ldots \quad (1.4)$$

Hence,

$$-\frac{d\,G_p(s)}{ds} = -G_p'(s) = -G_p'(p).\frac{dp}{ds} = +G_p'(p).\frac{1}{2\alpha p}$$

$$= G_p'(p).\frac{3\,Bi}{2Kp} \qquad \ldots \quad (1.5)$$

Then $$-\lim_{s\to 0} G_p'(s) = \frac{3a_2Bi}{K} = \frac{1}{K} \qquad \ldots \quad (1.6)$$

(first moment)

$$G_p''(p) = 2a_2 + 12a_4p^2 + 30a_6p^4 + \ldots$$

$$G_p''(s) = \frac{d}{dp}\left[\frac{G_p'(p)}{2\alpha p}\right]\frac{dp}{ds}$$

$$= -\frac{1}{2\alpha p}\left\{\frac{1}{2\alpha p^2}(2a_2p + 4a_4p^3 + 6a_6p^5 + \ldots)\right.$$

$$\left. - \frac{1}{2\alpha p^2}(2a_2p + 12a_4p^3 + 30a_6p^5 + \ldots)\right\}$$

$$= +\frac{1}{4\alpha^2p^3}[8a_4p^3 + 24a_6p^5 + \ldots]$$

i.e.

$$\lim_{s\to 0} G_p''(s) = \frac{2a_4}{\alpha^2} = \frac{2\,(Bi+5)}{5K^2} \qquad \ldots \quad (1.7)$$

$$G_p'''(p) = 24a_4 p + 120a_6 p^3 + \ldots$$

$$G_p'''(s) = \frac{d}{dp}\left[\frac{1}{\alpha^2}(2a_4 + 6a_6 p^2 + \ldots)\right]. \frac{dp}{ds}$$

$$-\lim_{s\to 0} G_p'''(s) = +\frac{12a_6 p}{\alpha^2}. \frac{1}{2\alpha p} = \frac{6a_6}{\alpha^3}$$

i.e.

$$-\lim_{s\to 0} G_p'''(s) = \frac{6\,(2h^2 + 14h + 35)}{35K^3} \quad \ldots \quad (1.8)$$

To evaluate the moments of the <u>overall</u> transfer function:-

From (1.1)

$$\lim_{s\to 0} G(s) = e^{-0}.\, e^{-\phi}\, e^{\phi} = 1 \quad \text{(zero'th moment)} \quad \ldots \quad (1.9)$$

From (1.1)

$$-G'(s) = G(s) - e^{-s}\, e^{-\phi} \exp[\phi G_p(s)].\, \phi G_p'(s)$$

$$= G(s)[1 - \phi.\, G_p'(s)]$$

Hence from (1.5) and (1.9):

$$-\lim_{s\to 0} G'(s) = 1 + V_H = \mu, \quad \ldots \quad (1.10)$$

the first moment

$$G''(s) = -G'(s)[1 - \phi\, G_p'(s)] + G(s).\phi.G_p''(s)$$

$$= [1 - \phi G_p'(s)]^2.G(s) + \phi\, G_p''(s).G(s)$$

Hence, from (1.6), (1.9) and (1.7):

$$\lim_{s\to 0} G''(s) = (1 + V_H)^2 + KV_H \cdot \frac{2(Bi+5)}{5K^2}$$

$$= \mu^2 + (\mu-1)^2 \frac{2(Bi+5)}{5KV_H} = \mu_2$$

the second moment.

The second moment about the mean, or variance is, from II.

$$\sigma^2 = \mu_2 - \mu^2 = \frac{2(\mu-1)^2 Bi}{5KV_H} + \frac{2(\mu-1)^2}{KV_H} \quad \ldots \quad (1.11)$$

$$G'''(s) = -2(1 - \phi G_p'(s)) .G(s) .\phi G_p''(s)$$

$$+ (1 - \phi G_p'(s))^2 G'(s) + \phi G_p'''(s).G(s)$$

$$+ \phi G_p''(s). G'(s)$$

$$= 3 \phi G_p''(s). G'(s) + \left[\frac{G'(s)}{G(s)}\right]^2. G'(s)$$

$$+ \phi G_p'''(s). G(s)$$

Hence $$-\lim_{s\to 0} G'''(s) = 3\mu(\mu-1)^2 \frac{Bi+5}{5KV_H} + \mu^3$$

$$+ 6(\mu-1) \frac{2Bi^2+14Bi+35}{35K^2}$$

$$= \mu_3 ,$$

the third moment.

The third moment about the mean, or kurtosis is given from equation II. by

$$\pi^3 = \mu_3 - 3\mu \sigma^2 - \mu^3$$

$$= (\mu-1).\frac{6}{35K^2} (2Bi^2+14Bi+35)$$

$$\ldots \quad (1.12)$$

2. Extended Axial Dispersion Model with Simplified Boundary Conditions

For z=1, from Appendix 1, equ. (2.3):-

$$G(s) = e^{m}$$

where $$m = \frac{Pe'}{2} - \frac{1}{2}\sqrt{\{Pe'^2 + 4Pe'[s + \phi(1 - G_p(s)]\}}$$

and $$\phi \equiv KV_H$$

write

$$X = Pe'^2 + 4Pe'[s + \phi(1 - G_p(s))]$$

Then $\lim_{s\to 0} X = Pe'^2$,

$$X' = 4Pe'(1 - \phi\, G_p')$$

$$\lim_{s\to 0} X' = 4Pe'(1 + V_H),$$

$$\lim_{s\to 0} \frac{X'}{\sqrt{X}} = 4(1+V_H)$$

$$\lim_{s\to 0} m = 0$$

Hence $\lim_{s\to 0} G(s) = 1$ zero'th moment . . . (2.1)

$$G'(s) = e^{m}.\, m' = G(s).\, m'$$

$$m' = -\frac{1}{2}\frac{d}{ds}\sqrt{X} = -\frac{X'}{4\sqrt{X}}$$

$$\boxed{\mu = -\lim_{s\to 0} G'(s) = 1 + V_H}\ , \qquad \ldots \quad (2.2)$$

the first moment or mean

$$\lim_{s\to 0} \frac{X'}{\sqrt{X}} = 4\mu . \quad , \quad \lim X' = 4Pe'\mu$$

$$X'' = - 4Pe' \phi G_p''$$

$$\lim_{s\to 0} X'' = - \frac{8Pe\ V_H\ (Bi+5)}{5K} \qquad \text{from (2.7)}$$

$$= - 8\sqrt{X}.\ (\mu-1)\ \frac{Bi+5}{5K}$$

$$X''' = - 4Pe' \phi G_p'''$$

$$\lim X''' = 24Pe'(\mu-1)\ \frac{(2Bi^2+14Bi+35)}{35K^2} \qquad \text{from (1.8)}$$

$$\frac{d^2m}{ds^2} = - \frac{d}{ds}\ \frac{X'}{4\sqrt{X}} = - \frac{2X''\ X + (X')^2}{8\ X\ \sqrt{X}}$$

$$= - \frac{X''}{4\sqrt{X}} + \frac{(X')^2}{8X\sqrt{X}}$$

i.e. $$\lim_{s\to 0} \frac{d^2m}{ds^2} = 2(\mu-1).\ \frac{Bi+5}{5K} + \frac{2}{Pe'}\ \mu^2$$

$$\frac{d^3m}{ds^3} = - \frac{2X'''X + X'X''}{8X\sqrt{X}} + \frac{4X'X''\ X\sqrt{X} - 3(X')^3\sqrt{X}}{16X^3}$$

$$= - \frac{X'''}{4\sqrt{X}} + \frac{X'X''}{8X\sqrt{X}} + \frac{X'X''\sqrt{X}}{4X^2} - \frac{3(X')^3\sqrt{X}}{16X^3}$$

Hence

$$\lim_{s\to 0} \frac{d^3m}{ds^3} = - 6(\mu-1).\ \frac{2Bi^2+14Bi+35}{35K^2} - \frac{12\mu(\mu-1)}{Pe'}\ \frac{(Bi+5)}{5K}$$

$$- \frac{12\mu^3}{Pe'^2}$$

Now $G''(s) = e^m[(m')^2 + m'']$

Hence

$$\mu_2 = \lim_{s\to 0} G''(s) = \mu^2 + \frac{2\mu^2}{Pe'} + 2(\mu-1)\frac{Bi+5}{5K}$$

The variance, $\sigma^2 = \mu_2 - \mu^2$

i.e.

$$\boxed{\sigma^2 = \frac{2\mu^2}{Pe'} + 2(\mu-1)\frac{Bi+5}{5K}} \quad \ldots \quad (2.3)$$

Now

$$G'''(s) = m'G''(s) + e^m[2m'm'' + m''']$$

$$= 3m'G''(s) - 2(m')^3 + G(s)m'''$$

Hence

$$\mu_3 = \lim_{s\to 0} G'''(s) = 3\mu\mu_2 - 2\mu^3 - \lim_{s\to 0} m'''$$

The skewness, $\pi^3 = \mu_3 - 3\mu\,\sigma^2 - \mu^3$

$$= \mu_3 - 3\mu\,\mu_2 + 3\mu^3 - \mu^3$$

$$= -\lim_{s\to 0} m'''$$

or

$$\boxed{\pi^3 = \frac{12\mu^3}{Pe'^2} + \frac{12\mu(\mu-1)}{Pe'}\frac{Bi+5}{5K} + 6(\mu-1).\frac{2Bi^2+14Bi+35}{35K^2}} \quad \ldots \quad (2.4)$$

$$Z''' = -\phi\, G_p'''(s)$$

$$G'''(s) = M\left\{\frac{4Z'Z''}{Z^3} - \frac{6(Z')^3}{Z^4} - \frac{Z'''}{Z^2} + \frac{2Z'Z''}{Z^3}\right\}$$

$$\lim_{s\to 0} G'''(s) = -\frac{12\mu(\mu-1).(Bi+5)}{M^2 5K} - \frac{6\mu^3}{M^3} - \frac{6(\mu-1).(2Bi^2+14Bi+35)}{M\ 35K^2}$$

Hence
$$\pi^3 = -M \lim_{s\to 0} G'''(s) - \frac{3\mu\sigma^2}{M} - \frac{\mu^3}{M}$$

$$= \frac{6\mu(\mu-1).(Bi+5)}{M\ 5K} + \frac{2\mu^3}{M^2}$$

$$+ \frac{6(\mu-1)\ (2Bi^2+14Bi+35)}{35K^2} \qquad \ldots \quad (3.5)$$

APPENDIX 3

PUBLISHED PAPERS BY C.P.JEFFRESON

RELEVANT TO THE PRESENT WORK

Paper 1- 'Dynamics of packed beds with intraphase heat or mass transfer.'

Paper 2- 'An approximation method for Fourier transform inversion applied to distributed parameter systems.' INSIDE BACK COVER.

Paper 3- 'A further note on "Dynamics of packed beds.."'

Paper 4- 'Dynamic testing - aunification.'

Chemical Engineering Science, 1968, Vol. 23, pp. 509–523. Pergamon Press. Printed in Great Britain.

Dynamics of packed beds with intraphase heat or mass transfer

C. P. JEFFRESON
Chemical Engineering Department, The University of Adelaide, South Australia

(*Received* 17 *June* 1967)

Abstract—An extension of the finite-stage model is proposed to describe the dynamic behaviour of packed bed heat exchangers and adsorbers. The model allows for axial dispersion, interphase resistance and intraparticle diffusion in the absence of gross radial transfer. A comparison between the proposed finite stage model and the axial dispersion model is made using the techniques of frequency response and moments analysis. Close correspondence is revealed between the two and it is concluded that (in the absence of decisive experimental data) either may be used. The finite stage model proposed has the advantage, however, that intraparticle diffusion effects may be much more simply allowed for.

1. INTRODUCTION

STUDIES of the dynamic behaviour of packed beds in which inter and intraphase heat and mass transfer occur may be justified by their relevance to the design and operation of packed bed adsorbers, chromatographic adsorption columns, thermal regenerators and packed bed chemical and nuclear reactors. The analysis presented here refers to packed beds in which negligible gross radial heat or mass transfer occurs and which radial fluid velocity variations may also be regarded as negligible. A simple extension of the finite stage or cell model of Kramers and Alberda[10] and others is presented and some of the predictions of this model compared with those of the more usual axial dispersion model. Detailed experimental verification is in progress at present.

(*a*) *Axial dispersion in the absence of interphase transfer*

A considerable amount of work has been reported concerning the effect of axial heat or mass transfer on the dynamics of packed beds. The work of Kramers and Alberda[10] is of considerable importance in this regard. They showed that if the frequency response of a series of perfect mixers is compared with that obtained from the axial dispersion model with negligible heat or mass transfer, then the dynamic behaviour of the two models may be forced in to close correspondence by relating the axial dispersion Peclet number P_{e_a} to the number of mixing stages N by the equation:

$$P_{e_a} \simeq \frac{N-1}{N} \cdot 2. \qquad (1)$$

Here P_{e_a} is defined with the distance between equivalent mixing stages as the characteristic dimension.

Whilst the predicted value of the axial Peclet number for long bed lengths has been fairly well verified in the literature for the turbulent flow of gases through packed beds[15], little evidence is available to verify Eq. (1). A highly significant paper by Mickley, Smith and Korshak[11] has, however, recently presented experimental evidence for the cell model in that eddy diffusivities in the voids of a packed bed were found to be considerably smaller than overall axial dispersion coefficients.

(*b*) *Interphase transfer—axial dispersion model*

Despite the intuitive appeal of the cell of finite stage model, most, if not all of the work carried out on the dynamics of beds with inter and intraphase heat and mass transfer has been interpreted in terms of the axial dispersion model. Analytical solutions have been in general quite complex and usually require extensive tabulation of special functions or digital computation for evaluation.

Some basic assumptions inherent in the axial dispersion formulation of the problem include:

(*i*) effectively uniform external fluid temperature or concentration over the length of a particle;
(*ii*) negligible inter particle conduction;
(*iii*) Fick's law type intraparticle transfer;
(*iv*) a linear adsorption isotherm over the range of concentrations considered (in the case of adsorption).

Assumption (*i*) is a natural one to make in the case of the proposed finite stage model.

Using the above assumptions, Rosen[13, 14] obtained analytically the response of outlet concentration to a step change in fluid concentration at the inlet where axial dispersion was negligible. The solution obtained appeared in the form of an infinite integral requiring numerical evaluation, convergence of which in general is slow. A simpler integral resulted when surface resistance was zero and approximate solutions were also obtained.

Deisler and Wilhelm[8] obtained the frequency response "transfer function" relating outlet fluid temperature to inlet fluid frequency variations allowing for axial dispersion but assuming negligible interphase resistance. The problem was again solved by Hagberg[9].

More recently Babcock, Green and Perry[2] obtained an exact solution to the problem of Deisler and Wilhelm. The solutions again involved infinite integrals and special hyperbolic functions. Numerical integration was necessary although approximate equations for the variance were obtained which showed that contributions to the variance of intraparticle diffusion and axial dispersion could be made regarded approximately additive over a limited range.

Chao and Hoelscher[6] obtained exact values for mean variance and skewness of the response of a packed bed in which interphase resistance and axial dispersion were present but particle diffusivity could be regarded as infinite. Their solutions are compared with the finite stage model solutions below as is the frequency response solution to the same problem of Pulsifer[12].

2. FORMULATION OF PROPOSED CELL MODEL

(*a*) *Basic equations*

Following Kramers and Alberda[10] the bed may be divided into a number of perfectly mixed cells separated by an axial distance H. In the following derivation temperature variations will be assumed to be of interest although an equivalent formulation for the case of linear adsorption may be readily obtained.

Then a heat balance may be written for the fluid of a given stage i assuming negligible radial heat conduction or velocity variation i.e.

$$H \,.\, \epsilon \,.\, \rho_f \,.\, c_f \,.\, \frac{\mathrm{d}T_i}{\mathrm{d}t'} = v_a \,.\, \epsilon \,.\, \rho_f \,.\, c_f \,.\, [T_{i-1} - T_i] + h_p \,.\, a_p \,.\, H \,.\, (1-\epsilon) \,.\, [T_{p_i} - T_i]$$

where T_i is the fluid temperature in the (well-mixed) stage i, T_{p_i} is the particle *surface temperature* at stage i and a_p is the area of particle per unit volume. Other symbols are defined in the Notation.

In the above equation, time may be normalised in units of overall bed holdup time $\bar{T}$ where

$$\bar{T} = \frac{L}{v_a} = \frac{N\mathrm{d}_p}{v_a} = \frac{MH}{v_a}.$$

The result is

$$\frac{\mathrm{d}T_i}{\mathrm{d}t} = N \,.\, T_{i-1} - N \,.\, T_i + KV_H[T_{p_i} - T_i] \qquad (2)$$

where V_H is the ratio of the volumetric heat capacity of the solid phase to that of the fluid phase at the particular volumetric porosity in the bed and K is a non dimensional heat transfer coefficient parameter defined by

$$K = \frac{h_p a_p}{\rho_s c_s} \cdot \bar{T}. \qquad (3)$$

One of the assumptions of this model is that particles in a given stage are surrounded by fluid of uniform temperature. It will be noted that this assumption is also made in the case of the continuous model although no physical justification is proposed.

The temperature $T_{p_i}(r, t)$ at any point within a

particle at stage i may be obtained by a convolution of the fluid temperature $T_i(t)$ at stage i with the temperature response at the same point to an impulsive change in external fluid temperature (Duhamel's Theorem). Zero initial conditions are assumed in each case. In Laplace Transform form using the convolution theorem we have for surface temperature ($r = 1$)

$$T_{p_i}(s) = G_p(s) \,.\, T_i(s) \tag{4}$$

where $G_p(s)$ is the Laplace transform of the impulse response i.e. the 'transfer function' between surface temperature and external fluid temperature. Taking transforms of Eq. (2) and substituting Eq. (4), the response of the fluid temperature at stage i to a perturbation in inflowing fluid from stage $i-1$ may be written again in transfer function notation as

$$\frac{T_i(s)}{T_{i-1}(s)} = \frac{N}{s+[1-G_p(s)]KV_H+N} = G(s). \tag{5}$$

The overall packed bed response, i.e. the response of stage N to temperature changes at the inlet $T_0(t)$ becomes, by repeated application of (5):

$$\frac{T_N(s)}{T_0(s)} = G_N(s) = (G(s))^N. \tag{6}$$

As is well known the steady state "frequency response" of this (linear) system may be obtained by substituting $j\omega$ for s in Eqs. (4) (5) and (6) where ω is the normalised frequency of the input and output sine waves.

(b) Particle transfer functions—non zero interphase resistance

The response of the particles to step or impulsive changes in external fluid may in general be expressed in open or closed form (5). The open form may frequently be convenient especially if convergence is rapid. In the case of the step response the general form of the response is

$$U(t,1) = 1-\sum_{n=1}^{\infty} K_n \exp(-\alpha_n^2 D_S t)$$

where the K_n, α_n are functions of some transcendental equation.

In the present notation, the general form of the transfer function $G_p(s)$ will be

$$G_p(s) = \sum_{n=1}^{\infty} \frac{K_n/\bar{T}}{(T_n/\bar{T})s+1}. \tag{7}$$

To date only two fluid particle transfer functions have been derived, one for spherical, the other for right cylindrical particles. The latter is rather inconvenient to use, an outline of the derivation is given in Appendix 1. The transfer function for spherical particles, may, be obtained after an appropriate transformation of variables, from Carslaw and Jaeger's solution[5] for the step response of an infinite slab one face of which is maintained at zero temperature the other being subjected to a 'radiation' boundary condition. The open solution has the same form as Eq. (7) where

$$\left.\begin{aligned} \frac{K_n}{\bar{T}} &= \frac{2h}{h^2-h+\beta_n^2} \\ \frac{T_n}{\bar{T}} &= \frac{1}{\alpha \,.\, \beta_n^2} \end{aligned}\right\} \tag{8a}$$

where $h = Rh_p/k_s$ is a form of the Biot number, β_n are the roots of

$$\left.\begin{aligned} &\beta\cot\beta+h-1=0 \\ &\text{and } \alpha \text{ is defined here by} \\ &\alpha = \frac{k_s}{\rho_s c_s R^2} \end{aligned}\right\} \tag{8b}$$

(c) Zero interphase resistance

The transfer function corresponding to Eq. (5) when the fluid-particle transfer coefficient may be regarded as infinite may be obtained by taking the limit as h tends to infinity of Eqs. (5) and (8). A similar result may be obtained by consideration of Carslaw and Jaeger's solution for this case relating average particle temperature to surface heat flux.

The results are

$$\frac{T_i(s)}{T_{i-1}(s)} = \frac{N}{s-3\alpha V_H N G_F(s)+N} \tag{9}$$

where

$$G_F(s) = \sum_{n=1} \frac{-2T_n/\bar{T}}{T_n/\bar{T}\cdot s+1}$$

and $T_n/\bar{T}$ is defined by Eq. (13) with

$$\beta_n = n\pi.$$

(*d*) *Infinite particle diffusivity*

When particle diffusivity may be regarded as infinite so that the particles are at uniform temperature, Eq. (5) still applies but the transfer function $G_p(s)$ may be given by the simple equation

$$G_p(s) = \frac{K}{s+K} \tag{10}$$

where K has been defined by Eq. (3).

(*e*) *Application to linear adsorption*

In the case of linear adsorption the concentration of the adsorbed or 'tracer' component under consideration in the solid phase expressed per unit of total bed volume may be related to the concentration in the fluid phase under conditions outlined in References [6, 13] by equations of the type:

$$\frac{1}{\epsilon\bar{T}}\frac{\mathrm{d}\bar{w}_i}{\mathrm{d}t} = \frac{1}{R_a}\left(c_i - \frac{w_i}{B}\right)$$

where B is the slope of the adsorption isotherm in consistent units, t is normalised time, w_i, c_i are the concentrations of tracer at the surface of the particles and in the fluid phase at stage i, $\bar{w}_i$ being volume averaged over the particles at stage i, and R_a is an interphase resistance term.
Writing

$$W_i = \frac{w_i}{c_0 B}$$

and

$$C_i = c_i/c_0$$

we have

$$\frac{\mathrm{d}\bar{W}_i}{\mathrm{d}t} = K(C_i - W_i) \tag{11}$$

where

$$K = \frac{\epsilon}{B}\cdot\frac{\bar{T}}{R_a}.$$

In general the results derived for heat transfer in Eqs. (2)–(10) inclusive, may be extended to linear adsorption, using the equivalences of Table 1.

Table 1

For adsorption	
Replace	By
T_i	C_i
T_{p_i}	W_i
V_H	B/ϵ
K	$\epsilon\bar{T}/R_aB$
α	$D_s\bar{T}/R$
h	$\epsilon R_a/3BD_s$ for spheres

In Eqs. (2)–(10) inclusive

APPLICATION OF MOMENTS ANALYSIS

(*a*) *Basic equations*

If a temperature or concentration pulse be applied to a packed bed the difference between the corresponding moments of the resulting outlet and inlet pulses may be related to the pulse resulting if an impulse could physically be applied to the inlet. These latter moments contain the fundamental parameters of the system. Bischoff and Levenspiel[3] have made extensive tabulations of moments for various boundary conditions for the dispersion model with negligible interphase transfer.

The techniques of moment analysis depends on the following property of linear systems. If $x(t)$ and $g(t)$ are distribution functions, i.e.,

$$g(t), x(t) = 0 \qquad t < 0,$$

and

$$\lim_{t\to\infty} x(t) = 0$$
$$\lim_{t\to\infty} g(t) = 0$$
$$\int_0^\infty g(t)\,\mathrm{d}t = \int_0^\infty x(t)\,\mathrm{d}t = 1.$$

$X(s)$ and $G(s)$ are their respective Laplace transforms and the distribution function $y(t)$ is formed by the convolution of $x(t)$ and $g(t)$, i.e.

$$Y(s) = X(s)\,.\,G(s)$$

then it may be readily shown (at least for $n = 1$, 2 and 3) that

$$\int_0^\infty (t-\mu_y)^n y(t)\,\mathrm{d}t = \int_0^\infty (t-\mu_x)^n x(t)\,\mathrm{d}t + \int_0^\infty (t-\mu_g)^n g(t)\,\mathrm{d}t \tag{12}$$

where

$$\int_0^\infty y(t)\,\mathrm{d}t = 1$$

μ_y, μ_x and μ_g are the first moments of their respective distribution e.g.

$$\mu_x = \int_0^\infty t \,.\, x(t)\, dt. \tag{13}$$

From Eq. (12), if $g(t)$ is the impulse response of the system then the first, second and third moments of the impulse response may be obtained from the difference between the moments of an arbitrary input pulse $x(t)$ and the resulting output pulse $y(t)$ provided both are normalised.

The moments of the impulse response contain the fundamental parameters of the system and for the proposed cell model may also be obtained by repeated application of Eq. (12). Thus from Eq. (6) we have

$$\int_0^\infty (t-\mu_N)^n g_N(t)\, dt = N \,.\, \int_0^\infty (t-\mu_1)^n g(t)\, dt \tag{14}$$

where

$$\mathscr{L} g(t) = G(s)$$

and

$$\mathscr{L} g_N(t) = G_N(s) = (G(s))^N.$$

The symbol $\mathscr{L}$ denoting the Laplace operator. Using Eq. (12) and the relation[17]:

$$\int_0^\infty t^n x(t)\, dt = \lim_{s\to 0} (-1)^n \frac{d^n X(s)}{ds^n}$$

we have

$$\mu_1 = \int_0^\infty t g(t)\, dt = \frac{1}{N}(1 + K \,.\, V_H \,.\, X),$$

$$\mu_N = N\mu_1$$

also

$$\int_0^\infty t^2 g(t)\, dt = \frac{(\mu_N - 1)}{N}\frac{Y}{X} + \frac{2\mu_N{}^2}{N}$$

and

$$\int_0^\infty t^3 g(t)\, dt = \frac{6\mu_N}{N^2}(\mu_N - 1)\frac{Y}{X} + \frac{6\mu_N{}^3}{N^3} + \frac{(\mu_N - 1)}{N}\cdot\frac{Z}{X}$$

yielding ultimately,

$$\begin{aligned}
\mu_N &= \int_0^\infty t g_N(t)\, dt = 1 + K \,.\, V_H \,.\, X \\
\sigma_N{}^2 &= \int_0^\infty t^2 g_N(t)\, dt = \frac{\mu_N{}^2}{N} + \frac{Y}{X}\cdot(\mu_N - 1) \\
\pi_N{}^3 &= \int_0^\infty (t-\mu_N)^3 g_N(t)\, dt \\
&= 3\frac{\mu_N}{N}\cdot(\mu_N - 1)\frac{Y}{X} + \frac{2\mu_N{}^3}{N^2} + (\mu_N - 1)\cdot\frac{Z}{X}
\end{aligned} \tag{15}$$

where for spherical particles,

$$\begin{aligned}
X &= \sum_{n=1}^{\infty} \frac{K_n}{\bar{T}}\left[\frac{T_n}{\bar{T}}\right] \\
Y &= 2\sum_{n=1}^{\infty} \frac{K_n}{\bar{T}}\left[\frac{T_n}{\bar{T}}\right]^2 \\
Z &= 6\sum_{n=1}^{\infty} \frac{K_n}{\bar{T}}\left[\frac{T_n}{\bar{T}}\right]^3
\end{aligned} \tag{16}$$

where K_n and T_n have been defined by Eq. (8).

In Eq. (15) and (16) two parameters, h and α, uniquely determine X, Y and Z. The corresponding parameters for linear adsorption are given in Table 1. Two further parameters, V_H and N are also required to specify Eqs. (15). We also have for spheres,

$$K = 3\alpha h.$$

General plots of Y/X and Z/X as a function of h and α are presented in Figs. 1 and 2.

In general, one of the parameters V_H, N, α or h needs to be known to determine the other three although a solution will not always result if the 'known' parameter is chosen arbitrarily. The central limit theorem (17) predicts that for N *large* the impulse response distribution $g_N(t)$ approaches a normal or Gaussian distribution. This results in very small values of the 'skewness or third moment $\pi_N{}^3$ and tends to limit the usefulness of the method to short bed lengths.

In computation of the values presented in Figs. 1 and 2, use may be made of the fact that the limiting (steady state) value of particle temperature in response to a unit step change in external fluid temperature is unity. This may be deduced from physical considerations since under steady state, the net transfer of heat to or from a paricle must be zero, i.e. the surface temperature must be unity. From this we have

$$\lim_{t\to\infty} \int_0^t g_p(t)\, dt = \sum_{n=1}^{\infty} \frac{Kn}{\bar{T}} = 1. \tag{16a}$$

The use of the infinite sum of Eq. (16a) as a stringent criterion for convergence of X, Y and Z may be justified since

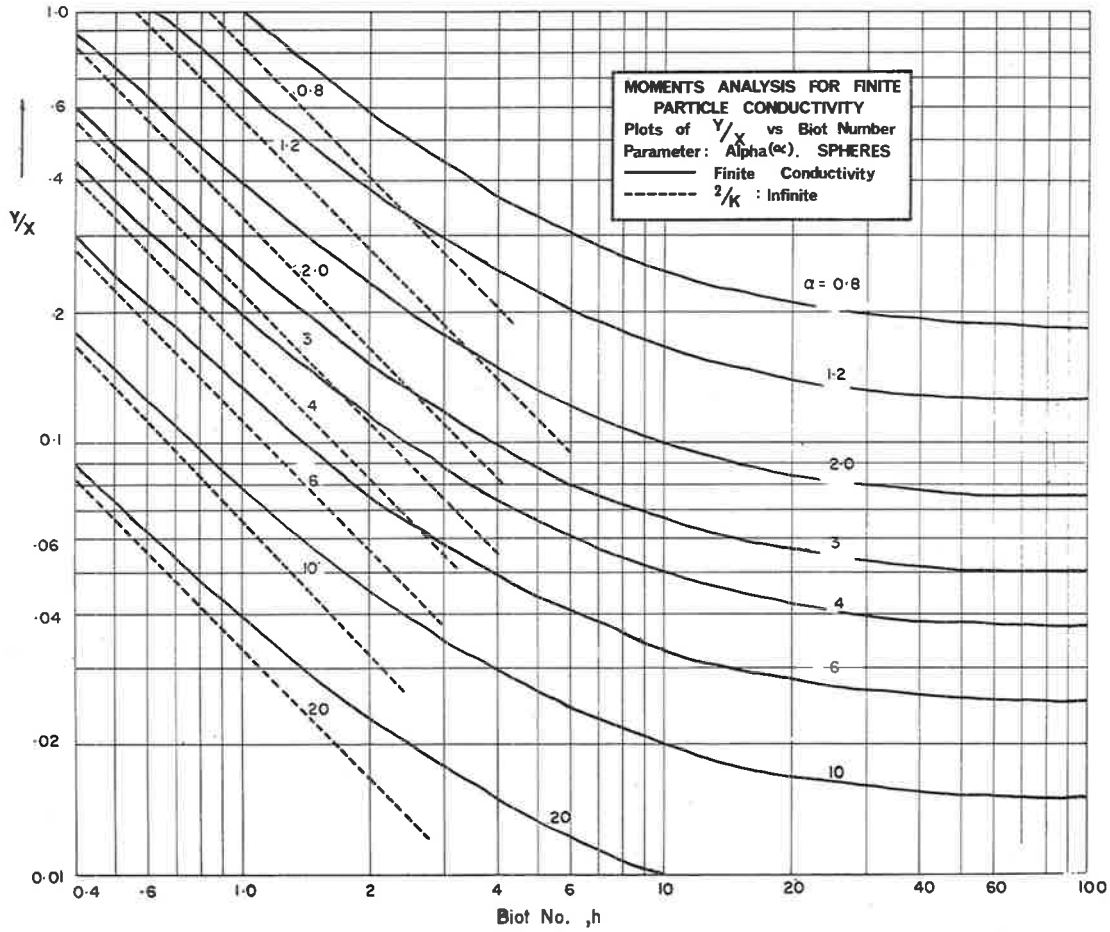

Fig. 1. Plots of Y/X vs. Biot number for spheres.

$$X = \frac{1}{\alpha} \sum_{n=1}^{\infty} \frac{Kn}{\bar{T}} \cdot \frac{1}{\beta_n^2}$$

$$Y = \frac{2}{\alpha^2} \sum \frac{Kn}{\bar{T}} \cdot \frac{1}{\beta_n^4}$$

and

$$Z = \frac{6}{\alpha^3} \sum \frac{Kn}{\bar{T}} \cdot \frac{1}{\beta_n^6}$$

and since the roots β of Eq. (8b) tend to infinity for $0 \leqslant h \leqslant \infty$, n large.

A further criterion for convergence verifiable numerically to any desired accuracy for any combination of α and h is the equation

$$X = \sum_{n=1}^{\infty} \frac{Kn}{\bar{T}} \cdot \frac{Tn}{\bar{T}} = \frac{1}{3\alpha h} = \frac{1}{K}. \qquad (16b)$$

It is found that the use of the first six roots β of Eq. (8b) given by Carslaw and Jaeger[5] give X, Y and Z to less than 1 per cent for the Biot number h less than 15, the error in X increasing to 7 per cent for $h = 100$. This is reduced to 0·1 per cent by taking the first twenty roots. The errors in Y/X and in Z/X are of the same order. In the preparation of Figs. 1 and 2 up to 200 roots have been taken for large values of h.

(*b*) *Reduction to infinite particle diffusivity*

As h becomes very small and α large the limiting values of X, Y and Z become

$$\left.\begin{aligned} X &= 1/K \\ Y &= 2/K^2 \\ Z &= 6/K^3 \end{aligned}\right\}. \qquad (17)$$

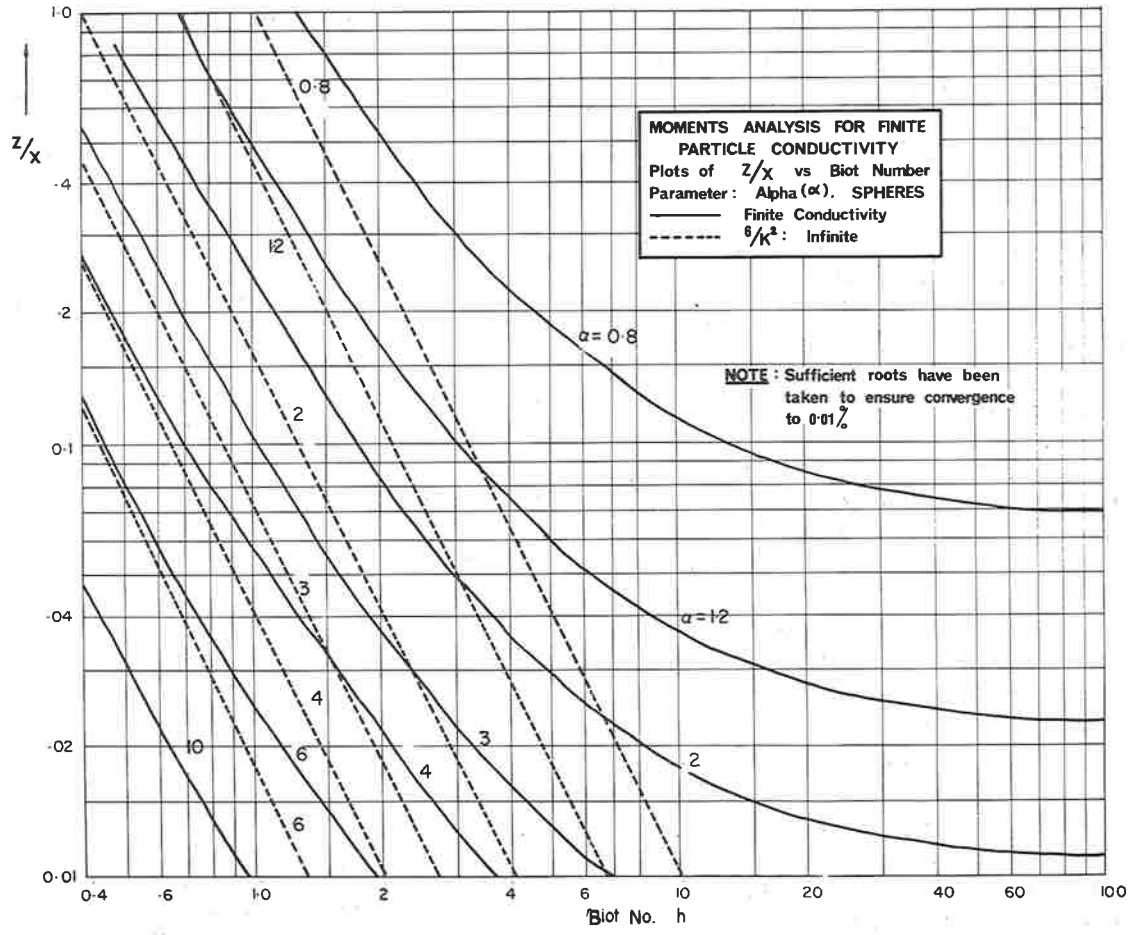

Fig. 2. Plots of Z/X vs. Biot number for spheres.

Equation (17) becomes

$$\mu_N = 1 + V_H$$

$$\sigma_N^2 = \frac{2}{K}(\mu_N - 1) + \frac{\mu_N^2}{N} \tag{18}$$

$$\pi_N^3 = \frac{6\mu_N}{NK}(\mu_N - 1) + \frac{2\mu_N^3}{N^2} + \frac{6(\mu_N - 1)}{K^2}.$$

Chao and Hoelscher[6] have derived the first three moments for the axial dispersion model of linear adsorption under the assumption of infinite particle diffusivity. Substituting the equivalences of Table 1, their results are, in heat transfer terminology:

$$\mu = 1 + V_H$$

$$\sigma^2 = \frac{2(\mu - 1)}{K} + \frac{2}{N \cdot P_{e_a}}\mu^2$$

$$\pi^3 = \frac{12\mu(\mu - 1)}{NK} + \frac{12\mu^3}{N^2 P_{e_a}^2} + \frac{6(\mu - 1)}{K^2}$$

where N is the bed length in particle diameters.

Substituting $P_{e_a} = 2M/N$ and noting that M refers to the number of 'effective' mixing stages,

$$\mu = 1 + V_H$$

$$\sigma^2 = \frac{2(\mu - 1)}{K} + \frac{\mu^2}{M} \tag{19}$$

$$\pi^3 = \frac{6\mu(\mu - 1)}{MK} + \frac{3\mu^3}{M^2} + \frac{6(\mu - 1)}{K^2}.$$

(*c*) *Discussion*

Equations (16b) and (18) indicate that the first moment of the impulse response of a packed bed depends only on the ratio of the packing thermal capacity to that of the fluid irrespective of whether intra-particle temperature gradients occur or not.

Comparison of Eq. (19) with Eq. (18) reveals that the mean and variance equations are exactly identical whilst the equation for skewness differ only in the term in μ.

When V_H (or B/ϵ) is small (as in the adsorption experiments of Chao and Hoelscher) the two calculated values of skewness rapidly converge when the number of stages exceeds 5–10 over a wide range of values of V_HK. In the case of the temperature response of beds packed with steel spheres however ($V_H \simeq 600$) the two values of skewness may remain 10–20 per cent below the axial dispersion skewness even for beds 200 mixing lengths long. Since this however requires an impossibly high value of heat transfer coefficient this is of littler consequence. For moderate values of V_HK as would be expected (up to 20) the two models rapidly converge for bed lengths exceeding 10. This is brought out in Table 2 below.

It may be expected that additional experimental data at low bed lengths will establish which of the models gives the best fit to the data in this region.

In the case of negligible interphase transfer, Aris [1] has shown that

$$\sigma^2 = \frac{2}{N \,.\, P_{e_a}} = \frac{1}{M} \qquad (20a)$$

whilst Chao and Hoelscher derived the result

$$\pi^3 = \frac{12}{N^2 P_{e_a}{}^2} = \frac{3}{M^2}. \qquad (20b)$$

The corresponding finite stage results are

$$\sigma^2 = \frac{1}{N} \qquad (21a)$$

$$\pi^3 = \frac{2}{N^2}. \qquad (21b)$$

It may be seen that Eqs. (20a) and (21a) require a Peclet number of two, a well known result, whilst Eqs. (20b) and (21b) require $P_{e_a} = \sqrt{6} = 2{\cdot}44$. The two models are hence incompatible and the result of Kramers and Alberda (Eq. (1)) cannot be derived from moments analysis.

4. APPLICATION TO FREQUENCY RESPONSE OF PACKED BEDS

(*a*) *Infinite particle diffusivity*

Equations (5), (6) and (7) provide relatively simple formulae for computation of the steady state frequency response of packed beds whether finite concentration or temperature gradients exist within the particles or not. As is well known, the substitution of complex frequency $j\omega$ for s will yield the steady state frequency response of the system in magnitude and phase.

The frequency response method has often been used to determine interphase transfer coefficients when particle diffusivity is effectively infinite. In this case Eq. (10) applies and it is of interest to compare the resulting response

Table 2. Ratio π^3_N/π^3 as a function of N and V_HK

	$\frac{1.\ V_H = 1}{V_H.K}$				$\frac{2.\ V_H = 600}{V_H.K}$			
N	1	5	10	100	1	5	10	100
1	0·809	0·779	0·778	0·778	0·846	0·697	0·672	0·668
2	0·889	0·837	0·834	0·834	0·941	0·720	0·683	0·669
5	0·966	0·911	0·906	0·905	0·989	0·846	0·744	0·673
10	0·989	0·952	0·947	0·944	0·997	0·941	0·848	0·681
20	0·995	0·989	0·972	0·970	0·999	0·986	0·952	0·742
50	0·997	0·993	0·988	0·987	0·999+	0·997	0·989	0·772
100	0·999	0·999	0·998	0·993	0·999+	0·999	0·997	0·870

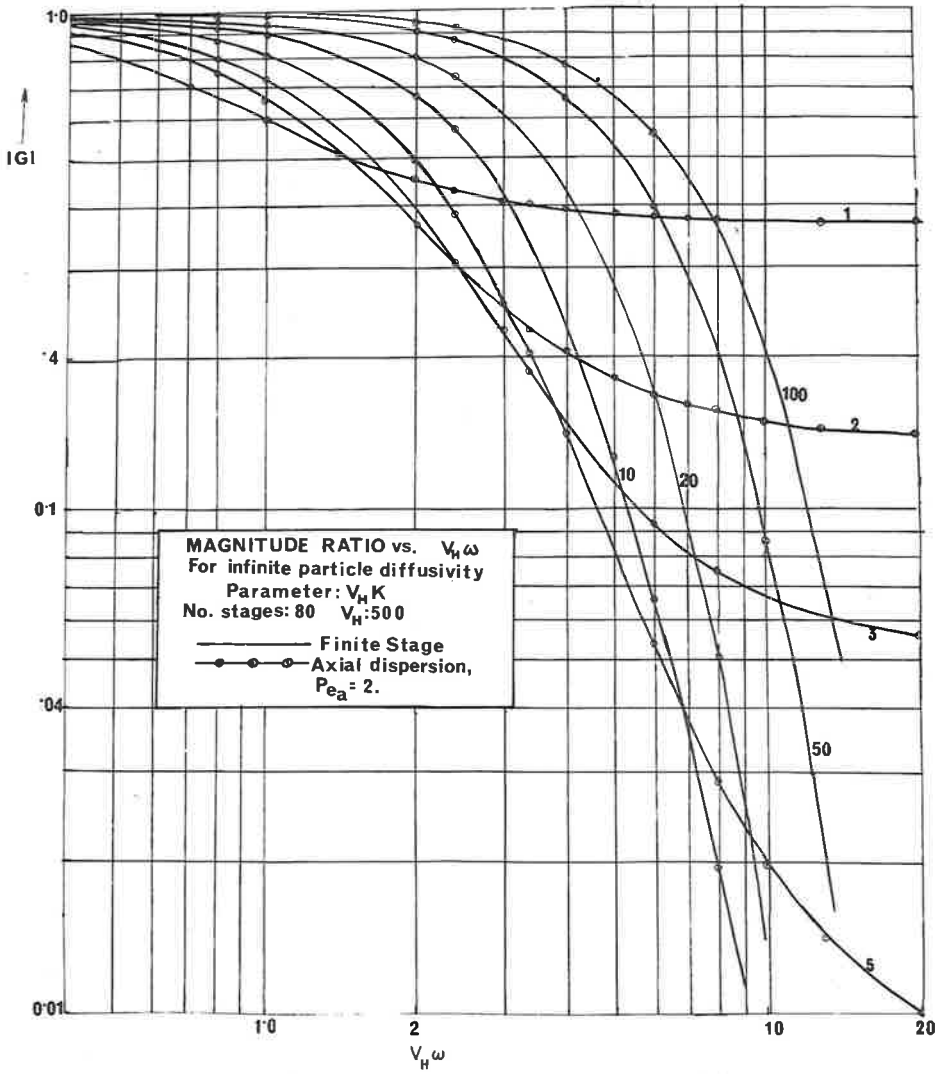

Fig. 3. Magnitude ratio curves for infinite particle internal diffusivity, spheres.

with that predicted for the axial dispersion model. Pulsifer[12] has obtained a solution in this case allowing for axial dispersion.

The solution obtained by Pulsifer in the present notation is

$$G(j\omega) = \frac{4\exp(\tfrac{1}{2}\gamma)\cdot(P+jQ)^{1/2}}{[1+(P+jQ)^{1/2}]^2\exp[1/2\gamma(P+jQ)^{1/2}]-[1-(P+jQ)^{1/2}]^2\exp[-1/2\gamma(P+jQ)^{1/2}]} \quad (22)$$

where

$$\gamma = 1/(NPe_a)$$

$$P = 1+4\gamma\frac{V_H K\omega^2}{K^2+\omega^2}$$

$$Q = 4\gamma\omega\left[1+\frac{V_H K^2}{K^2+\omega^2}\right].$$

Typical frequency responses computed for the two solutions are plotted in Figs. 3 and 4 for the range of frequencies normally encountered in heat transfer work. As in Pulsifer's original work, magnitude ratio and phase angle are plotted

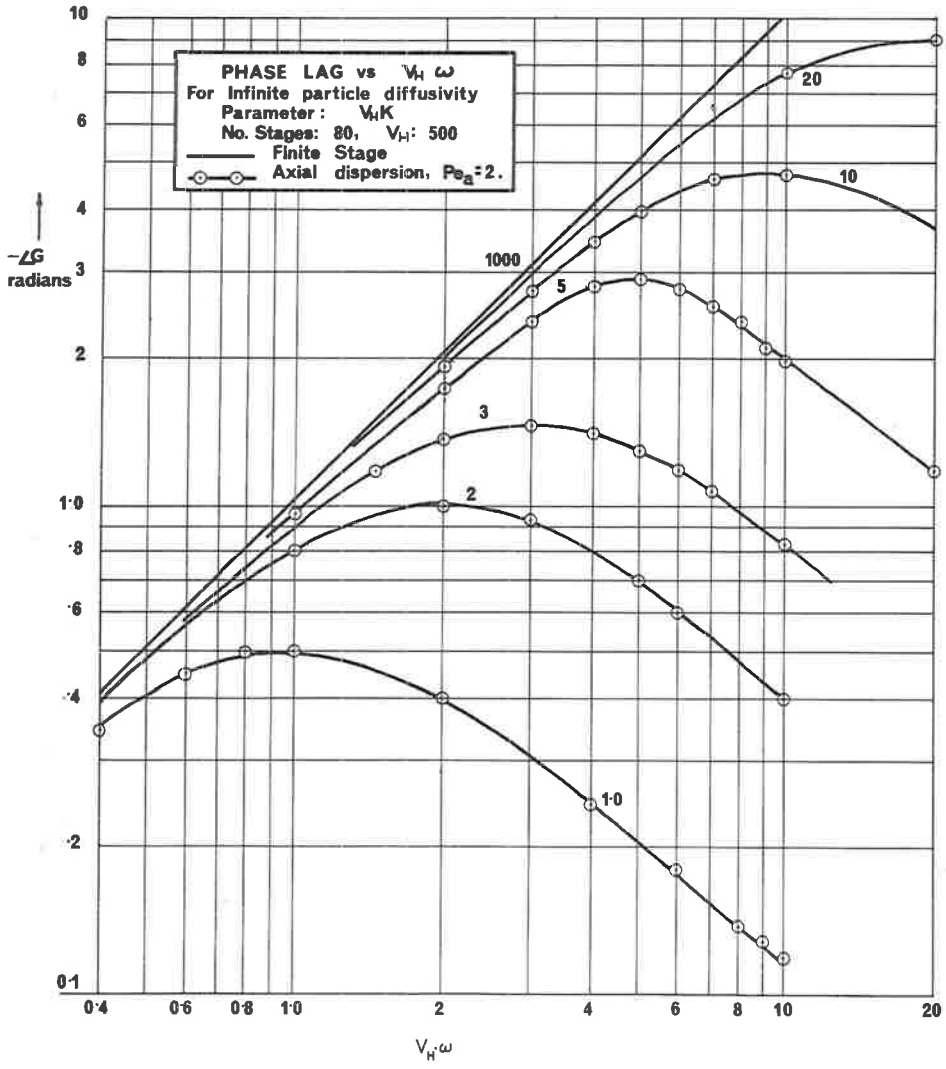

Fig. 4. Phase lag curves for infinite particle informal diffusivity, spheres.

against the frequency variable $N \cdot V_H \cdot \omega$ with $V_H \cdot K$ as a parameter. It will be noted that frequency ω is normalised with respect to overall bed holdup time $\bar{T}$. The degree of correspondence agrees generally with that predicted by moments analysis.

The effect of varying Peclet number at low bed lengths according to Kramers and Alberda's equation (Eq. (1) here) is shown in Fig. 5.

Typical plots showing the effects of finite particle conductivity are displayed in Fig. 6.

CONCLUSIONS

The modified finite stage model proposed agrees remarkably well with the axial dispersion model over a wide range of parameters. It has the added advantage however that intraparticle diffusion effects may be readily accounted for unlike the unwieldy axial dispersion solutions. In the range over which the two models disagree there is still insufficient evidence to suggest which of the two is the most 'valid'. In fact the work of Mickley, Smith and Korchak suggests

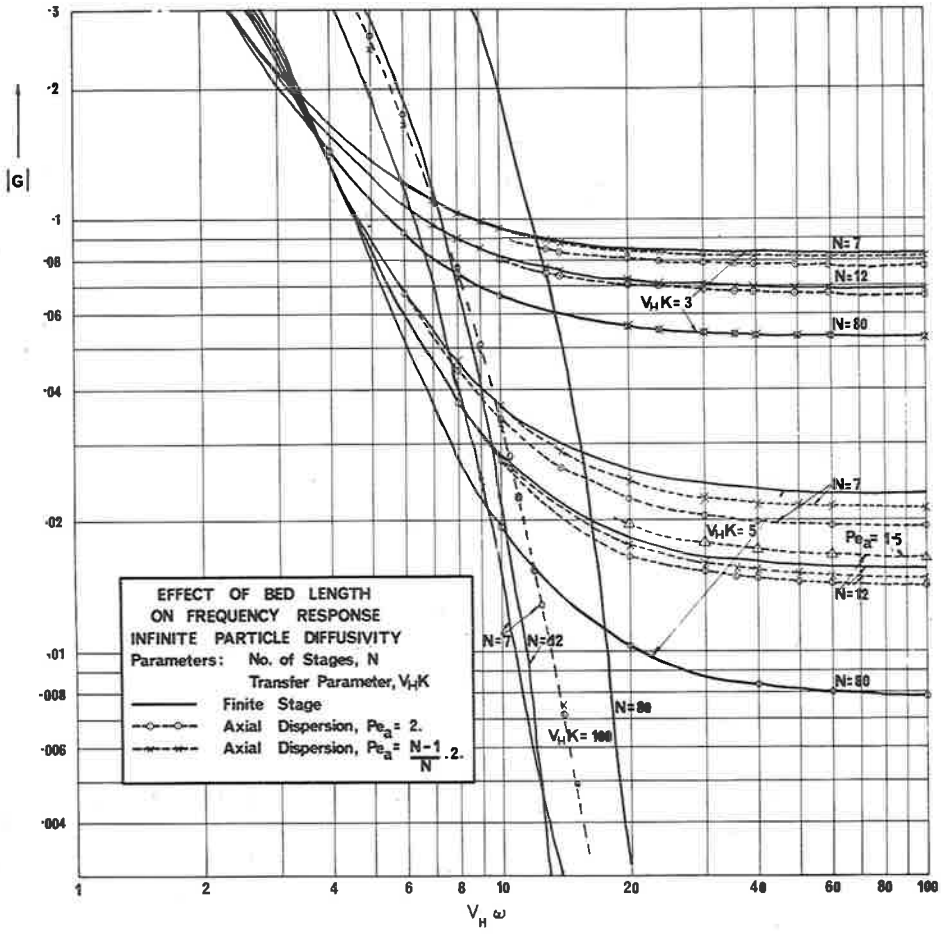

Fig. 5. Effects of bed length on frequency response, infinite particle diffusivity.

that, at least in the turbulent region, the finite stage model may be preferable. A suitable choice of parameters will nonetheless force the two models into close agreement even at low Reynolds numbers assuming that the continuous model in fact holds in this region. The ease of computation of the finite stage model should make it useful in simulation studies (where linearity may be assumed) by application of numerical inverse Fourier transformation together with convolution.

NOTATION

a_p ratio of surface area to volume of a particle

B slope of adsorption isotherm

c concentration of tracer component (for adsorption)

c_0 reference concentration of tracer component

C_i normalised concentration at stage i

c_s, c_f particle and fluid heat capacity respectively

D_s particle diffusivity

$G(s)$ transfer function of fluid temperature single stage impulse response

$G_p(s)$ surface temperature particle transfer function

$G_N(s)$ fluid temperature transfer function for N stage process

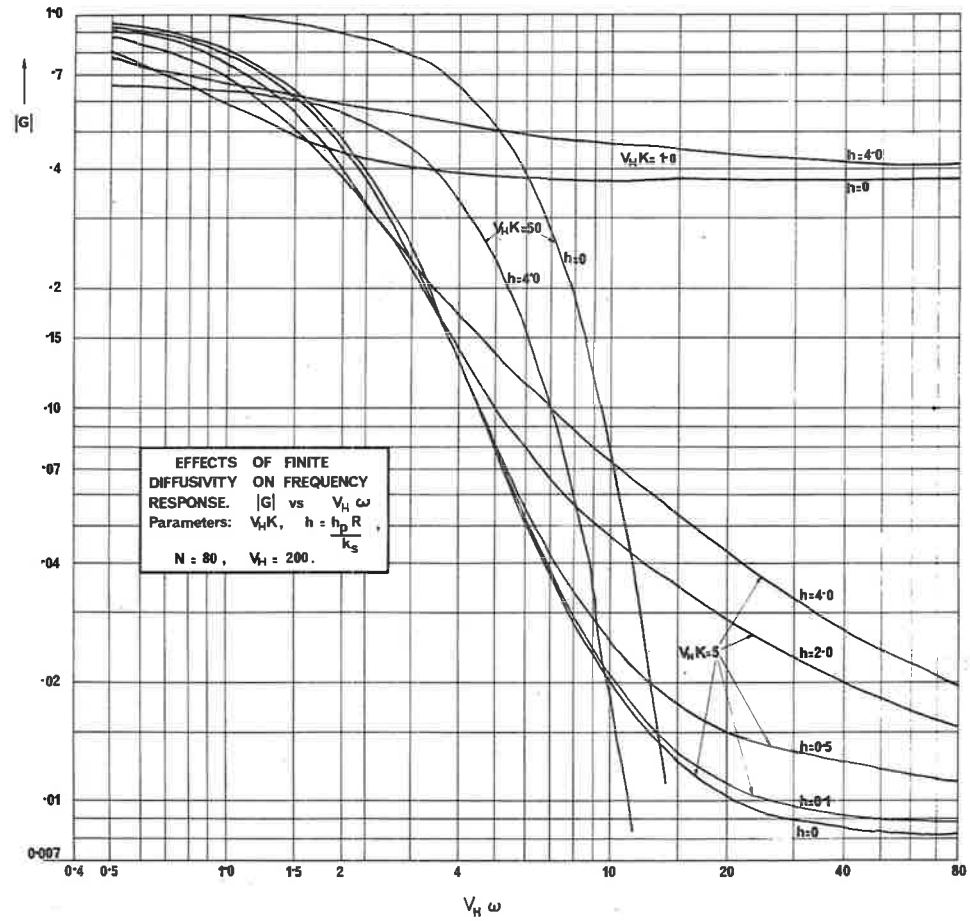

Fig. 6. Effects of finite particle diffusivity on frequency response.

$G_F(s)$ transform of particle surface flux $= \left[\frac{\partial T_{p_i}}{\partial r}\right]_{r=1}$

H distance between perfectly mixed stages

h 'Boit number' $= \frac{Rh_p}{k_s}$

h_p fluid–particle heat transfer coefficient

k_s solid conductivity for heat transfer

K_n gain term corresponding to nth root in particle transfer function $= 2h/(h^2-h+\beta_n{}^2)$ for spheres

L bed length

M number of effective stages in bed

N nominal number of stages = bed length/(particle diameter)

K particle heat transfer parameter $= h_p a_p \bar{T}/\rho_f c_f$

P_{e_a} axial Peclet number with H as characteristic dimension

R_a interphase resistance in adsorption

t normalised time in bed holdup time units

r normalised particle radius relative to outside radius

R Particle radius

$T_i(t)$ fluid temperature at stage i

$T_{p_i}(t)$ particle surface temperature at stage i

$\bar{T}$ average bed fluid holdup time

$\bar{T}_{p_i}(t)$ volumetrically average particle temperature at stage i

T_n time constant corresponding to nth root in particle transfer function $= 1/(\alpha\beta_n)$ for spheres

v_a interstitial fluid velocity
V_H ratio of bulk packing columetric heat capacity to fluid heat capacity $= (1-\epsilon)\rho_s c_s/\epsilon\rho_f c_f$
w point particle concentration of adsorbed tracer
$\bar{w}$ volumetrically averaged particle concentration
w_0 reference particle tracer concentration
W_i normalised surface concentration at stage $i = w/c_0$ B
X,Y,Z particle diffusion parameters defined by Eq. (16)
α diffusivity parameter for particles $= \bar{T}k_s/\rho_s c_s R^2$
β_n nth root of Eq. (8b)
γ $1/(N P_{e_a})$
ϵ bed external volumetric porosity
μ_g first moment of impulse responses distribution $g(t)$
μ_N first moment of N stage process impulse response (Eq. (13))
$\pi_N{}^3$ third moment of N stage process impulse response (Eq. (15))
ρ_f, ρ_s density, fluid and solid
$\sigma_N{}^2$ variance of N stage process impulse response (Eq. (15))
ω Frequency, normalised with respect to bed holdup time $\bar{T}$.

REFERENCES

[1] ARIS R., *Chem. Engng Sci.* 1960 **13** 1.
[2] BABCOCK R. E., GREEN D. W. and PERRY R. H., *A.I.Ch.E. Jl* 1966 **12** 922.
[3] BISCHOFF K. B. and LEVENSPIEL O., *Chem. Engng Sci.* 1962 **17** 245, 257.
[4] BRACEWELL R. M., *The Fourier Transform and Applications*. McGraw-Hill 1965.
[5] CARSLAW H. S. and JAEGER J. C., *Conduction of Heat in Solids*, 2nd Edn. Oxford University Press 1959.
[6] CHAO R. and HOELSCHER H. E., *A.I.Ch.E.Jl* 1966 **12** 271.
[7] DANCKWERTS P. V., *Chem. Engng Sci.* 1953 **2** 1.
[8] DEISLER P. F. and WILHELM R. H., *Ind. Engng Chem.* 1953 **45** 1219.
[9] HAGBERG C. G., Sc.D. Thesis, Washington University 1964.
[10] KRAMERS H. and ALBERDA G., *Chem. Engng Sci.* 1953 **2** 173.
[11] MICKLEY H. S., SMITH K. A. and KORCHAK E. I., *Chem. Engng Sci.* 1965 **20** 237.
[12] PULSIFER A. H., Ph.D. Thesis, Syracuse University 1965.
[13] ROSEN J. B., *J. chem. Phys.* 1952 **20** 387.
[14] ROSEN J. B., *Ind. Engng Chem.* 1954 **46** 1590.
[15] SINCLAIR R. J. and POTTER O. E., *Trans. Instn chem. Engrs* 1965 **43** T3.

APPENDIX

TRANSFER FUNCTION FOR CYLINDRICAL PARTICLES

Consider a right cylindrical particle surrounded by a uniform temperature fluid with a heat transfer coefficient h_p, Biot number h.

Then for heat flow within particles at stage i we have, in normalised coordinates dropping the subscript i from internal temperatures:

$$\frac{1}{\alpha}\frac{\partial T_P}{\partial t} = \frac{\partial^2 T_P}{\partial z^2} + \frac{\partial^2 T_P}{\partial r^2} + \frac{1}{r}\frac{\partial T_P}{\partial r}. \tag{A.1}$$

Boundary conditions are

$$\left.\begin{aligned} \text{for } r = 1, \quad & \frac{\partial T_P}{\partial r} = h\,(T_i - T_P) \\ \text{for } z = 1, \quad & \frac{\partial T_P}{\partial z} = h\,(T_i - T_P) \\ \text{for } z = 1, \quad & \frac{\partial T_P}{\partial z} = -h\,(T_i - T_P) \end{aligned}\right\}. \tag{A.2}$$

The 'product of solutions' method[5] may be applied to determine the response of the particle to a unit step change in external fluid temperature using Carslaw and Jaegers'[5] solutions for the temperature response of an infinite cylinder, with unit

initial temperature 'radiating' into a medium of zero temperature and the corresponding solution for an infinite slab. Thus for the infinite cylinder, $0 \leqslant r < 1$

$$\chi(r, t) = 2h \sum_{s=1}^{\infty} \frac{e^{-\alpha\phi_s^2 t} . J_0(r\phi_s)}{(h^2+\phi_s^2) . J_0(\phi_s)}. \tag{A.3}$$

Where ϕ_n are roots of

$$\phi J_0'(\phi) + hJ_0(\phi) = 0 \tag{A.4}$$

$J_0(\phi)$ is a Bessel function of zero order.
For the infinite slab $-1 < z < 1$

$$\Psi(z, t) = 2h \sum_{n=1}^{\infty} \frac{\cos(\zeta_n z)\, e^{-\alpha\zeta_n^2 t}}{[h^2+h+\zeta_n^2] \cos\zeta_n} \tag{A.5}$$

where ζ_n are roots of

$$\zeta \tan\zeta = h. \tag{A.6}$$

The unit step response of the finite cylinder $F(r, z, t) = 0$, $t < 0$ becomes

$$F(r, z, t) = 1 - \psi(z, t) . \chi(r, t).$$

The 'impulse response' then is given by

$$\begin{aligned} g_P(r, z, t) &= \frac{\partial}{\partial t} F(r, z, t) \\ &= -\Psi'(z, t) . \chi(r, t) - \Psi(z, t) . \chi'(r, t). \end{aligned} \tag{A.7}$$

The use of Duhamel's Theorem [5], Eq. (1.14) [10] allows the response to an arbitrary change in external fluid temperature to be computed by convolution with the impulse response.

The surface averaged temperature over the whole particle is of interest since a uniform external temperature has been assumed. Setting $z = \pm 1$ in Eq. (A.7) we have for an impulsive input,

$$T_P(t) = 2 \int_0^1 r g_P(r, t)\, dr.$$
$$\underset{\text{av. plane}}{}$$

Writing

$$\left.\begin{aligned} \frac{T_{n_1}}{\bar{T}} &= \frac{1}{\alpha\zeta_n^2}, \quad \frac{T_{n_2}}{T} = \frac{1}{\alpha\phi_n^2} \\ \frac{K_{n_1}}{\bar{T}} &= \frac{2h}{h^2+h+\zeta_n^2}, \quad \frac{K_{n_2}}{\bar{T}} = \frac{2h}{h^2+\phi_n^2} \end{aligned}\right\} \tag{A.8}$$

and carrying out the integration, using the recurrence relation for Bessel Functions and Eq. (A.4) gives

$$\begin{aligned} T_P(t) &= 2h\left[\sum_r \frac{K_{r_1}}{T_{r_1}} e^{-t\bar{T}/T_{r_1}}\right]\left[\sum_s \frac{K_{s_2}}{\bar{T}\phi_s^2} e^{-t\bar{T}/T_{s_2}}\right] \\ &\quad + 2h\left[\sum_r \frac{K_{r_1}}{\bar{T}} e^{-t\bar{T}/T_{r_1}}\right]\left[\sum_s \frac{K_{s_2}}{T_{s_2}\phi_s^2} e^{-t\bar{T}/T_{s_2}}\right] \end{aligned}$$
$$\underset{\text{av. plane}}{}$$

which reduces after further manipulation to

$$T_P(t) = 2h \sum_{r=1}^{\infty} \sum_{s=1}^{\infty} \frac{K_{r_1} K_{s_2}}{\phi_s^2 \bar{T}^2} \left(\frac{\bar{T}}{T_{rs}}\right) . e^{-t\bar{T}/T_{rs}} \tag{A.9}$$
$$\underset{\text{av. plane}}{}$$

where

$$\frac{1}{T_{rs}} = \frac{1}{T_r} + \frac{1}{T_s}$$

in a similar manner, the surface averaged temperature over the cylindrical surface becomes

$$\begin{aligned} T_P(t) &= \tfrac{1}{2} \int_{-1}^{1} g_P(z, t)\, dz \\ &= h \sum_{r=1}^{\infty} \sum_{s=1}^{\infty} \frac{K_{r_1} K_{s_2}}{\zeta_r^2 \bar{T}^2} \left(\frac{\bar{T}}{\bar{T}_{rs}}\right) e^{-t\bar{T}/T_{rs}}. \end{aligned} \tag{A.10}$$
$$\underset{\text{av. cyl.}}{}$$

The surface area weighted average of Eqs. (A.9) and (A.10) has again resulted in an equation of the form

$$T_r(t) = \sum_{n=1}^{\infty} \frac{Kn}{Tn} e^{-\bar{T}t/T_n}.$$

Details of the results of computations using cylindrical particles may be obtained by writing to the Chemical Engineering Department, University of Adelaide.

Résumé—On propose un prolongement du modèle à étages définis pour décrire le comportement dynamique d'échangeurs de température et d'absorbeurs de chaleur dans un lit garni. Le modèle tient compte de la dispersion axiale, de la résistance en interphase et de la diffusion entre les particules en l'absence de transfert radial. On compare le modèle proposé à étages définis et le modèle à dispersion axiale selon les techniques de la réponse de fréquence et de l'analyse des moments. Une étroite correspondance est ainsi révélée entre les deux modèles et on conclut que (en l'absence de données expérimentales décisives) il est possible d'utiliser l'une ou l'autre. Le modèle proposé à étages définis a l'avantage, toutefois, de tenir compte plus facilement des effets de diffusion entre les particules.

Zusammenfassung—Es wird eine Erweiterung des endlichen Stufenmodells vorgeschlagen, um das dynamische Verhalten von Füllkörperbett-Wärmeaustauschern und Absorbern zu beschreiben. Das Modell berücksichtigt axiale Dispersion, Zwischenphasenwiderstand und Diffusion innerhalb der Teilchen, in der Abwesenheit von Gesamtradialübertragung. Ein Vergleich zwischen dem vorgeschlagenen endlichen Stufenmodell und dem axialen Dispersionsmodell wird durchgeführt, und zwar unter Verwendung von Frequenz- und Moment-analyse. Es wird eine enge Übereinstimmung zwischen beiden festgestellt und es wird daraus geschlossen, dass (in der Abwesenheit massgeblicher experimenteller Daten) sowohl das eine wie das andere Modell verwendet werden könnte. Das vorgeschlagene, endliche Stufenmodell hat jedoch den Vorteil, dass es damit bedeutend einfacher ist, die Effekte der Diffusion innerhalb der Teilchen zu berücksichtigen.

adjacent to the film but this is weak as flow in the thin film is now slow. The film profile is symmetrical about the vertical axis of the drop being thinnest at the edge with a secondary minimum at the centre. This symmetry and the associated flow patterns persist up to the point of rupture of the film. Rupture occurs sooner when lycopodium powder is present in the film as this bridges the gap between the two bounding surfaces.

Tilting of the drop would seem to be associated with the existence of a thick film in the early stages of approach and this in turn with reverse flow into the film. If the film initially thins relatively quickly by symmetrical outward drainage tilt does not occur.

The extension to a liquid drop approaching a flat plate is obvious and all the stages illustrated in Fig. 3 have been observed, although circulation can only occur inside the drop in this case. Reverse flow in the film in the early stages of drainage provides an alternative explanation of the well known dimple. However, its persistence throughout the drainage can only be explained in terms of deformation of the interface by the pressure gradient sustaining the symmetrical outward flow [4]. The effect of the reverse flow is to make the dimple larger than it would have otherwise been.

Acknowledgement – The author would like to thank Professor W. Smith for his encouragement and the Science Research Council for a generous grant. The experimental work was carried out by Mr. R. J. Travis.

Reader in Chemical Engineering S. HARTLAND
University of Nottingham, England

REFERENCES

[1] HARTLAND S., *Trans. Instn chem. Engrs* 1967 **45** T97.
[2] HARTLAND S., *Trans. Instn chem. Engrs* 1967 **45** T102.
[3] HARTLAND S., *Chem. Engng Sci.* 1967 **22** 1675.
[4] HARTLAND S., Paper 20d, Tripartite Chemical Engineering Conference, Montreal, Canada, September 1968.
[5] HARTLAND S., *J. Colloid Science* 1968 **26** 383.
[6] HARTLAND S., *Trans. Instn chem. Engrs* 1968.
[7] GARNER F. H., *Trans. Instn chem. Engrs* 1950 **46** T275 **28** 88.

Chemical Engineering Science, 1969, Vol. 24, pp. 613–614. Pergamon Press. Printed in Great Britain.

A further note on "Dynamics of packed beds with intraphase heat or mass transfer"

(*Received* 10 *September* 1968)

1. INTRODUCTION

IN A RECENT paper in this Journal [1] the writer has derived the first moment, μ_N and the second and third moments about the mean, σ_N^2 and π_N^3 of the impulse response of a packed bed with inter- and intraphase heat or mass transfer using an extension of the finite stage model.

Comparison of these three moments with experimental results allows evaluation of the internal particle diffusivity, interphase transfer coefficient and thermal capacitance of the packing (or slope of the adsorption isotherm for adsorption experiments) provided the number of effective external mixing stages N is assumed unaffected by interphase transfer.

Expression of the particle transfer function $G_p(s)$ in closed form allows a great simplification in the determination of the particle Biot number h and eliminates the need to use Fig. 1 and 2 of the paper.

2. CLOSED FORM EXPRESSION OF MOMENTS

A closed form expression $Y_D(s)$ for the particle transfer function where external (interphase) resistance is absent has been derived by Rosen [2] and defined as the "system admittance for solid diffusion only". It is related to the particle transfer function $G_P(s)$ of [1] by the equation

$$G_P(s) = \frac{K}{K + Y_D(s)} \tag{1}$$

where K is a non-dimensional number proportional to the fluid–particle transfer coefficient,

$$Y_D(s) = \frac{K}{h}(p \cot p - 1), \tag{2}$$

and

$$p = j(s/\alpha)^{1/2}.$$

Here, $j = \sqrt{-1}$; s is the Laplace transform variable and K and h are related, through α, by:-

$$K = 3\alpha h.$$

In Reference [1] the first, second and third moments of the impulse response of the overall packed bed response are given as:

$$\mu_N = \int_0^\infty t g_N(t)\,dt = 1 + K \cdot V_H \cdot X,$$

$$\sigma_N^2 = \int_0^\infty (t - \mu_N)^2 g_N(t)\,dt = \frac{\mu_{N^3}}{N} + \frac{Y}{X}(\mu_N - 1) \tag{3}$$

and

$$\pi_N^3 = \int_0^\infty (t - \mu_N)^3 g_N(t)\,dt = \frac{3\mu_N}{N}(\mu_N - 1)\frac{Y}{X} + \frac{2\mu_N^3}{N^2} + (\mu_N - 1)\frac{Z}{X}.$$

It should be noted that X, Y and Z may be expressed in the form:

$$X = -\lim_{s\to 0}\frac{dG_P(s)}{ds}$$

$$Y = +\lim_{s\to 0}\frac{d^2G_P(s)}{ds^2} \qquad (4)$$

and

$$Z = -\lim_{s\to 0}\frac{d^3G_P(s)}{ds^3}.$$

If Eq. (1) is expanded as an infinite series in p and the appropriate derivatives and limits obtained, Eqs. (4) become:

$$X = \frac{1}{K}$$

$$Y = \frac{2(h+5)}{5K^2} \qquad (5)$$

$$Z = \frac{6(2h^2+14h+35)}{35K^3}.$$

3. ESTIMATION OF INTERNAL PARTICLE DIFFUSIVITY

Having obtained experimental estimates of the impulse response moments, the last two equations of Eq. (3) may be used to estimate Y/X and Z/X assuming the value N, of the number of external mixing stages is unaffected by interphase transfer.

Eliminating K between Y/X and Z/X yields

$$\gamma = \frac{Z/X}{(Y/X)^2} = \frac{15}{14}\cdot\frac{2h^2+14h+35}{(h+5)^2} \qquad (6)$$

allowing h and hence K to be obtained explicitly without recourse to successive approximations and Figs. 1 and 2 of [1].

A check on the consistency of the mathematical model, the experimental accuracy of the moments and/or the value of N chosen is provided by the inequality:

$$1{\cdot}5 \leqslant \gamma \leqslant 2{\cdot}14$$

for

$$0 \leqslant h \leqslant \infty.$$

It will be noted that Chao and Hoelscher [3] found it necessary to reduce the number of effective stages in order to make the second and third moments consistent. This indicates either

(a) the axial fluid phase dispersion coefficient is increased by interphase transfer

or

(b) significant particle diffusional resistance was present in their experiments (they assumed it to be zero)

and/or

(c) a more complex model than either the axial dispersion or the finite stage model is required to adequately describe the processes occurring in a packed bed since an identical result is obtained using the finite stage model moments.

In a similar way the continuous model of Chao and Hoelscher may be extended to the case of finite internal particle diffusivity yielding:

$$\mu = 1 + V_H$$

$$\sigma^2 = \frac{2\mu^2}{NP_{e_a}} + \frac{Y}{X}(\mu - 1) \qquad (7)$$

and

$$\pi^3 = \frac{6\mu(\mu-1)}{N\cdot P_{e_a}}\frac{Y}{X} + \frac{12\mu^3}{N^2P_{e_a}^2} + (\mu-1)\frac{Z}{X}$$

In Eq. (7), a simplified "plug-flow" entrance boundary condition was assumed.

Department of Chemical Engineering C. P. JEFFRESON
University of Adelaide
South Australia, Australia

NOTATION

- a_p ratio, particle surface area to volume
- c_s, c_f particle and fluid heat capacities respectively
- d_p particle diameter
- $G(s)$ overall bed transfer function, axial dispersion model
- $G_p(s)$ fluid-particle surface transfer function
- h Biot number $= d_p h_p/2k_s$
- h_p fluid–particle transfer coefficient
- K $= h_p a_p \bar{T}/\rho_f c_f$
- k_s particle conductivity
- N = ratio bed length to particle diameter
- $\bar{T}$ bed fluid holdup time
- t time, normalised with respect to $\bar{T}$
- X, Y, Z particle transfer parameters defined by Eqs. (4)
- $Y_D(s)$ particle "admittance" transfer function of Rosen [2]
- V_H Ratio, bulk packing volumetric heat capacity to bulk volumetric heat capacity of interstitial fluid.

REFERENCES

[1] JEFFRESON C. P., *Chem. Engng Sci.* 1968 **23** 509.
[2] ROSEN J. B., *J. Chem. Phys.* 1952 **20** 387.
[3] CHAO R. and HOELSCHER H. E., *A.I.Ch.E.Jl* 1966 **12** 271.

Chemical Engineering Science, 1970, Vol. 25, pp. 1319–1329. Pergamon Press. Printed in Great Britain.

Dynamic testing—a unification

C. P. JEFFRESON
Department of Chemical Engineering, The University of Adelaide, Adelaide, South Australia, Australia

(*First received* 15 *December* 1969; *in revised form* 18 *February* 1970)

Abstract—Fundamental relationships between frequency response, step response and moments analysis are used to unify and extend theories of dynamic testing by these methods. It is shown that conventional methods of least squares polynomial curve fitting in the frequency domain allow estimates to be made of the moments of the impulse response of a linear system and a method by which the moments may be obtained from a perfect step response is proposed. General integral formulae for step response prediction are also presented. A discussion of errors arising in "frequency domain" analysis leads to the conclusion that experimental design limits the amount of useful information which may be obtained from a pulse test, irrespective of the method of analysis used. An experimental technique which limits the effects of "tailing" is proposed.

INTRODUCTION

A NUMBER of workers have recently pointed out the practical disadvantages of the moments analysis of pulse experiments [1, 2]. Clements [1] has shown that curve fitting of the single parameter axial dispersion model to Fourier transformed pulse data i.e., to the "frequency response" of the system, leads to a lower root mean square error than is obtained using parameters from moments analysis. Errors arising in moments analysis are attributed to the undue weight placed on the "tail" of an experimental response which is the part most susceptible to drift and recorded inaccuracies.

Nonetheless, clear definition of the relationships between the frequency response and the moments of the impulse response of a system is likely to be of value. Since the moments of a linear system define the *shape* of impulse and step responses, such a clarification should allow at least qualitative translation from frequency to time domains.

In this paper some elementary results from mathematical statistics have been applied to the problem. The results obtained lead towards a unification of pulse, step and frequency response methods of dynamic testing so that a number of isolated data analysis techniques become special cases of the general theory.

A method of improving the reliability of pulse test experiments is suggested in the final section of the paper.

FUNDAMENTAL RELATIONSHIPS

The *impulse response* $g(t)$ of a stable linear system (or residence time distribution function of a linear flow system) may be regarded as a probability density function, i.e.

$$\int_{-\infty}^{\infty} g(t)\mathrm{d}t = \int_{0}^{\infty} g(t)\mathrm{d}t = \mu_0' \qquad (1)$$

where μ_0' is the zero'th moment or steady state *gain* of the system and $g(t) = 0,\ t < 0$ by definition of impulse response.

The characteristic function $G(j\omega)$ is defined in the present context by

$$\begin{aligned} G(j\omega) &= \int_{-\infty}^{\infty} g(t)\,.\,\mathrm{e}^{-j\omega t}\,.\,\mathrm{d}t \\ &= R(\omega) + jI(\omega) \\ &= G(j\omega)\,.\,\exp\left[j\angle G(j\omega)\right] \end{aligned} \qquad (2)$$

with inverse

$$g(t) = \frac{1}{2\pi}\int_{-\infty}^{\infty} G(j\omega)\,.\,\mathrm{e}^{j\omega t}\mathrm{d}\omega.$$

In Eqs. (2), $R(\omega)$ and $I(\omega)$ are the real and imaginary parts of the characteristic function or Fourier transform of $g(t)$. $|G(j\omega)|$ and $\angle G(j\omega)$

are the modulus and argument representations of $G(j\omega)$ and as is well known[12] define the frequency response of a linear stable system as a function of natural frequency ω. The complex variable $G(j\omega)$ may also thus be described as the "frequency response transfer function". The transform defined by Eq. (2) may also be regarded as a complex sum of Fourier sine and cosine transforms:

$$G(j\omega) = \int_0^\infty g(t) \cos \omega t \, dt - j \int_0^\infty g(t) \sin \omega t \, dt. \tag{3}$$

Substitution of the series expansions for $\cos \omega t$ and $\sin \omega t$ leads to the well known result [13]:

$$G(j\omega) = \mu_0' - \mu_2' \cdot \frac{\omega^2}{2!} + \mu_4' \cdot \frac{\omega^4}{4!} - \cdots \cdots + j\left[-\mu' \cdot \omega + \mu_3' \cdot \frac{\omega^3}{3!} - \mu_5' \cdot \frac{\omega^5}{5!} + \cdots\right], \tag{4}$$

where μ_n' is the n'th moment of $g(t)$ about the origin, i.e.

$$\mu_n' = \int_0^\infty t^n \cdot g(t) \cdot dt \tag{5}$$

$$\text{for } g(t) = 0, t < 0.$$

Equation (3) indicates that Fourier transformation of the impulse response $g(t)$ of a system effectively involves evaluation of *all* the moments of $g(t)$ about the origin.

Definition of the cumulants κ_n of a density function has been found useful in the theory of mathematical statistics[4]. They are defined by the expansion

$$\ln [G(j\omega)] = \sum_{n=0}^{\infty} \kappa_n \frac{(-j\omega)^n}{n!} \tag{6}$$

and can be found in terms of the moments μ_n' and in terms of the *central moments* μ_n of a distribution, where

$$\mu_n = \int_0^\infty (t - \mu_1')^n \cdot g(t) \cdot dt. \tag{7}$$

Kendall and Stuart[13] give tables of μ_n in terms of κ_j, and κ_n in terms of μ_j up to $n = 10$ when the steady state gain μ_0' is unity. These formulae for the first four cumulants are given in Eq. (8) below

$$\begin{aligned} \kappa_0 &= \ln \mu_0' = 0 \qquad \text{for} \qquad \mu_0' = 1 \\ \kappa_1 &= \mu_1' \\ \kappa_2 &= \mu_2 = \sigma^2 = \mu_2' - 2\mu_1'^2 + \mu_1'^2 \cdot \mu_0' \\ \kappa_3 &= \mu_3 = \pi^3 = \mu_3' - 3\mu_1'\mu_2' + 3\mu_1'^3 - \mu_1'^3\mu_0' \\ \kappa_4 &= \mu_4 - 3\mu_2^2 \end{aligned} \tag{8}$$

where σ^2 is defined as the variance of the impulse response distribution and π^3 is usually loosely called the "skewness".

It may be noted that for most flow systems the steady state gain μ_0 is unity although this may not be necessarily so. An example is the response of a packed bed to inlet temperature changes where heat loss occurs through the walls.

APPLICATIONS TO THE THEORIES OF PULSE AND FREQUENCY RESPONSE TESTING

1. *Introduction*

At present there are two principal methods for obtaining the parameters of a system by pulse testing. In both, a pulse input $x(t)$ is applied to a linear stable system under test and the output pulse $y(t)$ measured. Then certain parameters of the impulse response, $g(t)$, or its Fourier transform (frequency response transfer function) $G(j\omega)$ are estimated. Both methods rely on the existence of the following relation between input and output Fourier transforms:

$$Y(j\omega) = X(j\omega) \cdot G(j\omega) \tag{9}$$

or in the "time domain" where $x(t) = y(t) = 0$, $t < 0$,

$$y(t) = \int_0^t x(\tau) \cdot g(t - \tau) \cdot d\tau.$$

In the case of distributed parameter systems of interest to chemical engineers, there may be a number of space variables included in $G(j\omega)$.

In this section, application of the fundamental relationships derived earlier to these two methods—moments analysis and pulse to frequency response analysis—is discussed.

2. *Additivity of cumulants under convolution*

If the frequency response transfer function is expressed in modulus $|G(j\omega)|$ and argument form $\angle G(j\omega)$ and logarithms taken, we have:

$$\ln [G(j\omega)] = \ln |G(j\omega)| + j \angle G(j\omega).$$

Hence comparison with Eq. (6) yields:

$$\left.\begin{aligned} \ln |G(j\omega)| &= \kappa_0 - \kappa_2 \frac{\omega^2}{2!} + \kappa_4 \frac{\omega^4}{4!} - \kappa_6 \frac{\omega^6}{6!} + \\ \text{and } \angle G(j\omega) &= -\kappa_1 \omega + \kappa_3 \frac{\omega^3}{3!} - \kappa_5 \frac{\omega^5}{5!} + . \end{aligned}\right\} \quad (10)$$

Equations (10) allow a generalisation of a result, derived by Aris [3] to be made. Aris' derivation was applicable to the situation illustrated by Fig. 1(B). Here the output and the input pulses are related by Eq. (9). Aris showed that if μ'_{Y_1}, μ'_{G_1} and μ'_{X_1} are the first moments of $y(t)$, $g(t)$ and $x(t)$ respectively then

$$\mu'_{G_1} = \mu'_{Y_1} - \mu'_{X_1}.$$

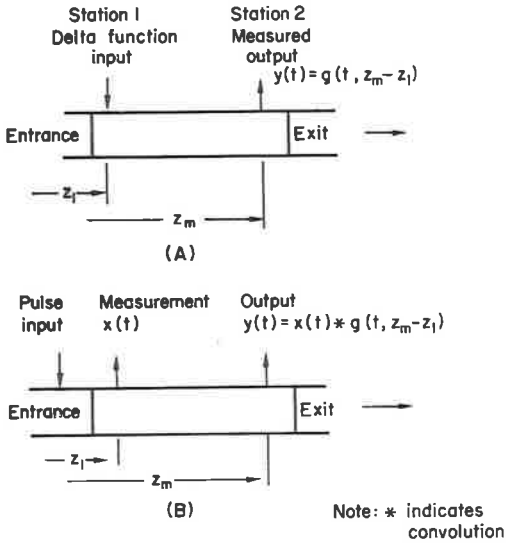

Figs. 1(A), (B). Pulse testing configurations of Aris [3].

Similarly, for the corresponding variances σ_Y^2, σ_G^2 and σ_X^2:

$$\sigma_G^2 = \sigma_Y^2 - \sigma_X^2.$$

These two equations provide the theoretical basis for obtaining estimates of the first two moments of the system from experimental pulse data.

Now, applying the properties of complex numbers to Eq. (9) we have:

$$\ln |Y(j\omega)| = \ln |X(j\omega)| + \ln |G(j\omega)|$$

$$\text{and} \qquad \angle Y(j\omega) = \angle X(j\omega) + \angle G(j\omega). \quad (11)$$

Since $x(t)$ and $y(t)$ are density functions and may thus also be represented by equations of the form of (10) it follows that the cumulants are all *additive under convolution*, i.e.

$$\kappa_{Y_n} = \kappa_{X_n} + \kappa_{G_n}. \quad (12)$$

Thus Aris' result is generalised for all the cumulants although, as pointed out in the Introduction, evaluation of moments of higher order than 2 will be (experimentally) prone to errors due to "tailing". The generalisation also indicates that there can be no difference between the moments obtained by injecting an impulse (Dirac, or delta) function input at station 1 of Fig. 1(A) and those obtained by measurement of an input passing station 1 of Fig. 1(B) provided the same inpulse response $g(t, x - x_m)$ describes both situations.

3. *Frequency domain analysis*

Estimation of the frequency response transfer function $G(j\omega)$ by numerical Fourier transformation of input and output pulses may be carried out by Eq. (9), i.e. from

$$G(j\omega) = \frac{Y(j\omega)}{X(j\omega)}.$$

In practice, this method leads to "breakdown" of the estimated transfer function at high fre-

quencies. This difficulty is discussed in Section 6 from the present point of view. Here, it will be assumed than an accurate estimate of $G(j\omega)$ is available either as a result of an accurate pulse to frequency conversion or by direct cyclic testing.

Examination of Eq. (10) reveals that the modulus of the transfer function $|G(j\omega)|$ (or "magnitude ratio" in cyclic testing) is expanded in terms of the even cumulants, the first two being the gain and variance of the system. The argument $\angle G(j\omega)$ or phase shift between output and input sine waves in cyclic testing, has been expanded in terms of the odd cumulants, the first two being the first moment and the skewness or third central moment. Since the impulse response of many distributed parameter flow systems tends towards a displaced Gaussian distribution of negligible skewness, the phase shift becomes that of a pure dead time, i.e.,

$$\angle G(j\omega) \simeq -\mu_1' \cdot \omega. \tag{13}$$

This explains why parameter estimation using the phase shift is so rarely of value in chemical engineering research although an estimate of the first moment may be useful. Figure 2 illustrates this with a typical flow system frequency response—that of a tracer injected into turbulent fluid in a pipeline. The Taylor theory as presented by Levenspiel [10] has been assumed.

4. *Comparison between moments and frequency domain analysis*

Equations (10) reveal that the application of conventional least-squares polynomial curve fitting to $|G(j\omega)|$ and $\angle G(j\omega)$ should result in estimates of the cumulants of the impulse response distribution function. When the frequency response transfer function has been obtained by pulse testing, *such estimates can be*

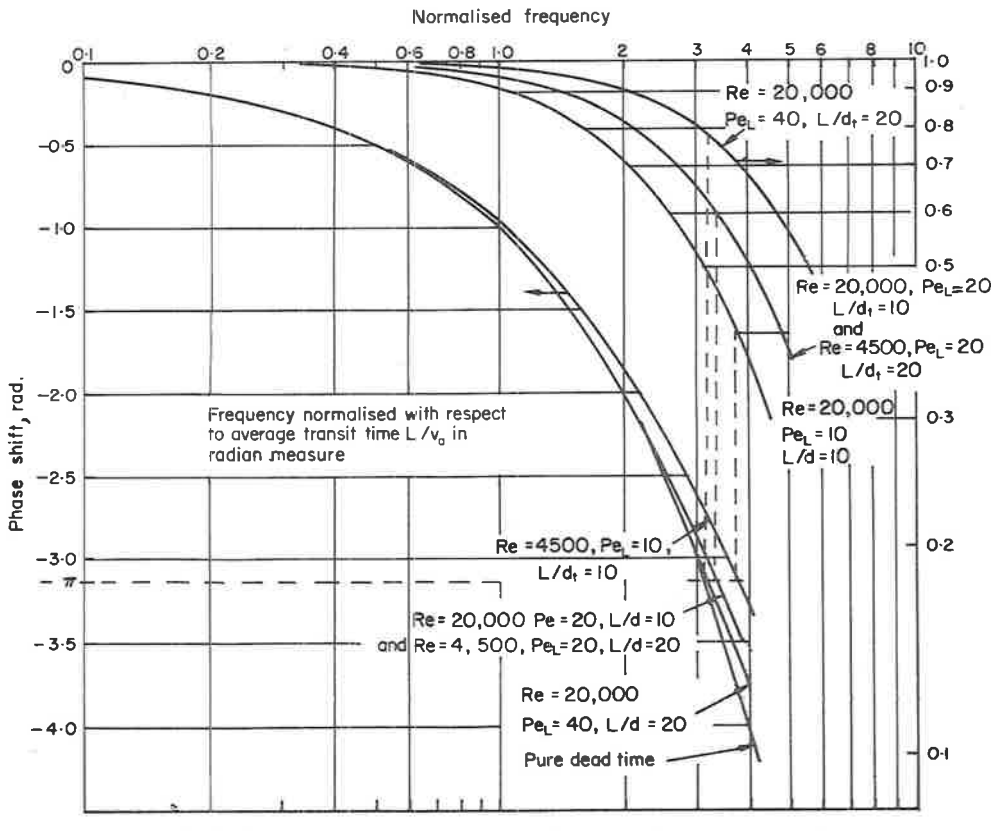

Fig. 2. Frequency response transfer functions—axial dispersion model.

no more accurate than those resulting from direct moments analysis.

The superiority of pulse to frequency response analysis over direct moments analysis reported by Clements[1] may thus be regarded as a result of averaging out the errors arising in successive cumulants. The values of parameters obtained by fitting a theoretical model to a frequency response transfer function, i.e. *frequency domain* analysis, must, from the present point of view, depend markedly on the frequency range of the comparison.

Consider for example, the model used by Clements in his comparison—the doubly infinite version of the single parameter dispersion model. We have for this system:

$$G(j\omega) = e^{Pe/2} \exp\left[-\tfrac{1}{2}\sqrt{\{Pe^2 + 4Pe(j\omega T)\}}\right]$$

where Pe is the effective axial Peclet number and T is the mean residence time.

The first four cumulants are relatively simple (see Appendix):

$$\kappa_0 = 0, \kappa_1 = T, \kappa_2 = \frac{2T^2}{Pe}, \kappa_3 = \frac{12T^3}{Pe^2}, \kappa_4 = \frac{120T^4}{Pe^3},$$

i.e. for $\omega T \leqslant 5$,

$$\ln|G| = -\frac{(T\omega)^2}{Pe} + \frac{5}{Pe^3}(T\omega)^4 - \ldots.$$

Values of Pe reported by Clements range from about 10 to 60. Consider the case where $Pe \simeq 20$.

Then,

$$\ln|G| = -0{\cdot}05(T\omega)^2 + 0{\cdot}000625(T\omega)^4 - \cdots$$

and $$\angle G = -T\omega + 0{\cdot}010(T\omega)^2 - \cdots$$

It may be seen that for a normalised frequency range of $0 < T\omega < 1$, the second term is more than 100 times smaller than the first.

Hence if parameter fitting is carried out over this range of frequencies, moments analysis must yield identical parameters to frequency domain analysis, *provided the experimental data actually fits the model proposed.*

At higher frequencies, the contribution of terms in ω^4, ω^6 etc., become larger. For example at $T\omega = 2$, the second term is now only one tenth that of the first. Since the effect of truncation of a tail of a pulse test is to reduce the values of all cumulants[2] and since the sign of the terms in Eqs. (10) alternate, it is possible that over one part of the frequency range covered, tail truncation errors will be positive, whilst over the other part, errors become negative. The fractional error in the higher cumulants will be greater than in the smaller[2] despite their smaller weighting.

It may be seen from the above that estimation of the reliable frequency range is of crucial importance—this is considered in Section 6. It is also evident that improvements in experimental technique which eliminate tail truncation should greatly improve the accuracy of both methods. This point is considered in the final section of the paper.

5. *Other frequency domain methods*

Pëtho[8] has recently derived the following relationships between frequency response and moments analysis:

$$\mu_1' = \lim_{\omega \to 0}\left[\frac{d\angle G}{d\omega}\right]$$

and

$$\sigma^2 = -\lim_{\omega \to 0}\left[\frac{d^2 \ln|G|}{d\omega^2}\right] \qquad (14)$$

where, as before, σ^2 is the variance of the impulse response density function.

Examination of Eqs. (10) reveals that these results may be generalised to yield

$$\kappa_{2n+1} = \lim_{\omega \to 0}(-1)^n \cdot \frac{d^{2n+1}\angle G}{d\omega^{2n+1}}$$

$$\kappa_{2n} = \lim_{\omega \to 0}(-1)^n \cdot \frac{d^{2n}\ln|G|}{d\omega^{2n}} \qquad (15)$$

$$n = 0, 1, 2, \ldots\ldots$$

From a practical point of view, computation of impulse response moments by differentiation

of an experimental frequency response in the region of zero frequency is likely to be even more prone to error than direct estimation of moments.

Another example of the generalisations which follow from Eq. (10) is provided by the work of Rosen and Winsche[9]. These investigators suggested that fluid–particle transfer coefficients in packed beds may be determined from the slope of a plot of the ratio $\ln|G|/\angle G$ against frequency, ω. This plot should be a straight line. Division of the series expansion of $\angle G$ into $|G|$ indicates that a straight line results when $\kappa_4 - \kappa_2\kappa_3$ is negligible over the frequency range of comparison. For heat transfer in packed beds this requires long bed lengths and low Reynolds numbers so that the conditions of the test are somewhat restricted.

6. *"Breakdown" of numerical transformations*

When input and output pulses $x(t)$ and $y(t)$ to a system are Fourier transformed numerically by evaluation of the trigonometric integrals of Eq. (3), the resultant transforms: $X(j\omega)$, $Y(j\omega)$ and $G(j\omega)$ (from Eq. 9) usually 'breakdown' at some frequency ω_{max}. Breakdown is evidenced by a degeneration into physically meaningless oscillations. One criterion for breakdown is the Sampling Theorem[11] which in effect states that breakdown occurs when the mesh size, δ, in a numerical integration becomes comparable with the half period, π/ω_{max}. We thus require that

$$\delta < \pi/\omega_{max};$$

for numerical stability.

Unfortunately, the Sampling Theorem is in fact only applicable to pulses, the transforms of which become zero for $\omega > \omega_{max}$. The maximum frequency obtainable depends on the numerical method used; however Lees and Dougherty have shown that stepped, trapezoidal and parabolic interpolation formulae all reduce to:

$$Y(j\omega) = \int_0^\infty y(t) \,.\, e^{-j\omega t}\, dt$$

$$\simeq [CF] \sum_{i=0}^{n} y(i\delta) \,.\, \exp(-j\omega i\delta) \,.\, \delta.$$

Here, the correction factors CF depend only on ω and δ. When the ratio $G(j\omega) = Y(j\omega)/X(j\omega)$ is evaluated, correction factors cancel so that different methods of numerical approximation have little effect. The empirical criterion developed by Lees and Dougherty:

$$\delta < \frac{0{\cdot}1\pi}{\omega_{max}} \qquad (16)$$

appears to work well in practice. Figure 3 illustrates the growth in error occurring in Simpson's $\frac{1}{3}$ rule integration of impulse data from a flow mixer[6]. The difference between integrations carried out with mesh spacings of δ and 2δ increases in magnitude near the point predicted by in equality (14). Similar results were obtained in other tests also reported in reference [6].

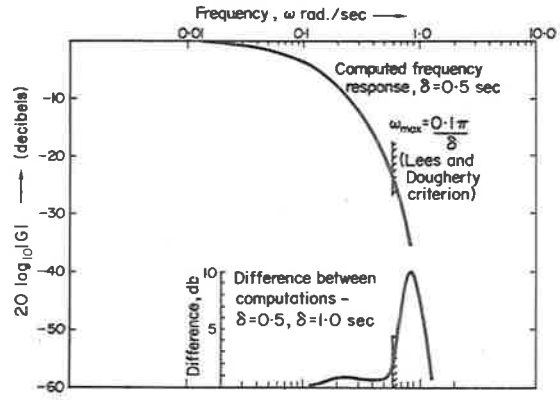

Fig. 3. Comparison of pulse to frequency response breakdown criteria.

An alternative viewpoint is that since trigonometric integration in effect involves simultaneous evaluation of *all* the moments of a pulse about its origin and since, from Eqs. (4) and (9) the contribution due to the higher moments increases as frequency increases, than breakdown may be regarded as caused by accumulation of errors in estimation of the higher order moments which are weighted by successively higher powers of

frequency. The fact that the terms in Eq. (9) alternate in sign would also be consistent with the oscillations frequently observed.

APPLICATIONS TO STEP TESTING THEORY

1. *Introduction*

When a perfect unit step function $U(t)$ is applied to a stable linear system of impulse response $g(t)$, where $U(t)$ is defined by

$$U(t) = \begin{cases} 0, t < 0 \\ 1, t \geq 0 \end{cases}$$

then the resultant step response $u(t)$ may be useful in parameter estimation. Future extension of the theory to 'imperfect step' testing would be useful, since it is rarely possible to apply a perfect step in temperature or concentration to a flow system. Such an extension has not been made here, unfortunately. It should be noted that numerical differentiation of input and output is impractical because of the large errors involved.

2. *Relation between step response and moments*

Consider first the perfect step response $u(t)$. Although neither $U(t)$ nor $u(t)$ are, strictly speaking, Fourier transformable (except in a limiting sense), the difference between the final value μ'_{G_0} (the gain of the system) and the response $u(t)$ is. Defining this difference as $\phi_G(t)$ where

$$\phi_G(t) = U(t)[\mu'_{G_0} - u(t)], \tag{17}$$

the Fourier transform of $\phi_G(t)$ may be obtained, noting that

$$u(t) = \int_0^t g(\tau) \, . \, d\tau$$

$$\text{and} \quad U(t) = \int_0^t \delta(\tau) \, . \, d\tau.$$

Here $\delta(t)$ is a Dirac, delta, or impulse function defined in reference [11].

The transform of $\phi_G(t)$ is:

$$\mathscr{F}[\phi_G(t)] = \mathscr{F}\left\{ \int_0^t [\delta(\tau) \, . \, \mu'_{G_0} - g(\tau)] \, d\tau \right\}. \tag{18}$$

The Fourier transform of $\delta(t)$ is unity and the Laplace transform integration theorem [11] may be extended to the Fourier transform of Eq. (18) provided, as in this case, the definite integral is still Fourier transformable.

Thus, if $\mathscr{F}[f(t)] = F(j\omega)$,

then

$$\mathscr{F} \int_0^t f(\tau) \, d\tau = F(j\omega)/j\omega,$$

provided $\int_0^t f(\tau) \, d\tau$ actually has a Fourier transform.

When this is applied to the Fourier transformable Function $\phi_G(t)$ one obtains

$$\mathscr{F}[\phi_G(t)] = [\mu'_{G_0} - R_G(\omega) - jI_G(\omega)]/j\omega \tag{19}$$

where

$$\mathscr{F}g(t) = R_G(\omega) + jI_G(\omega).$$

Fourier transformation of $\phi_G(t)$ was, essentially, the method used by Healy [7] to obtain the frequency response transfer function of a packed bed of spheres from its step response.

Substitution of Eq. (4) into (19) yields

$$\mathscr{F}[\phi_G(t)] = \mu'_{G_1} - \frac{\mu'_{G_3}}{3}\frac{\omega^2}{2!} + \frac{\mu'_{G_5}}{5} \cdot \frac{\omega^4}{4!} - \ldots\ldots + j\left[\frac{\mu'_{G_2}}{2} \cdot \omega + \frac{\mu'_{G_4}}{4} \cdot \frac{\omega^3}{3!} - \frac{\mu'_{G_6}}{6} \cdot \frac{\omega^5}{5!} + \ldots\ldots\right]. \tag{20}$$

Equation (20) states that the moments about the origin, μ'_{ϕ_n}, of the function $\phi(t)$ are related to the moments about the origin of the impulse response by equation (21):

$$\mu'_{\phi_n} = \frac{\mu'_{G_{n+1}}}{n+1}. \tag{21}$$

3. *Application of perfect step relations*

Equation (21) indicates that accurate moments will be more difficult to obtain from the step

response than from the impulse response since the magnitude of each moment is reduced by a factor $n+1$. This "loss of information" is a well known characteristic of step testing. Further information is lost when the *life expectation function* $\psi(t)$ of Zwietering[14] is measured experimentally since this is, in normalised time, related to the step response by

$$\psi(t) = \int_0^t \phi(\tau)\, d\tau.$$

The moments are again shifted, as in Eq. (21), and in this case, divided by $n+2$.

A particular case of Eq. (19) has, nonetheless, already been applied in the literature on breakthrough curve measurements in packed beds. Antonson and Dranoff[15] evaluated the integral of the difference between the breakthrough curve or step response and its final value, to obtain the distribution coefficient for ethane adsorption on molecular sieves. The integral referred to is, in fact, the zero'th moment about the origin μ'_{ϕ_0} of $\phi(t)$ and is, according to Eq. (21) equal to *first* moment of the impulse response. Equation (21) also indicates that the higher moments could be evaluated, although no doubt, similar inaccuracies to those occuring in pulse-type experiments would result.

4. *Inversion to obtain step response*

Equation (17) leads to a general integral formulae for the determination of a step response (or breakthrough curve of a packed bed) from the particular frequency response transfer function proposed.

Equation (17) may be re-arranged to yield:

$$u(t) = U(t)\{\mu'_{G_0} - \mathscr{F}^{-1}[\phi_R(\omega) + j\phi_I(\omega)]\} \quad (22)$$

where $\phi_R(\omega)$ and $\phi_I(\omega)$ denote real and imaginary parts of the Fourier transform of $\phi(t)$ and as before:

$$\phi_R(\omega) = I_G(\omega)/\omega$$
$$\phi_I(\omega) = [\mu'_{G_0} - R_G(\omega)]/\omega.$$

Rosen's integral form of the breakthrough curve of a linear adsorber[16] is a particular example of (22) where the inversion integral is evaluated numerically.

Slightly simpler versions of Eq. (22) are:

$$u(t) = 1 - 2\,\mathscr{F}^{-1}\frac{I_G(\omega)}{\omega}$$
$$= 1 - 2\,.\,\mathscr{F}^{-1}\left[\frac{\mu'_{G_0} - R_G(\omega)}{\omega}\right]$$

i.e.,

$$u(t) = 1 + \frac{2}{\pi}\int_0^\infty \frac{I_G(\omega)}{\omega}\cdot\cos\omega t\,.\,d\omega$$

and

$$u(t) = 1 - \frac{2}{\pi}\int_0^\infty \frac{\mu'_{G_0} - R_G(\omega)}{\omega}\cdot\sin\omega t\,.\,d\omega.$$

The above equations are derived from the fact that for a real physical system, $R_G(\omega)$ and $I_G(\omega)$ are even and odd functions of frequency respectively[11]. It should be noted that it is first necessary to obtain the limits

$$\lim_{\omega\to 0}\frac{I_G(\omega)}{\omega} \text{ and/or } \lim_{\omega\to 0}\frac{\mu'_{G_0} - R_G(\omega)}{\omega}$$

in order to carry out the integrations indicated.

EXPERIMENTAL DESIGN OF PULSE EXPERIMENTS

If the *input* pulse to a system does not return quickly to zero, but decays away slowly in an indefinite manner, the resultant output tail may be even more indefinite, so that errors due to drift and lack of resolution of recording instruments may be compounded.

Such "tailing" usually arises as a result of the finite capacity of fittings and lines. For example, Healy[7] applied temperature pulses to a packed bed through which air was flowing steadily, using a fine wire Nichrome heater. The initial rise and fall times of the input pulses were excellent, but the small capacitance of fittings resulted in a long input tail. Similar effects may be observed when small quantities of a saline solution are injected into a stream, in this case as

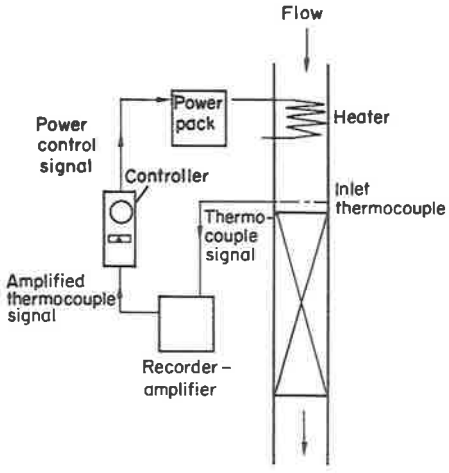

Fig. 4. Apparatus for control of drift.

a result of molecular diffusion from the injection apparatus. The problem may be compounded in the case of thermal pulse injection by slow changes in incoming fluid temperature.

A simple technique which has greatly improved experimental reproducibility in present work on packed bed dynamics is illustrated in Fig. 4. The measurement of input temperature is used, in a feedback manner, to control the input quantity so that its baseline remains slightly above the ambient or background before and after administering the pulse. Thus, the effects of tailing are eliminated and the control system may theoretically be used to administer a suitably shaped pulse. In practice, it has been found that manual pulse administration is necessary since controller settings suitable for "regulator" control of baseline drift may not be satisfactory during injection.

SUMMARY AND FURTHER WORK

The relationships derived between the frequency response and the moments of a system have allowed a number of isolated techniques of dynamic testing and analysis to be treated in a unified way. Such a unification should lead in the long run to a more rigorous analysis of errors and to improvements in experimental technique. The application of this approach to orthogonal polynomial methods of data reduction, for example the method of Dooge [17] is to be submitted in a later paper.

Acknowledgment—Acknowledgement is made to the Australian Institute of Nuclear Science and Engineering for support of the experimental program currently conducted in conjunction with this analysis.

NOTATION

$\mathscr{F}$ Fourier transform operator
$g(t)$ impulse response density function for stable linear systems
$G(j\omega)$ Fourier transform of impulse response or characteristic function of $g(t)$
$|G(j\omega)|$ modulus representation of $G(j\omega)$, i.e. magnitude ratio for cyclic tests
$\angle G(j\omega)$ argument representation of $G(j\omega)$ or phase shift between imput and output sine waves in a cyclic test
$R(\omega)$ real part of $G(j\omega)$
$I(\omega)$ imaginary part of $G(j\omega)$
t time
Pe Peclet number in dispersion model (see Appendix)
T mean residence time in dispersion model (Appendix)
$x(t)$ input pulse to a system under pulse test
$y(t)$ output pulse from a system under pulse test
$X(j\omega)$ Fourier transform of input pulse
$Y(j\omega)$ Fourier transform of output pulse
$u(t)$ response of system to perfect step input
$U(t)$ unit step function

Greek symbols

$\delta(t)$ impulse or Dirac function
δ mesh spacing for numerical integration
κ_n n'th cumulant of impulse response density function $g(t)$ (Eq. (6))
μ'_n or μ'_{Gn} n'th moment about origin of $g(t)$

μ_n	n'th moment about centre of mass μ of $g(t)$	$\psi(t)$	"life expectation" function of Zwietering[14]
$\sigma^2 \equiv \mu_2$	variance of impulse response density function	$\phi(t)$ or $\phi_a(t)$	difference between final value of step response and value at time t
ω	natural frequency		

REFERENCES

[1] CLEMENTS W. C., Jr., *Chem. Engng Sci.* 1969 **24** 957.
[2] CURL R. L. and McMILLAN M. L., *A.I.Ch.E.Jl* 1966 **12** 819.
[3] ARIS R., *Chem. Engng Sci.* 1959 **9** 266.
[4] ZELEB M. and SEVERO N. C., *Probability Functions* In *Handbook of Mathematical Functions* (Edited by ABRAMOWITZ M. and STEGAN I. A.). Dover 1965.
[5] LEES S. and DOUGHERTY R. C., *J. bas. Engng* 1967 **89** 445.
[6] OWENS L., *Honours Proj. Rep.*, Univ. Adelaide 1969.
[7] HEALY J. E., *U.S. At. Energy Comm. Rep.* No. RPI-3639-3, 1967.
[8] PËTHO Á., Submitted for publication.
[9] ROSEN J. B. and WINSCHE W. E., *J. chem. Phys.* 1950 **18** 1587.
[10] LEVENSPIEL O., *Chemical Reaction Engineering*. Wiley 1962.
[11] BRACEWELL R. N., *The Fourier Transform and its Applications*. McGraw-Hill 1965.
[12] DOETSCH G., *Guide to the Application of Laplace Transforms* (Translated and Edited by McFAIRBAIRN W.). Van Nostrand, London 1963.
[13] KENDALL M. G. and STUART A., *The Advanced Theory of Statistics*, Vol. 1, 2nd Edn. Griffin, London 1958.
[14] ZWIETERING T. N., *Chem. Engng Sci.* 1959 **11** 1.
[15] ANTONSON C. R. and DRANOFF J. S., *Chem. Engng Prog. Symp. Ser.* 1967 **63** (74) 61.
[16] ROSEN J. B., *Jl chem. Phys.* 1952 **20** 387.
[17] DOOGE J. C. I., *Jl S.I.A.M. Control* 1965 **2** 397.

APPENDIX

CUMULANTS OF DOUBLY-INFINITE SINGLE-PARAMETER AXIAL DISPERSION MODEL

The frequency response transfer function[1] for this system is

$$G(j\omega) = \exp\left\{\frac{Pe}{2}\left[1-\sqrt{\left(1+\frac{4j\omega T}{Pe}\right)}\right]\right\}. \qquad \text{(A1)}$$

Writing $z = 4j\omega T/Pe$, the series expansion for $(1+z)^{1/2}$ may be written:

$$(1+z)^{1/2} = 1+\tfrac{1}{2}z+\tfrac{1}{2}(\tfrac{1}{2}-1)z^2/2!+\tfrac{1}{2}(\tfrac{1}{2}-1)(\tfrac{1}{2}-2)z^3/3!+ \qquad \text{(A2)}$$

provided $|z| \leqslant 1$, i.e. $\omega T \leqslant Pe/4$.

Substituting (A2) into (A1) and taking logarithms:

$$\ln[G(j\omega)] = \frac{Pe}{2}[-\tfrac{1}{2}z-\tfrac{1}{2}(\tfrac{1}{2}-1)z^2/2!-\cdots\cdot]$$

$$= Pe\left[-\frac{1}{2^2}z+\frac{1}{2^3}\frac{z^2}{2!}-\frac{1.3}{2^4}\frac{z^3}{3!}+\cdots\cdot\right] |z| \leqslant 1.$$

Comparing with Eq. (6) term by term, i.e. with:

$$\ln[G(j\omega)] = \sum_{n=0}^{\infty}\frac{\kappa_n}{n!}(-1)^n(j\omega)^n \qquad \text{(A3)}$$

we obtain

$$\kappa_n = [1.3.5\ldots(2n-3)].\frac{2^{n-1}T^{n-1}}{Pe^{n-1}},\ n = 1, 2, -$$

$$\kappa_0 = 0$$

i.e. $\kappa_1 = 1$, $\kappa_2 = 2T/Pe$, $\kappa_3 = 12T^2/Pe^2$, $\kappa_4 = 120T^3/Pe^3$,

Résumé—Les relations fondamentales entre la réponse de fréquence, la réponse par degrés et les analyses de moments sont employées pour unifier et étendre les théories d'essais dynamiques par ces méthodes. On démontre que les méthodes conventionnelles de l'ajustement de courbe polynôme des moindres carrés dans le domaine de fréquence permet l'estimation de moments de réponse d'impulsions d'un système linéaire et on propose une méthode qui permet d'obtenir les moments d'une réponse par degré parfaite. Une formule d'intégration générale est également présentée pour la prédiction d'une réponse par degré. Une discussion des erreurs qui surviennent dans l'analyse du "domaine de fréquence" conduit à conclure que le modèle expérimental limite la quantité d'informations utiles que l'on peut obtenir d'un essai d'impulsions quelle que soit la méthode d'analyse employée. Une technique expérimentale qui limite les effets de "queues" est proposée.

Zusammenfassung—Es werden grundlegende Beziehungen zwischen Frequenzkennlinie, Stufenkennlinie und Momentenanalyse verwendet um Theorien der dynamischem Prüfung nach diesen Verfahren zu vereinheitlichen und auszubauen. Es wird gezeigt das konventionelle Verfahren des polynom-

ischen Kurvenanpassens mittles kleinster Quadrate im Frequenzgebiet Schätzungen der Momente der Impulsreaktion eines linearen Systemes gestatten, und es wird eine Methode vorgeschlagen mittels welcher die Momente aus einer perfekten Stufenkennlinie erhalten werden können. Ferner werden allgemeine integralformeln für die Voraussage von Stufenkennlinien dargelegt. Eine Erörterung der in der "Frequenzbereich" Analyse entstehenden Fehler führt zu dem Schlusse, dass das Ausmass an brauchbarer Information, die durch einen Impulsversuch erhalten werden kann, unabhängig von dem zur Verwendung gelangenden Analysenverfahren, durch die Versuchsanordnung begrenzt wird. Eine Versuchstechnik, die die Auswirkungen einer 'schleichenden Kennlinie' begrenzt, wird vorgeschlagen.

APPENDIX 4

ANALYSIS OF DYNAMIC AND STEADY-STATE WALL EFFECTS IN PACKED BED DYNAMIC TESTING

1. Physical Assumptions

(i) Temperatures external to the bed wall are uniform along the bed length. All temperatures and fluxes are referred to this datum so that in effect ambient temperature is set equal to zero.

(ii) The wall is assumed to be thin so that axial wall conduction is negligible.

(iii) Fluid temperatures in the bed are essentially radially uniform. This is based on experimental measurement of temperature gradients in the tube.

(iv) Since the wall is thin, heat transfer to the surroundings will be via a lumped heat transfer coefficient h_e, which will include wall resistance and external radiation and convection resistance.

2. Basic Equations

Writing a heat balance for well-mixed fluid in stage i (distance $i.d_p$ from bed inlet):

$$\varepsilon d_p . A_c . \rho_f c_f . \frac{dT}{dt'} = \varepsilon A_c . v_a . \rho_f c_f . [T_{i-1} - T_i]$$

$$+ h_p . a_p . A_c . d_p (1-\varepsilon) [Ts_i - T_i]$$

$$+ h_w . a_w . A_c . d_p [T_w - T_i] \quad \ldots \quad (2.1)$$

where A_c = tube cross sectional area,

h_w = fluid-wall heat transfer coefficient,

a_w = wall area per unit bed volume,

a_p = particle surface area per unit particle volume,

and

$a_w = 4/(M\, d_p)$ for a circular cross section,

and $a_p = 6/d_p$ for spherical or right cylindrical particles.

Defining wall and particle Stanton numbers St_w and St_p in the normal way and defining normalised time t with respect to bed holdup time L/v_a, i.e.

$$t = t' . \frac{v_a}{L} = \frac{t' . v_a}{N . d_p} \quad ,$$

equation (4.1) becomes:

$$\frac{dT_i}{dt} = N[T_{i-1} - T_i] + 6N\, St_p . (1-\varepsilon) [Ts_i - T_i]$$

$$+ \frac{4N}{M} . St_w . [Tw_i - T_i] \quad \ldots \quad (2.2)$$

The particle surface temperature Ts_i may be related, as before the fluid temperature T_i at stage i by the fluid-particle transfer function $G_p(s)$

$$\frac{T_{s_i}(s)}{T_i(s)} = G_p(s) \quad , \qquad \ldots \quad (2.3)$$

whilst the transfer function between wall surface temperature at stage i and fluid temperature will be defined as

$$\frac{T_{w_i}(s)}{T_i(s)} = K_w G_w(s) \qquad \ldots \quad (2.4)$$

In equation (2.3) we have

$$\lim_{s \to 0} G_p(s) = 1$$

which, by the final value theorem, shows that a unit step change in fluid temperature will result in a unit change in particle surface temperature, t large.

In equation (2.4) $G_w(s)$ will be defined in a similar way, the constant K_w, to be defined indicating that, because of heat loss, the final wall temperature (given a unit change in fluid temperature) will differ from unity.

These definitions allow equation (2.2) to be written, after Laplace transformation:

$$\frac{T_i(s)}{T_{i-1}(s)} = \frac{1}{s/N + 6St_p(1-\varepsilon)[1-G_p(s)] + \frac{4St_w}{M}[1-K_w G_w(s)] + 1} \qquad \ldots \quad (2.5)$$

It will be noted that for $M \to \infty$, equation (2.5) becomes the usual finite stage model. Hence the most important variable in

reducing wall effects is the width of the bed in particle diameters.

3. Wall Transfer Function and Steady State Heat Loss

Note assumption (iv). This does not eliminate the need to specify the wall volumetric thermal capacitance $\rho_w c_w$.

For the wall thickness τ over a distance d_p,

$$a_w.\tau.\rho_w c_w.\frac{dT_{wi}}{dt'}.d_p = h_w.d_p.a_w[T_i - Tw_i] - h_e.d_p.a_w.Tw_i$$

or taking transforms,

$$\left[\frac{\tau.\rho_w.c_w.v_a}{(h_w+h_e).d_p}.\frac{s}{N} + 1\right].\ T_{w_i}(s) = \frac{h_w}{h_w+h_e}.T_i(s) \qquad \ldots \quad (3.1)$$

Comparison with equation (2.4) reveals

$$K_w = \frac{h_w}{h_w+h_e}, \qquad \ldots \quad (3.2)$$

$$G_w(s) = \frac{1}{\Pi_w s + 1}$$

where Π_w is defined as the wall time constant, i.e.

$$\Pi_w = \frac{\tau.\rho_w c_w.v_a}{(h_w+h_e).Nd_p} \qquad \ldots \quad (3.3)$$

The wall time constant increases with increasing thickness τ and thermal capacity $\rho_w c_w$.

The steady state change in temperature δT_N for a steady change δT_o at the bed inlet becomes from equation (2.5) [raised to the

power N], allowing $s \to 0$,

$$\frac{\delta T_N}{\delta T_o} = \frac{1}{\left[\frac{4St_w}{M}[1-K_w] + 1\right]^N}$$

or

$$\boxed{\frac{\delta T_N}{\delta T_o} = \left[\frac{N}{N^*}\right]^N} \quad \ldots \quad (3.4)$$

where N^*, the 'effective number of stages' is defined by

$$N^* = N\left[1 + \frac{4St_w(1-K_w)}{M}\right]$$

$$= N\left[1 + \frac{4St_w}{M}\cdot\frac{h_e}{h_w+h_e}\right] \quad \ldots \quad (3.5)$$

When the wall coefficient controls heat transfer, i.e. $h_e \to \infty$, equation (3.5) becomes

$$N^* = N\left[1 + \frac{4St_w}{M}\right] \quad \ldots \quad (3.6)$$

or, when external and/or wall resistance controls, $h_w \to \infty$, equation (3.5) may be written:

$$N^* = N\left[1 + \frac{4St_e}{M}\right]$$

where $St_e = \frac{h_e}{G\,c_f}$ $\quad \ldots \quad (3.7)$

Re-writing equation (2.5) and substituting (3.7):

$$\frac{T_N(s)}{T_o(s)} = \left[\frac{1}{\frac{s}{N} + 6St(1-\varepsilon)[1-G_p(s)] + \frac{4}{M}St_w K_w[1-G_w(s)] + \frac{N^*}{N}}\right]^N$$

$\quad \ldots \quad (3.8)$

4. Effects of Normalisation of Response First Moment

As pointed out in chapter V, it is usual to normalise a break-through curve from zero to 1. or to normalise the area of an output curve to unity even when heat loss occurs. It is necessary to estimate the effect this may have on the resultant calculated moments.

The zero'th moment of impulse response before normalisation becomes

$$\mu_o' = \frac{\delta T_N}{\delta T_o} = \left[\frac{N}{N^*}\right]^N \qquad \ldots(4.1)$$

Normalising equation (3.8) with respect to the zero'th moment, an apparent transfer function $G_N^+(s)$ results which has a unity gain or unity zero'th moment:

$$G_N^+(s) = \left[\frac{N^*}{s + 6N^*St(1-\varepsilon)[1-G_p(s)] + \frac{4N^*St_w K_W}{M}[1-G_W(s)] + N^*}\right]^N \qquad \ldots(4.2)$$

Following a similar argument to that given in section V.D.3, a step change in input temperature of δT_o F^o will be assumed where the subscript zero denotes "zero'th stage."

Then in a similar manner to before;

$$\lim_{t\to\infty} \left[\begin{array}{c}\text{Total Convective} \\ \text{Heat input}\end{array} - \begin{array}{c}\text{Total Convective} \\ \text{Heat output}\end{array} - \begin{array}{c}\text{Total Wall} \\ \text{Heat Loss}\end{array}\right]$$

= Heat retained in packing, interstitial fluid AND wall as $t\to\infty$

$$\ldots(4.3)$$

The additional total heat input which is necessary to supply wall heat loss is given, using the notation of V.D.3, by:

$$W.\, c_f \int_o^\infty \delta T_o \frac{\mu_o' - 1}{\mu_o'}\, dt = \text{Total wall heat loss} \qquad \ldots(4.4)$$

The heat retained by the wall and packing at steady state will be estimated by assuming that wall and fluid reach essentially the same temperature, i.e. 'external' resistance is controlling. This assumption is conservative since temperature drop across the wall will result in a smaller quantity retained..

A further conservative assumption will be that the final length averaged temperature rise is δT_o, although this drops exponentially from δT_o to δT_N (steady state).

Then equations (4.3) and (4.4) yield:

$$\int_0^\infty [\mu_o' \ \delta T_o - \delta T_N (t)] \, dt = \mu_o' \ \delta T_o \, [Mc_s + M_f c_f + M_w c_w]$$

where $M_w \ c_w$ denotes the total wall 'capacitance' in (say) B.T.U. / ^oF.

In normalising the response $\delta T_N(t)$ to 0 to 1, we define

$$u^+(t) = \frac{\delta T_N (t)}{\mu_o' \ \delta T_o}, \text{ i.e.}$$

$$\int_0^\infty [1 - u^+ (t)] \, dt = \frac{Mc_s + M_f \ c_f}{Wc_f} + \frac{M_w \ c_w}{Wc_f} \qquad \ldots(4.5)$$

The first term on the R.H.S. of equation (4.5) is the first moment for zero heat loss, $(1 + V_H) \, L/v_a$, whilst the second term is the 'error' due to wall capacitance. The approximate relative size of this error will be calculated below:

5. Calculated Effects of Wall Heat Transfer - An Example

An alternative viewpoint is to note that for a (say) 10% 'heat loss' over a bed length N of 50, the ratio N*/N will be very close to unity (in this case $[N^*/N]^N = 1.010$, $N^*/N = 1.002$) so that

in equation (4.2), $N^* \simeq N$ to small error, and provided $\frac{4N^*}{M} \Sigma St_w K_w [1 - G_w(s)]$ is always small relative to

$$6N^* St (1-\varepsilon) [1 - Gp (s)] ,$$

all cumulants including $\kappa_1 = \mu_1'$ will be approximately those obtained for zero heat loss.

In order to place numerical values on the likely errors in present experiments a number of further assumptions will be made.

(i) External wall heat transfer coefficient may be regarded simply as k_s/τ where k_s is the wall thermal conductivity and τ is wall thickness. This is a conservative assumption since no thermal resistance between liner and copper wall is provided for.

(ii) Wall Stanton numbers are 80% of the particle Stanton number at a given flow as suggested by Beek [1953].

For the present experiments, we have

d_p = 6.2 and 3.1 mm.,

d_t = 3.77 ins.,

τ = 0.11 inch,

k_s = 0.096 BTU/(hr.ft.$^\circ$F)

(Unplasticised P.V.C.)

Equivalent $h_e = \frac{0.096}{0.11} \times 12 = 10.5$ BTU/(hr.ft.$^2{}^\circ$F)

Wall heat transfer coefficient = $0.8\, h_p$

$$h_w = 0.8.St.Pr.\, Re.\frac{k_f}{d_p}$$

where k_f = molecular conductivity.

In order to estimate the Stanton numbers at Reynolds numbers lower than the reliable Denton limit of 500, Brodkey's correlation referred to in section I.A.5 and plotted on figure I.A.2.1 will be assumed.

For the calculations of table AP.4.4.1 below, it has been assumed that $Pr = 0.74$, $k_f = 0.016$ B.T.U./(hr. ft. ^oF).

TABLE AP.4.5 1

Re_p	St_w	d_p = 6.2mm., M = 15.4			d_p = 3.1mm., M = 30.8		
		h_w	k_w	$\frac{N^*}{N}$	h_w	k_w	$\frac{N^*}{N}$
20	0.508	5.91	0.360	1.0844	11.8	0.520	1.0316
40	.332	7.74	0.42	1.0496	15.48	0.586	1.0281
80	.234	10.9	0.509	1.0298	21.8	0.667	1.0135
100	.204	11.9	0.531	1.0248	23.8	0.686	1.0083
200	.166	19.4	0.649	1.0151	38.8	0.782	1.00471
400	.0975	22.8	0.684	1.0080	45.6	0.807	1.00243
800	.0775	36.2	0.776	1.0045	72.4	0.868	1.00133
1,000	.0717	41.8	0.779	1.0041	83.6	0.884	1.00108
2,000	.0583	68.9	0.870	1.00197	137.8	0.927	1.000552
4,000	.0474	110.3	0.914	1.00105	220.6	0.953	1.00029
8,000	.0384	178.3	0.945	1.00055	357.6	0.966	1.00017
10,000	.0359	209.1	0.954	1.00043	418.2	0.975	1.000117

Table 5.1 may be used to calculate the 'heat loss ratio' (actually the zero'th moment μ_o') from equation (4.1) at varying bed lengths. Note however, that the error due to heat loss is, according to the present analysis, independent of bed length.

TABLE AP.4.5 2

STEADY STATE RATIO

$$\mu'_o = \frac{\text{Output Temperature Rise}}{\text{Input temperature Rise}}$$

Tube diameter = 3.77 inches

Re_p	L = 3.30 ins.		L = 12.55 ins.	
	M = 15.4	M = 30.8	M = 15.4	M = 30.8
20	.343	.432	.016	0.041
40	.520	.473	.083	0.058
80	.689	.696	.221	0.252
100	.718	.800	.283	0.428
200	.817	.881	.463	0.617
400	.897	.937	.664	0.779
800	.940	.965	.794	0.872
1,000	.946	.971	.810	0.895
2,000	.973	.984	.902	0.946
4,000	.984	.993	.946	0.971
8,000	.993	.995	.972	0.983
10,000	.994	.997	.978	0.988

Hence heat loss increases rapidly as Reynolds number falls below about 100 although N^*/N remains less than 1.05 (5% error) down to $Re_p = 40$ for the large diameter particles.

According to equation (4.2) the dynamic effect of the wall will be small over all frequencies when the ratio

$$\frac{2}{3M} \cdot \frac{St_w}{St(1-\varepsilon)} \cdot K_w \cdot \frac{1 - G_w(j\omega)}{1 - G_p(j\omega)}$$

is small for all frequencies, ω.

The value of Π_w in $G_w(j\omega)$ should be small in equation (3.3) which is similar to saying that $M_w c_w$ in equation (4.5) should be small relative to $Mc_s + M_f c_f$. Nonetheless, irrespective of the values of $G_w(j\omega)$ and hence of the thermal mass of the wall, we require $\alpha = 3M\ St\ (1-\varepsilon)/(2\ St_w.K_w)$ to be large for negligible wall error. This ratio has been calculated in table AP.5.3 and may be seen to be quite large over the entire range of the present experimental flows ($100 < Re_p < 1000$).

TABLE AP.4.5.3

RELATIVE IMPORTANCE OF WALL ON DYNAMIC RESPONSE ($\varepsilon = 0.37$)

Re_p	$6St(1-\varepsilon)$	M = 15.4		M = 30.8	
		$\frac{4St_w.K_w}{M}$	Ratio,α	$\frac{4St_w.K_w}{M}$	Ratio,α
20	2.40	0.0475	50.9	0.0237	102
40	1.57	0.0362	43.4	0.0181	87
80	1.10	0.0310	35.4	0.0155	71
100	0.065	0.0281	34.4	0.0140	70
200	0.785	0.0279	28.2	0.0139	56
400	0.461	0.0173	26.4	0.0086	53
800	0.366	0.0157	23.2	0.0078	46
1,000	0.338	0.0145	23.2	0.0072	45
2,000	0.276	0.0131	21.0	0.0065	42
4,000	0.224	0.0112	20.0	0,0056	40
8,000	0.181	.00943	19.2	0.0047	38
10,000	0.170	.00881	19.1	0.0044	38

Finally, the ratio of wall capacitance to bed capacitance i.e. $M_w c_w / M c_s$ may be calculated assuming the volumetric thermal capacity (in, say, BTU/(ft^3 ^{o}F)) of each to be equal. This is a reasonable assumption for most metals and plastics.

Then for τ = 0.11 inch, and d_t = 3.77 inch and porosity ϵ = 0.37,

$$\frac{M_w c_w}{M c_s} \simeq \frac{0.11 \times 3.77 \times \pi}{\pi \times (3.77)^2/4}$$

$$= 1/8.5$$

This suggests an error in the first moment of greater than 10%, however since as noted above (section 4.4) since most of the temperature drop would occur across the wall insulation, the quantity of heat held by the wall would be considerably less than indicated by the above calculation. Furthermore, the calculations of table 5.3 show (see equ.5.1) that even if wall and particle transfer functions are identical, then the ratio, α is likely to be sufficiently high to make wall effects negligible.

6. SUMMARY

A rigorous solution of the wall effect problem does not appear justified for the present experiments. The simplified analysis does lead to the conclusions that for a satisfactory design, which excludes wall effects we require that

(i) the ratio $M = d_t/d_p$ should be large
and that

(ii) wall thickness (including any insulation between bed and wall) should be minimised since the thermal capacitance of apparently thin walls may be quite large relative to that of the bed.

The first conclusion is not perhaps so obvious as the second. The analysis also suggests that although fractional heat loss increases markedly at low flowrates, the ralative dynamic wall effect indicated by the value of α in table 5.1 will decrease at lower flowrates.

A relatively 'perfect' test section would use a very thin stainless steel wall with external vacuum insulation, and no internal lagging (as in the present experiments or in the experiments of Heggs [1967]). In order to increase M, particle size needs to be very small relative to test section diameter although this usually leads to an undesirably high pressure drop through a section.

The effects of wall are also predicted to be independent of bed length.

According to the above analysis, wall effects may be expected to lead to a high value of first moment μ_1' when normalisation is carried out. If high values are not obtained, it seems reasonable to assume that the higher moments are correct, especially since in practice the higher order moments are normalised again with respect to the first.

APPENDIX 5

SYMMETRY CONSIDERATIONS IN FOURIER TRANSFORM INVERSION.

In chapters IV and V use is made of certain symmetry properties of Fourier transform. Although these may be found in texts on the Fourier transform (in particular Bracewell's [1965]) they are appended here for the convenience of the reader.

Following Bracewell, "any function f(t) can be split unambiguously into odd and even parts". If this is not so then let

$$f(t) = E_1(t) + \phi_1(t)$$
$$= E_2(t) + \phi_2(t)$$

where $E_1(t)$ and $E_2(t)$ are both even parts of f(t)

and $\phi_1(t)$ and $\phi_2(t)$ are odd parts of f(t)

Then "$E_1 - E_2 = \phi_2 - \phi_1$,

but $E_1 - E_2$ is even and $\phi_2 - \phi_1$ is odd, hence $E_1 - E_2$ must be zero".

Applying this to the impulse response g(t) defined in section II.A.2, where, it will be recalled, $g(t) = 0$, $t < o$, the even and odd parts of g(t) are

$$E(t) = \tfrac{1}{2}[\, g(t) + g(-t)]$$
$$\phi(t) = \tfrac{1}{2}[\, g(t) - g(-t)]$$
and $$g(t) = E(t) + \phi(t), \quad -\infty < t < \infty$$

It may be seen that for $t \geq o$, $E(t) = \phi(t) = \frac{1}{2}g(t)$ whilst for $t < o$, $E(t)$ is the 'positive' reflection of $g(t)$ about the t axis whilst $\phi(t) = -E(t)$, $t < o$.

The Fourier transform of $g(t)$ may now be written :

$$\mathcal{F}[g(t)] = \int_{-\infty}^{\infty} [E(t). + \phi(t)]\, e^{j\omega t}.\, dt$$

$$= \int_{o}^{\infty} g(t)\, e^{j\omega t}.dt, \text{ since } g(t) = o,\ t < o$$

$$= R(\omega) + j\, I(\omega)$$

Where $R(\omega)$ is the real part of $G(j\omega)$ and $I(\omega)$ the imaginary part.

But since sin ωt is odd and cos ωt even,

$$\int_{-\infty}^{\infty} E(t).\, e^{j\omega t}.\, dt = 2 \int_{o}^{\infty} E(t).\cos\omega t.dt$$

$$\int_{-\infty}^{\infty} \phi(t).\, e^{j\omega t}.dt = 2j \int_{o}^{\infty} \phi(t).\sin \omega t.\, dt,$$

or,

equating real and imaginary parts, the real part of $G(j\omega)$ is Fourier (cosine) transform of the even part of $g(t)$

whilst,

the imaginary part of $G(j\omega)$ is the Fourier (sine) transform of the odd part of $g(t)$.

It may be seen that <u>either</u> the real or the imaginary part of the $G(j\omega)$ contains all the information required to

compute $g(t)$.

Hence, for $t \geq 0$,

$$\int_{-\infty}^{\infty} R(\omega).\cos \omega t.\, d\omega = \int_{-\infty}^{\infty} I(\omega) \sin \omega t.\, d\omega = \tfrac{1}{2}\, g(t).$$

A similar argument may be applied to the function $\phi(t)$ defined in section IV.A.3.

It may also be noted, from equation II.A.2.4 that the real part $R(\omega)$ of $G(j\omega)$ is an even function of ω whilst the imaginary part $I(\omega)$ is an odd function.

APPENDIX 6

SOME 6400 FORTRAN PROGRAMS AND SUB-PROGRAMS

The inclusion of these programs is intended to allow duplication of theoretical results quoted in the Thesis, where desired.

INDEX

SOME 6400 FORTRAN PROGRAMS AND SUBPROGRAMS

1. Frequency Response Transfer Function Subroutine, FRESP2 for Spherical Particles.

General Description

This version is the one required to compute $I(\omega)/\omega$ for Fourier transform inversion to the step response or breakthrough curve (program FOURIN). A similar subprogram is used with program SEARCH as in section VII.G.2.

For real (i.e. non integer) values of N, the number of stages, the statement after 5 on page 3 is replaced by:

```
G1 = N/(OMEGA + (1.-GP)*PHI + N)
G1 = N*CLOG(G1)     $   G=CEXP(G1)
```

where N is defined as REAL and CLOG and CEXP are complex log and complex exponentiation functions available on 6400 FORTRAN. For the Chao and Hoelscher model, equation (AP.1.2.3) is used with CEXP instead of the statements after 5.

Main Symbol Equivalences.

PROGRAM	PHI	AH	VH	N	OMEGA	VAR	AMU3
THESIS	KV_H	Bi	V_H	N	$j\omega$	σ^{*2}	μ_3'

Explanatory Notes.

Statements to 17: Compute normalised variance σ^{*2} and μ_3', yielding the scale factors Z= SDEPHI = $\sqrt{\mu_1'/3}$ according to equ. (3) in the Addendum to Chapter IV.

Statements 17 to 10: compute maximum frequency of interest, WM.

Statements 10 to 3: Compute particle transfer functions G_p from equations(II.B.3.4 and .5) and (II.B.3.14).
GA in the program is the γ which appears in these equations.

SUBROUTINE FRESP2, Page 1.

```
      SUBROUTINE FRESP2(SDEPHI)
      COMMON/A/CA,CB,CC,NPR,NDUM,NT,SIGN,NPR2
      COMMON/D/W(1001),W2(1001),R2(1001),FILL(3003)
      COMMON/E/RB(1001),Z
      COMMON/F/DW,WM,NW,DWZ
      DIMENSION GMOD(1001),GARG(1001),GLOG(1001)
      COMPLEX OMEGA,GP,G,G2,C8,C9,C10,C11,C14,C15,YD
C     FINITE STAGE MODEL-CLOSED FORM.
C     OBTAINS MINUS IMAGINARY PART DIVIDED BY OMEGA.
      PI=3.141592653          $   C1=SQRT(PI)/2.
C     READ PARAMETERS IN MODEL.
      READ11,PHI,AH,VH,N
   11 FORMAT(3F10.0,I5)
      PRINT2,PHI,AH,VH,N
    2 FORMAT(1H1/*XPARAMETERS IN FINITE STAGE MODEL-CLOSED FORM */*XPHI
     C=*F10.2,5X*RIOT NUMBER=*E13.2,5X*VH=*F10.2,/10X*NO. OF STAGES=*I4)
C     COMPUTE NORMALISED MOMENTS OF G(T) AND OF E(1.-U(T))
C     NORMALISED VARIANCE.
      CORR1=VH/(VH+1.)        $   CORR4=CORR1*CORR1$   CORR2=1.+AH/5.
      CORR3=(2.*AH*AH+14.*AH+35.)/35.
      VAR=1./N+2.*CORR2*CORR4/PHI
C     NORMALISED THIRD CUMULANT.
      SKEW=2./(N*N)+6.*CORR2*CORR4/(N*PHI)+6.*CORR3*CORR4*CORR1/(PHI*PHI)
     1)
      SDG=SQRT(VAR)           $   AMU2=VAR+1.
      AMU3=SKEW+AMU2+2.*VAR   $   GAM2=SKEW/(VAR*VAR)
```

SUBROUTINE FRESP2. Page 2.

```
      VAREPHI=AMU3/3.          $   SDEPHI=SQRT(VAREPHI)
      SDIW=2./SDEPHI
C     PRINT MOMENTS.
      PRINT17,VAR,SKEW,GAM2,SDG,VAREPHI,SDEPHI,SDIW
   17 FORMAT(//5X*NORMALISED IMPULSE RESPONSE PARAMETERS*/*XVARIANCE=*E1
     13.5,10X*THIRD CUMULANT=*E13.5,/*XRATIO,GAMMA2=*E13.5,/20X*STANDARD
     2 DEVIATION OF IMPULSE RESPONSE=*F10.5,//5X*NORMALISED STEP RESPONS
     3E PARAMETERS*/*XVARIANCE OF EVEN PART OF PHI=*E13.5,10X*STD. DEVN.
     4=*E13.5,/*XFREQUENCY DOMAIN ESTIMATED STD. DEVN.=*F10.5)
C     COMPUTE MAXIMUM FREQUENCY VALUE.
      WM=SDIW*4.
C     SET UP W VALUES- NOTE W(I) NORMALISED WITH RESPECT TO (1+VH)*TH.
      DW=WM/(NW-1.)
      PRINT9,NW,DW,WM
    9 FORMAT(4/4X*NUMBER OF FREQUENCY VALUES=*I4,4X*W INCREMENT=*F10.5,4
     C/4X*MAXIMUM FREQUENCY NORMALISED WITH RESPECT TO 1+VH=*F10.3)
      W(1)=0                   $   DO10I=2,NW
   10 W(I)=W(I-1)+DW
      R2(1)=1.                 $   AK=PHI/VH
      DO1K=2,NW                $   OMEGA=W(K)*(0.,1.)/(1.+VH)
      IF(AH.EQ.0.)3,4
    4 C5=3.*W(K)*AH    /(2.*AK*(1.+VH))          $  GA=SQRT(C5)
      C6=COS(GA)               $   C7=SIN(GA)    $  C8=CMPLX(C6,-C7)
      C9=CMPLX(C6,C7)          $   C10=CMPLX(C7,C6)  $  C11=CMPLX(C7,-C6)
      C12=EXP(-GA)             $   C13=EXP(GA)
```

SUBROUTINE FRESP2. Page3.

```
      C14=(C12*CR+C13*C9)/(C12*C10+C13*C11)
      C15=(GA*(1.,-1.)*C14-1.)*AK/AH                    $   GP=AK/(AK+C15)
      GOTO5
    3 GP=AK/(AK+OMEGA)
    5 RYD=REAL(GP)              $   AIYD=AIMAG(GP)
      G=(N/(OMEGA+(1.-GP)*PHI     +N))**N
      IF(NPR2.EQ.1)12,8
   12 RG=REAL(G)                  $   AIG=AIMAG(G)     $  GMOD(K)=CABS(G)
      GARG(K)=ATAN2(AIG,RG)       $   GM=GMOD(K)       $  GLOG(K)=ALOG(GM)
      IF(GARG(K).GT.0.)7,8
    7 GARG(K)=GARG(K)-2.*PI
    8 G=-G/(OMEGA*(VH+1.))
    1 R2(K)=REAL(G)
      PRINT6,(W(I),R2(I),I=1,NW,4)
    6 FORMAT(//*XMINUS IMAGINARY PART OF FREQUENCY RESPONSE DIVIDED BY O
     CMEGA*/(4(10X*W*5X*-I(W)/W*10X)/(4(F11.4,F12.5,10X)))
C     PRINT OUT FREQUENCY RESPONSE IF DESIRED.
      IF(NPR2.EQ.1)13,14
   13 PRINT 15,(W(I),GLOG(I),GMOD(I),I=2,NW,4)
   15 FORMAT(//*XMAGNITUDE AND LOGMAGNITUDE RATIOS*//3(4X*OMEGA LOG. MOD
     C(G) *7X*MOD G*10X)/(3(F9.4,E13.5,XF12.5,9X)))
      GARG(1)=0.
      PRINT16,(W(I),GARG(I),I=1,NW,4)
   16 FORMAT(//*XPHASE SHIFTS*//4(4X*OMEGA*7X*ARG G*13X)/(4(F9.4,XF12.5,
     C12X)))
   14 RETURN
      END
```

2. Hermite Polynomial breakthrough Curve Program, FOURIN2 of Section IV.C.3.

General Description.

This program comprises the main, controlling program FOURIN2 and subroutines FRESP2, HERMITE, and INTERP. Subroutine HERMITE: using Z-multiplied frequency and time scales set up in FOURIN2, the subroutine evaluates coefficients a_{2n} of equation (IV.C.3.4) which are listed in Appendix 9, using equation (IV.C.3.3) and Simpson's 1/3rd rule. Hermite functions $H_{2n}(\omega).\exp(-\omega^2/4)$ are computed instead of Hermite polynomials, using recurrence relationships of equation (IV.C.3.2). H(1,I) represents the current even value of the Hermite function starting with $H_0(\omega)$ times $\exp(-\omega^2/4)$, whilst H(2,1) is the next (odd) Hermite function required for evaluating the next even Hermite function. FACT is the current value of (2n)! The value of RBAR(I) at each frequency is the approximation to $I(\omega)/\omega$ at frequency ω_1 of W(I), whilst ERINT(K) is the integral error-square of the K'th approximation.

After computing the frequency domain approximation up to statement 38, the inverse, E[1-u(t)] or G(I) is multiplied by 2, and converted to the step response u(t) in the main program. The corresponding time Hermite functions are called TH(1,I) and TH(2,I) in a similar way to H(1,I) and H(2,I) above.

Program FOURIN2

The main program uses FRESP2 to compute the scale factors Z, required to obtain a satisfactory approximation and also the maximum time value of interest as described in the Addendum to Chapter IV.

In obtaining the step response, G2(I) from twice the inverse of $I(\omega)/\omega$ as described above, the similarity theorem is first used :

$$G2(I) = 1. - G2(I)/Z.$$

Subroutine INTERP:

This a Lagrangian interpolation subroutine required to obtain , from ten points on the breakthrough curve in the vicinity of the required value, the times T^*_{05}, T^*_{10} , etc. Since interpolation is a fairly standard procedure, the subroutine is not listed here.

```
      PROGRAM FOURIN2(INPUT,TAPE 60=INPUT,OUTPUT)
C     MODIFIED TO COMPUTE SUITABLE VALUES OF SCALE FACTORS Z, FROM VARIANCE.
C     TIME SCALE NORMALISED WITH RESPECT TO (1.+VH)*TM.
C     USES LAGRANGIAN INTERPOLATION TO OBTAIN SPECIFIC TIMES.
C     PRINTS FREQUENCY RESPONSE IF REQUIRED.
C     CLOSED FORM FREQUENCY RESPONSE MODIFIED TO OBTAIN STEP RESPONSE
C     WITH ONE INVERSION.
C     MODIFIED TO ALLOW FOR VARIATIONS IN Z WITHOUT RECALLING FRESP2.
      COMMON/A/CA,CB,CC,NPR,N,NT,SIGN ,NPR2
      COMMON/B/H(2,1001),TH(2,201),ERINT(100)
      COMMON/C/T2(201),ET2(201)
      COMMON/D/W(1001),W2(1001),R2(1001),EW(1001),EW2(1001),E(1001)
      COMMON/E/RR(1001),Z
      COMMON/F/DW,WM,NW,DWZ
      COMMON/G/T(201),B(100),G2(201)
      DIMENSION R(20),FO(20)
      DIMENSION ZA(20),F(201),X(20)
C     SET UP CONSTANTS
      PI=3.141592653          $   CA=SQRT(PI)        $   CB=1/CA
      CC=SQRT(2.)*CB
C     READ PRINT AND PLOT PARAMETERS
C     READ NUMBER OF TERMS REQUIRED IN POLYNOMIAL,NUMBER OF FREQ. POINTS.
      READ1,NPR,NPR2,N,NW
C     NPR2=1 IF FREQUENCY RESPONSE TO BE PRINTED.
C     NPR=1 IF EACH WEIGHTED HERMITE POLYNOMIAL IS TO BE PRINTED
    1 FORMAT(10I5)
C     READ NUMBER OF TIME INCREMENTS.
   22 READ1,NT
      IF(EOF,60)2,3
    3 CALL FRESP2(SDEPHI)   $   NZ=1
      ZA(1)=SDEPHI
      TM=3.5*SDEPHI
      DO5K1=1,NZ              $   Z=ZA(K1)
C     DEFINE TIME VALUES.
      DT=TM/NT                $   T(1)=T2(1)=0.     $   DTZ=DT/Z
      DO10I=2,NT              $   T(I)=T(I-1)+DT
```

```
C     SET UP Z- MULTIPLIED FREQUENCY SCALES
      DWZ=DW*Z                $   W2(1)=0.          $   DO6I=2,NW
    6 W2(I)=W2(I-1)+DWZ       $   PRINT23,Z
   23 FORMAT(*1SCALE FACTOR APPROXIMATION=*,F10.3)
C     CALCULATE COEFFICIENTS B(2K) K=0,1,2,...., RBAR, AND INVERSE
C     FOURIER TRANSFORM FOR R2
      CALL HERMITE
C     PRINT RBAR(W)
      PRINT 18,(W(I),RR(I),I=1,NW,4)
   18 FORMAT(*0HERMITE APPROXIMATION TO FREQUENCY RESPONSE*/
     C 4(*       OMEGA      R BAR*,10X)/(4(F11.4,F10.5,10X)))
C     DEFINE G2(T) FOR ORIGINAL RANGE OF T,SUBTRACT FROM 1.,AND PRINT AS
C     STEP RESPONSE, AND COMPUTE F FACTORS.
      DO19I=1,NT              $   IF(T(I).EQ.0.)GOTO7
      F1=SQRT(T(I))           $   F(I)=1./F1-F1     $  G2(I)=1.-G2(I)/Z
      GOTO19
    7 F(I)=0.  $   G2(I)=1.-G2(I)/Z
   19 CONTINUE
      PRINT11,(T(I),F(I),G2(I),I=1,NT,4)
   11 FORMAT(*XINVERSE OF HERMITE APPROXIMATION TO STEP RESPONSE*/4(4X*T
     CIME*3X*F FACTOR STEP RESP.*4X)/(4(F8.4,E11.4,F11.5,4X)))
C     CARRY OUT LAGRANGIAN INTERPOLATION TO OBTAIN T02,T05,T10,T20,T40,T50,
C     T60AND T80.
      R(1)=0.02$R(2)=0.05$R(3)=0.10$R(4)=0.20$R(5)=0.40$R(6)=0.50
      R(7)=0.64R(8)=0.8$R(9)=0.9$R(10)=0.95
      NR=10                   $   NI=5
      CALL INTERP(R,FO,T,G2,NR,NI,NT)
      DO12I=1,NR              $   IF(FO(I).LE.+0.)GOTO13
      F1=SQRT(FO(I))          $   F(I)=1./F1-F1     $   GOTO12
   13 F(I)=0.
   12 CONTINUE
      PRINT14,(R(I),FO(I),F(I),I=1,NR)
   14 FORMAT(4/,42X*INTERPOLATED VALUES*//18X*FRACTIONAL RESPONSE*5X*INT
     1ERPOLATED TIME*5X*INTERPOLATED F FACTOR*//,(26XF6.3,12XE13.5,13XE1
     21.4,//))
    5 CONTINUE
      GOTO22
    2 STOP
      END
```

PROGRAM FOURIN2, Page 3.

```
      COMMON/A/CA,CB,CC,NPR,N,NT,SIGN
      COMMON/B/H(2,1001),TH(2,201),ERINT(100)
      COMMON/C/T(201),ET(201)
      COMMON/D/W2(1001),W(1001),R(1001),EW2(1001),EW(1001),E(1001)
      COMMON/E/RBAR(1001),Z
      COMMON/F/DW,WM,NX,DX
      COMMON/G/T2(201),A(100),G(201)
      DIMENSION EM(100)
      EQUIVALENCE(NX,NY)
C     MAXIMUM ERROR FOUND FOR EACH PARTIAL SUM
C     ERROR DISTRIBUTION ALSO COMPUTED FOR PLOTTING
C     NOTE-ERROR INTEGRAL CARRIED OUT OVER ORIGINAL BANDWIDTH
C     DEFINE HERMITE POLYNOMIALS FOR ALL W FOR N TERMS
      EW(1)=ET(1)=1.          $   DO22I=2,NX
   22 EW(I)=EXP(-W(I)*W(I)/4.)
      DO23I=2,NT
   23 ET(I)=EXP(-T(I)*T(I))
      DO1K=1,N                $   IF(K.GT.1)GOTO2   $   DO3I=1,NY
      H(1,I)=EW(I)            $   H(2,I)=W(I)*EW(I)
    3 RBAR(I)=0.              $   FACT=1.           $   GOTO4
    2 L=2*K-2                 $   M=L-1             $   DO5I=1,NY
      H(1,I)=W(I)*H(2,I)-M*H(1,I)
    5 H(2,I)=W(I)*H(1,I)-L*H(2,I)
C     PRINT IF REQUIRED
      IF(NPR.NE.1)GOTO6
      PRINT7, L,(W(I),H(1,I),I=1,NY,5)
    7 FORMAT(6X,*HERMITE POLYNOMIAL H(N), N =*,I3/
     C 4(*   ARGUMENT      POLYNOMIAL*,4X)/(4(F11.5,E16.3,4X)))
    6 FACT=FACT*L*M
C     CALCULATE COEFFICIENTS A(2K) USING SIMPSONS ONE THIRD RULE
    4 X=0.                    $   DO9I=1,2          $   DO9J=I,NX,2
    9 X=X+2.*I*R(J)*H(1,J)
      A(K)=(X-R(1)*H(1,1)-R(NX)*H(1,NX))*DX/3.
```

```
      A(K)=CC*A(K)/FACT
      ERINT(K)=0.              $   DO11I=1,NY
      RBAR(I)=RBAR(I)+A(K)*H(1,I)
      E(I)=RBAR(I)-R(I)
   11 ERINT(K)=ERINT(K)+E(I)*E(I)*DX
C     FIND MAXIMUM ERROR
      BV=1E-12                 $   BV=E(1)          $   DO38I=2,NY
      PQ=ABS(E(I))
   38 BV=AMAX1(BV,PQ)          $   EM(K)=BV
C     CALCULATE INVERSE FOURIER TRANSFORM G
      IF(K.GT.1)GOTO13         $   SIGN=1.          $   DO14I=1,NT
      TH(1,I)=ET(I)            $   TH(2,I)=2.*T(I)*ET(I)
   14 G(I)=2.*CB*A(1)*ET(I)                         $   GOTO1
   13 SIGN=-SIGN               $   DO16I=1,NT
      TH(1,I)=2.*T(I)*TH(2,I)-M*TH(1,I)
      TH(2,I)=2.*T(I)*TH(1,I)-L*TH(2,I)
   16 G(I)=G(I)+2.*A(K)*SIGN*TH(1,I)*CB
    1 CONTINUE
C     PRINT COEFFICIENTS B(2K),ERROR INTEGRALS AND MAXIMUM ABSOLUTE ERROR
      PRINT17,N,(A(I),ERINT(I),EM(I),I=1,N)
   17 FORMAT(*XNUMBER OF TERMS IN APPROXIMATION=*,I3//*XCOEFFICIENTS OF
     CINTEGRATION,ERROR INTEGRAL AND MAXIMUM ABSOLUTE ERROR*//3(8X,*B(2K
     C)*,3X,*ERROR INT.*,4X,*MAX.ERROR*)//(9E13.3))
      RETURN
      END
```

3. Hermite Polynomial Fourier Transform Program for Experimental Pulse Data, Program DITRAN3.

General Description.

This program, with associated subroutines, DATAG and GENFT accepts pulse input and output data read off the experimental records with the 'OSCAR' curve reader. An example of the data is given on page 8 of the program listing. After normalising input and output pulses in DATAG, each pulse is approximated by a Hermite function series (in GENFT) and the coefficients of each are punched out on cards. The cards may then be accepted by the model-fitting program SEARCH and the approximations reconstructed. The input data may be used also in program MOMENTS (which is a simple extension of DATAG and therefore not listed here). Program MOMENTS computes, in addition to the first moments, as in DATAG, the second and third absolute andcentral moments and also by linear interpolation, the corrected flowrate from the calibration curves for the rotameters.

Explanatory Notes.

Program DITRAN3: Comments read at statement 9 include data used in MOMENTS but not in DATAG. Maximum normalised frequency ω^* of interest is assumed to be 12. (statement after No. 1)

Subroutine DATAG: At statement 3, ZER(I) represents

the time value in millimeters of recorder chart or minutes of the first non-zero reading recorded for the input pulse I=1, or the output pulse I=2. DT(I) is the increment between readings also in mm. or mins., whilst N(I) is the number of readings and NTC the number of thermocouples in thermopile. 'OSCAR' punches, for each data point, two values, the first of which is an 'X' co-ordinate (not read by the program) and the second of which (the 'Y' value) is read as G(J,I), corresponding to pulse no. I and time value T(J). These readings are adjusted for OSCAR baseline and No. of thermocouples in the 'DO' loop ending at statement 5. In the statements after 6, the first moment, in input time scale units is designated as YI1(I), whilst the zero'th moment, or area is YI(I). The first moment requires that the zero'th moment should be unity, hence statement 11. The estimated impulse response moment AMU is the difference between input and output moments and this value is used to normalise the time scale in the 'DO' loop to statement 2.

The scale factors Z(1) and Z(2) for the Hermite approximation are chosen, from experience to be 10/(maximum time recorded).

Having called GENFT to compute Hermite approximations to each pulse, GF, the estimated frequency response response transfer function is computed, using complex arithmetic, from the inverse convolution operation:

$$G(j\omega^*) = \frac{Y(j\omega^*)}{X(j\omega^*)}$$

Subroutine GENFT.

In the 'DO' loop to statement 1, the time scale for each pulse is multiplied by the appropriate scale factor Z. Even values of the Hermite function starting with $H_o(t).\exp(-t^2/4)$ are denoted by H(1,I), whilst even functions are H(2,I). Even coefficients, a_{2k} are A(K,1) and the odd coefficients A(K,2). In computing the Fourier transform, even values are used to compute GFBR(I,IC), the real values of $G(j\omega)$ whilst odd values are used to obtain GFBI(I,IC), the imaginary part.

In the DO loop terminating at statement 15, the Similarity Theorem is used to recover the Fourier transform of the original pulses.

PROGRAM DITRAN3, Page 1.

```
      PROGRAM DITRAN3(INPUT,TAPE 60=INPUT,OUTPUT,PUNCH)
C     MODIFIED TO PUNCH COEFFICIENTS TO SIX SIGNIFICANT FIGURES.
C     MODIFIED TO COMPUTE SCALE FACTORS AND TO OUTPUT PUNCH CARD DATA
C     IN COMPATIBLE FORM.  INPUT ALSO NOW COMPATIBLE WITH MOMENTS PROGRAM.
C     USES DIFFERING NUMBER OF TERMS FOR INPUT AND OUTPUT APPROXIMATIONS.
C     DITRAN2 MODIFIED TO ELIMINATE PLOT.
C     THIS MODIFICATION PRINTS ERROR IN FINAL TIME DOMAIN APPROXIMATION.
C     MODIFIED TO ACCEPT A NUMBER OF SETS OF DATA FROM OSCAR
      COMMON/A/CB,CC,NP,NTP(5),IFP,NPLOT,Z(2),M(2),NW,W(402)
      DIMENSION A(48)
C     SET CONSTANTS
      PI=3.141592653          $   CA=SQRT(PI)          $   CB=2.*CA
      CC=1./(SQRT(2.)*CA)
      READ1,M(1),M(2),IFP,NW
C     M(1)=NUMBER OF TERMS INPUT PULSE
C     M(2)=NUMBER OF TERMS OUTPUT PULSE.
C     PARAMETER-
C          IFP=1,2, OR 3 IF TRANSFORM IS TO BE EXPRESSED IN REAL AND
C          IMAGINARY FORM, MODULUS AND ARGUMENT FORM, OR IN BOTH FORMS
C     NW=NUMBER OF FREQUENCY VALUES.  WMAX=12.
    9 READ7,A
      IF(EOF,60)3,4
    7 FORMAT(8A10)
    4 PRINT8,A
    8 FORMAT(1H1/6(5X8A10/))
    1 FORMAT(16I5)
C     DEFINE FREQUENCY POINTS
      DW=12./NW               $   W(1)=0.              $   DOSI=2,NW
    5 W(I)=W(I-1)+DW
C     READ BOTH SETS OF EXPERIMENTAL VALUES FOR G(T) AND USE THEIR
C     TRANSFORMS TO CALCULATE THAT FOR THE BASIC TRANSFER FUNCTION
      CALL DATAG              $   GOTO9
    3 STOP
      END DITRAN3
```

```
      SUBROUTINE DATAG
      COMMON/A/CR,CC,NP,NTP(5),IFP,NPLOT,Z(2),M(2),NW,W(402)
      COMMON/D/X(502),YE(502),YA(502) ,E(502)
      COMMON/F/T(502,2),G(502,2),GNB(502)
      COMMON/G/GFR(402),GFBR(402),GFI(402),GFBI(402),GFM(402),GFBM(402),
     C GFA(402),GFBA(402)
      DIMENSION ZER(2),DT(2),N(2),YI(2),PULSE(2),YI1(2)
      COMPLEX GF
      INTEGER PULSE
      DATA PULSE/5HINPUT,6HOUTPUT/
C     READ IN TWO SETS OF EXPERIMENTAL VALUES FOR G(T) AND CALCULATE
C     THE FOURIER TRANSFORM OF THE BASIC TRANSFER FUNCTION
      PRINT1
    1 FORMAT(1H1/* DIRECT FOURIER TRANSFORM PROGRAM WITH EXPERIMENTAL DA
     CTA*/)
C     G(T) CONSISTS OF A SET OF INPUT DATA AND A SET OF OUTPUT DATA
      DO11I=1,2
      READ3,ZER(I),DT(I),N(I),NTC
    3 FORMAT(2F10.4,I3,I2)
      NT=N(I)
      READ4,BASE
      PRINT27, PULSE(I),NT,ZER(I),DT(I),BASE
   27 FORMAT(*0NUMBER OF *,A7,*DATA POINTS =*,I4,5X,*ZERO =*,F10.4,5X,
     C *INCREMENT =*,F10.4,5X,*BASE =*,F10.4)
      READ30,(G(J,I),J=1,NT)
   30 FORMAT(9(4X,F4.2),8X)
    4 FORMAT(8F10.4)
      DO5J=1,NT
C     REDEFINE DATA WITH RESPECT TO BASE AND ADJUST FOR NUMBER OF
C     THERMOCOUPLES.
      G(J,I)=G(J,I)-BASE
    5 G(J,I)=G(J,I)/NTC
```

```
C       DEFINE TIME VALUES - SPACED DT UNITS APART
        T(1,I)=ZER(I)              $   DO6J=2,NT
    6   T(J,I)=T(J-1,I)+DT(I)
C       NORMALISE INPUT AND OUTPUT DATA.
        YI(I)=YI1(I)=0.            $   DO7K=1,2          $   DO7J=K,NT,2
        YI1(I)=YI1(I)+2.*K*G(J,I)*J*DT(I)
    7   YI(I)=YI(I)+2.*K*G(J,I)
        YI1(I)=(YI1(I)-G(1,I)*DT(I)- G(NT,I)*DT(I)*NT)*DT(I)/3.
        YI(I)=(YI(I)-G(1,I)-G(NT,I))*DT(I)/3.
   11   YI1(I)=YI1(I)/YI(I)
C       COMPUTE FIRST MOMENT OF IMPULSE RESPONSE,NORMALISE TIME SCALE,COMPUTE
C       SCALE FACTORS AND NORMALISE DATA.
        AMU=YI1(2)-YI1(1)
        PRINT8,AMU,(YI1(I),I=1,2)
    8   FORMAT(//*XESTIMATED FIRST MOMENT OF IMPULSE RESPONSE=*E13.5,//*XF
         CIRST MOMENT  OF INPUT PULSE=*E13.5,/*XFIRST MOMENT OF OUTPUT PULSE
         C=*E13.5,/*XRESULTS EXPRESSED IN ORIGINAL TIME SCALE UNITS*)
        DO2I=1,2                   $   DT(I)=DT(I)/AMU  $ZER(I)=ZER(I)/AMU
        NT=N(I)                    $   T(1,I)=ZER(I)    $   YI(I)=YI(I)/AMU
        DO10J=2,NT                 $   T(J,I)=T(J-1,I)+DT(I)
   10   G(J,I)=G(J,I)/YI(I)        $   Z(I)=10./T(NT,I)
        PRINT9,PULSE(I),YI(I),(T(J,I),G(J,I),J=1,NT)
    2   CONTINUE
    9   FORMAT(*0STRENGTH OF *,A7,*PULSE =*,F10.4//4(20X,*T*,9X,*G(T)*)
         C //(4(F21.4,F13.5)))
        PRINT12,Z,AMU
   12   FORMAT(*1EXPANSION - COMPRESSION SCALE FACTORS ---*,5X,*INPUT DATA
         C*,F10.4,5X,*OUTPUT DATA*,F10.4 ,//*XFIRST MOMENT  OF IMPULSE=*E13.
         Z5)
C       CALCULATE FOURIER TRANSFORMS OF INPUT DATA AND OUTPUT DATA
   25   DO28I=1,2     $   PRINT29,PULSE(I)
   29   FORMAT(*ORESULTS FOR *,A7,*DATA*)
        CALL GENFT(I+1,N(I),DT(I))          $   NT=N(I)
C       PRINT ERROR(T) AGAINST T.
   28   PRINT 31,PULSE(I),(T(J,I),E(J),J=1,NT)
```

```
   31 FORMAT(///*XERROR IN*,A7,*APPROXIMATION*,//4(20X,*T*,9X,*E(T)*)
     C//(4(8XE13.3,F13.3)))
C      CALCULATE BASIC FOURIER TRANSFORM TRANSFER FUNCTION = FOURIER
C      TRANSFORM OF OUTPUT/FOURIER TRANSFORM OF INPUT
       DO16I=1,NW                  $    IF(GFR(I).EQ.0.AND.GFI(I).EQ.0)GOTO17
       GF=(GFBR(I)+(0.,1.)*GFBI(I))/(GFR(I)+(0.,1.)*GFI(I))
       GFR(I)=REAL(GF)             $    GFI(I)=AIMAG(GF)
   17  IF(IFP.EQ.1)GOTO16          $    IF(GFM(I).GT.0)GOTO18
       GFM(I)=1.5                  $    GOTO23
   18  GFM(I)=GFBM(I)/GFM(I)
   23  GFA(I)=GFBA(I)-GFA(I)
   16  CONTINUE
       NTP(I)=M                    $    NP=1
C      PRINT BASIC FOURIER TRANSFORM TRANSFER FUNCTION
       IF(IFP.EQ.2)GOTO19
       PRINT20
   20  FORMAT(*0BASIC FOURIER TRANSFORM TRANSFER FUNCTION IN REAL AND IMA
     CGINARY FORM*//4(*    OMEGA*,8X,*REAL*,8X,*IMAG.*)/)
       PRINT21, (W(I),GFR(I),GFI(I),I=1,NW)
   21  FORMAT(4(F9.4,F12.5,F13.5))
       IF(IFP.EQ.1)RETURN
   19  PRINT22
   22  FORMAT(*0BASIC FOURIER TRANSFORM TRANSFER FUNCTION IN MODULUS AND
     CARGUMENT FORM*//4(*    OMEGA*,5X,*MODULUS*,5X,*ARGUMENT*)/)
       PRINT21, (W(I),GFM(I),GFA(I),I=1,NW)
       RETURN
       END DATAG
```

```
      SUBROUTINE GENFT(LT,NT,DT)
      COMMON/A/CP,CC,NP,NTP(5),IFP,NPLOT,ZZ(2),M(2),NW,W(402)
      COMMON/D/X(502),YE(502),YA(502) ,E(502)
      COMMON/F/T(502,2),G(502,2),GNB(502)
      COMMON/G/GFBR(402,2),GFBI(402,2),GFBM(402,2),GFBA(402,2)
      DIMENSION ET(500),H(2,500),FAC(2),A(100,2),EW(400),WH(2,400)
      DIMENSION EI(100),EM(100)
      COMPLEX OMEGA
C     GENERATE APPROXIMATIONS TO G(T) AND ITS FOURIER TRANSFORM
      IC=LT-1                    $   Z=ZZ(IC)
      DO1I=1,NT                  $   T(I,IC)=T(I,IC)*Z
    1 ET(I)=EXP(-T(I,IC)*T(I,IC)/4.)   $  EW(1)=1.
      DO14I=2,NW                 $   W(I)=W(I)/Z
   14 EW(I)=EXP(-W(I)*W(I))      $   MDO=M(IC)
      DO2K=1,MDO                 $   IF(K.GT.1)GOTO3
      DO4I=1,NT
      H(1,I)=ET(I)               $   H(2,I)=T(I,IC)*ET(I)
    4 GNB(I)=0.                  $   FAC(1)=FAC(2)=1.  $   GOTO6
    3 LA=2*K-3                   $   LB=LA+1           $   LC=LB+1
      FAC(1)=FAC(1)*LA*LB        $   FAC(2)=FAC(2)*LB*LC
      DO5I=1,NT
      H(1,I)=T(I,IC)*H(2,I)-LA*H(1,I)
    5 H(2,I)=T(I,IC)*H(1,I)-LB*H(2,I)
C     CALCULATE COEFFICIENTS A(2K),B(2K+1),K=0,1,2,...
    6 DO7L=1,2                   $   X=0.              $   DO8I=1,2
      DO8J=I,NT,2
    8 X=X+2.*I*G(J,IC)*H(L,J)
      A(K,L)=(X-G(1,IC)*H(L,1)-G(NT,IC)*H(L,NT))*DT*Z/3.
    7 A(K,L)=A(K,L)*CC/FAC(L)
C     CALCULATE GNBAR(T) FOR ALL T
      EI(K)=0.                   $   DO9I=1,NT         $   DO35L=1,2
   35 GNB(I)=GNB(I)+A(K,L)*H(L,I)      $  E(I)=GNB(I)-G(I,IC)
    9 EI(K)=EI(K)+(GNB(I)-G(I,IC))*(GNB(I)-G(I,IC))*DT
C     FIND MAXIMUM ERROR.
      BV=1E-12     $   BV=E(1)
      DO38I=2,NT   $   PQ=ABS(E(I))
```

```
   38 BV=AMAX1(BV,PQ)
      EM(K)=BV
C     CALCULATE FOURIER TRANSFORM OF G(T)
      IF(K.GT.1)GOTO16          $   SIGN=1.
      DO17I=1,NW
      WH(1,I)=EW(I)             $   WH(2,I)=2.*W(I)*EW(I)
      GFBR(I,IC)=WH(1,I)*A(1,1)*CB
   17 GFBI(I,IC)=-WH(2,I)*A(1,2)*CB                  $   GOTO2
   16 SIGN=-SIGN                $   DO19I=1,NW
      WH(1,I)=2.*W(I)*WH(2,I)-LA*WH(1,I)
      WH(2,I)=2.*W(I)*WH(1,I)-LB*WH(2,I)
      GFBR(I,IC)=GFBR(I,IC)+SIGN*WH(1,I)*A(K,1)*CB
   19 GFBI(I,IC)=GFBI(I,IC)-SIGN*WH(2,I)*A(K,2)*CB
    2 CONTINUE
      PRINT10,MDO,((A(K,I),I=1,2),EI(K),EM(K),K=1,MDO)
   10 FORMAT(*0NUMBER OF TERMS IN APPROXIMATION =*,I3//
     C*0COEFFICIENTS OF INTEGRATION ERROR INTEGRAL AND MAXIMUM ABSOLUTE
     CERROR*//2(10X*A(2K)*,8X,*B(2K+1)*,3X,*ERROR INT.*,4X,*MAX.ERROR*)
     C//(2(2P,2E15.3,0P,2E13.3)))
      PUNCH18,((A(K,I),I=1,2),K=1,MDO)
   18 FORMAT(6(5P,E11.0,2X)2X)
      DO11I=1,NT                $   YE(I)=G(I,IC)
   11 X(I)=T(I,IC)=T(I,IC)/Z
      PRINT12, (X(I),GNB(I),I=1,NT)
   12 FORMAT(///* APPROXIMATION TO G(T)*//4(20X,*T*,5X,*GNBAR(T)*)//
     C (4(F21.4,F13.5)))
```

```
      DO15I=1,NW                    $    W(I)=W(I)*Z
      GFBR(I,IC)=GFBR(I,IC)/Z
      GFBI(I,IC)=GFBI(I,IC)/Z
      IF(IFP.EQ.1)GOTO15
      OMEGA=GFBR(I,IC)+(0.,1.)*GFBI(I,IC)
      GFBM(I,IC)=CABS(OMEGA)
      IF(GFBI(I,IC).EQ.0.AND.GFBR(I,IC).EQ.0)GOTO37
      GFBA(I,IC)=ATAN2(GFBI(I,IC),GFBR(I,IC))       $   GOTO15
   37 GFBA(I,IC)=0.
   15 CONTINUE
      IF(IFP.EQ.2)GOTO21
      PRINT22
   22 FORMAT(*0APPROXIMATION TO FOURIER TRANSFORM IN REAL AND IMAGINARY
     CFORM*//4(*     OMEGA*,8X,*REAL*,8X,*IMAG.*)/)
      PRINT23, (W(I),GFBR(I,IC),GFBI(I,IC),I=1,NW)
   23 FORMAT(4(F9.4,F12.5,F13.5))
      IF(IFP.EQ.1)GOTO13
   21 PRINT24
   24 FORMAT(*0APPROXIMATION TO FOURIER TRANSFORM IN MODULUS AND ARGUMEN
     CT FORM*//4(*     OMEGA*,5X,*MODULUS*,5X,*ARGUMENT*)/)
      PRINT23, (W(I),GFBM(I,IC),GFBA(I,IC),I=1,NW)
   13 CONTINUE
      RETURN
      END GENFT
```

```
  20   40    3  100
RUN 7-25.4.69.6.9MM PERSPEX,EPS=0.368.   OSCAR 62    L=3.3,Q=19.05 (47K)
P=12.5PSIG. 186MM/MIN.,B=762.,T=67., INPUT DELTA=OUTPUT DELTA=2.5MM=0.815SEC.,
I/P=3T/C.,SPAN 2.5MV.,O/P=4T/C., SPAN=1.0MV.

  12.5      67.       19.05     .368       6.9       3.3       3.77      762.
  2
  0.        .815     23 6
   1.01
929 101 923 179 917 336 911 426 904 470 899 498 893 526 886 538 880 363PI  0162
874 266 867 210 861 167 855 150 849 139 843 128 837 118 831 114 824 108PI  0262
818 104 813 101 805 100 805 102 805 099                                PI  0362
  0.        .815     15325
  0.
923 001 917 014 911 050 905 083 898 121 893 158 885 192 880 218 873 223PO  0162
867 218 860 215 855 205 849 201 843 193 836 185 831 181 824 176 819 167PO  0262
813 162 806 159 800 154 792 148 784 143 779 142 773 137 768 135 762 133PO  0362
755 127 750 125 743 122 737 122 732 116 724 115 719 113 713 111 705 105PO  0462
702 103 694 101 688 100 682 097 675 095 670 093 663 091 658 090 651 087PO  0562
644 085 639 082 633 080 625 077 620 075 614 073 608 071 601 069 595 067PO  0662
588 065 582 064 576 063 570 061 563 061 558 059 553 059 544 057 540 055PO  0762
533 055 526 054 521 052 513 052 508 051 499 048 495 045 489 045 483 044PO  0862
478 043 472 041 464 040 459 039 453 040 446 037 440 036 434 035 428 034PO  0962
422 033 415 033 411 031 403 031 399 027 393 027 385 025 380 023 374 023PO  1062
367 023 362 023 356 023 351 023 343 021 338 020 332 019 324 019 320 019PO  1162
313 018 305 018 301 015 293 015 288 015 281 015 275 014 268 014 263 014PO  1262
257 013 252 013 244 012 239 011 233 008 225 011 220 009 213 010 207 010PO  1362
201 007 195 007 187 007 181 005 176 005 171 006 163 005 157 005 151 005PO  1462
144 004 140 004 133 005 126 003 120 003 115 003 110 003 103 003 095 003PO  1562
091 003 083 003 078 003 071 003 064 002 059 003 053 002 045 001 041 001PO  1662
034-000 034 003 034 000 034 002 034 002 034 000 034 001 034 000 033 000PO  1762
```

4. PROGRAM DANCKW(Used in Computing Figure II.B.3.1)

General Description-

This program computes the (complex) ratio of the frequency response computed with the full Danckwerts' boundary conditions at inlet and outlet of the bed to the frequency response computed with the simplified conditions of Chao and Hoelscher, (Appendix 1.2). The ratio, denoted by R3 in the program, is printed out in real and imaginary form and in modulus form (MR3) for 17 frequency values. The modulus form is plotted in Figure II.B.3.1.

The Biot number is assumed to be zero so that the particle transfer function $G_p(j\omega)$ becomes:

$$G_p(j\omega) = \frac{K}{j\omega + K} = \frac{KV_H}{j\omega V_H + KV_H} ,$$

where KV_H in the program is written as PHI. The frequency scale chosen is $\omega^* = \omega(1+V_H)$ i.e., ω^* is normalised relative to the centre of mass of the impulse response. Hence, $j\omega V_H = j\omega^* . \frac{V_H}{1 + V_H}$ = OMEGA in the program.

The other ratio, called R1 refers to the frequency response transfer function computed with the incomplete Danckwerts' boundary conditions used in Appendix 7, i.e.,

$$G(j\omega^*) = R_1(j\omega^*) . G(j\omega^*)$$

where $G_1(\omega^* j)$ is defined by the Chao and Hoelscher equn., (AP.1.2.3) and

$$R_1(j\omega^*) = \frac{2}{1 + \sqrt{X}/Pe'}$$

Here, X is defined by equation (AP.1.1.13):

$$X = Pe'^2 + 4.Pe' \, (j\omega + KV_H(1-G_p))$$

$$\text{i.e., } X = Pe' + 4.Pe' \left\{ \frac{OMEGA}{V_H} + \frac{KV_H . OMEGA}{OMEGA + KV_H} \right\}$$

In computing $R_3(j\omega^*)$, equation AP.1.1.13 is written in the alternative form:

$$G(j\omega^*) = R_3(j\omega^*) \, . \, G_1(j\omega^*),$$

where $$R_3(j\omega^*) = \frac{4.Pe'.\sqrt{X}}{(Pe'+\sqrt{X})^2} \cdot \frac{1}{1 - \exp(\mp\sqrt{X}) . \left\{\frac{Pe'-\sqrt{X}}{Pe'-\sqrt{X}}\right\}^2}$$

The third ratio, R2, computed in the program has no theoretical significance.

```
C     PROGRAM TO COMPUTE COMPLEX CORRECTION FACTORS FOR DANCKWERTS
C     BOUNDARY CONDITIONS.
      DIMENSION W(17)
      COMPLEX OMEGA,PHI2,X,X1,R1,R2,CORRN,R3
      REAL N,MR1,MR2,MR3
      READ1,(W(I),I=1,17)
    1 FORMAT(16F5.0)
    2 READ1,PHI,PE,N,VH
      IF(EOF,60)3,4
    4 PED=N*PE                $FAC=PHI/PED          $   G=1.+1./VH
      PRINT5,PHI,PE ,N,VH
    5 FORMAT(1H1/5X*PHI=*F10.5,5X*PECLET NUMBER=*F5.2,//*XNUMBER OF STAG
     1ES=*F5.2,5X*HEAT CAPACITY RATIO=*F5.1,//)
      PRINT7
    7 FORMAT(10X*XFREQUENCY*3X*REAL R1*3X*IMAG.R1*4X*MOD.R1*3X*REAL R2*3
     2X*IMAG.R2*4X*MOD.R2*3X*REAL R3*3X*IMAG.R3*4X*MOD.R3*)
      DO6J=1,17             $   W1=W(J)/G          $   OMEGA=(0.,1.)*W1
      PHI2=OMEGA*(1./VH+PHI/(OMEGA+PHI))    $   X=PED*PED+4.*PED*PHI2
      X=CSQRT(X)            $   X1=X/PED           $   R1=2./(1.+X1)
      RR1=REAL(R1)          $   AR1=AIMAG(R1)      $   MR1=CABS(R1)
      R2=R1*R1*X1           $   RR2=REAL(R2)       $   AR2=AIMAG(R2)
      MR2=CABS(R2)          $   CORRN=(1.-X1)/(1.+X1)
      CORRN=CORRN*CORRN     $   CORRN=CORRN*CEXP(-X)
      CORRN=1./(1.-CORRN)   $   R3=R2*CORRN        $   RR3=REAL(R3)
      AR3=AIMAG(R3)         $   MR3=CABS(R3)
      PRINT8,W(J),RR1,AR1,MR1,RR2,AR2,MR2,RR3,AR3,MR3
    8 FORMAT(10X,10F10.5,//)
    6 CONTINUE
      Y=SQRT(PED*PED+4.*PED*PHI)                    $   YR1=2./(1.+Y/PED)
      YR2=YR1*YR1*Y/PED/(1-(1.-Y/PED)*(1.-Y/PED)/(1.+Y/PED)/(1.+Y/PED)*E
     1XP(-Y))
      F1=1.+ALOG(YR1)/PHI   $   F2=1.+ALOG(YR2)/PHI
      PRINT9,YR1,YR2,F1,F2
    9 FORMAT(///*XREAL CORRECTION FACTORS*//*XR1=*E13.5,10X*R2=*E13.5,//
     1/*XCORRESPONDING F FACTORS*//*XF1=*E13.5,10X*F2=*E13.5)
      GOTO2
    3 STOP
```

5. Sub-Program, CYL For Finite Cylinder Frequency Response Transfer Function. (Written by R.Wilkshe under direction

This subroutine evaluates the particle frequency response transfer function from the formulae given in the Appendix of Paper 1 In Appendix 3. It incorporates root finding by Newton's method to the obtain the roots of

$$\phi \cdot J'_o(\phi) + Bi \cdot J_o(\phi) = 0.,$$

and

$$\zeta \cdot \tan \zeta = Bi$$

where $J'_o(\phi)$ and $J_o(\phi)$ are the Bessel functions defined in the Paper.

In order to speed up root evaluation (which takes up much of the time of the program), the first six roots of each are read in using Carslaw and Jaeger's tabulations. It is necessary to stop root evaluation when:

for reasons of economy, the desired limit on computer time has been exceeded (statement 20)

or as at statement 14, the desired upper limit of 1000 roots has been exceeded

or as at statement 19, when $\Sigma\Sigma K_{rs}/\bar{T}$ is within 0.1% of the theoretical value of unity.

It was found that small errors in evaluating G_p using th convergence criterion above led to a much larger error in th overall transfer function G since, in effect, $G_p(S)$ is raise to the N'th power where N is the bed length, particularly as frequency tends to zero. Because of the excessive runnin time of this program, very few computations were performed.

Subroutine CYL, Page 1

```
      SUBROUTINE CYL
C  SUBROUTINE EVALUATES REAL PART OF FINITE STAGE FREQUENCY RESPONSE FOR
C  CYLINDRICAL PARTICLES.
      DIMENSION PHI(1000),ZETA(1000),PHI2(1000),ZETA2(1000),PHI3(1000),
     *  CZETA3(1000),K(4)
      COMMON/A/R(400),OMG(400),GOP(400),WMAX2,VH,AH,PH,N
      COMPLEX GOP,OMEGA,GN
      INTEGER WMAX2
      READ100,KA,LTMAX
  100 FORMAT(I2,I3)
C     LTMAX=MAXIMUM CENTRAL PROCESSOR TIME IN SECONDS TO BE SPENT ON
C     ROOT EVALUATION.
      PRINT 101,VH,AH,PH,N
  101 FORMAT(1H1,/10X*SUBROUTINE CYL*//5X*VH =*F10.3,5X*BIOT NUMBER AH =
     1*F10.3,5X*PHI =*F10.5,5X*NUMBER OF STAGES N =*I4)
      DO 1 I = 1,WMAX2
    1 GOP(I)=(0.,0.)
      XK=PH/VH $ ALPHA=XK/(3.*AH)
      AH2=AH*AH $ CONST=2.6666667*AH2*AH $ AH2PAH=AH2+AH
      PI=3.141592653          $   MARK=0              $   SIGMA=0.
      CONINV=1./CONST         $   CON=.0001*CONINV
      PRINT 102,XK,ALPHA
  102 FORMAT(5X,*HEAT TRANSFER PARAMETER K =* F15.8,5X,*DIFFUSIVITY PARA
     1METER ALPHA =*F15.8,/)
      READ 103,(PHI(I),I=1,6),(ZETA(I),I=1,6)
C     FIND START CP TIME
      CALL LTIME(K)           $   LT=K(1)
  103 FORMAT(6F10.4,/6F10.4)
      I=1
    3 IM1=I-1 $ IR=0
      IF(I.LE. 6)8,4
    4 Z1=ZETA(IM1)+PI
      GO TO 5
    8 Z1=ZETA(I)
    5 Z1G=GRATER(Z1)
```

```
      SINZ1=SIN(Z1G)
      COSZ1=COS(Z1G)
      Z2=Z1-(Z1*SINZ1-AH*COSZ1)/(Z1/COSZ1+SINZ1)
      IF(ABS(Z2-Z1).LT.5.E-5)10,6
    6 Z1=Z2
      IR=IR+1
      IF(IR.GE. 8)7,5
    7 PRINT 104,I,Z1,ZETA(IM1)
  104 FORMAT(X*ROOT EVALUATION ROUTINE ERROR AT I =*I3* FOR ZETA(I) -
     1ITERATION BOUND EXCEEDED*/10X*Z1= *F15.8,10X,*ZETA(I-1) =*F15.8)
      STOP
   10 ZETA(I)=Z2
      IR=0
      IF(I.LE. 6)9,15
   15 P1=PHI(IM1)+PI
      GO TO 11
    9 P1=PHI(I)
   11 CALL RES01JY(P1,B0P1,B1P1,Y0,Y1)
      P2=P1+(AH*P0P1-P1*B1P1)/(AH*B1P1+P1*B0P1)
      IF(ABS(P2-P1).LT.5.E-5)16,12
   12 P1=P2
      IR=IR+1
      IF(IR.GE. 8)13,11
   13 PRINT 106,I,P1,PHI(IM1)
  106 FORMAT(X*ROOT EVALUATION ROUTINE ERROR AT I =*I3* FOR PHI(I) -
     2 ITERATION BOUND EXCEEDED*/10X*P1 =* F15.8,10X,*PHI(I-1) = *F15.8)
      STOP
   16 PHI(I) =P2
   17 PHI2(I) =PHI(I)*PHI(I)  $ ZETA2(I) =ZETA(I)*ZETA(I)
      PHI3(I)=1./(PHI2(I)*(AH2+PHI2(I)))
      ZETA3(I)=1./(ZETA2(I)*(AH2PAH+ZETA2(I)))
```

```
      DO 19 J =1,I
      IIJ=I+1-J
      P2PZ2=ZETA2(IIJ)+PHI2(J)
      AP2Z2=ALPHA*P2PZ2
      TMRS=P2PZ2*PHI3(J)*ZETA3(IIJ)
      DO 18 KW=2,WMAX2        $   OMEGA=(0.,1.)*OMG(KW)
   18 GOP(KW)=GOP(KW)+TMRS*AP2Z2/(OMEGA    +AP2Z2)
   19 SIGMA=SIGMA+TMRS
      IF(ABS(SIGMA-CONINV).LT.CON)22,20
   20 CALL LTIME(K)           $   LTD=K(1)-LT
      IF(LTD.GT.LTMAX)2,14
    2 PRINT105,LTD,I
  105 FORMAT(X*SERIES DOES NOT CONVERGE BEFORE*I4*SECONDS CP TIME*/3X*I=
     C*I4)
      GOTO24
   14 IF(I-1000)21,23,23
   21 I=I+1
      GOTO 3
   22 MARK = MARK+1
      PRINT 108,I
  108 FORMAT(10X*SERIES CONVERGENCE LIMIT REACHED, I =*I3)
      IF(MARK-2)20,24,24
   23 PRINT 109
  109 FORMAT(X*SERIES DOES NOT CONVERGE BEFORE 1000 TERMS*)
   24 SIG = CONST*SIGMA
      PRINT110,SIG
  110 FORMAT(//10X*SIGMA K/TBAR=*E12.5)
      DO 25 KW=2,WMAX2        $   OMEGA=(0.,1.)*OMG(KW)
      GOP(KW)=CONST*GOP(KW)
      GN=N/(OMEGA    +(1.-GOP(KW))*PH+N)
      GN=GN**N
   25 R(KW)=REAL(GN)
      RETURN
      END
```

6. Program SEARCH

General Description

This program compares frequency responses (obtained in the form of coefficients in Hermite polynomial expansions from DITRAN3, subroutine GENFT) with theoretica frequency responses. Three integral errors are computed the main one of interest (referred to in chapter VII) being SC, the integral error square between either real parts of the predicted output pulses/as or, in this version, between the real parts of the estimated frequency response transfer functions.

Subroutines are DATAG2, which reconstructs the experimental frequency responses and MODEL2 which, in this case, computes the theoretical finite stage model and the corresponding error criteria.

It is believed that these programs should be self-explanatory, in view of earlier notes to the other program Subroutine MODEL2, referred to in the program, is merely another version of FRESP2 and is therefore not listed.

```
      PROGRAM SEARCH(INPUT,TAPE 60=INPUT,OUTPUT)
C     RECTANGULAR PARAMETER SEARCH PROGRAM ON BIOT NUMBER AND PHI
C     MODIFIED TO USE VARIANCE AS CONTROLLING PARAMETER.
C     FINITE STAGE MODEL IN CLOSED FORM.
C     MODIFIED TO ALLOW N TO BE REAL.
      COMMON/A/NW,W(402),Y(402),Y2(402),GMOD(402),GARG(402),EXGR(402),TH
     CGR(402)
      COMMON/B/AH(20),PHI(20,20),SIGSQ(20),SA(20,20),SB(20,20),SC(20,20)
     C,VH,DW
      REAL N
      DIMENSION A(32)
      READ3,NPSP,NW,WMIN,WMAX
C     PRINT EVERY NPSP-TH APPROXIMATION
C     N=NUMBER OF STAGES (MAY BE REAL IN THIS VERSION).
    3 FORMAT(2I5,6F10.0)
    1 READ8,A                    $   PRINT10,A
   10 FORMAT(1H1/4(5X8A10/))
    8 FORMAT(8A10)
      IF(EOF,60)2,17
C     DEFINE FREQUENCY POINTS,VH*OMEGA
   17 DW=(WMAX-WMIN)/NW          $   W(1)=WMIN          $   DO9I=2,NW
    9 W(I)=W(I-1)+DW             $   CALL DATAG2
C     IMAX = MAXIMUM NUMBER OF VALUES OF VARIANCE,PARAMETER I.
C     JMAX = MAXIMUM NUMBER OF VALUES OF BIOT NUMBER.,PARAMETER,J.
      READ3,IMAX,JMAX,VH,SIGSQ(1),AH(1),DELSIG,DELH,N
      NP=K=0
C     SET UP ARRAYS OF PARAMETERS FOR PARAMETER SEARCH
      DO5I=2,IMAX
    5 SIGSQ(I)=SIGSQ(I-1)+DELSIG
      DO6J=2,JMAX
    6 AH(J)=AH(J-1)+DELH
C     SET UP ARRAYS OF VALUES OF BIOT NUMBER,PHI.
      CORRN=VH/(1.+VH)           $   CORRN=CORRN*CORRN
      DO19I=1,IMAX               $   DO19J=1,JMAX
   19 PHI(I,J)=2.*CORRN*(1.+AH(J)/5.)/(SIGSQ(I)-1./N)
C     CARRY OUT PARAMETER SEARCH AND FIND MINIMUM ERRORS.
```

```
      SV1=SV2=1.E300
      DO4I=1,IMAX              $    DO4J=1,JMAX        $    NP=NP+1$    K=K+1
      CALL MODFL2(I,J,N)       $    SV1=AMIN1(SA(I,J),SV1)
      SV2=AMIN1(SB(I,J),SV2)$       IF (NP.NE.NPSP)GOTO4
      PRINT7,K,VH,N,SIGSQ(I),AH(J),PHI(I,J),SA(I,J),SB(I,J),SC(I,J)
    7 FORMAT(///*XTRIAL NUMBER*I3,3X*VH=*F10.2,*NUMBER OF STAGES=*F10.2,
     C/*XNORMALISED VARIANCE=*F11.5,5X*BIOT NUMBER=*E10.2,5X*KVH=*E13.5,
     C//*XMAGNITUDE RATIO-*/17X*INTEGRAL ERROR SQUARE=*E13.4,/7X*INTEGRA
     CL RELATIVE ERROR SQUARED=*E13.4,/*XREAL PART OF TRANSFER FUNCTIONS
     C-*/33X*INTEGRAL ERROR SQUARED=*E13.4)
      PRINT12,(W(L),Y(L),GMOD(L),L=1,NW)
   12 FORMAT(//*XMAGNITUDE RATIOS*//4(4X,*OMEGA*,6X,*MOD G*,2X,*THEOR.MO
     CDG*2X)/(4(F9.4,X2F11.5,2X)))
      PRINT11,(W(L),Y2(L),GARG(L),L=1,NW)
   11 FORMAT(//*XPHASE SHIFTS*//4(4X,*OMEGA*,6X,*ARG G*,4X,*TH.ARG G*2X)/
     C/(4(F9.4,X2F11.5,2X)))
      PRINT18,(W(L),EXGR(L),THGR(L),L=1,NW)
   18 FORMAT(//*XREAL PARTS OF FREQUENCY RESPONSE TRANSFER FUNCTIONS*//4
     C(4X*OMEGA*5X*REAL G*2X*TH. REAL G*2X)/(4(F9.4,X2F11.5,2X)))
      NP=0
    4 CONTINUE
C     PRINT SUMMARY OF RESULTS FOR BOTH ERROR CRITERIA
      PRINT16,SV1,SV2
   16 FORMAT(///2X*MINIMUM SIMPLE SUM OF ERROR SQUARE=*E12.4,//2X*MINIMU
     CM SUM OF RELATIVE ERROR SQUARE=*E12.4,//)
      PRINT10,A
      PRINT14,VH,N,K
   14 FORMAT(16X*SUMMARISED RESULTS*/*XHEAT CAPACITY RATIO=*F10.2,5X*NO.
     C OF STAGES=*F10.2,/12X*TOTAL NUMBER OF TRIALS=*I3,///16X*SIGMA SQU
     CARED*5X*BIOT NO.*10X*PHI*11X*SA*11X*SB*11X*SC*)
      PRINT13,((SIGSQ(I),AH(J),PHI(I,J),SA(I,J),SB(I,J),SC(I,J),I=1,IMAX
     C),J=1,JMAX)
   13 FORMAT((16X6E13.5))
      GOTO1
    2 STOP
      END SEARCH
```

PROGRAM SEARCH, Page 3.

```
      SUBROUTINE DATAG2
C     MODIFICATION OF DATAG1
      COMMON/A/NW,W(402),GFBR(402,2),GFBI(402,2),GR(402),RG(402)
      DIMENSION N(2),A(100,2),WH(2,400),EW(400),Z(2),PULSE(2)
      COMPLEX GM,GF
      INTEGER PULSE
      DATA PULSE/5HINPUT,6HOUTPUT/
C     SET CONSTANTS
      PI=3.141592653        $   CA=SQRT(PI)          $   CB=2.*CA
      CC=1./(SQRT(2.)*CA)
      DO1I=1,2              $   READ2,N(I),Z(I)      $   N1=N(I)
    2 FORMAT(I5,2F10.0)
      READ3,((A(K,IC),IC=1,2),K=1,N1)                $   IF(W(1).NE.0.)GOTO4
      EW(1)=1.              $   GOTO5
    4 EW(1)=EXP(-W(1)*W(1)/Z(I))
    5 DO6J=2,NW             $   W(J)=W(J)/Z(I)
    6 EW(J)=EXP(-W(J)*W(J)) $   DO7K=1,N1            $   IF(K.GT.1)GOTO8
    3 FORMAT(6(E11.0,2X)2X)
      SIGN=1.               $   DO9J=1,NW
      WH(1,J)=EW(J)         $   WH(2,J)=2.*W(J)*EW(J)
      GFBR(J,I)=WH(1,J)*A(1,1)*CB
```

```
 9 GFBI(J,I)=-WH(2,J)*A(1,2)*CB                    $    GOTO7
 8 SIGN=-SIGN              $    LA=2*K-3             $    LB=LA+1
   LC=LB+1                 $    DO10J=1,NW
   WH(1,J)=2.*W(J)*WH(2,J)-LA*WH(1,J)
   WH(2,J)=2.*W(J)*WH(1,J)-LB*WH(2,J)
   GFBR(J,I)=GFBR(J,I)+SIGN*WH(1,J)*A(K,1)*CB
10 GFBI(J,I)=GFBI(J,I)-SIGN*WH(2,J)*A(K,2)*CB
 7 CONTINUE
   DO11J=1,NW              $    W(J)=W(J)*Z(I)
   GFBR(J,I)=GFBR(J,I)/Z(I)
11 GFBI(J,I)=GFBI(J,I)/Z(I)
 1 CONTINUE
13 DO12I=1,NW
   GF    =(GFBR(I,2)+(0.,1.)*GFBI(I,2))/(GFBR(I,1)+(0.,1.)*GFBI(I,1))
   GR(I)=REAL(GF)          $    R=GR(I)             $    AI=AIMAG(GF)
   GFBR(I,1)=CABS(GF)      $    GFBR(I,2)=ATAN2(AI,R)
12 CONTINUE
   PRINT20,(PULSE(I),N(I),Z(I),I=1,2)
20 FORMAT(*XNUMBER OF TERMS IN *,A7,*APPROXIMATION=*I4,/*XSCALE FACTO
  CR=*F10.4,//)
   RETURN
   END DATAG2
```

7. Subprogram ECOND Used in Computing Equivalent Conductivity Model Time and Frequency Responses.

General Description.

This subroutine evaluates the equivalent conductivity model time and frequency response functions. The only parameter, apart from the normalised time and frequency values, is PE which is equivalent to Pe_a in the model.

Subroutine ECOND.

```
      SUBROUTINE ECOND(PE)
      COMMON/A/W(201),T(201),NT,NW
      COMMON/B/GMOD(201),GARG(201),THEO(201)
      COMMON/R/GRE(201),GRE(201),GRS(201),S1,S2,DELW
      COMPLEX OMEGA,G,CE
      GARG(1)=0.                $   GMOD(1)=1.
C     PART 1 EVALUATES FREQUENCY RESPONSE.
      CA=PE/2.                  $   CB=PE*PE          $   DO1I=2,NW
      OMEGA=(0.,1.)*W(I)        $   CE=CSQRT(CB+4.*PE*OMEGA)
      G=EXP(CA)*CEXP(-CE/2.)    $   AIG=AIMAG(G)      $   RG=REAL(G)
      GMOD(I)=CABS(G)           $   GARG(I)=ATAN2(AIG,RG)
      GRE(I)=RG
    1 CONTINUE
C     PART 2 COMPUTES STEP RESPONSE.
      DO7J=1,NT                 $   IF(T(J).EQ.0.)GOTO2
      CB=T(J)/PE                $   CB=2.*SQRT(CB)    $   IF(T(J)-1.)3,4,5
    3 CC=(1.-T(J))/CB           $   CALL ERF(CC,0.,CD,AH,ER)
      THEO(J)=1.-CD             $   GOTO6
    4 THEO(J)=1.                $   GOTO6
    5 CC=(T(J)-1.)/CB           $   CALL ERF(CC,0.,CD,AH,ER)
      THEO(J)=1.+CD
    6 CC=(1.+T(J))/CB           $  CALL ERF(CC,0.,ER,AH,CD)
      THEO(J)=(THEO(J)+EXP(CA)*CD)/2.           $   GOTO7
    2 THEO(J)=0.
    7 CONTINUE
      RETURN
      END ECOND
```

APPENDIX 7
DERIVATION OF F FACTORS

1. F - FACTORS FOR HEAT TRANSFER TO SPHERES OF UNIFORM SURFACE TEMPERATURE

i) Finite Stage Model

The derivation here is an alternative one to that of Epstein [1958], generalised to allow for varying effective axial dispersion Peclet number.

Writing a steady state balance over stage i, a distance iH from the bed inlet, where H is the distance between 'perfect mixers', the fluid temperatures δT_i are defined as deviations from the (assumed constant) particle surface temperature throughout the bed:

$$G\, c_f\, (\delta T_{i-1} - \delta T_i) = h_p \cdot a_p\, (1-\varepsilon)\, H\, T_i \qquad \ldots(7.1)$$

or substituting $KV_H = \dfrac{h_p}{Gc_f} \cdot a_p\, (1-\varepsilon)\, L = St.a_p\, (1-\varepsilon)\, N\, d_p$

where $L = N\, d_p = MH$,

$$\frac{\delta T_i}{\delta T_{i-1}} = \frac{1}{1 + KV_H/M}$$

For a bed of length L, i.e. for a bed of M perfect mixers in length,

$$\frac{\delta T_M}{\delta T_o} = \frac{1.}{[1 + KV_H/M]^M} \qquad \ldots(7.2)$$

where δT_o is the temperature perturbation of the 'zero'th' stage above the sphere surface temperature, i.e. the inlet fluid temperature referred to sphere temperature as datum.

For perfect plug flow, the usual 'LMTD' solution is obtained from:

$$\frac{d\delta T}{dz} + (KV_H)\ \delta T\ (z) = 0 \qquad \ldots(7.3)$$

with boundary condition

$$\lim_{z \to o} \delta T(z) = \delta T_o = \text{inlet temperature.}$$

where, as elsewhere, z is the distance from the bed inlet, normalised with respect to overall bed length.

The solution of equation (7.3) for z = 1, i.e. for $\delta T(z) \equiv \delta T_M$, becomes

$$\frac{\delta T_M}{\delta T_o} = \frac{1}{[\exp KV_H/M]^M} \qquad \ldots(7.4)$$

Equations (7.2) and (7.4) may forced into correspondence if KV_H in equations (7.3) and (7.4) is regarded as a 'pseudo' KV_H, $KV_{H\ calc}$ such that

$$F = \frac{KV_{H\ calc}}{KV_H} = \frac{St_{calc}}{St}$$

where KV_H and St refer to the 'true' values used in the finite stage solution. Hence equation (7.4) becomes

$$\frac{\hat{\delta}T_M}{\hat{\delta}T_o} = \frac{1}{[\exp F.\ KV_H/M]^M} \qquad \ldots(7.5)$$

Comparing equations (7.2) and (7.5) we obtain,

$$F = \ln [1 + KV_H/M] \ .\ \frac{1}{KV_H/M} \qquad \ldots(7.6)$$

Now, $$\frac{KV_H}{M} = St.ap\ (1-\varepsilon).\ \frac{N}{M}\ .\ d_p = 6St.(1-\varepsilon).\ \gamma$$

for $a_p = 6/d_p$

where γ is the ratio defined by Aris (section I.A.2)

i.e., for $Pe = 2/\gamma$, equation (I.A.2.3),

$$KV_H/M = 12\ St\ (1-\varepsilon)/Pe.$$

Hence
$$F = \frac{\ln [1 + 12St\ (1-\varepsilon)\ /Pe]}{12\ St\ (1-\varepsilon)\ /Pe} \qquad ...(7.7)$$

which is equation (III.A.2.3) of chapter III.

To show that equations (III.A.1.2) and (III.A.2.3) are identical, define, following Epstein:

$$R = \delta T_o/\delta T_M$$

so that equation (7.2) becomes

$$\ln R = M \ln [1 + KV_H/M]$$

i.e.
$$\frac{\ln R}{M} = \ln [1 + KV_H/M]$$

or
$$R^{1/M} = 1 + KV_H/M$$

Hence, from equation (7.6)

$$F = \frac{\ln R}{M.(R^{1/M} - 1)} \qquad ...(7.8)$$

which is equation (III.A.1.2) when $Pe = 2$ or $M = N$.

Equations (7.7) and (7.8) extend Epstein's solution to allow for variable Peclet number or number of effective mixing stages.

ii) Continuous Model with Danckwert's Boundary Conditions

The steady state two phase continuous model allowing for axial dispersion is obtained from equation (II.B.2.2) by setting $\partial T/\partial t = 0$,. Since T_S is assumed constant along the length of the bed,

$$\frac{\partial T}{\partial z} = \frac{\partial\, \delta T}{\partial z}$$, yielding:

$$\frac{d^2\delta T}{dz^2} - NPe\,\frac{d\delta T}{dz} - NPe.\ KV_H.\ \delta T(z) = 0 \qquad \ldots(7.9)$$

where as before

$$\delta T(z) = T(z) - T_S.$$

The general solution of equation (7.9) is

$$\delta T(z) = C_1.\ \exp\,(m_1 z) + C_2.\ \exp\,(m_2 z) \qquad \ldots(7.10)$$

where C_1 and C_2 are constants and m_1, m_2 are the roots of

$$m^2 - NPe.\ m - NPe.\ KV_H = 0$$

$$m_1 = \frac{NPe}{2} - \frac{1}{2}\sqrt{(N^2Pe^2 + 4\ NPe.\ KV_H)}$$

and m_2 is the positive root.

The exit condition

$$\lim_{z \to \infty} \delta T(z) = 0 \text{ or finite,}$$

(valid for long beds) yields $C_2 = 0$.

Assuming the Danckwerts' [1953] inlet condition where δT_o is the inlet temperature difference:

$$\delta T_o = \left[\ \delta T(z) - \frac{1}{NPe}\ .\ \frac{d\delta T}{dz}\ \right]_{z \to 0+}$$

we obtain by substitution,

$$C_1 = \frac{\delta T_i}{1 - m_1/(NPe)} = \delta T_i\ .\ \frac{NPe}{m_2}$$

Hence, from equation (7.10):

$$\frac{\delta T(z)}{\delta T_o} = \frac{\exp\,(m_1 z)}{1 - m_1\,/(NPe)} .$$

Setting $z = 1$ for bed outlet $\delta T(z) = \delta T_M$,

$$\frac{\delta T_M}{\delta T_o} = \frac{\exp m_1}{1 - m_1\,/(NPe)}$$

Comparing with the plug flow solution equation (7.4): i.e. with

$$\frac{\delta T_M}{\delta T_o} = \exp(-F.\ KV_H)$$

$$F\ KV_H = - m_1 + \ln\ [1 - m_1\,/(NPe)]$$

$$F = \left[\sqrt{\left[1+\frac{24}{Pe}.\ St\ (1-\varepsilon)\right]} - 1\right] . \frac{Pe}{12\ St\ (1-\varepsilon)} + C \quad \ldots(7.11)$$

The first term in equation (7.11) is the R.H.S. of equation III.A.2.4) and is independent of bed length whilst the second term, C, may be regarded as a correction for the Danckwerts' boundary condition where:

$$C = \ln\left\{\frac{1}{2}\left[\sqrt{\left[1+\frac{24}{Pe}.\ St(1-\varepsilon)\right]} + 1\right]\right\} . \frac{1}{6N\ St(1-\varepsilon)} \quad \ldots(7.12)$$

The correction term C decreases as bed length N increases. As an example of the size of the correction, take St = 0.1, N = 10, Pe = 2, ε = 0.33, Then $KV_H = 4$ and:

$$F = 0.85 + C$$

where $C = 0.017$.

In view of the uncertainty concerning actual physical conditions at the inlet to a bed it appears that such a small correction is unjustified.

2 Steady State Fluid-Wall Heat Transfer

In appendix 4, an approximate analysis of the effects of wall heat loss and thermal capacitance has been carried out assuming radial gradients in the bed to be neglibile. Point measurements within the experimental test section did not reveal significant temperature gradients.

Nonetheless the following calculations were carried out to test this assumption and incidentally to derive F factors for wall heat loss measurements in order to show that the magnitude of axial dispersion corrections are likely to be similar to corrections required for fluid-particle heat transfer.

The complete analytical solution to the problem of steady state wall heat transfer has been presented by Olbrich, Agnew and Potter [1966]* when fluid and solid temperatures are assumed equal, using the Danckwerts' boundary condition at the inlet:

$$\delta T(z,r) = \sum_{i=1}^{\infty} \psi_i(r) \cdot \phi_i(z) \qquad \ldots(7.13)$$

where r has been normalised with respect to bed radius and z with respect to bed length, and $T(z,r)$ is the bed temperature referred to the constant wall temperature as datum.

* The references to this section are listed at the end of the appendix.

$$\psi_i(r) = \frac{2\,b.\,J_o(n_i r)}{(b^2+n_i)\,J_o(n_i)} \qquad \ldots(7.14)$$

$$\phi_i(z) = \frac{\exp\,[-z\,NPe\,(\gamma_i-1)]}{\gamma_i} \qquad \ldots(7.15)$$

$$\text{and}\quad \gamma_i = \frac{1}{2}\left[1+\sqrt{\left(1+\frac{8\,n_i^2}{Pe_r.M_w Pe}\right)}\right] \qquad \ldots(7.16)$$

In equations (7.14), (7.15) and (7.16), b is defined by

$$b = \frac{h_w.M_w d_p}{2\,ke_r}\ ,$$

and ke_r is the equivalent radial conductivity in the bed.

The n_i are roots of

$$n_i\,J_1(n_i) - b.\,J_o(n_i) = 0 \qquad \ldots(7.17)$$

and Pe_r, the radial equivalent Peclet number, has bed radius $M_w d_p/2$ as characteristic dimension:

$$Pe_r = \frac{C_f.G.M_w d_p}{2\,ke_r} = \frac{b}{St_w} \qquad \ldots(7.18)$$

The average temperature across a section, $\overline{T}(z)$, is obtained from

$$\delta\overline{T}(z) = 2\int_0^1 r.\,\delta T(z,r)\,dr$$

$$= \sum_{i=1}^{\infty} \phi_i(z).\ [\psi_i(r)]_{r=1}.\ \frac{2b}{n_i^2} \qquad \ldots(7.19)$$

Definition of an F factor to account for axial conduction requires that equations (7.18) and (7.19) be satisfactorily approximated by the first term of the series, since from equations (7.15) and (7.16), this results in temperatures $\delta\overline{T}(z)$ and $\delta T(z,r)$ which are exponential functions of length z.

As pointed out by Kunii et al. [1968], this assumption is valid when the effective bed Biot number b approaches zero, i.e.when $M_w d_p$ is small and/or the ratio h_w/ke_r is small.

In this case $2b \simeq n_i^2$ and

$$\delta\bar{T}(z) \simeq \phi_1(z) \cdot \psi_1(r)\Big|_{r=1} = \delta T(z,r)\Big|_{r=1} \qquad \ldots(7.20)$$

i.e., the average bed temperature is equal to that at the bed periphery (r=1) and radial gradients are effectively absent.

A stringent condition for the first term of equation (7.19) to dominate the solution is set by

$$\lim_{b \to 0} \sum_{i=1}^{\infty} \frac{2b}{n_i^2} \cdot \psi_i(r)\Big|_{r=1} = \lim_{b \to 0} \sum_{i=1}^{\infty} \frac{4b^2}{n_i^2(b^2+n_i^2)}$$

$$= \lim_{b \to 0} \frac{4b^2}{n_1^2(b^2+n_1^2)} = 1 \qquad \ldots(7.21)$$

Equation (7.20) then becomes

$$\delta\bar{T}(z) = \frac{\exp\left[-z\, N\, Pe(\gamma_1 - 1)\right]}{\gamma_1} \qquad \ldots(7.22)$$

where

$$\gamma_1 = \lim_{b \to 0} \frac{1}{2}\left[\sqrt{\left(1 + \frac{8\, n_i^2}{Pe_r M_w Pe}\right)}\right]$$

$$= \frac{1}{2}\left[1 + \sqrt{\left(1 + \frac{16\, St_w}{M_w\, Pe}\right)}\right] \qquad \ldots(7.23)$$

A simple plug flow solution, assuming radial gradients to be absent except in the wall boundary region, may be obtained by solving equation (7.24) below with the usual simplified inlet boundary condition

$$\lim_{z \to 0} \delta T(z) = \delta T_o = \text{inlet temperature}$$

$$\frac{d\,\delta T}{dz} + \phi_w \cdot \delta T(z) = 0 \qquad \ldots(7.24)$$

where $\phi_w = \frac{4N}{M_w} \cdot St_w$,

and $M_w = d_T/d_p$.

It may be seen that equation (7.24) is identical to equation (7.3) with ϕ_w replacing KV_H. Similarly, for axial dispersion and/or conduction equation (7.9) is appropriate with ϕ_w replacing KV_H.

The solution of equation (7.24) is

$$\delta T(z) = \exp\left[-\phi_w . z\right]$$

which may be compared with equation (7.22) to yield

$$F = \left[\sqrt{\left(1 + \frac{16\ St_w}{M_w\ Pe}\right)} - 1\right] . \frac{M_w\ Pe}{8\ St_w} + C_w \qquad \ldots(7.25)$$

where in a similar way to before, C_w is a Danckwerts' boundary condition correction factor and the first term of equation (7.25) may be obtained from equation (7.11) substituting ϕ_w for KV_H i.e. replacing $6St(1-\varepsilon)$ by $4St_w / M_w$.

The correction factor decreases, as before, with increasing bed length, in this case N:

$$C_w = \frac{M_w}{4 .N.St_w} \cdot \ln \gamma_1 \qquad \ldots(7.26)$$

and despite the presence of M_w in the numerator decreases with increasing M_w since ln γ_1 decreases more rapidly than M_w increases. C_w is also identical with C of equation (7.12) if KV_H is replaced by $4St_w/Mw$.

Approximate values of b for typical situations may be estimated from the correlations of Kunii et al.

i.e., $$b = St_w . Pe_r$$

where $$St_w = 0.2\ Pr^{-2/3} . Re_p^{-0.20} \qquad 40 < Re_p < 800 \qquad ...(7.27)$$

and $$Pe_r = \frac{0.5\ M_w . Re_p . Pr}{12 + 0.084\ Re_p} \qquad 40 < Re_p < 8000 \qquad ...(7.28)$$

A few values of b/M_w have been calculated below, (extending the range of Re_p somewhat outside the valid range), to give an indication of the approximate values to be expected.

VALUES OF b/M_w ESTIMATED FROM EQUATIONS (7.27) and (7.28)

Re_p	b/M_w
40	.094
100	.176
400	.239
1000	.246
4000	.194
10000	.168

Using Carslaw and Jaeger's [1959] table of roots of equation (7.17) the value of $\frac{4\,b^2}{n_1^2\,(b^2 + n_1^2)}$ may be calculated for a number of values of b. As pointed out above, the condition

$$\frac{4\,b^2}{n_1^2\,(b^2+ n_1^2)} \simeq 1$$

leads to an identical F factor to that obtained when radial gradients are assumed absent. Hence provided this condition is satisfied, it may be assumed that radial gradients may be ignored or are very small.

Values of $4b^2 / [n_1^2\,(b^2 + n_1^2)]$ are tabulated in the following table. It may be seen that even when M_w is as high as 20 and Re_p = 10000, so that b ≃ 2.1, this condition is satisfied to 5%, i.e. for the present range of experimental parameters radial gradients are not likely to be of importance.

VALUES OF THE RADIAL CONTRIBUTION TO THE FIRST TERM IN EQUATION (7.19)

i.e. $\psi_1(r)\big]_{r=1} \cdot \frac{2b}{n_1^2}$

b	n_1	$\psi_1(r)\big]_{r=1} \cdot \frac{2b}{n_1^2}$
0	0	1.0000
.10	.3960	1.000
.20	.6170	.9990
.40	.8516	.9969
.60	1.0184	.9938
.80	1.1490	.9892
1.0	1.2558	.9842
2.0	1.5994	.9537

REFERENCES FOR APPENDIX 7.

CARSLAW, H.S. and JAEGER, J.C., 'Conduction of Heat in Solids', Second Edn.,Oxford,1959,p 493.

DANCKWERTS, P.V., Chem.Engineering Sci., 2 : 1 (1953)

KUNII, D., SUZUKI, M. and ONO, N., Jl. Chem.Engineering of Japan, 1 : 21 (1968)

OLBRICH, W.E., AGNEW, J.B. and POTTER, O.E., Trans.Instn.Chem.Engrs., 44: T207 (1966)

APPENDIX 8

DERIVATION OF MAXIMUM ERROR BOUNDS FOR DIRECT AND INVERSE FOURIER TRANSFORMATION.

The use of the Hermite polynomial approximation method for Fourier transformation and inversion yields an estimate of the integral error squared in both frequency and time domains and allows a plot of error in the approximation to be made

(i) against frequency for Fourier transform inversion as in chapter IV,

(ii) against time for transformation of pulse data as in chapters V and VII.

This information tells us nothing (except in a qualitative way) about the maximum error in the inverse for (i) or in the frequency domain for (ii).

The object of this appendix is to derive an inequality which relates the desired maximum error to the integral error squared. The derivation is not a rigorous one but appears to give realistic yet conservative estimates in the majority of cases.

(i) Transform Inversion.

It is assumed that for $|\omega| > \omega_e$ the real part of the transform to be inverted is effectively zero. In the Fourier transform computations of section IV.C.1 we define the integral

error square to be

$$\bar{\varepsilon}^2(\omega) = \int_0^{\omega_c} [R(\omega) - \bar{R}(\omega)]^2 \, d\omega$$

$$= \int_0^{\omega_c} [\varepsilon(\omega)]^2 \, d\omega \qquad \ldots(8.1)$$

where $R(\omega)$ is the real part of the transform to be inverted and by appendix 5

$$\mathcal{F}^{-1} R(\omega) = E [g(t)]$$

where E denotes the even part of and $g(t)$ is the time function to be obtained.

In a similar manner,

$$\mathcal{F}^{-1} \varepsilon(\omega) = E [\varepsilon(t)] \qquad \ldots(8.2)$$

where $\varepsilon(t)$ is the time distribution of error.

If the error were distributed uniformly over all frequencies, i.e. if

$$\varepsilon(\omega) = \varepsilon , \quad -\infty < \omega < \infty$$

then the time distribution of error $\varepsilon(t)$ would be a Dirac or delta function having infinite magnitude but area ε, i.e.

$$\varepsilon(t) = \varepsilon . \delta(t)$$

It seems reasonable therefore, to assume that if we <u>assume</u>

$$\varepsilon(\omega) = \begin{cases} \varepsilon , |\omega| < \omega_c \\ 0 , |\omega| > \omega_c \end{cases} \qquad \ldots(8.3)$$

then the time distribution will be a maximum. Bracewell[1965] has derived the inverse Fourier transform of a function having the form of equation (8.3). In the present definition of the Fourier transform (equ. II.A.2.3) which differs from Bracewell's we obtain

$$\mathcal{F}^{-1}\varepsilon(\omega) = \frac{\varepsilon.\omega_c}{\pi} \cdot \frac{\sin \omega_c t}{\omega_c t} = E\,[\varepsilon(t)] \qquad \ldots(8.4)$$

For the frequency domain error distribution implied by equation (8.3), $\bar{\varepsilon}^2(\omega)$ defined by equation (8.1) becomes

$$\bar{\varepsilon}^2(\omega) = \varepsilon^2 . \omega_c \qquad \ldots(8.5)$$

From equation (8.4), the maximum value of $\varepsilon(t)$ is given by

$$\varepsilon(t)_{max} = 2 . \frac{\varepsilon.\omega_c}{\pi} \qquad \ldots(8.6)$$

Substituting in equation (8.5) we obtain

$$\varepsilon(t)_{max} = \frac{2}{\pi} \sqrt{\omega_c . \bar{\varepsilon}^2(\omega)}$$

$$\text{or} \quad \varepsilon(t) \leq 0.637 \sqrt{[\ \omega_c . \bar{\varepsilon}^2(\omega)\ ]} \qquad \ldots(8.7)$$

where $\bar{\varepsilon}^2(\omega)$ is defined by equation (8.1).

(ii) Direct Fourier Transformation

We define in this case the integral error square of the time approximation $\bar{g}(t)$ to $g(t)$ by

$$\bar{\varepsilon}^2(t) = \int_0^{T_{max}} [\ g(t) - \bar{g}(t)\ ]^2\, dt$$

$$= \int_0^{T_{max}} [\ \varepsilon(t)\ ]^2 . dt \qquad \ldots(8.8)$$

where it is assumed that

$$g(t) = \bar{g}(t) = 0 \text{ for } t > T_{max}.$$

We wish to estimate the maximum error in either $R_\varepsilon(\omega)$ or $I_\varepsilon(\omega)$ the real and imaginary parts, respectively, of the Fourier transform of $\varepsilon(t)$.

Assuming in a similar manner to before that

$$\varepsilon(t) = \begin{cases} \bar{\varepsilon} & 0 < t < T_{max} \\ 0 & t > T_{max}, \\ & t < 0 \end{cases} \qquad \ldots(8.9)$$

We obtain $R_\varepsilon(\omega)$ from the Fourier transform of the even part of $\varepsilon(t)$

$$E\,\varepsilon(t) = \begin{cases} \varepsilon/2 & |t| < T_{max} \\ 0 & |t| > T_{max} \end{cases}$$

The resultant transform by the Reciprocity theorem may be obtained from equation (8.4) and is

$$R_\varepsilon(\omega) = 2\pi \cdot \varepsilon \cdot \frac{T_{max}}{\pi} \cdot \frac{\sin(T_{max}.\omega)}{T_{max}\ \omega} \qquad \ldots(8.10)$$

and has a maximum value :

$$R_\varepsilon(\omega)_{max} = 2\varepsilon \cdot T_{max} \qquad \ldots(8.11)$$

Equations (8.8) and (8.9) yield

$$\bar{\varepsilon}^2(t) = \varepsilon^2 . T_{max}$$

$$\text{i.e. } R_\varepsilon(\omega) \leq 2\sqrt{T_{max} . \bar{\varepsilon}^2(t)} \quad \ldots(8.12)$$

which is of a similar form to equation (8.7).

COEFFICIENTS, AND INTEGRAL ERRORS FOR HERMITE POLYNOMIAL EXPANSIONS OF BREAKTHROUGH CURVES FOR PARAMETER COMBINATIONS OF TABLE IV.C.5.1

For method of reconstruction, see section IV.C.6., or Program FOURIN2 in Appendix 6.

NOTE: alterations to Biot numbers in the tables were necessary because of an incorrect Format statement in the program. The values as altered are nonetheless correct.

BREAKTHROUGH CURVE COEFFICIENTS (Contd.)

PARAMETERS IN FINITE STAGE MODEL, VH=1000.
KVH= 25, BIOT NUMBER= 0, LENGTH N= 25, VARIANCE= 1.198E-01
STD. DEVN. OF IMPULSE RESPONSE= 3.462E-01, SCALE FACTOR IN APPROXN= .6787
MAXIMUM FREQUENCY IN INTEGRATION= 11.79 MAXIMUM TIME= 2.38
COEFFICIENTS OF HERMITE APPROXIMATION TO I(W)/W AND INTEGRAL SQUARE ERROR-

K	B(2K)	ERROR INT.	K	B(2K)	ERROR INT.	K	B(2K)	ERROR INT.
1	7.788E-01	1.002E-01	2	-1.979E-01	1.333E-03	3	6.552E-03	3.300E-05
4	-1.330E-04	1.686E-05	5	1.743E-05	1.464E-06	6	4.043E-07	7.206E-07
7	3.107E-08	1.375E-07	8	9.296E-10	3.744E-08	9	2.838E-11	7.670E-09
10	1.268E-14	7.541E-09	11	-3.946E-14	9.655E-09	12	-1.674E-15	5.825E-09
13	4.485E-18	6.119E-09	14	2.142E-18	5.902E-09	15	2.484E-20	4.904E-09
16	-1.911E-21	5.365E-09	17	-2.819E-23	4.473E-09	18	1.525E-24	4.808E-09
19	1.495E-26	4.295E-09	20	-1.072E-27	4.279E-09	21	-5.172E-31	4.255E-09

PARAMETERS IN FINITE STAGE MODEL, VH=1000.
KVH= 25, BIOT NUMBER= .10, LENGTH N= 25, VARIANCE= 1.214E-01
STD. DEVN. OF IMPULSE RESPONSE= 3.485E-01, SCALE FACTOR IN APPROXN= .6800
MAXIMUM FREQUENCY IN INTEGRATION= 11.76 MAXIMUM TIME= 2.38
COEFFICIENTS OF HERMITE APPROXIMATION TO I(W)/W AND INTEGRAL SQUARE ERROR-

K	B(2K)	ERROR INT.	K	B(2K)	ERROR INT.	K	B(2K)	ERROR INT.
1	7.794E-01	9.933E-02	2	-1.969E-01	1.337E-03	3	6.551E-03	3.742E-05
4	-1.529E-04	1.613E-05	5	1.710E-05	1.311E-06	6	3.670E-07	6.990E-07
7	3.060E-08	1.333E-07	8	9.088E-10	3.776E-08	9	2.863E-11	7.738E-09
10	2.889E-14	7.443E-09	11	-3.868E-14	9.561E-09	12	-1.669E-15	5.786E-09
13	3.826E-18	6.037E-09	14	2.120E-18	5.842E-09	15	2.516E-20	4.838E-09
16	-1.888E-21	5.300E-09	17	-2.834E-23	4.411E-09	18	1.507E-24	4.745E-09
19	1.508E-26	4.232E-09	20	-1.061E-27	4.221E-09	21	-6.660E-31	4.191E-09

BREAKTHROUGH CURVE COEFFICIENTS (Contd.)

PARAMETERS IN FINITE STAGE MODEL, VH=1000.
KVH= 50, BIOT NUMBER= 0, LENGTH N= 50, VARIANCE= 5.992E-02
STD. DEVN. OF IMPULSE RESPONSE= 2.448E-01, SCALE FACTOR IN APPROXN= .6286
MAXIMUM FREQUENCY IN INTEGRATION= 12.73 MAXIMUM TIME= 2.20
COEFFICIENTS OF HERMITE APPROXIMATION TO I(W)/W AND INTEGRAL SQUARE ERROR-

K	B(2K)	ERROR INT.	K	B(2K)	ERROR INT.	K	B(2K)	ERROR INT.
1	7.512E-01	1.453E-01	2	-2.371E-01	3.395E-03	3	8.455E-03	1.245E-03
4	1.143E-03	6.422E-05	5	3.192E-05	1.255E-05	6	-7.911E-07	9.709E-06
7	-1.043E-07	3.160E-06	8	-4.768E-09	5.895E-07	9	-1.196E-10	8.526E-08
10	1.262E-13	8.978E-08	11	1.628E-13	1.095E-07	12	5.952E-15	5.943E-08
13	-3.157E-17	6.620E-08	14	-7.622E-18	6.151E-08	15	-7.369E-20	5.163E-08
16	6.711E-21	5.607E-08	17	8.785E-23	4.682E-08	18	-5.257E-24	5.009E-08
19	-4.526E-26	4.497E-08	20	3.624E-27	4.441E-08	21	-9.974E-31	4.456E-08

PARAMETERS IN FINITE STAGE MODEL, VH=1000.
KVH= 50, BIOT NUMBER= .10, LENGTH N= 50, VARIANCE= 6.072E-02
STD. DEVN. OF IMPULSE RESPONSE= 2.464E-01, SCALE FACTOR IN APPROXN= .6293
MAXIMUM FREQUENCY IN INTEGRATION= 12.71 MAXIMUM TIME= 2.20
COEFFICIENTS OF HERMITE APPROXIMATION TO I(W)/W AND INTEGRAL SQUARE ERROR-

K	B(2K)	ERROR INT.	K	B(2K)	ERROR INT.	K	B(2K)	ERROR INT.
1	7.516E-01	1.445E-01	2	-2.365E-01	3.312E-03	3	8.399E-03	1.190E-03
4	1.117E-03	6.218E-05	5	3.178E-05	1.096E-05	6	-7.009E-07	8.734E-06
7	-9.823E-08	2.922E-06	8	-4.568E-09	5.638E-07	9	-1.170E-10	8.402E-08
10	1.965E-14	8.471E-08	11	1.556E-13	1.044E-07	12	5.819E-15	5.712E-08
13	-2.731E-17	6.285E-08	14	-7.383E-18	5.875E-08	15	-7.432E-20	4.905E-08
16	6.483E-21	5.339E-08	17	8.730E-23	4.446E-08	18	-5.083E-24	4.764E-08
19	-4.528E-26	4.266E-08	20	3.513E-27	4.222E-08	21	-2.209E-31	4.225E-08

BREAKTHROUGH CURVE COEFFICIENTS (Contd.)

PARAMETERS IN FINITE STAGE MODEL, VH=1000.
KVH= 100, BIOT NUMBER= 0, LENGTH N= 100, VARIANCE= 2.996E-02
STD. DEVN. OF IMPULSE RESPONSE= 1.731E-01, SCALE FACTOR IN APPROXN= .6031
MAXIMUM FREQUENCY IN INTEGRATION= 13.26 MAXIMUM TIME= 2.11
COEFFICIENTS OF HERMITE APPROXIMATION TO I(W)/W AND INTEGRAL SQUARE ERROR-

K	B(2K)	ERROR INT.	K	B(2K)	ERROR INT.	K	B(2K)	ERROR INT.
1	7.339E-01	1.812E-01	2	-2.605E-01	1.002E-02	3	1.178E-02	5.861E-03
4	2.411E-03	6.035E-04	5	2.252E-05	5.775E-04	6	-8.842E-06	2.219E-04
7	-5.722E-07	2.466E-05	8	-1.282E-08	5.713E-06	9	2.339E-10	4.933E-06
10	2.261E-11	1.480E-06	11	3.942E-13	6.861E-07	12	-1.427E-14	7.056E-07
13	-6.686E-16	3.305E-07	14	4.189E-18	3.631E-07	15	6.332E-19	2.380E-07
16	-2.983E-22	2.398E-07	17	-4.810E-22	1.806E-07	18	1.078E-24	1.858E-07
19	3.030E-25	1.430E-07	20	-2.602E-27	1.539E-07	21	-1.422E-28	1.216E-07

PARAMETERS IN FINITE STAGE MODEL, VH=1000.
KVH= 100, BIOT NUMBER= .10, LENGTH N= 100, VARIANCE= 3.036E-02
STD. DEVN. OF IMPULSE RESPONSE= 1.742E-01, SCALE FACTOR IN APPROXN= .6035
MAXIMUM FREQUENCY IN INTEGRATION= 13.26 MAXIMUM TIME= 2.11
COEFFICIENTS OF HERMITE APPROXIMATION TO I(W)/W AND INTEGRAL SQUARE ERROR-

K	B(2K)	ERROR INT.	K	B(2K)	ERROR INT.	K	B(2K)	ERROR INT.
1	7.341E-01	1.806E-01	2	-2.601E-01	9.865E-03	3	1.172E-02	5.746E-03
4	2.389E-03	5.806E-04	5	2.291E-05	5.537E-04	6	-8.647E-06	2.137E-04
7	-5.613E-07	2.385E-05	8	-1.275E-08	5.124E-06	9	2.160E-10	4.505E-06
10	2.181E-11	1.362E-06	11	3.943E-13	6.009E-07	12	-1.323E-14	6.284E-07
13	-6.478E-16	2.902E-07	14	3.353E-18	3.155E-07	15	6.046E-19	2.076E-07
16	3.216E-22	2.058E-07	17	-4.566E-22	1.558E-07	18	5.637E-25	1.585E-07
19	2.886E-25	1.220E-07	20	-2.185E-27	1.309E-07	21	-1.375E-28	1.025E-07

BREAKTHROUGH CURVE COEFFICIENTS (Contd.)

PARAMETERS IN FINITE STAGE MODEL, VH=1000.
KVH= 250, BIOT NUMBER= 0, LENGTH N= 250, VARIANCE= 1.198E-02
STD. DEVN. OF IMPULSE RESPONSE= 1.095E-01, SCALE FACTOR IN APPROXN= .5877
MAXIMUM FREQUENCY IN INTEGRATION= 13.61 MAXIMUM TIME= 2.06
COEFFICIENTS OF HERMITE APPROXIMATION TO I(W)/W AND INTEGRAL SQUARE ERROR-

K	B(2K)	ERROR INT.	K	B(2K)	ERROR INT.	K	B(2K)	ERROR INT.
1	7.219E-01	2.138E-01	2	-2.757E-01	2.204E-02	3	1.534E-02	1.499E-02
4	3.535E-03	3.685E-03	5	-1.382E-05	3.675E-03	6	-2.254E-05	1.365E-03
7	-1.302E-06	3.445E-04	8	-7.494E-09	3.375E-04	9	2.398E-09	1.856E-04
10	1.071E-10	5.915E-05	11	-8.554E-14	6.011E-05	12	-1.445E-13	4.524E-05
13	-2.774E-15	3.020E-05	14	1.197E-16	3.342E-05	15	3.895E-18	2.307E-05
16	-9.029E-20	2.621E-05	17	-3.329E-21	1.977E-05	18	7.453E-23	2.195E-05
19	1.940E-24	1.786E-05	20	-5.942E-26	1.880E-05	21	-6.082E-28	1.702E-05

PARAMETERS IN FINITE STAGE MODEL, VH=1000.
KVH= 250, BIOT NUMBER= .10, LENGTH N= 250, VARIANCE= 1.214E-02
STD. DEVN. OF IMPULSE RESPONSE= 1.102E-01, SCALE FACTOR IN APPROXN= .5878
MAXIMUM FREQUENCY IN INTEGRATION= 13.61 MAXIMUM TIME= 2.06
COEFFICIENTS OF HERMITE APPROXIMATION TO I(W)/W AND INTEGRAL SQUARE ERROR-

K	B(2K)	ERROR INT.	K	B(2K)	ERROR INT.	K	B(2K)	ERROR INT.
1	7.221E-01	2.134E-01	2	-2.755E-01	2.187E-02	3	1.530E-02	1.485E-02
4	3.523E-03	3.623E-03	5	-1.330E-05	3.615E-03	6	-2.237E-05	1.340E-03
7	-1.293E-06	3.344E-04	8	-7.658E-09	3.271E-04	9	2.360E-09	1.801E-04
10	1.056E-10	5.732E-05	11	-7.542E-14	5.816E-05	12	-1.422E-13	4.381E-05
13	-2.738E-15	2.921E-05	14	1.176E-16	3.233E-05	15	3.836E-18	2.231E-05
16	-8.859E-20	2.534E-05	17	-3.278E-21	1.912E-05	18	7.314E-23	2.122E-05
19	1.911E-24	1.727E-05	20	-5.836E-26	1.818E-05	21	-6.003E-28	1.645E-05

BREAKTHROUGH CURVE COEFFICIENTS (Contd.)

PARAMETERS IN FINITE STAGE MODEL, VH=1000.
KVH= 20, BIOT NUMBER= 0, LENGTH N= 25, VARIANCE= 1.398E-01
STD. DEVN. OF IMPULSE RESPONSE= 3.739E-01, SCALE FACTOR IN APPROXN= .6951
MAXIMUM FREQUENCY IN INTEGRATION= 11.51 MAXIMUM TIME= 2.43
COEFFICIENTS OF HERMITE APPROXIMATION TO I(W)/W AND INTEGRAL SQUARE ERROR-

K	B(2K)	ERROR INT.	K	B(2K)	ERROR INT.	K	B(2K)	ERROR INT.
1	7.863E-01	8.966E-02	2	-1.868E-01	1.456E-03	3	6.636E-03	1.201E-04
4	-3.473E-04	1.058E-05	5	1.417E-05	3.897E-07	6	-9.381E-08	3.490E-07
7	2.252E-08	4.294E-08	8	4.223E-10	2.217E-08	9	2.344E-11	3.751E-09
10	6.958E-14	3.281E-09	11	-2.163E-14	4.299E-09	12	-1.149E-15	2.651E-09
13	-8.823E-19	2.612E-09	14	1.346E-18	2.598E-09	15	1.946E-20	2.092E-09
16	-1.180E-21	2.314E-09	17	-2.056E-23	1.897E-09	18	9.441E-25	2.056E-09
19	1.128E-26	1.808E-09	20	-6.761E-28	1.822E-09	21	-1.324E-30	1.783E-09

PARAMETERS IN FINITE STAGE MODEL, VH=1000.
KVH= 20, BIOT NUMBER= .250, LENGTH N= 25, VARIANCE= 1.448E-01
STD. DEVN. OF IMPULSE RESPONSE= 3.805E-01, SCALE FACTOR IN APPROXN= .6992
MAXIMUM FREQUENCY IN INTEGRATION= 11.44 MAXIMUM TIME= 2.45
COEFFICIENTS OF HERMITE APPROXIMATION TO I(W)/W AND INTEGRAL SQUARE ERROR-

K	B(2K)	ERROR INT.	K	B(2K)	ERROR INT.	K	B(2K)	ERROR INT.
1	7.880E-01	8.725E-02	2	-1.842E-01	1.504E-03	3	6.683E-03	1.488E-04
4	-3.910E-04	9.965E-06	5	1.366E-05	4.899E-07	6	-2.219E-07	2.639E-07
7	2.000E-08	2.247E-08	8	2.388E-10	1.573E-08	9	2.042E-11	2.209E-09
10	4.163E-14	1.999E-09	11	-1.542E-14	2.618E-09	12	-9.106E-16	1.608E-09
13	-1.321E-18	1.564E-09	14	1.029E-18	1.568E-09	15	1.577E-20	1.251E-09
16	-8.993E-22	1.387E-09	17	-1.635E-23	1.133E-09	18	7.194E-25	1.230E-09
19	9.046E-27	1.077E-09	20	-5.179E-28	1.088E-09	21	-1.232E-30	1.060E-09

BREAKTHROUGH CURVE COEFFICIENTS (Contd.)

PARAMETERS IN FINITE STAGE MODEL, VH=1000.
KVH= 80, BIOT NUMBER= 0, LENGTH N= 100, VARIANCE= 3.495E-02
STD. DEVN. OF IMPULSE RESPONSE= 1.869E-01, SCALE FACTOR IN APPROXN= .6074
MAXIMUM FREQUENCY IN INTEGRATION= 13.17 MAXIMUM TIME= 2.13
COEFFICIENTS OF HERMITE APPROXIMATION TO I(W)/W AND INTEGRAL SQUARE ERROR-

K	B(2K)	ERROR INT.	K	B(2K)	ERROR INT.	K	B(2K)	ERROR INT.
1	7.369E-01	1.741E-01	2	-2.564E-01	8.236E-03	3	1.105E-02	4.574E-03
4	2.154E-03	3.749E-04	5	2.661E-05	3.388E-04	6	-6.638E-06	1.383E-04
7	-4.484E-07	1.718E-05	8	-1.171E-08	1.431E-06	9	5.529E-11	1.498E-06
10	1.427E-11	5.551E-07	11	3.809E-13	1.127E-07	12	-3.990E-15	1.446E-07
13	-4.486E-16	6.641E-08	14	-3.808E-18	4.548E-08	15	3.401E-19	4.131E-08
16	5.518E-21	2.340E-08	17	-2.328E-22	2.583E-08	18	-3.782E-24	1.598E-08
19	1.559E-25	1.681E-08	20	1.409E-27	1.283E-08	21	-9.226E-29	1.094E-08

PARAMETERS IN FINITE STAGE MODEL, VH=1000.
KVH= 80, BIOT NUMBER= .250, LENGTH N= 100, VARIANCE= 3.620E-02
STD. DEVN. OF IMPULSE RESPONSE= 1.903E-01, SCALE FACTOR IN APPROXN= .6084
MAXIMUM FREQUENCY IN INTEGRATION= 13.15 MAXIMUM TIME= 2.13
COEFFICIENTS OF HERMITE APPROXIMATION TO I(W)/W AND INTEGRAL SQUARE ERROR-

K	B(2K)	ERROR INT.	K	B(2K)	ERROR INT.	K	B(2K)	ERROR INT.
1	7.377E-01	1.724E-01	2	-2.554E-01	7.850E-03	3	1.088E-02	4.299E-03
4	2.094E-03	3.338E-04	5	2.740E-05	2.954E-04	6	-6.160E-06	1.229E-04
7	-4.213E-07	1.591E-05	8	-1.139E-08	1.040E-06	9	2.356E-11	1.087E-06
10	1.266E-11	4.484E-07	11	3.740E-13	7.401E-08	12	-2.181E-15	9.365E-08
13	-4.052E-16	5.077E-08	14	-5.124E-18	2.500E-08	15	2.855E-19	3.059E-08
16	6.436E-21	1.295E-08	17	-1.872E-22	1.915E-08	18	-4.562E-24	9.211E-09
19	1.286E-25	1.311E-08	20	2.077E-27	7.807E-09	21	-8.243E-29	9.072E-09

BREAKTHROUGH CURVE COEFFICIENTS (Contd.)

PARAMETERS IN FINITE STAGE MODEL, VH=1000.
KVH= 200, BIOT NUMBER= 0, LENGTH N= 250, VARIANCE= 1.398E-02
STD. DEVN. OF IMPULSE RESPONSE= 1.182E-01, SCALE FACTOR IN APPROXN= .5894
MAXIMUM FREQUENCY IN INTEGRATION= 13.57 MAXIMUM TIME= 2.06
COEFFICIENTS OF HERMITE APPROXIMATION TO I(W)/W AND INTEGRAL SQUARE ERROR=

K	B(2K)	ERROR INT.	K	B(2K)	ERROR INT.	K	B(2K)	ERROR INT.
1	7.233E-01	2.093E-01	2	-2.739E-01	2.002E-02	3	1.487E-02	1.340E-02
4	3.392E-03	2.991E-03	5	-7.629E-06	2.988E-03	6	-2.042E-05	1.091E-03
7	-1.190E-06	2.360E-04	8	-9.308E-09	2.275E-04	9	1.961E-09	1.275E-04
10	9.032E-11	3.992E-05	11	3.026E-14	3.963E-05	12	-1.174E-13	3.017E-05
13	-2.353E-15	1.982E-05	14	9.507E-17	2.202E-05	15	3.224E-18	1.513E-05
16	-7.084E-20	1.718E-05	17	-2.741E-21	1.293E-05	18	5.867E-23	1.435E-05
19	1.604E-24	1.165E-05	20	-4.726E-26	1.229E-05	21	-5.165E-28	1.107E-05

PARAMETERS IN FINITE STAGE MODEL, VH=1000.
KVH= 200, BIOT NUMBER= .250, LENGTH N= 250, VARIANCE= 1.448E-02
STD. DEVN. OF IMPULSE RESPONSE= 1.203E-01, SCALE FACTOR IN APPROXN= .5898
MAXIMUM FREQUENCY IN INTEGRATION= 13.56 MAXIMUM TIME= 2.06
COEFFICIENTS OF HERMITE APPROXIMATION TO I(W)/W AND INTEGRAL SQUARE ERROR=

K	B(2K)	ERROR INT.	K	B(2K)	ERROR INT.	K	B(2K)	ERROR INT.
1	7.237E-01	2.083E-01	2	-2.735E-01	1.956E-02	3	1.475E-02	1.304E-02
4	3.358E-03	2.840E-03	5	-6.188E-06	2.838E-03	6	-1.992E-05	1.033E-03
7	-1.164E-06	2.172E-04	8	-9.692E-09	2.059E-04	9	1.862E-09	1.160E-04
10	8.656E-11	3.616E-05	11	5.600E-14	3.566E-05	12	-1.113E-13	2.724E-05
13	-2.259E-15	1.781E-05	14	8.960E-17	1.981E-05	15	3.075E-18	1.359E-05
16	-6.653E-20	1.543E-05	17	-2.610E-21	1.161E-05	18	5.516E-23	1.289E-05
19	1.529E-24	1.045E-05	20	-4.456E-26	1.103E-05	21	-4.960E-28	9.920E-06

BREAKTHROUGH CURVE COEFFICIENTS (Contd.)

PARAMETERS IN FINITE STAGE MODEL, VH=1000.
KVH= 15, BIOT NUMBER= 0, LENGTH N= 25, VARIANCE= 1.731E-01
STD. DEVN. OF IMPULSE RESPONSE= 4.160E-01, SCALE FACTOR IN APPROXN= .7223
MAXIMUM FREQUENCY IN INTEGRATION= 11.08 MAXIMUM TIME= 2.53
COEFFICIENTS OF HERMITE APPROXIMATION TO I(W)/W AND INTEGRAL SQUARE ERROR=

K	B(2K)	ERROR INT.	K	B(2K)	ERROR INT.	K	B(2K)	ERROR INT.
1	7.973E-01	7.516E-02	2	-1.703E-01	1.849E-03	3	7.109E-03	3.143E-04
4	-5.769E-04	1.206E-05	5	1.278E-05	3.729E-06	6	-8.866E-07	1.359E-07
7	7.924E-09	9.799E-08	8	-9.151E-10	3.777E-09	9	3.639E-13	3.823E-09
10	-3.189E-13	1.627E-09	11	2.227E-14	1.915E-09	12	6.513E-16	1.345E-09
13	1.236E-18	1.306E-09	14	-9.886E-19	1.267E-09	15	-1.178E-20	1.052E-09
16	8.430E-22	1.157E-09	17	1.368E-23	9.590E-10	18	-6.849E-25	1.034E-09
19	-7.295E-27	9.192E-10	20	4.854E-28	9.206E-10	21	5.301E-31	9.095E-10

PARAMETERS IN FINITE STAGE MODEL, VH=1000.
KVH= 15, BIOT NUMBER= 0.50, LENGTH N= 25, VARIANCE= 1.864E-01
STD. DEVN. OF IMPULSE RESPONSE= 4.317E-01, SCALE FACTOR IN APPROXN= .7331
MAXIMUM FREQUENCY IN INTEGRATION= 10.91 MAXIMUM TIME= 2.57
COEFFICIENTS OF HERMITE APPROXIMATION TO I(W)/W AND INTEGRAL SQUARE ERROR=

K	B(2K)	ERROR INT.	K	B(2K)	ERROR INT.	K	B(2K)	ERROR INT.
1	8.014E-01	7.020E-02	2	-1.642E-01	2.033E-03	3	7.365E-03	3.848E-04
4	-6.378E-04	1.549E-05	5	1.340E-05	6.326E-06	6	-1.152E-06	2.629E-07
7	4.833E-09	2.488E-07	8	-1.437E-09	1.589E-08	9	-7.221E-12	1.280E-08
10	-5.561E-13	5.816E-09	11	3.865E-14	7.202E-09	12	1.309E-15	5.015E-09
13	4.264E-18	4.756E-09	14	-1.856E-18	4.680E-09	15	-2.452E-20	3.830E-09
16	1.571E-21	4.230E-09	17	2.744E-23	3.478E-09	18	-1.277E-24	3.764E-09
19	-1.485E-26	3.322E-09	20	9.121E-28	3.344E-09	21	1.615E-30	3.279E-09

BREAKTHROUGH CURVE COEFFICIENTS (Contd.)

PARAMETERS IN FINITE STAGE MODEL, VH=1000.
KVH= 30, BIOT NUMBER= 0, LENGTH N= 50, VARIANCE= 8.653E-02
STD. DEVN. OF IMPULSE RESPONSE= 2.942E-01, SCALE FACTOR IN APPROXN= .6509
MAXIMUM FREQUENCY IN INTEGRATION= 12.29 MAXIMUM TIME= 2.28
COEFFICIENTS OF HERMITE APPROXIMATION TO I(W)/W AND INTEGRAL SQUARE ERROR-

K	B(2K)	ERROR INT.	K	B(2K)	ERROR INT.	K	B(2K)	ERROR INT.
1	7.644E-01	1.224E-01	2	-2.186E-01	1.746E-03	3	7.155E-03	2.022E-04
4	4.320E-04	3.363E-05	5	2.493E-05	2.165E-06	6	6.755E-07	8.421E-08
7	9.924E-09	2.425E-08	8	-2.591E-10	1.757E-08	9	-2.183E-11	5.749E-09
10	-6.431E-13	1.492E-09	11	1.373E-15	1.572E-09	12	7.969E-16	1.218E-09
13	1.777E-17	7.395E-10	14	-5.336E-19	8.479E-10	15	-2.335E-20	5.641E-10
16	3.286E-22	6.354E-10	17	1.959E-23	4.702E-10	18	-2.682E-25	5.199E-10
19	-1.205E-26	4.081E-10	20	2.405E-28	4.405E-10	21	4.796E-30	3.754E-10

PARAMETERS IN FINITE STAGE MODEL, VH=1000.
KVH= 30, BIOT NUMBER= 0.50, LENGTH N= 50, VARIANCE= 9.319E-02
STD. DEVN. OF IMPULSE RESPONSE= 3.053E-01, SCALE FACTOR IN APPROXN= .6565
MAXIMUM FREQUENCY IN INTEGRATION= 12.19 MAXIMUM TIME= 2.30
COEFFICIENTS OF HERMITE APPROXIMATION TO I(W)/W AND INTEGRAL SQUARE ERROR-

K	B(2K)	ERROR INT.	K	B(2K)	ERROR INT.	K	B(2K)	ERROR INT.
1	7.674E-01	1.175E-01	2	-2.142E-01	1.575E-03	3	6.970E-03	1.085E-04
4	2.957E-04	2.957E-05	5	2.305E-05	2.661E-06	6	7.264E-07	2.570E-07
7	2.019E-08	1.019E-08	8	2.739E-10	7.445E-10	9	-4.298E-12	9.421E-10
10	-4.925E-13	6.488E-10	11	-1.726E-14	2.274E-10	12	-1.177E-16	1.479E-10
13	1.638E-17	2.675E-10	14	5.332E-19	1.537E-10	15	-7.784E-21	2.160E-10
16	-5.877E-22	1.748E-10	17	3.286E-24	1.984E-10	18	4.607E-25	1.735E-10
19	-3.102E-27	1.972E-10	20	-2.806E-28	1.647E-10	21	3.637E-30	1.978E-10

BREAKTHROUGH CURVE COEFFICIENTS (Contd.)

PARAMETERS IN FINITE STAGE MODEL, VH=1000.
KVH= 150, BIOT NUMBER= 0, LENGTH N= 250, VARIANCE= 1.731E-02
STD. DEVN. OF IMPULSE RESPONSE= 1.316E-01, SCALE FACTOR IN APPROXN= .5923
MAXIMUM FREQUENCY IN INTEGRATION= 13.51 MAXIMUM TIME= 2.07
COEFFICIENTS OF HERMITE APPROXIMATION TO I(W)/W AND INTEGRAL SQUARE ERROR-

K	B(2K)	ERROR INT.	K	B(2K)	ERROR INT.	K	B(2K)	ERROR INT.
1	7.256E-01	2.026E-01	2	-2.711E-01	1.717E-02	3	1.413E-02	1.119E-02
4	3.166E-03	2.123E-03	5	1.176E-06	2.123E-03	6	-1.729E-05	7.632E-04
7	-1.025E-06	1.309E-04	8	-1.137E-08	1.156E-04	9	1.380E-09	6.767E-05
10	6.803E-11	2.056E-05	11	1.776E-13	1.933E-05	12	-8.191E-14	1.511E-05
13	-1.797E-15	9.584E-06	14	6.310E-17	1.073E-05	15	2.346E-18	7.307E-06
16	-4.574E-20	6.275E-06	17	-1.972E-21	6.205E-06	18	3.921E-23	6.883E-06
19	1.164E-24	5.547E-06	20	-3.153E-26	5.880E-06	21	-3.947E-28	5.241E-06

PARAMETERS IN FINITE STAGE MODEL, VH=1000.
KVH= 150, BIOT NUMBER=0.50, LENGTH N= 250, VARIANCE= 1.864E-02
STD. DEVN. OF IMPULSE RESPONSE= 1.365E-01, SCALE FACTOR IN APPROXN= .5934
MAXIMUM FREQUENCY IN INTEGRATION= 13.48 MAXIMUM TIME= 2.08
COEFFICIENTS OF HERMITE APPROXIMATION TO I(W)/W AND INTEGRAL SQUARE ERROR-

K	B(2K)	ERROR INT.	K	B(2K)	ERROR INT.	K	B(2K)	ERROR INT.
1	7.265E-01	2.000E-01	2	-2.699E-01	1.617E-02	3	1.385E-02	1.043E-02
4	3.078E-03	1.854E-03	5	4.253E-06	1.853E-03	6	-1.617E-05	6.647E-04
7	-9.649E-07	1.041E-04	8	-1.193E-08	8.734E-05	9	1.191E-09	5.230E-05
10	6.072E-11	1.571E-05	11	2.234E-13	1.435E-05	12	-7.047E-14	1.137E-05
13	-1.616E-15	7.086E-06	14	5.288E-17	7.965E-06	15	2.063E-18	5.397E-06
16	-3.775E-20	6.102E-06	17	-1.724E-21	4.567E-06	18	3.170E-23	5.063E-06
19	1.022E-24	4.066E-06	20	-2.652E-26	4.320E-06	21	-3.548E-28	3.830E-06

BREAKTHROUGH CURVE COEFFICIENTS (Contd.)

PARAMETERS IN FINITE STAGE MODEL,VH=1000.
KVH= 50, BIOT NUMBER= 2,LENGTH N= 250, VARIANCE= 5.989E-02
STD. DEVN. OF IMPULSE RESPONSE= 2.447E-01, SCALE FACTOR IN APPROXN= .6285
MAXIMUM FREQUENCY IN INTEGRATION= 12.73 MAXIMUM TIME= 2.20
COEFFICIENTS OF HERMITE APPROXIMATION TO I(W)/W AND INTEGRAL SQUARE ERROR-

K	B(2K)	ERROR INT.	K	B(2K)	ERROR INT.	K	B(2K)	ERROR INT.
1	7.512E-01	1.453E-01	2	-2.371E-01	3.400E-03	3	8.467E-03	1.244E-03
4	1.143E-03	6.307E-05	5	3.162E-05	1.236E-05	6	-7.930E-07	9.508E-06
7	-1.033E-07	3.080E-06	8	-4.707E-09	5.747E-07	9	-1.180E-10	8.359E-08
10	1.196E-13	8.783E-08	11	1.606E-13	1.073E-07	12	5.887E-15	5.835E-08
13	-3.080E-17	6.490E-08	14	-7.535E-18	6.036E-08	15	-7.326E-20	5.064E-08
16	6.634E-21	5.501E-08	17	8.719E-23	4.592E-08	18	-5.199E-24	4.914E-08
19	-4.497E-26	4.410E-08	20	3.585E-27	4.357E-08	21	-8.837E-31	4.370E-08

PARAMETERS IN FINITE STAGE MODEL,VH=1000.
KVH= 50, BIOT NUMBER= 5,LENGTH N= 250, VARIANCE= 8.384E-02
STD. DEVN. OF IMPULSE RESPONSE= 2.896E-01, SCALE FACTOR IN APPROXN= .6489
MAXIMUM FREQUENCY IN INTEGRATION= 12.33 MAXIMUM TIME= 2.27
COEFFICIENTS OF HERMITE APPROXIMATION TO I(W)/W AND INTEGRAL SQUARE ERROR-

K	B(2K)	ERROR INT.	K	B(2K)	ERROR INT.	K	B(2K)	ERROR INT.
1	7.635E-01	1.240E-01	2	-2.201E-01	1.725E-03	3	7.013E-03	2.414E-04
4	4.677E-04	4.376E-05	5	2.832E-05	3.145E-06	6	8.123E-07	1.378E-07
7	1.245E-08	4.364E-08	8	-3.328E-10	3.250E-08	9	-2.901E-11	1.116E-08
10	-8.623E-13	3.139E-09	11	2.865E-15	3.375E-09	12	1.132E-15	2.598E-09
13	2.385E-17	1.654E-09	14	-8.112E-19	1.875E-09	15	-3.260E-20	1.274E-09
16	5.341E-22	1.435E-09	17	2.774E-23	1.076E-09	18	-4.386E-25	1.191E-09
19	-1.695E-26	9.479E-10	20	3.799E-29	1.016E-09	21	6.445E-30	8.824E-10

BREAKTHROUGH CURVE COEFFICIENTS (Contd.)

PARAMETERS IN FINITE STAGE MODEL, VH=1000.
KVH= 20, BIOT NUMBER= 5, LENGTH N= 100, VARIANCE= 2.096E-01
STD. DEVN. OF IMPULSE RESPONSE= 4.578E-01, SCALE FACTOR IN APPROXN= .7530
MAXIMUM FREQUENCY IN INTEGRATION= 10.62 MAXIMUM TIME= 2.64
COEFFICIENTS OF HERMITE APPROXIMATION TO I(W)/W AND INTEGRAL SQUARE ERROR=

K	B(2K)	ERROR INT.	K	B(2K)	ERROR INT.	K	B(2K)	ERROR INT.
1	8.099E-01	6.092E-02	2	-1.522E-01	2.319E-03	3	7.596E-03	5.643E-04
4	-7.690E-04	2.709E-05	5	1.435E-05	1.654E-05	6	-1.837E-06	1.116E-06
7	-3.328E-09	1.109E-06	8	-2.970E-09	1.134E-07	9	-2.850E-11	7.680E-08
10	-1.405E-12	3.417E-08	11	8.812E-14	4.321E-08	12	3.209E-15	3.072E-08
13	1.768E-17	2.808E-08	14	-4.458E-18	2.794E-08	15	-6.361E-20	2.263E-08
16	3.637E-21	2.511E-08	17	7.026E-23	2.048E-08	18	-3.025E-24	2.223E-08
19	-3.832E-26	1.949E-08	20	2.175E-27	1.972E-08	21	5.479E-30	1.919E-08

PARAMETERS IN FINITE STAGE MODEL, VH=1000.
KVH= 50, BIOT NUMBER= 0, LENGTH N= 250, VARIANCE= 4.392E-02
STD. DEVN. OF IMPULSE RESPONSE= 2.096E-01, SCALE FACTOR IN APPROXN= .6150
MAXIMUM FREQUENCY IN INTEGRATION= 13.01 MAXIMUM TIME= 2.15
COEFFICIENTS OF HERMITE APPROXIMATION TO I(W)/W AND INTEGRAL SQUARE ERROR=

K	B(2K)	ERROR INT.	K	B(2K)	ERROR INT.	K	B(2K)	ERROR INT.
1	7.422E-01	1.627E-01	2	-2.493E-01	5.899E-03	3	9.962E-03	2.920E-03
4	1.744E-03	1.676E-04	5	3.000E-05	1.218E-04	6	-3.768E-06	5.728E-05
7	-2.807E-07	9.781E-06	8	-9.006E-09	5.199E-07	9	-8.741E-11	1.354E-07
10	5.748E-12	1.848E-07	11	3.061E-13	8.154E-08	12	4.194E-15	3.388E-08
13	-2.087E-16	6.309E-08	14	-8.951E-18	3.791E-08	15	6.453E-20	4.603E-08
16	8.766E-21	4.015E-08	17	-8.385E-24	4.104E-08	18	-6.654E-24	3.801E-08
19	1.917E-26	4.017E-08	20	4.101E-27	3.483E-08	21	-3.852E-29	4.008E-08

BREAKTHROUGH CURVE COEFFICIENTS (Contd.)

PARAMETERS IN FINITE STAGE MODEL, VH=1000.
KVH= 20, BIOT NUMBER= 0, LENGTH N= 100, VARIANCE= 1.098E-01
STD. DEVN. OF IMPULSE RESPONSE= 3.314E-01, SCALE FACTOR IN APPROXN= .6702
MAXIMUM FREQUENCY IN INTEGRATION= 11.94 MAXIMUM TIME= 2.35
COEFFICIENTS OF HERMITE APPROXIMATION TO I(W)/W AND INTEGRAL SQUARE ERROR-

K	B(2K)	ERROR INT.	K	B(2K)	ERROR INT.	K	B(2K)	ERROR INT.
1	7.744E-01	1.065E-01	2	-2.040E-01	1.397E-03	3	6.749E-03	1.941E-05
4	1.707E-05	1.916E-05	5	1.837E-05	2.064E-06	6	5.678E-07	5.965E-07
7	2.859E-08	1.024E-07	8	8.384E-10	2.058E-08	9	2.020E-11	4.169E-09
10	-1.243E-13	5.141E-09	11	-3.600E-14	6.334E-09	12	-1.327E-15	3.723E-09
13	8.407E-18	4.165E-09	14	1.816E-18	3.903E-09	15	1.675E-20	3.344E-09
16	-1.652E-21	3.614E-09	17	-2.071E-23	3.065E-09	18	1.315E-24	3.265E-09
19	1.056E-26	2.962E-09	20	-9.108E-28	2.918E-09	21	7.117E-31	2.945E-09

PARAMETERS IN FINITE STAGE MODEL, VH=1000.
KVH= 20, BIOT NUMBER= 2, LENGTH N= 100, VARIANCE= 1.497E-01
STD. DEVN. OF IMPULSE RESPONSE= 3.869E-01, SCALE FACTOR IN APPROXN= .7033
MAXIMUM FREQUENCY IN INTEGRATION= 11.37 MAXIMUM TIME= 2.46
COEFFICIENTS OF HERMITE APPROXIMATION TO I(W)/W AND INTEGRAL SQUARE ERROR-

K	B(2K)	ERROR INT.	K	B(2K)	ERROR INT.	K	B(2K)	ERROR INT.
1	7.899E-01	8.481E-02	2	-1.815E-01	1.556E-03	3	6.724E-03	1.837E-04
4	-4.383E-04	9.267E-06	5	1.291E-05	7.933E-07	6	-3.664E-07	1.786E-07
7	1.674E-08	9.489E-09	8	2.543E-11	9.392E-09	9	1.662E-11	9.358E-10
10	1.235E-14	8.980E-10	11	-8.059E-15	1.154E-09	12	-6.241E-16	7.064E-10
13	-1.898E-18	6.644E-10	14	6.500E-19	6.788E-10	15	1.138E-20	5.306E-10
16	-5.639E-22	5.917E-10	17	-1.135E-23	4.783E-10	18	4.512E-25	5.219E-10
19	6.392E-27	4.522E-10	20	-3.292E-28	4.603E-10	21	-1.128E-30	4.436E-10

BREAKTHROUGH CURVE COEFFICIENTS (Contd.)

PARAMETERS IN FINITE STAGE MODEL;VH=1000.
KVH= 10, BIOT NUMBER= 2,LENGTH N= 50, VARIANCE= 2.994E-01
STD. DEVN. OF IMPULSE RESPONSE= 5.472E-01, SCALE FACTOR IN APPROXN= .8241
MAXIMUM FREQUENCY IN INTEGRATION= 9.71 MAXIMUM TIME= 2.88
COEFFICIENTS OF HERMITE APPROXIMATION TO I(W)/W AND INTEGRAL SQUARE ERROR-

K	B(2K)	ERROR INT.	K	B(2K)	ERROR INT.	K	B(2K)	ERROR INT.
1	8.294E-01	4.138E-02	2	-1.218E-01	3.776E-03	3	1.020E-02	6.139E-04
4	-7.647E-04	8.167E-05	5	3.466E-05	2.039E-05	6	-1.945E-06	3.046E-06
7	5.804E-08	1.006E-06	8	-2.759E-09	1.620E-07	9	6.563E-11	5.551E-08
10	-2.101E-12	1.350E-08	11	7.213E-14	2.887E-09	12	-8.418E-16	2.122E-09
13	2.721E-17	9.762E-10	14	-1.415E-18	4.463E-10	15	8.000E-21	5.132E-10
16	4.074E-22	5.626E-10	17	1.202E-23	4.238E-10	18	-6.057E-25	4.366E-10
19	-2.182E-27	4.138E-10	20	3.353E-28	4.072E-10	21	-3.038E-31	4.116E-10

PARAMETERS IN FINITE STAGE MODEL;VH=1000.
KVH= 10, BIOT NUMBER= 5,LENGTH N= 50, VARIANCE= 4.192E-01
STD. DEVN. OF IMPULSE RESPONSE= 6.475E-01, SCALE FACTOR IN APPROXN= .9215
MAXIMUM FREQUENCY IN INTEGRATION= 8.68 MAXIMUM TIME= 3.23
COEFFICIENTS OF HERMITE APPROXIMATION TO I(W)/W AND INTEGRAL SQUARE ERROR-

K	B(2K)	ERROR INT.	K	B(2K)	ERROR INT.	K	B(2K)	ERROR INT.
1	8.530E-01	2.508E-02	2	-8.629E-02	6.128E-03	3	1.349E-02	6.054E-04
4	-5.765E-04	3.010E-04	5	7.184E-05	3.830E-05	6	-9.747E-07	3.387E-05
7	2.187E-07	4.908E-06	8	9.764E-10	4.784E-06	9	3.732E-10	5.223E-07
10	-1.991E-12	6.131E-07	11	-4.303E-14	6.594E-07	12	-1.682E-14	3.340E-07
13	3.027E-17	3.469E-07	14	1.145E-17	3.695E-07	15	3.225E-19	2.701E-07
16	-1.324E-20	3.004E-07	17	-2.382E-22	2.492E-07	18	9.276E-24	2.722E-07
19	1.589E-25	2.329E-07	20	-7.383E-27	2.376E-07	21	-2.757E-29	2.285E-07

BREAKTHROUGH CURVE COEFFICIENTS (Contd.)

PARAMETERS IN FINITE STAGE MODEL, VH=1000.
KVH= 100, BIOT NUMBER= 2, LENGTH N= 250, VARIANCE= 3.194E-02
STD. DEVN. OF IMPULSE RESPONSE= 1.787E-01, SCALE FACTOR IN APPROXN= .6048
MAXIMUM FREQUENCY IN INTEGRATION= 13.23 MAXIMUM TIME= 2.12
COEFFICIENTS OF HERMITE APPROXIMATION TO I(W)/W AND INTEGRAL SQUARE ERROR-

K	B(2K)	ERROR INT.	K	B(2K)	ERROR INT.	K	B(2K)	ERROR INT.
1	7.351E-01	1.783E-01	2	-2.588E-01	9.260E-03	3	1.148E-02	5.308E-03
4	2.306E-03	4.976E-04	5	2.432E-05	4.673E-04	6	-7.900E-06	1.835E-04
7	-5.193E-07	2.101E-05	8	-1.241E-08	3.278E-06	9	1.509E-10	3.098E-06
10	1.883E-11	9.780E-07	11	3.918E-13	3.424E-07	12	-9.459E-15	3.857E-07
13	-5.695E-16	1.692E-07	14	3.649E-19	1.717E-07	15	4.985E-19	1.168E-07
16	2.517E-21	1.050E-07	17	-3.664E-22	8.305E-08	18	-1.265E-24	7.821E-08
19	2.353E-25	6.130E-08	20	-6.886E-28	6.376E-08	21	-1.197E-28	4.821E-08

PARAMETERS IN FINITE STAGE MODEL, VH=1000.
KVH= 10, BIOT NUMBER= 0, LENGTH N= 50, VARIANCE= 2.196E-01
STD. DEVN. OF IMPULSE RESPONSE= 4.686E-01, SCALE FACTOR IN APPROXN= .7597
MAXIMUM FREQUENCY IN INTEGRATION= 10.53 MAXIMUM TIME= 2.66
COEFFICIENTS OF HERMITE APPROXIMATION TO I(W)/W AND INTEGRAL SQUARE ERROR-

K	B(2K)	ERROR INT.	K	B(2K)	ERROR INT.	K	B(2K)	ERROR INT.
1	8.103E-01	5.989E-02	2	-1.505E-01	2.536E-03	3	8.179E-03	5.029E-04
4	-7.234E-04	2.745E-05	5	1.728E-05	1.219E-05	6	-1.587E-06	6.813E-07
7	6.963E-09	6.519E-07	8	-2.318E-09	4.685E-08	9	-1.133E-11	3.930E-08
10	-1.090E-12	1.567E-08	11	6.446E-14	1.925E-08	12	2.079E-15	1.391E-08
13	1.189E-17	1.271E-08	14	-3.049E-18	1.255E-08	15	-4.133E-20	1.023E-08
16	2.503E-21	1.134E-08	17	4.662E-23	9.259E-09	18	-2.057E-24	1.004E-08
19	-2.523E-26	8.823E-09	20	1.473E-27	8.912E-09	21	3.330E-30	8.695E-09

BREAKTHROUGH CURVE COEFFICIENTS (Contd.)

PARAMETERS IN FINITE STAGE MODEL, VH=1000.
KVH= 100, BIOT NUMBER= 0, LENGTH N= 250, VARIANCE= 2.396E-02
STD. DEVN. OF IMPULSE RESPONSE= 1.548E-01, SCALE FACTOR IN APPROXN= .5980
MAXIMUM FREQUENCY IN INTEGRATION= 13.38 MAXIMUM TIME= 2.09
COEFFICIENTS OF HERMITE APPROXIMATION TO I(W)/W AND INTEGRAL SQUARE ERROR=

K	B(2K)	ERROR INT.	K	B(2K)	ERROR INT.	K	B(2K)	ERROR INT.
1	7.300E-01	1.906E-01	2	-2.654E-01	1.284E-02	3	1.282E-02	7.921E-03
4	2.749E-03	1.087E-03	5	1.414E-05	1.076E-03	6	-1.228E-05	3.903E-04
7	-7.558E-07	4.619E-05	8	-1.292E-08	2.679E-05	9	6.251E-10	1.812E-05
10	3.844E-11	5.243E-06	11	3.386E-13	3.997E-06	12	-3.680E-14	3.421E-06
13	-1.063E-15	1.938E-06	14	2.332E-17	2.207E-06	15	1.215E-18	1.463E-06
16	-1.486E-20	1.629E-06	17	-9.844E-22	1.209E-06	18	1.301E-23	1.329E-06
19	5.958E-25	1.049E-06	20	-1.200E-26	1.126E-06	21	-2.314E-28	9.675E-07

PARAMETERS IN FINITE STAGE MODEL, VH=1000.
KVH= 100, BIOT NUMBER= 1, LENGTH N= 250, VARIANCE= 2.795E-02
STD. DEVN. OF IMPULSE RESPONSE= 1.672E-01, SCALE FACTOR IN APPROXN= .6014
MAXIMUM FREQUENCY IN INTEGRATION= 13.30 MAXIMUM TIME= 2.10
COEFFICIENTS OF HERMITE APPROXIMATION TO I(W)/W AND INTEGRAL SQUARE ERROR=

K	B(2K)	ERROR INT.	K	B(2K)	ERROR INT.	K	B(2K)	ERROR INT.
1	7.326E-01	1.842E-01	2	-2.621E-01	1.088E-02	3	1.212E-02	6.478E-03
4	2.520E-03	7.327E-04	5	1.977E-05	7.126E-04	6	-9.906E-06	2.663E-04
7	-6.275E-07	2.909E-05	8	-1.286E-08	9.962E-06	9	3.458E-10	7.773E-06
10	2.708E-11	2.253E-06	11	3.763E-13	1.317E-06	12	-2.056E-14	1.247E-06
13	-7.785E-16	6.304E-07	14	9.495E-18	7.142E-07	15	7.952E-19	4.659E-07
16	-4.317E-21	4.978E-07	17	-6.211E-22	3.692E-07	18	4.367E-24	3.958E-07
19	3.846E-25	3.064E-07	20	-5.196E-27	3.315E-07	21	-1.672E-28	2.722E-07

BREAKTHROUGH CURVE COEFFICIENTS (Contd.)

PARAMETERS IN FINITE STAGE MODEL, VH=1000.
KVH= 20, BIOT NUMBER= 1, LENGTH N= 50, VARIANCE= 1.398E-01
STD. DEVN. OF IMPULSE RESPONSE= 3.738E-01, SCALE FACTOR IN APPROXN= .6950
MAXIMUM FREQUENCY IN INTEGRATION= 11.51 MAXIMUM TIME= 2.43
COEFFICIENTS OF HERMITE APPROXIMATION TO I(W)/W AND INTEGRAL SQUARE ERROR=

K	B(2K)	ERROR INT.	K	B(2K)	ERROR INT.	K	B(2K)	ERROR INT.
1	7.861E-01	8.978E-02	2	-1.869E-01	1.475E-03	3	6.693E-03	1.169E-04
4	-3.432E-04	9.923E-06	5	1.373E-05	3.505E-07	6	-9.557E-08	3.083E-07
7	2.117E-08	3.768E-08	8	3.968E-10	1.935E-08	9	2.186E-11	3.315E-09
10	6.866E-14	2.879E-09	11	-2.033E-14	3.772E-09	12	-1.075E-15	2.330E-09
13	-8.764E-19	2.294E-09	14	1.262E-18	2.282E-09	15	1.824E-20	1.837E-09
16	-1.105E-21	2.032E-09	17	-1.928E-23	1.666E-09	18	8.845E-25	1.806E-09
19	1.058E-26	1.588E-09	20	-6.335E-28	1.600E-09	21	-1.244E-30	1.566E-09

PARAMETERS IN FINITE STAGE MODEL, VH=1000.
KVH= 20, BIOT NUMBER= 2, LENGTH N= 50, VARIANCE= 1.597E-01
STD. DEVN. OF IMPULSE RESPONSE= 3.997E-01, SCALE FACTOR IN APPROXN= .7115
MAXIMUM FREQUENCY IN INTEGRATION= 11.24 MAXIMUM TIME= 2.49
COEFFICIENTS OF HERMITE APPROXIMATION TO I(W)/W AND INTEGRAL SQUARE ERROR=

K	B(2K)	ERROR INT.	K	B(2K)	ERROR INT.	K	B(2K)	ERROR INT.
1	7.933E-01	8.036E-02	2	-1.764E-01	1.671E-03	3	6.850E-03	2.458E-04
4	-5.098E-04	9.799E-06	5	1.250E-05	1.847E-06	6	-6.167E-07	1.079E-07
7	1.205E-08	2.027E-08	8	-4.037E-10	2.113E-09	9	8.963E-12	2.329E-10
10	-1.154E-13	7.536E-11	11	5.999E-15	5.326E-12	12	-3.581E-17	6.484E-12
13	-1.094E-18	9.007E-12	14	-1.061E-19	5.220E-12	15	1.089E-21	6.708E-12
16	9.128E-23	6.180E-12	17	-1.367E-25	6.355E-12	18	-7.633E-26	5.959E-12
19	2.939E-28	6.358E-12	20	4.755E-29	5.614E-12	21	-4.879E-31	6.432E-12

PARAMETERS IN FINITE STAGE MODEL, VH=1000.
KVH= 10, BIOT NUMBER= 2, LENGTH N= 25, VARIANCE= 3.194E-01
STD. DEVN. OF IMPULSE RESPONSE= 5.652E-01, SCALE FACTOR IN APPROXN= .8399
MAXIMUM FREQUENCY IN INTEGRATION= 9.52 MAXIMUM TIME= 2.94
COEFFICIENTS OF HERMITE APPROXIMATION TO I(W)/W AND INTEGRAL SQUARE ERROR=

K	B(2K)	ERROR INT.	K	B(2K)	ERROR INT.	K	B(2K)	ERROR INT.
1	8.333E-01	3.817E-02	2	-1.159E-01	4.101E-03	3	1.072E-02	6.084E-04
4	-7.452E-04	1.026E-04	5	4.012E-05	2.055E-05	6	-1.852E-06	4.817E-06
7	7.989E-08	9.525E-07	8	-2.325E-09	3.586E-07	9	1.059E-10	5.179E-08
10	-2.093E-12	2.745E-08	11	5.711E-14	1.232E-08	12	-2.855E-15	3.137E-09
13	2.603E-17	3.638E-09	14	2.771E-19	3.794E-09	15	4.712E-20	2.298E-09
16	-1.304E-21	2.559E-09	17	-2.099E-23	2.186E-09	18	6.771E-25	2.386E-09
19	1.819E-26	1.978E-09	20	-6.465E-28	2.046E-09	21	-3.982E-30	1.928E-09

PARAMETERS IN FINITE STAGE MODEL, VH=1000.
KVH= 20, BIOT NUMBER= 0, LENGTH N= 50, VARIANCE= 1.198E-01
STD. DEVN. OF IMPULSE RESPONSE= 3.461E-01, SCALE FACTOR IN APPROXN= .6785
MAXIMUM FREQUENCY IN INTEGRATION= 11.79 MAXIMUM TIME= 2.37
COEFFICIENTS OF HERMITE APPROXIMATION TO I(W)/W AND INTEGRAL SQUARE ERROR=

K	B(2K)	ERROR INT.	K	B(2K)	ERROR INT.	K	B(2K)	ERROR INT.
1	7.785E-01	1.005E-01	2	-1.981E-01	1.373E-03	3	6.664E-03	2.887E-05
4	-1.225E-04	1.517E-05	5	1.656E-05	1.276E-06	6	3.843E-07	6.048E-07
7	2.846E-08	1.156E-07	8	8.556E-10	3.083E-08	9	2.564E-11	6.406E-09
10	8.606E-15	6.326E-09	11	-3.629E-14	8.088E-09	12	-1.529E-15	4.884E-09
13	4.265E-18	5.139E-09	14	1.964E-18	4.953E-09	15	2.260E-20	4.120E-09
16	-1.753E-21	4.506E-09	17	-2.573E-23	3.759E-09	18	1.399E-24	4.039E-09
19	1.363E-26	3.611E-09	20	-9.835E-28	3.596E-09	21	-4.294E-31	3.578E-09

PARAMETERS IN FINITE STAGE MODEL, VH=1000.
KVH= 10, BIOT NUMBER= 0, LENGTH N= 25, VARIANCE= 2.396E-01
STD. DEVN. OF IMPULSE RESPONSE= 4.895E-01, SCALE FACTOR IN APPROXN= .7758
MAXIMUM FREQUENCY IN INTEGRATION= 10.31 MAXIMUM TIME= 2.72
COEFFICIENTS OF HERMITE APPROXIMATION TO I(W)/W AND INTEGRAL SQUARE ERROR-

K	B(2K)	ERROR INT.	K	B(2K)	ERROR INT.	K	B(2K)	ERROR INT.
1	8.155E-01	5.445E-02	2	-1.428E-01	2.824E-03	3	8.640E-03	5.552E-04
4	-7.547E-04	3.759E-05	5	2.083E-05	1.543E-05	6	-1.777E-06	9.888E-07
7	1.466E-08	8.586E-07	8	-2.678E-09	5.327E-08	9	-2.442E-12	5.220E-08
10	-1.415E-12	1.735E-08	11	7.409E-14	2.002E-08	12	1.961E-15	1.529E-08
13	1.662E-17	1.351E-08	14	-3.233E-18	1.321E-08	15	-4.094E-20	1.087E-08
16	2.546E-21	1.205E-08	17	4.868E-23	9.808E-09	18	-2.128E-24	1.064E-08
19	-2.589E-26	9.351E-09	20	1.514E-27	9.448E-09	21	3.489E-30	9.214E-09

PARAMETERS IN FINITE STAGE MODEL, VH=1000.
KVH= 10, BIOT NUMBER= 1, LENGTH N= 25, VARIANCE= 2.795E-01
STD. DEVN. OF IMPULSE RESPONSE= 5.287E-01, SCALE FACTOR IN APPROXN= .8078
MAXIMUM FREQUENCY IN INTEGRATION= 9.90 MAXIMUM TIME= 2.83
COEFFICIENTS OF HERMITE APPROXIMATION TO I(W)/W AND INTEGRAL SQUARE ERROR-

K	B(2K)	ERROR INT.	K	B(2K)	ERROR INT.	K	B(2K)	ERROR INT.
1	8.247E-01	4.548E-02	2	-1.288E-01	3.443E-03	3	9.670E-03	6.008E-04
4	-7.684E-04	6.359E-05	5	2.963E-05	1.878E-05	6	-1.916E-06	1.974E-06
7	4.113E-08	9.489E-07	8	-2.788E-09	8.215E-08	9	3.810E-11	5.239E-08
10	-1.845E-12	1.125E-08	11	7.399E-14	5.980E-09	12	3.466E-16	5.805E-09
13	2.260E-17	4.222E-09	14	-2.195E-18	3.663E-09	15	-1.295E-20	3.282E-09
16	1.331E-21	3.635E-09	17	2.750E-23	2.913E-09	18	-1.257E-24	3.136E-09
19	-1.231E-26	2.801E-09	20	8.418E-28	2.813E-09	21	1.256E-30	2.766E-09

PARAMETERS IN FINITE STAGE MODEL, VH=1000.
KVH= 50, BIOT NUMBER= 0, LENGTH N= 100, VARIANCE= 4.992E-02
STD. DEVN. OF IMPULSE RESPONSE= 2.234E-01, SCALE FACTOR IN APPROXN= .6201
MAXIMUM FREQUENCY IN INTEGRATION= 12.90 MAXIMUM TIME= 2.17
COEFFICIENTS OF HERMITE APPROXIMATION TO I(W)/W AND INTEGRAL SQUARE ERROR-

K	B(2K)	ERROR INT.	K	B(2K)	ERROR INT.	K	B(2K)	ERROR INT.
1	7.457E-01	1.558E-01	2	-2.446E-01	4.761E-03	3	9.334E-03	2.144E-03
4	1.501E-03	1.067E-04	5	3.134E-05	5.678E-05	6	-2.384E-06	3.095E-05
7	-2.003E-07	6.773E-06	8	-7.332E-09	6.572E-07	9	-1.213E-10	6.384E-08
10	2.697E-12	1.417E-07	11	2.522E-13	1.244E-07	12	6.050E-15	5.754E-08
13	-1.175E-16	8.257E-08	14	-9.394E-18	6.637E-08	15	-2.118E-20	6.318E-08
16	8.683E-21	6.442E-08	17	5.665E-23	5.751E-08	18	-6.705E-24	5.895E-08
19	-2.222E-26	5.607E-08	20	4.396E-27	5.294E-08	21	-1.861E-29	5.602E-08

PARAMETERS IN FINITE STAGE MODEL, VH=1000.
KVH= 50, BIOT NUMBER= 1, LENGTH N= 100, VARIANCE= 5.790E-02
STD. DEVN. OF IMPULSE RESPONSE= 2.406E-01, SCALE FACTOR IN APPROXN= .6269
MAXIMUM FREQUENCY IN INTEGRATION= 12.76 MAXIMUM TIME= 2.19
COEFFICIENTS OF HERMITE APPROXIMATION TO I(W)/W AND INTEGRAL SQUARE ERROR-

K	B(2K)	ERROR INT.	K	B(2K)	ERROR INT.	K	B(2K)	ERROR INT.
1	7.501E-01	1.474E-01	2	-2.386E-01	3.640E-03	3	8.643E-03	1.395E-03
4	1.211E-03	6.746E-05	5	3.135E-05	1.758E-05	6	-1.078E-06	1.231E-05
7	-1.200E-07	3.627E-06	8	-5.171E-09	5.985E-07	9	-1.200E-10	7.844E-08
10	5.137E-13	9.645E-08	11	1.771E-13	1.132E-07	12	6.011E-15	5.992E-08
13	-4.448E-17	6.954E-08	14	-7.948E-18	6.331E-08	15	-6.661E-20	5.414E-08
16	7.063E-21	5.832E-08	17	8.405E-23	4.918E-08	18	-5.520E-24	5.231E-08
19	-4.227E-26	4.737E-08	20	3.772E-27	4.648E-08	21	-3.618E-30	4.703E-08

APPENDIX 10

CYCLIC METHOD ERROR ANALYSIS

1. INTRODUCTION

In this appendix some of the errors which may arise in application of the cyclic method of dynamic testing are analysed in detail. The analysis refers basically to the method which uses high frequency testing to obtain the limiting value predicted by the Rosen and Schumann models (Chapter II.B.4) i.e.:

$$\lim_{\omega \to \infty} |G(j\omega)| = \exp\left[-6NSt\,(1-\varepsilon)\right] \qquad \ldots(1.1)$$

Equation (1.1) may be used to determine the range of parameters N, St, ε for which such a limiting magnitude ratio is measurable. Assuming the heat transfer correlation of figure I.A.2.1 for Stanton number, we obtain the following calculated limiting magnitude ratios:-

TABLE AP.10. 1.1

LIMITING MAGNITUDE RATIO ACCORDING TO THE SCHUMANN MODEL FOR THE CYCLIC TEST METHOD, ε = 0.37.

Re_p	MAGNITUDE RATIO AT BED LENGTHS, N, INDICATED (ε= 0.37)		
	N = 5	N = 10	N = 20
20	6×10^{-6}	4×10^{-11}	1×10^{-21}
100	0.008	6×10^{-5}	5×10^{-9}
400	0.100	0.010	1×10^{-4}
2000	0.230	0.050	0.003
10000	0.427	0.183	0.033

It may be seen that in order to obtain a measurable magnitude ratio, bed length must be short and flow high. Table AP.10.1.2 summarises the published experimental conditions of three research organisations using this method.

TABLE AP.10.1.2

EXPERIMENTAL CONDITIONS USED
IN THREE CYCLIC METHOD INVESTIGATIONS

	National Engineering Laboratory, G.B. Meek [1963]	Brookhaven National Laboratory, U.S.A. Lindauer, [1967]	A.A.E.C. Australia Szomanski, [1968]
Section Shape	Square	Square	Square
W/dp	Matrix: A=5, B=5, C=15, D=10	25.4, 14.5, 8	6
L/d_p	Matrix: A=12, B≈7½, C=12, N=12	5.25 to 12.9	12
Reynolds Number Range (approx)	640 - 4200	23 - 18200	10,000-40,000

Examination of the calculations of section III.D, reveals that fluid phase axial dispersion corrections are likely to be negligible over the range of Reynolds numbers usually investigated by this method.

2. DETAILED ERROR ANALYSIS

Heat transfer coefficients obtained by the above investigators are generally considerably higher than predicted by the Denton correlation. The reason appears to lie in the sensitivity of high frequency measurements to attenuation introduced by bed supports, wall capacitance and heat loss, recorder limitations and measurement lags.

Szomanski and co-workers [1968] appear to be the first to attempt to correct systematically for these errors.

Thus it has been assumed that if r_T is the total experimental attenuation and r_E is the error attenuation then

$$r_S = r_T / r_E \qquad \ldots(2.1)$$

where r_S is the specimen attenuation the error attenuation is obtained from empty bed measurements. The validity of the above assumption will be examined in the following sections.

(i) Errors which are Reduced by Increasing Bed Lengths

The attenuation which is introduced by temperature probes, bed supports or recorder bandwidth limitations is constant at a given 'real' frequency ω'. In analysing the results of a cyclic test, a normalised frequency scale ω is introduced where

$$\omega = \omega' . \bar{T} . (V_H + 1).$$

$\bar{T}$ = bed holdup time L/V_a

and V_H is, Saunders and Ford's heat capacity ratio.

Hence the effect of increasing $\bar{T}$ is to make the attenuation introduced by these causes less important. Unfortunately, as indicated earlier (Table 10.1.1) bed lengths are required to remain short in order to obtain a measurable output amplitude.

If input and output are attenuated by the same amount (for example, where both input and output thermoprobes are immersed in the free stream) equation (2.1) applies and the errors cancel out in any case. Unfortunately, the attenuation resulting from bed supports is present only in the output signal and furthermore cannot be predicted from empty bed measurements.

Tables V1.B.2.1 and V1.B.2.3 list time constants obtained by cooling experiments on 0.0067 inch thermocouple wires.

1. Table 2.2, immersed in a packed bed, dp = 6.2 m.m, $\varepsilon \simeq 0.4$ and
2. Table 2.1, in the free stream above the bed.

It will be noted that the measurements differ by about 45%. Similar differences are likely between mesh screens in free air and mesh screens supporting a bed.

Calculation of Nusselt numbers from the wire time constants in Section V1.B.2 indicated that thin probes in a packed bed may be used to measure fluid temperature directly - i.e.measurements downstream of the supports are avoided.

The importance of bed support 'time constants' increases both as the bed length is reduced and as the Reynolds number increases. Table AP.10.2.1 shows the maximum calculated allowable time constant in seconds if the bed response is to be attenuated by no more than 10.6% at a normalised frequency of 10, the frequency beyond which the Schumann model predicts a constant magnitude ratio.

TABLE AP.10.2.1

MAXIMUM ALLOWABLE BED SUPPORT TIME CONSTANT

Assumptions: Heat transfer correlation of figure I.A.2.1, particle diameter = 6.2 mm., packing heat capacity of 30 BTU/(ft^3) (^oF), fluid specific heat 0.23 BTU/(lb) (^oF).

Particle Reynolds Number	MAXIMUM ALLOWABLE TIME CONSTANT IN SECONDS AT INDICATED BED LENGTH		
	N = 10	N = 20	N = 50
180	7.6	15.2	38.0
360	3.8	7.6	19.0
720	1.9	3.8	9.5
1440	0.95	1.9	4.7
2880	0.475	0.95	2.4
5760	0.237	0.47	1.2
11520	0.118	0.24	0.59

(ii) Errors Not Reduced by Increasing Bed Length

Neither direct heat loss nor wall capacitance effects are reduced by increasing the bed length, although it has been shown in appendix 4 that a reduction in error occurs as the number of particles, M, across a given section is increased. As would be expected, the dynamic effect of the wall depends markedly on the fluid-wall heat transfer coefficient h_w. At a given mass flow, assuming a tube to particle diameter d_T/d_p of about 10, the results of Chan and Lawther [1967] show that fluid-wall coefficients will be about six or eight times the empty tube coefficient for a given empty section mass flowrate.

It is apparent without further analysis that attenuation due to wall capacity and heat loss cannot be predicted from measurements on the empty bed.

A detailed analysis of the dynamic effects of wall heat loss is very difficult if temperature gradients within the bed are to be provided for.

Assumptions made in the treatment in appendix 4 were:-

(a) fluid temperature gradients within the bed are small
(b) the wall is sufficiently thin to allow axial wall heat conduction to be ignored.

(iii) Results of Wall Effect Analysis

According to section AP.4.4, wall effect is largely a function of the tube to particle diameter ratio, $M = d_T/d_p$. The values of α defined in AP.4.5 should be high for negligible wall effect. Taking the low flow end of Szomanski's work as an example ($Re_p = 10{,}000$, $M = 6$) the value of α calculated falls to about 7.4. Hence for this and higher flowrates, the dynamic effect of the wall becomes quite important, especially at high frequencies. It also is apparent that a simple correction of the type given by equation (2.1) is not likely to have meaning.

It should also be noted that the results of Meek [1961] obtained using values of M of 10 and 15 are closer to the correlation of Denton than are his matrix A and B results (M = 5).

A more detailed analysis of his results is made difficult by the fact that the walls of his test section were very heavy (i.e., $M_w.c_w / M\ c_s$ defined in Appendix 4 (AP.4.5) was large and that the last layer of particles was welded together, thus increasing the effects of radial heat transfer.

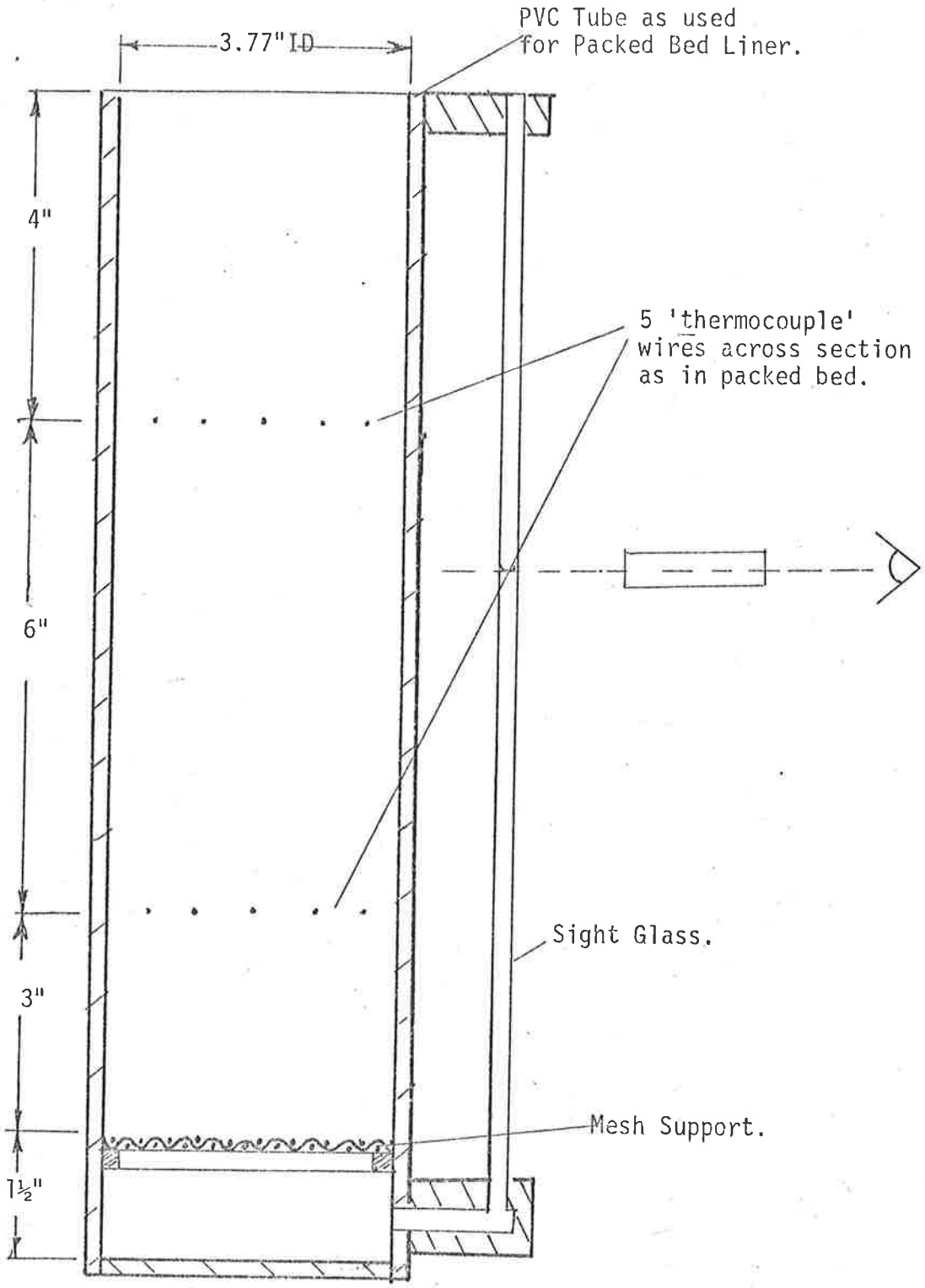

Figure AP.11.1
SIMULATED TEST SECTION
USED FOR POROSITY MEASUREMENTS
IN PACKED BEDS, KEROSENE
DISPLACEMENT

APPENDIX 11

PHYSICAL PROPERTIES

1. Porosity Measurements

In order to establish the effect of the bed thermocouples on local porosity and to obtain average porosity data an incremental fluid addition approach was adopted.

A length of the same P.V.C. liner used for the test section was made up as shown on figure AP.11.1 with external sight glass and identical packing support grid to that used in the experiments.

The simulated test section was packed in the manner described in VI.A.2.e, i.e. packing was forced into the bed by suction except in the case of the perspex packed section where the walls were hand poured since this was the method used in experiments.

Simulated thermocouple wires were installed with the same diametric spacing as shown in figure VI.C.4.4. Kerosene was added in 3 ml. increments through the sight glass and level recorded after each addition through an accurate travelling telescope. Plots of level against volume added are shown on figures AP.II.1.2, 1.3 and 1.4.

It may be seen that porosity increases to a limiting value as the level increases above the support mesh. Blanks were run on the empty tube and corrections made for the volume of the sight glass. It may also be noted that thermocouple wires have negligible effect on the local porosity except for a region of 3 mm. on either side.

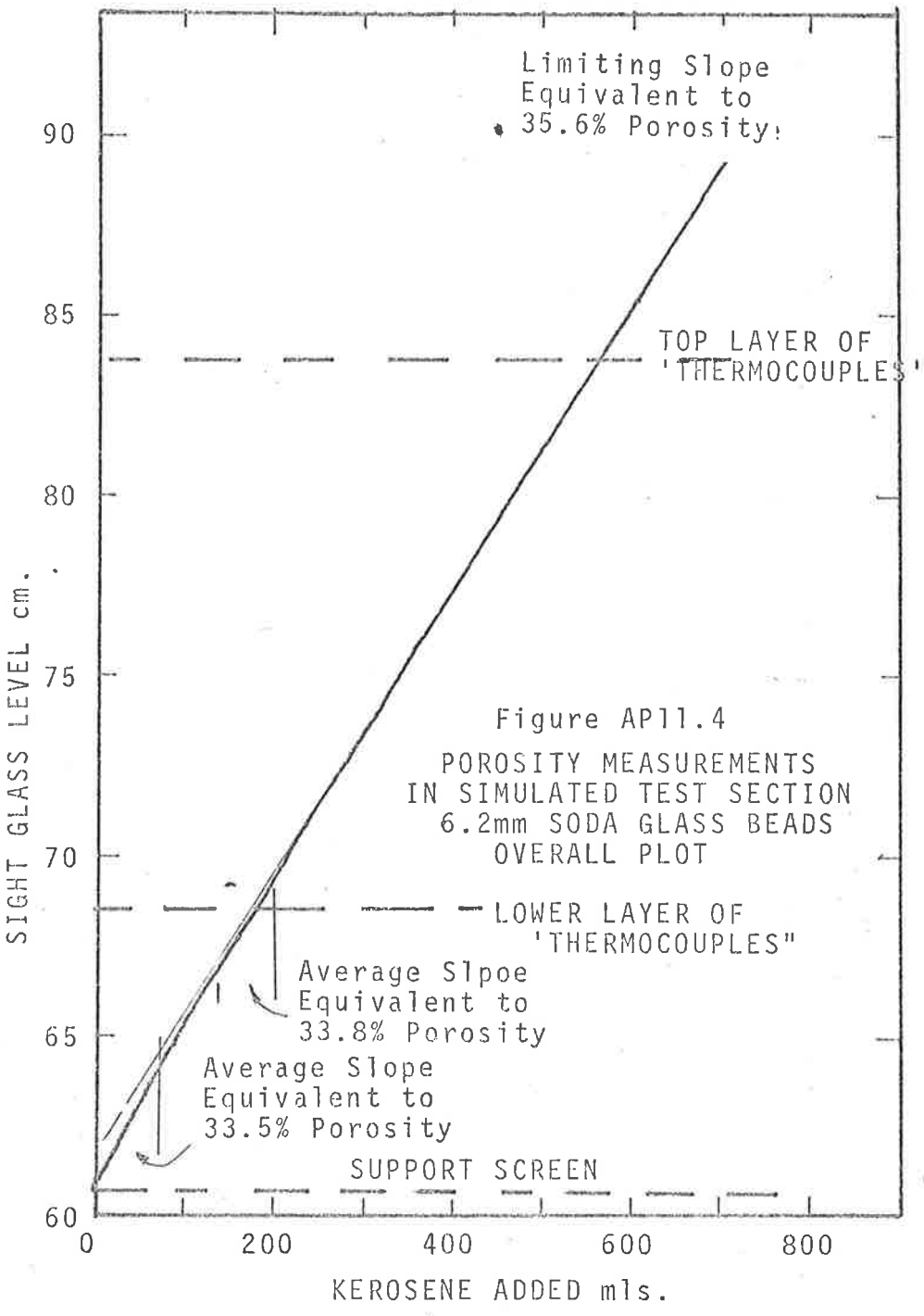

Figure AP11.4

POROSITY MEASUREMENTS
IN SIMULATED TEST SECTION
6.2mm SODA GLASS BEADS
OVERALL PLOT

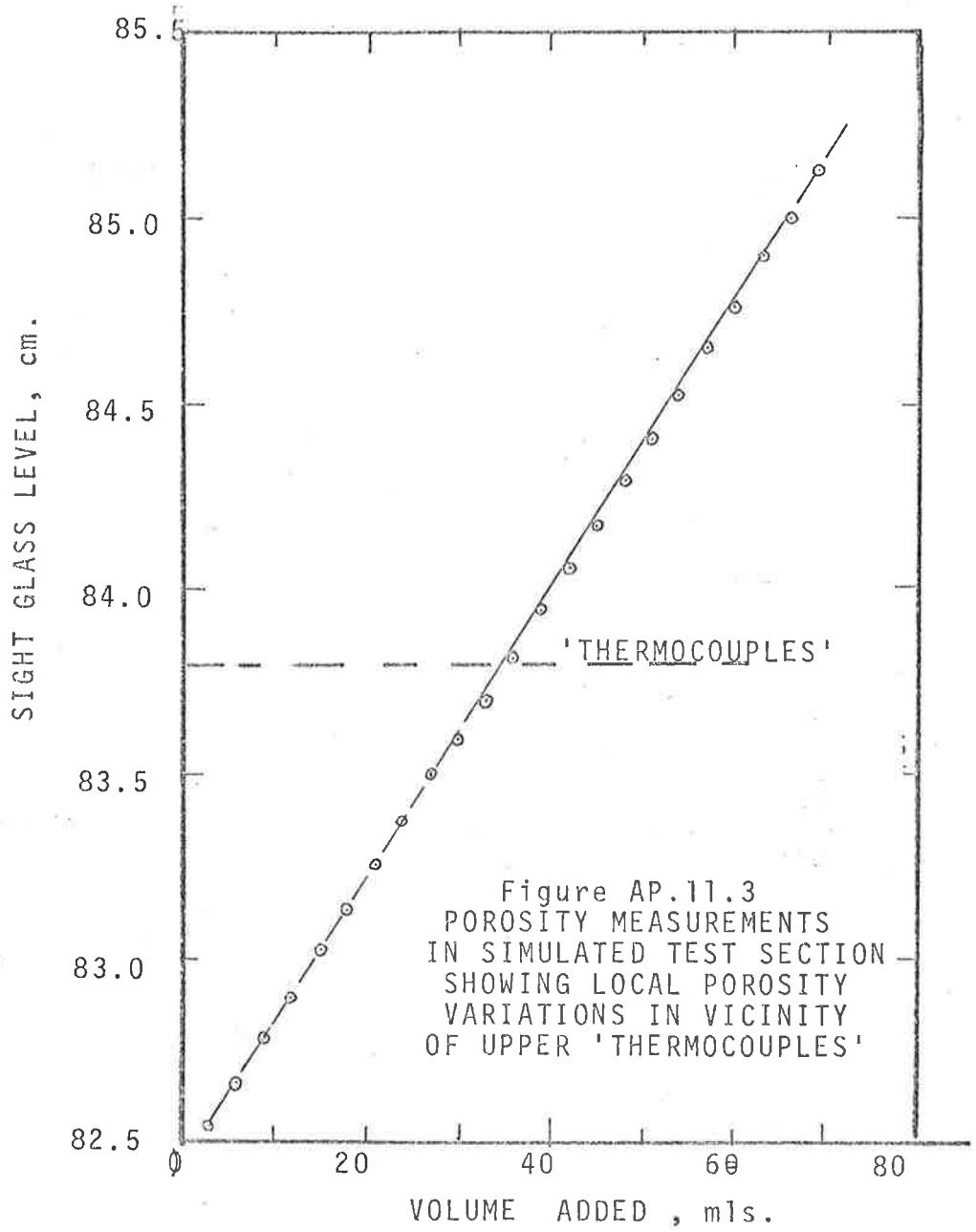

Figure AP.11.3
POROSITY MEASUREMENTS
IN SIMULATED TEST SECTION
SHOWING LOCAL POROSITY
VARIATIONS IN VICINITY
OF UPPER 'THERMOCOUPLES'

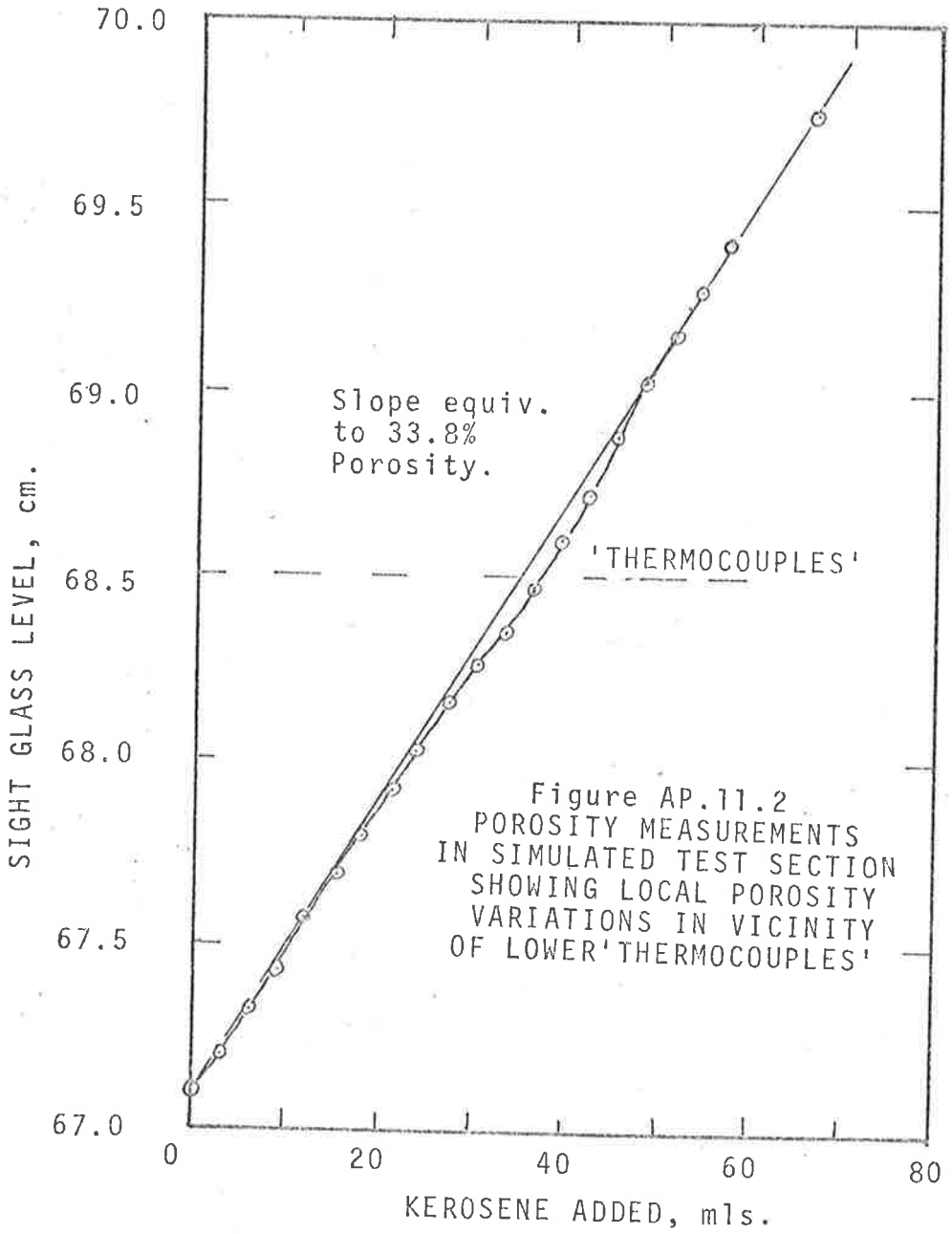

Figure AP.11.2
POROSITY MEASUREMENTS
IN SIMULATED TEST SECTION
SHOWING LOCAL POROSITY
VARIATIONS IN VICINITY
OF LOWER 'THERMOCOUPLES'

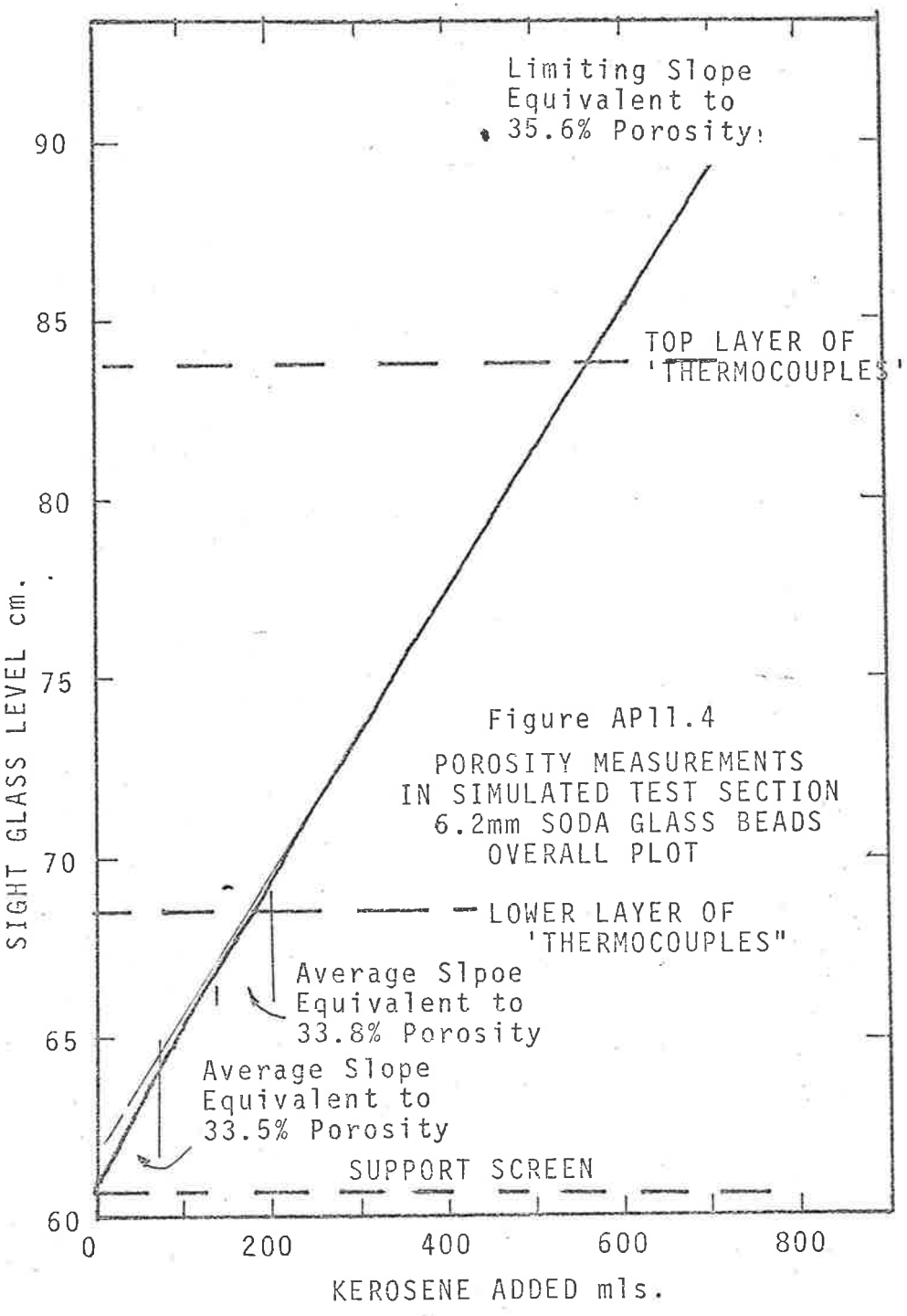

Figure AP11.4

POROSITY MEASUREMENTS
IN SIMULATED TEST SECTION
6.2mm SODA GLASS BEADS
OVERALL PLOT

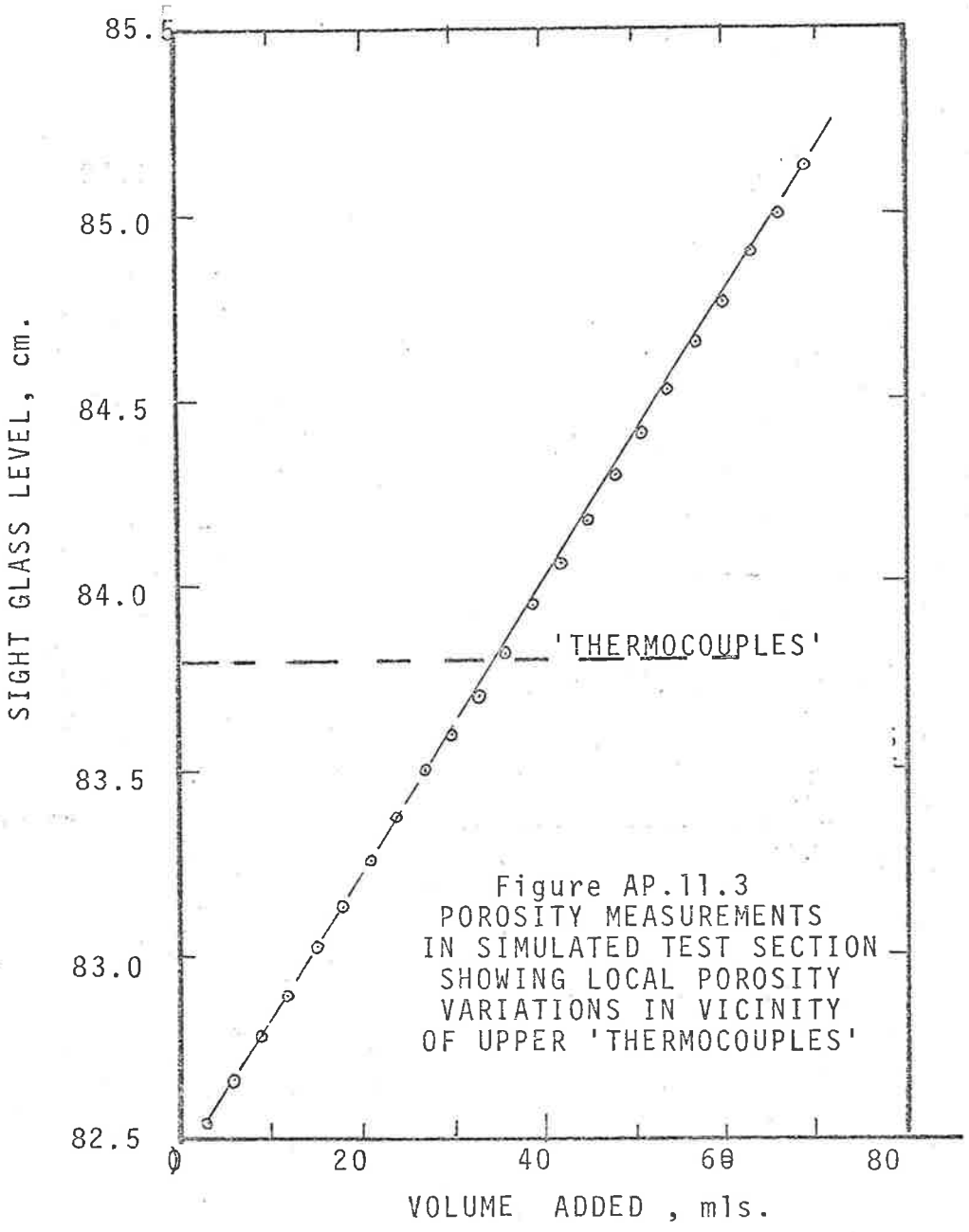

Figure AP.11.3
POROSITY MEASUREMENTS
IN SIMULATED TEST SECTION
SHOWING LOCAL POROSITY
VARIATIONS IN VICINITY
OF UPPER 'THERMOCOUPLES'

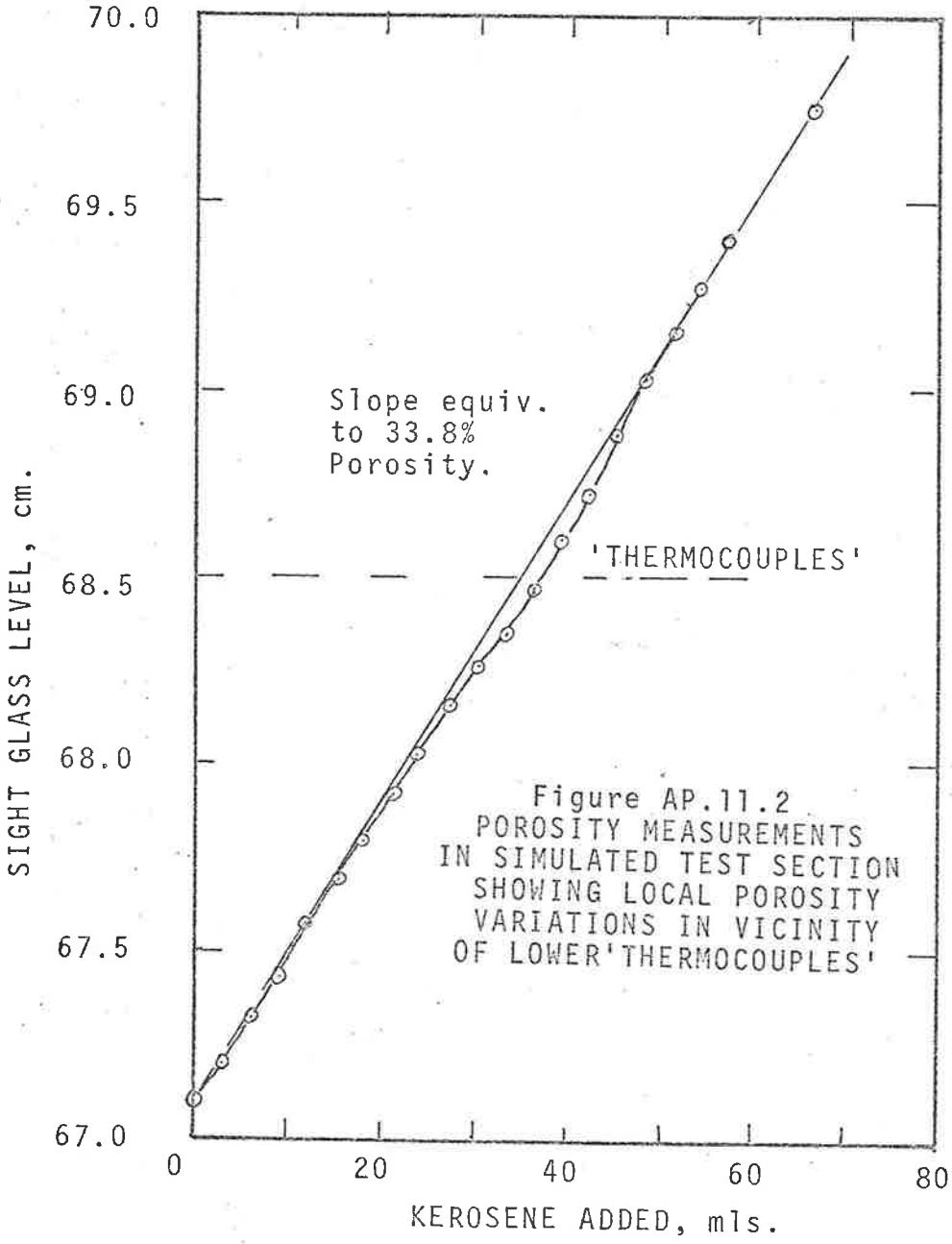

Figure AP.11.2
POROSITY MEASUREMENTS
IN SIMULATED TEST SECTION
SHOWING LOCAL POROSITY
VARIATIONS IN VICINITY
OF LOWER 'THERMOCOUPLES'

Only one detailed traverse was carried out for each packing size, however overall porosity determinations were carried out on repeat packings with the results tabulated (table AP.11.1.1).

TABLE AP.11.1.1

POROSITY DETERMINATIONS

Bed diameter by displacement = 3.77 inches

Particle	Size mm	Average bulk Porosity, above support zone
Soda Glass	6.2	0.346
Nominal 6 mm		0.345
'Englass'		0.346
Acrylic (Perspex)	6.9	0.368
Nom.7.0 mm.		0.369
		0.368
Lead, Nominal 4 mm.	4.04	0.368

In the case of the 4 mm lead experiments, porosity was also determined by weighing the amount of packing poured into the actual test section between measurement stations.

2. SPECIFIC HEAT

Specific heat was determined by heating a weighed quantity of beads in a heavy steel cylindrical container in a temperature controlled oven, A thermocouple was inserted loosely in the centre of the beads and another soldered to the base of the container.

When both temperatures had stabilised as noted by a Cambridge workshop potentiometer, the container was quickly removed from the oven and a brass stopper at the base of the container quickly removed. The beads were dropped into a weighed quantity of distilled water contained in a Dewar flask and the temperature rise noted with another chromel alumel thermocouple after mixing had stabilised temperature. Thermocouples were exchanged between oven and flask after each determination and specific heat calculated from a heat balance. Results are shown in Table AP.11.2.1.

TABLE AP.11.2.1

HEAT CAPACITY DETERMINATIONS

Water assumed 1 cal/gm^{o}C)

Particle	Size m m	Heat Capacity cal/(gm^{o}C)	Water Temperature Initial ^{o}F	Final ^{o}F
Soda glass	6.2	0.1834	70.9	95.0
		0.1855	71.2	95.8
		0.1832	70.3	95.1
		0.1840	74.8	99.0
		0.1850	95.9	100.0
	Mean:	0.184		
Acrylic (Perspex)	6.9	0.3555	85.1	106.2
		0.3593	80.6	102.7
		0.3547	82.3	103.7
		0.3437	80.4	101.7
		0.3499	77.6	99.3
	Mean:	0.353		

COMMONWEALTH OF AUSTRALIA
DEPARTMENT OF SUPPLY

DEFENCE STANDARDS LABORATORIES

8/148
TS69-249
MAW

REPORT
ON

18th June, 196

THERMAL CONDUCTIVITY OF GLASS SAMPLE

Submitted by: Chemical Engineering Department,
University of Adelaide, S.A.

Reference: Letter CPJ/DC dated 21st May, 1969.

Description: Two specimens of a sample of soda glass in disk form measuring approximately 7.6 cm diameter and 0.36 cm thick. The sample was submitted for measurement of thermal conductivity at a mean temperature about 20°C.

Test Conditions: The sample was tested in the "as received" condition in a guarded disk apparatus of the type described in Section 3 of Appendix A, B.S. 874:1956 "Definitions of heat insulating terms and methods of determining thermal conductivity".

RESULTS OF TEST:

Thickness	cm	0.362
Density (mean of specimens)	g/cm^3	2.61
Hot plate temperature	°C	23
Cold plate temperature	°C	17
Mean test temperature	°C	20
Thermal conductivity	W/cm deg C	0.0098

Note: It is estimated that the error in the thermal conductivity measurement does not exceed 8 per cent.

= 6.79 BTU/(hr)(ft²)(°F/inch)

= 0.566 BTU/(hr)(ft)(°F)

3. THERMAL CONDUCTIVITY

Because of the difficulty and expense of the determinations only one determination was carried out - on the 6.2 mm soda glass beads. The value for the acrylic or Perspex beads was taken from the thesis of Babcock [1962].

A number of slabs were cast although only two were used because of difficulty in melting the beads without excessive bubble formation. The beads were placed in a 4" dia. platinum mold supported in refractory sand which was enclosed in a refractory crucible. Temperature was raised to 850 ^{o}C and maintained at this temperature until all beads were melted. This temperature resulted in less than 0.1% (est) by volume of occluded air and gas formation. The platinum was then stripped away and specimens ground to 7.6 cm dia. by 0.36 cm thick optically flat discs and thermal conductivity determined by the Defence Standards Laboratory using a guarded hot plate apparatus. A copy of the test certificate is shown in figure AP.11.3.1.

Mean thermal conductivity at about 68^{o}F was 0.566 BTU/(hr.ft.^{o}F) ± 8%.

4. OTHER PHYSICAL PROPERTIES - Packings

Mean diameter was determined by counting approximately 500 balls into a beaker on a Mettler balance.

Result:	6 mm soda glass	6.20 mm
	7 mm acrylic	6.90 mm
	4 mm lead	4.05 mm

Specific gravity was determined by displacement of distilled water to eliminate occlusion of air bubbles.

6.2 mm soda glass: 2.579, 2.586, 2.585
mean: 2.583 gm/cc

6.9 mm perspex: 1.195, 1.192, 1.192, 1.193
mean: 1.193 gm/cc

4.0 mm lead: 11.16

Air

A constant Prandtl number of 0.74 was assumed, with a viscosity taken from the alignment chart in Perry, Chemical Engineers' Handbook Fourth Edition of 0.0185 centipoises (assumed temperature- 70°F). Specific heat was taken to be that of dry air since air was passed through a silica gel dryer before use. The value of 0.240 BTU/(lb°F) was taken from the psychrometric table in Perry (op.cit.) between 70 and 80°F. Thermal conductivity was calculated from the Prandtl number to be 0.0141 BTU/(hr.ft.°F).

In calculating density, a molecular weight of 28.96 was assumed with compressibility of unity.

SYMBOLS USED

NOTE: A number of symbols used in appendixes have been defined locally and do not appear in this table.

a_n (Ch.IV) n'th coefficient in Hermite or Laguerre polynomial expansion.

a_p Ratio of surface area to volume of a particle (= $6/d_p$ for spheres or right cylinders)

Bi Biot number for spheres with particle radius R as characteristic dimension = $h_p\ R/k_S = h_p\ d_p/\ 2k_S$

c_i (Ch.I) steady state concentration stage i.

C_n (Ch.IV) normalising factor in orthogonality relation for polynomials = $n!\ (2\pi)^{\frac{1}{2}}$ for Hermite polynomials.of order n.

c_f Fluid heat capacity BTU /(lb.^{o}F).

c_S Solid packing heat capacity BTU /(lb.^{o}F).

d_p Particle diameter, ft.

D_S Particle diffusivity, ft.^{2}/hr

D_e (Ch.I) equivalent 'eddy' diffinivity or dispersivity in packed bed ft.^{2}/hr.

D_m 'Molecular' diffusivity = $k_f\ /(\rho_f.c_f)$ for thermal diffusion.

d_h or d_e Equivalent or 'hydraulic' diameter $2.\ \varepsilon.\ dp\ /[3(1-\varepsilon)]$,ft.

d_T Tube diameter. ft.

$E(t)$ (Ch.IV) even part of a function

E 'Even part of' operator, $E[f(t)] = E(t)$

$\mathcal{F}$ Fourier transform operator, e.g. $\mathcal{F}[f(t)] = F(j\omega)$

$F(j\omega)$ Fourier transform of function, $f(t)$.

F (Ch.I) flux of heat or matter.

F (Ch.III) Epstein F factor = St calc / St.

F (Chapters IV,V,VII) Babcock parameter = $\sqrt{t^*} - 1/\sqrt{t^*}$

G Superficial mass velocity through packed bed = $\varepsilon . v_a . \rho_f$

$G(s)$ Laplace transform transfer function = $\mathcal{L}[g(t)]$ (section II.A.1)

$G_p(s)$ Laplace transform fluid particle surface temperature transfer function.

$G_N(s)$ Laplace transform transfer function relating fluid temperature, N'th stage to inlet fluid temperature variations.

$G(j\omega)$ Fourier transform or 'frequency response' transfer function.

$|G(j\omega)|$ Modulus representation of $G(j\omega)$, i.e. magnitude ratio for cyclic tests.

$\underline{/G(j\omega)}$ Argument representation of $G(j\omega)$, or phase shift between output and input sine waves for a cyclic test.

$g(t)$ Impulse response of a linear system, for packed bed response of bed at normalised time t, usually at outlet (z = 1) to an impulse function inlet temperature variation.

$g(t,z)$ Impulse response as above where z = 1.

H (Ch.II) distance between perfectly-mixed stages, finite stage model.

$H_n(\omega)$ (Ch.IV) Hermite polynomial of n'th order, argument ω.

h_w Surface averaged wall heat transfer coefficient, BTU /(hr.ft^2. ^oF)

h_p Surface-averaged fluid particle heat transfer coefficient BTU /(hr.ft^2. ^oF)

$I(\omega)$ Imaginary part of frequency response transfer function $= \emptyset\ [G(j\omega)]$

$I_1(t)$ Modified Bessel function, first kind, argument t.

j $\sqrt{-1}$

j_H Colburn j_H factor = St. $Pr^{2/3}$.

$J_n(t)$ Bessel function, order n, argument t.

k_m or k_f Fluid molecular thermal conductivity, BTU/(hr.ft.^oF).

k_{eddy} (Ch.I) equivalent eddy thermal conductivity BTU/(hr.ft.^oF).

k_S Solid thermal conductivity, BTU/(hr.ft.^oF).

K Fluid-particle heat transfer parameter = $h_p\ a_p\ \overline{T}\ /\ \rho_S\ c_S$

K_n (Ch.II) gain term corresponding to n'th root in particle transfer function = $2Bi/(Bi^2 - Bi + \beta_n)$.

KV_H Fundamental packed bed heat transfer parameter, product of K and V_H, . KV_H = St. a_p. L. $(1-\varepsilon)$.

L Overall bed length = M.H = N.d_p, ft.

$\mathcal{L}$ Laplace transform operator.

M (Ch.II) number of effective stages in a bed, finite stage model.

M_w (Ch.III) bed diameter expressed in particle diameters, d_T/d_p

M Mass of solid packing in a bed, lbs.

M_f Mass of fluid retained in interstices of a packed bed.

N Bed length in particle diameters see also equns.(VII.B.7.1 and (VII.B.7.2).

Nu Nusselt number hd/k_f

ϕ 'Odd part of' operator, e.g. $\phi\,[G(j\omega)] = I(\omega)$ where $G(j\omega) = R(\omega) + j\ I(\omega)$.

Pe_m 'True' or fluid molecular conduction axial Peclet number $= v_a\, d_p / D_m$

Pe Axial fluid dispersion equivalent Peclet number with particle diameter as characteristic dimension.

Pe' Axial fluid dispersion equivalent Peclet number with bed length as characteristic dimension $= N.Pe$.

Pe_r Equivalent radial dispersion Peclet number based on particle diameter.

Pe_a Equivalent conductivity model equivalent axial dispersion Peclet number, defined by equations (II.D.2.3) et.sequ.

Pr Prandtl number $c_f.\,\mu_f / k_f$

$p(s)$ Laplace transform parameter used in Rosen particle transfer function $= j\,(s/\alpha)^{\frac{1}{2}}$

t^+ Time normalised with respect to heat capacity ratio for packed beds,

$$t^+ = t/V_H = t'/(\overline{T}.\ V_H)$$

$\overline{T}$ Mean fluid residence time, L/v_a.

T (Ch.VI) thermocouple time constant, sec.

$T_i(t)$ Temperature at stage i and normalised time t for finite stage model, i = 0,1, ... N.

$T_o(t)$ Temperature at inlet of a bed (i.e. at 'stage zero') for finite stage model.

$Tp_i(t)$ Particle surface temperature at stage i, finite stage model.

T_n Time constant corresponding to n'th root of particle transfer function = $1/\alpha\beta_n$ for spheres.

$\delta T_f(z,t)$ Changes in fluid temperature at normalised distance z from bed inlet, normalised time t.

$\delta T_w(z,t)$ Changes in wall temperature at normalised distance z from bed inlet, normalised time t.

ΔT_{LM} Steady state logarithmic mean temperature difference.

$U(t)$ Unit step function defined by: $U(t) = 1,\ t \geq 0$

$U(t) = 0,\ t < 0$

$u(t)$ Response of packed bed (at normalised distance z = 1) to a unit step function input temperature variation, all initial conditions zero (i.e., $T(z,t) = 0,\ 0 \leq z \leq 1,\ t < 0$)

v_a Axial mean interstitial velocity in a packed bed = $G/(\varepsilon.\rho_f)$.

V_H 'Heat capacity ratio' between solid and fluid in a packed bed $= \dfrac{\rho_S.\ c_S.\ (1-\varepsilon)}{\rho_f.\ c_f.\varepsilon}$

W Total weight flow rate of fluid through a packed bed $= G.A_c$ lb/hr.

X (Ch.II.,app.2) discriminant of Laplace transformed characteristic equations.

$x(t)$ Usually 'input' variation to a system where $x(t) = 0$, $t < 0$.

$X(j\omega)$ Fourier transform of variable $x(t)$.

$y(t)$ Usually 'output' variation from a system in response to input variation $x(t)$ where $y(t) = 0$, $t < 0$.

$Y(j\omega)$ Fourier transform of, $y(t)$.

$Y_D(s)$ 'Admittance' function of J.B.Rosen eqn.(II.B.3.5)

z' 'Real' distance ususlly from packed bed inlet, ft.

z Distance normalised with respect to overall bed length, $L, = z'/L$.

Z Scale factor, used in Hermite polynomial approximation.

GREEK SYMBOLS

α Diffusivity parameter for particles $= \bar{T}\, k_S/\rho_S\, c_S\, R^2$ i.e. $\alpha = K/3Bi$.

β (Ch.I) ratio, axial fluid-solid-fluid conductivity to total effective axial donductivity.

β_n n'th root of $\beta.\omega + \beta + Bi - 1 = 0$.

γ (Ch.I) particle diameter normalised distance between perfect mixers, cell or finite stage model i.e. $\gamma = H / d_p = N/_M$.

γ (Section II.B.8) parameter used in computing Rosen fluid particle admittance function.

γ_1 Usual statistical measure of skewness of a density function. Equn.(II.E.1.1)

γ_2 Alternative measure of skewness used in packed bed modelling equation (II.E.1.2)

$\delta(t)$ Delta, Dirac or impulse function defined by $\delta(t) = 0, \quad t < 0, t > 0, \quad \int_{-\infty}^{\infty} \delta(t)\, dt = 1.$

δ (Ch.V) mesh spacing for a numerical integration.

ε Bulk volumetric porosity = (volume of void space in a packed bed) / (total volume of bed).

θ Occassionally used to denote t^*.

κ_n n'th cumulant of impulse response density function g(t) where time scale normalised relative to mean fluid holdup time $\overline{T}$.

κ_n^* As above, time scale normalised relative to $\overline{T}.\ (1+V_H)$.

μ_f fluid viscosity, lb./(hr.ft.)

μ Used to denote μ_1', first absolute moment of impulse response density function g(t) where time scale is normalised relative to $\overline{T}$.

$\mu(t)$ First absolute moment as above in 'real time' units min.

μ'_n n'th absolute moment (moment about origin) of impulse response density function, time scale normalised relative to $\overline{T}$, n = 0,1,2...

μ^* First absolute moment, time scale normalised relative to $\overline{T}.\ (1 + V_H)$.

μ_n n'th central moment of impulse response density function, i.e. n'th moment about $t = \mu_1'$ where time scale normalised relative to $\overline{T}\ \ (1+ V_H)$.

μ_{ϕ_n} (Ch.V) n'th central moment of density function $\phi(t) = \mu_0' - u(t)$, where $\lim_{t \to \infty} u(t) = \mu_0'$,
$\phi(t) = 0, \ t < 0.$

μ_{G_n} or μ'_{G_n} Occasionally used to denote μ_n or μ'_n . respectively.

π^3 Third central moment i.e. μ_3 or 'skewness' of impulse response density function, time scale normalised relative to $\overline{T}$.

$\pi^3(t)$ Third central moment as above, in 'real time' units, min.^{3}

π^{*3} Third central moment of impulse response density function, time scale normalised relative to first moment $\mu(t)$ i.e. relative to $\overline{T}\ (1+V_H)$ for packed beds.

π 3.141596 ....

Π Time constant (app.4)

ρ_f Density of fluid, lb/cu.ft.

ρ_S Density of solid, lb/cu.ft.

σ^2, σ Variance (i.e. second central moment μ_2) and 'standard deviation' respectively of impulse response function g(t), time scale normalised relative to $\overline{T}$.

$\sigma^2(t)$ Variance of density function in real time units min.^{2}

σ^{*2} Variance of impulse response density function g(t)*, time scale normalised relative to $\overline{T}.(1+V_H)$.

τ Wall thickness,ft.

$\phi(t)$ $= \mu'_o - u(t)$, $\phi(t) = 0$, $t < 0$, where $\lim_{t \to \infty} u(t) = \mu'_o$.

$\psi(t)$ 'Life expectation' function of Zweitering

$$= \int_0^t . \phi(t) \quad dt. \quad \text{(ch.V)}$$

ω' Natural frequency in real time i.e. radians per min.

ω Normalised natural frequency, normalised relative to $\overline{T}$.

ω^* Normalised natural frequency, normalised relative to $\overline{T} . (1+V_H)$.

REFERENCES.

ABRAMOWITZ, M. and STEGUN, I.A., Editor 'Handbook of Mathematical Functions', Dover, 1965. Refce a. p927. Refce b. p355

AMUNDSON, N.R., Ind. and Engng Chem. 48 : 26 and 48 35 (1956).

ANDERSSEN, A.S. and WHITE, E.T., Can. Jl. Chem. Engng. 47 : 58 (1969).

ANTONSON, C.R. and DRANOFF, J.S., Chem. Engng Prog. Symp. Ser. 63 No. 74 6 1 (1967).

ANZELIUS, A. Z. angeu. math. u. Mech., 6 : 291 (1926).

ARGO, W.B. Ph.D. Thesis 'Reaction Kinetics and heat transfer in packed beds', Purdue University, 1953.

ARGO, W.B. and SMITH, J.M., Chem. Engng Prog., 49: 443 (1953).

ARIS, R., Chem. Engng. Sci., 9: 266 (1959).

ARIS, R. ,Chem. Engng. Sci., 13 : 1 (1960)

ARIS, R. and AMUNDSON, N.R., A.I.Ch.E.Jl, 3 : 280 (1957)

ARSAC, J., 'Fourier Transforms and the Theory of Distributions' trans. Nussbann A. and Heim G.C., Prentice Hall, 1966.

BABCOCK, R.E. 'Longitudinal dispersion of thermal energy in unconsolitated packed beds', Ph.D. Thesis, Univ. Oklahoma, 1964.

BABCOCK, R.E., GREEN, D.W. and PERRY, R.H., A.I.Ch.E.Jl., 12 : 922 (1966)

BABCOCK, R.E., PERRY, R.H. and CROSSER, O.K., Chem. Engng. Progr. Symp. Ser., 63 : No. 77 102 (1967)

BAR-ILAN M. and RESNICK, W., Ind. and Engng Chem., 49 : 313 (1957)

BARKER, J.J., Ind. and Engng. Chem. 57 : 43 (1965).

BARON, J. Chem. Engng. Progr. 48 : 118 1952.

BAUMEISTER, E.B. and BENNETT, C.O., A.I. Ch.E.Jl 4 : 69 (1958).

BEEK, J., Adv. in Chem. Engng., 3 229 (1962).

BENNETT C.O. and MYERS, J.E., 'Momentum Heat and Mass Transfer' McGraw-Hill, 1962.

BISCHOFF, K.B. and LEVENSPIEL, O., Chem. Engng Sci., 17 245, 257 (1962).

BRADSHAW, R.D. and MEYERS, J.E., A.I.Ch.E.Jl., 9 : 590 (1963)

BRODKEY, R.S., 'Final Report by the Ohio State University Research Foundation to U.S. Atomic Energy Commission' Contract No. AT(11-1) - 774, Oct. 1964.

BRODKEY, R.S. in 'Mixing, Theory and Practice' UHL V.W. and GRAY, J.B. Editors Vol.1 Chapter 2, 1966.

**BRACEWELL next page

REFERENCES. (Cont'd)

BRACEWELL, R.N., 'The Fourier Transform and its Applications', McGraw-Hill, 1965.

Refce. a : p.69 et seq.

Refce. b : p.121.

BROWNLEE, K.A., 'Industrial Experimentation', Fourth Edn., H.M.S.O. 1949.

CARBERRY, J.J., A.I.Ch.E. Jl. 4 13M (1958).

CAIRNS, E.J. and PRAUSNITZ, J.M., Chem. Engng. Sci. 12 : 20 (1960).

CARSLAW, H.S. and JAEGER, J.C., 'Conduction of Heat in Solids' Second Edn., Oxford, 1959.

CHAN, B.K.C. and LAWTHER, K.R., Aust. Atomic Energy Comm. Rep. AAEC/TM 389, May, 1967.

CHAO, R.,Ph.D. Thesis, JohnsHopkins Univ. Baltimore, 1965.

CHAO, R. and HOELSCHER, H.E., A.I.Ch.E.Jl, 12 : 271 (1966).

CHILTON, T.H. and COLBURN, A.P., Ind. and Engng Chem., 27:285 (1935).

CHUKHANOV, Z.F., Int. Jl. Heat Mass Transf. 6 : 691 (1963).

CHUKHANOV, Z.F., and SHAPATINA, E.A., Inzv. Akad. Nauk. SSR Otd. Tekhn. Nauk.No. 7, 746 (1945). Quoted by HEGGS [1967].

CLEMENTS, W.C., jr., Chem. Engg. Sci., 24 : 957 (1969).

COLBURN, A.P.,Trans. A.I.Ch.E.Jl.29 : 174 (1933).

COLWELL, C.J. and DRANOFF, J.S., A.I.Ch.E.Jl. 12 : 304 (1966).

CURL, R.L. and McMILLAN, M.L.,A.I.Ch.E.Jl., 12 : 819 (1966).

DANCKWERTS, P.V., Chem. Engng. Sci., 2 : 1 (1953).

DAYTON, R.W., FAWCETT, S.L., GRIMBLE, R.E. and SEALANDER, C.E., Battelle Memorial Inst. Rep. BMI - 747, 1952.

De ACETIS, J. and THODOS, G., A.I.Ch.E.Jl 4 : 69 (1958).

DEANS, H.A. and LAPIDUS, L., A.I.Ch.E.Jl., 6 : 663 (1960).

DENTON, W.H. Proc. of Genl. Discussion of Heat Transfer, Inst. M.E. (London) and A.S.M.E. 370 (1951).

DENTON, W.J., ROBINSON, C.H. and TIBBS, R.S., A.E.R.E. Report R4346, 1953.

DIESLER, P.F. and WILHELM, R.H., Ind. and Engng Chem. 45 : 1219 (1953).

DOETSCH, G., 'Guide to the Application of Laplace Transforms' (Trans. and Ed'd. by M. FAIRBAIRN W.) Van Nostrand, London, 1953.

Refce. a : p. 69.
Refce. b : p. 84.

REFERENCES. (Cont'd)

DOOGE, J.C.I., Jl. S.I.A.M. Control 2 : 397 (1965).

EDWARDS, J.F. and J.F. RICHARDSON, Chem. Engng. Sci., 23109 (1968).

EICHHORN, J. and WHITE, R.R., Chem. Engng. Prog. Symp. Ser. 48 No.4 11 (1952).

EPSTEIN, N., Canadian Jl. of Chem. Engng, 36 210 (1958).

FELLER, W., 'An Introduction to Probability Theory and its Applications' Vol.I, Second Edn., Wiley, 1957 (Chapter XIV.5).

GAMSON, B.W., THODOS, G. and HOUGEN, O.A., Trans. Am. Inst. Chem. Engrs. 39 : 1 (1943).

GILLESPIE, B.M., CRANDALL, E.D. and CARBERRY, J.J., A.I.Ch.E.Jl., 14 : 483 (1968).

GOMEZPLATA, A. and BROWN, R.W., A.I.Ch.E.Jl. 14 : 657 (1968).

GREEN, D.W., PERRY, R.H. and BABCOCK, R.E., A.I.Ch.E.Jnl., 10 : 645 (1964).

GUNN, D.J., Chem. Engng. Sci., 25 : 53 (1970).

GUNN, D.J. and PRYCE, C., Trans. Instn. Chem. Engrs. 47 : T341 (1969).

GUPTA, A.S. and THODOS, G, Chem. Engng. Progr. 58 : 58 (1962).

GUPTA, A.S. and THODOS, G., A.I.Ch.E.J 9 : 751 (1963).

GUPTA, A.S. and THODOS, G., Ind. and Engng Chem. (Fundamentals) 3 : 218 (1964).

HANDLEY, D. and HEGGS, P.J., Trans. Instn. Chem. Engrs. 46 : T251 (1968).

HART, J.A. and SZOMANSKI,E., Instn. Engrs. Aust., Mech. and Chem. Trans. MC4 : (1) 38 (1968).

HAYS,J.R. CLEMENTS, W.C. jr. and HARRIS, T.R., A.I.Ch.E.Jl., 13 : 374 (1967).

HEALEY, J.E., U.S. At. Energy Comm. Rep. No. RPI-3639-3, 1967.

HEGGS, P.J. 'Transfer processes in packings used in thermal regenerators,' Ph.D. Thesis, Univ. Leeds, 1967.

HEGGS, P.J. Canadian Jl., Chem. Engng, 47 373 (1969).

HERZFELD,J.,Ed., "Temperature,its measurement and control inScience and Industry', Vol. 3, Part 2, American Institute of Physics,

JEFFRESON, C.P., Chem. Engng. Sci., 23: 509 (1968) (Paper 1, Appendix 3).

REFERENCES. (cont'd)

JEFFRESON, C.P., Instn. Engrs. Aust. Elec. Engng. Trans. EE5 : 77 (1969). (Paper 2, Appendix 3).

JEFFRESON, C.P., Chem. Engng. Sci., 24 : 613 (1969) (Paper 3, Appendix 3).

JEFFRESON, C.P., "Dynamic Testing - a unification', to be published, 1970 Chem. Engng. Sci. (Manuscript CE5 - 1127) Paper 4 Appendix 3).

JEFFRESON, C.P. 'The use of unstirred vessel to improve controllability of mixing processes'. Proc. "Chemeca 70' Chemical Engineering Conference Sydney - Melbourne, Aug. 1970 Paper 7.7 (Paper 5, Appendix 3).

JOLLS, K.R. and HANRATTY, T.J., A.I.Ch.E.Jl, 15 199 (1969).

KENDALL, M.G. and STUART,A.,'The Advanced Theory of Statistics', Vol.1, 2nd Edn. Griffin, London 1958, p 69 et seq.

KLINKENBERG, A., Indl. and Engg. Chem. 46 : 2285 (1954).

KLINKENBERG, A. and HARMENS, A., Chem. Engng. Sci., 11 : 260 (1960).

KLINKENBERG, A. and MOOY, H.H., Chem. Engng. Progr. 44 : 17 (1948)

KOULMEYER, G.F. A.I.Ch.E.Jl., 14 : 499 (1968).

KRAMERS, H. and ALBERDA, G., Chem. Engng. Sci., 2 : 173 (1953).

KUCERA, E., Jl. Chromatog. 19 : 237 (1965).

KUNII, D. and SMITH, J.M. A.I.Ch.E.Jl. 6 : 71 (1960).

KUNII, D. and SMITH, J.M., A.I.Ch.E.Jl., 7 : 29 (1961).

KUNII, D. SUZUKI, M. and ONO, N., Jl. Chem.Engng. of Japan, 2 : 21 (1968).

LAI, C[illegible]=LIANG and ROTU, J.A. Chem. Engng. Sci., 22 : 1299 (1967).

LAVENDER, W.J. and PEI, D.C.T., Int. Jl. Heat Mass Transf. 10 : 529 (1967).

LECLAIR, B.P. and HAMIELEC, A.E., Proc. Triparfite Chem. Engng. Conf. (Preprint) Session 39, Sept. 1968.

LEES, S. and DOUGHERTY, R.C., A.S.M.E. Trans. Ser. D. (Jl. Basic Engng.) 89 : 445 (1967).

LEVENSPIEL,O., Chemical Reaction Engineering, Wiley 1962.

LEVENSPIEL, O, and BISCHOFF, K.B., Chem. Engng. Sci., 17 : 245 (1962).

LINDAUER, G., A.I.Ch.E.Jl 13 : 1181 (1967).

REFERENCES. (Cont'd)

LITTMAN, H. and BARILE, R.G., Chem. Engng. Progr. Symp. Ser. 62 : No. 67 10 (1966).

LITTMAN, H. BARILE, R.G. and PULSIFER, A.H., Indl. and Engng. Chem. Fundamentals 7 : 554 (1968).

McADAMS, W.H., 'Heat Transmission' Ch. 10, section 1A, Third Edition McGraw-Hill, 1954.

McCONNACHIE, J.T.L. and THODOS, G., A.I.Ch.E.Jnl. 9 60 (1963).

MALLING, G.F. and THODOS, G., Int. Jl. Heat Mass Transfer, 10 489 (1967).

MASUMUNE, S. and SMITH, J.M., Ind. Engng Chem. Fund., 2 136 (1963).

MEEK, R.M.G., International Developments in Heat Transfer, Proc. of the 1961-62 Heat Transfer Conf., p 770, A.S.M.E. 1963.

MICKLEY, H.S., SMITH, K.A. and KORCHAK, E.I., Chem. Engng. Sci., 20 237 (1965).

MORAN, P.A.P., "An Introduction to Probability Theory' Section 6.4 et sequ. Oxford U.P. 1968.

NAGY, B.S., 'Introduction to Real Functions and Orthogonal Expansions' Oxford, 1965.

OSTERGAARD, K. and MICHELSEN, M.L., Tripartite Conf. Montreal 1968; Can. Jl. Chem. Engng., 47 107 (1969).

PETHO,A, a) Chem. Engng. Sci., 22 : 1793 (1967).

PETHO,A, b) 'A frequency response analysis method to determine the mean and variance of residence time distributions' personal comm. 1969, submitted for publications

PRICE, J., Aust. Atomic Energy Comm. Rep. AAEC/TM332, July 1966, Instn. Engrs. Aust. Mech. and Chem. Trans., MC4 : 7 (1968).

PULSIFIER, A.H., Ph.D. Thesis, Syracuse University, 1965.

RANZ, W.E., Chem. Engng. Progr., 48 247 (1952).

RIDGWAY, K. and TARBUCK, K.J., Jl. Pharm. Pharmacol, 18 (Suppl.) 168S (1966).

RIDGWAY, K. and TARBUCK, K.J., Chem.Engng. Sci., 23 1147 (1968).

RIMPELL, A.E., CAMP, D.T., KOSTECKI, J.A. and CANJAR, L.N., A.I.Ch.Engng.Jl. 14 19 (1968).

ROSEN, J.B., Jl. Chem. Phys., 20 (1), 387 (1952).

ROSEN, J.B., Ind. Engng. Chem. 46 1590 (1954).

REFERENCES. (Cont'd)

ROSEN, J.D. and WINSCHE, W.E., Jl.Chem.Phys. 18 1587 (1950).

ROWE, P.N. and CLAXTON, K.T., Trans.Inst.Chem.Engrs. 43 T321 (1965).

SATER, V.E. and LEVENSPIEL, O., Ind.Engng.Chem. Fund, 5 86 (1966).

SAUNDERS, O.A. and FORD, H., Jl.Iron Steel Inst. 141 : 291 (1940).

SCHNEIDER, P. and SMITH, J.M., A.I.Ch.Engng.Jnl.,14 762 (1968).

SCHUMANN, T.E.W., Jl. Franklin Inst., 208 405 (1929).

SCHWARTZ, R.M. and SMITH, J.M., Indl. and Engng. Chem., 45 : 1209 (1953).

[illegible]DEL, H.-P., Chemie. Eng. Techn. 37 : 1125 (1965).

SZOMANSKI, E. and MANINS, P.C., Aust. Atomic Energy Commission Report TM465 July 1968.

TURNER, G.A., A.I.Ch.E.Jnl. 13 678 (1967).

WADSWORTH, J., NRC Report MT - 39, Sept., 1958.

WADSWORTH, J., NRC Report MT-41, Feb., 1960.

WADSWORTH, J., International Developments in Heat Transfer, Proc. of the 1961-62 Heat Transfer Conf. p 760, A.S.M.E. 1963.

WILLIAMSON, J.E., BAZAIRE, K.E. and GEANKOPLIS = C.J., Ind. Engng. Chem. Fundamentals, 2 126 (1963).

Van CAUWENBERGHE, A.R., Chem. Engng. Sci., 21 : 203 (1966).

ZWEITERING, T.N., Chem. Engng. Sci. 11 1 (1959).

Inside Cover Back Pocket

Reprint

of Paper published in

THE ELECTRICAL ENGINEERING TRANSACTIONS

OF

THE INSTITUTION OF ENGINEERS, AUSTRALIA

Jeffreson, C. P. (1969). An approximation method for fourier transform inversion applied to distributed parameter systems. *Electrical Engineering Transactions of the Institution of Engineers, Australia. March*, 77-84.